

Appendix 1

Soil Data Report for 17th Street Canal

Introduction

This is a data report detailing the data collected by the Interagency Performance Evaluation Task Force (IPET) to support the analysis of the I-wall section that breached at the 17th Street Canal as a result of Hurricane Katrina on August 29, 2005. The location of the 17th Street Canal is shown in Figure 1-1. The site of the breach, located on the east bank near the north end of the canal, is also noted on Figure 1-1.

The data will be used in the Floodwall and Levee Performance Analysis task as part of its effort to determine how the flood protection structures performed in the face of the forces to which they were subjected by Hurricane Katrina, and to compare this performance with the design intent, the actual as-built condition, and observed performance. This effort includes understanding why certain structures failed catastrophically and why others did not. The effort will determine, in detail, how the levees and floodwalls performed during Hurricane Katrina. These studies will be documented in a series of reports. The series of reports will start with data reports detailing the data collected on the site conditions at 17th Street Canal, London Avenue Canal, Orleans Canal, and Inner Harbor Navigation Canal, as noted on Figure 1-1.

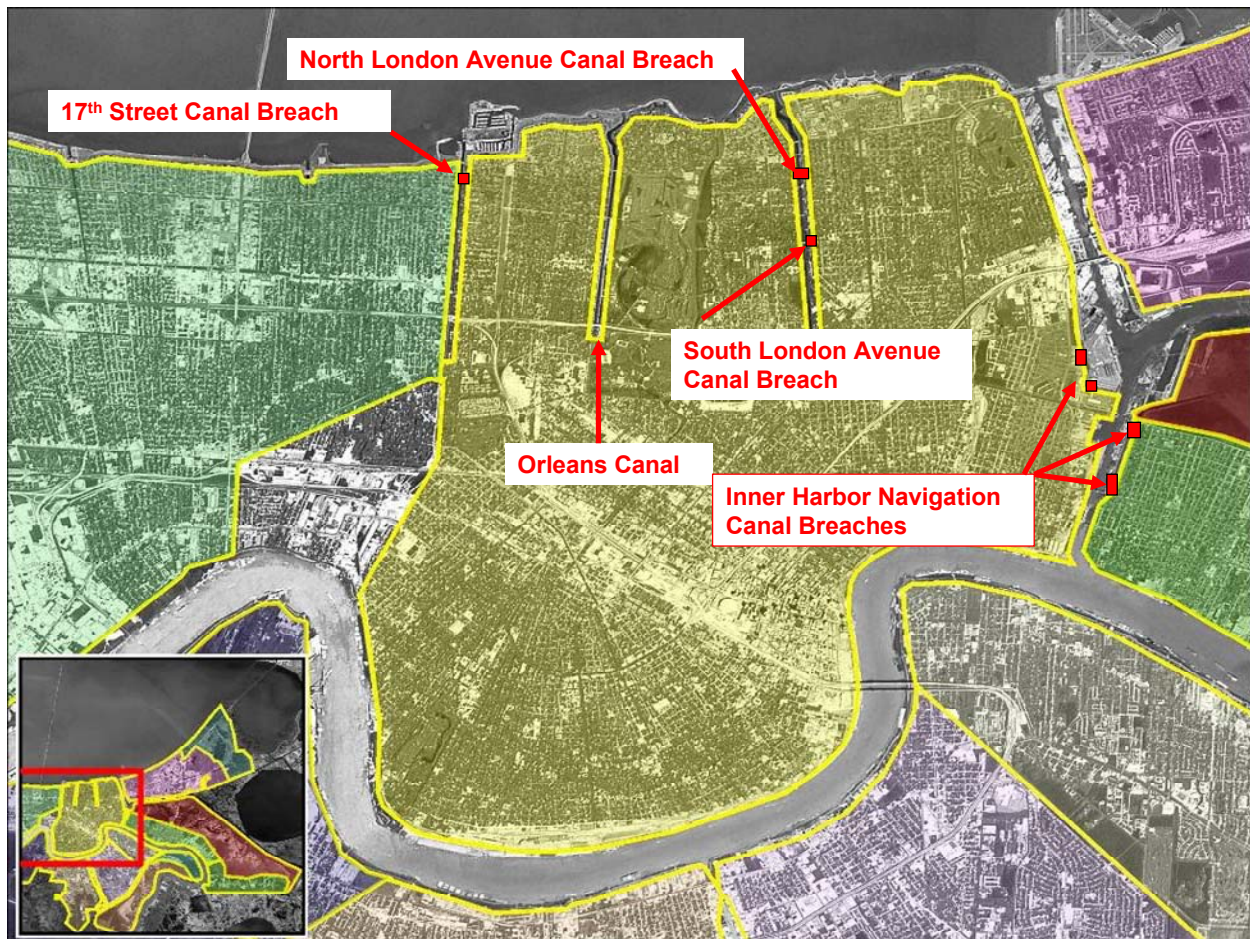


Figure 1-1. Location of Orleans Parish canals

The key data obtained for the breach site and documented as part of this report include:

- a. Geology of the area.
- b. Description of soil stratigraphy.
- c. Representative pre-Katrina cross section through the breach area.
- d. Soil undrained shear strength profiles.

These data were obtained from a variety of sources, including the project's General Design Memorandum, design documents, and surveys prepared prior to Katrina. In addition, this report contains information obtained from field and laboratory investigations and surveys conducted after the Hurricane Katrina event. This report was prepared with the intent to provide numerical and physical modelers with the information needed to build their models.

Geology

Introduction

Before examining the individual failure areas at the 17th Street Canal, a review of the geology is presented to familiarize the reader with the broader context of the geology of the delta plain, its stratigraphy, and the soils comprising the foundations at the different failure areas. For comparison purposes, the general geology of the 17th Street, Orleans, and London Avenue Canals levee breaches is reviewed. The geology of the New Orleans area has been determined from detailed mapping studies of the Louisiana Coastal Plain (LCP), from a review of the published literature, from data collection activities at each of the failure sites by an IPET study team, and from an evaluation of preexisting and recently drilled engineering borings from each of the failure areas.

Previous Studies

A review of the past geologic literature from the New Orleans area identifies the US Army Corps of Engineers (USACE) as being actively involved with much of the regional and focused geologic studies that have been performed in the eastern LCP or deltaic plain (Dunbar and others, 1994 and 1995; Dunbar, Torrey, and Wakeley, 1999; Fisk, 1944; Kemp and Michel, 1967; Kolb, Smith, and Silva, 1975; Kolb, 1964; Kolb and Van Lopik, 1958a and 1958b; Kolb and Schultz, 1954; Kolb and Saucier, 1982; May and others, 1984; Michel, 1967; Saucier, 1963, 1984, and 1994; and Schultz and Kolb, 1950). Many of these studies and associated geologic maps are available from a USACE-sponsored website on the geology of the Lower Mississippi Valley that is accessible to the public at lmvmapping.erdc.usace.army.mil.

Geologic History and Principal Physiographic Features of the New Orleans Area

To better understand the soils beneath the 17th Street, Orleans, and London Avenue Canals, and the engineering properties of these soils, a brief summary of the geologic history of the New Orleans area is presented. Detailed descriptions of the geologic history are presented in Saucier (1964 and 1994); Kolb, Smith, and Silva (1975); Kolb and Saucier (1982); and Kolb and Van Lopik (1958).

The geology and stratigraphy of the New Orleans area are young in terms of its age. Generally, sediments comprising the New Orleans area are less than 7,000 years old. Formation of the present day New Orleans began with the rise in global sea level, beginning about 12,000 to 15,000 years before the present. The rise in sea level was caused by melting of continental glaciers in the Northern Hemisphere and the release of ice-bound water to the oceans. At the maximum extent of continental glaciation, eustatic sea level was approximately 300 ft (~100 m) lower than the present level. In addition, the ancestral coastal shoreline was much farther south of its current location, probably near the edge of the continental shelf.

The underlying Pleistocene surface throughout much of coastal Louisiana was subaerial, and exposed to oxidation, weathering, and erosion. These conditions led to the development of a well-

developed drainage network across its surface, and created a distinct soil horizon in terms of its engineering properties. The Pleistocene horizon is easily recognizable in borings because of its distinct physical properties as compared to the overlying Holocene fill (i.e., oxidized color, stiffer consistency, higher shear strength, lower water content, and other physical properties.). The axis of the main valley or entrenchment of the Mississippi River was located west of New Orleans, in the vicinity of present day Morgan City, LA (Figure 1-2). Consequently, development of the early Holocene deltas was concentrated near the axis of Mississippi entrenchment when sea level rise began to stabilize sometime between 5,000 to 7,000 years before the present. New Orleans is located on the eastern edge of this buried entrenchment or alluvial valley.

The Pleistocene surface in the New Orleans area is variable, but generally ranges between 50 and 75 ft below sea level as determined from detailed mapping and examination of boring data (Kolb and Van Lopik 1958; Kolb, Smith, and Silva 1974; Saucier 1994; and Dunbar and others 1994 and 1995). Various sea level curves for the Louisiana coast are presented and discussed in Kolb, Smith, and Silva (1975) and Tornquist and Gonzalez (2002). These curves generally indicate that sea level transgression in the New Orleans area generally occurred between 6,000 to 9,000 years before the present, based on the mapped depths to the top of the Pleistocene surface.

As the rate of the sea level rise declined and stabilized, it led to the development of five, short-lived delta complexes across the Louisiana coast by deposition of Mississippi River sediments (Figure 1-2). Individual delta complexes are composed of numerous, branching distributary channels. These channels transport and deposit fluvial sediments along the margin of the delta and build land seaward into shallow coastal water. Distributary channels from the St. Bernard delta are responsible for filling the shallow Gulf waters in the greater New Orleans area (Frazier 1967).

Bayou Sauvage is a major distributary involved in the filling of the shallow Gulf waters in the New Orleans area (Figure 1-3). This channel extends eastward from the Mississippi River and is composed of Bayous Metairie, Gentilly (or Gentilly Ridge), and Sauvage. Natural levees of this distributary channel form a pronounced physiographic feature in the northern New Orleans area (Figure 1-3). Similarly, Mississippi River's natural levees are some of the highest land elevations found in New Orleans, and these were the first areas to be settled by the early inhabitants in the 1700s. Distributary channels in New Orleans are pronounced physiographic features, and are associated with the St. Bernard delta complex as determined from radiocarbon dating of organic sediments (Frazier, 1967; Kolb and Van Lopik 1958; McFarlan 1961; Britsch and Dunbar 1999; and Smith, Dunbar, and Britsch 1986).

Equally important to the development and filling history of the New Orleans area is the presence of a buried, barrier beach ridge which formed approximately 4,500 to 5,000 years before the present. This beach extends northeast in the subsurface along the southern shore of Lake Pontchartrain (Figure 1-4). Sea level was 10 to 15 ft lower than the current level when the beach ridge formed. A stable sea level permitted sandy sediments from the Pearl River to the east to be concentrated by longshore drift, and formed a sandy spit or barrier beach complex in the New Orleans area as shown by Figure 1-3 (Saucier 1994).

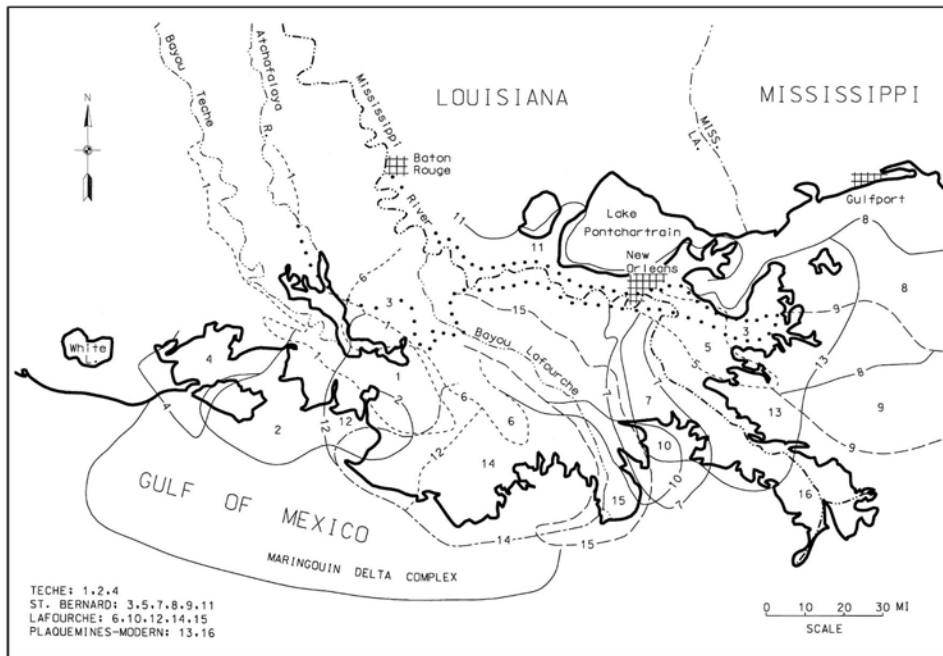
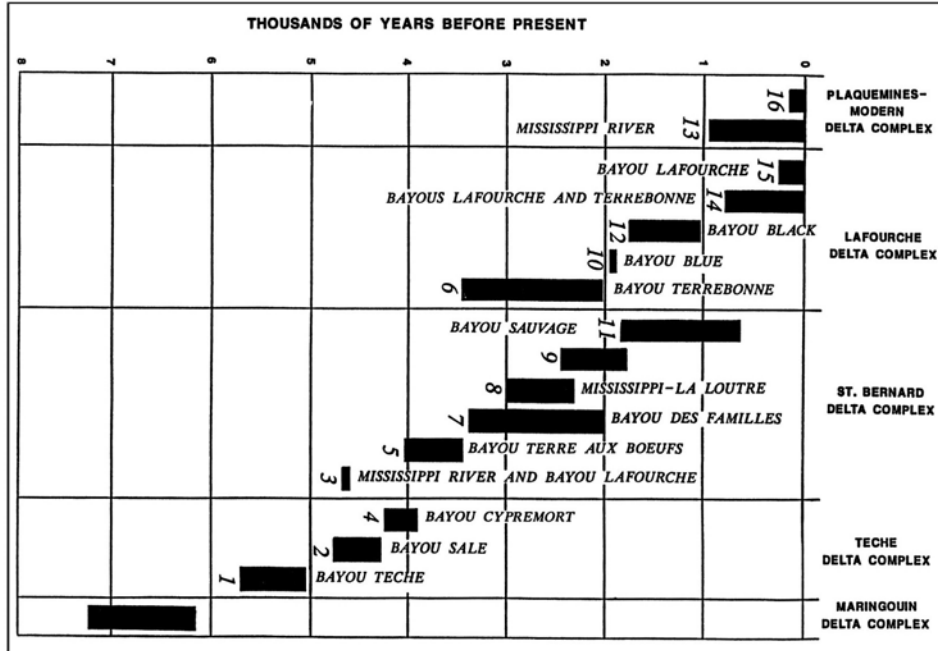


Figure 1-2. Location and approximate chronology of the Mississippi River Deltas, major distributary channels are numbered, note Bayou Sauvage (No. 11) which extends across the New Orleans area and forms the Bayou Metairie/Gentilly Ridge (after Frazier, 1967). Morgan City, LA, located along axis of maximum Mississippi River entrenchment

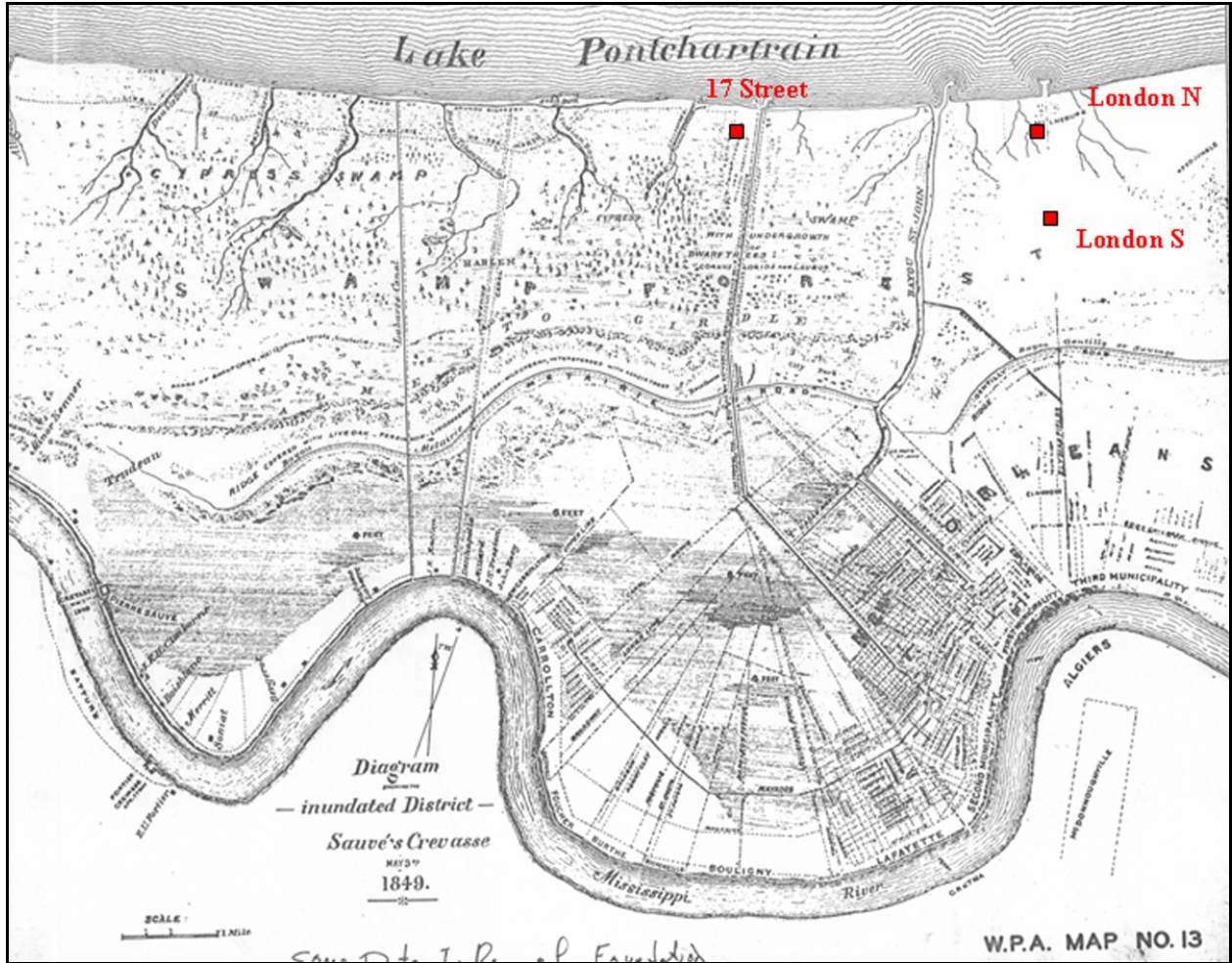


Figure 1-3. New Orleans area map from 1849 showing city limits and topography. Note the location of Bayous Metairie and Gentilly (i.e., Bayou Sauvage) and the identified cypress swamp north of the city at this time (Work Projects Administration 1943).

The presence of the barrier beach affected sedimentation patterns and the subsequent locations for advancing distributary channels in the New Orleans area. The beach complex likely prevented the Mississippi River and later St. Bernard distributaries from completely filling Lake Pontchartrain with sediment. Consequently, foundation soils beneath the 17th Street, Orleans, and London Avenue Canal breaches are affected by their proximity to the buried beach complex. As shown by Figure 1-4, the breach at the 17th Street Canal is located on the protected or land side of the beach ridge, while both of the London canal breaches are located over the thickest part or axis of this ridge complex. The beach ridge cuts across the Orleans Canal with the north portion on the landside and south portion over the axis of this ridge complex.

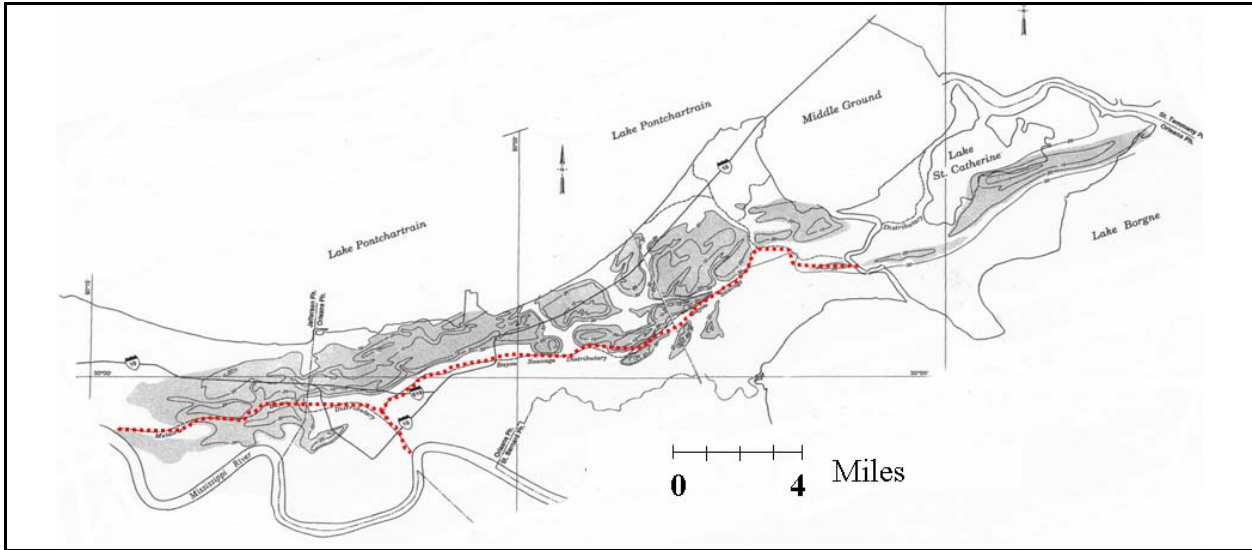


Figure 1-4a. Pine Island buried beach complex in the New Orleans Area (from Saucier 1994). Course of Bayou Sauvage (i.e., Bayous Metairie and Gentilly) identified in red. Note the presence of the barrier beach prevented this distributary course from extending northward into present day Lake Pontchartrain and filling the lake. Canal breaches are identified in blue with 17th Street breach behind the thickest part of the beach ridge, while both the London North and South breaches are on the axis of the barrier. See Figure 1-3b for close-up of canal areas.

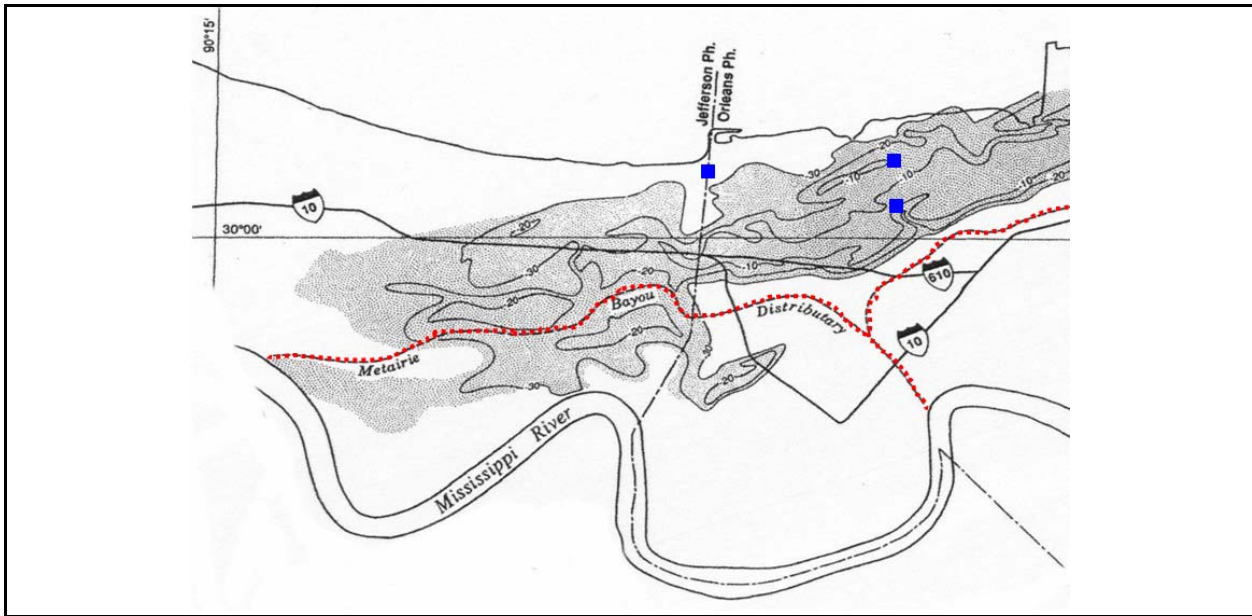


Figure 1-4b. Close-up view of the buried beach ridge, and the locations of the canal breaches to the buried beach (after Saucier 1994). The 17th Street breach is located behind the axis of the beach ridge while the London Canal breaches are located on the axis of the ridge. Bayou Metairie is identified in red and forms the Bayou Sauvage distributary course (No. 11) in Figure 1-2.

Surface and Subsurface Geology of the New Orleans Area

A geologic map of the New Orleans area is presented in Figure 1-5 and identifies the major environments of deposition at the surface in the vicinity of the 17th Street, Orleans, and London Avenue Canals. Located on the surface of the New Orleans area are natural levee and point bar deposits adjacent to the Mississippi River, abandoned distributary courses (Bayou Sauvage-Metairie north of the Mississippi River and Bayou des Families south of the Mississippi River, respectively), and extensive marsh-swamp deposits at the surface (see also Figure 1-3). Land reclamation occurred in the 1920's along the shore of Lake Pontchartrain by dredging, and this area is identified as spoil deposits.

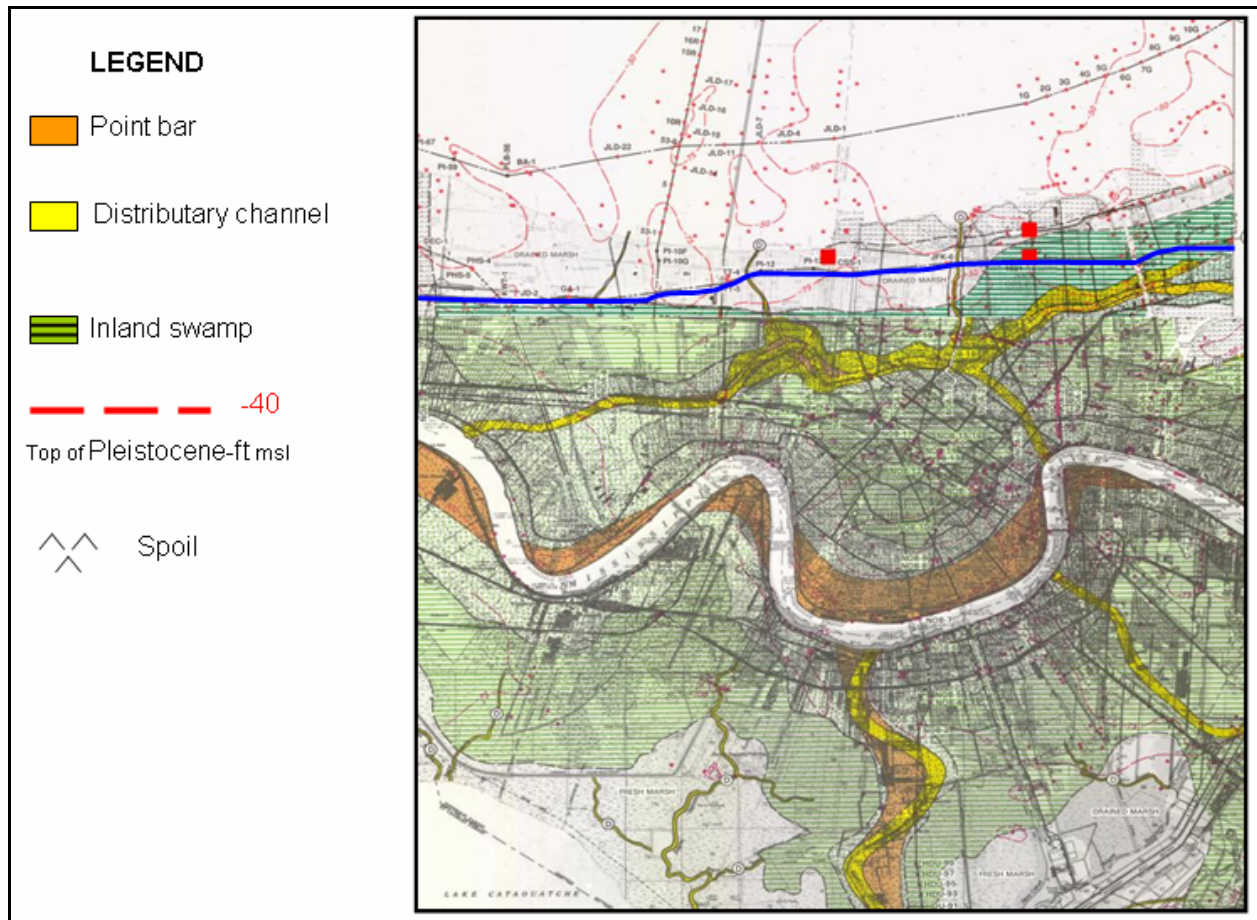


Figure 1-5. Geology map of the New Orleans and Spanish Fort Quadrangles showing the distribution of environments at surface. Elevation of the Pleistocene surface shown in red along with borings used to map this surface. Cross-section C-C' in blue extends through 17th Street and London Canal Areas (areas identified in red). See website lmvmapping.erd.c.usace.army.mil for nearby maps and other cross-sections identified. Portion of cross-section C-C' above is presented as Figure 1-6 (from Dunbar and others 1994 and 1995).

A portion of cross-section C-C from the Spanish Fort Quadrangle is presented as Figure 1-6 to identify the general subsurface stratigraphy beneath the 17th Street and London canal breaches. Boring data from this section identify distinct depositional environments in the

subsurface that are stacked vertically and form a stratigraphic record of the filling history during the Holocene period. Major stratigraphic units in the subsurface, beginning with the oldest, include the Pleistocene (older fluvial and deltaic deposits), bay sound/estuarine, relic beach (Pine Island Beach ridge) lacustrine/interdistributary, and marsh/swamp deposits. A summary description of the different depositional environments in the New Orleans area is presented in Appendix 2 (from Dunbar, Torrey, and Wakeley, 1999). Additionally, detailed descriptions of the different depositional environments are contained in Saucier (1994), Kolb (1962), and Kolb and Van Lopik (1958).

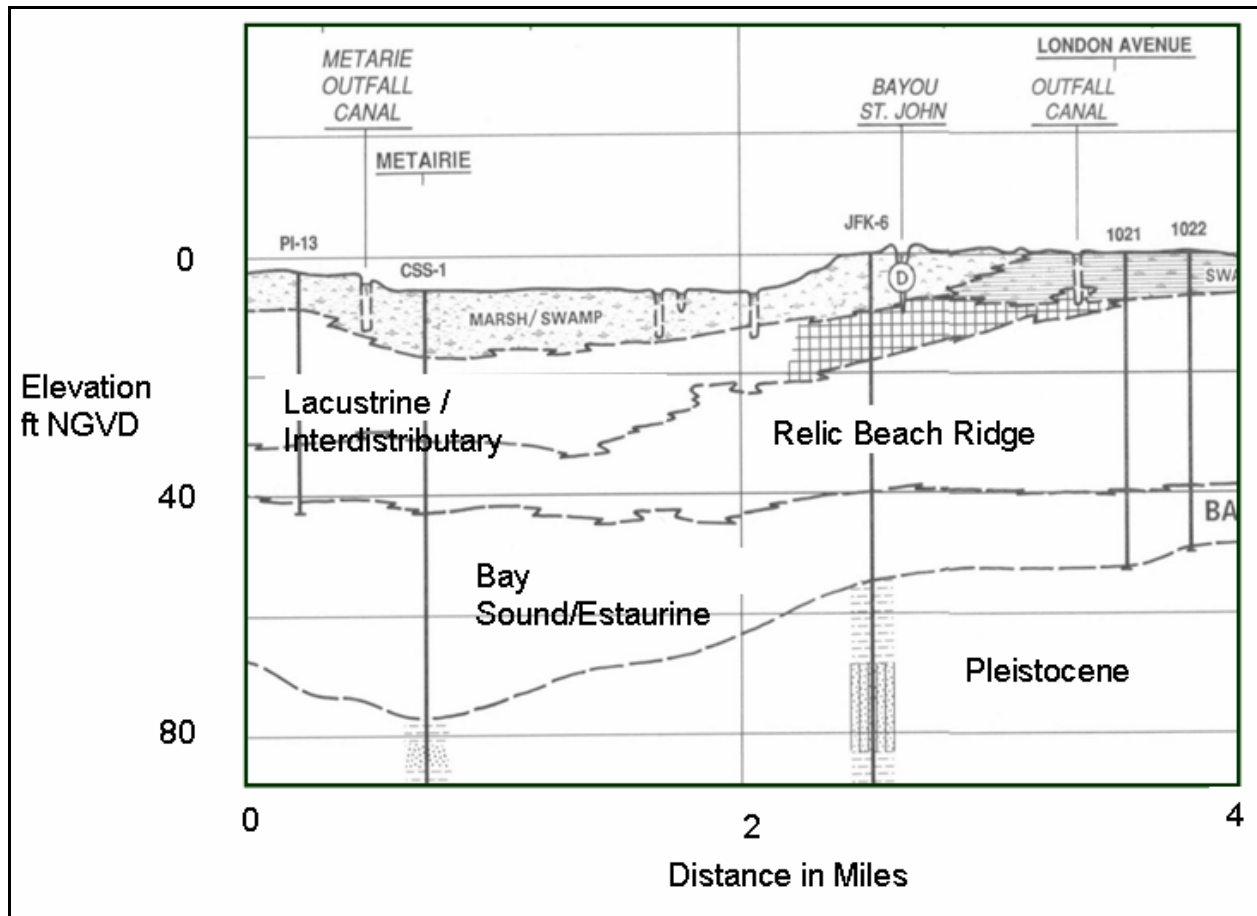


Figure 1-6. Portion of cross section C-C" from the Spanish Fort Quadrangle which extends through the 17th and London Canal breaches and identifies the stratigraphic environments in the subsurface (from Dunbar and others 1995)

Besides mapping the horizontal and vertical limits of the various environments of deposition, relationships between these environments and key engineering properties of the respective soils have been developed. These relationships have been tabulated and are published in Kolb (1962), Montgomery (1974), and Saucier (1994). A summary of these engineering relationships is presented in Appendix 2. Similarly, relationships have been developed from the engineering properties and laboratory soil test data from 17th Street, Orleans, and London Avenue Canals.

These data are presented in later sections of this summary as related to discussions of their engineering significance.

Geologic information from the New Orleans area helped the IPET focus its investigation and collection of data for the 17th Street, Orleans, and London Avenue Canal breaches. An understanding of the geology was an important first step to systematically collecting and evaluating stratigraphic and engineering data from these breach areas.

Development of Cross Sections

Pre-Katrina Sections

A significant amount of information was obtained from General Design Memorandum No. 20 – 17th Street Outfall Canal – Volume 1 (GDM No. 20) in the development of pre-Katrina cross sections. This document was completed in March 1990 in preparation for upgrading the New Orleans levee system to provide increased flood protection against a stronger revised design hurricane.

Figures 1-7 and 1-8 show longitudinal profiles of the east and west bank levees of the northern half of the 17th Street Outfall canal, respectively. These figures, obtained from GDM No. 20, show boring locations and the soil types obtained during the explorations for the project upgrade. It is noted that odd numbered borings are located on the west bank, and even numbered borings are located on the east bank. Noted on the figures is the location of the breach site which is situated on the east bank of the canal between Stations 560+50 and 564+50.

A more detailed representation of the soil stratigraphy profile along the centerline in the breach area is shown in Figure 1-9. This profile was constructed using additional soil data acquired during the post-Katrina soil exploration conducted during September through October 2006. The additional borings included B1, B2, B3, B4, B5, NO-1-05U, and NO-2-05U. A plan view showing the locations of both old and new borings is shown in Figure 1-10. The new borings were needed because only the two old borings, B62 and B64 (reported in GDM No. 20), were in the immediate vicinity of the breach. The new borings extended the depth of the investigation in this area from approximately Elevation -50 ft NGVD to Elevation -115 ft NGVD. Additionally, data from cone penetration testing, from the new exploration program, were used to supplement soil data from the old and new borings and refine the stratigraphy in the breach area. Since the levee was destroyed in the breach area during the storm, the new borings, B1 through B4, were drilled from a barge in the canal and were offset from the centerline. Data acquired from these borings were projected back to the centerline in an effort to improve the interpretation of the stratigraphy.

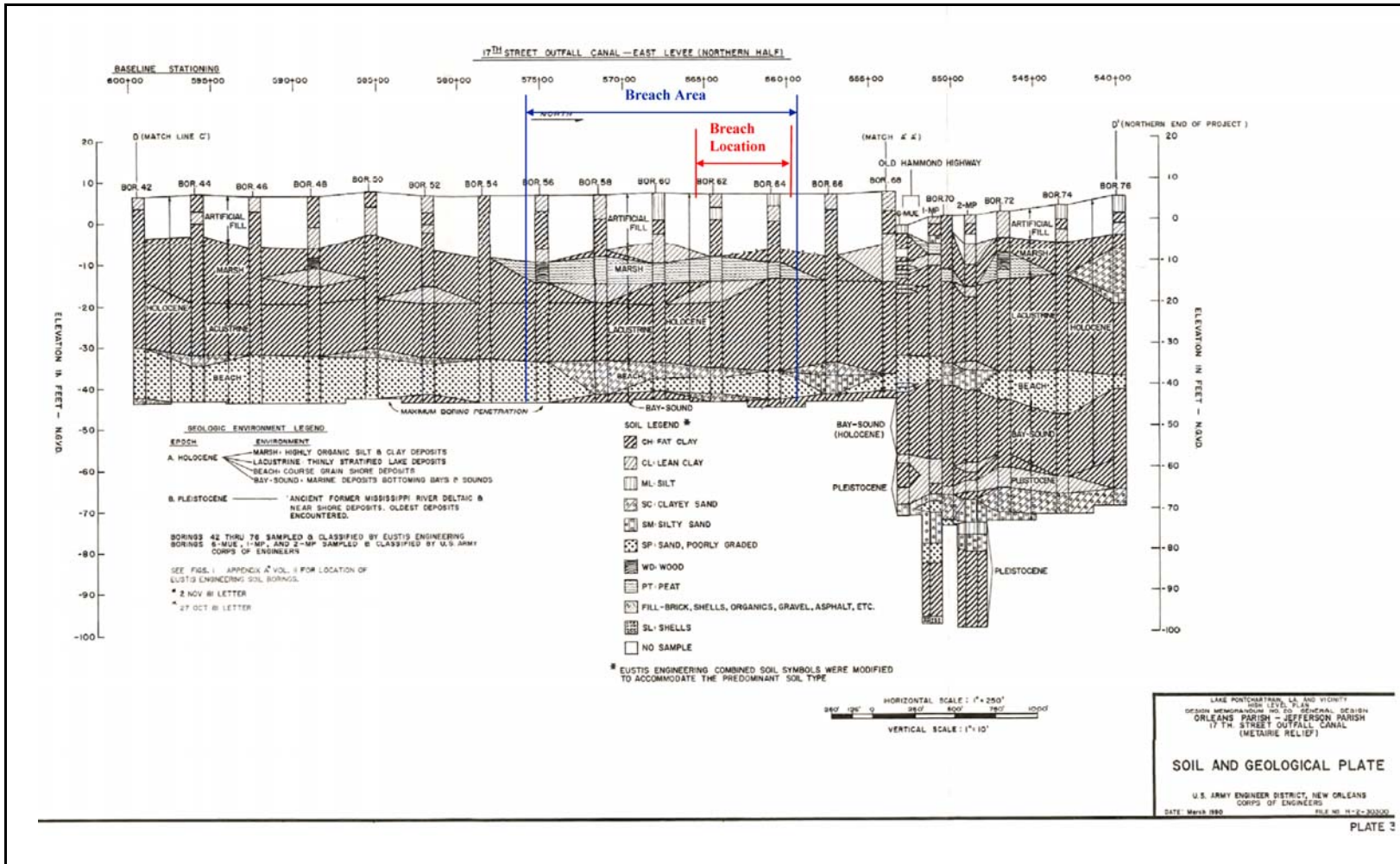


Figure 1-7. Geological Profile showing Breach Area (East Levee)

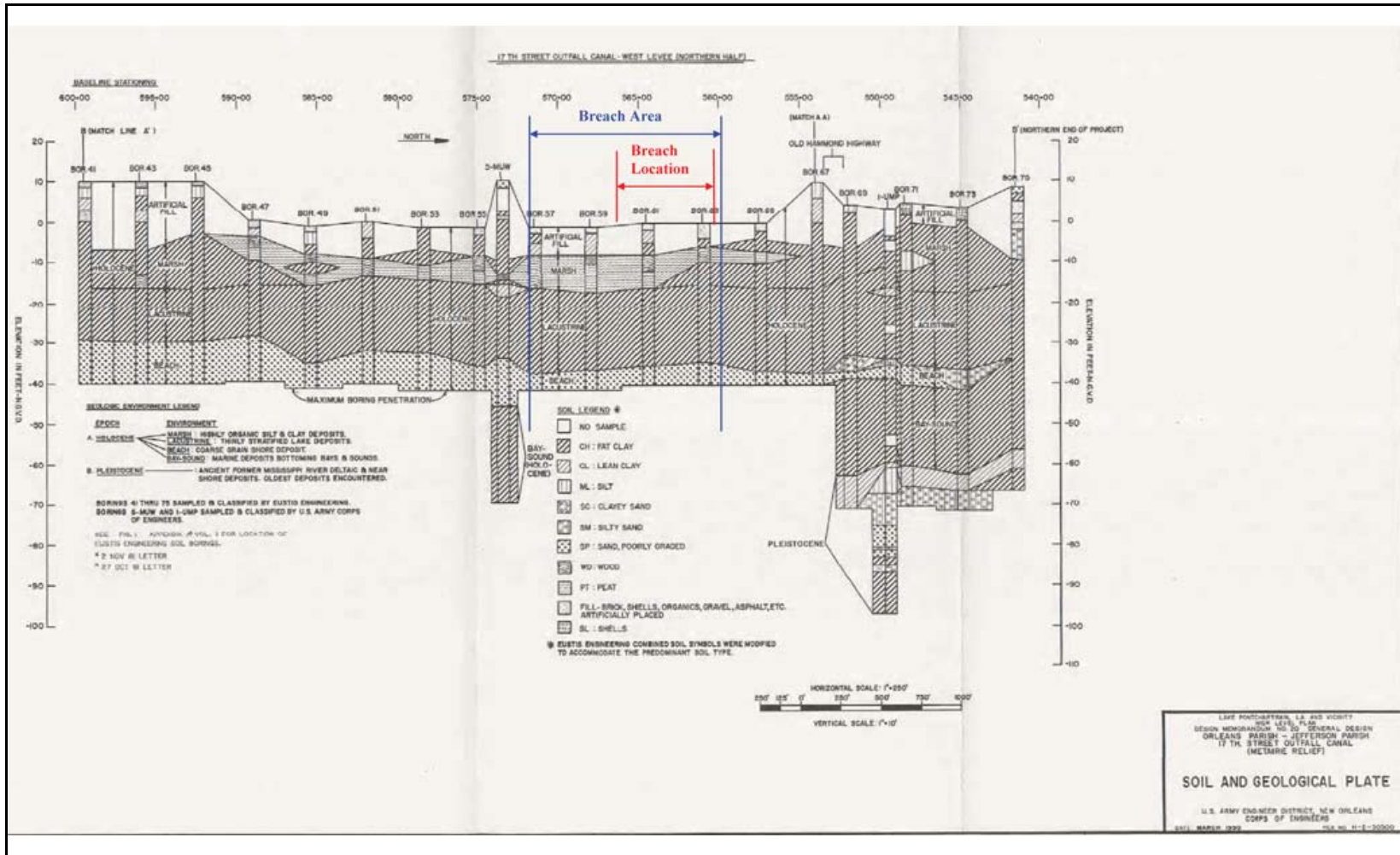


Figure 1-8. Geological Profile showing Breach Area (West Levee)

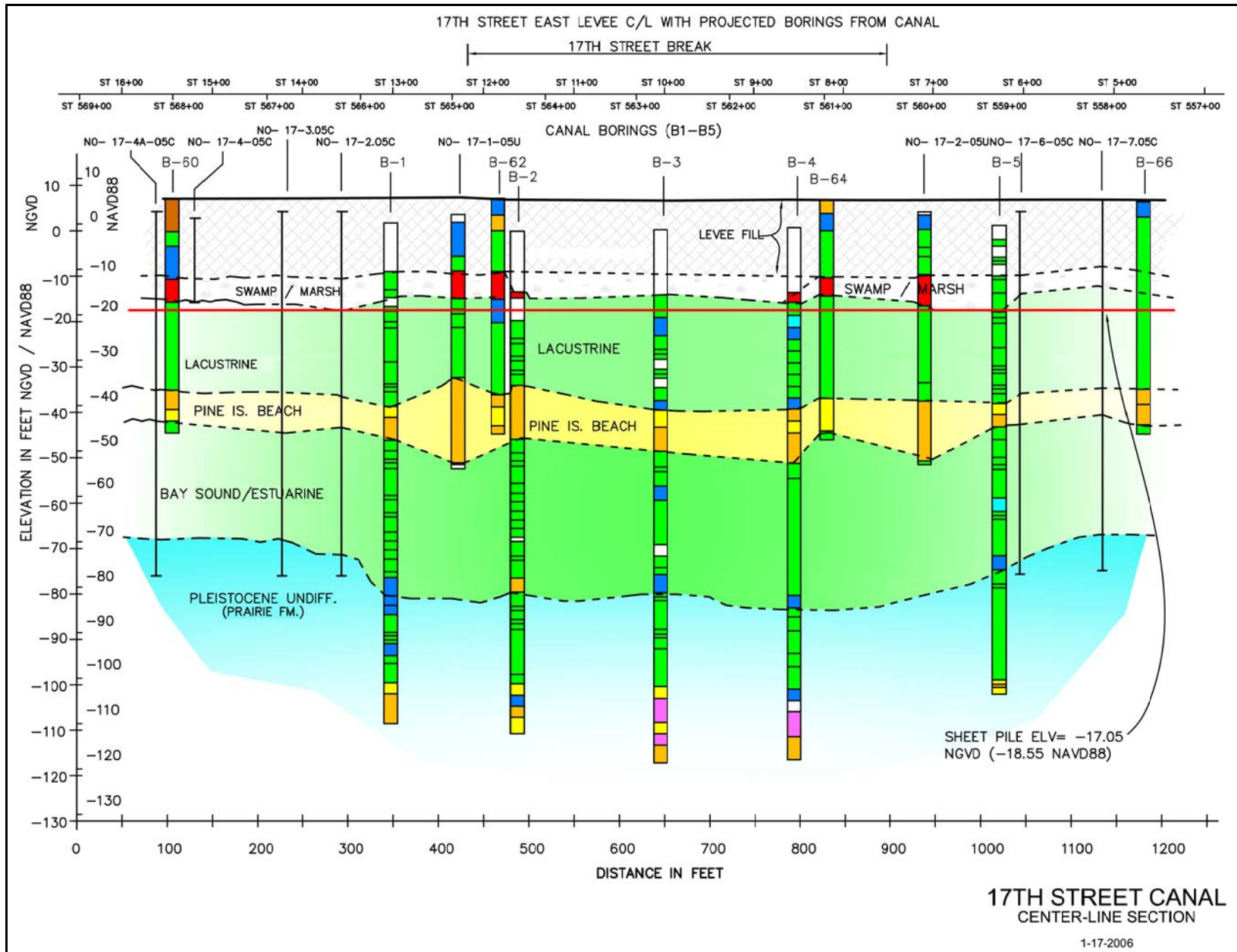


Figure 1-9. Centerline (CL) Cross-section of Breach

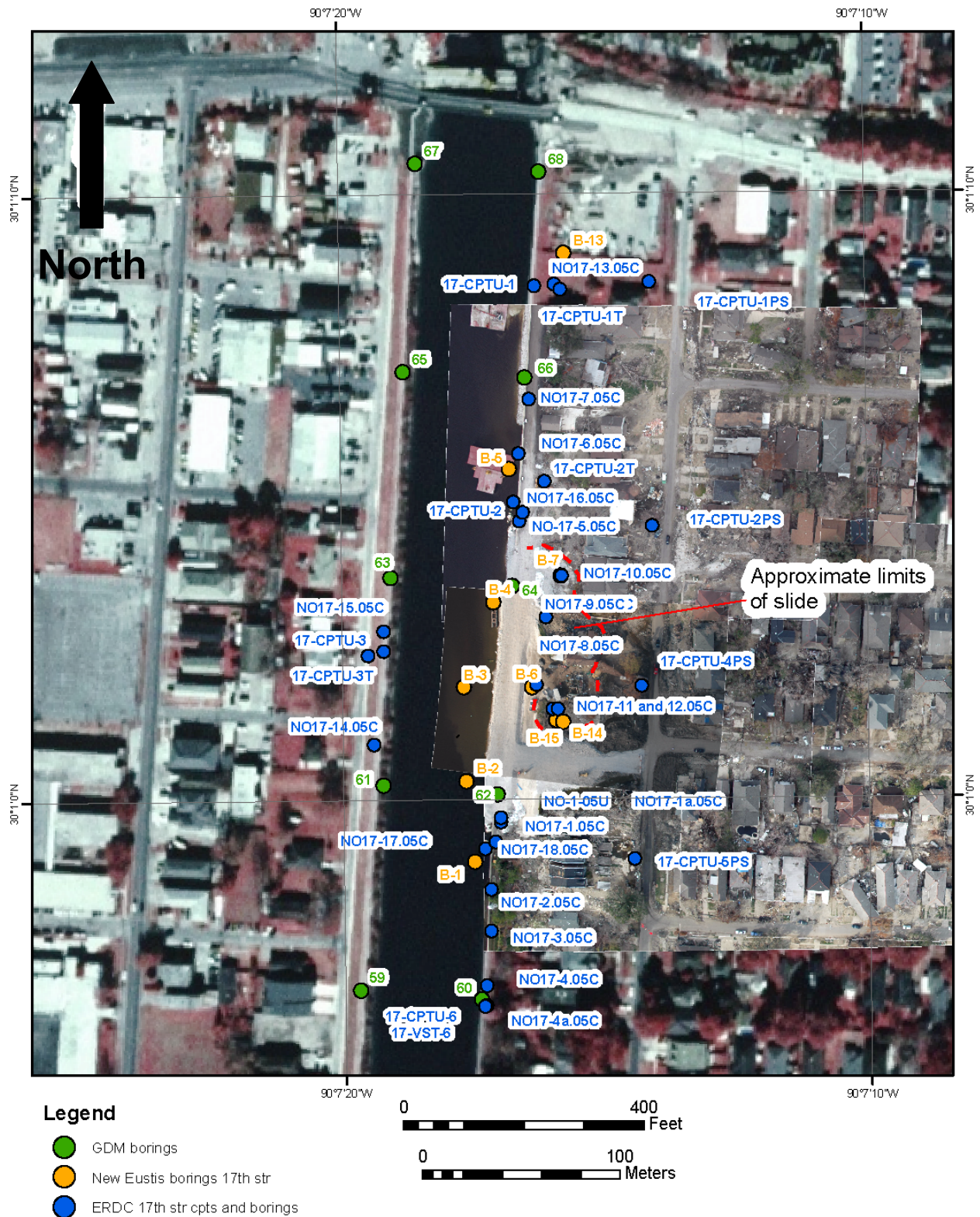


Figure 1-10. Boring and CPT Location Map

The information presented on Figure 1-9 yielded the following interpretation of the subsurface stratigraphy in the breach area. The subsurface in the breach area was simplified into six basic groups of soil types over the depth of the investigation:

Layer	Approximate Elevation of Top of Layer, ft (NGVD)	Approximate Elevation of Bottom of Layer (NGVD)	Soil Type	Consistency
Embankment	6.5	-10	Clayey (CL's and CH)	Stiff
Marsh	-10	-15	Organic/Peat	Very Soft
Lacustrine	-15	-35	Clays (CH)	Very Soft
Beach Sand	-35	-45	Sand	
Bay Sound/Estuarine	-45	-75	Clayey (CH)	Stiff to V. Stiff
Pleistocene (Undifferentiated) Prairie Formation	-75		Clays – Generally CH with some sand	Stiff

An additional word about the Marsh deposit may be useful. The marsh is represented as an organic soil and a peat-type material. Examination of the drilling logs suggests that since wood was encountered at the top part of the layer, this layer may be more fibrous near the top and more amorphous at the bottom of the layer. Further investigation of the peat layer may be necessary to better quantify the differences between the top and bottom of the layer.

Transverse Cross Sections through the Breach Site

Three representative transverse cross sections through the levee breach site were prepared from the data at hand. These three sections were developed from Station 8+30, Station 10+00, and Station 11+50. Station 8+30 is the most northerly station of the three. These cross sections were prepared with the intent that they represent the conditions that existed *immediately before* the arrival of Katrina. Data from a pre-Katrina airborne LIDAR (Light Detection and Ranging) survey on the New Orleans Levee System that was conducted during the year 2000 were used to improve the surface topography in the breach area from that presented in the GDM No. 20 and the design documents. The LIDAR data is the best data available for establishing the cross sections before Katrina, because accurate ground survey data were not available during the preparation of this report. The surveys generate points of X, Y, and Z data that are accurate to the nearest foot. A typical LIDAR section is shown in Figure 1-10. The LIDAR surveys were particularly useful in establishing the levee dimensions, slope, and toe elevations on the protected side of the floodwall. Unfortunately, the LIDAR system cannot penetrate through water, so it was not possible to use this technology to acquire the ground topography in the canal. A hydrographic survey was obtained *immediately after* Katrina, on August 31, 2006, to obtain the surface elevations of the canal between the floodwalls on the east and west banks. The data obtained from the hydrographic surveys are reflected in the cross-sections described in the next paragraph.

The three representative cross sections for Station 8+30, Station 10+00, and Station 11+50 are shown in Figures 1-11, 1-12, and 1-13, respectively. Three sections were prepared because the levee dimensions are variable in the breach area on the east bank. Each cross section shows the conditions across the entire canal from the west bank to the east bank where the breach site is located. A degree of interpretation was necessary, particularly pertaining to the east bank protected side, to complete the cross sections because of the lack of soil boring data in this area. Thus, the marsh/peat layer was interpreted to be thinner under the centerline of the levee than at the toe due to consolidation from the surcharge caused by the weight of the levee. Also, an interpretation was made to include a 2- to 3-ft layer of topsoil over the top of the peat in this area. This effect may be cultural in nature because the protected side of the east bank was located in a residential area with houses having well-kept lawns.

It is also noted that the levee cross section at Station 11+50, the southernmost section of the three and shown in Figure 1-13, is the location where the post-Katrina surveys showed that the most scour occurred while water was flowing through the breach.

Uncertainties

Many uncertainties pertaining to the subsurface in the breach area will be difficult, if not impossible, to resolve because the levee in this area was destroyed and drastically changed due to emergency relief efforts. There was a lack of subsurface information on the protected side of the levee during the 1990 levee raising project described in GDM No. 20. There are efforts planned by the IPET to obtain more information in the vicinity immediately north and south of the breach area to better define soil strengths and thickness of the top soil and peat layers.

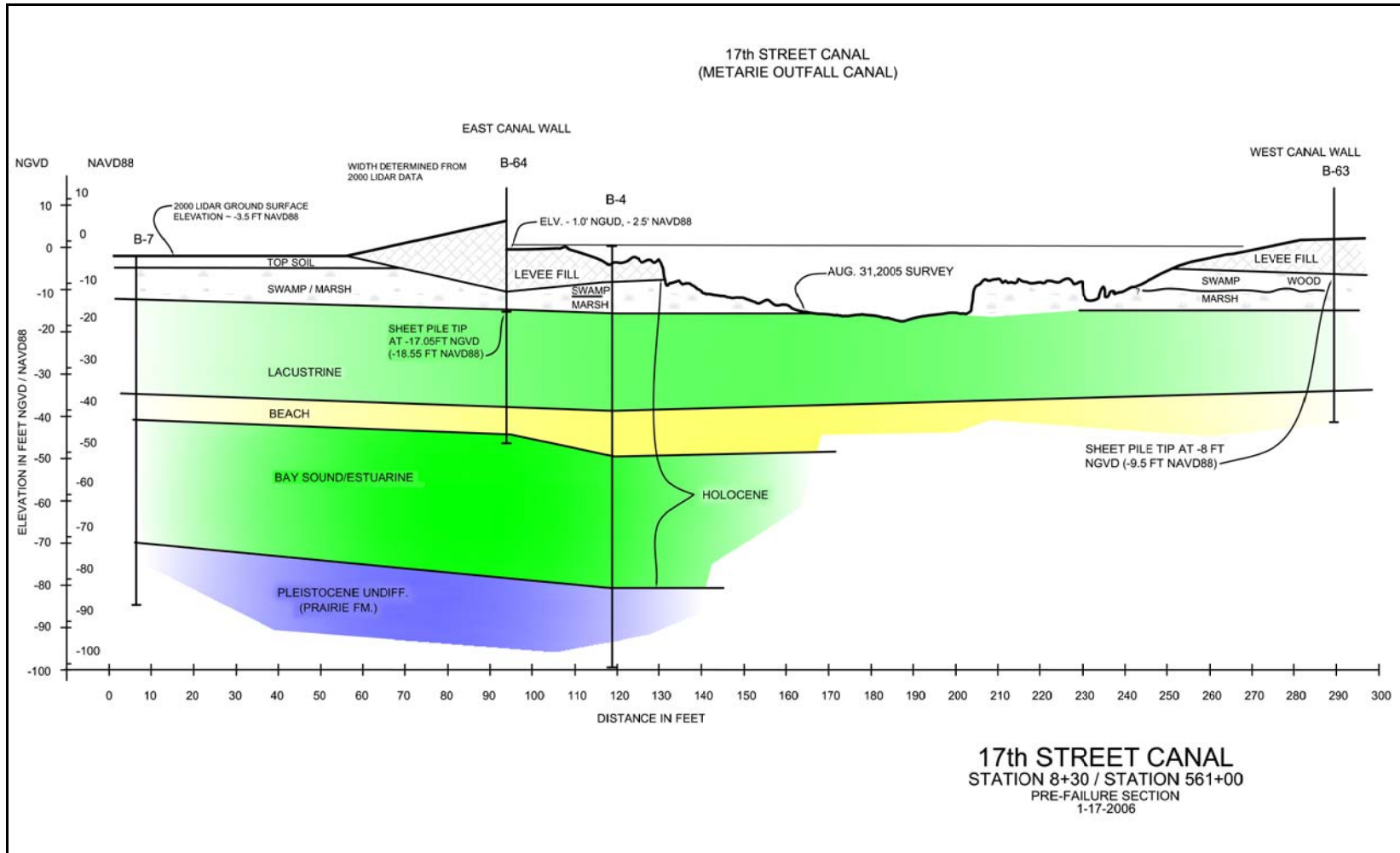


Figure 1-11. Prefailure Cross-Section at Sta 8+30 (New Stationing)/ Sta. 561+00 (GDM Stationing)

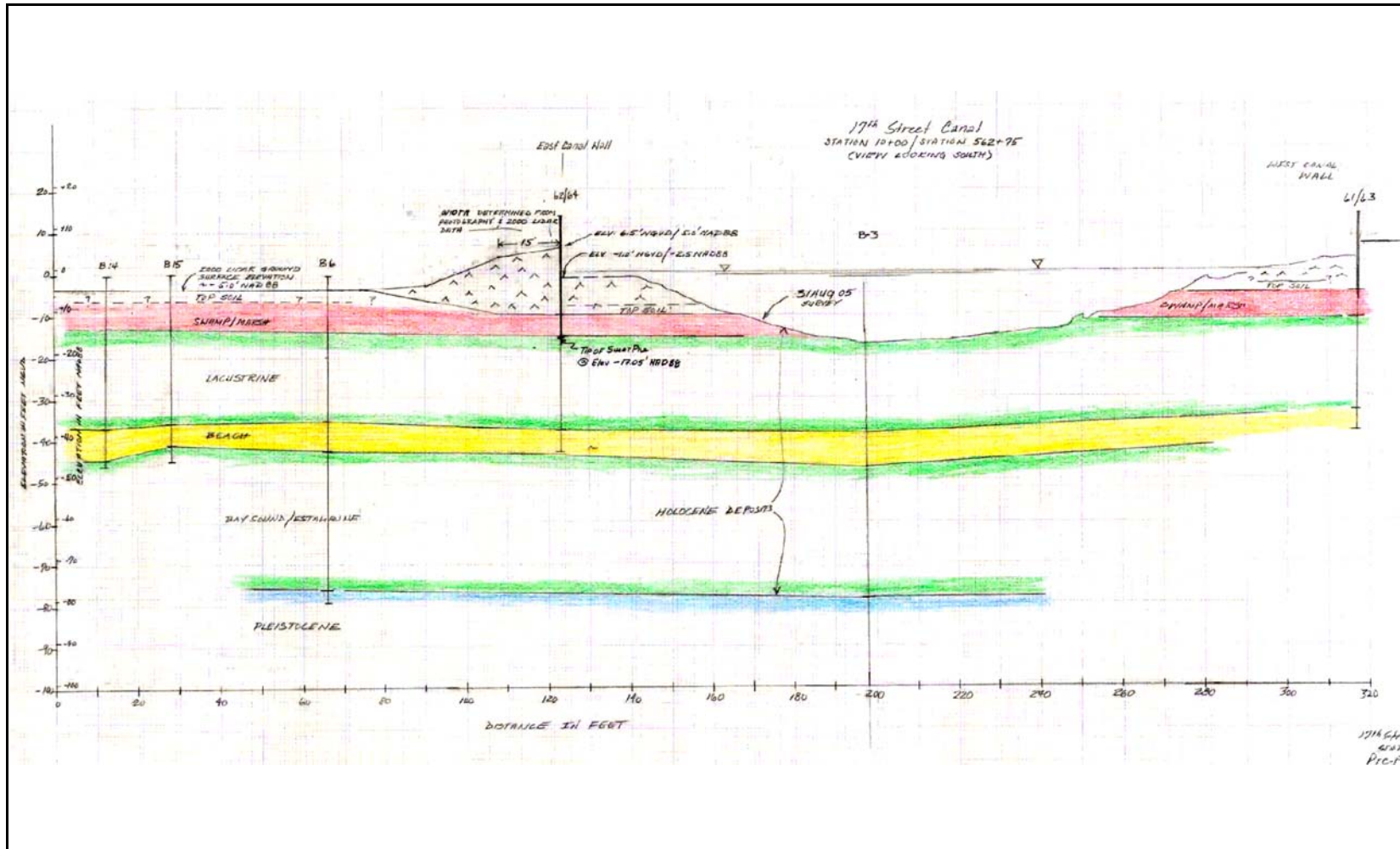


Figure 1-12. Prefailure Cross-Section at Sta 10+00 (New Stationing)/ Sta. 562+75 (GDM Stationing)

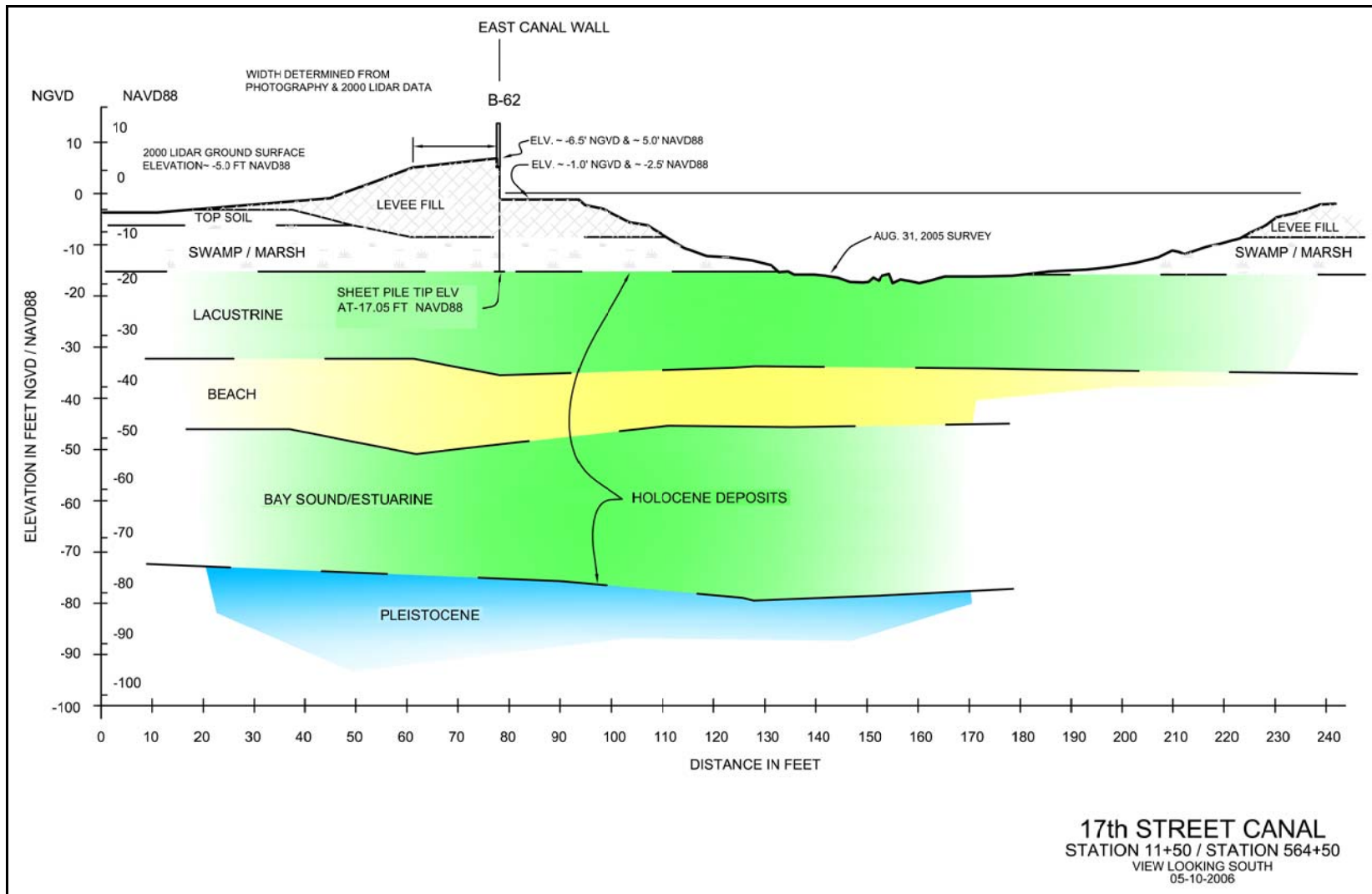


Figure 1-13. Prefailure Cross-Section at Sta 11+50 (New Stationing)/ Sta. 564+50 (GDM Stationing) (Note: Most scour occurred near this station)

Soil Properties

Introduction

The following is a summary of the current soil data available in the breach area of the 17th Street Canal. The soil data for the breach include all borings and cone penetrometer tests (CPT) in the breach area. This area was chosen because the geology and soil types are very similar to the soil types and geology found at the breach area. The breach area and breach location are shown in Figure 1-7. In addition, some soil data from the west levee will be used for the breach area because of similar geology and soil types. This area is shown in Figure 1-8.

The stratigraphy in the breach area is divided into Levee Embankment, Marsh Stratum, Lacustrine Stratum, and Beach Sand Stratum. The data for each stratum are presented below. These data consist of GDM borings, new borings (taken in 2005), and CPTs. Additional testing (consolidation tests, Atterberg Limits, UU triaxial tests w/ pore pressures) and investigations (CPTs and field vane shear test) were performed in 2006. Data from the investigations and lab testing are presented in later in the report.

Levee Embankment

Data on the levee embankment consist of five borings shown in the 1990 General Design Memorandum (GDM) and four cone penetrometer tests (CPT). Of the five GDM borings, four borings collected 3-in. (diameter) undisturbed samples, and one boring collected 5-in. (diameter) undisturbed samples. From the 3-in. samples, four unconfined compression (UC) tests were performed, and five one-point unconsolidated-undrained triaxial compression tests (UU-1), confined at existing overburden pressure, were performed. From the 5-in. samples, four one-point unconsolidated-undrained triaxial compression tests (UU-1), confined at existing overburden pressure, were performed. From these laboratory tests, moisture content and wet unit weights were determined. The moisture contents (%w) in the breach area are shown in Figure 1-14. In addition, these moisture content data were also plotted (Figure 1-15) with the moisture content data collected for the entire east levee on the canal. Also, the moisture content data for the entire west levee on the canal are shown in Figure 1-16.

The wet unit weight data in the breach area are shown in Figure 1-17. Wet unit weight data from the breach area plotted with wet unit weight data for the entire east levee are shown in Figure 1-18. Wet unit weight for the entire west levee on the canal is shown in Figure 1-19.

The undrained shear strength determined from the laboratory tests conducted on samples in the breach area is shown in Figure 1-20. Interpretation of the undrained shear strength from the CPTs using Mayne's method is plotted with laboratory test results in Figure 1-21. Interpretation of the undrained shear strength from the CPTs using the bearing capacity equation ($N_k=15$) is plotted with laboratory test results in Figure 1-22. These interpretations were provided by Dr. Thomas Brandon (Virginia Tech). Undrained shear strength data in the breach area plotted with undrained shear strength data for the entire east levee are shown in Figure 1-23. Undrained shear strength data for the entire west levee are shown in Figure 1-24.

Marsh Stratum

The data for the marsh stratum will be divided into two groups: Data on the marsh stratum under the levee embankment, and data on the marsh stratum at the toe of the levee.

Under the Levee Embankment

Data on the marsh stratum under the levee embankment consist of five borings shown in the 1990 General Design Memorandum (GDM) and four cone penetrometer tests (CPT) taken on the east levee. Of the five GDM borings, four borings collected 3-in. (diameter) undisturbed samples and one boring collected 5-in (diameter) undisturbed samples. From the 3-in. samples, five unconfined compression (UC) tests were performed. From the 5-in. samples, no shear strength data were available. From these laboratory tests, moisture content and wet unit weights were determined. The moisture contents (%w) in the breach area are shown in Figure 1-25. In addition, this moisture content data were also plotted (Figure 1-26) with the moisture content data collected for the entire east levee on the canal. Also, the moisture content data for the entire west levee on the canal are shown in Figure 1-27.

The wet unit weight data in the breach area are shown in Figure 1-28. Wet unit weight data from the breach area plotted with wet unit weight data for the entire east levee are shown in Figure 1-29. Wet unit weight for the entire west levee on the canal are shown in Figure 1-30.

The undrained shear strength determined from the laboratory tests conducted on samples in the breach area is shown in Figure 1-31. Interpretation of the undrained shear strength from the CPTs using Mayne's method is plotted with laboratory test results in Figure 1-32. Interpretation of the undrained shear strength from the CPTs using the bearing capacity equation ($N_k=15$) is plotted with laboratory test results in Figure 1-33. These interpretations were provided by Dr. Thomas Brandon (Virginia Tech). Undrained shear strength data in the breach area plotted with undrained shear strength data for the entire east levee are shown in Figure 1-34. Undrained shear strength data for the entire west levee are shown in Figure 1-35.

At the Toe of Embankment

Data on the marsh stratum under the toe of the levee embankment consist of five borings taken in 2005 on the protected side, four borings taken in 2005 on the canal side, three borings on the west levee toe shown in the 1990 GDM. Of the borings on the protected side of the east levee, four borings collected 5-in. (diameter) undisturbed samples, and one boring collected 3-in. (diameter) undisturbed samples. Of the borings on the canal side of the east levee, three borings collected 5-in. (diameter) undisturbed samples, and one boring collected 3-in. (diameter) undisturbed samples. Of the three GDM borings taken on the protected side of the west levee, two borings collected 3-in. (diameter) samples, and one boring collected 5-in. (diameter) undisturbed samples. From the 3-in. samples, four unconfined compression (UC) tests were performed, and two one-point unconsolidated-undrained triaxial compression tests (UU-1), confined at existing overburden pressure, were performed. From the 5-in. samples, 14 UC tests were performed, and six unconsolidated-undrained triaxial compression tests (Q) were

performed. From these laboratory tests, moisture content and wet unit weights were determined. The moisture contents (%w) in the breach area are shown in Figure 1-36. In addition, this moisture content data were also plotted (Figure 1-37) with the moisture content data collected for the entire east levee on the canal. Also, the moisture content data for the entire west levee on the canal are shown in Figure 1-38.

The wet unit weight data in the breach area are shown in Figure 1-39. Wet unit weight data from the breach area plotted with wet unit weight data for the entire east levee are shown in Figure 1-40. Wet unit weight for the entire west levee on the canal is shown in Figure 1-41.

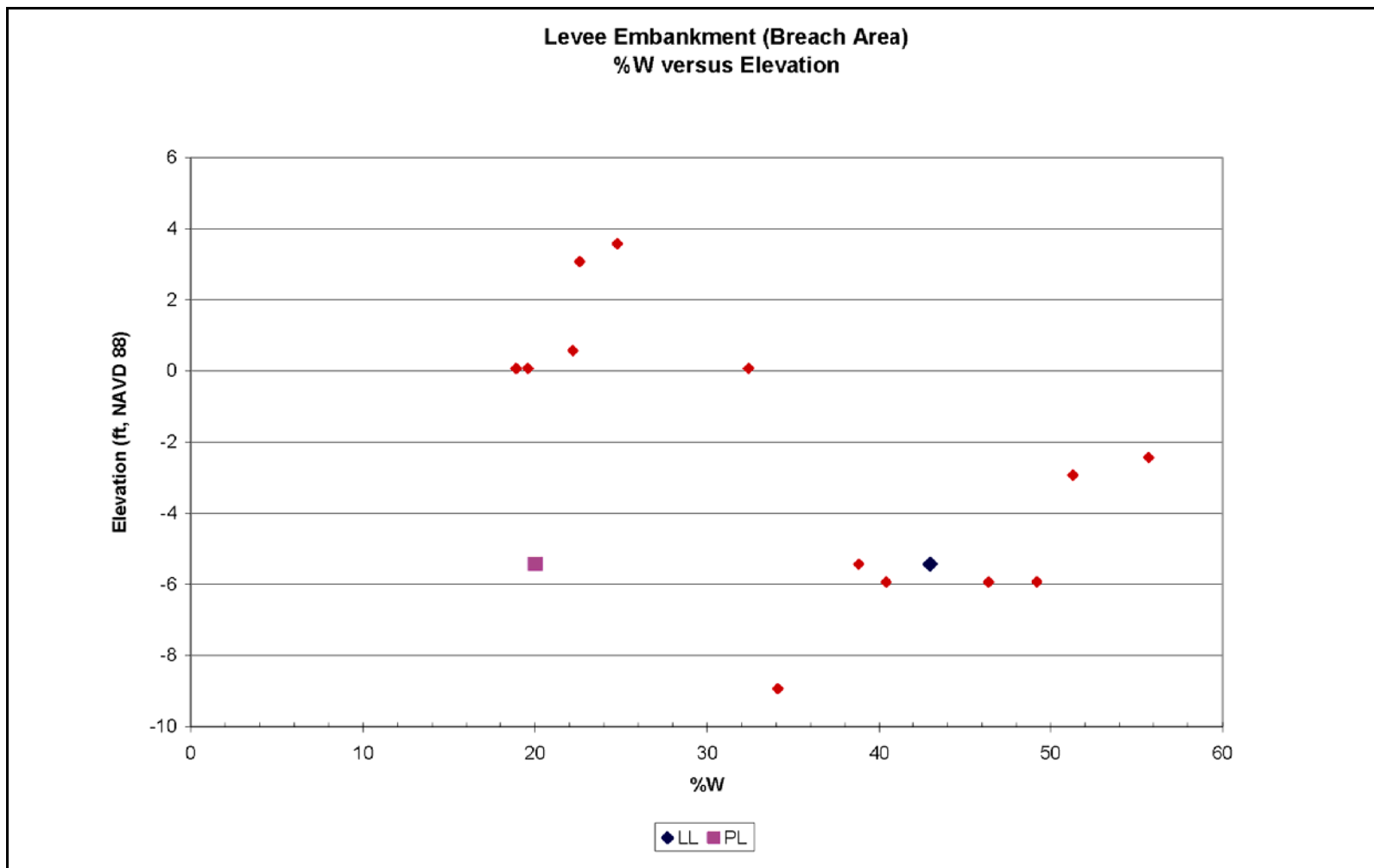


Figure 1-14. Levee Embankment (Breach Area), %w versus Elevation

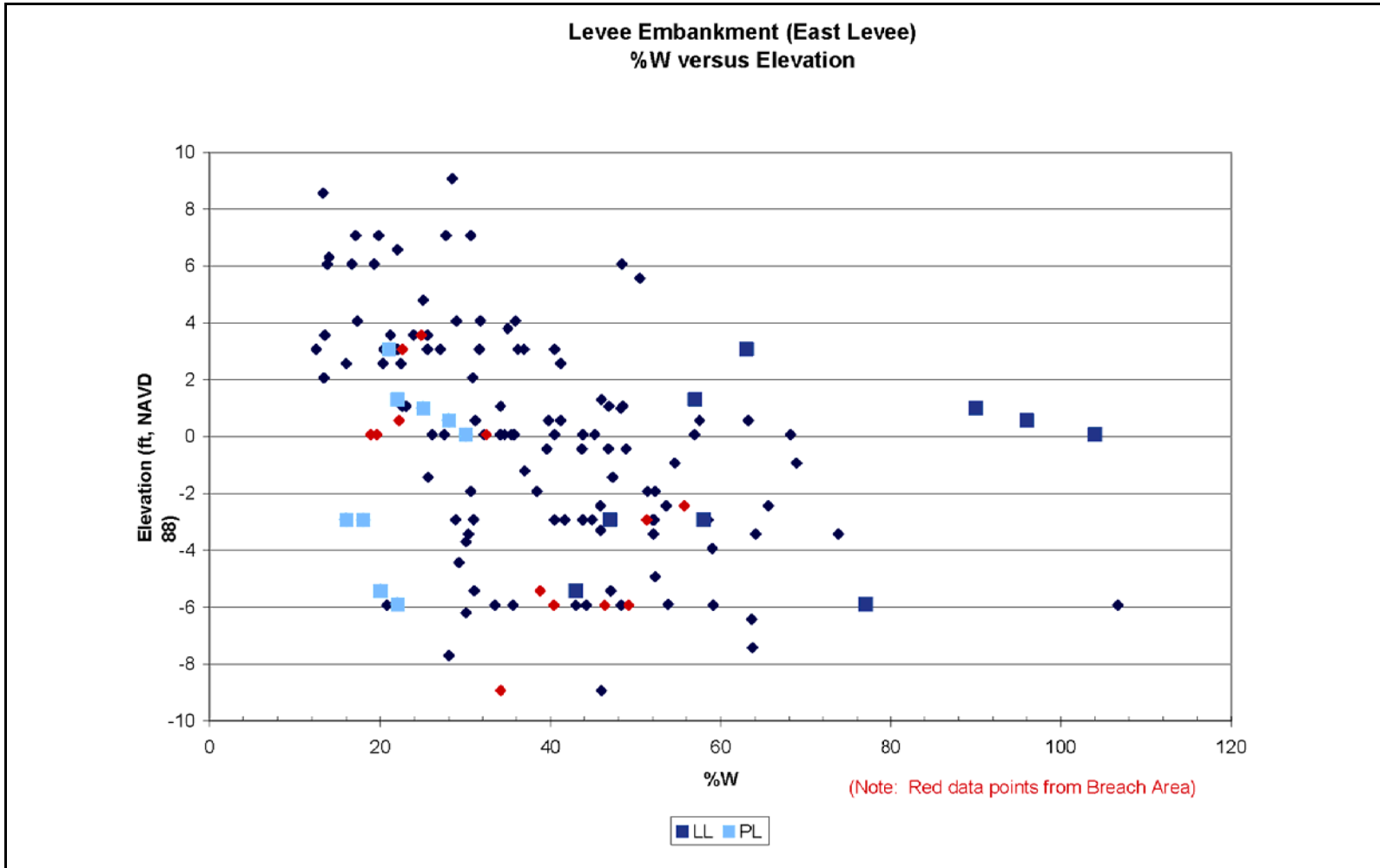


Figure 1-15. Levee Embankment (East Levee), %w versus Elevation

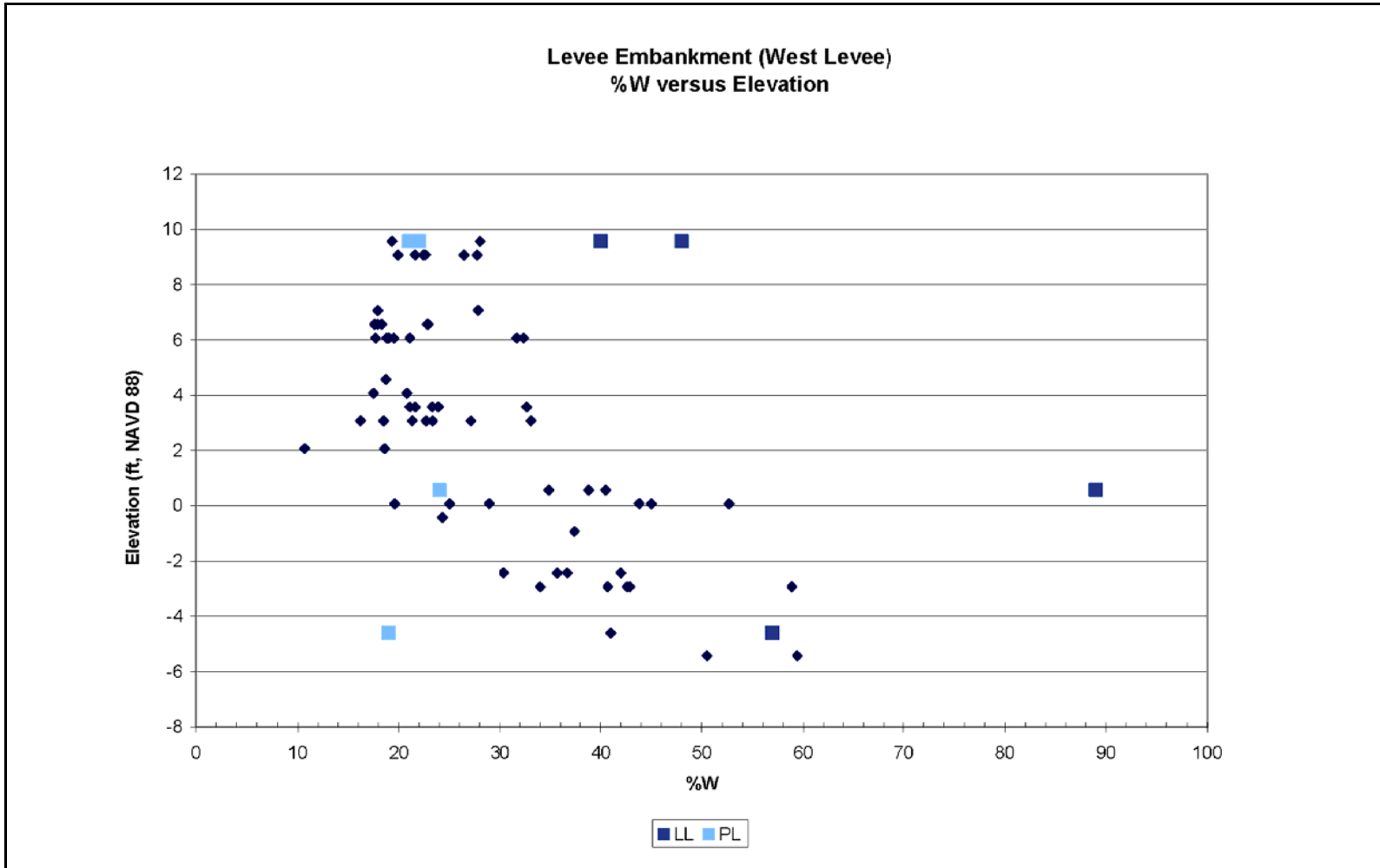


Figure 1-16. Levee Embankment (West Levee), %w versus Elevation

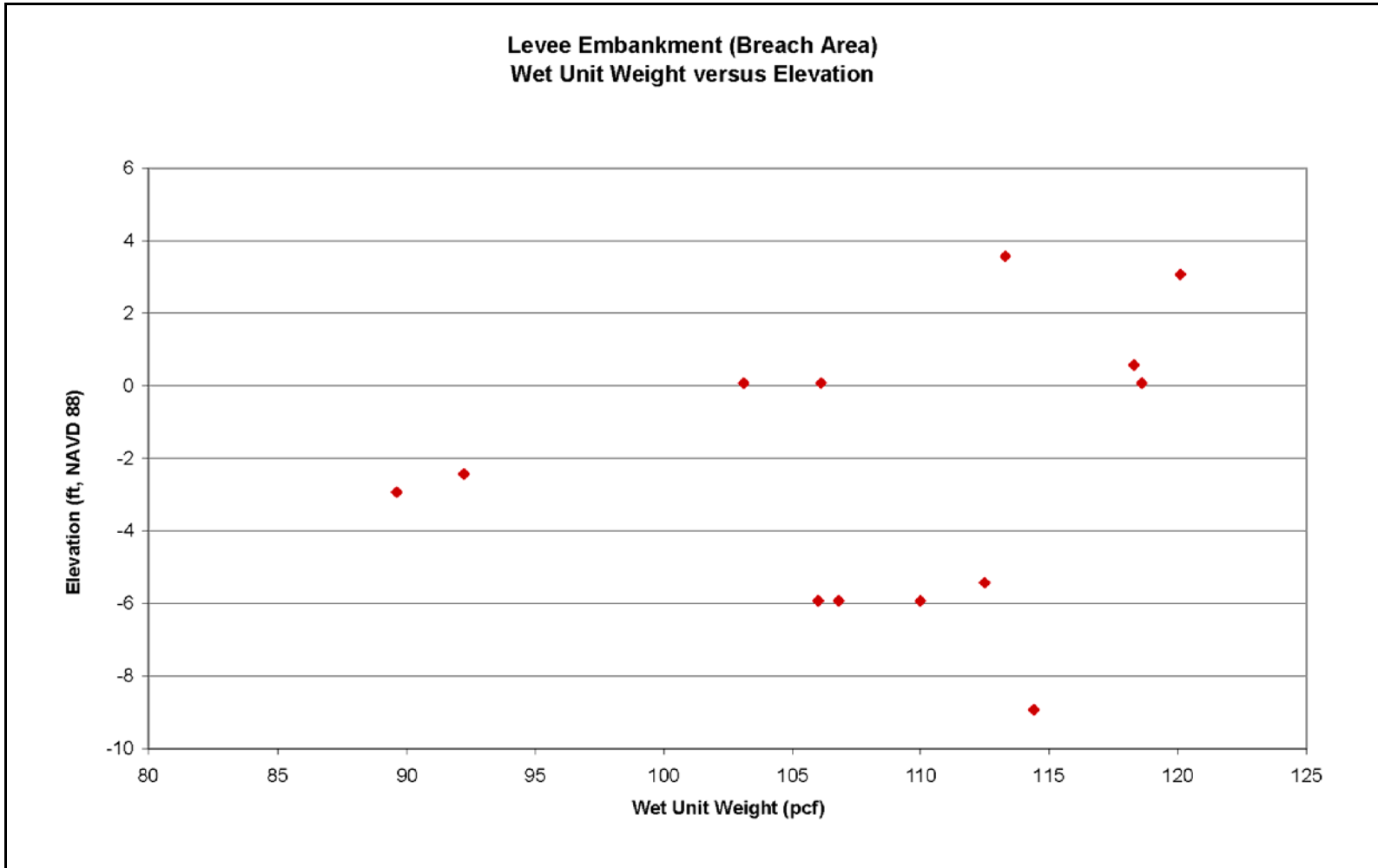


Figure 1-17. Levee Embankment (Breach Area), Wet Unit Weight versus Elevation

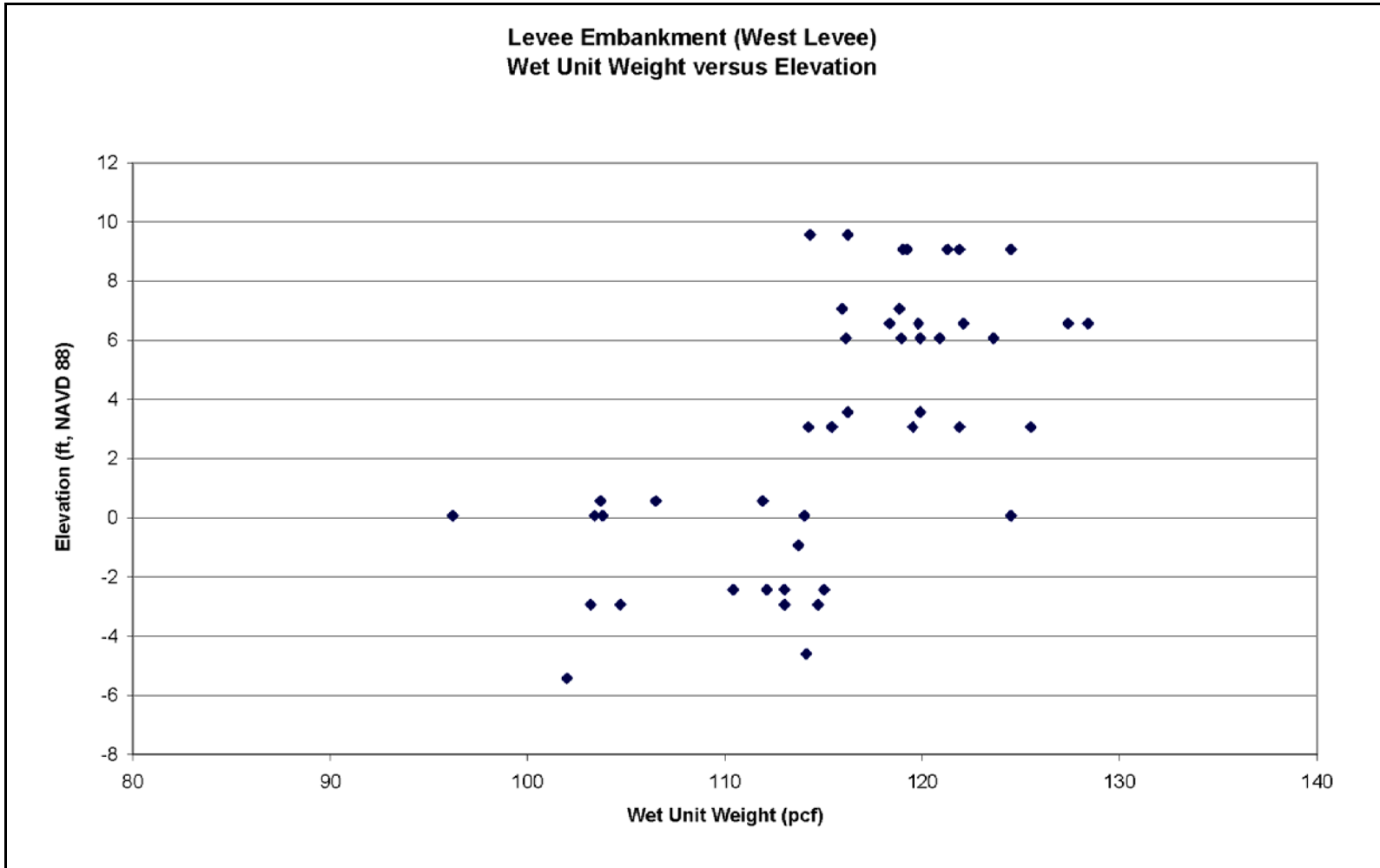


Figure 1-19. Levee Embankment (West Levee), Wet Unit Weight versus Elevation

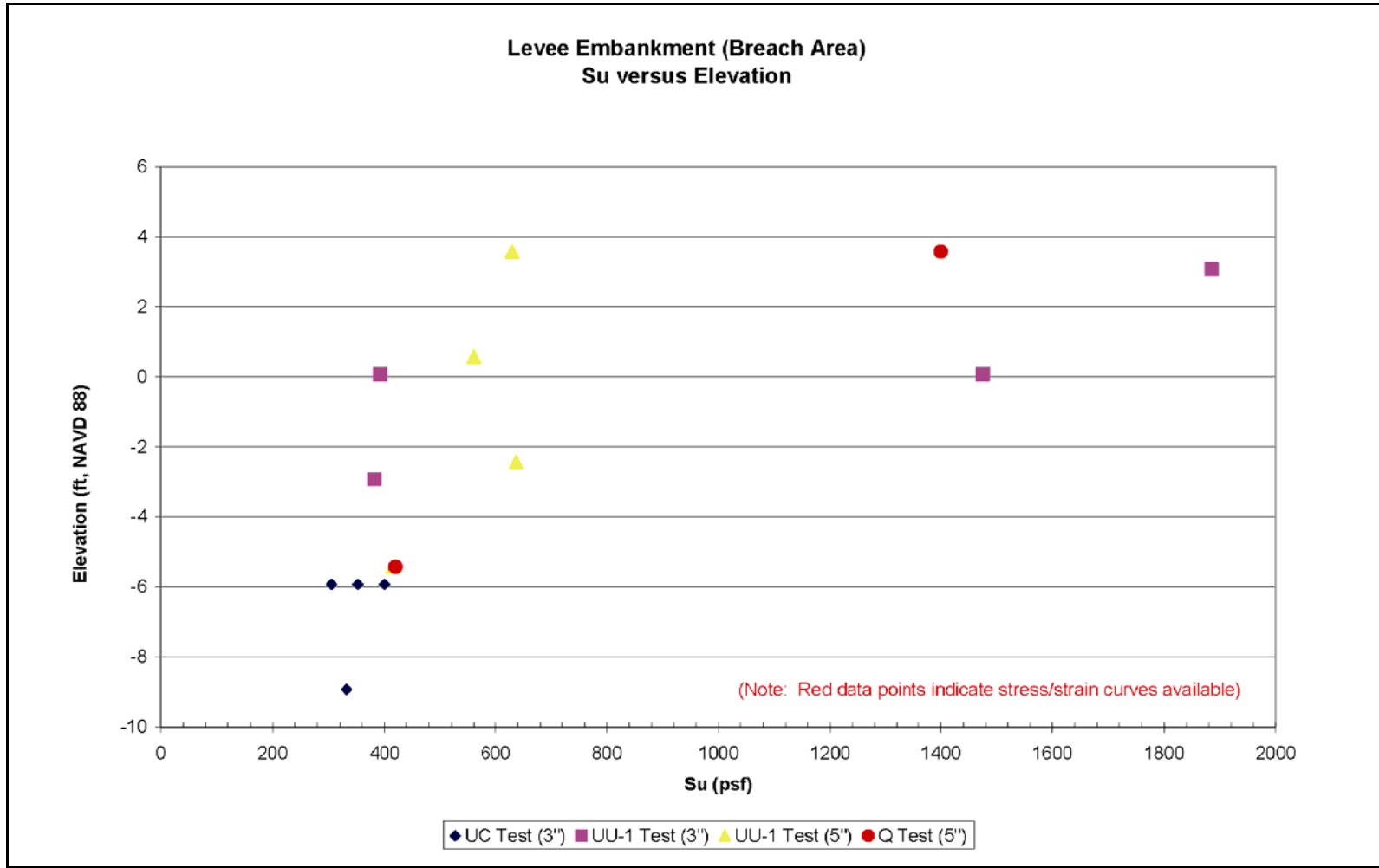


Figure 1-20. Levee Embankment (Breach Area), Su versus Elevation

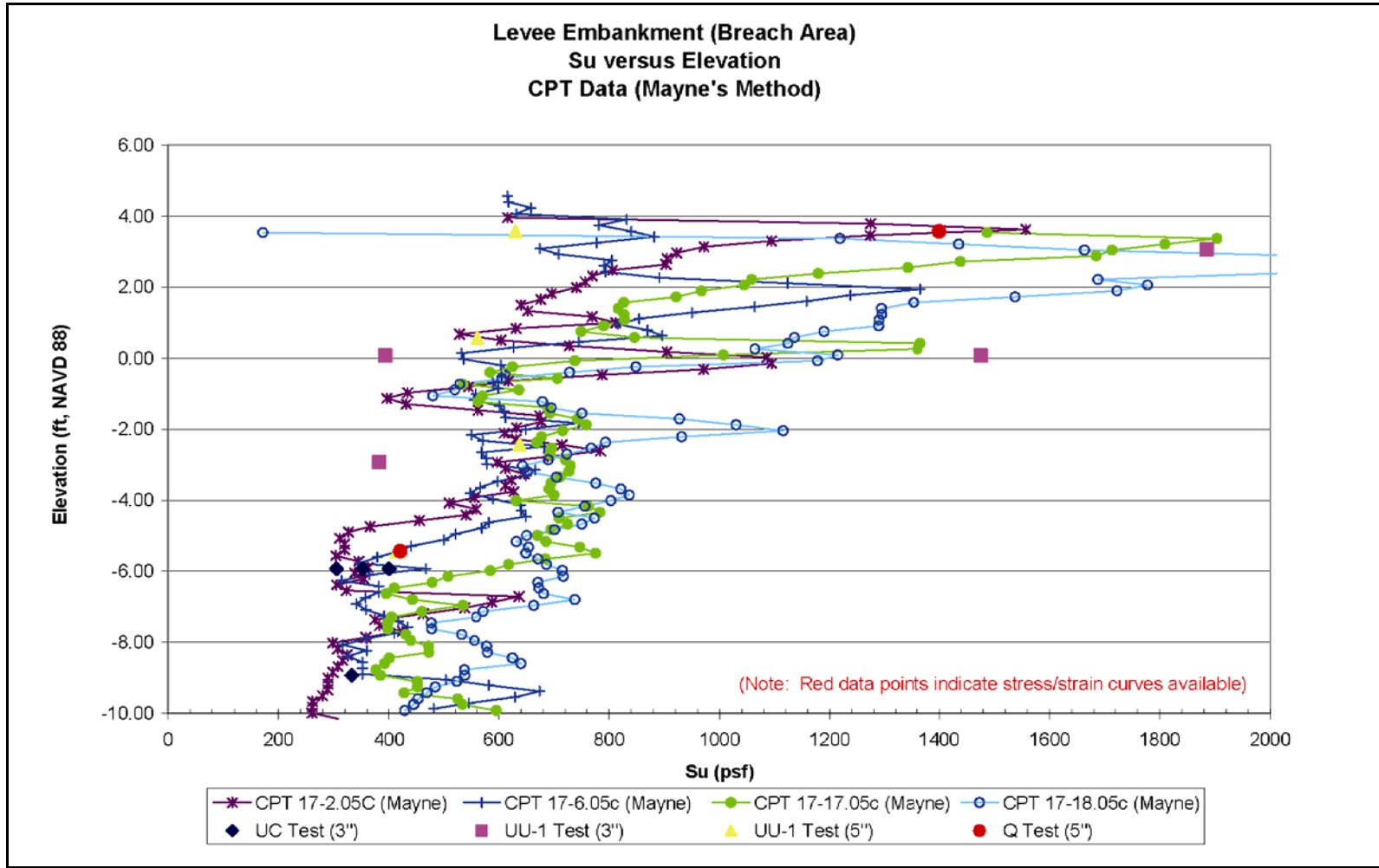


Figure 1-21. Levee Embankment, Su versus Elevation (CPT Data – Mayne's Method)

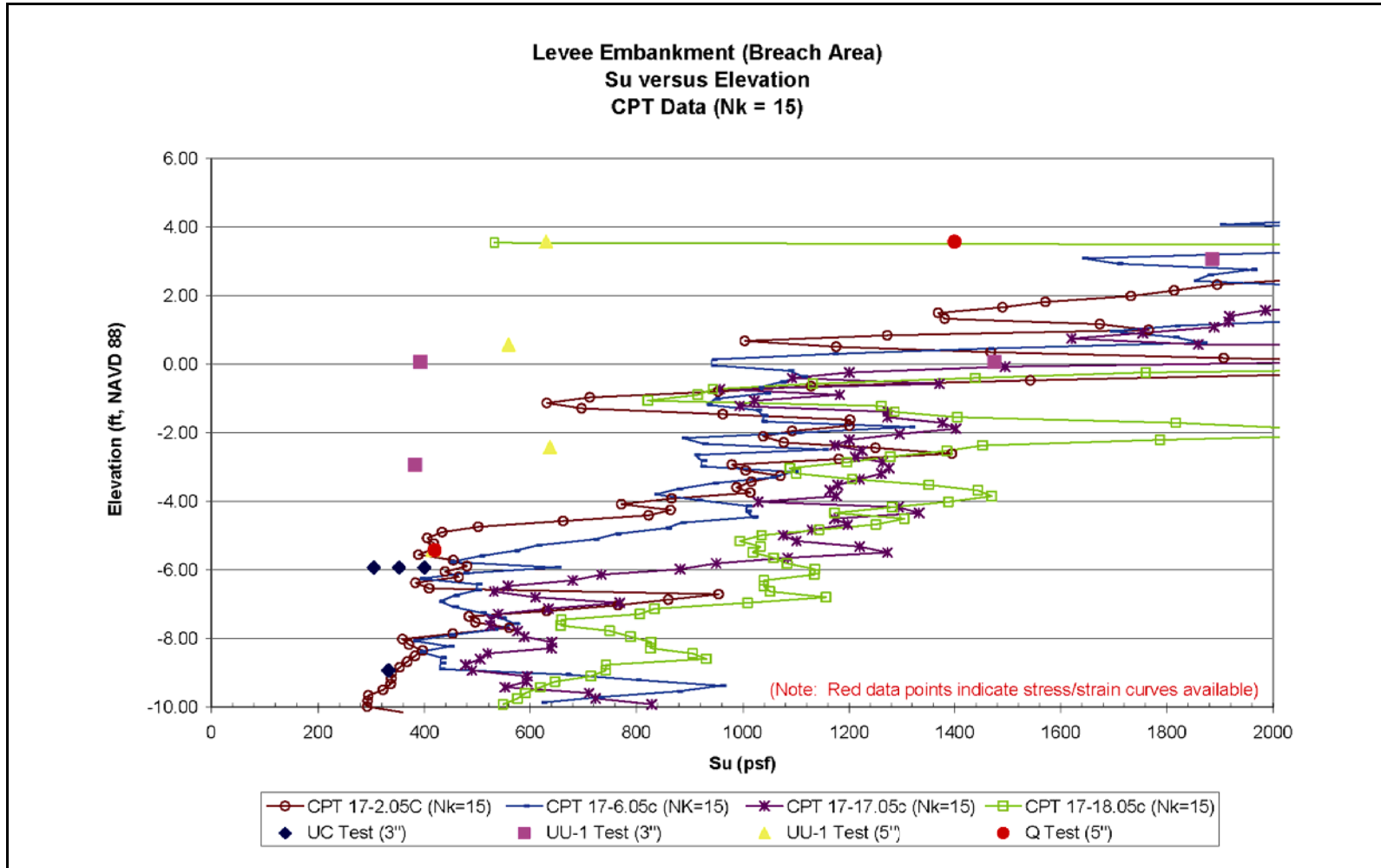


Figure 1-22. Levee Embankment (Breach Area), Su versus Elevation (CPT Data – Nk=15)

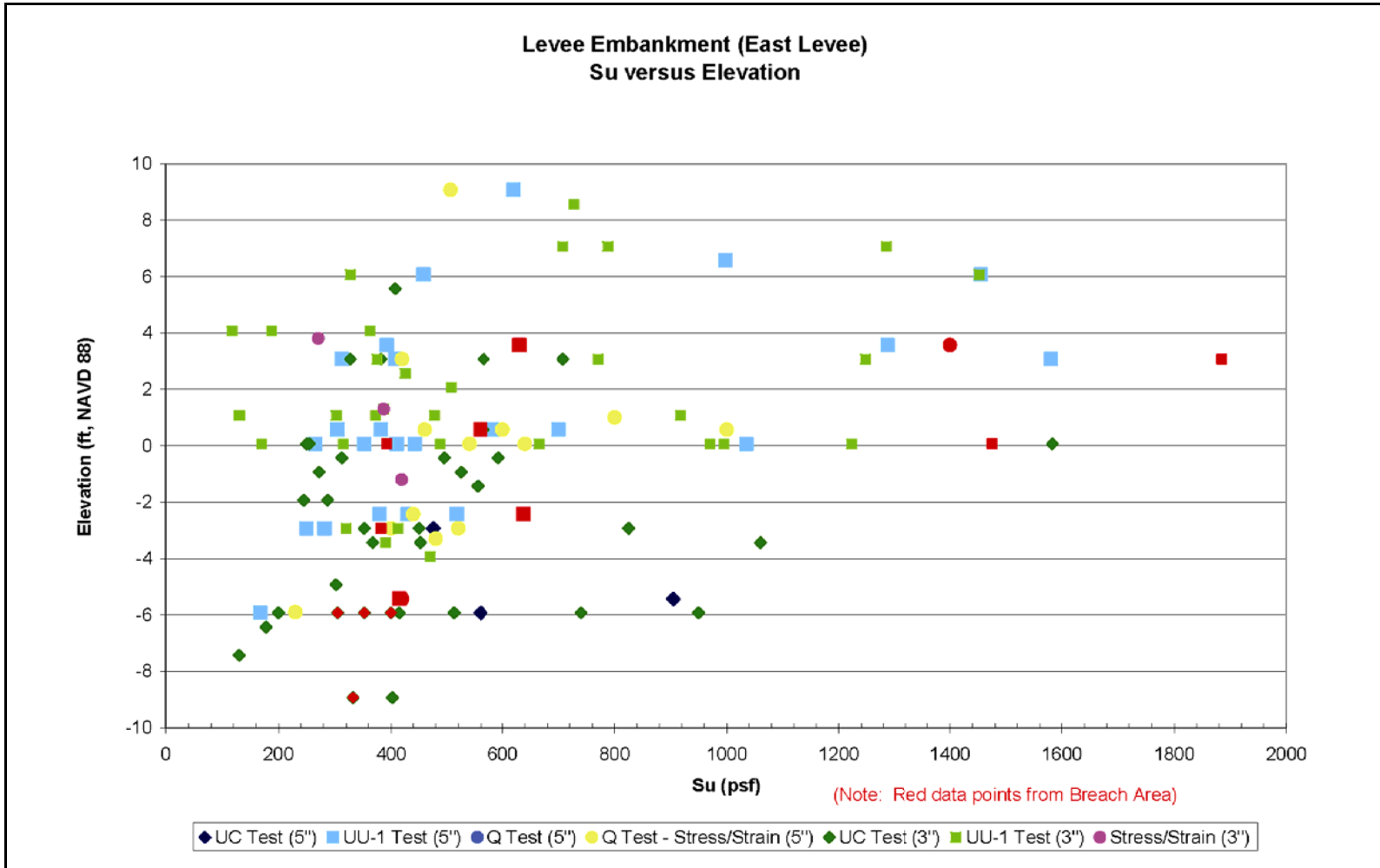


Figure 1-23. Levee Embankment (East Levee), Su versus Elevation

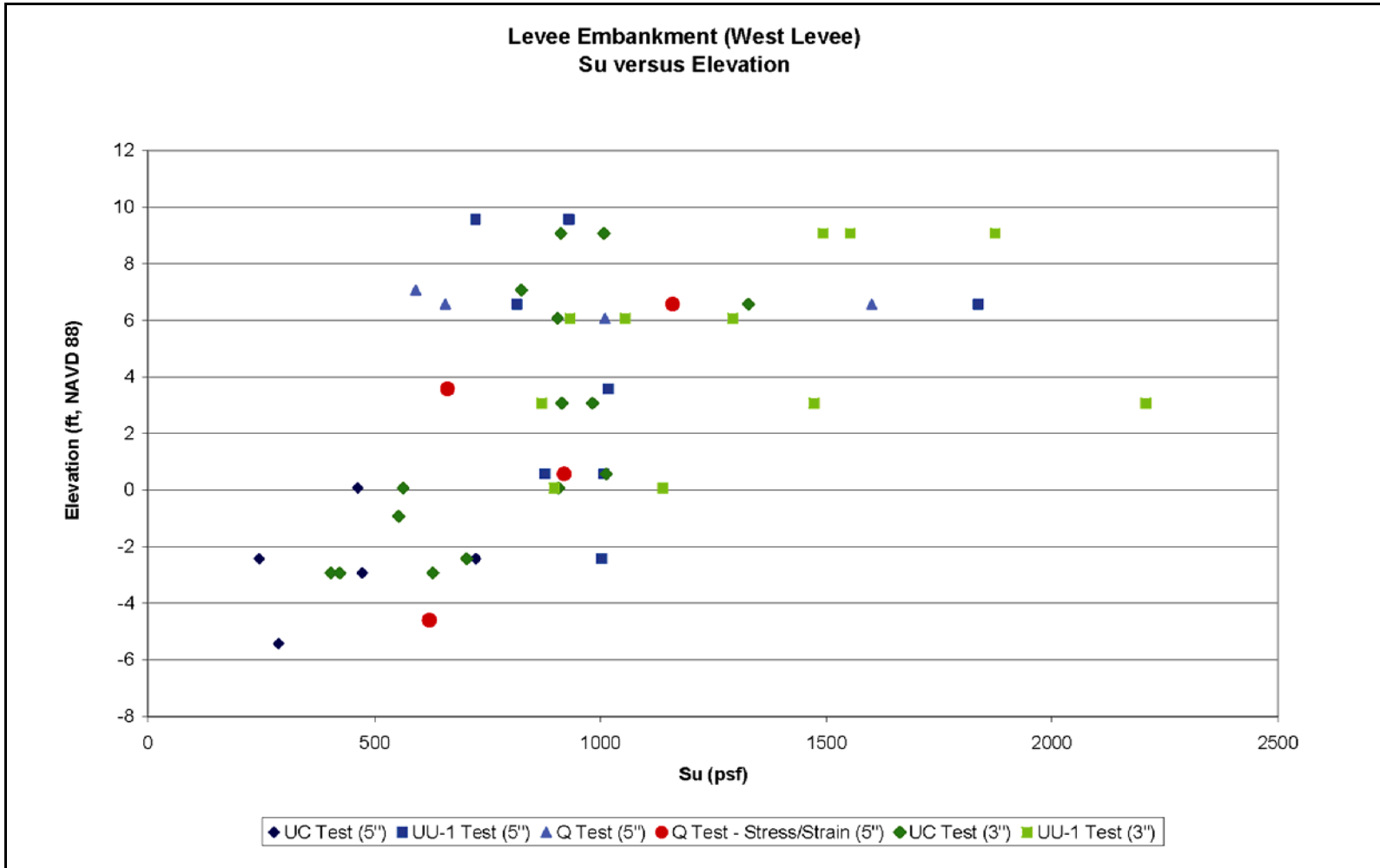


Figure 1-24. Levee Embankment (West Levee), Su versus Elevation

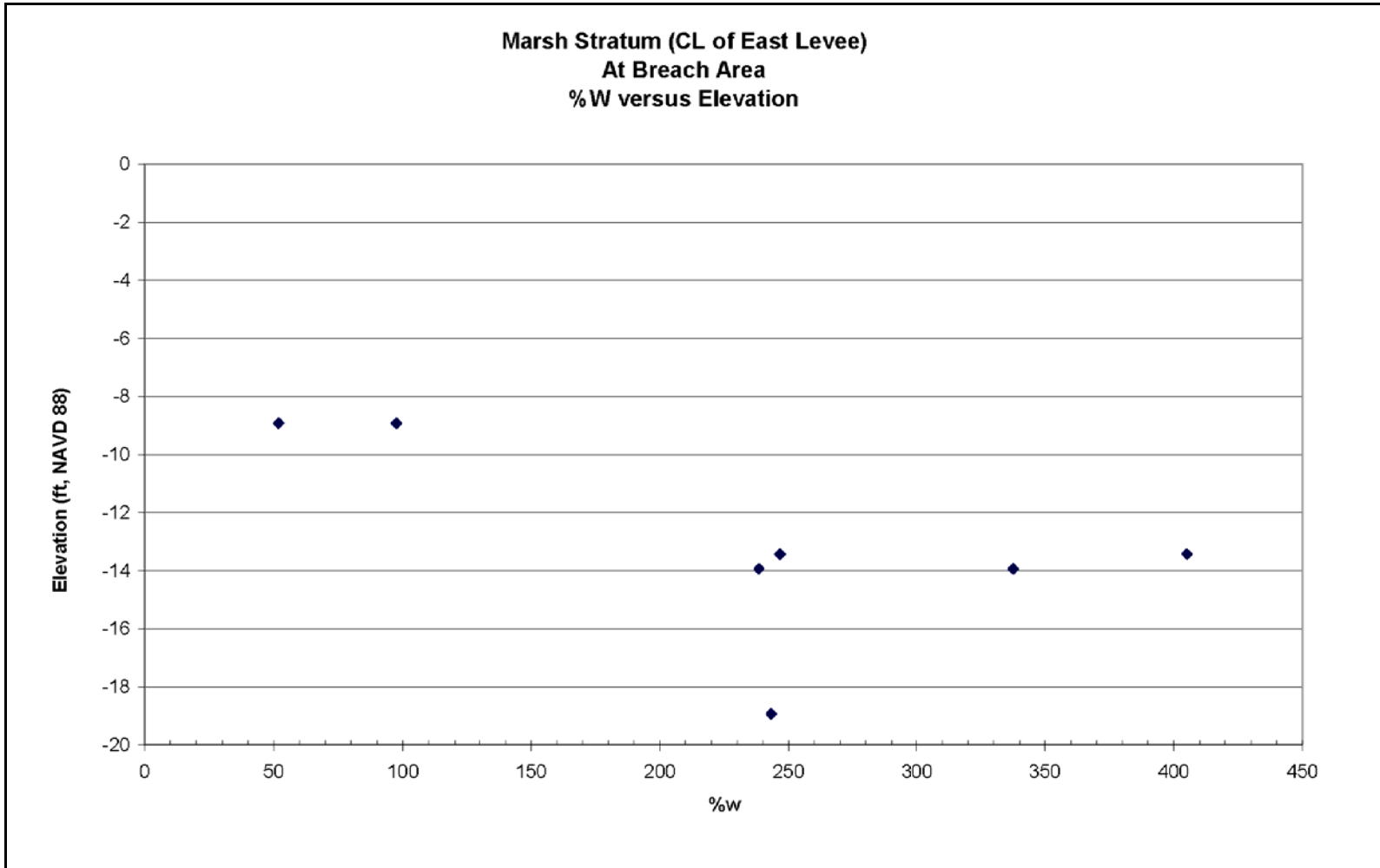


Figure 1-25. Marsh Stratum (CL of East Levee – At Breach Area), %w versus Elevation

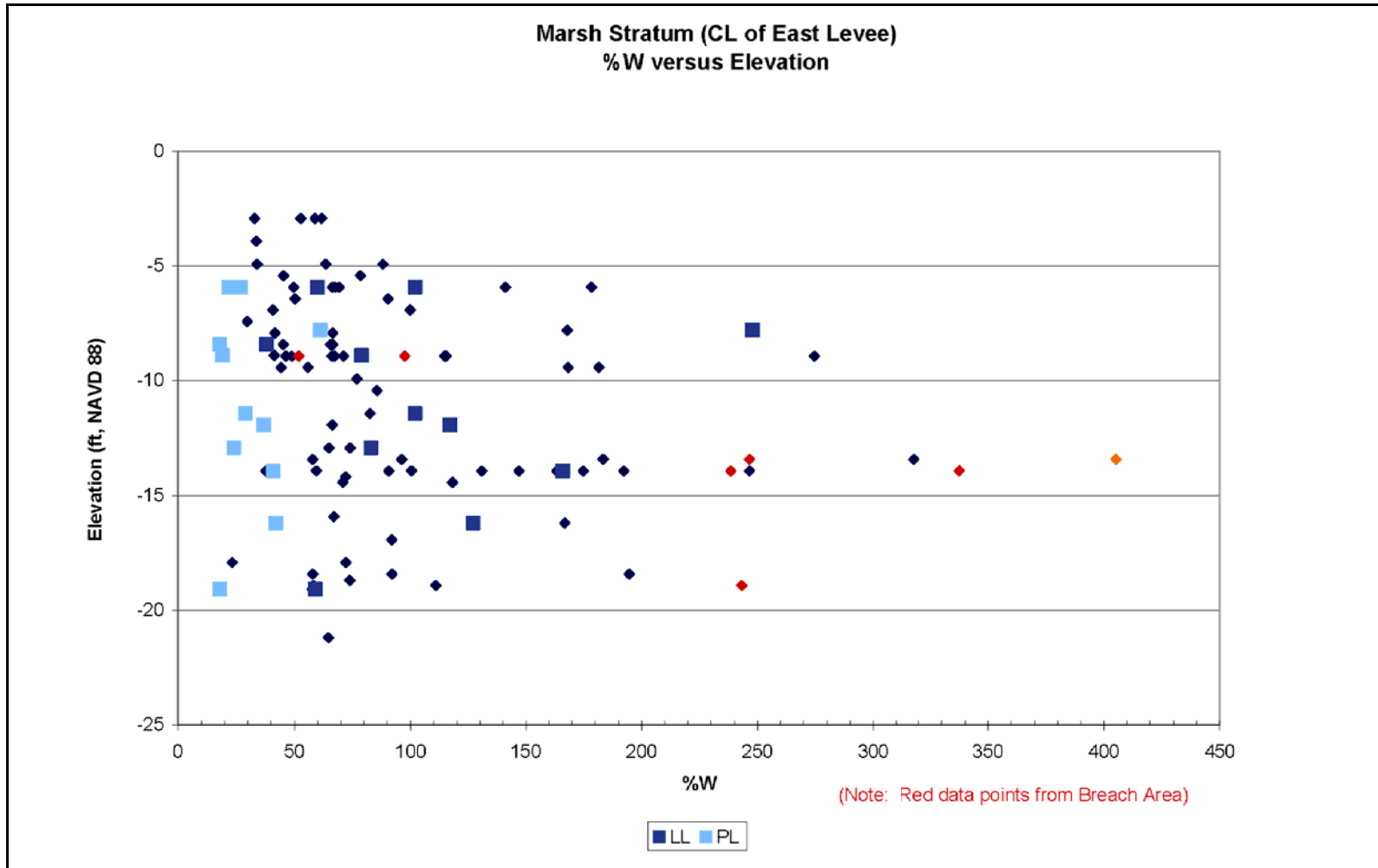


Figure 1-26. Marsh Stratum (CL of East Levee), %w versus Elevation

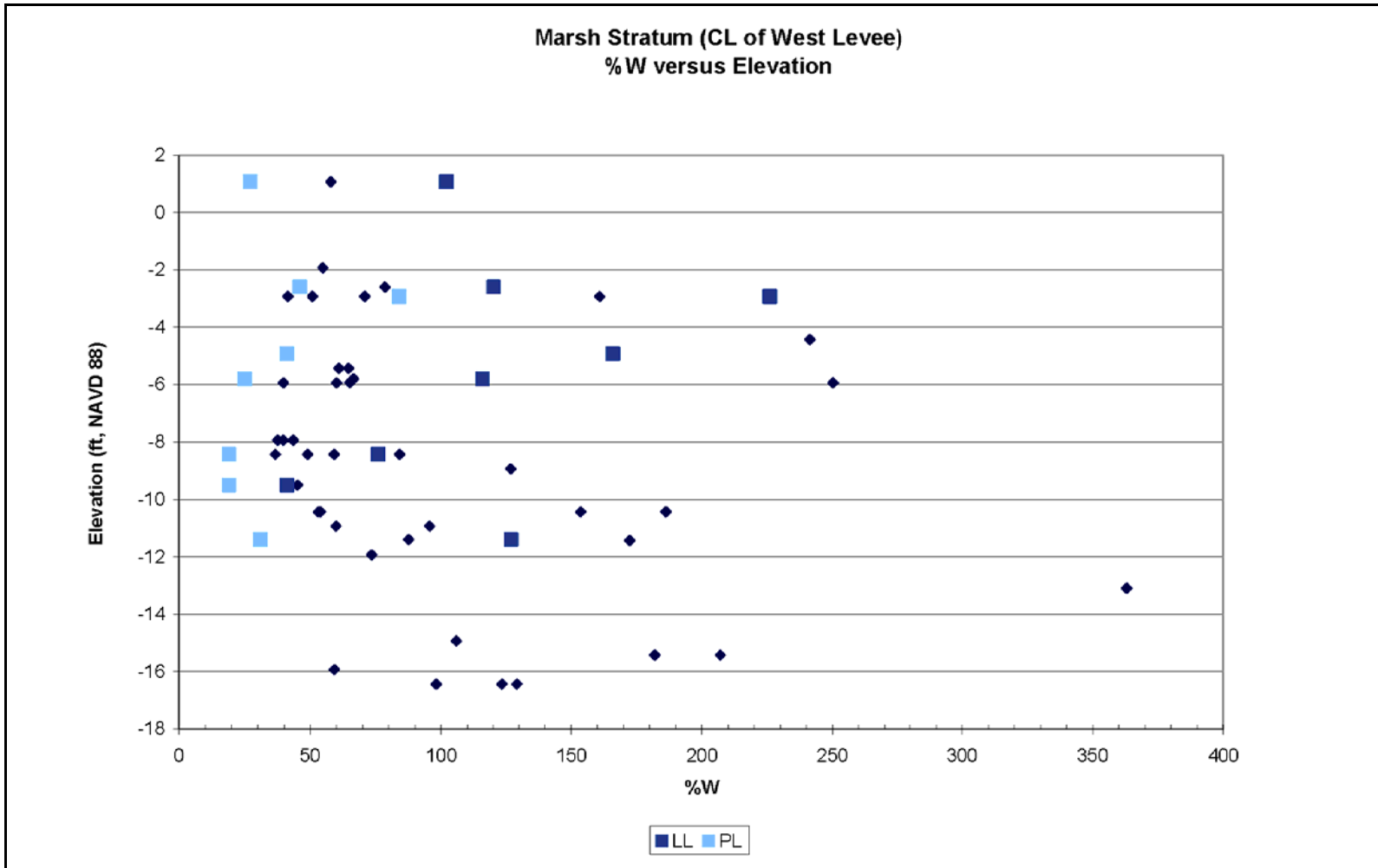


Figure 1-27. Marsh Stratum (CL of West Levee), %w versus Elevation

**Marsh Stratum (CL of East Levee)
At Breach Area
Wet Unit Weight versus Elevation**

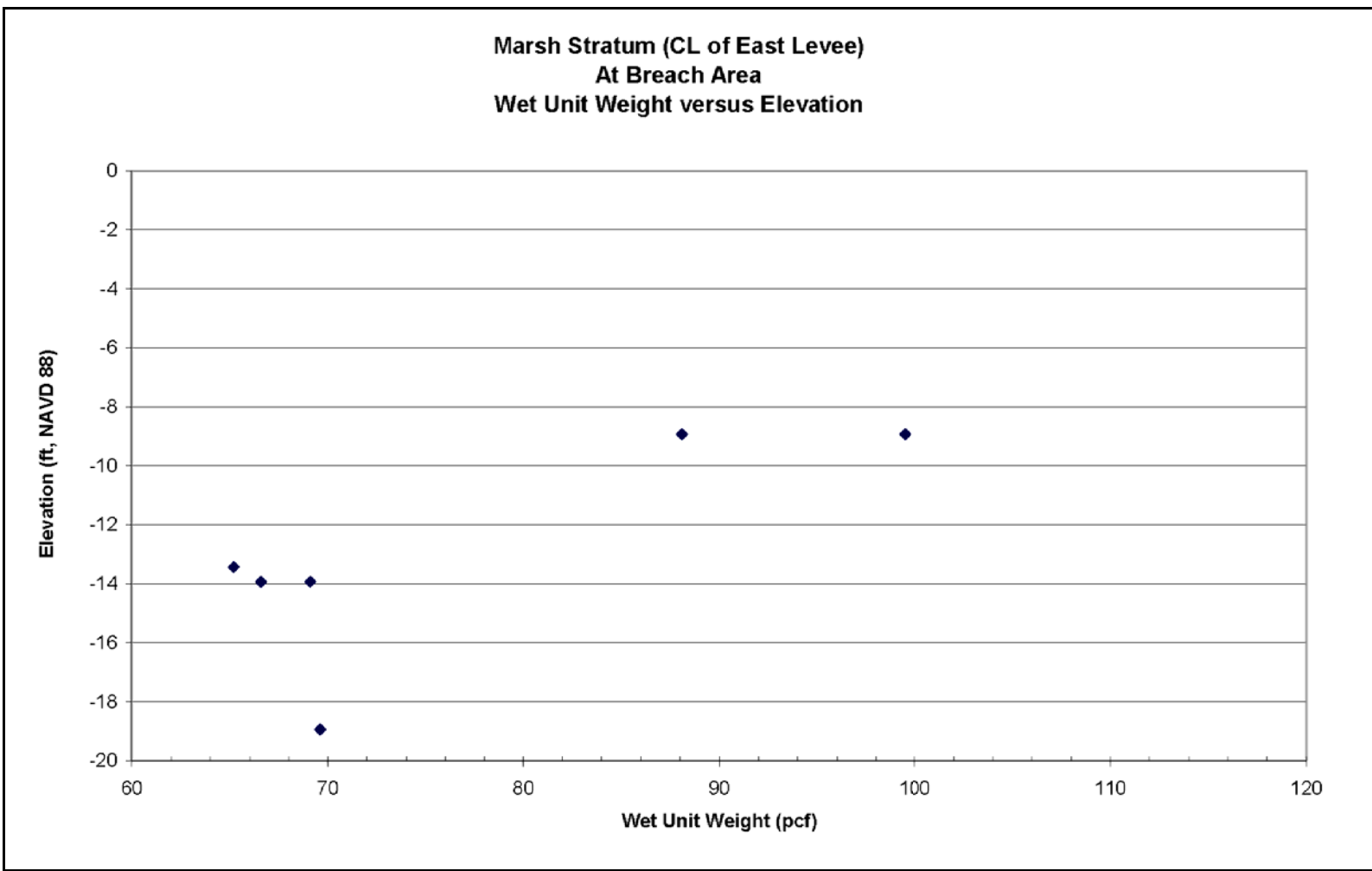


Figure 1-28. Marsh Stratum (CL of East Levee – At Breach Area), Wet Unit Weight versus Elevation

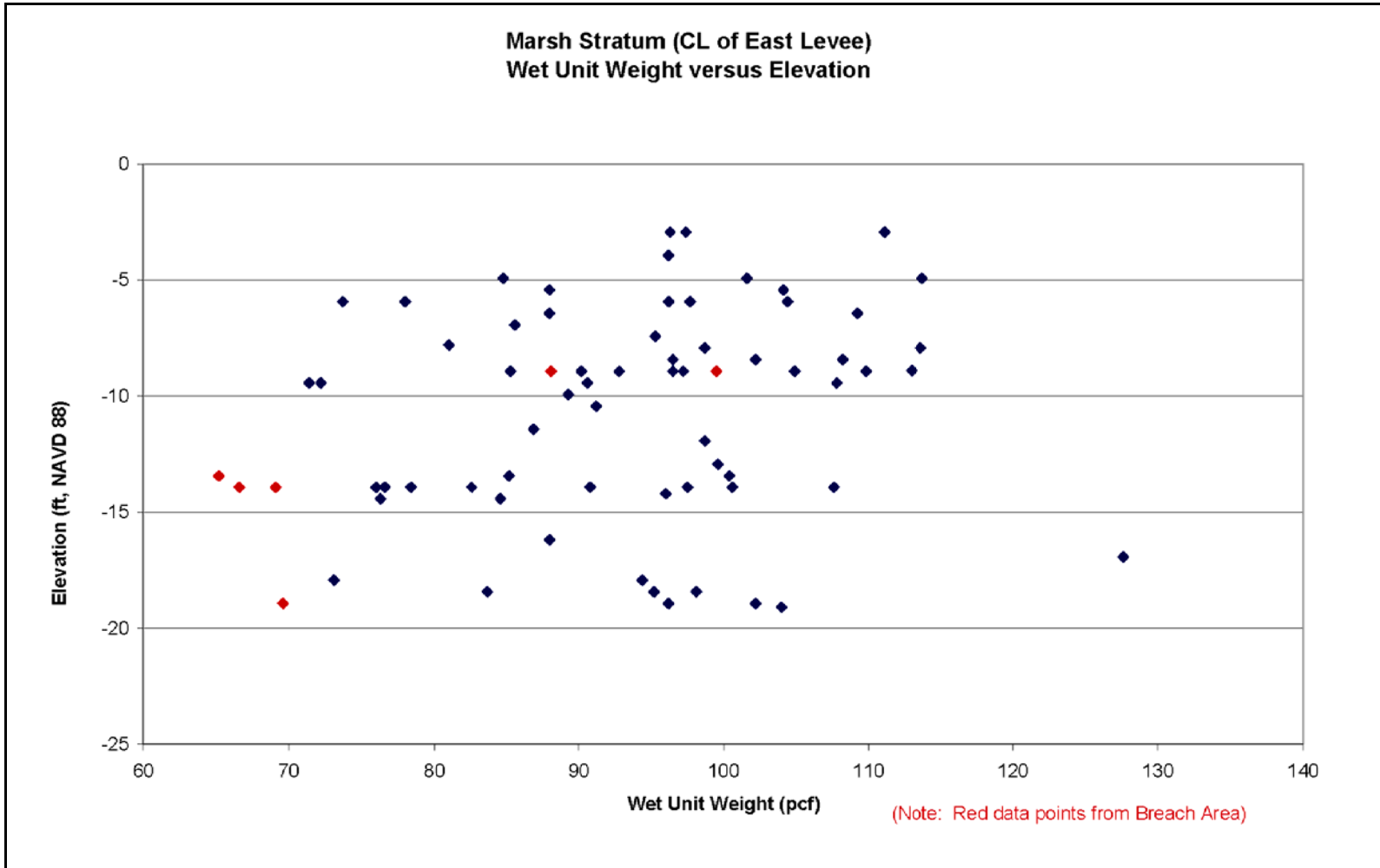


Figure 1-29. Marsh Stratum (CL of East Levee), Wet Unit Weight versus Elevation

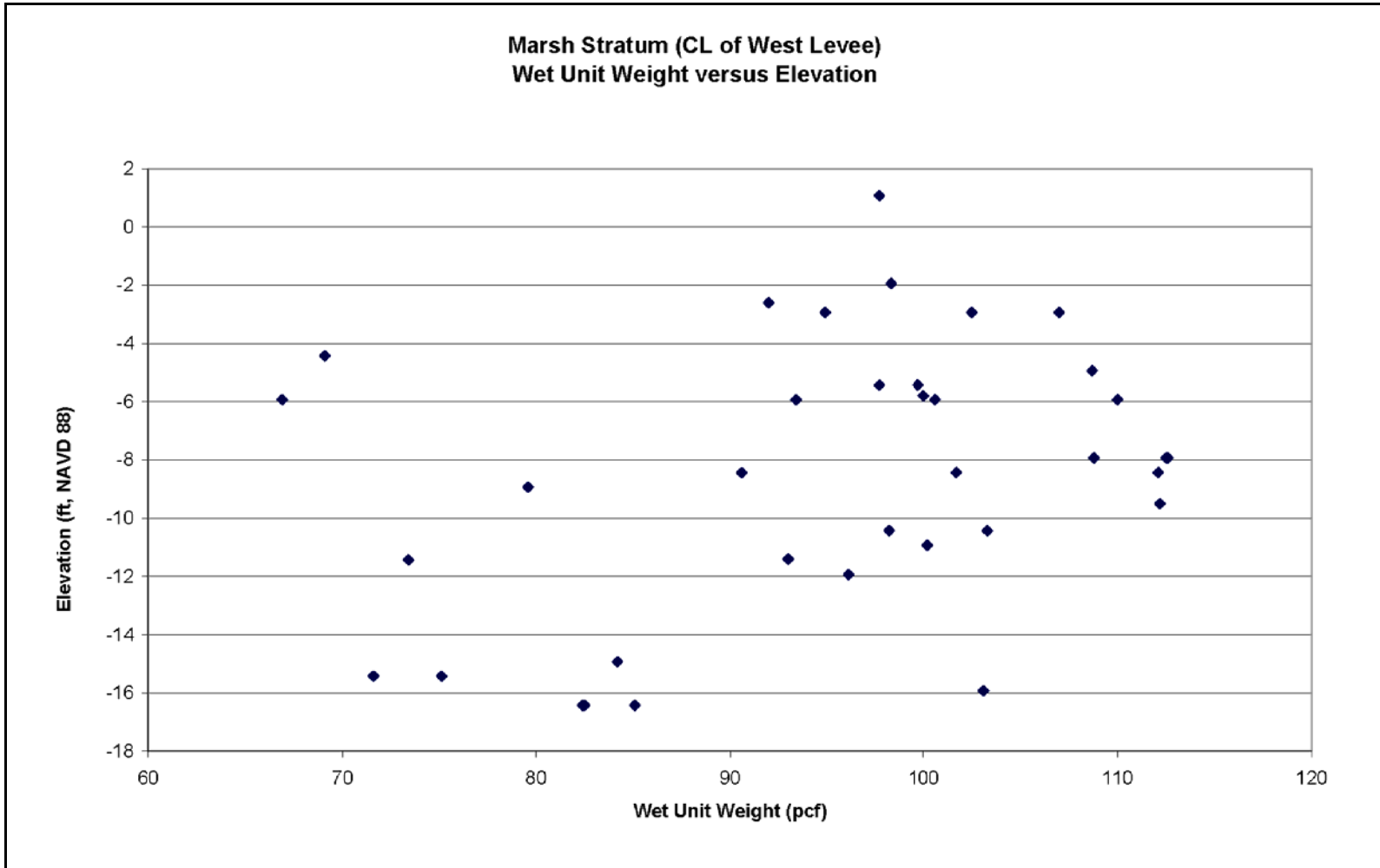


Figure 1-30. Marsh Stratum (CL of West Levee), Wet Unit Weight versus Elevation

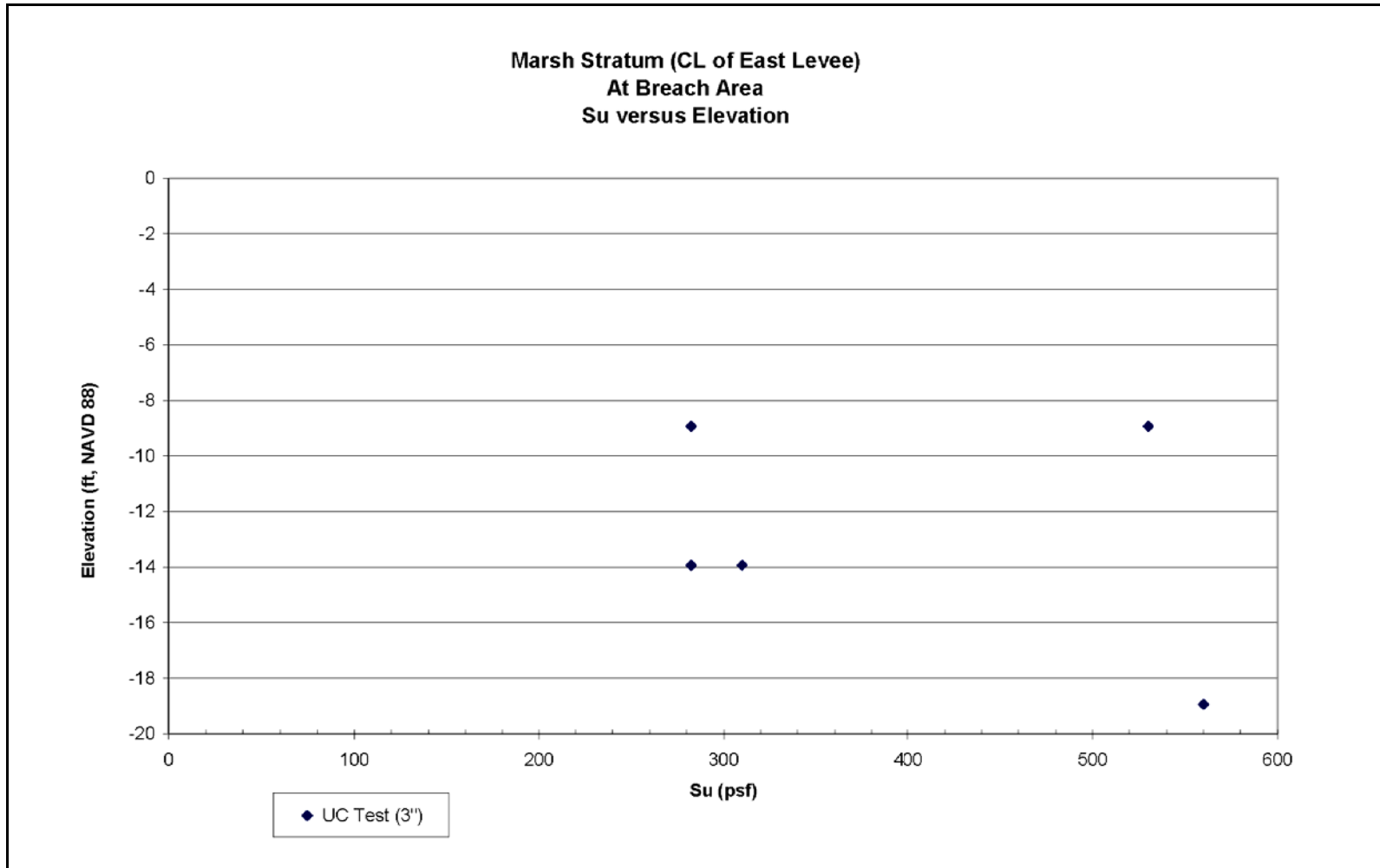


Figure 1-31. Marsh Stratum (CL of East Levee – At Breach Area), Su versus Elevation

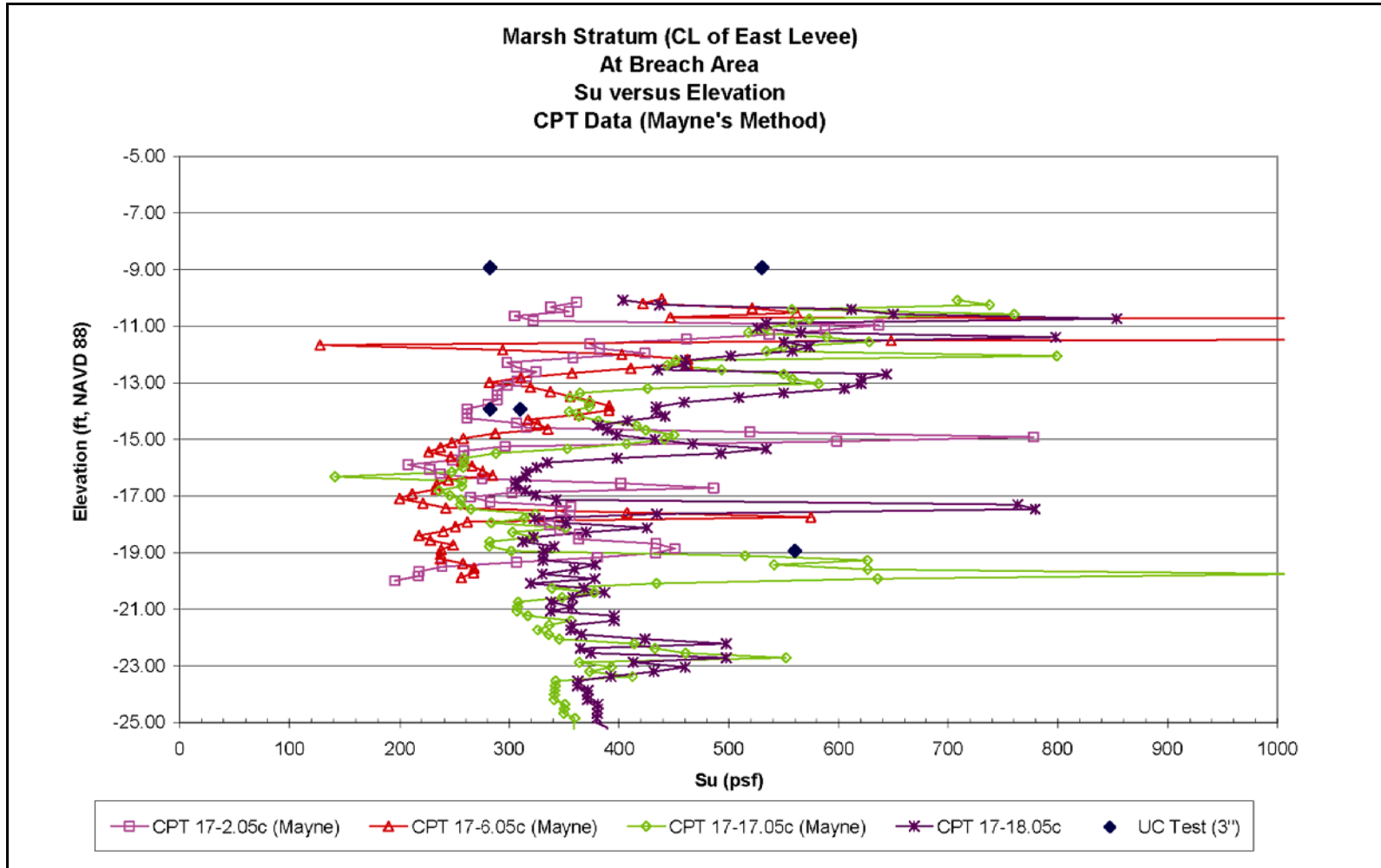


Figure 1-32. Marsh Stratum (CL of East Levee – At Breach Area), Su versus Elevation (CPT Data – Mayne's Method)

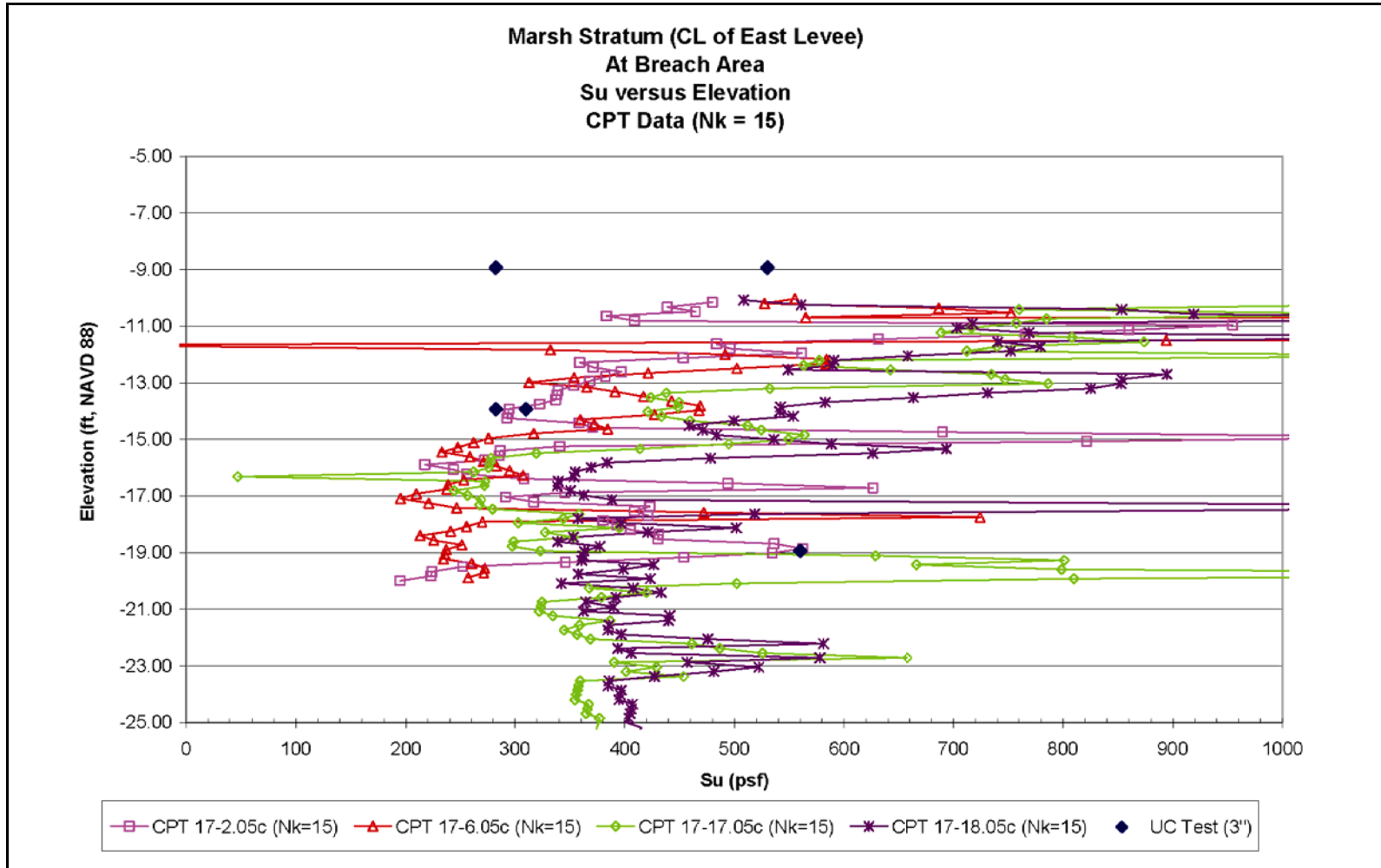


Figure 1-33. Marsh Stratum (CL of East Levee), Su versus Elevation (CPT Data – Nk=15)

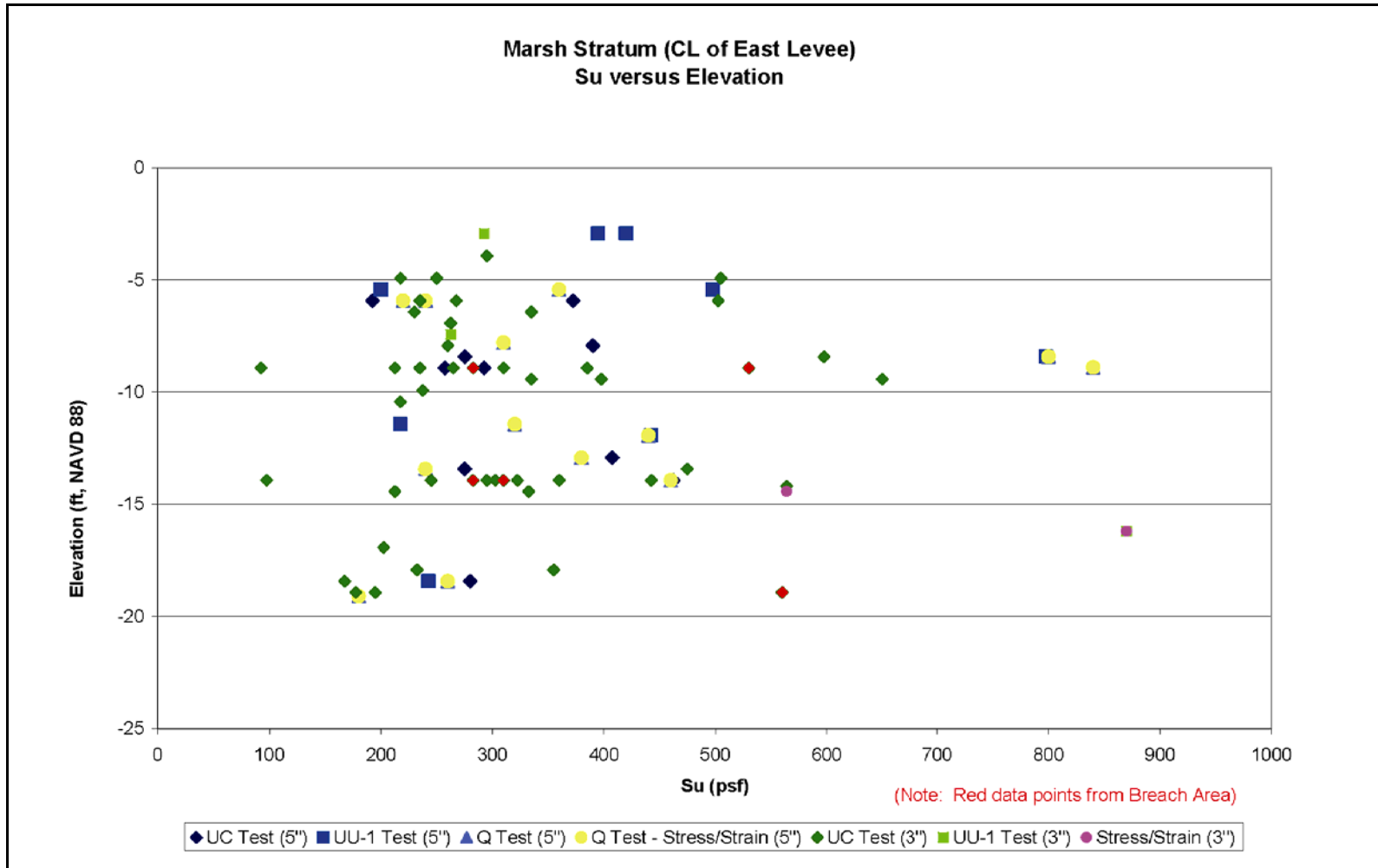


Figure 1-34. Marsh Stratum (CL of East Levee), Su versus Elevation

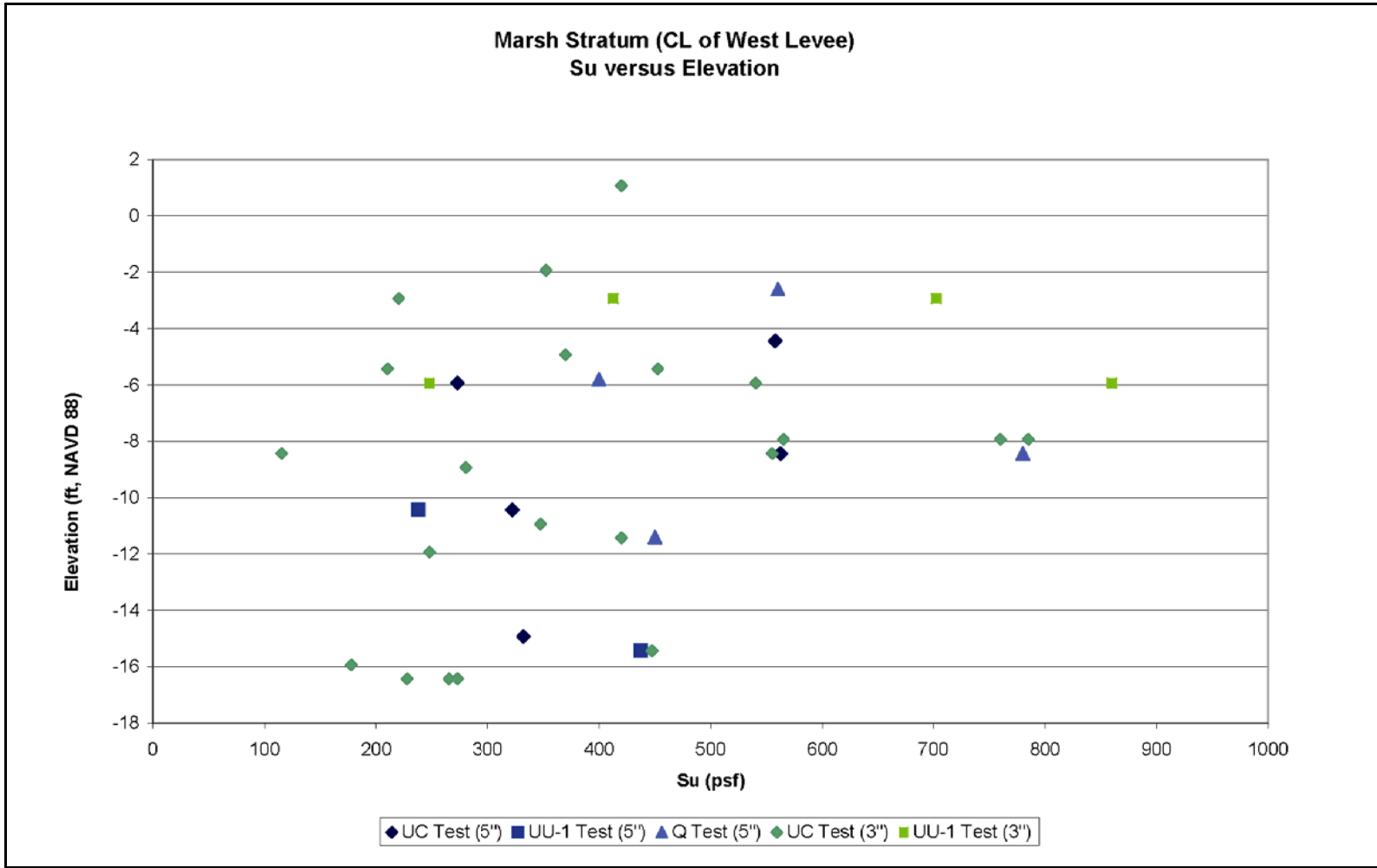


Figure 1-35. Marsh Stratum (CL of West Levee), Su versus Elevation

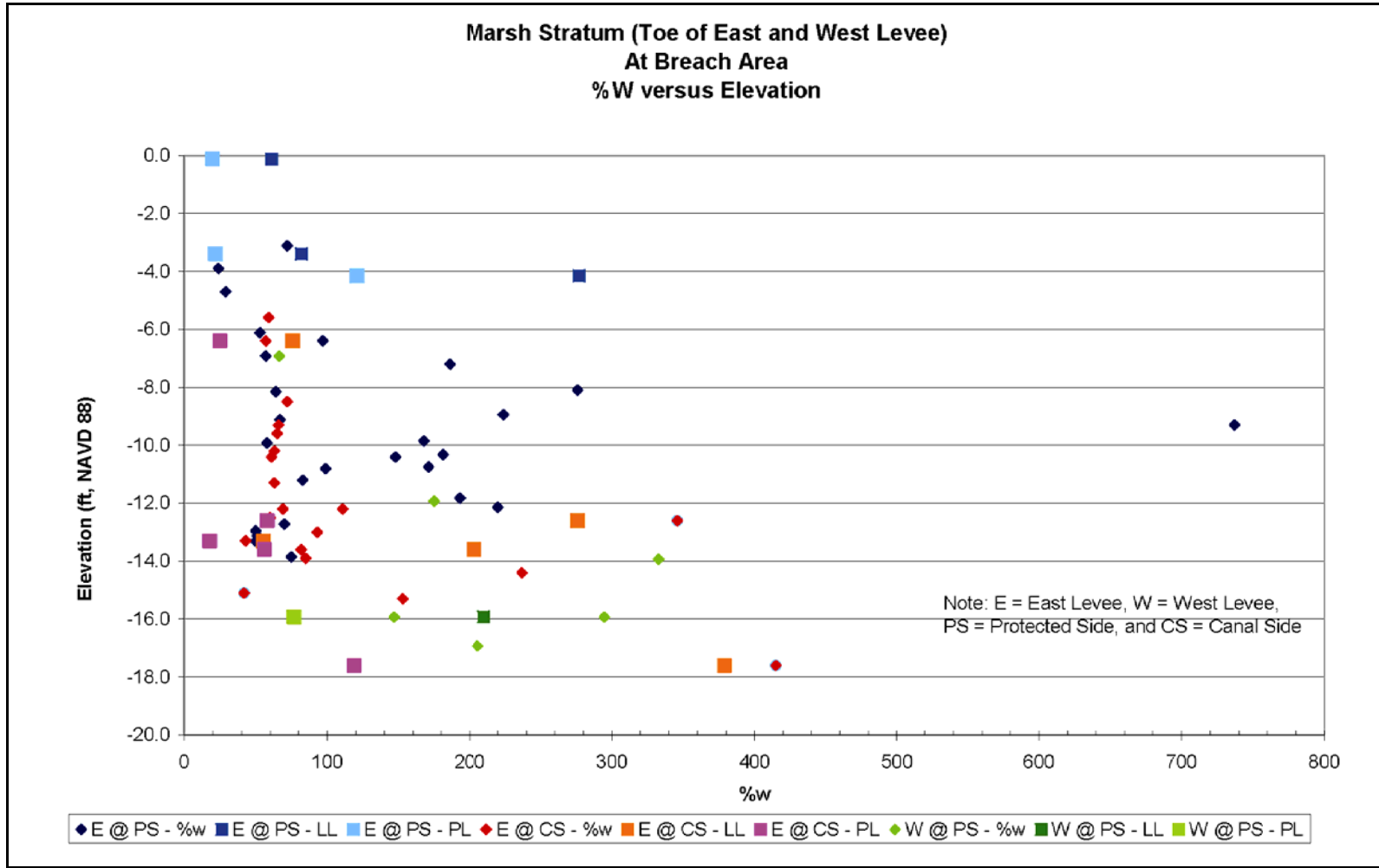


Figure 1-36. Marsh Stratum (Toe of East and West Levee – At Breach Area), %w versus Elevation

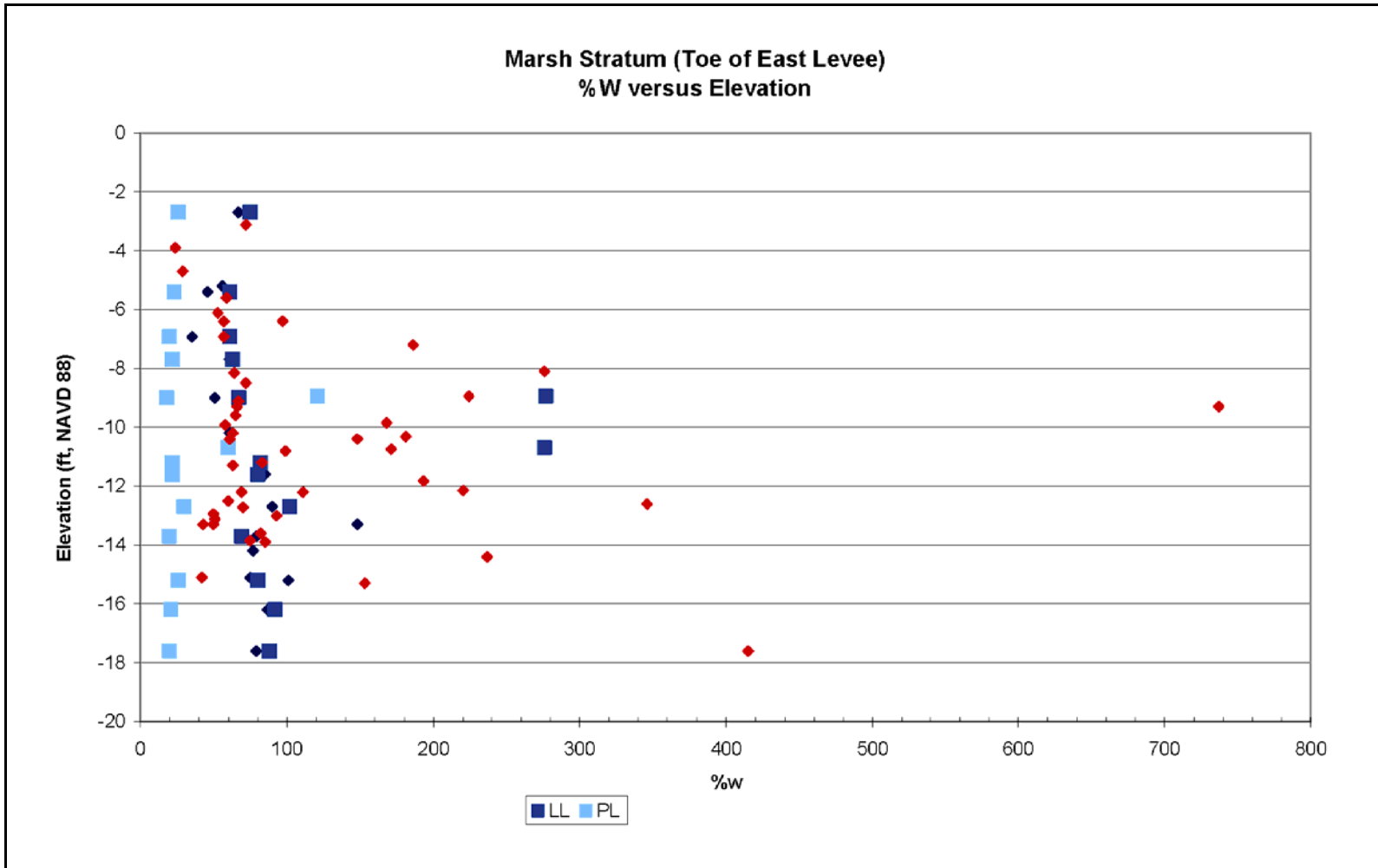


Figure 1-37. Marsh Stratum (Toe of East Levee), %w versus Elevation

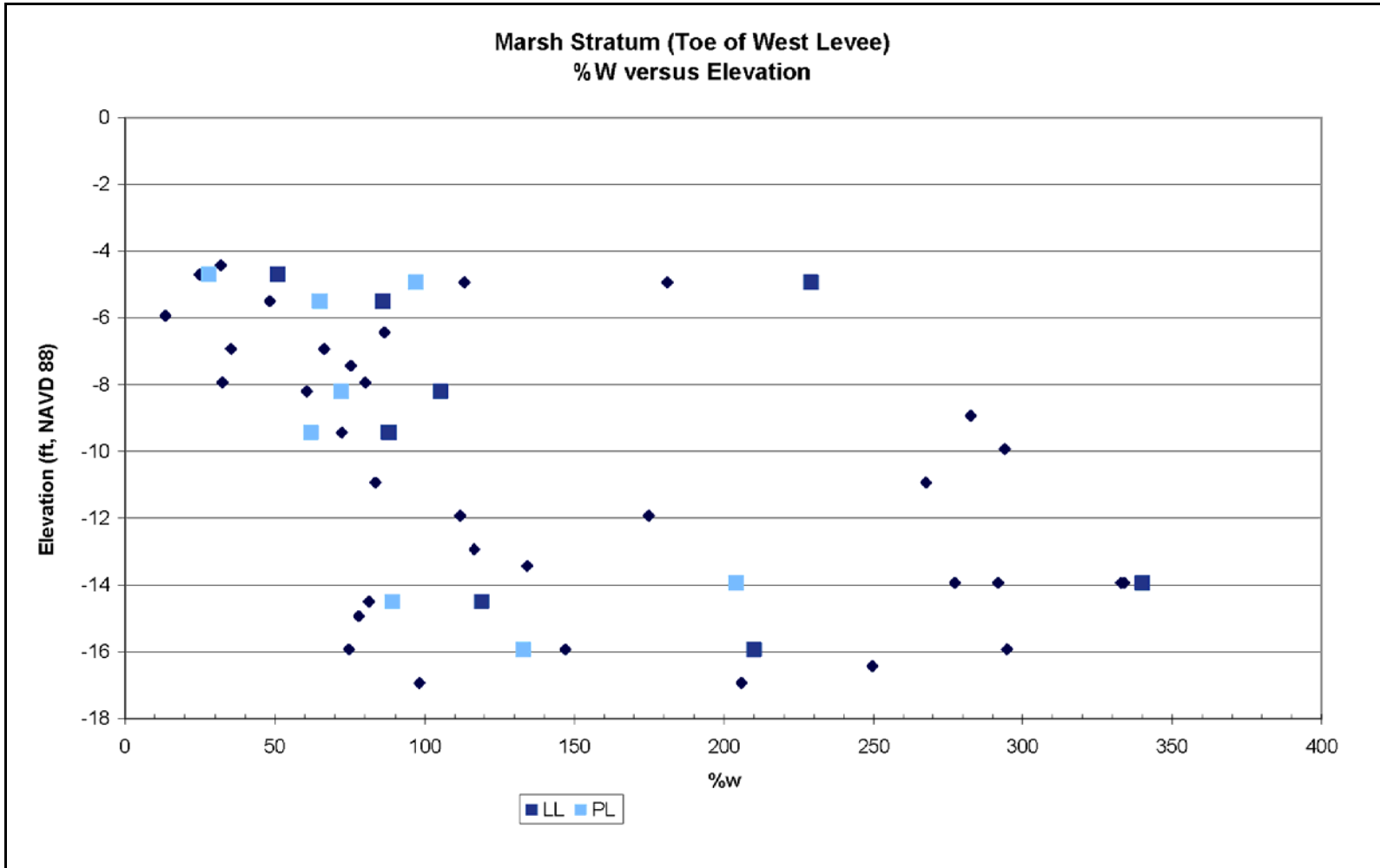


Figure 1-38. Marsh Stratum (Toe of West Levee), %w versus Elevation

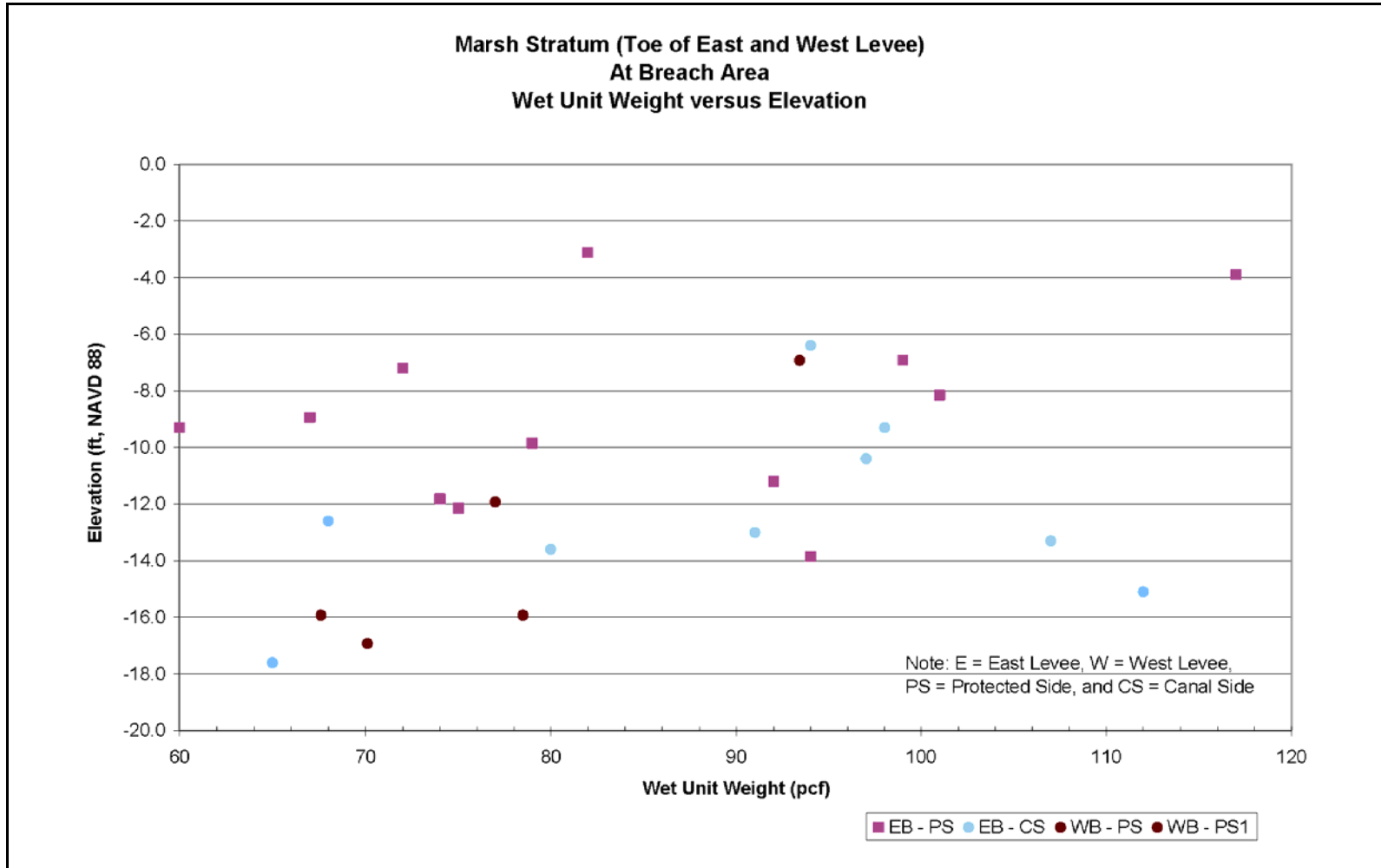


Figure 1-39. Marsh Stratum (Toe of East and West Levee – At Breach Area), Wet Unit Weight versus Elevation

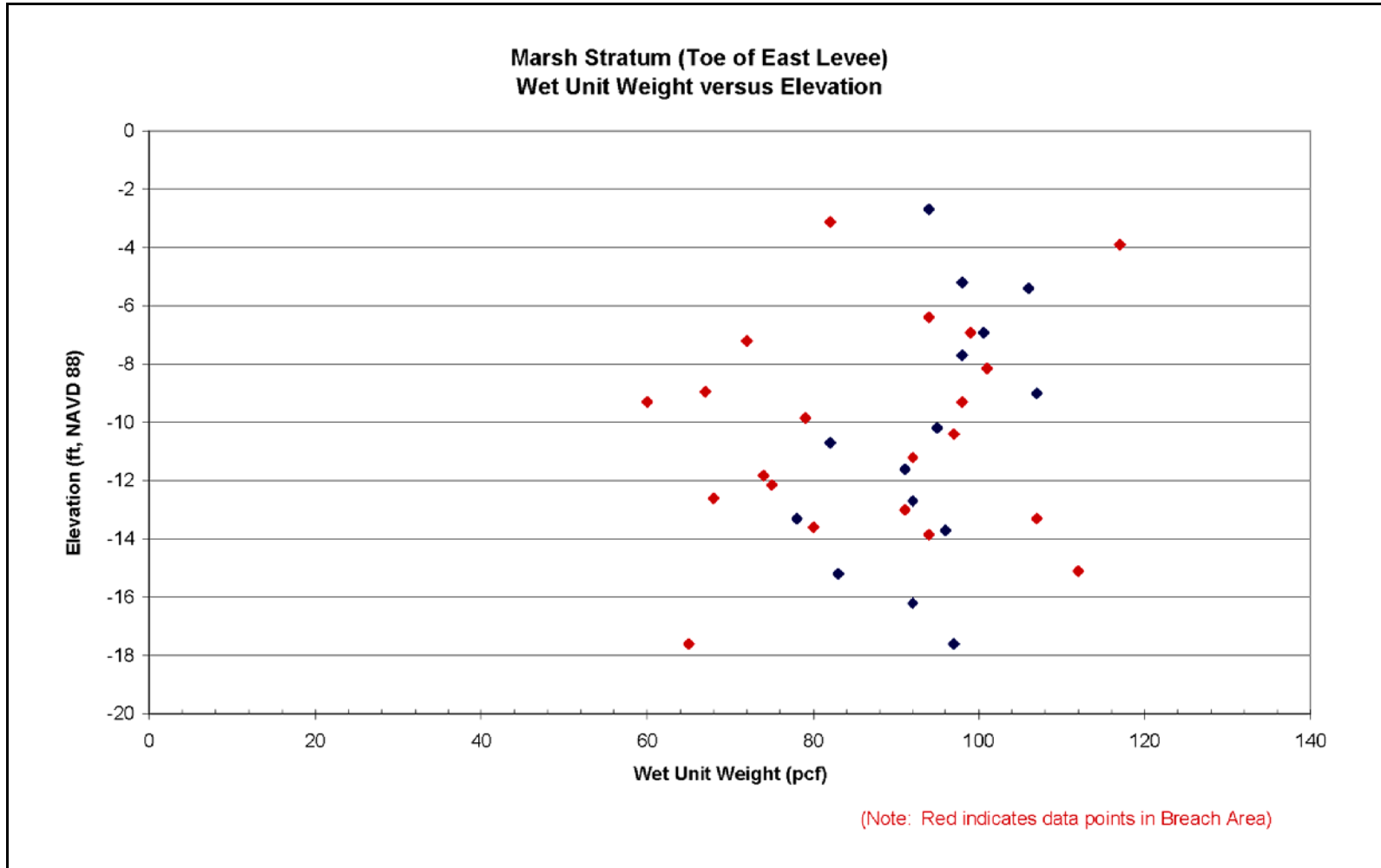


Figure 1-40. Marsh Stratum (Toe of East Levee), Wet Unit Weight versus Elevation

The undrained shear strength determined from the laboratory tests conducted on samples in the breach area is shown in Figure 1-42. Undrained shear strength data in the breach area plotted with undrained shear strength data for the entire east levee are shown in Figure 1-43. Undrained shear strength data for the entire west levee are shown in Figure 1-44.

Lacustrine Stratum

The data for the lacustrine stratum will be divided into two groups: data from under the levee embankment, and data from the toe of the levee.

Under the Levee Embankment

Data on the lacustrine stratum under the levee embankment consist of five borings shown in the 1990 GDM, and four cone penetrometer tests (CPT) taken on the east levee. Of the five GDM borings, four borings collected 3-in. (diameter) undisturbed samples, and one boring collected 5-in. (diameter) undisturbed samples. From the 3-in. samples, ten unconfined compression (UC) tests were performed. From the 5-in. samples, four UC tests were performed, and two one-point unconsolidated-undrained triaxial compression tests (UU-1), confined at existing overburden pressures, were performed. From these laboratory tests, moisture content and wet unit weights were determined. The moisture contents (%w) in the breach area are shown in Figure 1-45. The wet unit weight data in the breach area are shown in Figure 1-46.

Interpretation of the undrained shear strength from the CPTs using the bearing capacity equation ($N_k=15$) is plotted with laboratory test results in Figure 1-47. These interpretations were provided by Dr. Thomas Brandon (Virginia Tech).

At the Toe of Embankment

Data on the marsh stratum under the toe of the levee embankment consist of five borings taken in 2005 on the protected side, four borings taken in 2005 on the canal side, and three borings on the west levee toe shown in the 1990 GDM. Of the borings on the protected side of the east levee, four borings collected 5-in. (diameter) undisturbed samples, and one boring collected 3-in. (diameter) undisturbed samples. Of the borings on the canal side of the east levee, three borings collected 5-in. (diameter) undisturbed samples, and one boring collected 3-in. (diameter) undisturbed samples. Of the three GDM borings taken on the protected side of the west levee, two borings collected 3-in. (diameter) samples, and one boring collected 5-in. (diameter) undisturbed samples. From the 3-in. samples, 14 UC tests were performed, and five one-point unconsolidated-undrained triaxial compression tests (UU-1), confined at existing overburden pressure, were performed. From the 5-in. samples, 25 UC tests were performed, 19 unconsolidated-undrained triaxial compression tests (Q), and 7 one-point unconsolidated-undrained triaxial compression tests (UU-1), confined at existing overburden pressure, were performed. From these laboratory tests, moisture content and wet unit weights were determined. The moisture contents (%w) in the breach area are shown in Figure 1-48. The wet unit weight data in the breach area are shown in Figure 1-49.

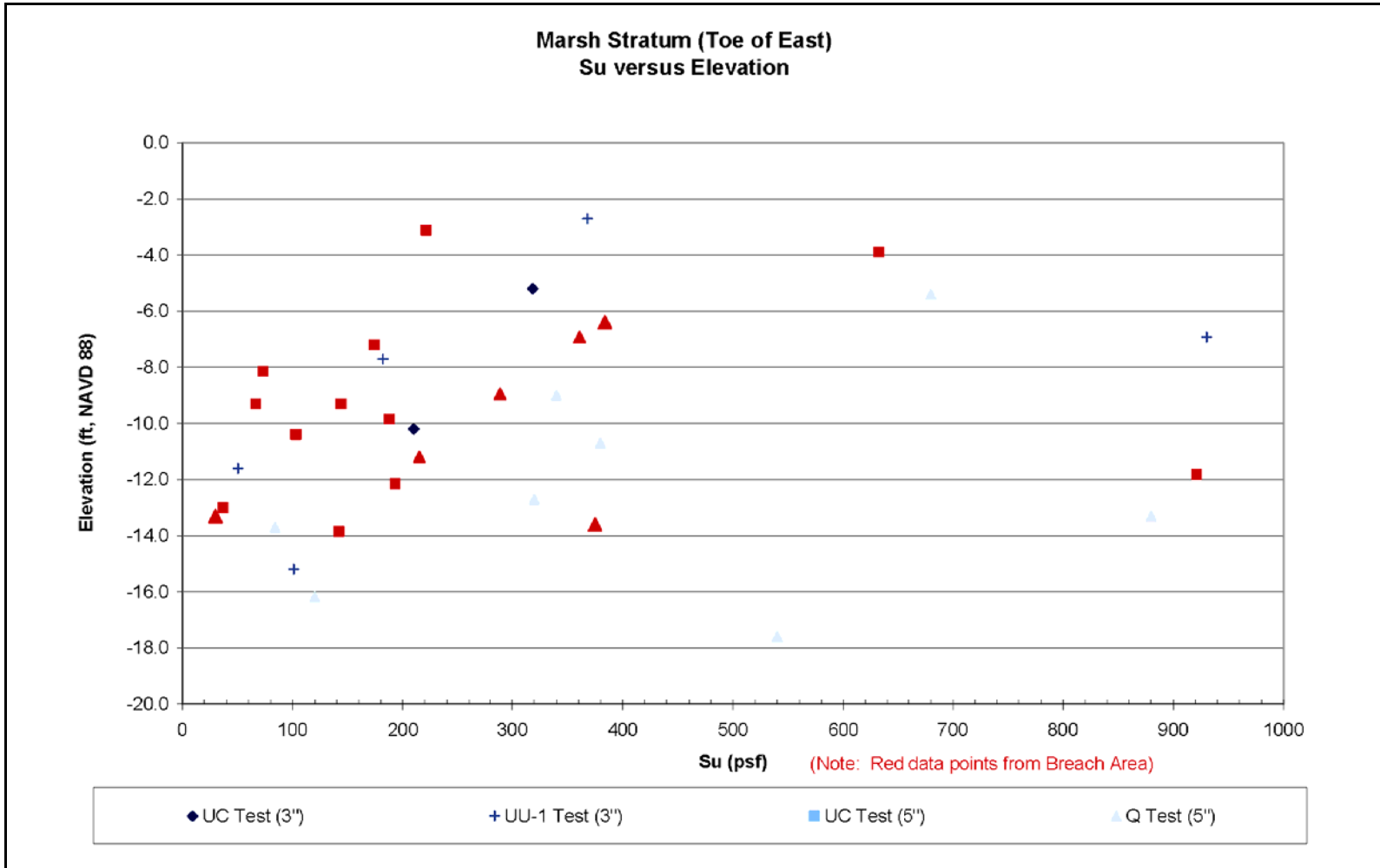
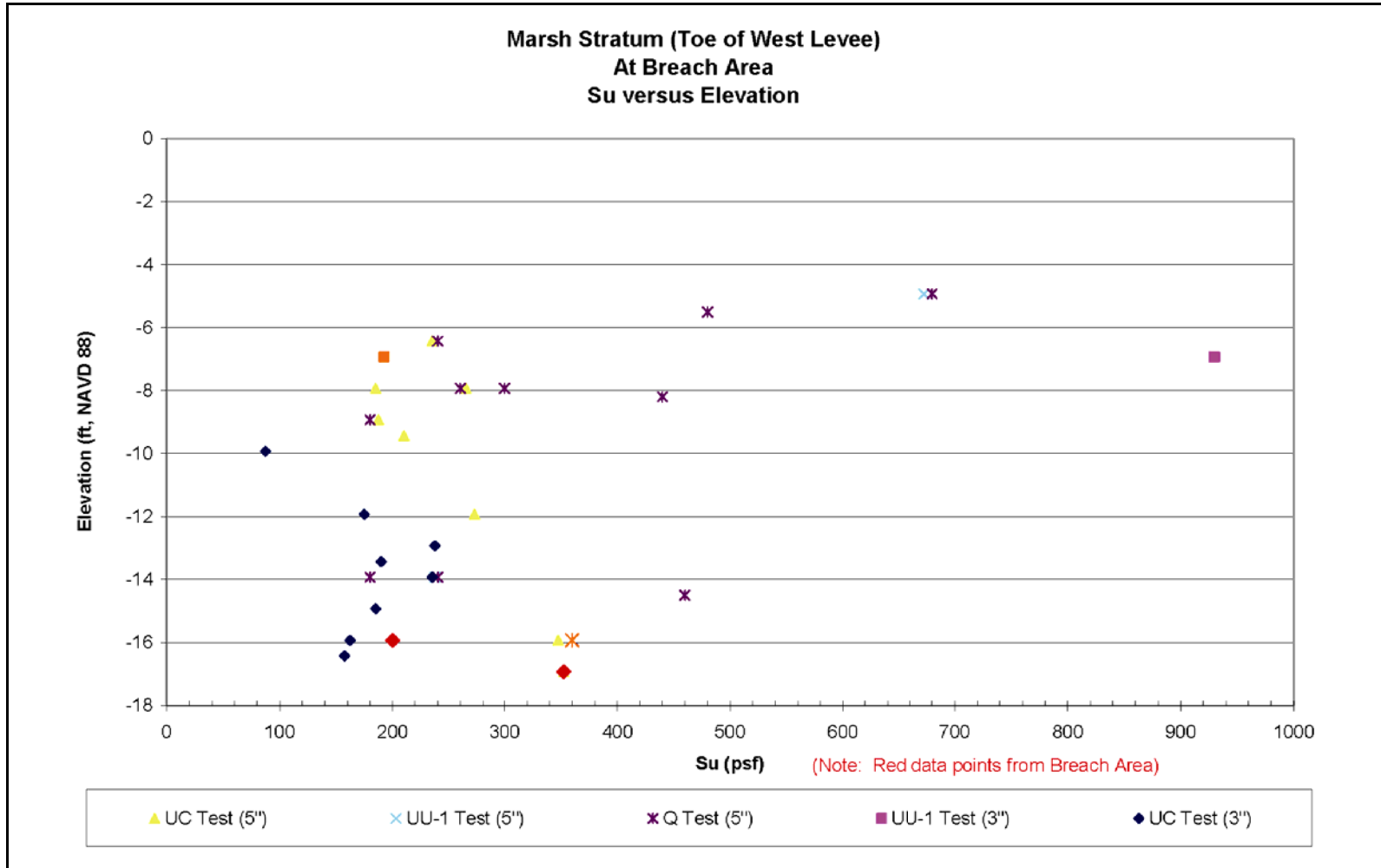


Figure 1-43. Marsh Stratum (Toe of East Levee), Su versus Elevation



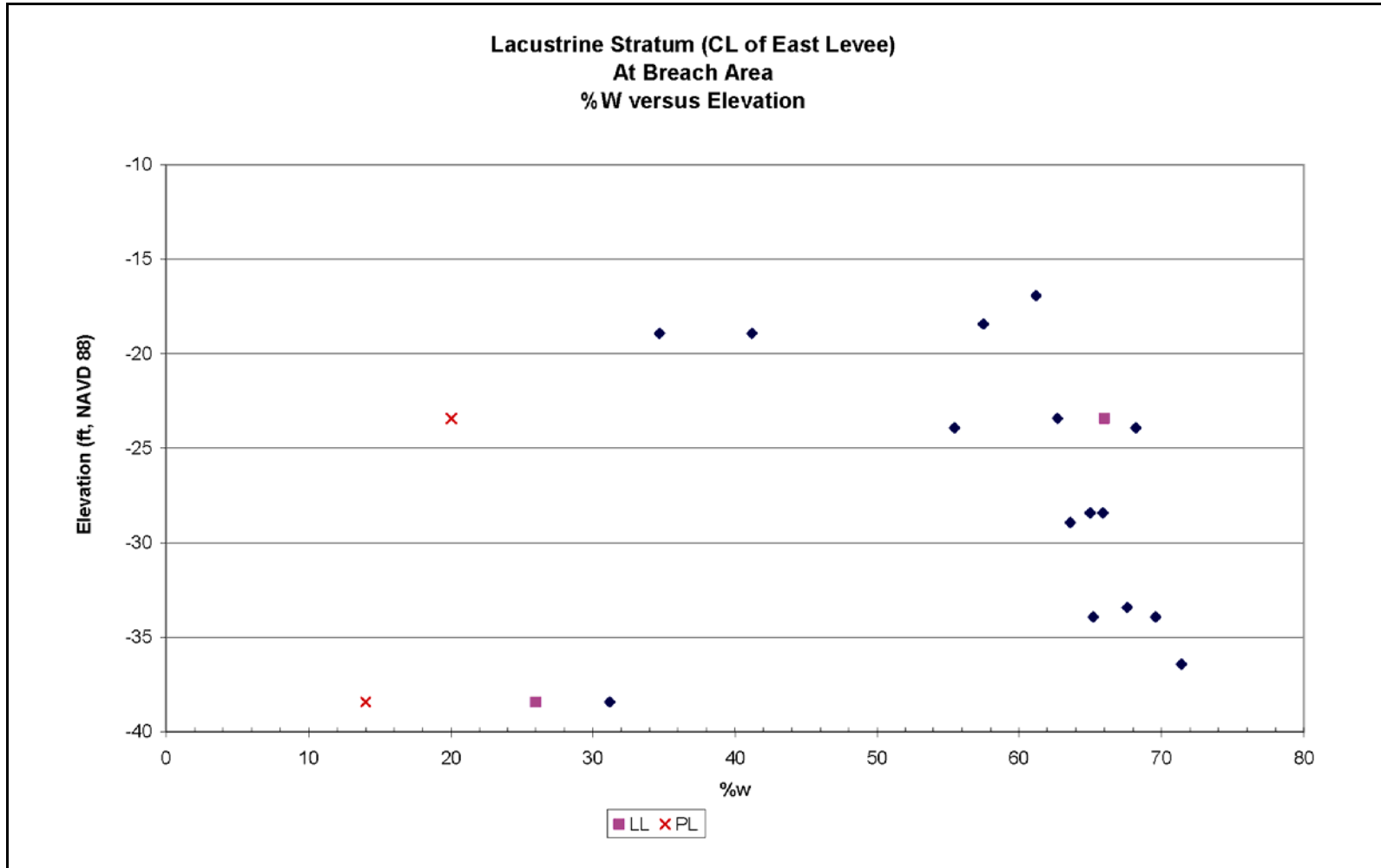


Figure 1-45. Lacustrine Stratum (CL of East Levee – At Breach Area), %w versus Elevation

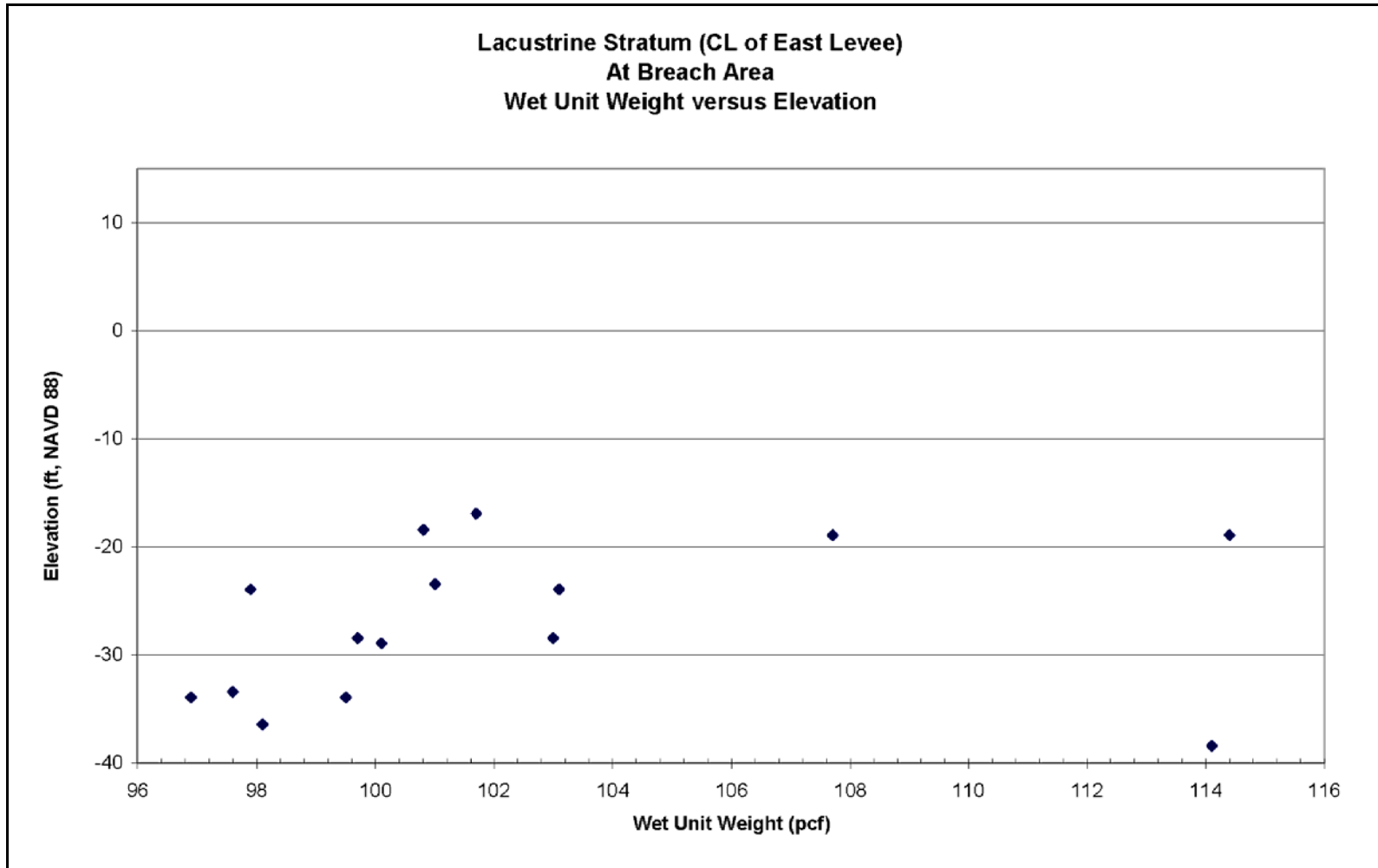


Figure 1-46. Lacustrine Stratum (CL of East Levee – At Breach Area), Wet Unit Weight versus Elevation

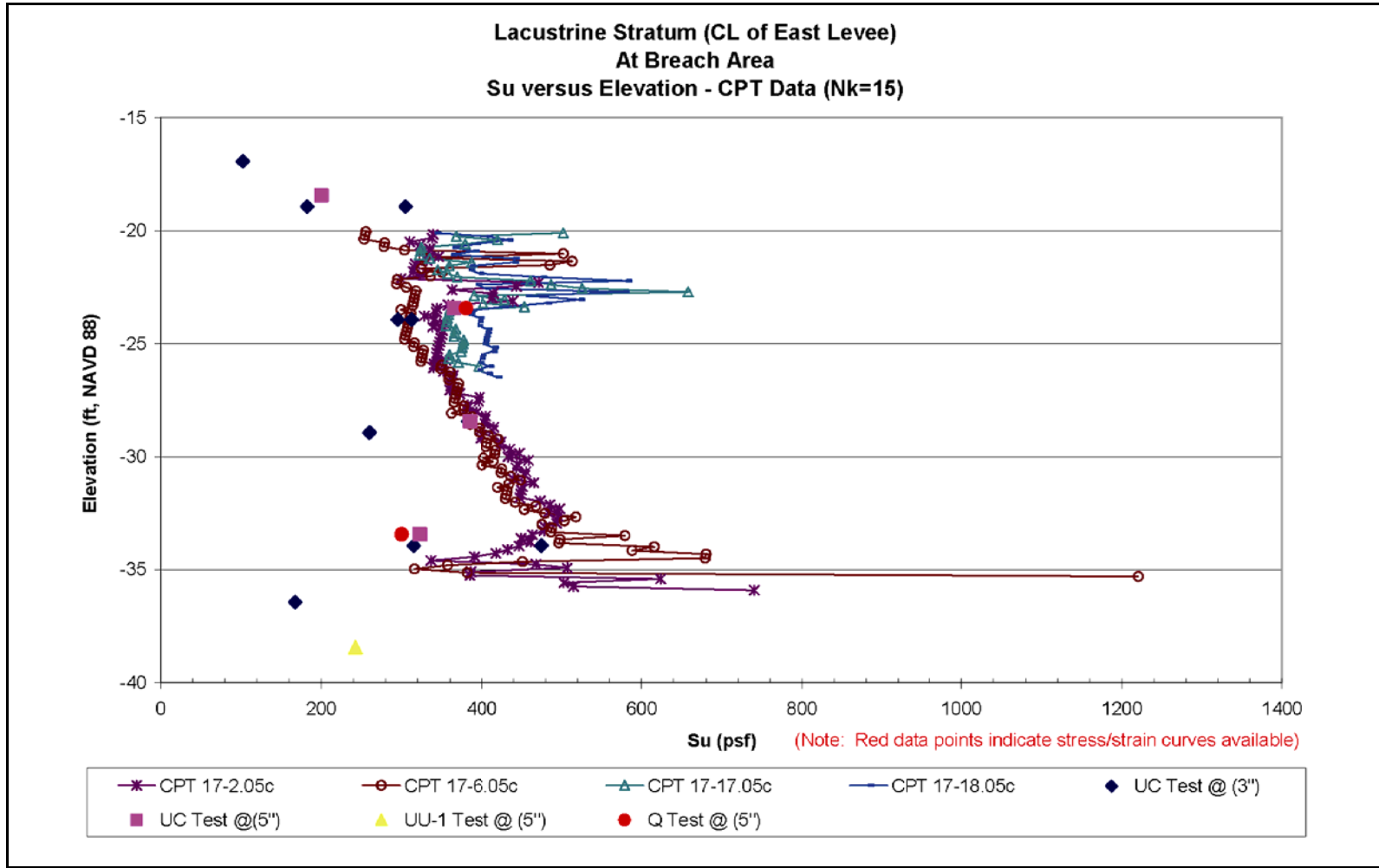


Figure 1-47. Lacustrine Stratum (CL of East Levee – At Breach Area), Su versus Elevation (CPT Data – Nk=15)

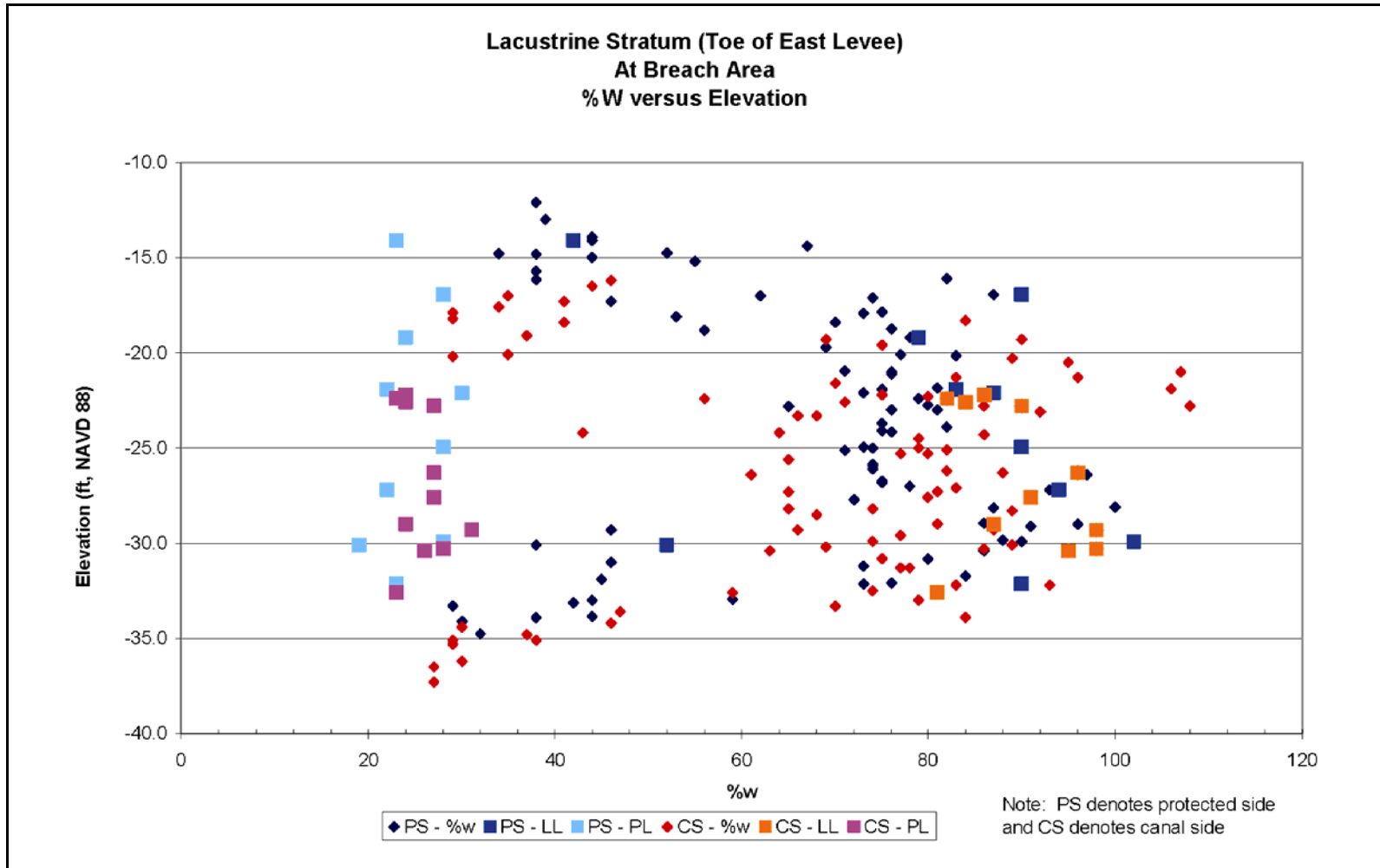


Figure 1-48. Lacustrine Stratum (Toe of East Levee – At Breach Area), %w versus Elevation

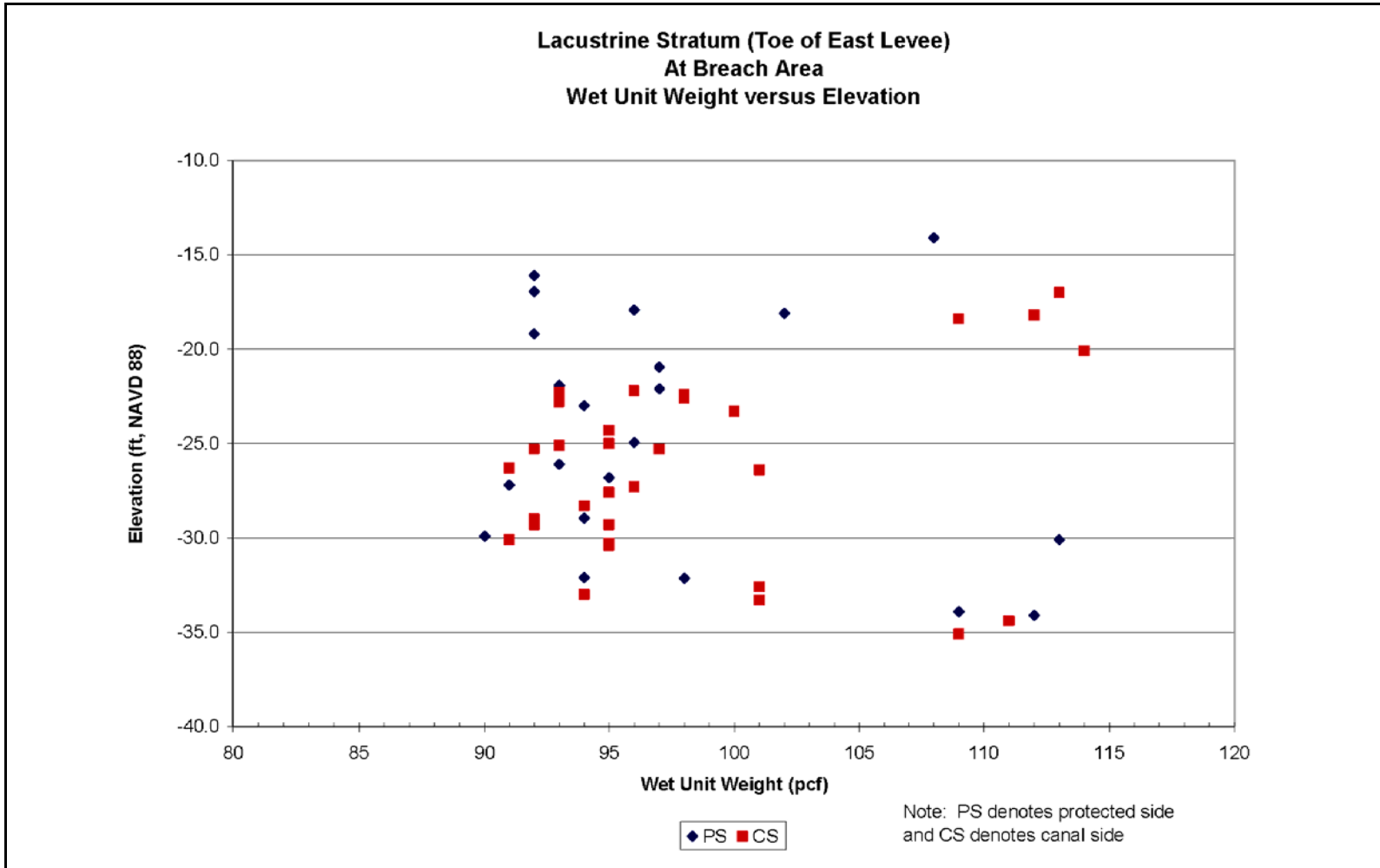


Figure 1-49. Lacustrine Stratum (Toe of East Levee – At Breach Area), Wet Unit Weight versus Elevation

The undrained shear strength determined from the laboratory tests conducted on samples in the breach area is shown in Figure 1-50. The S_u/P ratio for the shear strengths samples is shown in Figure 1-51.

Beach Sand Stratum. Forty standard penetration tests (SPT) were conducted in the beach sand stratum in the breach area. The field (uncorrected) standard penetration number for the beach sand stratum is shown in Figure 1-52. Interpretation of the SPT number from the CPTs will be provided later. Dissipation tests with the CPT were conducted at this stratum at 17-2.05c and 17-6.05c. At 17-2.05c, the head in the sand was about 7.8 ft below the top of the hole or at elevation -3.68 (NAVD 88). At 17-6.05c, the head in the sand was about 6 ft below the top of the hole or at elevation -1.3 (NAVD 88).

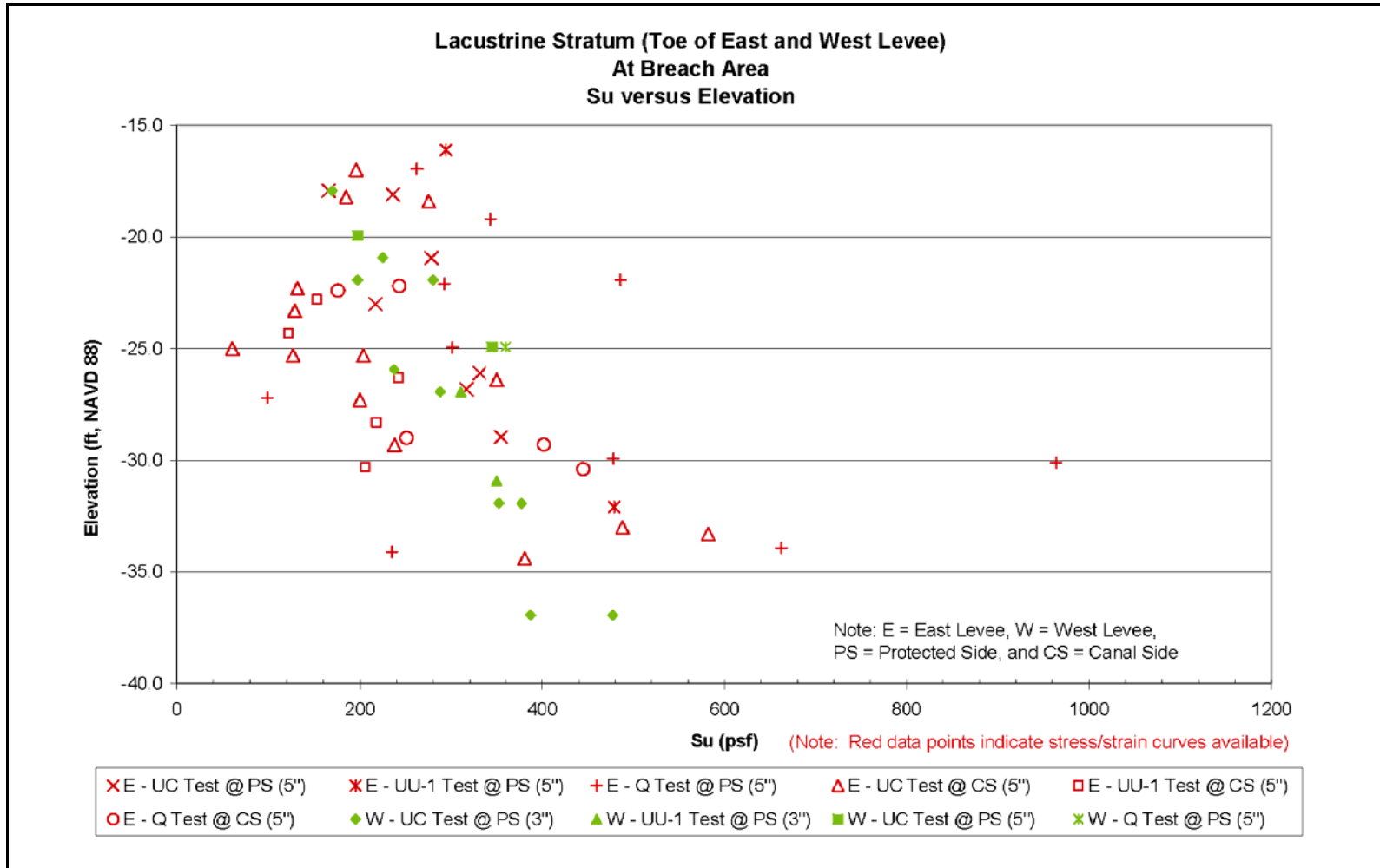


Figure 1-50. Lacustrine Stratum (Toe of East and West Levee – At Breach Area), Su versus Elevation

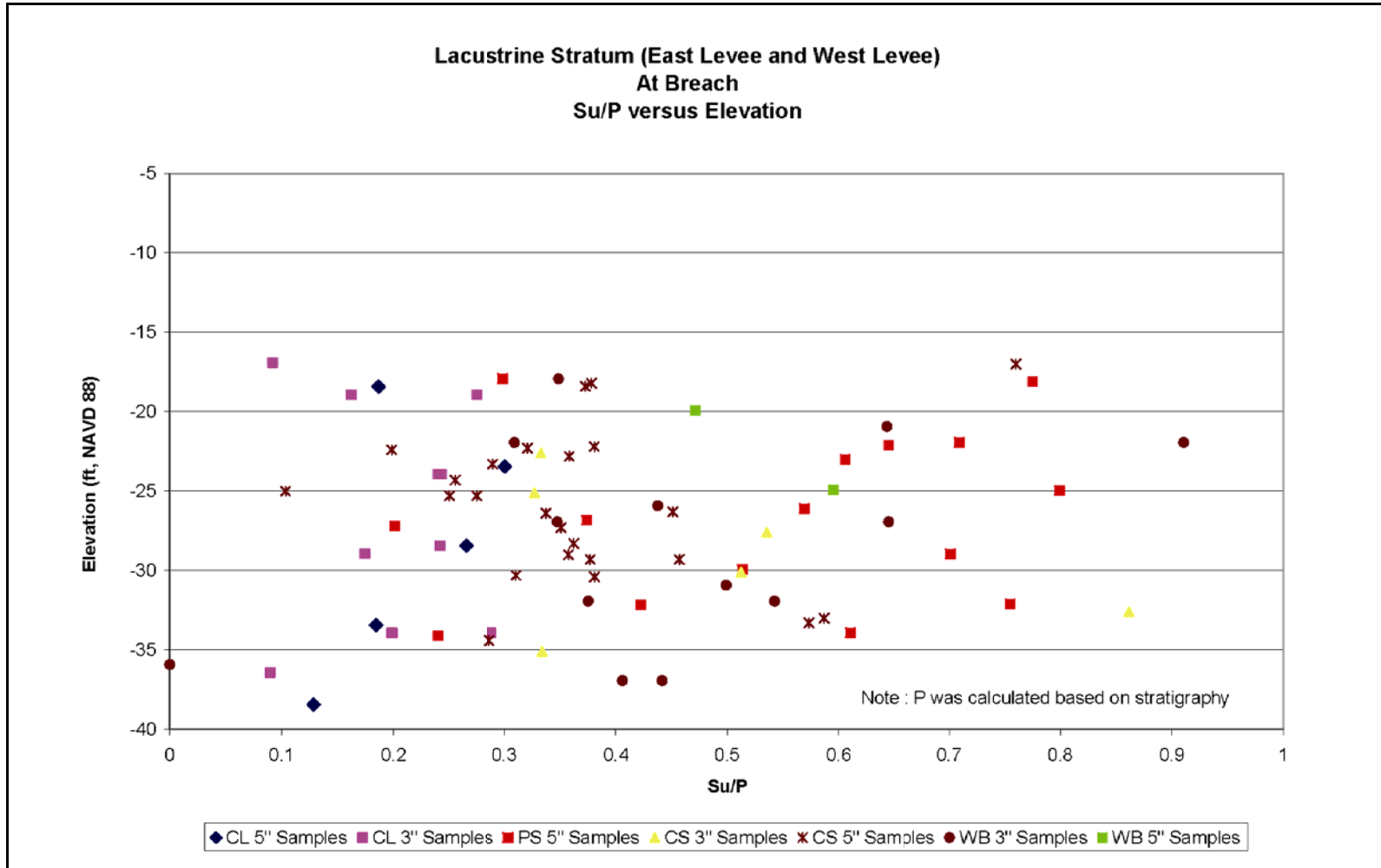


Figure 1-51. Lacustrine Stratum (East and West Levee), Su/P ratio versus Elevation

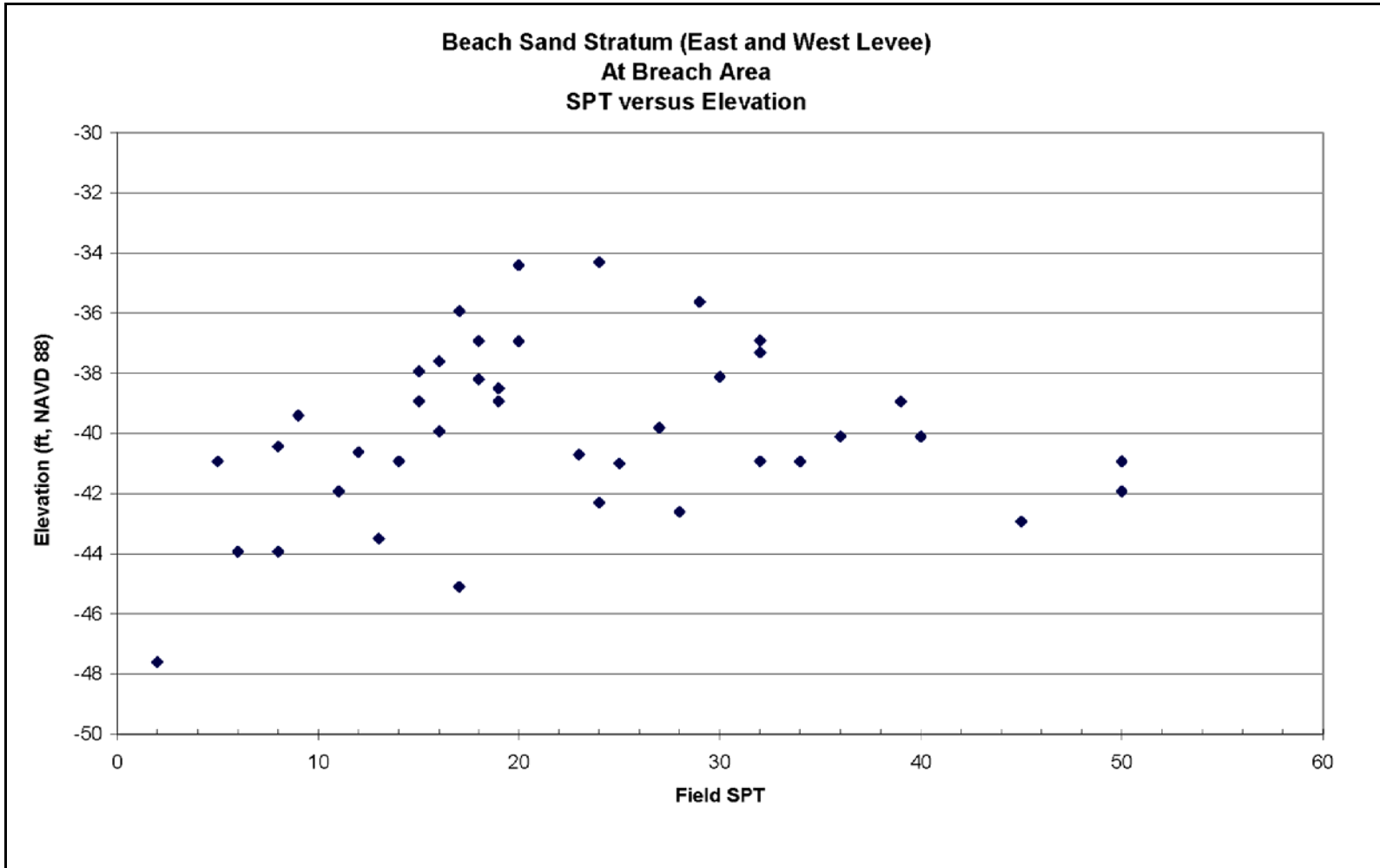


Figure 1-52. Beach Sand Stratum (East and West Levee – At Breach Area), Field SPT versus Elevation

Appendix 2

Description of New Orleans Area Geology, Environments of Deposition, and General Engineer Properties of these Environments

1 Introduction¹

The following summary describes the geology and the Holocene history of the New Orleans area, and the relationships between the associated environments of deposition and general engineering properties. This information has been extracted from a technical report on the geological and geotechnical aspects of the Celotex Levee failure, which occurred along the west bank of the Mississippi River in 1985 in the greater New Orleans area (Figure 2-1). Only the geology sections are presented in this Appendix. This information serves as background information for evaluation of the various canal failures during Hurricane Katrina.

The geologic portions of the Celotex Report are presented in Chapter 2 and Appendix A. Chapter 2 describes the geologic history and geology of the New Orleans area as determined from a review of the technical literature, an evaluation of numerous engineering borings, aerial photo interpretation, and preparation of several detailed cross-sections (Figures 2-2 through 2-5 of Chapter 2, see enclosed). Appendix A of this same report provides detailed descriptions and information about the engineering properties of the depositional environments that are present at the surface and in the subsurface. Chapter 2 and Appendix A are presented here in their original order of presentation because of their logical arrangement in the text. The descriptions of the environments are important when examining soil types and physical properties from the respective environments.

Additionally, various references are identified in the text and are presented at the end of this summary appendix. Many of the Corps of Engineer cited publications and maps for the New Orleans area are now presented at the ERDC website on the Geology of the Lower Mississippi Valley (see lmvmapping.erd.usace.army.mil).

A final note, the lacustrine environment is not identified in the summary description and is an important lithostratigraphic unit. This environment is unique to this area because of the protection afforded by the now buried Pine Island beach complex during the filling of the New Orleans area with subsequent sediment by the various Mississippi River distributary channels during the Middle to Late Holocene. The lacustrine environment has been mapped for the back or northern side of the beach ridge in various GDMs, while the front or seaward side has been mapped as being interdistributary. This distinction is primarily a matter of semantics, as opposed

¹ This appendix was extracted from Dunbar, J. B., Torrey, V. H., III, Wakeley, L. D., 1999. "A Case History of Embankment Failure, Geological and Geotechnical Aspects of the Celotex Levee Failure, New Orleans, Louisiana," Technical Report GL-99-11, Engineer Research and Development Center, Waterways Experiment Station, Vicksburg, MS.

to any significant differences between lithology and/or engineering properties of these respective two environments. For purposes of this discussion and overall context, these two environments are nearly identical. The discussion of the intertributary environment will be representative for the lacustrine environment identified throughout many of the GDMs.

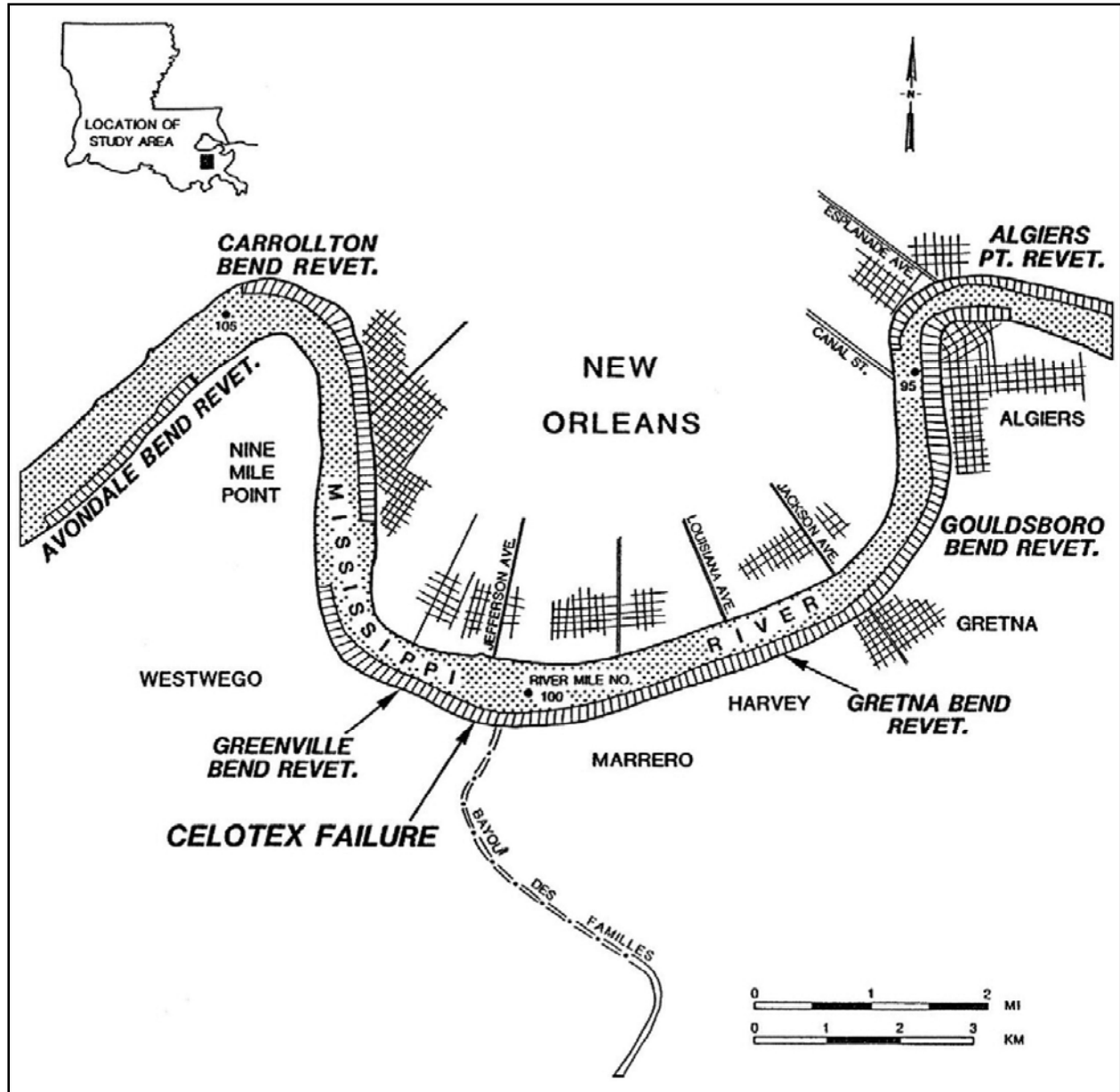


Figure 2-1. Map of study area showing location of the Celotex levee failure

2 Geology

Physiography

The study area is located in the southern portion of the lower Mississippi Valley and is a part of the Mississippi River's deltaic plain. Broad natural levees associated with the Mississippi River and Bayou des Familles, a prehistoric distributary channel, are the most prominent physiographic features in this area. Surface topography is generally of low relief with surface elevations ranging from approximately 25 ft (7.6 m) NGVD along the levee crests to sea level throughout much of the study area. Over a significant part of the New Orleans Metropolitan area the surface elevation is at or below sea level.

In the New Orleans area, the meander pattern of the Mississippi River is distinctive, making four nearly right angle turns which have changed very little during the past 100 years (Figure 2-1). The width of the Mississippi River within the study area (river mile 91.0 to 106.0 (146.45 to 170.59 km)) varies from 1,750 to 2,700 ft (533 to 823 m). The river thalweg elevations through this reach range from -70 ft (-21 m) to about -190 ft (-58 m) NGVD. The top of the bank elevation through the study reach averages about 10 ft (3 m) NGVD. Channel bendways are characterized by deep "permanent" scour pools separated by shallower crossings. Revetment protection along the river corresponds to the deeper scour pools at Avondale, Carrollton, Greenville, Gretna, Gouldsboro, and Algiers (Figure 2-1).

Geologic Setting and History

The scope of this study permits a summary of the major events to explain the significance of the engineering geology in the study area. The general geologic chronology that has been defined for the Mississippi River's deltaic plain is based upon thousands of engineering borings drilled during the past 50 years, hundreds of radiometric age determinations of organic deltaic sediments, and numerous geologic studies conducted in this region (Fisk 1944; Kolb and Van Lopik 1958a and 1958b; Kolb 1962; Kolb, Smith, and Silva 1975; Autin et al. 1991; Frazier 1967; Saucier 1969 and 1974; May et al. 1984; Dunbar et al. 1994 and 1995; Smith, Dunbar, and Britsch 1986). Boring data identify a diverse surface and subsurface geology that is related to the different course shifts by the Mississippi River and associated deltaic advances during the Holocene (last 10,000 years).

To better understand the geology of the area, it is first necessary to briefly review the geologic history of coastal Louisiana since the late Pleistocene (17,000 to 10,000 years ago). Approximately 17,000 years ago, glaciers covered much of North America and sea level was approximately 300 ft (91 m) below the present level (Kolb, Smith, and Silva 1975). The Gulf shoreline was much farther seaward than at its present location.

The ancestral Mississippi River and its tributaries below Baton Rouge, LA, were entrenched into the underlying Pleistocene surface and had developed a broad drainage basin, approximately 25 miles (40 km) wide, which extended southeasterly beneath the present deltaic plain (Kolb and Van Lopik 1958a). Geologic mapping (Kolb and Van Lopik 1958a and 1958b; May et al. 1984) indicates that the axis of the valley entrenchment occurs in the vicinity of Houma, LA, approximately 45 miles (72 km) southwest of New Orleans.

The underlying Pleistocene surface represents deposits from a much older Mississippi River deltaic plain sequence and associated nearshore environments. These sediments were deposited during the previous interglacial cycle (Sangamon interglacial period), approximately 125,000 to 70,000 years ago. Fisk (1944) collectively called these Pleistocene sediments the Prairie Formation. Sediments of the Prairie Formation outcrop at the surface just north of Lake Pontchartrain.

Sea level began rising approximately 17,000 years ago because of glacial melting and reached its present level between 4,000 and 6,000 years before the present. Rising sea level corresponds to a period of valley-wide aggrading of the ancestral alluvial valley by the existing fluvial systems. Melting glaciers released large quantities of sediment to the Pleistocene drainage system and filled the entrenched valley with coarse sediments (sand and gravel). A dense network of shallow and swiftly flowing braided stream courses formed within the ancestral alluvial valley because of overloading by the massive influx of glacial outwash. Along the length and width of the Lower Mississippi Valley, basal substratum sands are present in the subsurface which represent the relic braided stream or outwash plain sediments from glacial melting (Fisk 1944; Kolb et al. 1968; Krinitzsky and Smith 1969; Saucier 1964 and 1967; Smith and Russ 1974). The change in deposition from a braided system to a meandering Mississippi River system occurred approximately 12,000 years before the present (Saucier 1969; and Krinitzsky and Smith 1969).

Advent of the modern sea level began creation of the modern deltaic plain and led to the present land surface. Present day coastal Louisiana is the product of numerous, but generally short lived, seaward prograding delta systems. These deltas are subsequently reworked by coastal transgressive processes and modified. Five major deltaic systems have been built seaward during the past 6,000 years as shown by Figure 2-2 (after Frazier 1967). Each delta system consists of several major distributary channels and numerous individual delta lobes (Figure 2-3). The relative ages of these delta systems are generally well established by radiocarbon dating techniques. Limits of the different delta systems and the chronology of the major distributary channels associated with each system are summarized in Figures 2-2 and 2-3 (after Frazier 1967).

The first advance of a major delta system into the New Orleans area occurred with the St. Bernard system. The present course of the Mississippi River through the New Orleans area

was established during the active St. Bernard delta. Partial Mississippi River flow continued to pass through the New Orleans reach following abandonment of the St. Bernard system for the Lafourche delta complex. During the active Lafourche system, the Mississippi River flowed southward at Donaldsonville, through Bayou Lafourche, and to the Gulf of Mexico. After abandonment of the Lafourche system approximately 500 years ago, nearly full Mississippi River flow returned to the present day course.

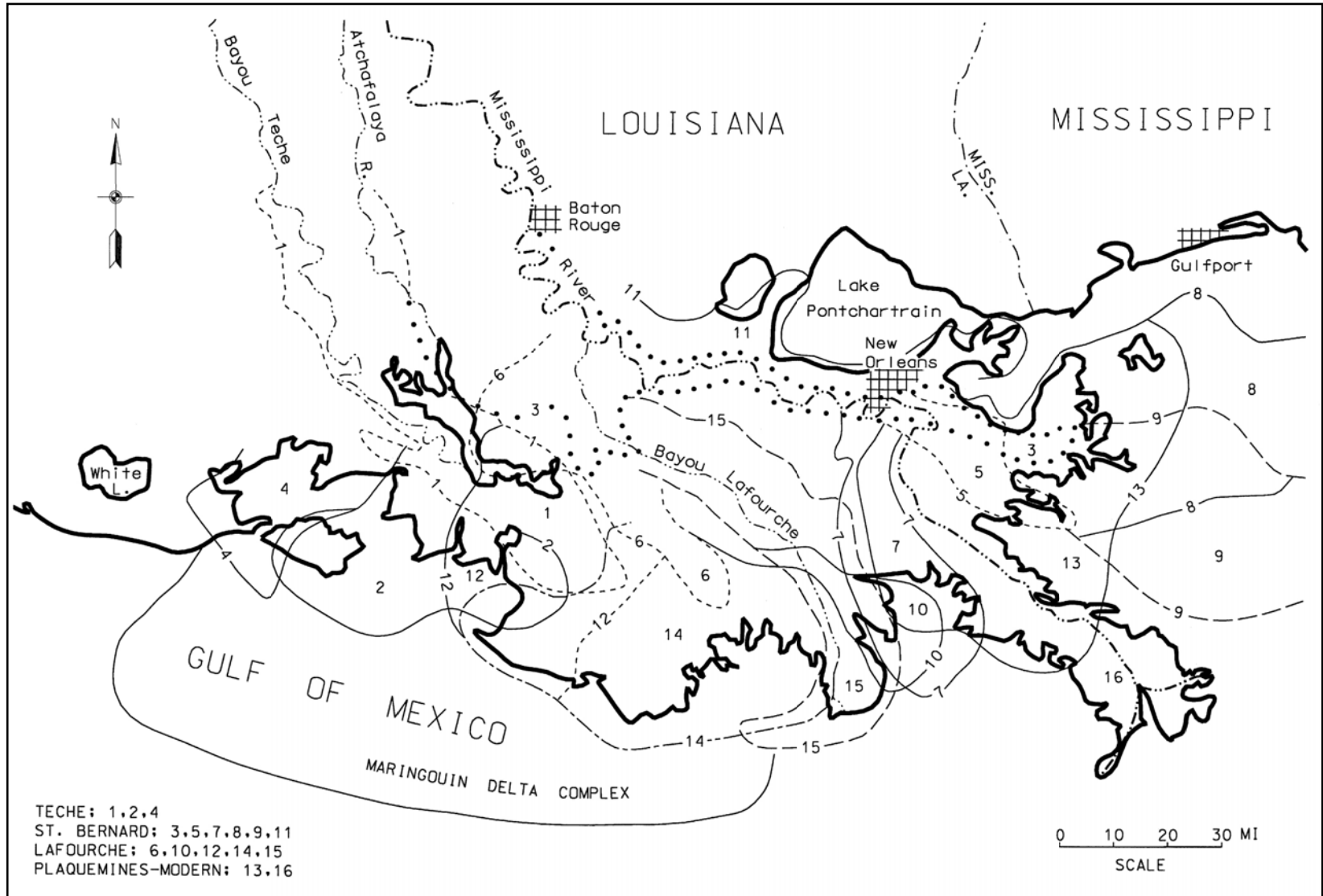


Figure 2-2. Holocene delta and distributary systems (after Frazier 1967)

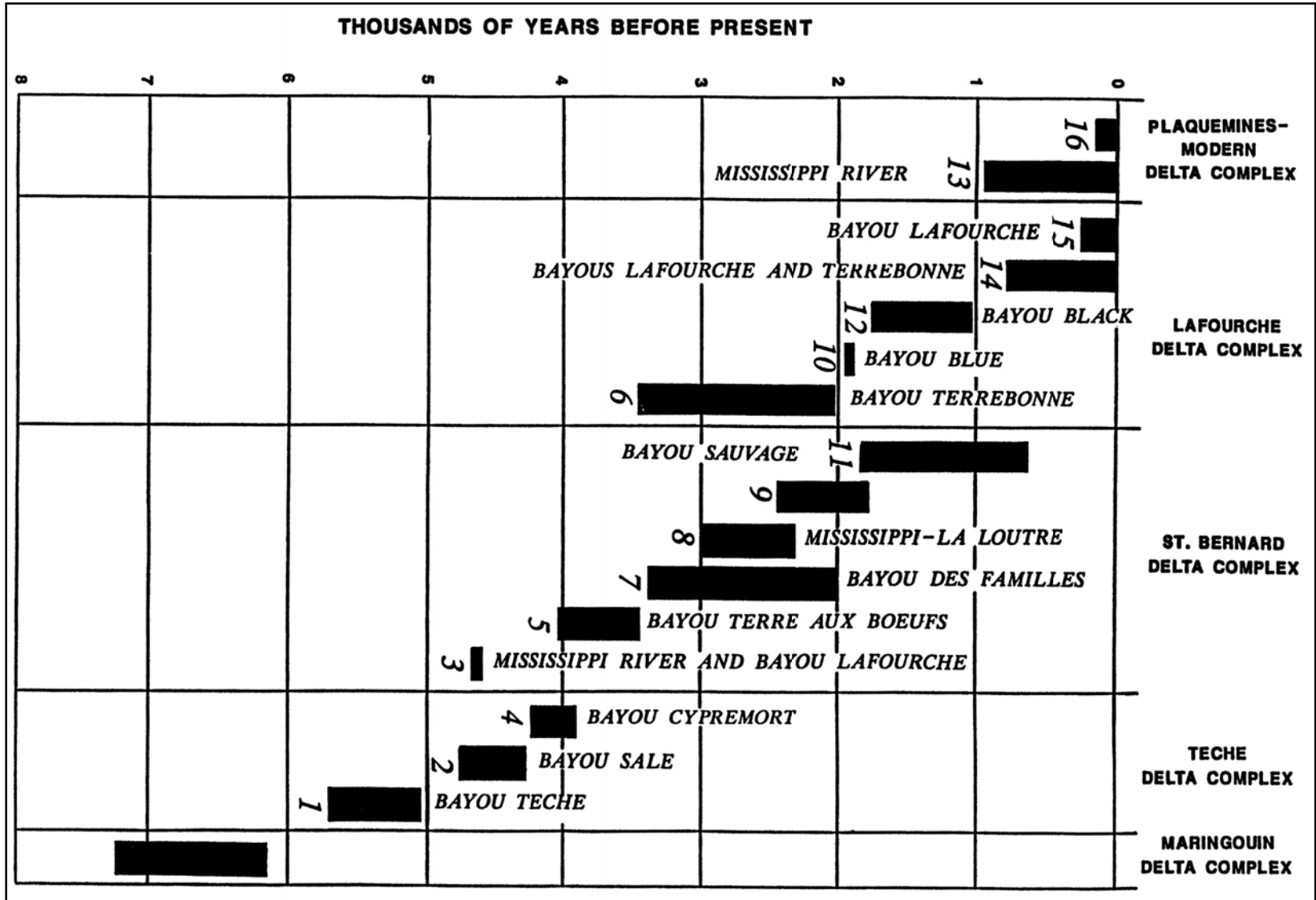


Figure 2-3. General chronology of Mississippi River delta and distributary systems (after Frazier 1967)

Geologic Structure

The study area is part of the seaward thickening wedge of Quaternary sediments which dip gently gulfward and fill the Gulf of Mexico geosyncline. Major structures within this sedimentary prism are piercement salt domes and growth faults. In the study area there are no buried salt domes. The vast majority of Louisiana's salt domes are located south and west of the New Orleans area (New Orleans Geological Society 1962 and 1983; and Halbouty 1967).

Faulting has been identified in the subsurface throughout the deltaic plain and in the Pleistocene deposits exposed at the surface north of Lake Pontchartrain (Wallace 1966; and Snead and McCulloh 1984). These faults are not tectonically active. Instead, they are related to sedimentary loading of the Gulf of Mexico basin. Faulting has been identified in the Pleistocene sediments beneath Lake Cataouatche (approximately 8 miles (12.8 km) southwest of New Orleans) and beneath Lake Pontchartrain (Wallace 1966; and Kolb, Smith, and Silva 1975). Fisk (1944) identified several normal faults in the buried Pleistocene sediments beneath New Orleans. He interpreted these faults based on the orientation of stream courses, lake shores, and the Mississippi River. The presence of these faults based solely on this type of evidence is speculative without more detailed stratigraphic evidence to support their existence. Non-tectonic geomorphic and stratigraphic processes can produce these types of linear features without faulting as the underlying mechanism. A detailed engineering study of Pleistocene sediments in the New Orleans area by Kolb, Smith, and Silva (1975) did not identify subsurface faults near the Celotex failure site or for the general New Orleans area. Their study identified only one fault in the New Orleans area (in Lake Pontchartrain) and was based on combined boring and geophysical (subbottom profiling) data.

No faults were identified during this investigation in the study area. Surface faults in Holocene sediments are difficult to detect, because unconsolidated sediments tend to warp rather than shear. Geologic mapping and boring data evaluated during the course of this study did not identify any surface or subsurface faulting in the study area.

Geology and Environments of Deposition

Surface geology

The first objective of this investigation was to map and define the surface and subsurface geology of the study area. Definition of the geology was accomplished by examination and interpretation of historic aerial photography, subsurface data (engineering borings and electrical logs), different hydrographic survey periods, historic maps, and by review of the available geologic literature (Autin et al. 1991; Eustis Engineering Company 1984; Frazier 1967; Kemp 1967; Kolb 1962; Kolb and Van Lopik 1958a and 1958b; Kolb, Smith, and Silva 1975; Kolb and Saucier 1982; Miller 1983; Saucier 1963; Self and Davis 1983). A map of the surface geology for the study area is presented in Figure 2-4.

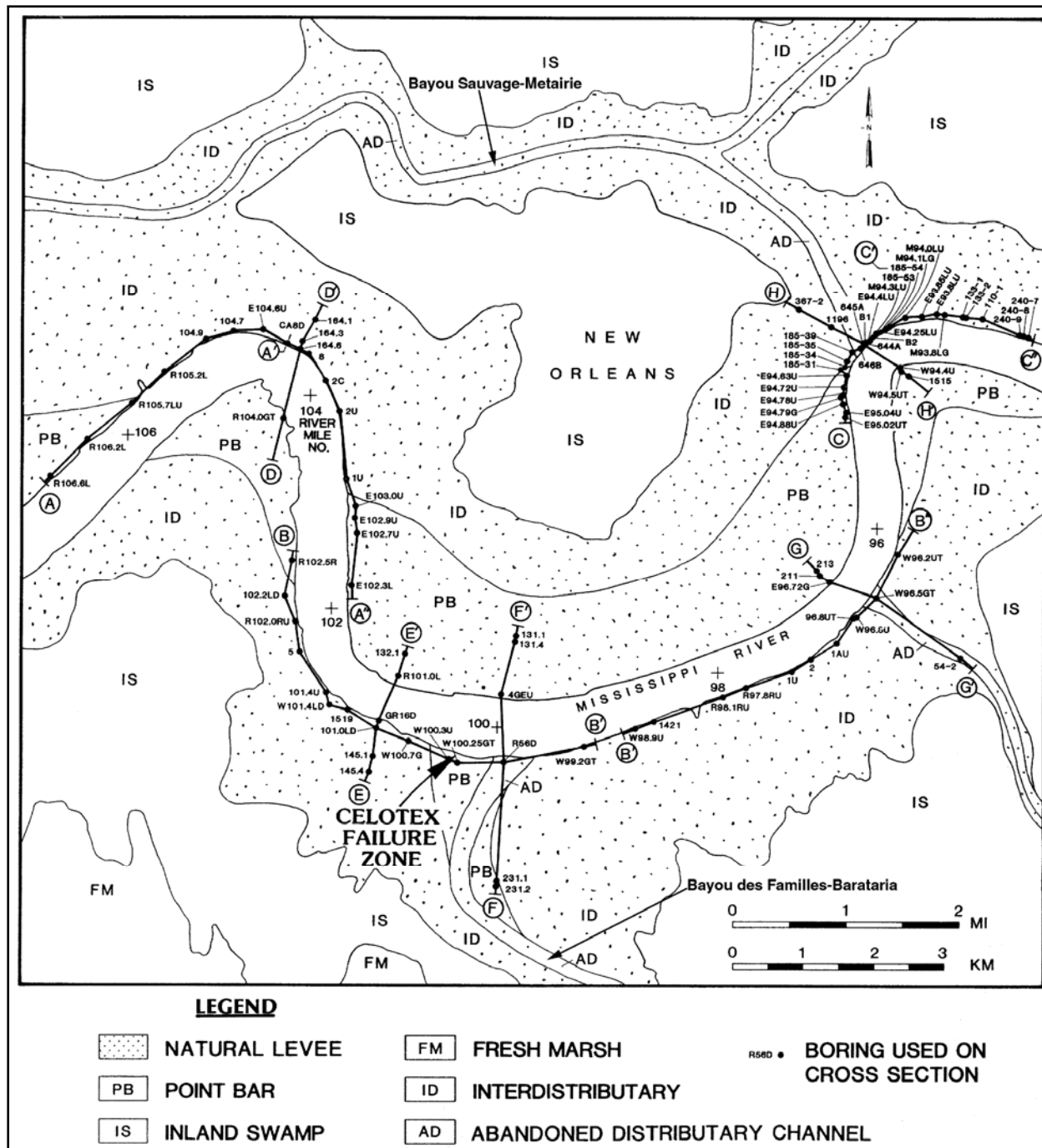


Figure 2-4. Geologic map of the study area showing boring and cross section locations

Environments of deposition mapped at the surface in Figure 2-4 include natural levee, point bar, inland swamp, fresh marsh, and several abandoned distributary channels. A complete description of the different environments of deposition present in the study area is contained in Appendix A. Natural levee deposits identified on the geologic map in Figure 2-4 are shown with the underlying environment of deposition. The surface geology consists primarily of Mississippi

River natural levee and point bar deposits, several abandoned distributary channels, and their associated fluvial and deltaic deposits.

Formation of the study area is directly related to the past and present courses of the Mississippi River and its abandoned distributary channels. Abandoned distributary channels within the study area are associated with two major distributary systems, Bayou des Familles-Barataria and Bayou Sauvage-Metarie Bayou (Figure 2-4). Bayou Des Familles-Barataria is a major St. Bernard distributary channel or Mississippi River course which extends due south from the Mississippi River at the Celotex failure site to Barataria, LA. This distributary system was active from approximately 2,000 to 3,400 years before the present (Frazier 1967).

The second major distributary course mapped in the study area is Bayou Sauvage-Metarie Bayou. According to Frazier (1967), this course was active from about 800 to 1,800 years before the present (Figure 2-3). However, Saucier (1963) and Kolb and Van Lopik (1958a) indicate that this system may have been active even earlier. Radiocarbon dates from organic sediments beneath the natural levees of Metarie Bayou range from 2,300 to 2,600 years before the present and indicate that a marsh surface was developed within this area. Metarie Bayou intersects the Mississippi River at Kenner and extends eastward, branching into two segments north of Algiers Point. The northern branch extends northeast toward Chef Menteur, Louisiana, as Bayou Sauvage. The southern branch, labeled Unknown Bayou by Saucier (1963), intersects the Mississippi River at Algiers Point (Figures 2-1 and 2-4), follows the Mississippi River between Algiers Point and Gretna, and then extends due southeast where it intersects the Mississippi River at 12 Mile Point.

Subsurface geology

Eight geologic cross sections were constructed from borings collected and evaluated during this study. The locations of the cross sections are shown on the geologic map in Figure 2-4. Cross sections A through H are presented as Figures 2-5a through 2-5k, respectively. The longer cross sections are presented as two separate sections or figures for illustration purposes. A legend of symbols and soil types identified on the sections is presented in Figure 2-5l. Sections were constructed such that each revetment reach includes sections parallel and perpendicular to the river bank. Parallel sections were constructed for only the cutbank or concave side as this is the side for maximum erosion and potential bank instability. The majority of soil types shown on the geologic sections are classified according to the Unified Soil Classification System (USCS). Borings not using the USCS (e.g., borings from private engineering companies) are shown with their textural soil types identified. The geologic cross sections show the vertical and horizontal limits of the various environments of deposition adjacent to the river as well as the soil types that form these different environments. Depositional environments present in the subsurface include interdistributary, intradelta, and nearshore gulf. A general description of these environments is contained in Appendix A. For readers desiring further engineering soils data beyond what is presented in this report, a detailed summary of soil engineering properties for the various environments of deposition is presented by Kolb (1962) and Montgomery (1974).

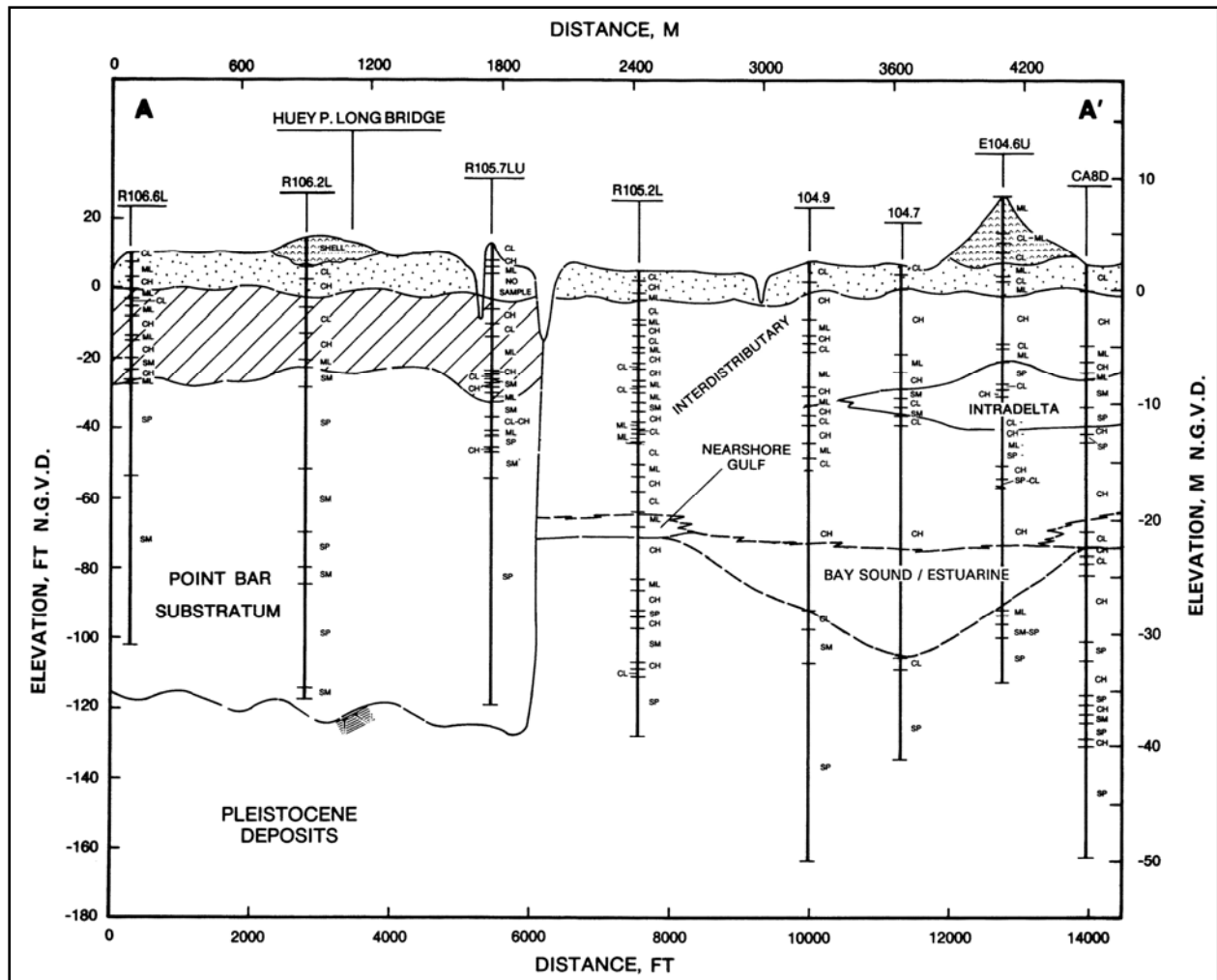


Figure 2-5a. Geologic cross section A-A' (see Figure 2-5l for symbol legend)

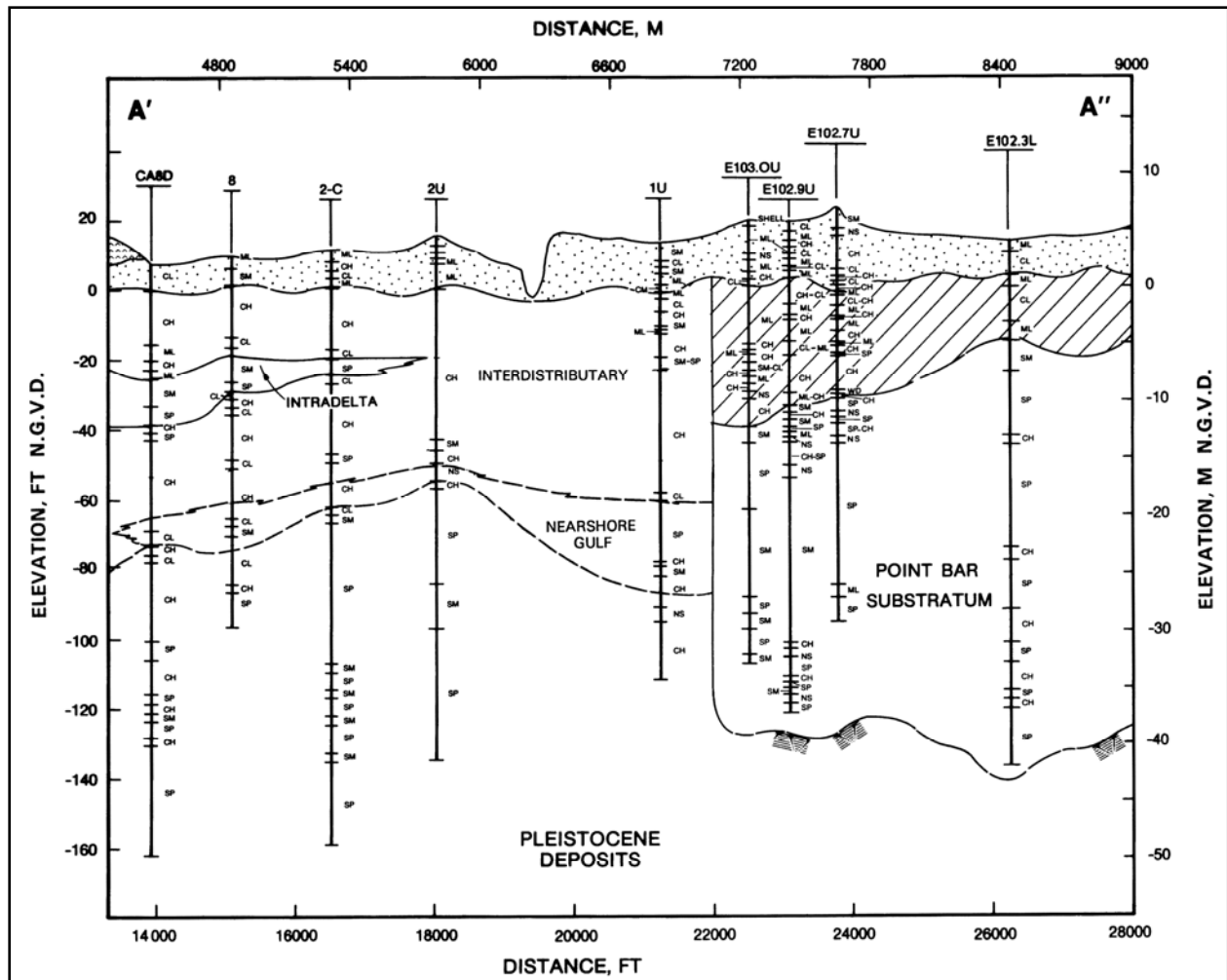


Figure 2-5b. Geologic cross section A'-A'' (see Figure 2-5l for symbol legend)

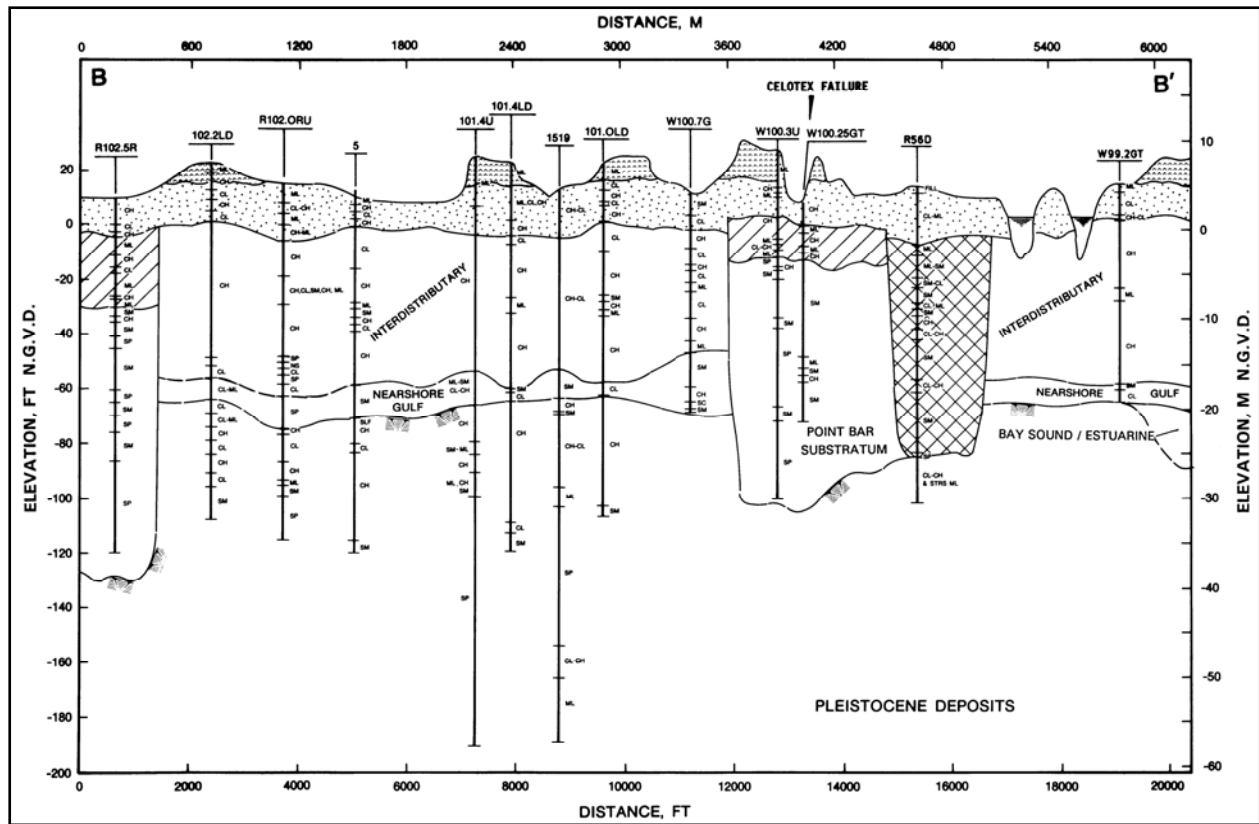


Figure 2-5c. Geologic cross section B-B' (see Figure 2-5l for symbol legend)

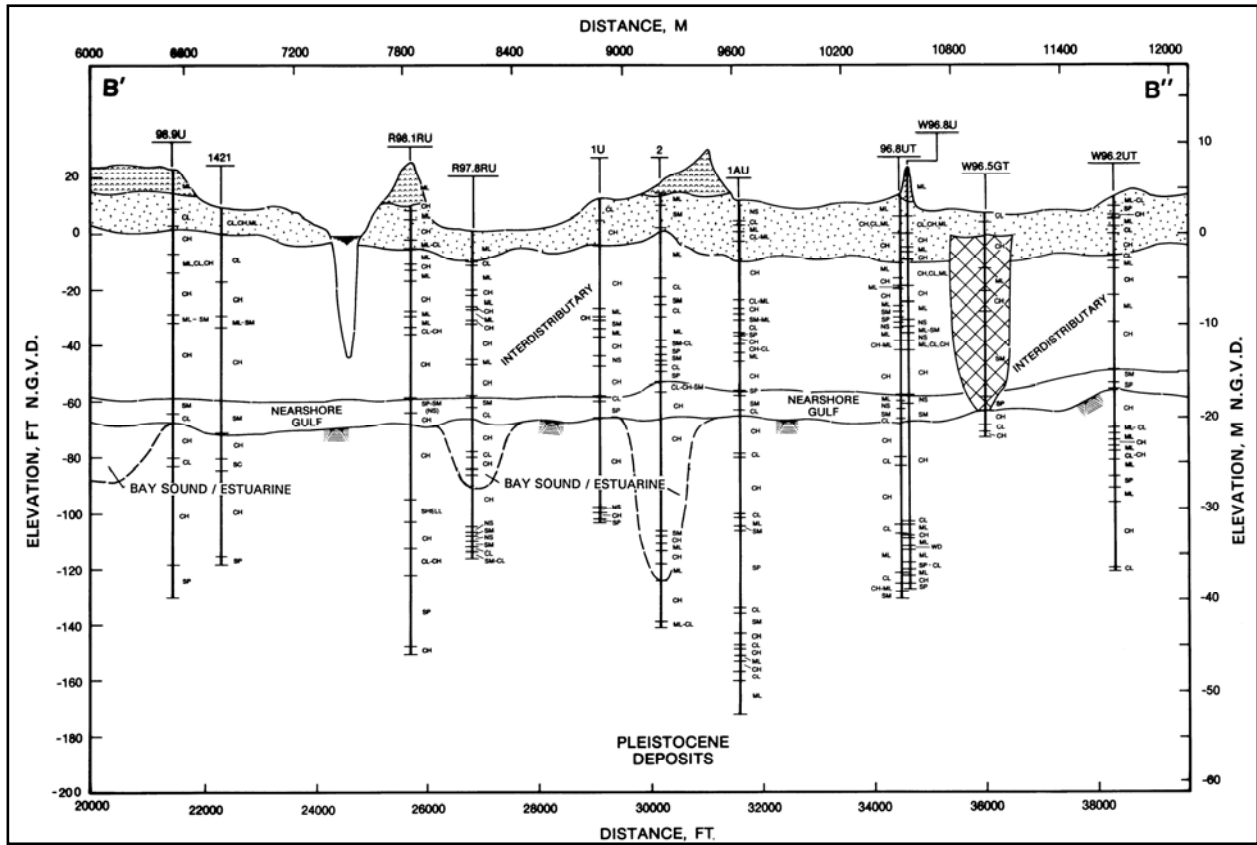


Figure 2-5d. Geologic cross section B'-B'' (see Figure 2-5f for symbol legend)

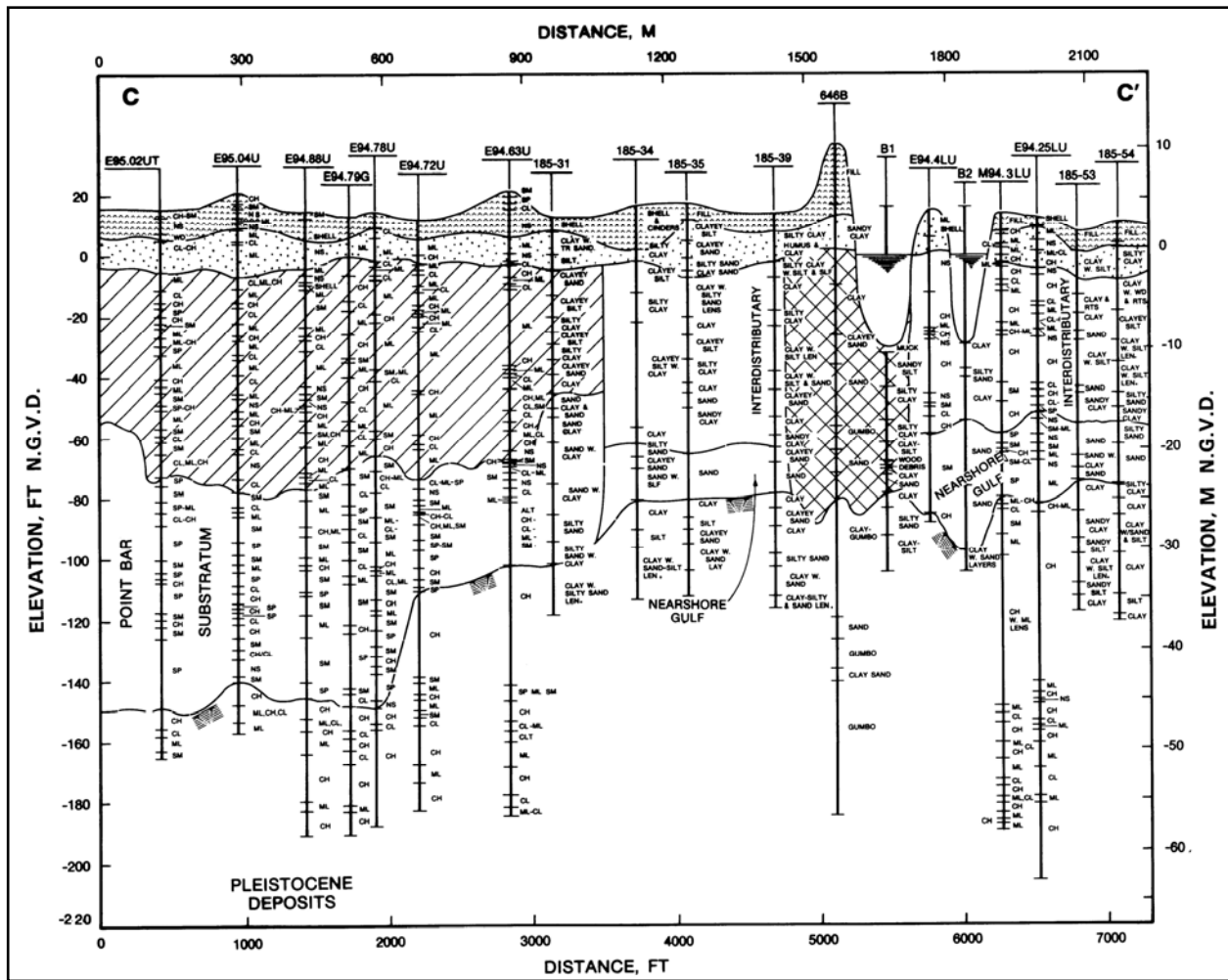


Figure 2-5e. Geologic cross section C-C' (see Figure 2-5f for symbol legend)

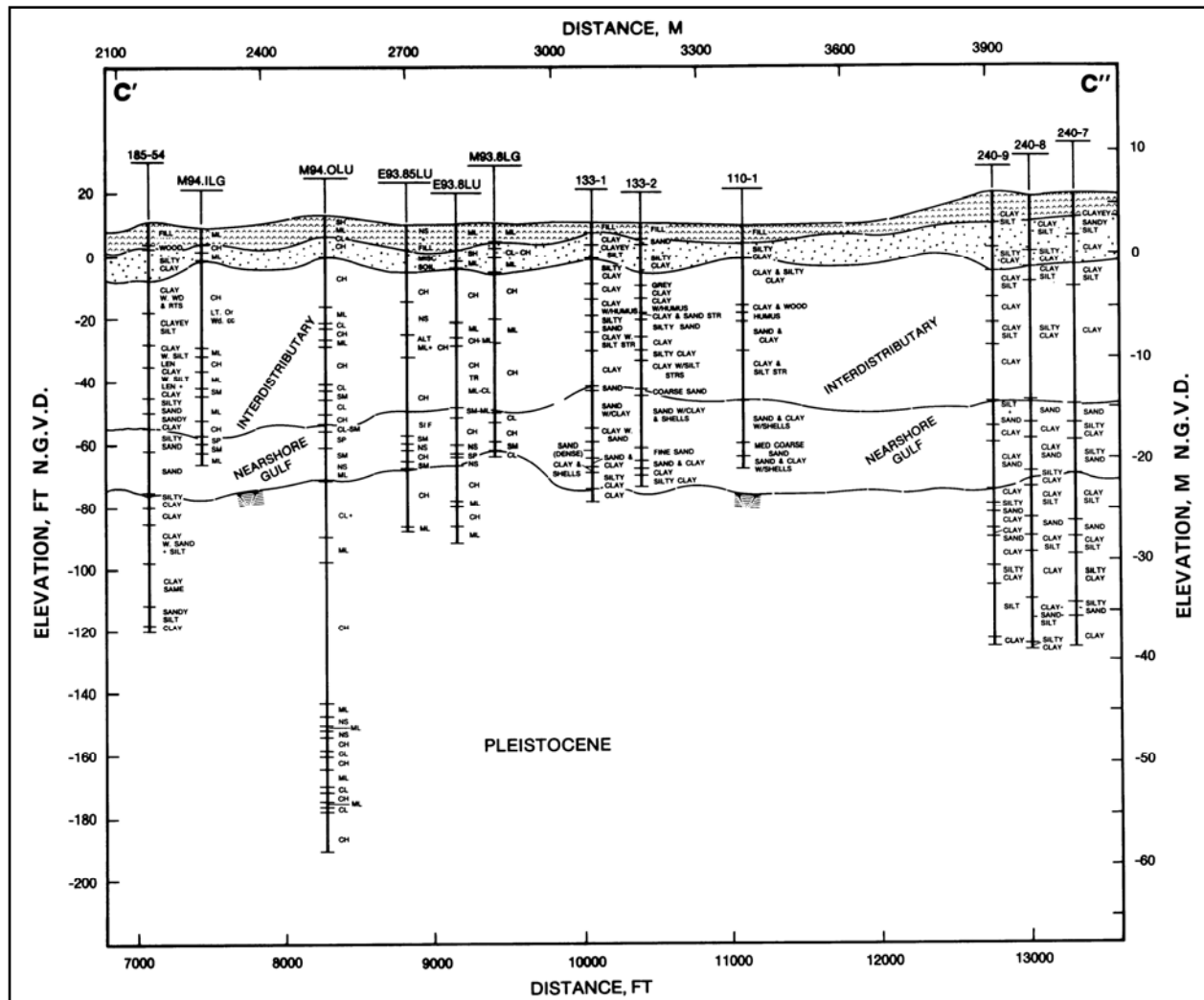


Figure 2-5f. Geologic cross section C'-C'' (see Figure 2-5i for symbol legend)

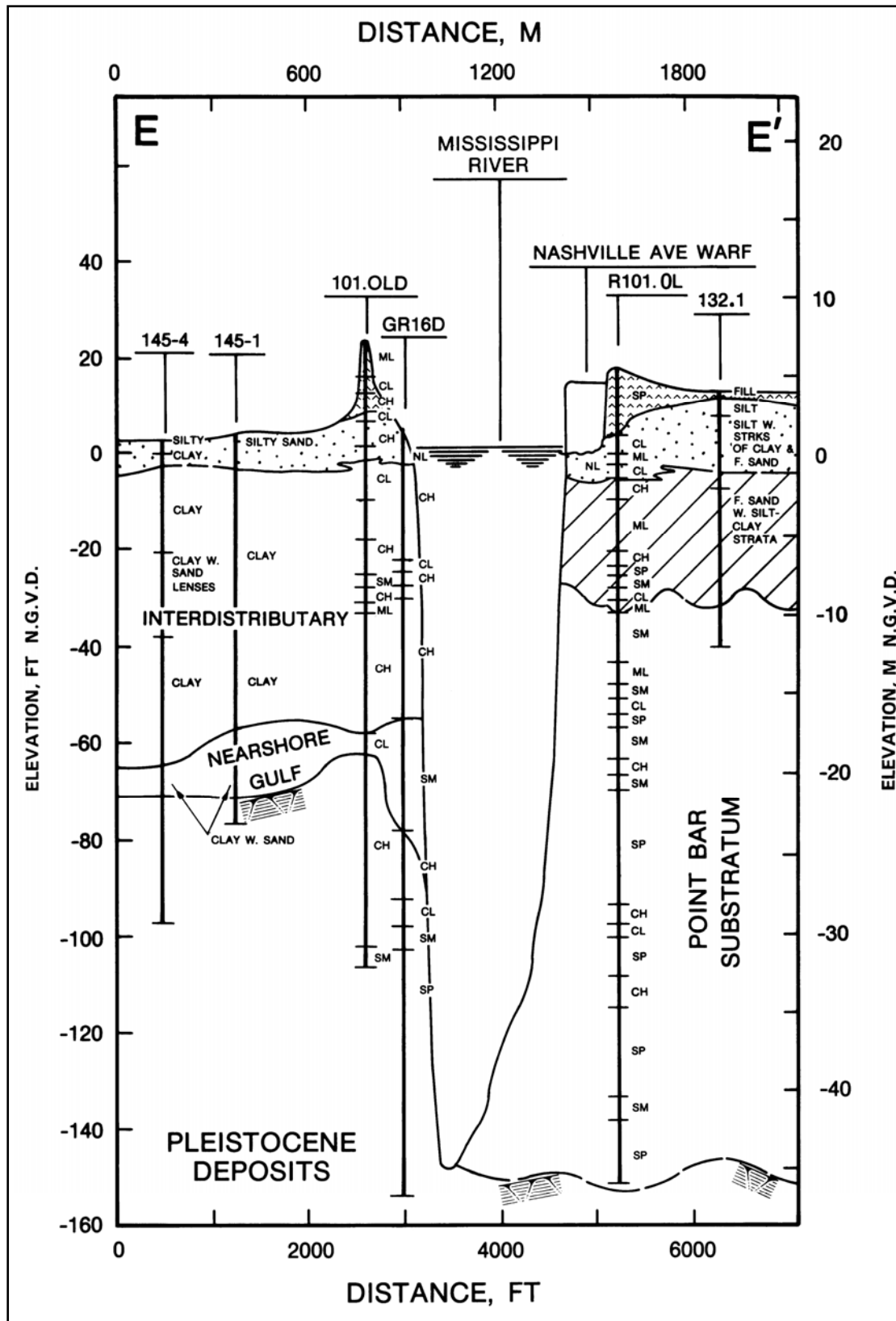


Figure 2-5h. Geologic cross section E-E' (see Figure 2-5l for symbol legend)

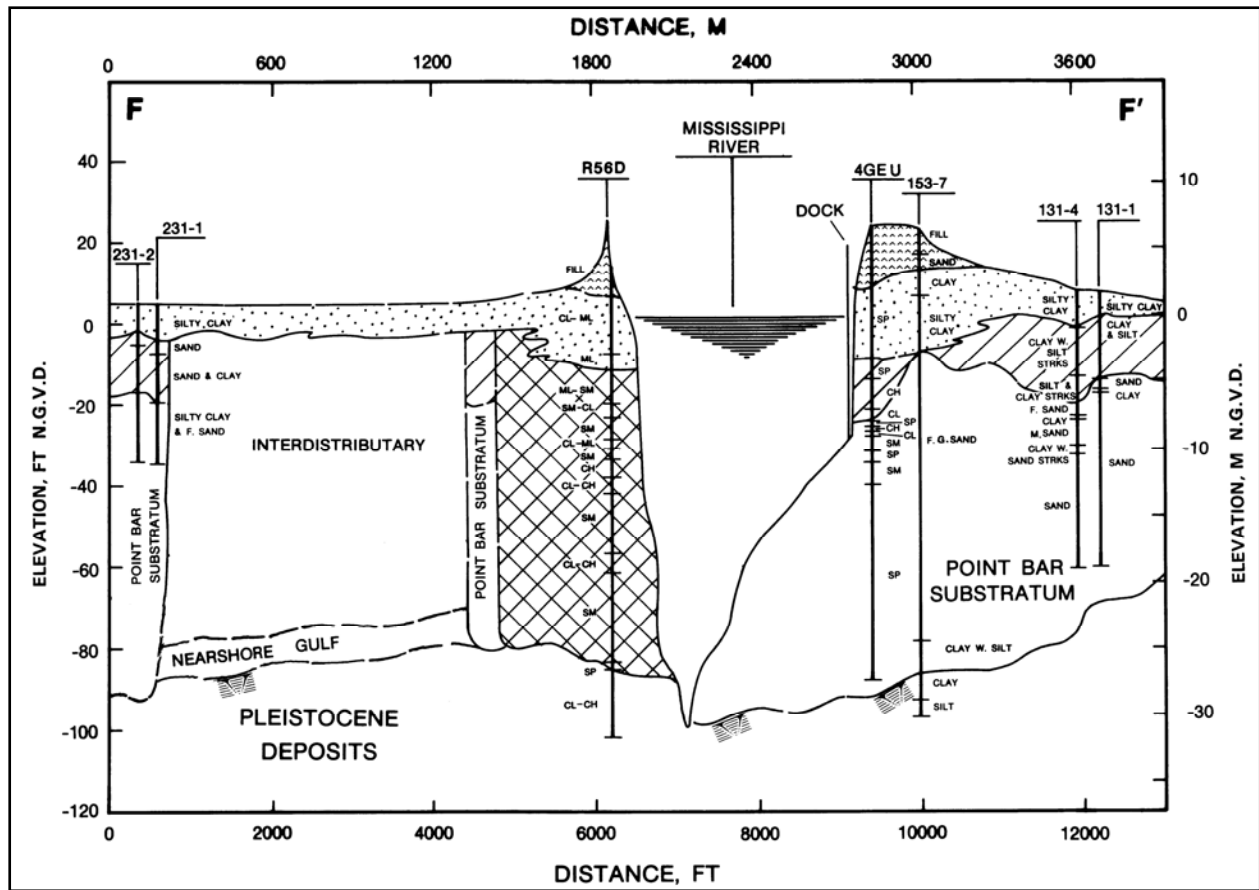


Figure 2-5i. Geologic cross section F-F' (see Figure 2-5l for symbol legend)

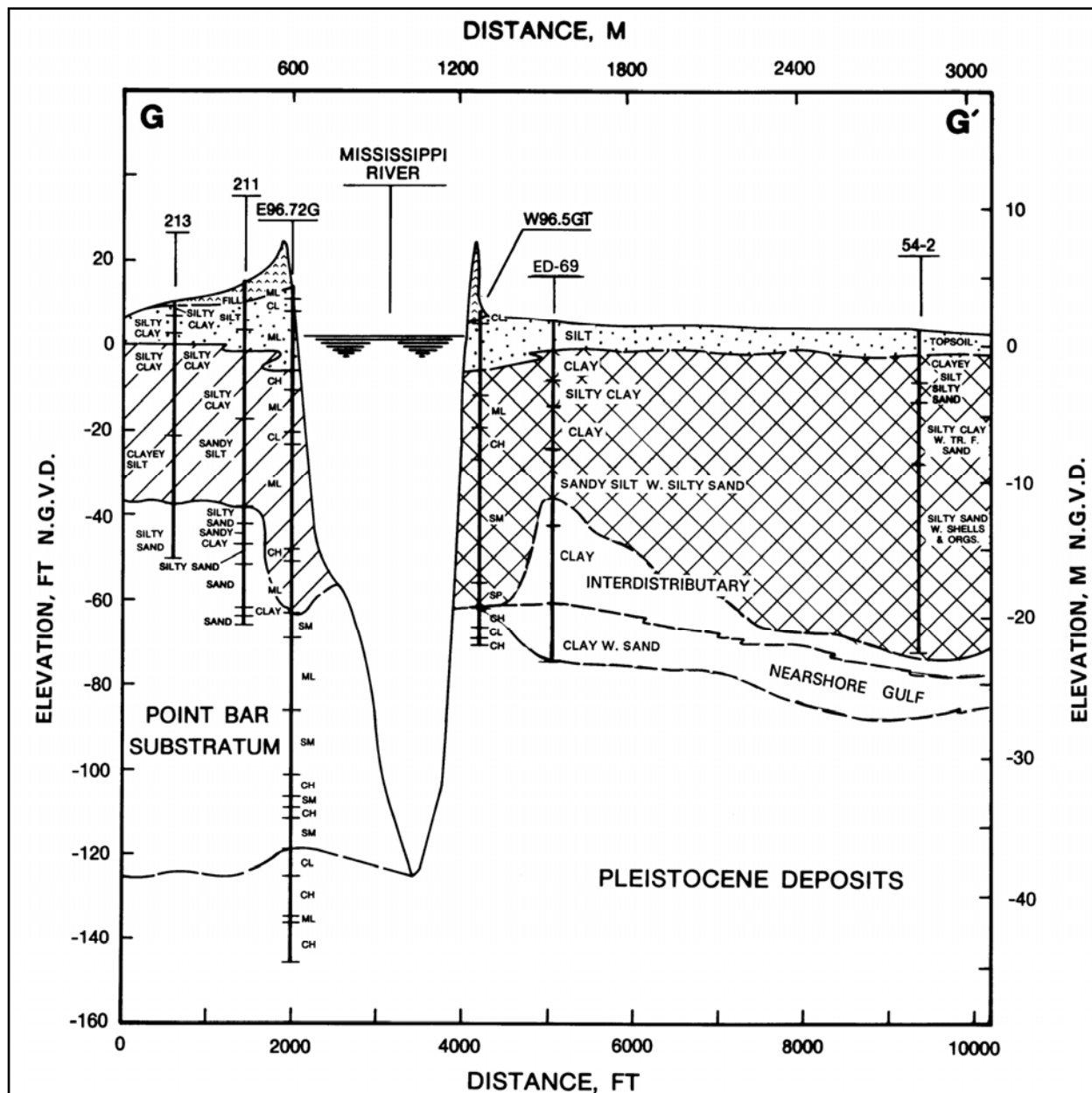


Figure 2-5j. Geologic cross section G-G' (see Figure 2-5i for symbol legend)

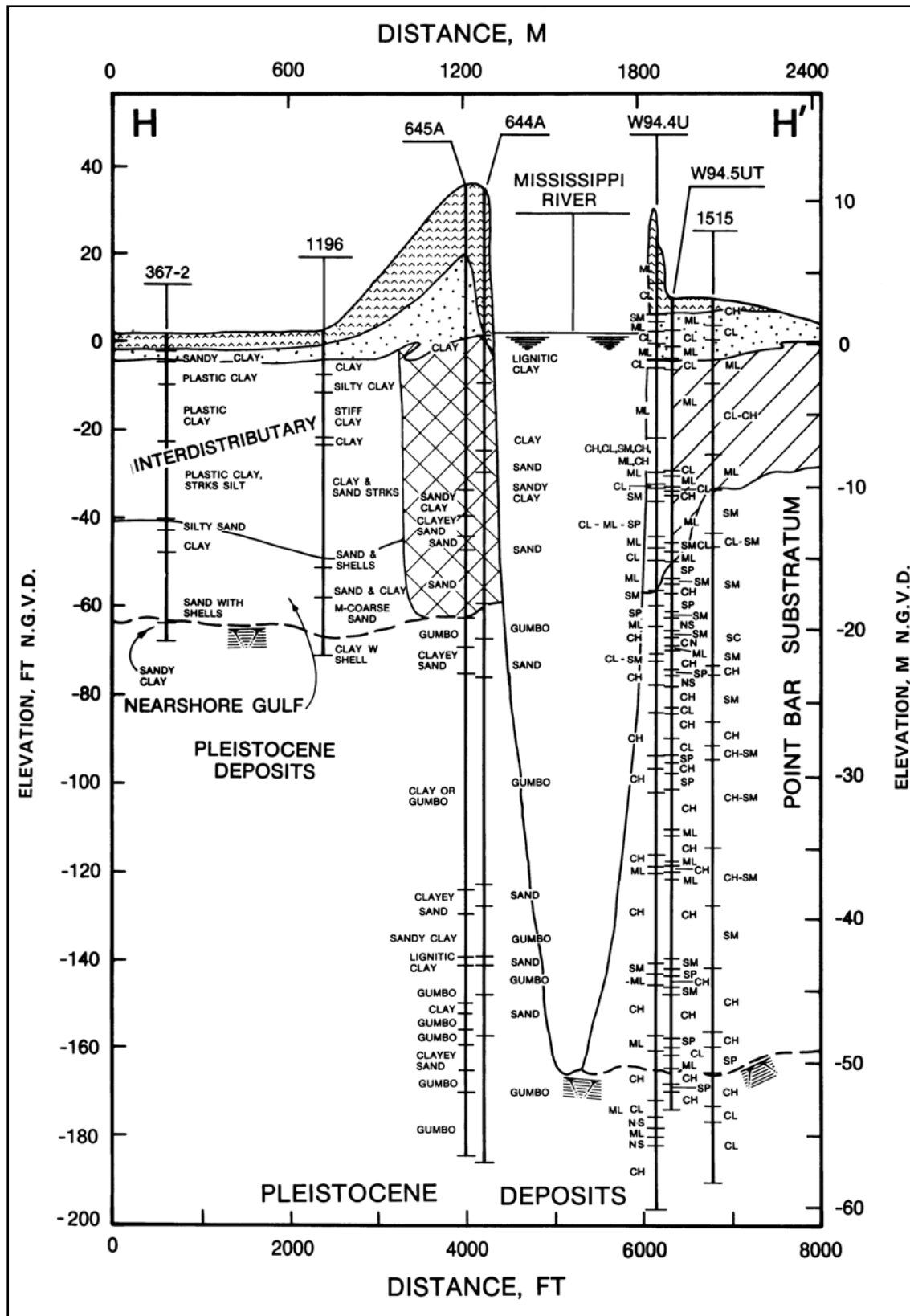
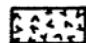

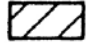
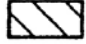



Figure 2-5k. Geologic cross section H-H' (see Figure 2-5l for symbol legend)

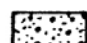

LEGEND

ENVIRONMENTS OF DEPOSITION

TOPSTRATUM DEPOSITS

-  LEVEE FILL
-  NATURAL LEVEE
-  POINTBAR
-  BACKSWAMP
-  ABANDONED COURSE

SUBSTRATUM DEPOSITS

-  UNDIFFERENTIATED
SAND AND GRAVEL
-  UPPER FINE-GRAINED
PLEISTOCENE SURFACE

SOIL TYPES (USCS)

- | | |
|-------------------------------------|-----------------------------------|
| CH — CLAY | SP — POORLY GRADED SAND |
| CL — SILTY CLAY,
SANDY CLAY | SW — WELL-GRADED SAND |
| ML — SILT, SANDY SILT,
CLAY SILT | GM — SILTY SAND-GRAVEL |
| SC — CLAYEY SAND | GW — WELL-GRADED
SAND-GRAVEL |
| SM — SILTY SAND | GP — POORLY GRADED
SAND-GRAVEL |

Figure 2-5l. Legend for the geologic sections of Figures 2-5a through 2-5k

Beneath the nearshore gulf sequence is the Pleistocene surface. The nearshore gulf sediments represent the deposits formed by the transgression of sea level onto the Pleistocene surface. These sediments were deposited under shallow-water conditions, before the advancement of the two major St. Bernard distributary systems into the study area. Establishment of the St. Bernard distributary systems into the study area produced the interdistributary sediments that were deposited into shallow-water, freshwater areas between the active distributary channels. Interdistributary sediments over time filled these shallow areas, and emergent vegetation in the form of fresh marsh began developing when interdistributary filling approached sea level. Closer to the active distributary systems, overbank deposition from the active distributary channels developed well drained natural levees and inland swamps.

A generalized contour map of the Pleistocene surface is presented in Figure 2-6 (Kolb, Smith, and Silva 1975). In general, the Pleistocene surface throughout the study area dips to the south and southwest at approximately 3 ft per mile (1 m per 1.6 km). Surface elevations on this surface are variable due to erosion by the preexisting Pleistocene drainage system and later Holocene scouring by past and present courses of the Mississippi River and its distributaries. Elevations of the Pleistocene surface range from -50 ft (-15 m) NGVD to greater than -150 ft (-46 m) NGVD in the bendways of the present Mississippi River channel.

Pleistocene deposits are characterized by a significant increase in stiffness and shear strength as compared to the overlying Holocene sediments. Pleistocene soils are fairly resistant to erosion from fluvial scouring. Where these soils occur in the riverbank, they represent a “hard point” which restrains the river’s migration and deepening. Pleistocene deposits in the bed and bank of the river have had a significant influence on the river’s ability to meander through the study area. There has been very little migration of the channel during the past 100 years as determined from comparison of old hydrographic surveys in Chapter 3 of this report.

Each of the different depositional environments present in the study area has distinct physical characteristics reflected by differences in soil types and associated engineering properties. Therefore, the geology of the study area will have a major influence on river scouring, lateral migration, and bank stability.

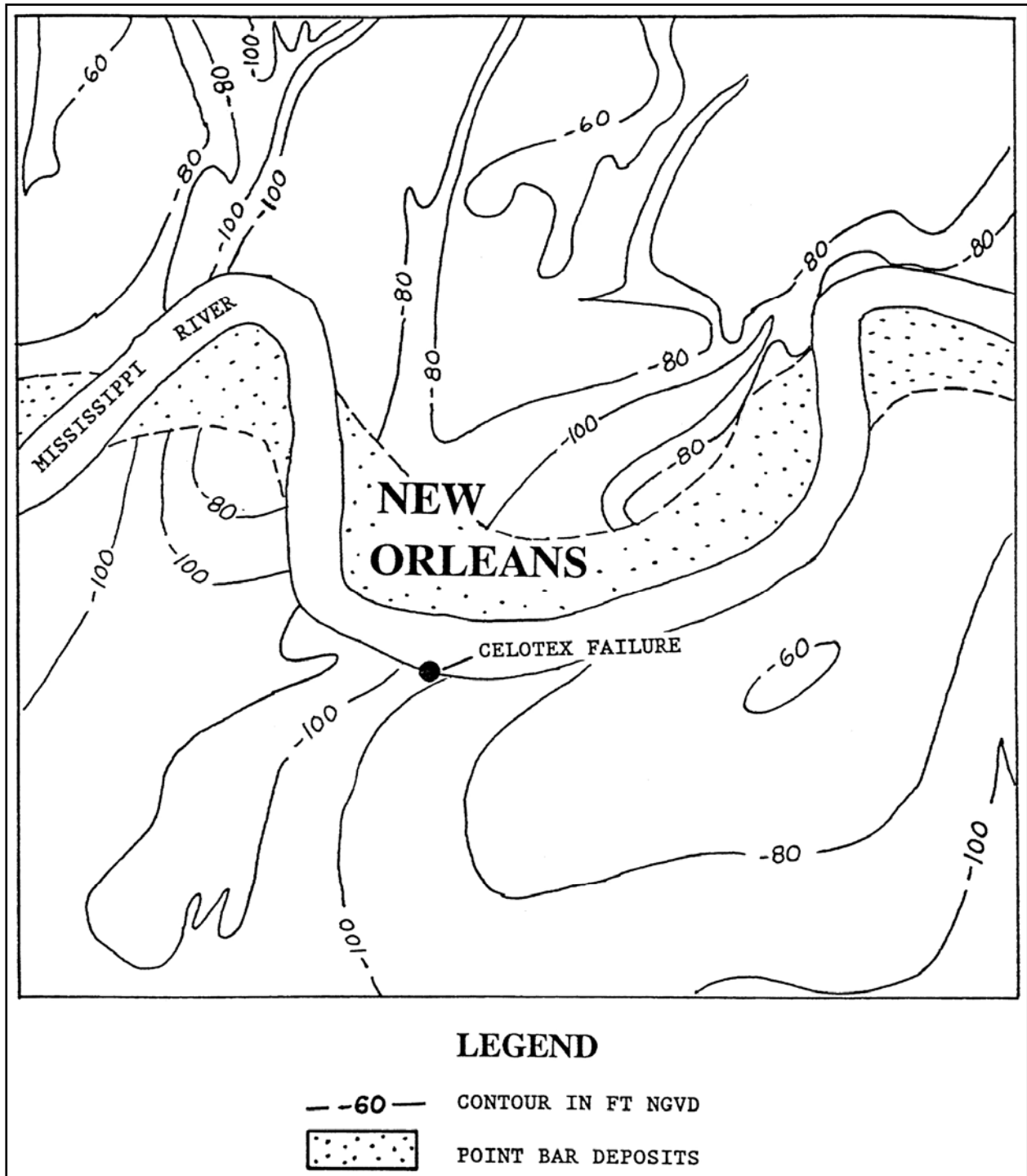


Figure 2-6. Generalized contour map of the Pleistocene surface (modified after Kolb, Smith, and Silva 1975)

Geology of Selected Revetment Reaches

Celotex failure site and Greenville Bend revetment

This riverbank reach extends from river mile 98.3 to 102.0 (158.2 to 164.1 km) on the right descending bank. The subsurface geology of the Celotex failure site is shown by cross sections B-B' (Figure 2-5c) and F-F' (Figure 2-5i). The locations of these sections are shown in Figure 2-4. Areal photography and boring data identify a point bar sequence (Figure 2-4 and 2-5c) associated with Bayou des Familles (Figure 2-5i). This distributary channel was a major course of the Mississippi River during the active St. Bernard delta complex.

The exact intersection and lateral limits of Bayou des Familles at the Mississippi River are not well defined from areal photography because this area has been extensively developed by industrial and residential construction. The position and lateral extent of the Bayou des Familles channel at the Mississippi River was interpreted from available historic charts, maps, and boring data.

Soil types within the point bar-abandoned distributary sequence are primarily coarse-grained, consisting mainly of silty sands (SM) and well sorted or poorly graded sands (SP). The available boring data indicate that the point bar-abandoned distributary sequence extends approximately 100 ft (30.5 m) below the ground surface before encountering the oxidized and erosion-resistant Pleistocene surface.

The geology immediately upstream and downstream from the Bayou des Familles point bar sequence consists of interdistributary deposits underlain by a generally coarser nearshore gulf sequence (CL, ML, SM, and SC). Soil types are variable within these two depositional environments. Interdistributary sediments consist primarily of clay (CL and CH) with disseminated organics.

Carrollton Bend and Carrollton Bend revetment

This bank reach extends from about river mile 102.0 to 105.0 (164 to 169 km) and encompasses the Carrollton Bend revetment which is on the left descending bank. The subsurface geology of the Carrollton Bend reach is shown on cross sections A-A' (Figure 2-5a), A'-A'' (Figure 2-5b), and D-D' (Figure 2-5g) (see Figure 2-4 for section locations). The geology consists of natural levee, interdistributary, intradelta, and nearshore gulf sediments. Soil types are variable within the individual environments as shown by the cross sections. The Pleistocene surface ranges between elevations -50 to -75 ft (-15.2 to -22.9 m) NGVD. Where the Mississippi River has entrenched itself into the Pleistocene, the river has formed thick point bar sediments in excess of 120 ft (36.6 m) deep.

Gretna Bend and Gouldsboro revetments

This revetted bank lies between river miles 95.5 and 98.3 (153.6 and 158.2 km). The Gretna Bend and Gouldsboro revetments are contiguous from upstream to downstream, respectively, along the right descending bank. The subsurface geology of the Gretna Bend and Gouldsboro Revetment reach is shown by cross sections B'-B'' (Figure 2-5d) and G-G' (Figure 2-5j) (see Figure 2-4 for section locations). The geologic sequence is similar to the two upstream revetment reaches already described. The Pleistocene surface ranges between elevations -55 to -70 ft (-16.8 to -21.3 m) NGVD and is overlain by nearshore gulf, interdistributary, and natural levee sediments.

As shown by the surface geology map in Figure 2-4, there is an abandoned distributary channel which intersects the Mississippi River and extends southeast at approximately river mile 96.5 (155.3 km). The existence of this former distributary channel is indicated by the presence of well-developed natural levees several miles southeast of the Mississippi River. The intersection of this distributary channel with the present Mississippi River is indicated by boring W96.5GT. At this location, a thick sand sequence was encountered in the subsurface.

Algiers Point revetment

This revetment reach lies between river mile 93.7 and 95.5 (150.8 and 153.7 km) on the right descending bank. The subsurface geology of Algiers Point is shown by cross sections C-C' (Figure 2-5e), C'-C'' (Figure 2-5f), and H-H' (Figure 2-5k). The permanent scour pool along Algiers Point is one of the deepest of the Mississippi River entrenchment below Baton Rouge. River thalweg elevations have historically been between -175 and -200 ft (-53.3 and -61 m) NGVD. At Algiers, along the point bar side of the river, fluvial scouring has created a 170-ft (51.8-m) thick point bar sequence (see cross section H-H' of Figure 2-5k). Soil types are variable within this thick sequence, but are primarily coarse-grained.

Along the concave or left bank of the river, the subsurface geology at Algiers Point consists of interdistributary sediments, separated by point bar deposits and an abandoned interdistributary channel (see Figure 2-4 and cross section C-C' of Figure 2-5e). These sediments are underlain by the Pleistocene surface. The lateral and vertical limits of the different depositional environments are shown by the surface geology map and the respective geologic cross sections. Soil types are highly variable as defined by the sections.

The abandoned distributary channel shown in Figure 2-4 is a former St. Bernard distributary which branches from the main Bayou Sauvage-Metarie Bayou course northwest of Algiers Point. The intersection of this distributary channel at the Mississippi River is defined by coarse-grained sediments in the subsurface in borings located within the former distributary channel (see sections C-C' of Figure 2-5e and H-H' of Figure 2-5k).

References

- Autin, W. J., Burns, S. F., Miller, B. J., Saucier, R. T., and Snead, J. I. (1991). "Chapter 18: Quaternary geology of the Lower Mississippi Valley." Vol K-2, *The Geology of North America*. The Geological Society of North America, Boulder, CO, 547-581.
- Bates, R. L., and Jackson, J. A. (1987). *Glossary of Geology*, 3rd ed., American Geological Institute, Alexandria, VA.
- Clough, G. W. (1966). "Ground water level in silty and sandy Mississippi River upper banks," Mississippi River Commission, Corps of Engineers, Vicksburg, MS. (Mr. F. J. Weaver, Lower Mississippi Valley Division, was a principal assistant in this study).
- Cullinan, T. A. (1969). "Contributions to the geology of Washington and St. Tammany Parishes, Louisiana," U.S. Army Engineer District, New Orleans, LA.
- Dunbar, J. B., Blaes, M., Dueitt, S., and Stroud, K. (1994). "Geological investigation of the Mississippi River deltaic plain, Report 2 of a Series," Technical Report GL-84-15, U.S. Army Engineer Waterways Experiment Station, Vicksburg, MS.
- Dunbar, J. B., Blaes, M., Dueitt, S., and May, J. (1995). "Geological investigation of the Mississippi River deltaic plain, Report 3 of a Series," Technical Report GL-84-15, U.S. Army Engineer Waterways Experiment Station, Vicksburg, MS.
- Dunbar, J. B., and Torrey, V. H. (1991). "Geologic, geomorphological and geotechnical aspects of the Marchand Levee failure, Marchand, Louisiana," Miscellaneous Paper GL-91-17, U.S. Army Engineer Waterways Experiment Station, Vicksburg, MS.
- Eustis Engineering Company. (1984). "Geotechnical investigation: Soil stratification and foundation conditions for residential development," Report for City of New Orleans, Sewerage and Water Board of New Orleans, New Orleans, LA.
- Fisk, H. N. (1944). "Geological investigation of the alluvial valley of the Lower Mississippi River," U.S. Army Corps Engineers, Mississippi River Commission, Vicksburg, MS.
- Frazier, D. E. (1967). "Recent deltaic deposits of the Mississippi River: Their development and chronology." Gulf Coast Association of Geological Societies. Transactions 17th annual meeting. San Antonio, TX.
- Halbouty, M. T. (1967). *Salt Domes, Gulf Region, United States and Mexico*. Gulf Publishing Company, Houston, TX.
- Hvorslev, M. J. (1956). "A review of the soils studies," Potamology Investigations Report No. 12-5, U.S. Army Engineer Waterways Experiment Station, Vicksburg, MS.

Kemp, E. B. (1967). "Geologic setting of New Orleans." Guidebook New Orleans, LA and vicinity field trip. The Geological Society of America and Associated Societies, Annual meetings.

Kolb, C. R. (1962). "Distribution of soils bordering the Mississippi River from Donaldsonville to Head of Passes," Technical Report No. 3-601, U.S. Army Engineer Waterways Experiment Station, Vicksburg, MS.

Kolb, C. R., and Saucier, R. T. (1982). "Engineering geology of New Orleans," Geological Society of America, Reviews in Engineering Geology 5, 75-93.

Kolb, C. R., Smith, F. L., and Silva, R. C. (1975). "Pleistocene sediments of the New Orleans-Lake Pontchartrain area," Technical Report S-75-6, U.S. Army Engineer Waterways Experiment Station, Vicksburg, MS.

Kolb, C. R., Steinriede, W. B., Krinitzsky, E. L., Saucier, R. T., Mabrey, P. R., Smith, F. L., and Fleetwood, A. R. (1968). "Geological investigation of the Yazoo Basin, Lower Mississippi Valley," Technical Report 3-480, U.S. Army Engineer Waterways Experiment Station, Vicksburg, MS.

Kolb, C. R., and VanLopik, J. R. (1958a). "Geology of the Mississippi River Deltaic Plain," Technical Report No. 3-483, Vol 1 and 2, U.S. Army Engineer Waterways Experiment Station, Vicksburg, MS.

_____. (1958b). "Geological investigation of the Mississippi River-Gulf Outlet Channel," Miscellaneous Paper No. 3-259, U.S. Army Engineer Waterways Experiment Station, Vicksburg, MS.

Krinitzsky, E. L. (1965). "Geological influences on bank erosion along meanders of the Lower Mississippi River," Potamology Investigations, Report 12-15, U.S. Army Engineer Waterways Experiment Station, Vicksburg, MS.

Krinitzsky, E. L., and Smith, F. L. (1969). "Geology of backswamp deposits in the Atchafalaya Basin, Louisiana," Technical Report S-69-8, U.S. Army Engineer Waterways Experiment Station, Vicksburg, MS.

Krinitzsky, E. L., Turnbull, W. J., and Weaver, F. J. (1966). "Bank erosion in cohesive soils of the Lower Mississippi Valley," Vol 92, No. SM1, Journal of Soil Mechanics and Foundations Division, Proceedings American Society of Civil Engineers, 121-136.

May, J. R., Britsch, L. D., Dunbar, J. B., Rodriguez, J. P., and Wlosinski, L. B. (1984). "Geological investigation of the Mississippi River Deltaic Plain," Technical Report GL-84-15, U.S. Army Engineer Waterways Experiment Station, Vicksburg, MS.

Miller, W. (1983). "Stratigraphy of newly exposed quaternary sediments, Eastern Orleans Parish, Louisiana," Tulane Studies in Geology and Paleontology 17(3, 4), 85-104.

Montgomery, R. L. (1974). "Correlation of engineering properties of cohesive soils bordering the Mississippi River from Donaldsonville to Head of Passes, LA," Miscellaneous Paper S-74-20, U.S. Army Engineer Waterways Experiment Station, Vicksburg, MS.

New Orleans Geological Society. (1962). "Salt domes of South Louisiana," Vol 1 and 2, J. C. Stipe and J. P. Spillers, ed., New Orleans, LA.

_____. (1983). "Salt domes of South Louisiana," Vol 3, S. J. Waguespack, ed., New Orleans, LA.

Padfield, C. J. (1978). "The stability of riverbanks and flood embankments," Final Technical Report, U.S. Army European Research Office, London, England.

Saucier, R. T. (1963). "Recent geomorphic history of the Pontchartrain Basin, Louisiana," Technical Report 16, Part A, United States Gulf Coastal Studies, Coastal Studies Institute, Contribution No. 63-2, Louisiana State University, Baton Rouge, LA.

_____. (1964). "Geological investigation of the St. Francis Basin," Technical Report 3-659, U.S. Army Engineer Waterways Experiment Station, Vicksburg, MS.

_____. (1967). "Geological investigation of the Boeuf - Tensas Basin Lower Mississippi Valley," Technical Report 3-757, U.S. Army Engineer Waterways Experiment Station, Vicksburg, MS.

_____. (1969). "Geological investigation of the Mississippi River area, Artonish to Donaldsonville, Louisiana," Technical Report S-69-4, U.S. Army Engineer Waterways Experiment Station, Vicksburg, MS.

Saucier, R. T. (1974). "Quaternary geology of the Lower Mississippi Valley," Arkansas Archeological Survey, Research Series No. 6, Fayetteville, AR.

_____. (1977). "The Northern Gulf Coast during the Farmdalian Substage: A search for evidence," Technical Report S-69-4, U.S. Army Engineer Waterways Experiment Station, Vicksburg, MS.

Saucier, R. T., and Kolb, C. R. (1967). "Alluvial geology of the Yazoo Basin, Lower Mississippi Valley," 1:250,000 map, U.S. Army Engineer Waterways Experiment Station, Vicksburg, MS.

Self, R. P., and Davis, D. W. (1983). "Geology of the New Orleans area," The Compass of Sigma Gamma Epsilon 60(2), 29-38.

Smith, F. L., and Russ, D. P. (1974). "Geological investigation of the Lower Red River-Atchafalaya Basin area," Technical Report S-74-5, U.S. Army Engineer Waterways Experiment Station, Vicksburg, MS.

Smith, L. M., Dunbar, J. B., and Britsch, L. D. (1986). "Geomorphological investigation of the Atchafalaya Basin, Area West, Atchafalaya Delta, and Terrebonne Marsh, Vol 1 and 2," Technical Report GL-86-3, U.S. Army Engineer Waterways Experiment Station, Vicksburg, MS.

Snead, J. I., and McCulloh, R. P. (1984). "Geologic map of Louisiana, scale 1:500,000, Baton Rouge, LA."

Torrey, V. H., III. (1988). "Retrogressive failures in sand deposits of the Mississippi River, Report 2, Empirical evidence in support of the hypothesized failure mechanism and development of the levee safety flow slide monitoring system," Technical Report GL-88-9, U.S. Army Engineer Waterways Experiment Station, Vicksburg, MS.

Torrey, V. H., III, Dunbar, J. B., and Peterson, R. W. (1988). "Retrogressive failures in sand deposits of the Mississippi River, Report 1, Field investigations, laboratory studies and analysis of the hypothesized failure mechanism," Technical Report GL-88-9, U.S. Army Engineer Waterways Experiment Station, Vicksburg, MS.

Torrey, V. H., III, and Weaver, F. J. (1984). "Flow failures in Mississippi riverbanks." Proceedings IV International Symposium on Landslides. Vol 2, Toronto, Canada, 355-360.

Turnbull, W. J., Krinitzky, E. L., and Weaver, F. J. (1966). "Bank erosion in soils of the Lower Mississippi Valley." Proceedings of the American Society of Civil Engineers, Journal of the Soil Mechanics and Foundation Division, 92(SM1), 121-136.

U.S. Army Corps of Engineers. (1909). "Survey of the Mississippi River, Chart Nos. 69 and 70," Mississippi River Commission, Vicksburg, MS.

U.S. Army Corps of Engineers. (1921). "Survey of the Mississippi River, Chart Nos. 69 and 70," Mississippi River Commission, Vicksburg, MS.

_____. (1950). "Piezometer observations at Reid Bedford Bend and indicated seepage forces," Potamology Investigations Report No. 5-4, Vicksburg, MS.

U.S. Army Corps of Engineers. (1975). "Master index, upper and lower Mississippi River surveys for period 1879-80 to 1928 and some historic maps prior to this period," Vol 2, Mississippi River Commission, Vicksburg, MS.

U.S. Army Engineer District, New Orleans. (1938). "Maps of the Mississippi River, Angola, La., to the Head of Passes," New Orleans, LA.

_____. (1952). "Mississippi River hydrographic survey, 1949-1952, Angola, La., to Head of Passes and South and Southwest Passes and Pass A Loutre," New Orleans, LA.

_____. (1965). "Mississippi River hydrographic survey, 1961-1963, Black Hawk, La., to Head of Passes and South and Southwest Passes and Pass A Loutre," New Orleans, LA.

_____. (1976). "Mississippi River hydrographic survey, 1973-1975, Black Hawk, La., to Head of Passes and South and Southwest Passes and Pass A Loutre," New Orleans, LA.

_____. (1984). "Mississippi River levees, Item M-181.1 to 180.2-L, Marchand Levee setback, final report," New Orleans, LA (internal report, unpublished).

_____. (1986). "Mississippi River levees, Item M-100.4-R, Celotex Levee and Batture restoration, final report," New Orleans, LA (internal report, unpublished).

_____. (1988). "Mississippi River hydrographic survey, 1983-1985, Black Hawk, La., to Head of Passes and South and Southwest Passes and Pass A Loutre," New Orleans, LA (internal report, unpublished).

Wallace, W. E. (1966). "Fault and salt map of South Louisiana," Gulf Coast Association of Geological Societies, Vol 16.

Appendix A

Environments of Deposition

General

This appendix provides a general description of the environments of deposition which produced the surface and subsurface geology encountered in the study reach. The distribution of surface deposits is shown by the geologic map in Figure 2-4 of the main text. Subsurface limits of the various depositional environments are shown by the cross sections in Figures 2-5a through 2-5k. A geologic legend is presented in Figure 2-5l that identifies symbols used in the geologic cross sections.

In addition to the general descriptions of the individual environments of deposition, this appendix also provides a very generalized indication of the engineering properties for each environment. Correlation of engineering properties and soil types to the different environments of deposition is based primarily on work by Kolb (1962)¹ and is summarized in Table A1. Additionally, Montgomery (1974) expanded upon Kolb's original work for several of the major depositional environments which form the bulk of the land area in the deltaic plain. Montgomery's work is summarized in Table A2 and provides further engineering data on the following selected environments of deposition: natural levee, point bar, backswamp, prodelta, intradelta, and inter-distributary deposits.

In terms of their engineering significance, the biggest contrast occurs between the Pleistocene and Holocene age sediments as shown by the engineering data in Table A1. Pleistocene sediments have higher cohesive strengths, lower water contents, and are much denser than Holocene soils. Holocene deposits in contrast are less consolidated, have higher water contents, and are more variable in density.

¹ References are listed following the main text.

	DEPOSITIONAL TYPES	LITHOLOGY PER CENT	PREDOMINANT SOIL TEXTURES ⁽¹⁾	NATURAL WATER CONTENT PER CENT DRY WEIGHT	UNIT WEIGHT LB./CU FT	SHEAR STRENGTH ⁽²⁾		REMARKS	
						COHESIVE STRENGTH LB./SQ FT	ANGLE OF INTERNAL FRICTION IN DEGREES		
RECENT ENVIRONMENTS	NATURAL LEVEES		CH, CL, ML & SM			VALUES RANGE TO APPROXIMATELY 2600 CHARACTERISTIC RANGE 800-1200	ML 20-35	Disposed in narrow bands flanking the Mississippi River and its abandoned courses and distributaries. Consist of intertonguing layers of fat and lean clays and sands silt along the Mississippi River and its abandoned courses. Substratum levee materials along abandoned distributaries usually much finer. Thickness varies from 20 to 60 feet. Thin flings in V at sea level. Thickness along distributaries usually on the order of 5 ft or less.	
	POINT BAR SANDY		ML, SM & SP		INSUFFICIENT DATA	INSUFFICIENT DATA	SP 25-35	Usually found flanking the more prominent bands of the present and abandoned courses to a depth of more than 100 ft. Consist of a bedded sequence 2 1/2 to 7 1/2 ft thick of silty sand, sandy silt, and sand increasing with depth. The substratum consists of essentially clean sand.	
	POINT BAR SILTY		CL & ML		INSUFFICIENT DATA	INSUFFICIENT DATA	---	ML 20-30	An unusually fine-grained point bar deposit consisting almost entirely of silt. Identified just upstream from Deshaensville and at Laplace.
	PRODELTA CLAYS		CH				---	0	A homogeneous fat clay in offshore areas and at depth. Contains increasing amounts of lean clay disposed in thin layers near the mouth of active distributaries. Thickness normally varies with depth to Pleistocene. Thicknesses range between 50 and 600 ft.
	INTRADELTA		CH, ML & SM		INSUFFICIENT DATA	INSUFFICIENT DATA	---	---	Relatively coarse sediments bottoming bays and sounds. Thickness ranges from 3 to 20 ft and averages 15 ft. Because of the ramming of bottom sediments by improving marine organisms shells have a mottled appearance due to the inclusion of lumps or pockets of coarse material in a fine matrix or fine material in a coarse matrix.
	INTERDISTRIBUTARY		CH				---	0	Forms clay wedges between major distributaries. Clay may be interrupted by silty or sandy materials associated with normal small distributaries. Minor amounts of silt and fine sands typically occur in very thin but distinct layers between clay strata giving deposit a "stratified" appearance. Thickness similar to intradelta above.
	ABANDONED DISTRIBUTARY		CH & CL	INSUFFICIENT DATA	INSUFFICIENT DATA	INSUFFICIENT DATA	---	---	Forming belts of clayey sediments from a few feet to more than 1,000 ft in width and from less than 10 to more than 50 ft in depth. A wedge of coarser material is normally found at the upstream end, the wedge of material may range from fine sand for the larger distributaries to silty clays for the smaller.
	ABANDONED COURSE		CH & SP	INSUFFICIENT DATA	INSUFFICIENT DATA	INSUFFICIENT DATA	---	---	Forming belts of fairly coarse sediment in abandoned Mississippi River courses. Average width 7,500 ft. Depth may be 75 to 150 ft. Lower portion of course filled with sandy material which thins in an upstream direction. Upper portion filled with silt and clay.
	SWAMP		CH			INSUFFICIENT DATA	---	---	Tree-covered organic deposits flanking the lower borders of the marsh and subject to fresh-water inundation, also mangrove swathed areas found landward of the barrier beaches and fringing the mainland. Deposits average 3 to 10 ft thick.
	MARSH		PT	VALUES RANGE TO APPROXIMATELY 800	INSUFFICIENT DATA	VERY LOW	---	---	Forms 90 per cent of the land surface in the deltaic plain. Ranges from wetland organic coarses to fine to firm organic silts and clays. Maximum thickness 100 ft or more normally associated with areas of greater subsidence. Average thickness 10 ft.
	SAND BEACH		SP	SATURATED	INSUFFICIENT DATA	0	---	30-35	Border the open gulf except in areas of active deltaic advance. May be a mile or more in width and more than 10 miles in length. Beach sand may pile as high as 20 ft above gulf level and extend to depths of 10 ft below gulf level. Beach sand beaches reach a thickness of 15 ft in some offshore areas.
	BAY-SOUND		ML & SM				---	15-30	Relatively coarse portion of subsequent delta. Intrinsically intertongued deposits. Disposed in broad wedges about abandoned courses and major distributaries. Thickness of intertongues associated with present Mississippi on order of 200 ft. Thickness of intradelta associated with abandoned courses much less, averaging between 20 to 100 ft.
	NEARSHORE GULF		SP	SATURATED	INSUFFICIENT DATA	0	---	25-35	Found at the borders of the open areas seaward of the sand or barrier beaches. Thickness appears to increase with distance from shore—maximum thickness believed to be on order of 5 ft. Distinctive blanket of this material occurs directly above Pleistocene.
	ESTUARINE		SP	SATURATED	INSUFFICIENT DATA	0	---	30-40	Sandy facies correlative with nearshore gulf deposits but filling minor valleys entrenched into underlying Pleistocene surface.
BACKSWAMP		CH & CL			VALUES RANGE TO APPROXIMATELY 1745 CHARACTERISTIC RANGE 450-1450	---	0	Thick clay overlying substratum sands upstream from Collage Point. Occasional lenses of shell are found indicating intertonguing fluvial-marine deposits.	
SUBSTRATUM		SP	SATURATED	INSUFFICIENT DATA	0	---	30-40	Massive sand and gravel deposits filling entrenched valley and grading laterally into nearshore gulf deposits. Material becomes coarser with depth. Maximum thickness on the order of 500 ft in deepest portion of entrenched valley.	
PRE-RECENT	PLEISTOCENE		CH & CL			VALUES RANGE TO APPROXIMATELY 3500 CHARACTERISTIC RANGE 900-1700	---	0	Ancient former deltaic plain of Mississippi River. Consists of environments of deposition and associated lithologies similar to those found in recent deltaic plain. Depth to this surface, eroded surface increases in a southerly and westerly direction in southeastern Louisiana.

Table A1. Engineering Properties of Depositional Environments from the Mississippi River Deltaic Plain (from Kolb 1962)

Deposit	Grain Size and Organic Content	Natural Water Content %	Liquid Limit %	Plasticity Index %	Liquidity Index	Dry Density pcf	Specific Gravity	Void Ratio e_o	s_u/p_o Ratio	Shear Strength			
										Q_u		S	
										c T/sq ft	R T/sq ft	ϕ deg	β deg
Natural levee		18-83 (45)	29-129 (66)	2-90 (42)	0.14-1.18 (0.54)	50-92 (76)	2.62-2.74 (2.69)	0.82-6.16 (1.46)	--	0.08-0.68	0.01-0.50 (0.20)	8-22 (13)	16-31 (24)
Point bar (silty)		26-79 (44)	31-87 (54)	7-63 (33)	0.22-1.60 (0.74)	54-98 (78)	2.65-2.77 (2.69)	0.70-2.12 (1.12)	0.14-0.37 (0.27)	0.11-1.24	0.01-0.50 (0.20)	8-22 (13)	16-31 (24)
Backswamp (organic)	Insufficient data	42-367 (127)	58-397 (152)	43-218 (106)	0.16-1.41 (0.70)	16-73 (43)	2.10-2.74 (2.46)	1.36-6.73 (3.11)	--	0.03-0.27	0.00-0.40 (0.14)	7-20 (13)	13-35 (22)
Backswamp (inorganic)		31-98 (59)	27-148 (83)	19-86 (56)	0.03-1.26 (0.55)	48-91 (65)	2.52-2.75 (2.68)	0.85-2.57 (1.62)	0.07-0.76 (0.26)	0.1-0.72	0.00-0.50 (0.13)	4-27 (12)	13-36 (21)
Prodelta		31-70 (53)	39-100 (79)	16-72 (51)	0.12-1.08 (0.51)	49-90 (72)	2.67-2.80 (2.72)	0.84-2.06 (1.32)	0.11-0.39 (0.22)	0.18-0.85	0.01-0.50 (0.20)	8-22 (13)	16-31 (24)
Intradelta		24-132 (58)	25-212 (77)	5-164 (52)	0.39-1.52 (0.69)	33-98 (67)	2.57-2.76 (2.70)	0.64-2.84 (1.57)	0.07-0.65 (0.29)	0.05-0.4	0.01-0.50 (0.20)	8-22 (13)	16-31 (24)
Inter-distributary		24-113 (57)	38-179 (82)	19-162 (59)	0.13-1.03 (0.61)	45-94 (66)	1.59-2.74 (2.64)	1.01-2.59 (1.58)	0.22-0.85 (0.37)	0.2-0.5	0.01-0.50 (0.20)	8-22 (13)	16-31 (24)

LEGEND	
Clay (0.005 mm)	Silt (0.05-0.005 mm)
Sand (2.0-0.05 mm)	Organic material

Notes: (1) Numbers in parentheses are average values.
 (2) Insufficient consolidated-undrained and drained shear strength data were available for the natural levee, point bar, prodelta, intradelta, and interdistributary deposits. The data shown represent all five deposits.
 (3) Insufficient data were available to clearly establish the amount of organic matter typically occurring in each deposit.
 (4) Shear strengths are given in cohesion (c), tons per square foot and angle of internal friction (ϕ) in degrees.
 Q_u denotes unconsolidated-undrained triaxial compression tests.
 R denotes consolidated-undrained triaxial compression tests.
 S denotes consolidated drained direct shear tests.
 (5) Grain-size characteristics based on references 2 and 10.

Table A2. Engineering properties of selected depositional environments from the Mississippi River deltaic plain (from Montgomery, 1974)

The biggest contrast in Holocene soils occurs between the high- and low- energy depositional environments. High-energy environments are generally associated with maximum fluvial and/or wave activity and are mainly composed of coarse-grained sediments. These environments include point bar, substratum, abandoned course, abandoned distributary, beach, nearshore gulf, estuarine/bay sound, and intradelta deposits (Table A1). Low-energy environments are composed primarily of fine-grained sediments and include marsh, swamp, natural levee, prodelta, and interdistributary. Only the environments of deposition that are present in the study area are examined in the following section. The environments are presented and described by their order and distribution of occurrence. Deltaic environments not present in the study area but identified in Table A1 are described in further detail by Kolb (1962) or Kolb and Van Lopik (1958a,b) for readers desiring further information.

Surface Environments of Deposition

Natural levee

Natural levees are vertical accretion deposits formed when the river overtops its banks during flood stage and sediment suspended in the flood flow is deposited immediately adjacent to the channel. The resulting landform is a low, wedge-shaped ridge decreasing in thickness away from the channel. The limits of natural levee deposits in the study area are shown in Figure 2-4 of the main report. Natural levee deposits are mapped in Figure 2-4 with the underlying environment of deposition (i.e., interdistributary, point bar, or inland swamp). Natural levee deposits cover approximately 40 percent of the study area and involve the Mississippi River and abandoned distributary channels from the active St. Bernard delta complex (i.e., Bayou des Familles-Barataria, Metairie Bayou, Bayou Sauvage, and two unnamed bayous).

Natural levee widths in the study area vary from about 3/4 to approximately 2 miles wide along the Mississippi River, and between 1/4 and 1/2 mile wide along the abandoned St. Bernard distributary channels (Figure 2-4). Natural levees are thickest adjacent to the main channel, ranging from 10 to 20 ft in thickness (Figures 2-5a to 2-5k). Their thickness decreases away from the river, eventually merging with inland swamp deposits.

Natural levee deposits in the study area are composed primarily of clay and silt with minor sand lenses. Soils associated with natural levee deposits are identified in Figures 2-5a through 2-5k of the main report. These deposits are generally coarser-grained near the channel, composed of silt (ML) and silty clay (CL), and become finer-grained (i.e., CL and CH) further from the river. Color varies from reddish brown or brown near surface to grayish brown, and medium to dark gray with depth. Darker colored natural levee soils are due to the higher organic content. Organic content is generally low and is in the form of small roots and occasionally disseminated wood fragments. Larger wood fragments are uncommon as oxidation has reduced organic materials to a highly decomposed state. Frequently associated with natural levee deposits are small calcareous nodules, formed as a result of groundwater percolating through the permeable soils and precipitated from solution. Natural levee soils are well-drained, have low-water contents, and generally have a stiff to very stiff consistency (Tables A1 and A2).

Inland swamp

Before describing characteristics of inland swamps and their distribution in the study area, a clarification of terminology is in order. Usage of the term inland swamp is restricted to the deltaic plain, whereas the term backswamp is restricted to the Mississippi River alluvial valley. Mapping by May et al. (1984) adopted the usage of the term inland swamp and defined the upvalley margin of this environment. Inland swamps are not bounded by valley margins or older meander belt ridges as in the alluvial valley. Instead, inland swamps in the deltaic plain are areas of high ground and woody vegetation formed because of the high sediment rates from advancing distributary channels.

Kolb (1962) recognized that the term backswamp was inappropriate for the deltaic plain and had reservations about using this term to describe swamp sediments below Donaldsonville, LA. May et al. (1984) have placed the boundary between backswamp and inland swamp near the vicinity of Houma, LA. The boundary separating the two swamp types occurs at the junction of Bayou Teche and Bayou LaFourche, two former Mississippi River courses. Consequently, the summary descriptions and engineering properties in Tables A1 and A2 for backswamp are more appropriate to inland swamp as the samples were derived primarily from inland swamp sediments. The primary distinction here is in process and the ultimate nature of the sediments derived by these processes. In theory, inland swamp sediments are considered to be much finer-grained than backswamp sediments since they are transported by smaller-scale distributary channels to locations on the deltaic plain that are well removed from the main channel. As shown by Figure 2-3 in the main report, primary Mississippi River flow was not confined to a single main channel during the period of active Holocene delta building but rather was shared by several smaller major distributary courses.

Inland swamps are vertical accretion deposits that receive sediment during times of high-water flow, when the natural levees are crested and suspended sediment in the flood waters is deposited in areas well removed from the main distributary channel. Inland swamp environments are low, often poorly drained, tree-covered areas flanking the main distributary channel. Inland swamps are low areas that are settling basins for flood flow and sediment, and represent one of the final stages in land building by the passing delta front. Sediment supply is sufficient to elevate the land surface to above sea level and allow woody vegetation to develop and become stable.

Inland swamps are the dominant surface environment in the study area and comprise approximately 50 percent of the Holocene deposits depicted in Figure 2-4. The surface of the inland swamp environment begins at about the 0 ft NGVD elevation. These deposits are approximately 10 to 15 ft thick with the base of this sequence grading into marsh and interdistributary sediments between -10 to -15 ft NGVD (Dunbar et al. 1994).

Inland swamps are composed of uniform, very fine-grained soils, primarily silty clay (CL) and clay (CH). Sand (SM and SP) and silt (ML) may be present but is considered a minor constituent of the total depositional sequence (Table A1 and A2, and Figures 2-5a through 2-5k of the main report). These deposits typically contain moderate to high organic contents in the form of decayed roots, leaves, and wood. Disseminated pyrite is a common but a very minor

constituent of these soils and is commonly found in more poorly drained areas which promotes reducing conditions. Inland swamp soils may become well drained during times of low water and undergo short periods of oxidation, lending a mottled appearance to the soil. Inland swamp soils are gray, dark gray, or occasionally black. Inland swamp soils have generally high-water contents, between 30 and 90 percent, as shown by Tables A1 and A2 (backswamp environment).

Point bar

Point bar deposits are lateral accretion deposits formed as a river migrates across its flood plain. River channels migrate across their floodplain by eroding the outside or concave bank and depositing a sandbar on the inside or convex bank. With time the convex bar grows in size and the point bar is developed. Associated with the point bar are a series of arcuate ridges and swales. The ridges are formed by lateral channel movement and represent relic lateral bars separated by low lying swales. The swales are locations for fine-grained sediments to accumulate. Point bar deposits are as thick as the total depth of the river that formed them. These deposits become coarser-grained with increasing depth. Maximum grain size is associated with the river's bedload (coarse sand and fine gravel) while the fine-grained soils occur near the surface. The basal or coarse-grained portion of the point bar sequence is deposited by lateral accretion while the fine-grained or upper portion of the point bar sequence is deposited by vertical accretion.

Point bar deposits in the study area are considered to be young, generally less than 3,500 years old. They began forming along Bayou des Familles-Barataria when the St. Bernard delta system was active but did not fully develop along the main river until the present Mississippi River course began forming less than 1,000 years before the present.

Soil types in a point bar sequence grade upward from coarse-grained sands and fine gravels near the base to clays near the surface. These deposits are variable, but in the study area are generally composed of at least 50 percent poorly graded fine sand (Figures 2-5a through 2-5h and Tables A1 and A2). Point bar deposits are separated into two distinct units, a predominantly fine-grained upper sequence or point bar top stratum, and a coarse-grained lower sequence or point bar substratum. Soil types associated with each unit are identified in the geologic sections in Figures 2-5a through 2-5f of the main report.

Abandoned course

An abandoned course as the name implies is a relic fluvial course that is abandoned in favor of a more hydraulically efficient course. An abandoned course contains a minimum of two meander loops and forms when the river's flow path is diverted to a new position on the river's floodplain. This event usually is a gradual process that begins by a break or a crevasse in the river's natural levee during flood stage. The crevasse forms a temporary channel that may, over time, develop into a more permanent channel. Eventually, the new channel diverts the majority of flow and the old channel progressively fills. Final abandonment begins as coarse sediment fills the abandoned channel segment immediately downstream from the point of diversion. Complete

filling of the abandoned course is a slow process that occurs by overbank deposition. The complete filling process may take several hundreds or even thousands of years to complete.

The Bayou des Familles-Barataria abandoned course is a prominent physiographic feature that extends due south from the Mississippi River at approximately river mile 100 (Figures 2-1 and 2-4 of the report). The abandoned course extends well beyond the limits of the study area and continues south to Barataria Bay (May et al. 1984, Dunbar et al. 1994). It contains broadly developed natural levees which are easily identified on aerial photography and topographic maps. Well developed natural levees and a meandering plan form distinguish the abandoned course from its short lived predecessor, the crevasse channel.

Boring information from the greater New Orleans area indicates channel fill from the Bayou des Familles abandoned course consists primarily of thick sand deposits capped by a thin layer of silt and clay. Detailed boring information from the abandoned course at its confluence with the Mississippi River is presented in Figures 2-5c and 2-5i of the main report. Engineering properties of abandoned course sediments are not sufficiently categorized in Table A1 due to lack of boring data. However, these sediments are considered to be similar in composition to sandy point bar deposits for which data are present.

Abandoned distributary channel

Distributary channels are channels that diverge from the trunk channel dispersing or “distributing” flow away from the main course. By definition, distributary channels do not return flow to the main channel on a delta plain (Bates and Jackson 1987). Distributary channels originate initially as crevasse channels during high flow periods when the main channel is unable to accommodate the larger discharge. If the flood is of sufficient duration, a permanent distributary channel is soon established through the crevasse. Abandonment of a distributary channel or distributary network occurs either as a major course shift upstream or the distributary becomes over extended and loses its gradient advantage in favor of a much shorter distributary channel. Complete abandonment usually occurs because of an improved gradient advantage by the new distributary.

Distributary channel abandonment closely parallels the abandonment of a course. During abandonment, the base of the channel is filled with poorly sorted sands, silts, and organic debris. As the channel continues to fill, the flow velocities are decreased, and the channel is filled by clay, organic ooze, and peats. Abandoned distributaries in the study area are approximately their original width, but only a fraction of their original depth due to infilling. Abandoned distributary channels in the study area are Metairie Bayou, Bayou Sauvage, and two unnamed distributaries that intersect the Mississippi River on the east and west banks (Figure 2-4). These distributary channels have all been partially or completely filled with sediments.

Often the distal ends of abandoned distributaries have been buried due to subsidence, destroyed by coastal erosion, or closer to the trunk channel, buried by later natural levee deposits (Figure 2-4). Metairie Bayou in the northern portion of the study area has been buried by later Mississippi River natural levee deposits and altered by the historic activities of man north of the

river. Natural levees are ideal for urban development since these areas are topographically higher than the surrounding area.

Abandoned distributaries are recognized on aerial photographs by their natural levees and the urban development associated with these levees. In the subsurface, distributary sediments are recognized by soil types (Table A1) and sedimentary structures characteristic of channel fill deposits. Engineering properties of abandoned distributary sediments are not sufficiently categorized in Table A1 due to lack of boring data. Upper channel fill consists of parallel and wavy laminated silts and silty clays, interbedded with highly burrowed clays with high-water contents. Distorted bedding, slump structures, organic layers, and minor shell material are also common in abandoned distributary deposits.

Freshwater marsh

In the southwestern portion of the study area there is an area of freshwater marsh, a nearly flat expanse where grasses and sedges are the only vegetation. Organic sedimentation plays an important role in the formation of marsh deposits. Peats, organic oozes (mucks), and humus are formed as the marsh plants die and are buried. Decay is largely due to anaerobic bacteria in stagnant water. Vegetative growth and sedimentation maintain the surface elevation at a fairly constant level, and the marsh deposits thicken as a result of subsidence over time. When marsh growth fails to keep pace with subsidence, the marsh surface is eventually inundated by water.

Peats are the most common form of marsh strata remains, and they consist of black fibrous masses of decomposed plants. Detrital organic particles, carried in by marsh drainage, and vegetative tissues form the mucks. Mucks are watery oozes that can support little or no weight. Sedimentation occurs in the marsh when floodwater overtops the natural levees, depositing clays and silts onto the marsh surface. Sediments are also transported to the marsh during lunar tides, wind tides, and hurricane tides when sediment laden marine waters inundate the marsh surface.

Marsh sediments are found in the subsurface as peats (Figures 2-5b through 2-5k) and represent a time during the Holocene where the land surface was at sea level and supporting marsh vegetation. Often marsh deposits grade vertically upward in a prograding delta system into inland swamp, followed by natural levee deposits. The reverse sequence is also true (i.e., marsh, natural levee, inland swamp, marsh). Engineering properties of marsh sediments are identified in Table A1.

Subsurface Environments of Deposition

Interdistributary

Interdistributary deposits are sediments deposited in low areas between active distributary channels, usually under brackish water conditions. Sediment laden waters overtop the natural levees of distributary channels during flood stage and deposit the coarsest sediment (silt) near the channel. The finer sediment (silty clay and clay) is transported away from the active

distributary channel and settles out of suspension as interdistributary deposits. In this manner, considerable thicknesses of clay are deposited as the distributary builds seaward. Interdistributary clays often grade downward into prodelta clays and upward into the highly organic clays of swamp and marsh deposits.

Interdistributary deposits are found throughout the study area in the subsurface (Figures 2-5b through 2-5k of the main report). These deposits range in thickness from 30 to 60 ft and start between 0 to -10 ft NGVD as shown by the cross sections in Figures 2-5b through 2-5k. Interdistributary deposits consist of saturated gray clays which are highly bioturbated and contain some silt laminae. Shell fragments and minor amounts of organic debris are also commonly distributed throughout the interdistributary sequence as shown by Tables A1 and A2.

Buried beach

Interdistributary sediments associated with Metairie Bayou, an abandoned St. Bernard distributary in the northern edge of the study area, overlie and grade laterally with buried beach deposits. Buried beach deposits are part of the Pine Island Beach trend, an early Holocene beach trend associated with active sedimentation from the Pearl River (Saucier 1963). Approximately 5,000 years ago, when sea level was slightly lower than the present, longshore drift created a southwest to northeast trending offshore spit or barrier beach complex in the New Orleans area. Sediments forming the spit were derived from sandy fluvial sediments transported by the Pearl River. This spit originated at the river's mouth and extended southwest to the vicinity of New Orleans. This buried beach complex forms the southern shore of Lake Pontchartrain and acted as a natural barrier for filling of Lake Pontchartrain by advancing distributary channels during the active St. Bernard stage of delta growth.

Metairie Bayou (Figure 2-4) follows the seaward edge of the Pine Island Beach trend and was blocked from entering the main body of Lake Pontchartrain by the higher topography of the relic beach. Instead, Metairie Bayou follows the relic beach trend northeast toward the coastal mainland as the Bayou Sauvage distributary channel. Coastal drainage into Lake Pontchartrain from the Pleistocene uplands breached the beach ridge and formed "The Rigolets," a pass into Lake Pontchartrain at the eastern edge of the deltaic plain (Figure A1 from Saucier 1963).

The beach trend grades laterally into intradelta and abandoned distributary deposits (Figure A1). Boring data identifies the buried beach deposits as consisting of uniform, fine to medium grained, quartz sand, ranging in color from gray to tan, and white upon exposure at the surface (Saucier 1963). Beach sand is generally well sorted and contains shell fragments.

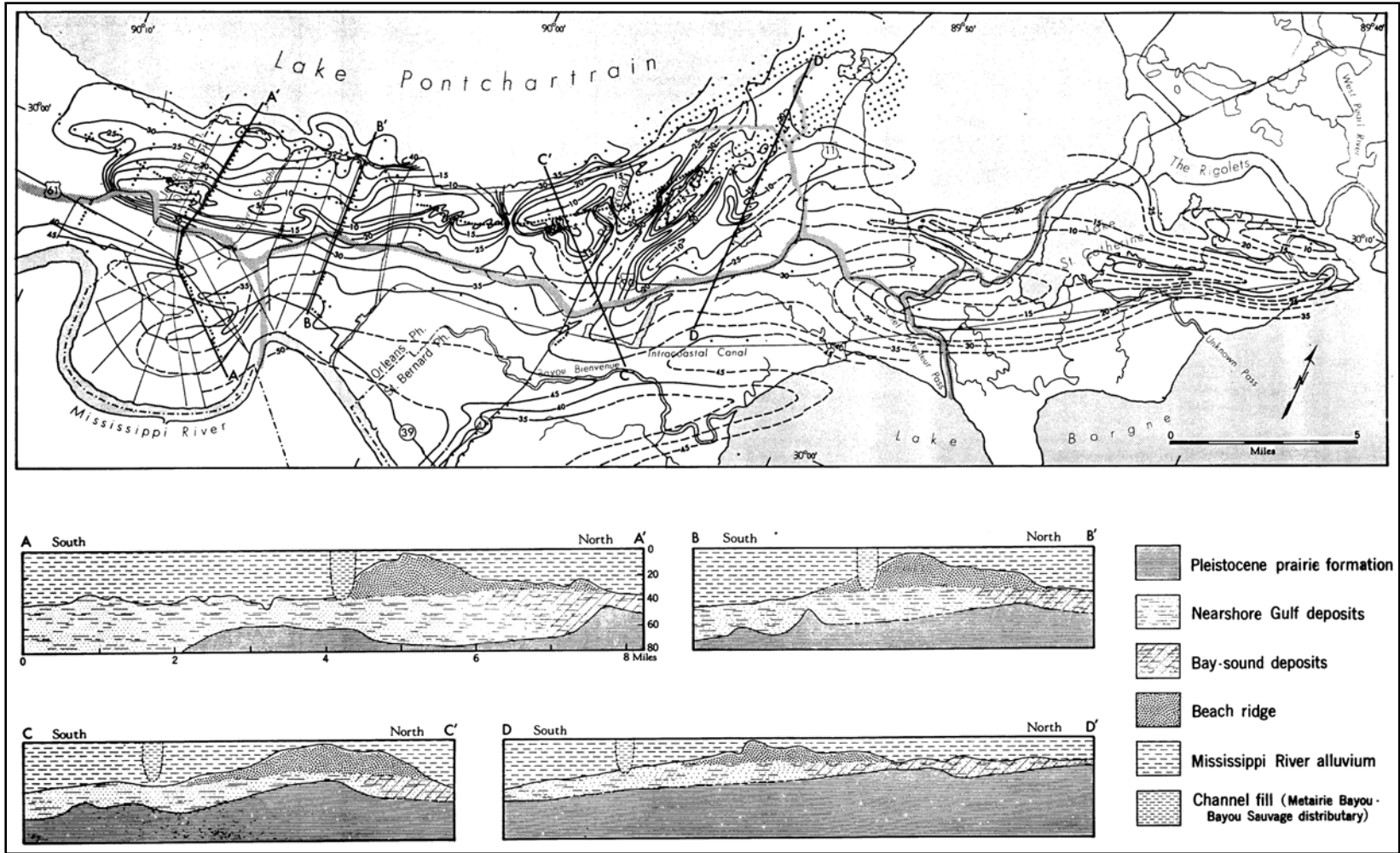


Figure A1. Topography of the buried Pine Island beach trend (Saucier 1963)

Intradelta

Intradelta deposits form at the mouth of distributary channels and consist of coarse-grained or sandy sediments. At the mouth of a distributary, the water velocity decreases upon entering open water, depositing coarse-grained sediments from suspension as distributary mouth bars. The coarse sediments are deposited on the bar crest or as fans along the sides of the bars. As the distributary is built seaward, it may cut through or split around the bar. The process is then repeated in each of the smaller, branching distributary channels. These deposits interfinger and merge with interdistributary clays.

Intradelta deposits are identified in the subsurface in borings near the Mississippi River (Figures 2-5a, 2-5b, 2-5e, and 2-5g). They consist primarily of clean sands and silty sands with some silts. Intradelta deposits are thickest nearer the distributary channels or channel source areas. Engineering properties of intradelta sediments are summarized in Tables A1 and A2.

Nearshore gulf

Nearshore gulf deposits are generally coarse-grained sediments formed by the transgression and interaction of the rising Holocene sea level with the drowned Pleistocene surface. Nearshore gulf deposits represent sediments eroded, transported, and deposited at the land/sea level interface, often at maximum wave energy and under storm conditions. These deposits generally consist of coarse-grained sediments and are primarily characterized by sand and shell hash. Available engineering data is presented in Table A1. The subsurface distribution of this depositional environment is shown by the cross sections in Figures 2-5a through 2-5k of the main report. Generally, this environment directly overlies the Pleistocene surface throughout the deltaic plain region.

Estuarine and bay sound

Both of these environments are marine and are a minor environment in the subsurface (see Figures 2-5a through 2-5l). Both of these environments directly overlie the Pleistocene surface. These two environments were formed early during the Holocene, or perhaps even Late Pleistocene, when sea level advanced onto the Pleistocene surface. As sea level advanced, it drowned the existing Pleistocene drainage network and created small estuaries and bays.

An estuary is a river valley where fresh water comes into contact with sea water (Bates and Jackson 1987). A bay sound is a partly enclosed brackish water body which is sheltered from direct access to the Gulf and is dominated by both fluvial and marine processes. Since the bay sound is partly restricted from the Gulf, the depositional energy and associated geomorphic processes are less severe than those associated with the nearshore gulf environment. Sediments deposited within an estuary or bay sound environment have a much greater range in grain size than sediments deposited within the nearshore gulf environment (Table A1). Silt and clay are usually more common within the estuarine and the bay sound environment than the nearshore gulf environment as shown by Table A1.

Substratum

Substratum or “braided stream/outwash plain” deposits related to glacial melting and sea level rise are not present in the study area. Substratum deposits as identified in this report are coarse-grained sediments associated with the point bar environment. The term substratum as used in this report and on the cross sections in Figures 2-5a through 2-5k is used in conjunction with and is a modifier of the point bar environment. Point bar substratum deposits are typically the lateral accretion or coarse-grained component of the point bar sequence. The upper boundary occurs at the base of the fine-grained or vertical accretion component of the point bar sequence and is defined by the first nearly continuous silty sand (SM) contact.

Pleistocene

Pleistocene deposits are present only in the subsurface and are correlative to the Prairie Formation. The Prairie Formation is the youngest of Fisk’s (1944) four major interglacial fluvial and deltaic sequences and was deposited during Sangamonian time, approximately 70,000 to 125,000 years ago. The Prairie Formation is similar in origin to the Holocene age deposits which overlie the Prairie. They were both envisioned by Fisk (1944) as fining upward from a coarse-grained substratum to a fine-grained top stratum. Both are products of rising sea level and deposition following continental glaciation. However, detailed analysis of glacial chronology from the midwest, combined with detailed geologic mapping from the Lower Mississippi Valley in recent years, indicates that the four-cycle model of Pleistocene glaciation and the accompanying interglacial deposition are an oversimplification (Autin et al. 1991). Recent studies indicate that the geology of the Prairie Formation in the study area is highly complex (Cullinan 1969; Kolb, Smith, and Silva 1975; Saucier 1977; Dunbar et al. 1994).

Lithologic and stratigraphic data on the Prairie Formation are based on surface exposures north of Lake Pontchartrain in St. Tammy, St. Helena, Tangipahoa, and Washington Parishes, Louisiana, and foundation engineering borings from the greater New Orleans metropolitan area. Pleistocene age soils outcropping on the north shore of Lake Pontchartrain were mapped by Cullinan (1969) as being typically light gray, light brown, or yellowish orange in color and composed of muddy, fine sandstones or fine to very fine sandy siltstones. Beneath the Holocene sediments in the New Orleans area, numerous engineering borings drilled into the Pleistocene surface identify the Prairie as being composed primarily of clay and silty clay and having the following characteristics (Kolb and VanLopik 1958a,b, Kolb 1962): (a) oxidized tan, yellow, or greenish gray color, (b) a marked decrease in water content, (c) distinctive stiffening in soil consistency and a general increase in shear strength, and (d) the presence of concretions. Pleistocene age soils forming the subsurface in the New Orleans area are usually easily distinguished from Holocene age soils by their sharp contrast in engineering properties, lithology, and stratigraphy. Soil color, water content, and shear strength are the most diagnostic criteria distinguishing Pleistocene from Holocene soils (Table A1).

Between the fine-grained Pleistocene sediments beneath the New Orleans area and the more coarse-grained sediments that outcrop at the surface north of Lake Pontchartrain, there is a transition which may be due to variations within environments of deposition or stratigraphy during

the Late Pleistocene. The New Orleans area Pleistocene soils may have formed under several depositional settings, including inland swamp, interdistributary, bay sound, and/or estuarine environments, while the coarser-grained soils north of Lake Pontchartrain are perhaps related to mainland beach and terrestrial fluvial environments draining the Pleistocene uplands. The Prairie surface is a highly complex stratigraphic sequence that consists of multiple depositional facies which formed over a period of several tens of thousands of years, followed by thousands of years of subaerial oxidation and erosion during maximum glacial episodes and lowered sea levels, and then later burial by Holocene sediments.

The Pleistocene surface dips gently to the south and southwest at about 3 to 5 ft per mile (Figure 2-6 of the main report). Elevations on the Pleistocene surface range from approximately -60 ft NGVD in the northern portions of the study area to more than -100 ft NGVD south of the Mississippi River. The base of the Prairie Formation beneath the Celotex failure site occurs somewhere between elevation -500 and -600 ft NGVD (Cullinan 1969).

Appendix 3

17th Street Canal Strength Evaluation

Objectives

The analysis of strength data described in the following sections had three objectives:

1. To develop a “shear strength model” for use in stability analyses and soil-structure interaction analyses of the I-walls at the 17th Street Canal, using all data available as of April 7, 2006. This strength model includes strengths for the levee fill, the marsh layer, the clay, and the sand in the foundation.
2. To compare this strength model to the strengths that were used for design of the I-walls in the area where the breach occurred.
3. To compare the strengths in the breach area with strengths in other sections of the 17th Street Canal I-wall.

Stratigraphy

The northern section of the 17th Street Canal where the breach occurred encompasses Stations 8+30, 10+00, and 11+50, on which this strength evaluation focuses.

The levee fill is compacted CL and CH material, with an average Liquid Limit of about 45. The average moist unit weight of the fill is about 109 pcf.

Beneath the fill is a layer of “marsh” material (or peat) 5 ft to 10 ft thick. The marsh layer is composed of organic material from the cypress swamp that occupied the area, together with silt and clay deposited in the marsh. The average moist unit weight of the marsh layer is about 80 pcf. Water contents of the marsh layer are as high as 737%. The average water content is approximately 112%. The marsh layer is fibrous at the top, and more amorphous near the bottom, indicating more advanced decomposition of the older organic materials at depth.

Beneath the marsh layer is a layer of lacustrine clay with an average Liquid Limit of about 95%. The clay is normally consolidated throughout its depth, having been covered and kept wet

by the overlying marsh layer. The average moist unit weight of the clay is about 109 pcf, and the average water content is approximately 65%.

Beneath the clay is a layer of Pine Island Beach sand, a silty sand with Standard Penetration blow counts ranging from 2 to 50. This layer is not involved in observed or calculated mechanisms of instability, and its strength is therefore of little importance in stability analyses, except as a more resistant layer beneath the clay.

Sources of Information on Shear Strengths

A considerable number of borings were drilled in the breach area and in neighboring areas before the failure. Additional borings have been drilled, cone penetration tests have been performed, and test pits have been excavated since the failure.

Several hundred unconfined compression tests, UU tests performed using only one confining pressure rather than a range of confining pressures (called UU-1 tests), and conventional UU tests performed using a range of confining pressures have been conducted on the soils at the site. Tests were performed on specimens trimmed from three-inch and five-inch diameter samples. Statistical analyses have been performed on the data from these tests to compute minimum, maximum, and average values of strength for the levee fill, the marsh layer, and the clay.

Four cone penetration tests with pore pressure measurements (CPTU tests) were performed near the area of the breach after the failure. These have proven to be very useful for evaluating the undrained strength of the clay, and for distinguishing the clay from the overlying marsh layer and the underlying sand.

The evaluation described here focused on undrained shear strengths of the levee fill, the marsh layer and the clay. Because the water loads that resulted in failure of the I-walls increased over a period of hours, there is little doubt that the levee fill and the clay beneath the marsh layer were undrained during the event. Determining whether the marsh layer should be modeled as drained or undrained will require laboratory consolidation tests to determine how quickly it drains when subjected to changes in load. Those tests are being performed at this time. The discussion below considers only undrained strength of the marsh layer. If it is determined that the drained strength, or partially drained strength, is more appropriate for the marsh layer, additional strength tests and slope stability analyses will be needed.

Shear Strength of Levee Fill

Data is available from two borings in the breach area (Borings 62 and 64) and several more in the neighborhood of the breach. In all, about 125 strength tests were performed on the levee fill material. Much of the fill is below the static water table, and an $s_u = c$, $\phi_u = 0$ strength interpretation is therefore appropriate.

The measured shear strengths of the levee fill material scatter very widely, from about 120 psf to more than 5,000 psf. With such widely scattered values, an average value may not be

meaningful, and considerable judgment is needed to select a representative value. Placing greatest emphasis on data from UU tests on five-inch diameter samples, $s_u = 900$ psf appears to be a reasonable value to represent the levee fill strength. This strength can be compared to a value of 500 psf used in the design analyses.

Shear Strength of the Marsh Layer

The marsh layer is stronger beneath the levee crest where it had been compressed under the weight of the levee, and weaker at the toe of the levee and beyond, where it has not been compressed so heavily. The same types of tests were used to measure marsh layer strengths as were used for fill strengths, and tests were performed on three-inch and five-inch diameter samples. Tests were also performed on two-inch diameter samples, but these were not included in the evaluation described here, because it was considered that such small samples would likely be too disturbed to be representative of field conditions.

The measured shear strengths scatter very widely, from about 50 psf to about 920 psf. Values of $s_u = 400$ psf beneath the levee crest, and $s_u = 300$ psf beneath the levee toe appear to be reasonably representative of the measured values. These strengths can be compared to a value of 280 psf used in the design analyses.

Shear Strength of Clay

The clay is normally consolidated, and its undrained shear strength increases with depth. Figure 3-1 shows variations of undrained shear strength with depth determined using Mayne's method (Mayne 2003)¹ for determining undrained shear strength from CPTU test results. Mayne's method uses the relationship among undrained strength, effective overburden pressure, and preconsolidation pressure that was proposed by Ladd (1991)², and has been found to give more reasonable values of undrained shear strength than use of constant values of the cone factors N_k or N_{kt} .

Whereas other methods of interpreting undrained shear strength from cone results are based on bearing capacity theory, Mayne's method considers tip resistance in relation to pore pressure and overburden pressure. For this reason it does not correspond to a single value of N_{kt} .

With Mayne's method, the undrained shear strength is related to cone tip resistance by the equation

$$s_u = 0.091(\sigma'_v)^{0.2} (q_t - \sigma_v)^{0.8} \quad (3-1)$$

¹ Mayne, P. W. (2003). "Class 'A' Footing Response Prediction from Seismic Cone Tests," Proceedings, Deformation Characteristics of Geomaterials, Vol. 1, Lyon, France.

² Ladd, C. C. (1991) "Stability Evaluation During Staged Construction," Terzaghi Lecture, ASCE Journal of Geotechnical Engineering, 117 (4), 540-615.

where s_u = undrained shear strength, σ'_v = effective vertical stress, q_t = total cone tip resistance adjusted for pore pressure effects, and σ_v = total vertical stress.

The undrained shear strength calculated with this method is based on that measured using Direct Simple Shear (DSS) tests. This strength is lower than that measured by conventional triaxial compression tests and greater than that measured by triaxial extension tests. Ladd (1991) has suggested that this is a reasonable average value for design purposes.

For the soft and very soft clay along the 17th Street Canal, the values of undrained shear strength are very close to values calculated using $N_{kt} = 15$, a value often used for computing undrained strengths of soft clays from CPTU test results.

As shown in Figure 3-1, the variations of undrained strength with depth within the clay computed using Equation 3-1 are very nearly the same for all four CPTU tests. The straight line representing the average undrained shear strength in the clay has a slope of 11 psf per foot of depth. This rate of strength increase with depth compares to values of 8.4 psf per foot to 13.5 psf per foot determined using laboratory strength test results for samples from borings B-1, B-2, B-3, B-4, and B-6, which appeared to have the most consistent test results.

The rate of increase of strength with depth is directly related to the s_u/p' ratio for the clay, and its buoyant unit weight, as follows:

$$\frac{s_u}{p'} = \frac{\text{rate of increase of } s_u \text{ with depth}}{\text{rate of increase of } p' \text{ with depth}} = \frac{\Delta s_u / \Delta z}{\gamma_{\text{buoyant}}} \quad (3-2)$$

The value of γ_{buoyant} for the clay is $109 \text{ pcf} - 62.4 \text{ pcf} = 46.6 \text{ pcf}$. Thus the value of s_u/p' is:

$$\frac{s_u}{p'} = \frac{11 \text{ psf per ft}}{46.6 \text{ pcf}} = 0.24 \quad (3-3)$$

which is a reasonable value for this normally consolidated clay.

These values provide a good basis for establishing undrained strength profiles in the clay. The undrained strength at the top of the clay is equal to 0.24 times the effective overburden pressure at the top of the clay, and the undrained strength increases with depth in the clay at a rate of 11 psf per foot.

In the IPET strength model the undrained shear strength of the clay is equal to 0.24 times the effective overburden pressure. The clay strength thus varies with lateral position, being greatest beneath the levee crest where the effective overburden pressure is greatest, and varying with depth, increasing at a rate of 11 psf per foot at all locations.

This model does not consider details of the stress distribution beneath the levee, which would result in “load spread” effects. These effects would result in rotation of principal stresses beneath

the levee, and in the added stress due to the levee load that would decrease with depth. Including these complex effects would complicate the model considerably. In our opinion, such refinement would make the model impractical, and is not justified. The model described in the previous paragraphs uses a simple stress distribution beneath the levee that satisfies vertical equilibrium, and it reflects the fact that the undrained strength is proportional to consolidation pressure, certainly the most important aspect of the strength of the clay.

The computer programs SLIDE³ and UTEXAS⁴ use two-dimensional interpolation to compute strengths that vary in both the horizontal and vertical direction, as is the case with the IPET strength model described above. This feature of these computer programs provides a convenient means for representing the New Orleans levee clay strengths in stability analyses. Provided that a sufficient number of interpolation points are used, the two computer programs give the same horizontal and vertical variations of shear strength.

Shear Strength of Sand

Correlations with Cone Penetration tip resistance were used to estimate a value of $\phi' = 35$ degrees for the silty sand beneath the clay. As noted previously, the sand layer is not involved in observed or computed failure mechanisms, and the value of ϕ' assigned to it therefore has no influence on computed factors of safety.

Comparison with Strengths Used in Design

The design analyses used undrained strengths for the levee fill, the marsh layer, and the clay, and a drained friction angle to characterize the strength of the sand layer beneath the clay, as does the strength model described above. Thus the design strengths are directly comparable to the IPET strengths discussed here.

The values of strength for the levee fill, the marsh layer, and the sand that were used in the design analyses for the 17th Street Canal I-wall, Stations 552+70 to 635+00 (new Stations 0+00 to 82+30) are shown in Table 3-1. This interval includes the breach area, which extends approximately from new Station 7+50 to new Station 12+20.

The design strength values shown in Table 3-1 are taken from Plate 56 of the 17th Street Canal Geotechnical Design Memorandum (GDM)⁵. Also shown in Table 3-1 are the values of strength from the IPET strength model.

It can be seen that the strengths for the levee fill, the marsh layer and the sand used in design are consistently lower than those estimated using all of the data available in April 2006.

³ Available from Rocscience Inc., 31 Balsam Avenue, Toronto, Ontario, Canada M4E 3B5

⁴ Available from Shinoak Software, 3406 Shinoak Drive, Austin TX 78731

⁵ Design Memorandum No. 20, General Design, Orleans Parish – Jefferson Parish, 17th Street Outfall Canal, U.S. Army Engineer District, New Orleans, March 1990.

The values of strength for the clay vary with depth and laterally, as discussed above. The values of undrained strength used in design are compared with those described above in Figures 3-2, 3-3, and 3-4. These figures show the strengths for the IPET strength model discussed previously as dotted lines, superimposed on photocopies of the GDM figure. Minor variations in the strengths at Stations 8+30, 10+00 and 11+50 occur because the thicknesses of the levee fill and marsh layer are slightly different in the three cross sections, and the effective stresses at the top of the clay are therefore slightly different.

In each of the three cases the rate of increase of strength with depth (11 psf per foot) are essentially the same in the IPET strength model as for the design strengths. The GDM strength model assumed a maximum strength of 380 psf in the clay layer, while the IPET model allowed the strength to increase past 380 psf. Beneath the levee crest, the design strengths are very close to those determined from the IPET strength model. At the toe of the levee, however, the IPET strengths are considerably lower than those used in design. This is the most significant finding that has emerged from this evaluation of shear strengths.

Comparison of Strengths within the Breach Area with Strengths Elsewhere

Field observations and preliminary analyses show that the shear strength of the clay has a greater effect on stability than the strengths of the levee fill, the marsh layer, or the sand. Critical slip surfaces intersect only small sections within the marsh layer and the levee fill, and do not intersect the sand layer beneath the clay at all. Therefore the strengths of these materials have small influence on stability, and minor variations in these strengths from section to section would not control the location of the failure. For this reason, the comparison of strengths in the breach area with strengths elsewhere has been focused mainly on the undrained strength of the clay.

Within the breach area, only two borings drilled before the failure (Borings 62 and 64) are available. The strengths measured on undisturbed specimens from these borings are listed in Table 3-2.

The strengths summarized in Table 3-2 can be compared with the strengths of specimens from borings to the north and south of the breach, which are summarized in Tables 3-3 and 3-4. For the purpose of comparing relative strengths, it was assumed that the strength was constant with depth.

The average strengths from Tables 3-2, 3-3, and 3-4 are compared in Table 3-5 and Figure 3-5.

Although the data is sparse, it is fairly consistent, and it appears that the clay strengths in the areas north and south of the breach are somewhat higher than those in the breach.

Based on the average values shown in Table 3-5 and Figure 3-5, the undrained strengths of the clay in the areas adjacent to the breach are 20% to 30% higher than those in the breach area.

Strength differences of this magnitude are significant. They indicate that the reason the failure occurred where it did is very likely that the clay strengths in the breach area were lower than in adjacent areas to the north and south.

At the time of completion of this report the results of some vane shear tests and cone penetration tests are not yet available. Those results will be reflected in a revision of this report if that is found necessary.

Table 3-1 Comparison of Strengths of Levee Fill, Marsh Layer and Sand Used in Design for Stations 552+70 to 635+00 with the IPET Strengths		
Material	Strengths used for design	IPET strength model
Levee fill	$s_u = 500$ psf, $\phi = 0$	$s_u = 900$ psf, $\phi = 0$
Marsh layer	$s_u = 280$ psf, $\phi = 0$	$s_u = 400$ psf, $\phi = 0$ beneath levee crest $s_u = 300$ psf, $\phi = 0$ beneath levee toe
Sand	$\phi' = 30$ degrees	$\phi' = 35$ degrees

Table 3-2 Undrained Strengths of Clay for Specimens from the Breach			
Boring 62			
Depth	Test type	s_u	Average
24 ft	UC	305 psf	280 psf
34 ft	UC	260 psf	
42 ft	UU-1	178 psf (very loose clayey sand – ignore)	
Boring 64			
Depth	Test type	s_u	Average
22 ft	UC	103 psf	240 psf
33.5 ft	UC	383 psf	
41.5 ft	UC	168 psf (likely disturbed – ignore)	

Table 3-3 Undrained Strengths of Clay for Specimens from Borings North of the Breach			
Boring 66			
Depth	Test type	s_u	Average
28.5 ft	UC	235 psf	317 psf
38.5 ft	UC	398 psf	
Boring 68			
Depth	Test type	s_u	Average
33 ft	UC	340 psf	353 psf
33 ft	UU	360 psf	
39 ft	UU	360 psf	
42.5 ft	UU-1	250 psf (likely sand, not clay – ignore)	
42.5 ft	UU	240 psf (likely sand, not clay - ignore)	

**Table 3-4
Undrained Strengths of Clay for Specimens from Borings South of the Breach**

Boring 60			
Depth	Test type	s_u	Average
24 ft	UC	200 psf	326 psf
29 ft	UC	365 psf	
29 ft	UU	380 psf	
34 ft	UC	385 psf	
39 ft	UC	323 psf	
39 UU	UU	300 psf	
44 ft	UU-1	243 psf (loose clayey sand – ignore)	
Boring 58			
Depth	Test type	s_u	Average
24 ft	UC	183 psf	324 psf
29 ft	UC	313 psf	
39 ft	UC	475 psf	
Boring 56			
Depth	Test type	s_u	Average
29 ft	UC	295 psf	305 psf
39 ft	UC	315 psf	

**Table 3-5
Comparison of Undrained Strengths from Breach Area Borings with Strengths from Borings North and South of the Breach**

Area	Range of s_u	Average s_u
Breach (Borings 62 and 64)	240 psf to 280 psf	260 psf
North of breach (Borings 66 and 68)	317 psf to 353 psf	335 psf
South of breach (Borings 56, 58 and 60)	305 psf to 326 psf	318 psf

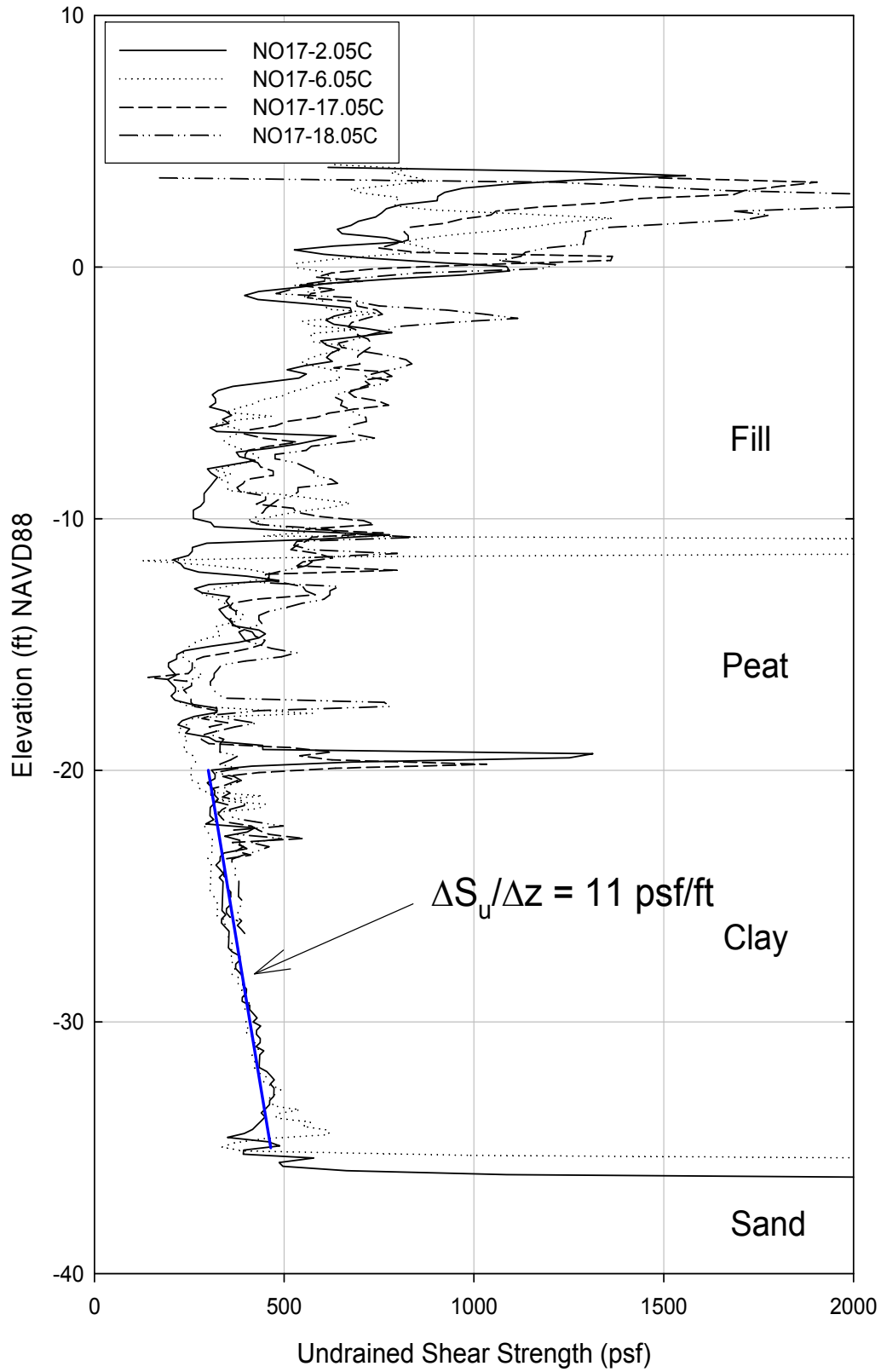


Figure 3-1. Undrained Shear Strength Calculated from CPTU Tests using Mayne's Method

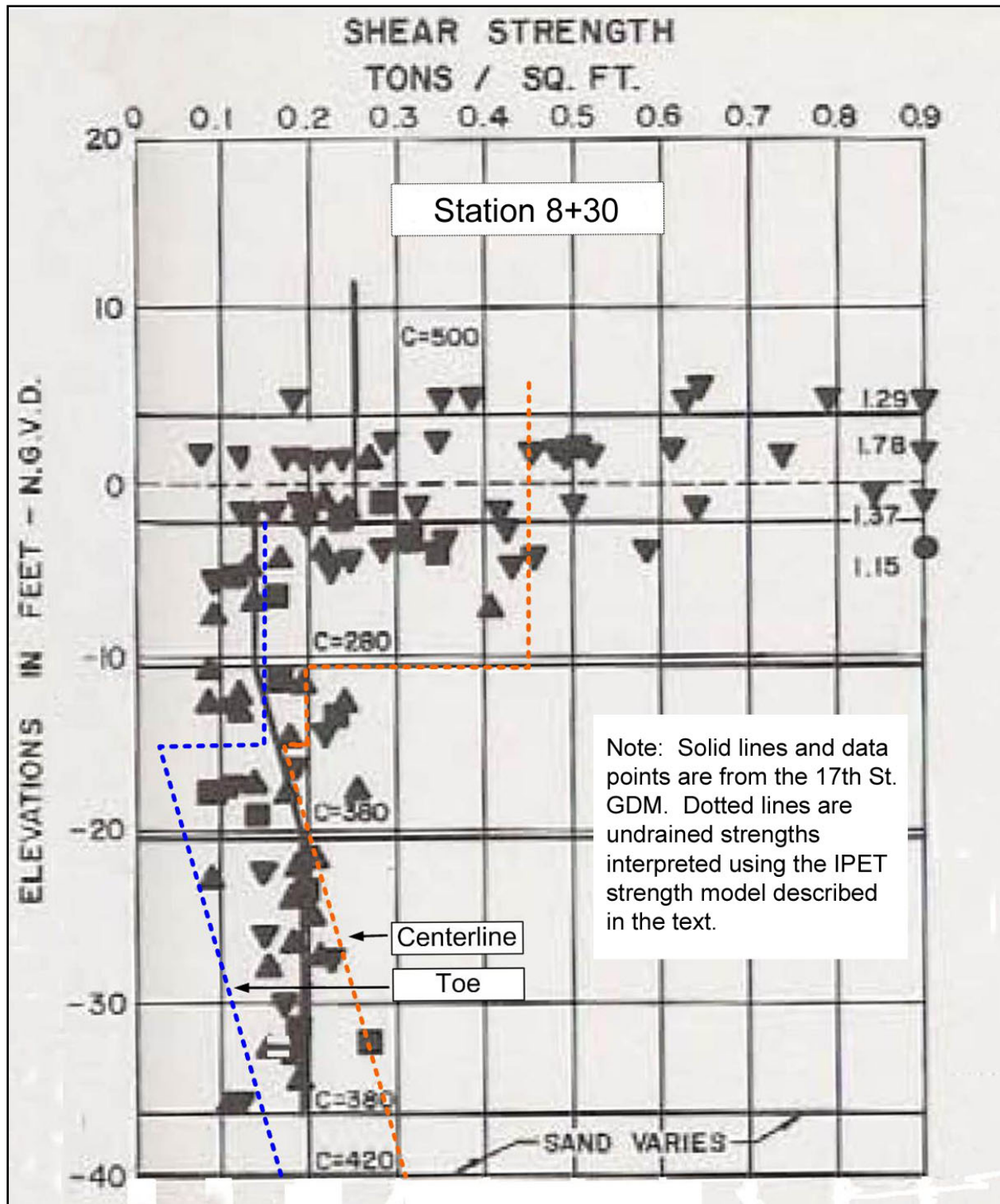


Figure 3-2. Comparison of Undrained Strength Profiles used for 17th Street I-Wall Design with Strength Profiles Interpreted from the IPET Strength Model for Station 8+30

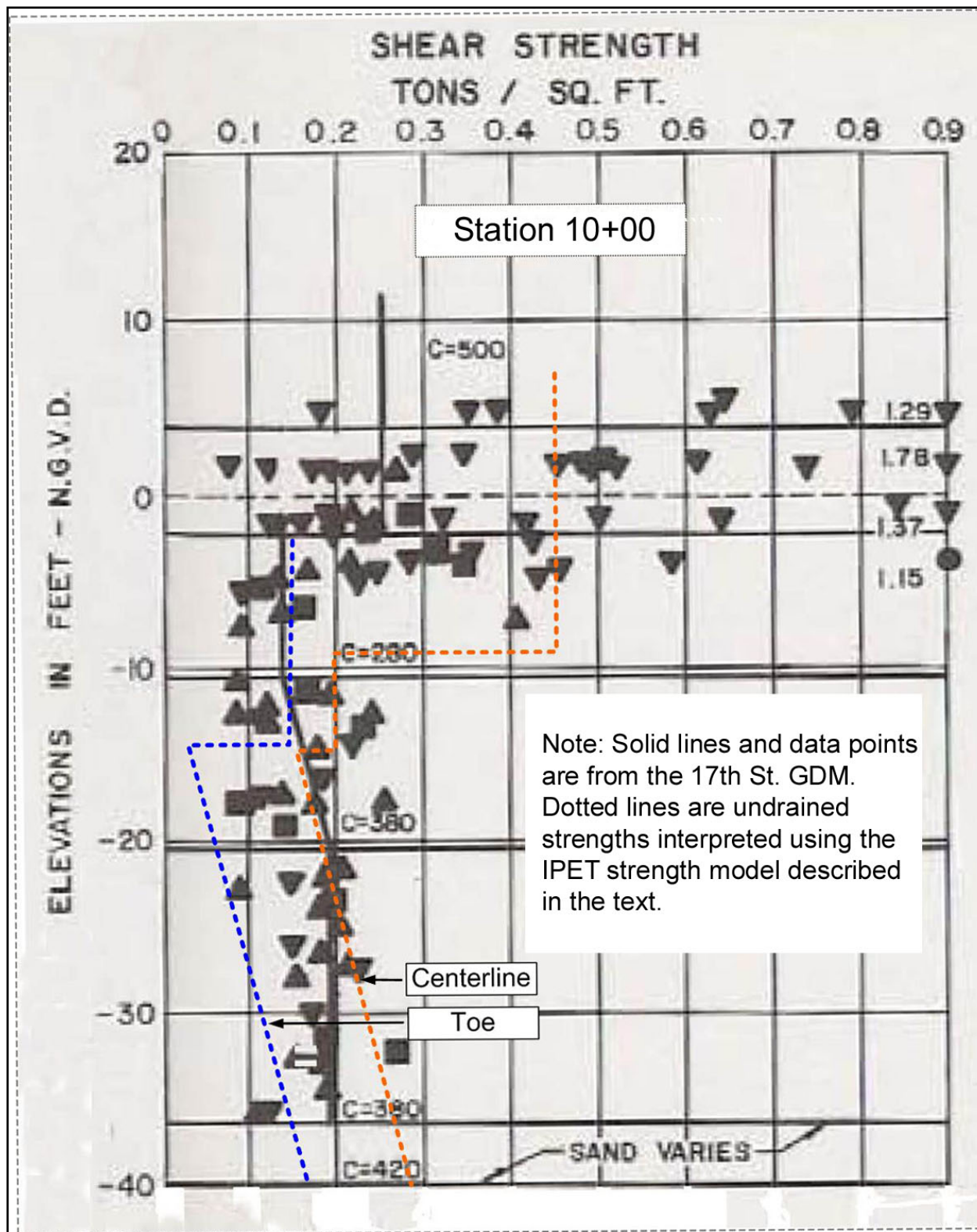


Figure 3-3. Comparison of Undrained Strength Profiles used for 17th Street I-Wall Design with Strength Profiles Interpreted from the IPET Strength Model for Station 10+00

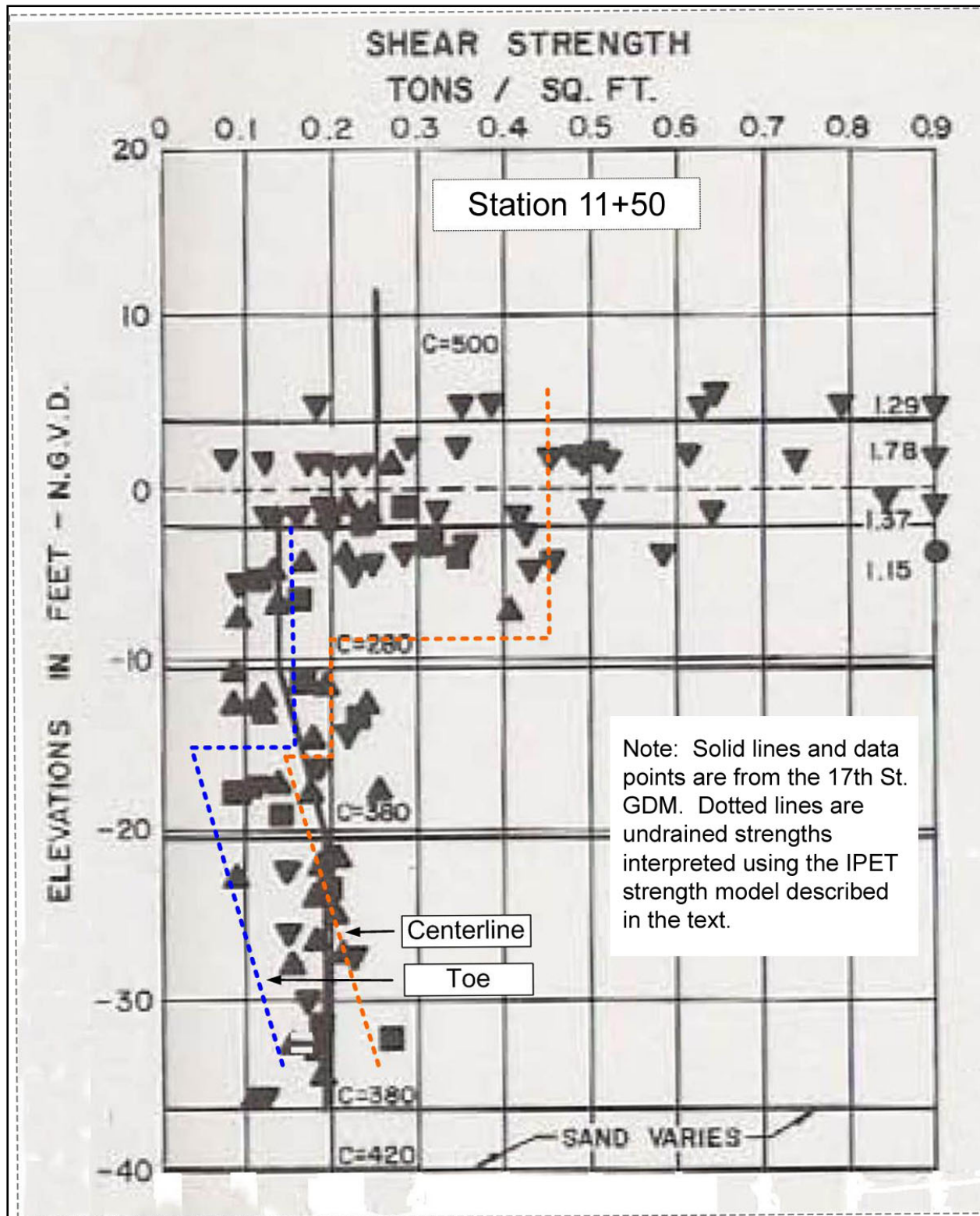


Figure 3-4. Comparison of Undrained Strength Profiles used for 17th Street I-Wall Design with Strength Profiles Interpreted from the IPET Strength Model for Station 11+50

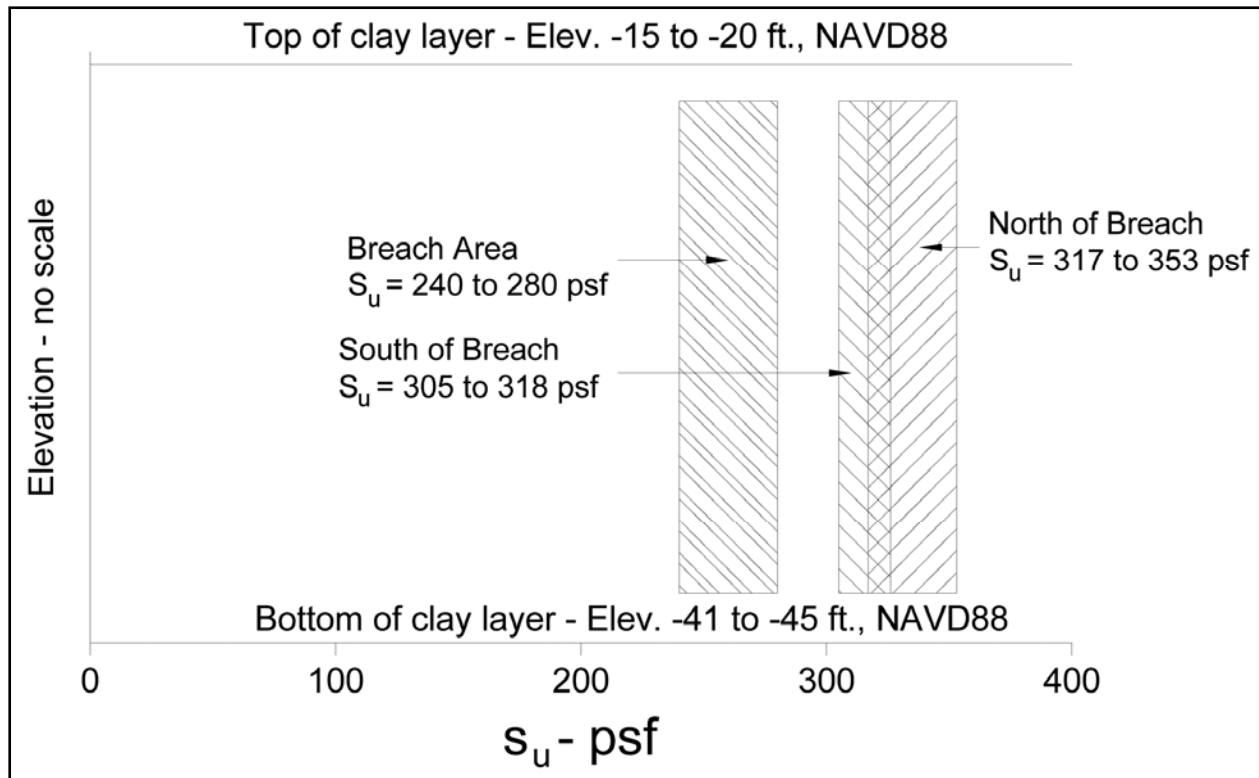


Figure 3-5. Comparison of Undrained Strengths from Breach Area Borings with Strengths from Borings North and South of Breach

Appendix 4

17th Street Canal

Slope Stability Analyses

Objectives

The analyses of stability described in the following sections were performed to answer these questions:

1. What are the factors of safety for the 17th Street Canal I-wall based on the IPET shear strength model, and how do the factors of safety vary with water level in the canal?
2. How are these factors of safety affected by assuming that a crack forms between the canal side of the wall and the levee fill, as the water level rises on the canal side of the wall?
3. What water level is needed for a factor of safety equal to 1.0, and how does this differ for Stations 8+30, 10+00, and 11+50?
4. How do factors of safety calculated using the New Orleans District Method of Planes compare to factors of safety calculated using Spencer's Method?
5. How do factors of safety calculated for design compare with those calculated using the IPET shear strength model and Spencer's Method?
6. How do factors of safety calculated for the breach area compare to factors of safety calculated for adjacent reaches of the I-wall, north and south of the breach area?
7. What are the probabilities of failure in the breach and adjacent areas?

Conditions Analyzed

Fifteen slope stability analyses (Cases 1 through 15 in Table 4-1) were performed for cross sections at Stations 8+30, 10+00, and 11+50. The shear strength profiles for these analyses are

shown in Figures 2, 3, and 4 of the shear strength evaluation report. These strengths are identified as “IPET” in Table 4-1.

Five slope stability analyses (Cases 16 through 20 in Table 4-1) were performed using the cross section and strength profile used in the 17th Street Canal design memorandum¹. These are identified as “GDM 20” in Table 4-1.

Average values of moist unit weight were used in the analyses: $\gamma_{\text{sat}} = 109$ pcf for the levee fill, $\gamma_{\text{sat}} = 80$ pcf for the marsh layer, and $\gamma_{\text{sat}} = 109$ pcf for the clay beneath the marsh layer, based on values measured in laboratory tests on undisturbed samples.

The critical slip surfaces found in the analyses did not extend down to the sand beneath the clay, and the sand strength and unit weight therefore did not influence the results of the analyses.

The analyses were performed for undrained conditions in the levee fill, the marsh layer, and the clay beneath the marsh layer. Based on available information, it appears that the values of permeability of all three of these materials were low enough so that dissipation of excess pore pressures during the rise of the water level in the canal would have been negligible, and would have had at most a minor influence on stability.

Analyses were performed for two conditions regarding contact between the I-wall and the adjacent soil on the canal side of the wall. These are indicated by “yes” or “no” in the column labeled “Crack” in Table 4-1. The term “crack” as used in herein refers to a vertical separation between the wall and the canal-side levee fill, not a local failure of either the wall or the fill soil.

- For the “no crack” analyses, it was assumed that the soil on the canal side of the wall was in intimate contact with the wall. Water pressures were applied to the surface of the levee fill, and to the I-wall where it projected above the crown of the levee, but were not applied to the face of the wall below the crown of the levee.
- For the “crack” analyses, it was assumed that the I-wall was separated from the levee fill on the canal side of the wall as the water level in the canal rose and caused the wall to deflect away from the canal. Full hydrostatic water pressures were applied to the I-wall, from the water level in the canal to the bottom of the wall.

Analyses were performed for the following canal water levels:

- Elevation 7.0 ft, the approximate water level at the time when the I-wall initially began to lean². It is estimated that the water level in the 17th Street Canal at the time the I-wall began to lean was 6.7 ft to 7.7 ft.
- Elevation 10.0 ft, the water level used as the principal design loading condition (converted here to NAVD88 datum).

¹ General Design Memorandum #20 – 17th Street Outfall Canal – Volume 1 (GDM20).

² All elevations here are referred to NAVD88 datum.

- The elevations that resulted in computed factors of safety equal to 1.0 at 8+30, 10+00, and 11+50. These were different elevations for the three stations.
- Elevation 11.5 ft, the elevation that resulted in a computed factor of safety equal to 1.0 for the GDM20 cross section and strength. This was analyzed only for the GDM20 design cross section and strength model.

The analyses described here were performed using the computer program SLIDE³, and factors of safety were checked using UTEXAS4⁴. Critical circular slip surfaces were located for each case, using the search routines available in SLIDE and UTEXAS4. The analyses were performed using Spencer's method⁵, which satisfies all conditions of equilibrium. Methods that satisfy all conditions of equilibrium have been shown to result in values of factor of safety that are not influenced appreciably by the details of the assumptions they involve⁶.

In all, 20 cases were analyzed. The conditions analyzed and results of these analyses are summarized in Table 4-1. The critical circles for these cases are shown in Figures 4-1 through 4-15, and 4-17 through 4-21.

Effect of Canal Water Level

The higher the water level in the canal, the lower was the calculated factor of safety, all other things being equal. This can be seen for the no crack or no gap condition by comparing Cases 1 and 3, for Station 8+30. Raising the canal water level from elevation 7.0 ft to elevation 10.0 ft results in a decrease in the computed factor of safety of 0.34, from 1.75 to 1.41. For Station 10+00, raising the water level from elevation 7.0 to 10.0 results in a decrease in factor of safety of 0.29 (Cases 6 and 8). For Station 11+50, the reduction is 0.31 (Cases 11 and 13).

Raising the water level also reduces the factor of safety for the cracked or gap condition, as can be seen by comparing Cases 2 and 4, Cases 7 and 9, and Cases 12 and 14. The reduction in the value of F for these cases varies from 0.21 to 0.28.

Effect of a Crack or Gap on the Canal Side of the Wall

Assuming that a gap formed on the canal side of the wall, and that hydrostatic water pressure acted through the full depth of the gap, causes a very significant reduction in the value of the calculated factor of safety.

³ Available from Rocscience Inc., 31 Balsam Avenue, Toronto, Ontario, Canada M4E 3B5

⁴ Available from Shinoak Software, 3406 Shinoak Drive, Austin, TX 78731

⁵ Spencer, E. (1967) "A Method of Analysis of the Stability of Embankments Assuming Parallel Inter-Slice Forces," *Geotechnique*, Institution of Civil Engineers, Great Britain, Vol. 17, No. 1, March, pp. 11-26.

⁶ Duncan, J. Michael, and Wright, Stephen G. (2005), *Soil Strength and Slope Stability*, John Wiley and Sons, New York, 293 pp.

For Station 8+30, with the canal water level at elevation 7.0 ft, the calculated factor of safety for the cracked condition is 1.32, as compared to 1.75 for the uncracked condition. With the water level at 10.0 ft, introducing a gap reduces the factor of safety from 1.41 to 1.04.

For Station 10+00, with the canal water level at elevation 7.0 ft, the calculated factor of safety for the cracked condition is 1.21, as compared to 1.57 for the uncracked condition. With the water level at 10.0 ft, introducing a gap reduces the factor of safety from 1.28 to 0.98.

For Station 11+50, with the canal water level at elevation 7.0 ft, the calculated factor of safety for the cracked condition is 1.21, as compared to 1.60 for the uncracked condition. With the water level at 10.0 ft, introducing a gap reduces the factor of safety from 1.29 to 1.00.

The “no crack” and “full crack” conditions considered here represent the extremes that are possible. The centrifuge model tests of the 17th Street I-wall showed that a gap did form full-depth at the back of the wall, consistent with the “full crack” condition considered here.

It seems likely that the failure was progressive, with a gradual reduction in factor of safety as the water rose, followed by a more sudden further reduction in factor of safety when the gap formed and water filled it. This appears to be a key factor in the mechanism of failure.

For the canal water level at elevation 10.0 ft, the calculated factor of safety is lowest at Station 10+00. This is approximately the same location where an eyewitness report indicates that the breach open to its full width just prior to 9:00 AM on August 29. The eyewitness reported that failure began at Station 11+00 where the I-wall initially started leaning prior to 7:00 AM. Subsequently, failure spread to other locations in the breach area.

A sequence of events consistent with the eyewitness report and the calculated results is this:

- As the canal water level rose, a gap did not form until the water reached an average elevation (not accounting for wave effects) of 6.7 ft to 7.7 ft, and the factor of safety before the gap formed was above 1.0.
- When the average water level reached elevation 6.7 ft to 7.7 ft, the I-wall began to lean, a gap formed between the I-wall and the levee fill on the canal side of the wall, resulting in a reduction in the factor of safety, and the wall began to fail at the location where the factor of safety was lowest.
- As the water in the canal rose to approximately elevation 10.0 ft, the breach fully opened resulting in a sudden surge of water into the protected area.

Static Water Level for Factor of Safety Equal to 1.0

The canal water level was varied to determine the static water level at which the calculated factor of safety would be equal to 1.0, with a gap. Calculated water levels for factors of safety equal to 1.0 for the cracked condition vary from 9.8 ft to 10.6 ft, as compared with a water level of 6.7 ft to 7.7 ft when the I-wall began leaning based on the eyewitness report. It appears that

water level in the canal rose until the breach fully open just prior to 9:00 AM when the elevation in the canal was between 9.5 and 10.5 ft.

An additional factor to be considered is the fact that the analyses discussed so far used circular slip surfaces. Additional analyses have been performed using noncircular slip surfaces with UTEXAS4. A comparison of the critical circular surface with the critical noncircular surface is shown in Figure 4-22. Although the critical noncircular surface is very similar in shape and position to the critical circle, the factor of safety for the noncircular surface is 6% lower. This 6% lower factor of safety corresponds to a water level for $F = 1.00$ that is 0.8 ft lower than the $F = 1.00$ water level found using circular slip surfaces.

These considerations can be summarized as follows:

- Static average water level at the time the I-wall started leaning = 6.7 ft to 7.7 ft.
- Effective water level at the time when the breach fully opened = 9.5 ft to 10.5 ft.
- Water level for $F = 1.00$ based on noncircular slip surfaces = 9.0 ft.

Considering the uncertainties involved in the time of failure and the magnitude of the wave effects, it appears that the best estimate of the water level at the time of failure is in good agreement with the water level for $F = 1.00$ determined using noncircular slip surfaces. As a result, it can be concluded that the IPET strength model is a reasonable characterization of the shear strengths in the 17th Street Canal breach area.

Comparison of Spencer's Method with the Method of Planes

Cases 16 through 20 of Table 4-1 used the design cross section and the shear strengths used in design. The cross section is shown in Figure 4-16, which is taken from Plate 62 of GDM20. The shear strengths are shown in Figures 2, 3, and 4 of the shear strength evaluation report (the design strength profile is the same in all three figures). This cross section and these shear strengths were used as the basis for design of the wall from Wall Stations 554+00 to 568+00, which includes the area where the breach occurred.

The factor of safety computed using the Method of Planes⁷ for these conditions was 1.30, with the canal water level at 10.0 ft NAVD88 (11.5 ft NGVD29), and no gap on the canal side of the wall. The factor of safety for this same condition computed using Spencer's Method (Case 18 in Table 4-1) was 1.45.

⁷ A study of the Method of Planes, undertaken by IPET at the request of the New Orleans District Task Force Guardian, indicates that the Method of Planes gives lower factors of safety than more accurate methods of analysis, such as Spencer's method. The magnitude of the difference between the two varies from case to case.

Comparison of Design Analyses with Analyses Performed Using the IPET Strength Model and Spencer's Method

The design analyses were based on these conditions:

1. The analyses were performed for the cross section shown in Figure 4-16.
2. The design strength profile shown in Figures 2, 3, and 4 of the shear strength evaluation report were used in the analyses. The same strengths were used under the embankment crest, under the slope, and beyond the toe of the levee.
3. The Method of Planes was used to calculate the factor of safety.
4. The wall was assumed to be in contact with the levee fill soil on the canal side (the “no crack” or “no gap” condition).
5. The water elevation was assumed to be at 10.0 ft NAVD88 (11.5 ft NGVD29).

As noted previously, for these conditions a factor of safety equal to 1.30 was calculated using the Method of Planes. Five variations on these conditions were analyzed using Spencer's Method. These are shown in Table 4-1 as Cases 16 through 20.

With the water level at 10.0 ft NAVD88, and a gap between the wall and the soil on the canal side, the factor of safety calculated using Spencer's Method is 1.24. The water level required to reduce the factor of safety to 1.0 is 11.5 ft NAVD88.

It appears that the most important difference between the conditions used as the basis for design and the conditions defined in this report is related to the strengths of the marsh layer and clay soils beneath the slopes and beyond the toe of the levee. The design strengths and the IPET strengths are very nearly the same beneath the crest of the levee. However, beneath the levee slopes, and beyond the toe, the design strengths were higher than the IPET strengths.

Comparison of Factors of Safety in the Breach Area with Those in Areas to the North and the South

In order to examine the effect on stability of the higher strengths in the sections north and south of the breach that were discussed in the strength evaluation report, stability analyses were performed using shear strengths for the clay and the marsh layer that were 20% higher than those estimated for the breach area. This 20% higher strength was based on the data available for the area south of the breach. North of the breach a greater difference in clay strength (about 30%) was indicated by the available strength data.

The analyses with higher strengths were performed for Station 10+00, with a gap at the canal side of the wall, full hydrostatic water pressure in the gap, and canal water levels at elevations

7.0 ft and 10.0 ft. The results of these analyses are shown in Table 4-2, together with the comparable results from Table 4-1.

For the canal water level at elevation 7.0 ft, a 20% increase in clay strength results in a 15% increase in factor of safety. A 20% increase in marsh layer strength results in 4% increase in factor of safety. For the canal water level at elevation 10.0 ft, a 20% increase in clay strength results in a 13% increase in factor of safety. A 20% increase in marsh layer strength results in 5% increase in factor of safety.

The factors of safety shown in Table 4-2 for increased clay and marsh layer strengths are consistent with the fact that failure did not occur in these areas. However, it appears that the margin of safety was very small.

Probabilities of Failure

Probabilities of failure have been estimated using an approximate technique based on the Taylor Series method. The coefficient of variation of the average clay strength and the average marsh layer strength were estimated to be 20%. The data available is sparse, and the scatter in measured values is influenced significantly by sample quality as well as variations in properties from one location to another. The estimated values of COV = 20% is thus largely based on judgment. Even so, it is useful to examine what probabilities of failure would be associated with this level of uncertainty concerning shear strengths.

The Taylor Series numerical method^{8,5} was used to estimate the standard deviation (σ_F) and the coefficient of variation of the factor of safety (COV_F), using these formulas:

$$\sigma_F = \sqrt{\left(\frac{\Delta F_{clay\ strength}}{2}\right)^2 + \left(\frac{\Delta F_{peat\ strength}}{2}\right)^2} \quad (4-1)$$

$$COV_F = \frac{\sigma_F}{F_{MLV}} \quad (4-2)$$

where $\Delta F_{clay\ strength}$ = difference between the values of the factor of safety calculated with the clay strength increased by one standard deviation and decreased by one standard deviation from its most likely value. $\Delta F_{marsh\ layer\ strength}$ is determined in the same way. F_{MLV} is the “most likely value” of factor of safety, computed using the IPET shear strengths.

Values of F_{MLV} and COV_F have been calculated for Station 10+00 and for areas adjacent to the breach, which were assumed for this purpose to have strengths 20% higher than the IPET

⁸Wolff, T. F. (1994). “Evaluating the reliability of existing levees.” Report, Research Project: Reliability of Existing Levees, prepared for U.S. Army Engineer Waterways Experiment Station Geotechnical Laboratory, Vicksburg, Miss.

strength model. The results are listed in Table 4-3, together with the corresponding values of probability of failure based on an assumed lognormal distribution of factor of safety.

For Station 10+00, the calculated probabilities of failure are 12% for a water level of 7.0 ft, and 58% for a water level of 10.0 ft. These values are reasonable, considering that the water level (including wave effects) was 8.7 ft to 9.7 ft at the time of failure. For adjacent areas with higher strengths, the probabilities of failure are lower, but still too high to offer confidence in the ability of the I-wall to survive water levels higher than about 7.0 ft.

Summary

The results of the analyses described in the preceding sections are consistent with the performance of the I-wall in the breach area, indicating that the IPET strength model and the mechanism of failure provide a suitable basis for evaluating the performance of the 17th Street Canal I-wall during Hurricane Katrina.

Calculated factors of safety are about 25% lower when it is assumed that a gap develops between the wall and the levee fill on the canal side of the wall. The results calculated assuming that a gap formed, and that full hydrostatic water pressure acted in the gap, are consistent with field observations and centrifuge test results, indicating a high likelihood that a gap did form in the areas where the wall failed. Centrifuge model tests of the 17th Street I-wall showed that a gap did form full-depth at the back of the wall, consistent with the “full crack” condition considered here.

The New Orleans District Method of Planes is a conservative method of slope stability analysis. A study of the Method of Planes undertaken by IPET at the request of the New Orleans District Task Force Guardian indicates that the Method of Planes gives lower factors of safety than more accurate methods of analysis, such as Spencer’s method. The magnitude of the difference between the two varies from case to case

The factors of safety calculated in the design analyses were higher than the factors of safety calculated for the conditions that are believed to best represent the actual shear strengths, geometrical conditions, and loading at the time of failure. The principal differences between the design analyses and the conditions described in this report relate to (1) the gap between the wall and the levee soil on the canal side of the wall, and (2) the fact that the design analyses used the same strength for the clay and the marsh layer beneath the levee slopes, and for the area beyond the levee toe, as for the zone beneath the crest of the levee. The IPET strength model has lower strengths beneath the levee slopes and beyond the toe.

Factors of safety for areas adjacent to the breach, where clay strengths are higher, were about 15% higher than those calculated for the breach area. These differences in calculated factor of safety are not large, and it thus appears that the margin of safety was small in areas that did not fail. It is possible that cracks or gaps did not form in those areas.

Estimates of probability of failure for water a level of 7.0 ft NAVD88 are about 12% in the breach area, and 1% in adjacent areas with clay strengths 20% higher. For a water level of 10.0 ft, the estimated probability of failure is 58% in the breach area and 16% in adjacent areas.

Table 4-1 Results of Slope Stability Analyses for Stations 8+30, 10+00, and 11+50 of the 17th Street Canal Floodwall							
Case	Section	Slip Surface	Method	Strength Model	Crack	Water Elev. Ft. NAVD88	F
1	8+30	Crit. Circle	Spencer's	IPET	no	7.0	1.75
2	8+30	Crit. Circle	Spencer's	IPET	yes	7.0	1.32
3	8+30	Crit. Circle	Spencer's	IPET	no	10.0	1.41
4	8+30	Crit. Circle	Spencer's	IPET	yes	10.0	1.04
5	8+30	Crit. Circle	Spencer's	IPET	yes	10.6	1.00
6	10+00	Crit. Circle	Spencer's	IPET	no	7.0	1.57
7	10+00	Crit. Circle	Spencer's	IPET	yes	7.0	1.21
8	10+00	Crit. Circle	Spencer's	IPET	no	10.0	1.28
9	10+00	Crit. Circle	Spencer's	IPET	yes	10.0	0.98
10	10+00	Crit. Circle	Spencer's	IPET	yes	9.8	1.00
11	11+50	Crit. Circle	Spencer's	IPET	no	7.0	1.60
12	11+50	Crit. Circle	Spencer's	IPET	yes	7.0	1.21
13	11+50	Crit. Circle	Spencer's	IPET	no	10.0	1.29
14	11+50	Crit. Circle	Spencer's	IPET	yes	10.0	1.00
15	11+50	Crit. Circle	Spencer's	IPET	yes	10.1	1.00
16	GDM 20	Crit. Circle	Spencer's	GDM 20	no	7.0	1.77
17	GDM 20	Crit. Circle	Spencer's	GDM 20	yes	7.0	1.60
18	GDM 20	Crit. Circle	Spencer's	GDM 20	no	10.0	1.45
19	GDM 20	Crit. Circle	Spencer's	GDM 20	yes	10.0	1.24
20	GDM 20	Crit. Circle	Spencer's	GDM 20	yes	11.5	1.00

Table 4-2 Factors of Safety Calculated for Stations 10+00 Geometry Using Clay Strength and Marsh Layer Strength 20% Higher than the IPET Strengths of these Materials							
Case	Section	Slip Surface	Method	Strength Model	Crack	Water Elev. Ft. NAVD88	F
7	10+00	Crit. Circle	Spencer's	IPET	yes	7.0	1.21
7A	10+00	Crit. Circle	Spencer's	clay + 20%	yes	7.0	1.40
7B	10+00	Crit. Circle	Spencer's	clay - 20%	yes	7.0	1.02
7C	10+00	Crit. Circle	Spencer's	marsh + 20%	yes	7.0	1.26
7D	10+00	Crit. Circle	Spencer's	marsh - 20%	yes	7.0	1.16
9	10+00	Crit. Circle	Spencer's	IPET	yes	10.0	0.98
9A	10+00	Crit. Circle	Spencer's	clay + 20%	yes	10.0	1.12
9B	10+00	Crit. Circle	Spencer's	clay - 20%	yes	10.0	0.84
9C	10+00	Crit. Circle	Spencer's	marsh + 20%	yes	10.0	1.04
9D	10+00	Crit. Circle	Spencer's	marsh - 20%	yes	10.0	0.93

**Table 4-3
Calculated Probabilities of Failure for Station 10+00 and Adjacent Areas**

Area	Water level (ft) NAVD88	F _{MLV}	COV _F	Probability of failure
Sta. 10+00	7.0	1.21	16%	12%
Sta. 10+00	10.0	0.98	15%	58%
Adjacent	7.0	1.47	15%	1%
Adjacent	10.0	1.17	15%	16%

F_{MLV} = most likely value of factor of safety
COV_F = coefficient of variation of factor of safety

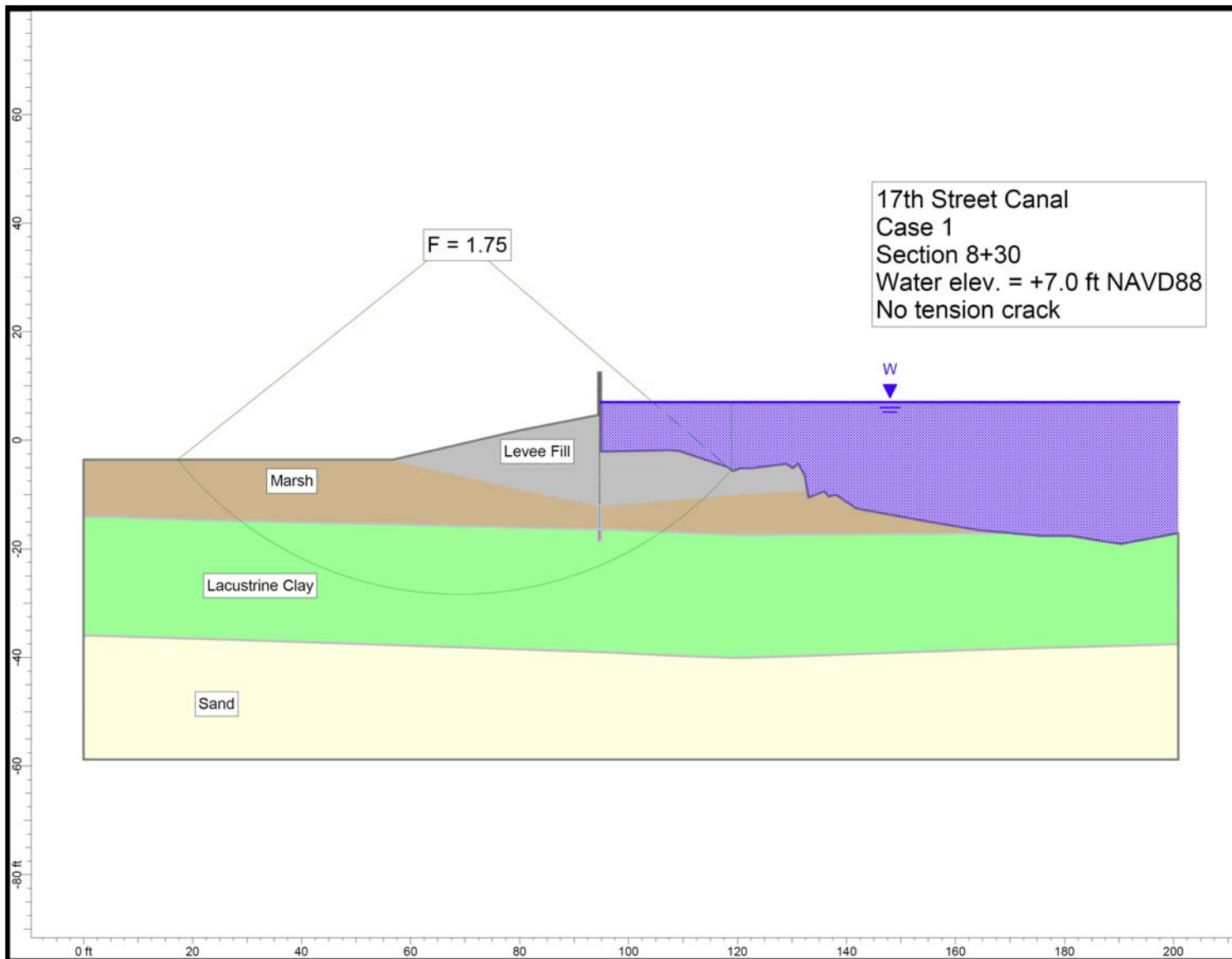


Figure 4-1. Critical Circle for 17th Street Canal Station 8+30 – Water Elevation 7.0 ft, No Tension Crack

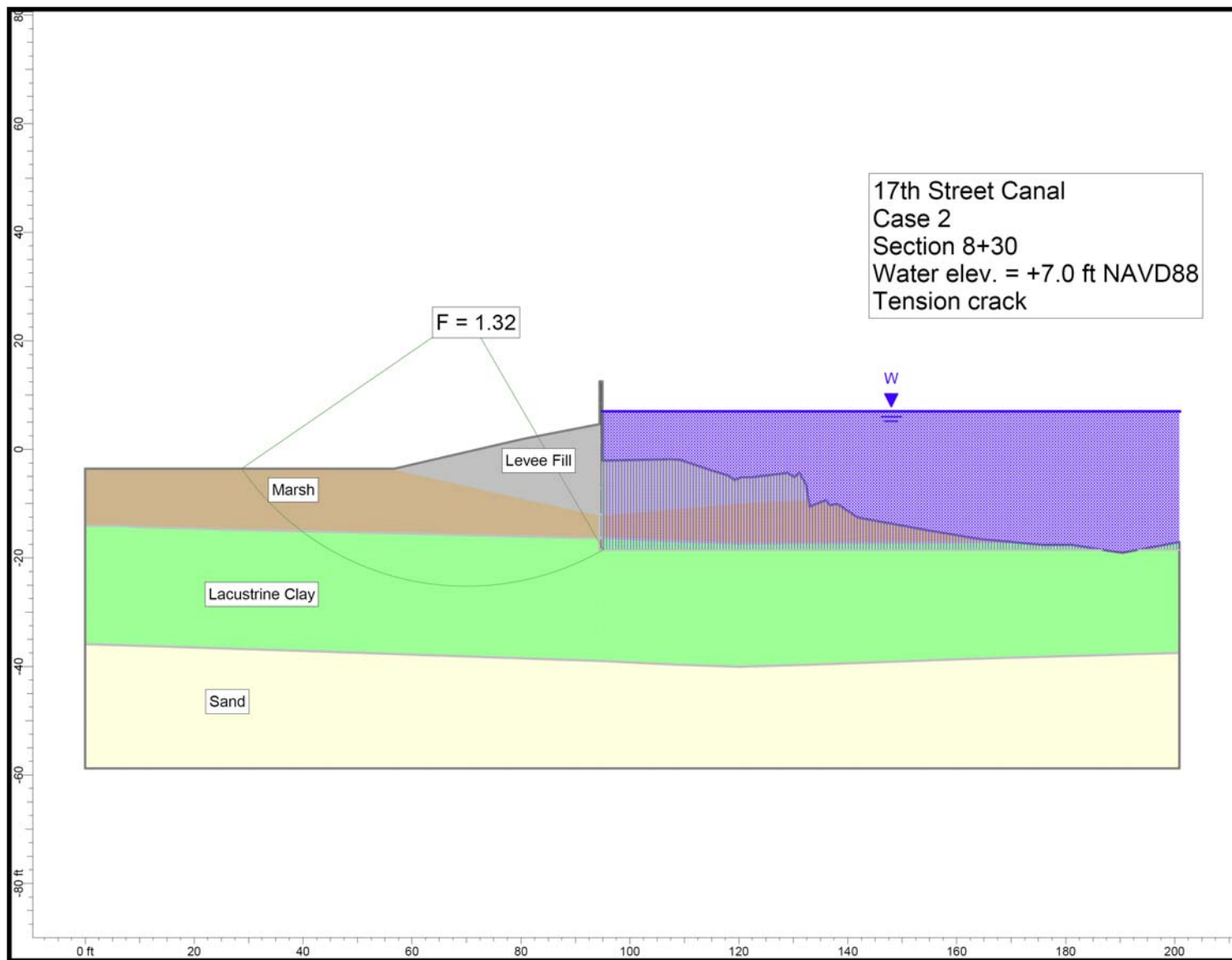


Figure 4-2. Critical Circle for 17th Street Canal Station 8+30 – Water Elevation 7.0 ft, Tension Crack

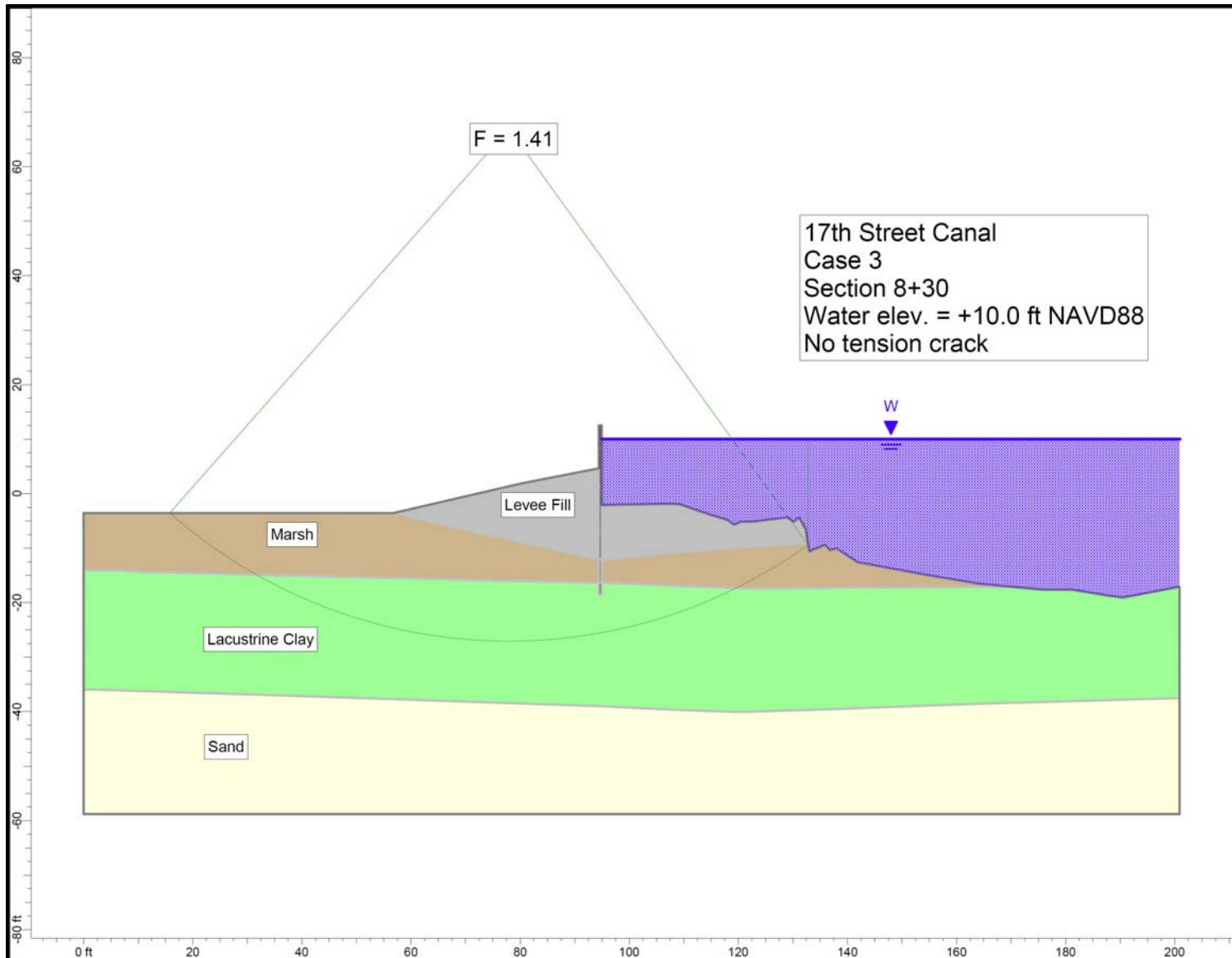


Figure 4-3. Critical Circle for 17th Street Canal Station 8+30 – Water Elevation 10 ft, No Tension Crack

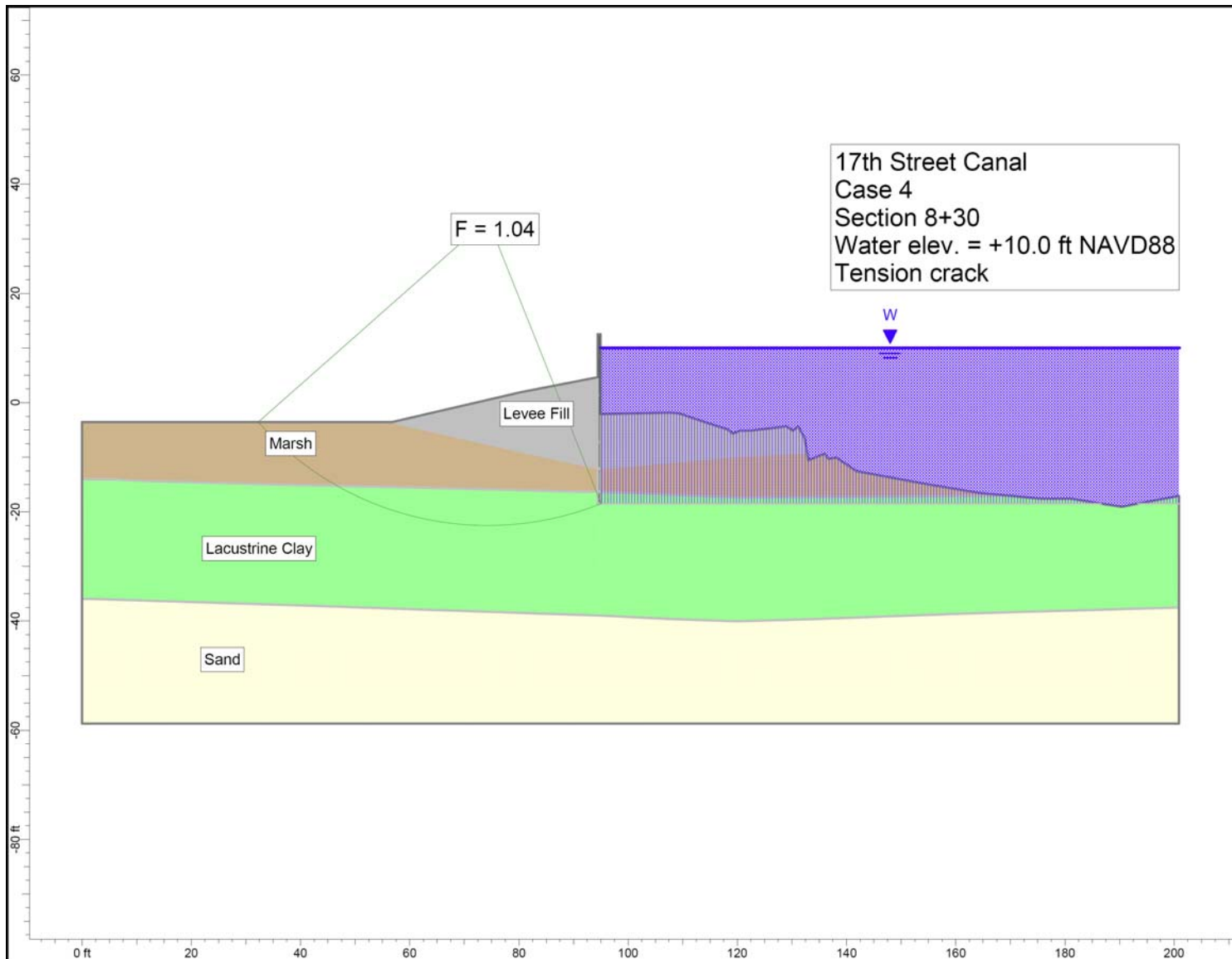


Figure 4-4. Critical Circle for 17th Street Canal Station 8+30 – Water Elevation 10 ft, Tension Crack

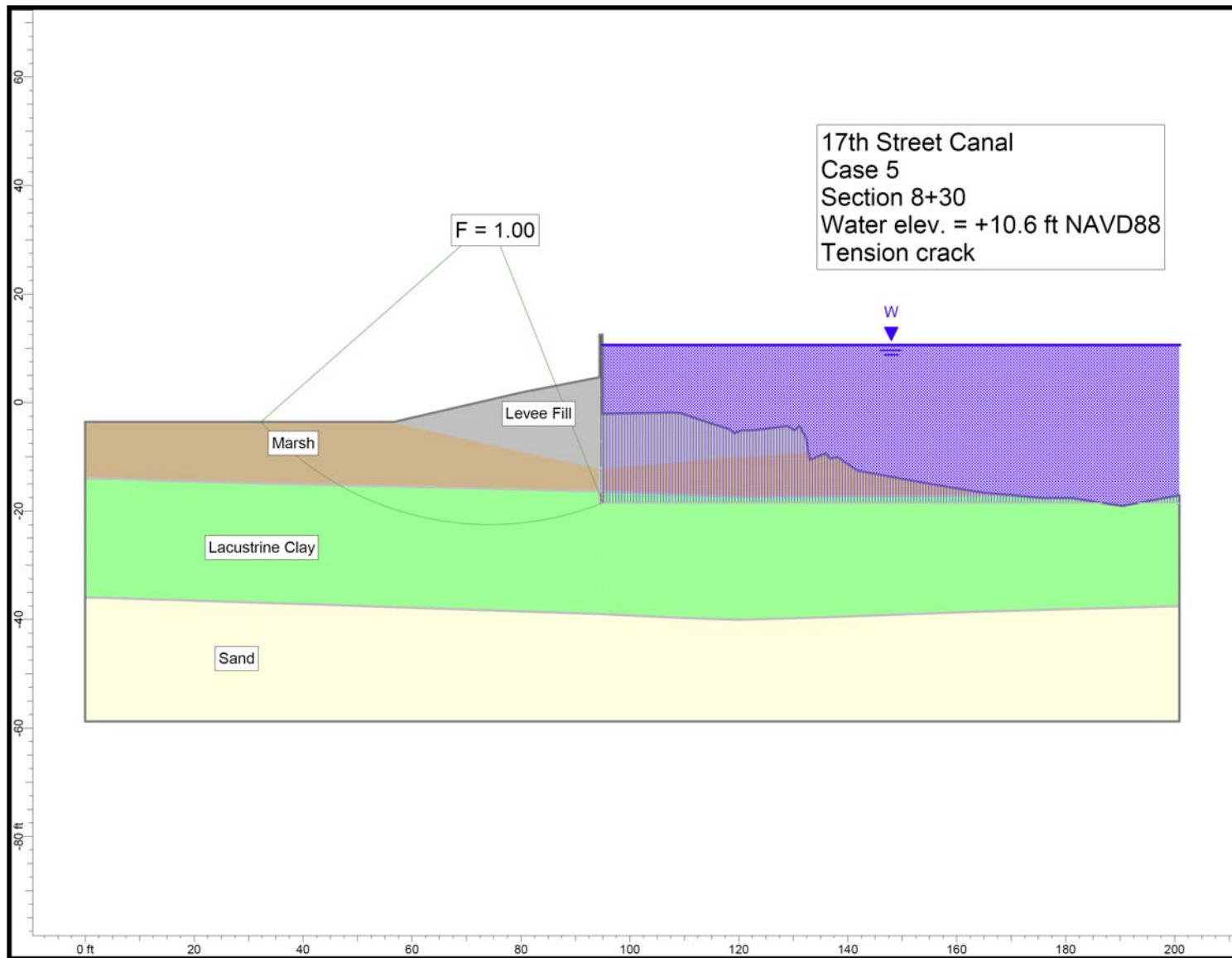


Figure 4-5. Critical Circle for 17th Street Canal Station 8+30 – Water Elevation 10.6 ft, Tension Crack.

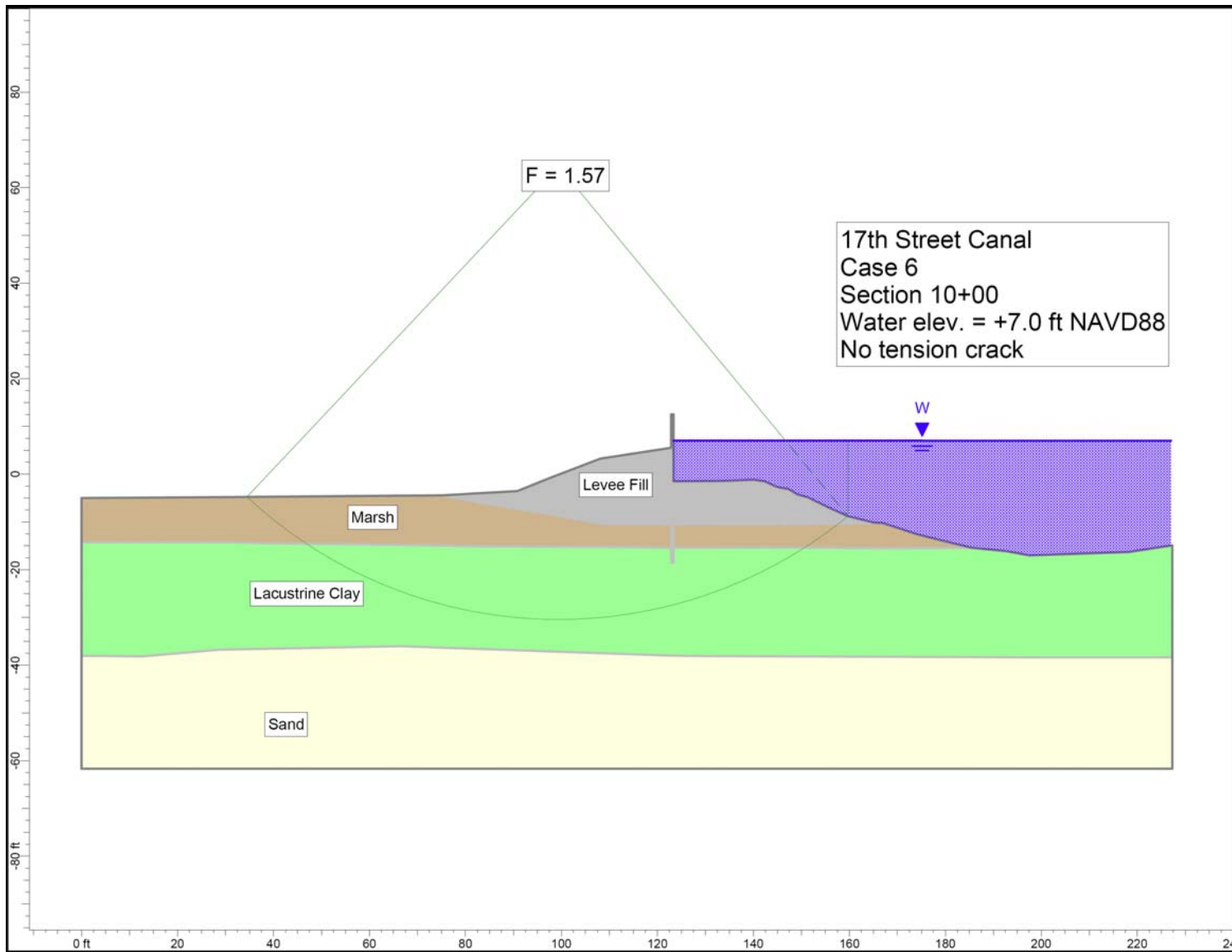


Figure 4-6. Critical Circle for 17th Street Canal Station 10+00 – Water Elevation 7.0 ft, No Tension Crack

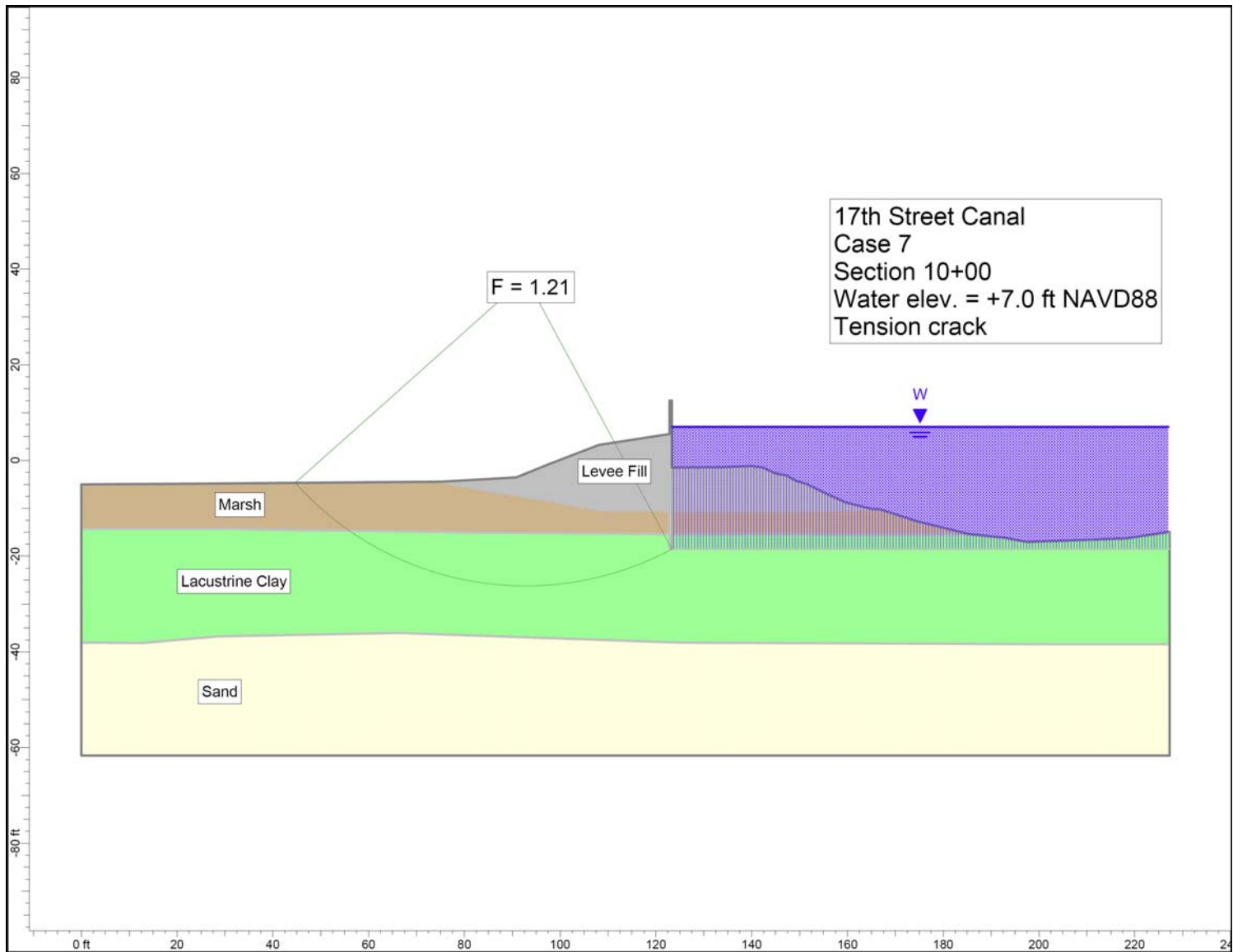


Figure 4-7. Critical Circle for 17th Street Canal Station 10+00 – Water Elevation 7.0 ft, Tension Crack

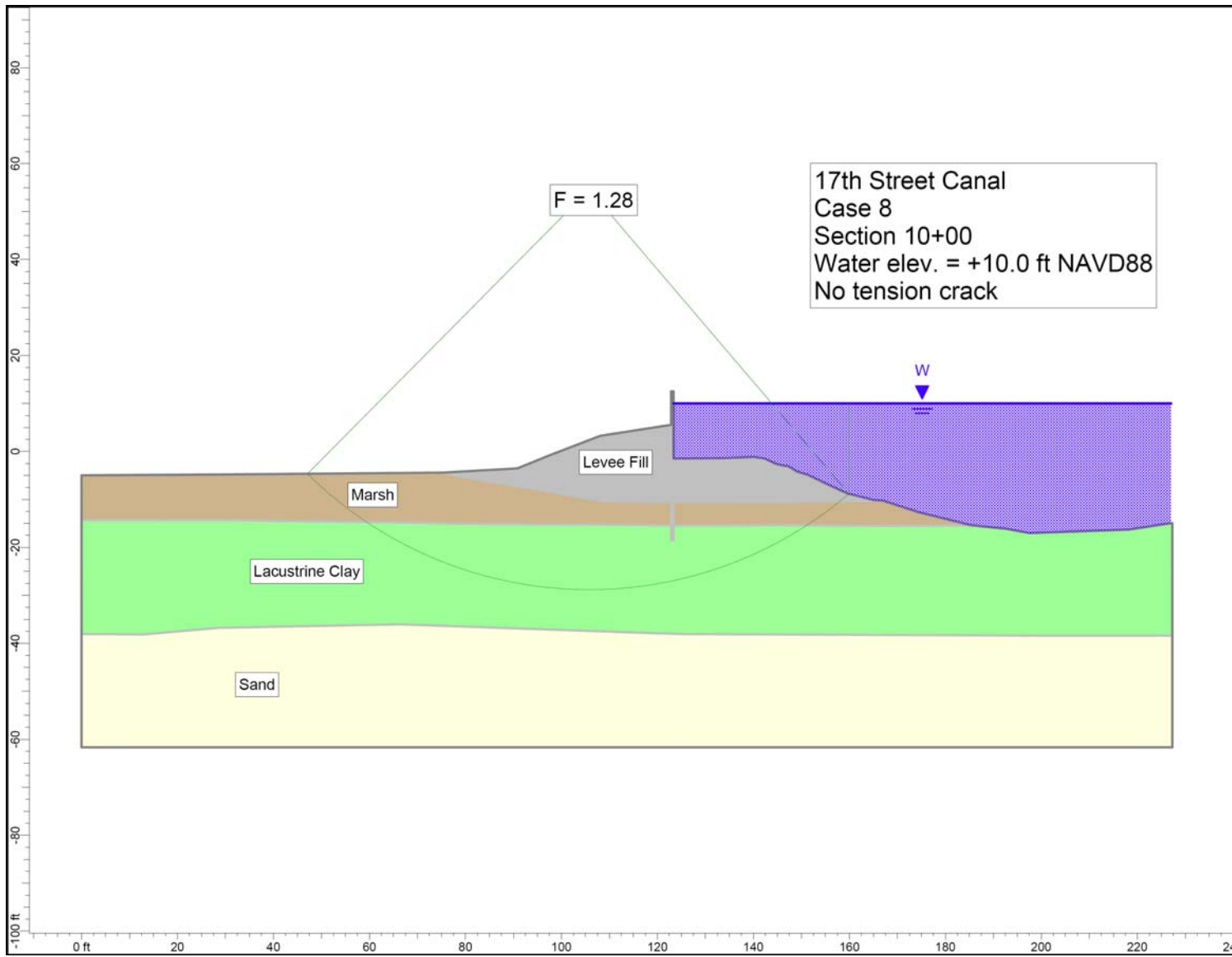


Figure 4-8. Critical Circle for 17th Street Canal Station 10+00 – Water Elevation 10 ft, No Tension Crack

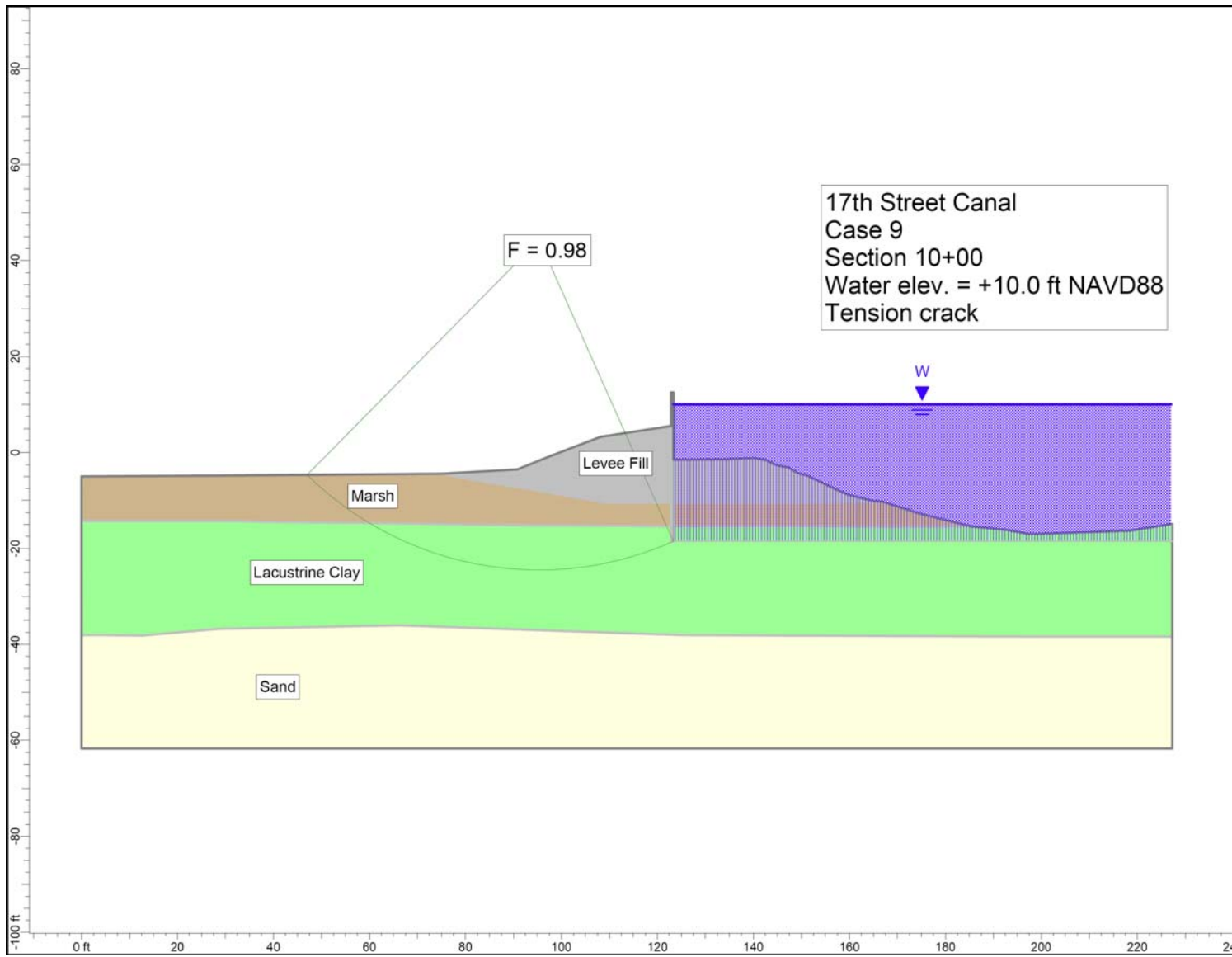


Figure 4-9. Critical Circle for 17th Street Canal Station 10+00 – Water Elevation 10 ft, Tension Crack

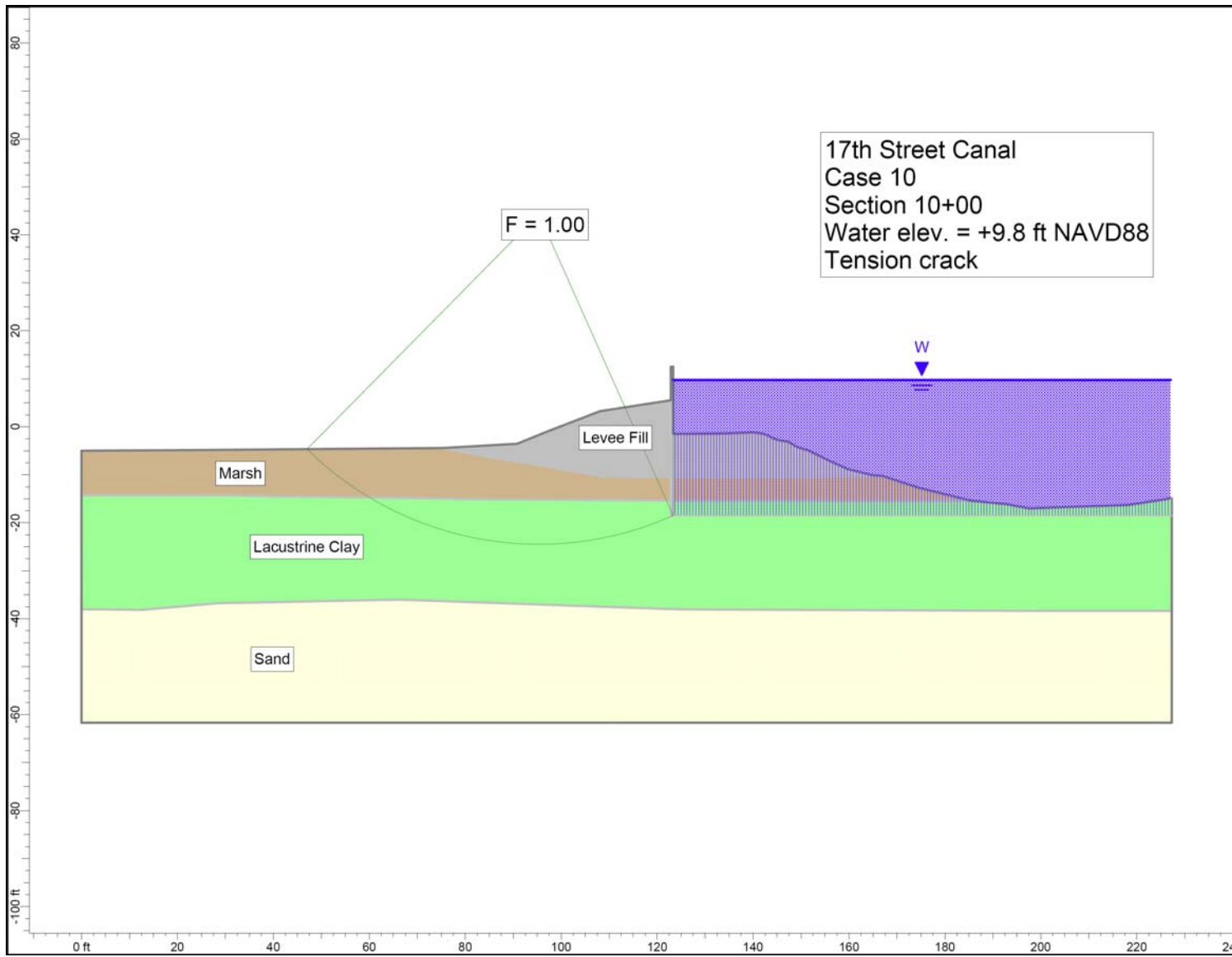


Figure 4-10. Critical Circle for 17th Street Canal Station 10+00 – Water Elevation 9.8 ft, Tension Crack

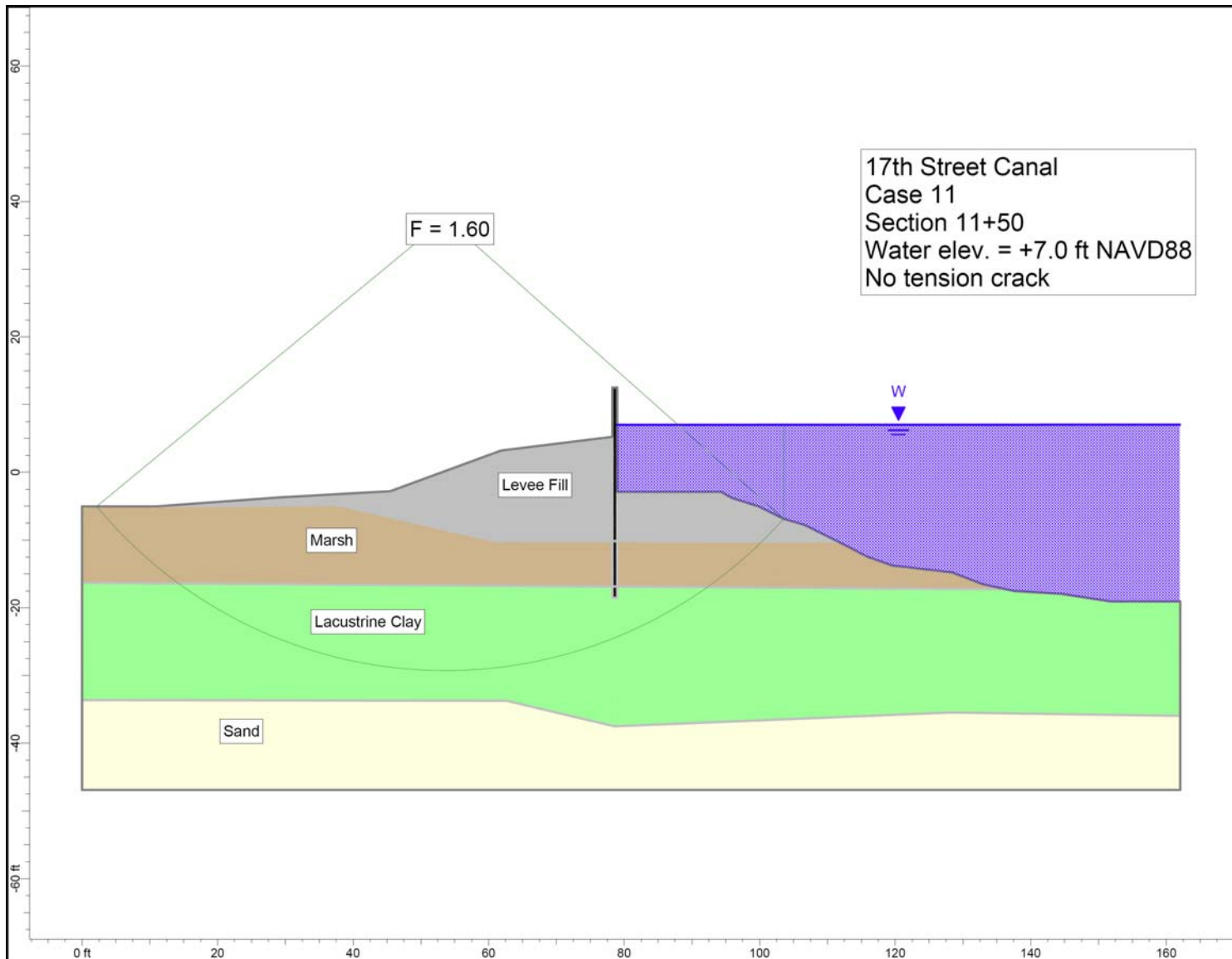


Figure 4-11. Critical Circle for 17th Street Canal Station 11+50 – Water Elevation 7 ft, No Tension Crack

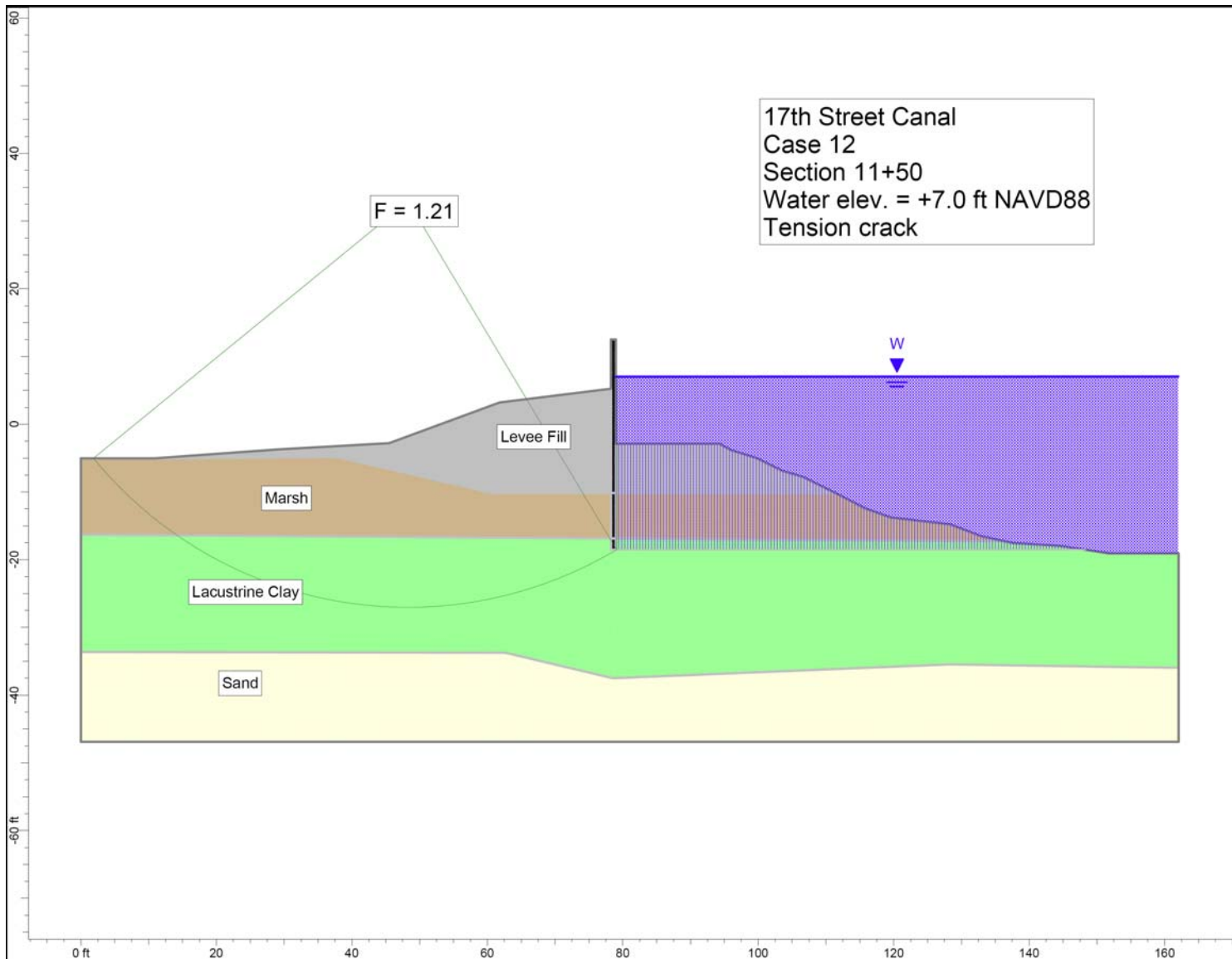


Figure 4-12. Critical Circle for 17th Street Canal Station 11+50 – Water Elevation 7 ft, Tension Crack

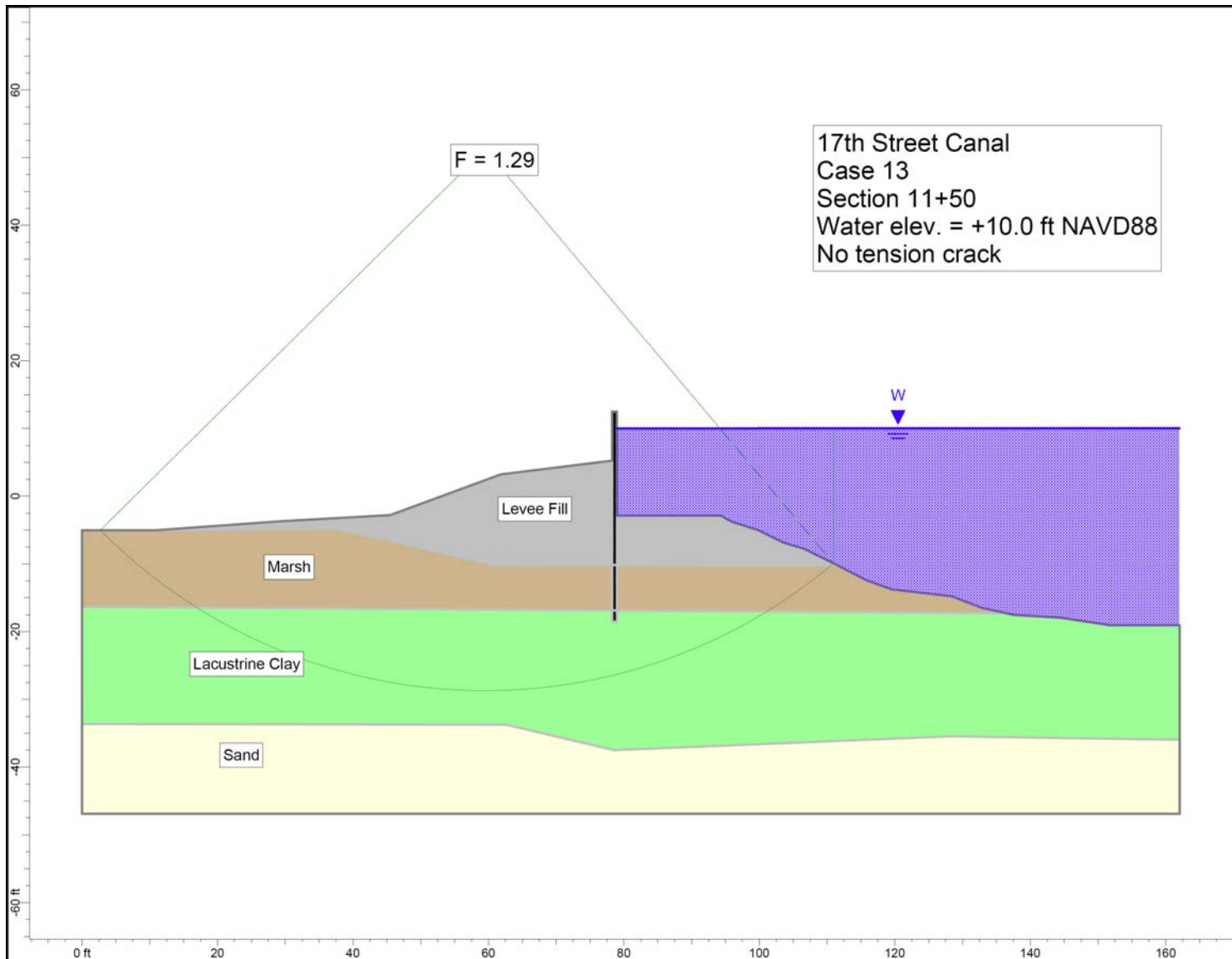


Figure 4-13. Critical Circle for 17th Street Canal Station 11+50 – Water Elevation 10 ft, No Tension Crack

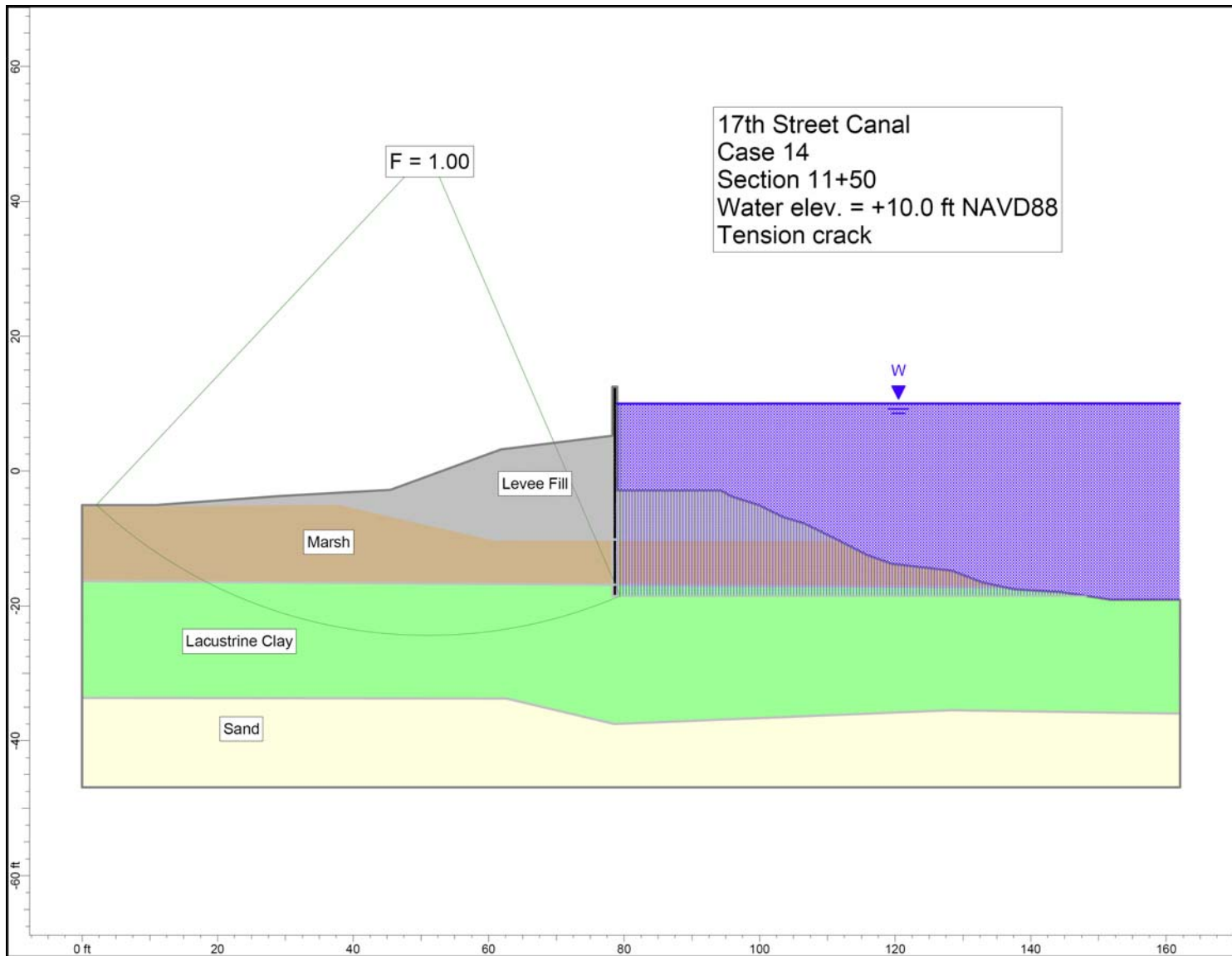


Figure 4-14. Critical Circle for 17th Street Canal Station 11+50 – Water Elevation 10 ft, Tension Crack

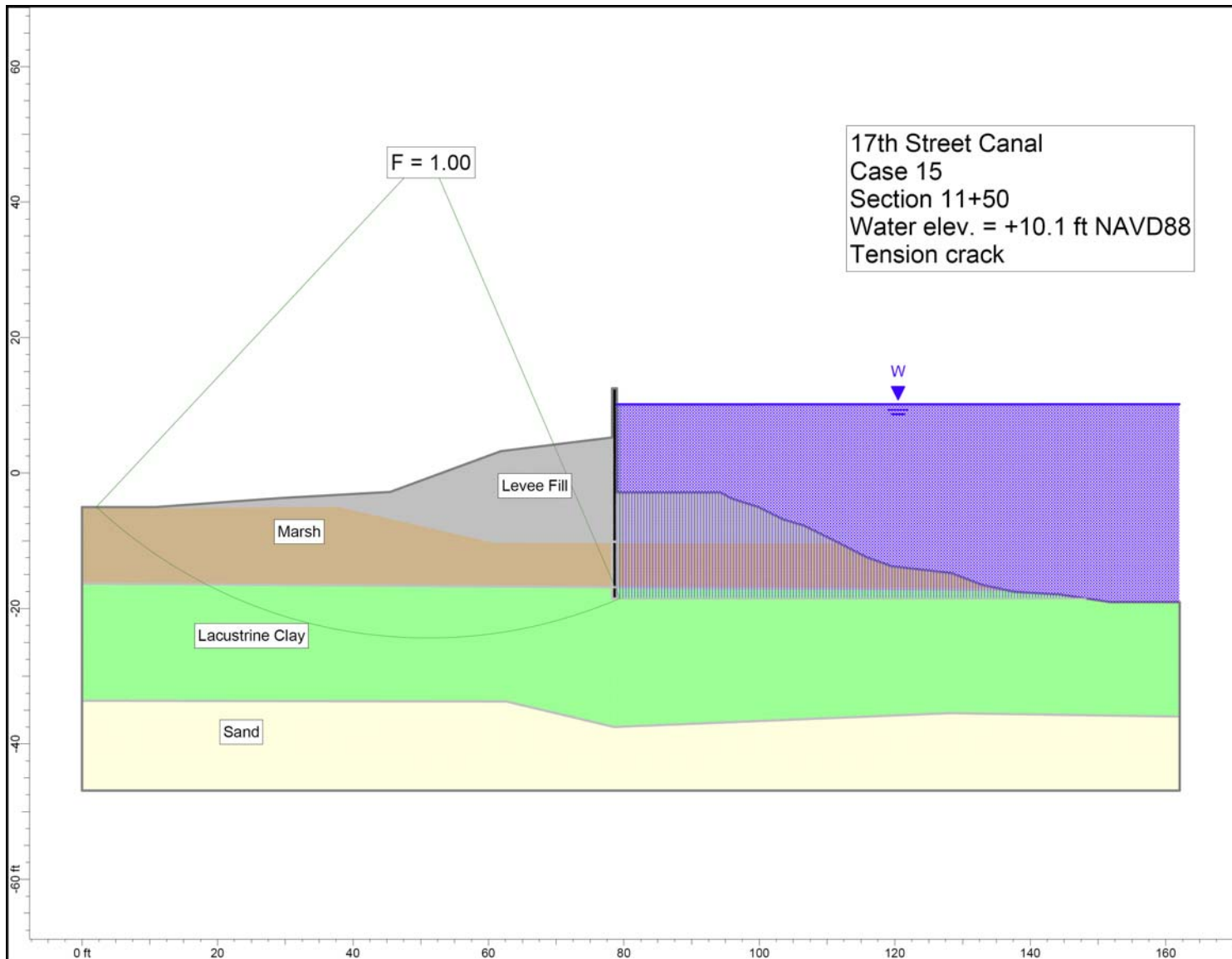


Figure 4-15. Critical Circle for 17th Street Canal Station 11+50 – Water Elevation 10.1 ft, Tension Crack

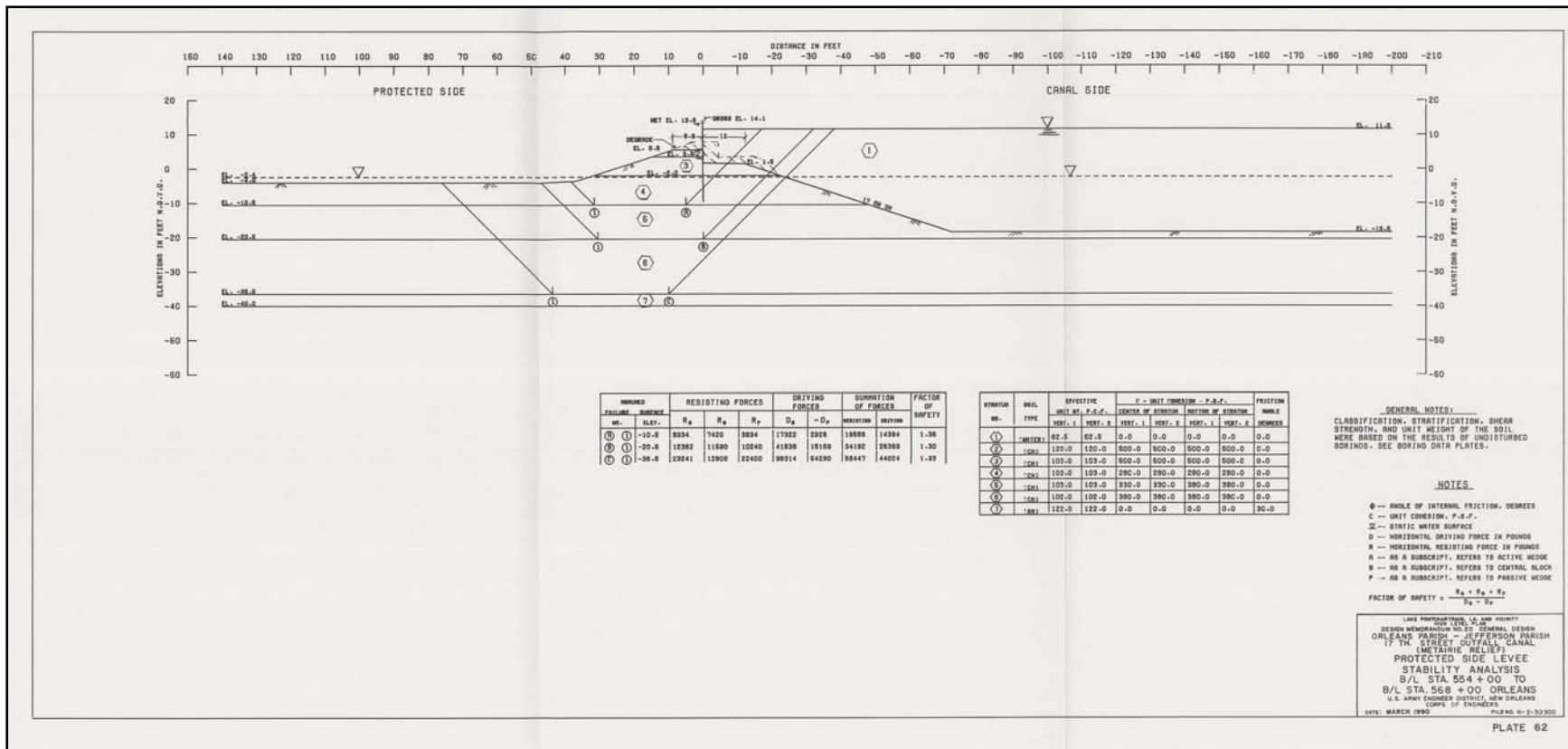


Figure 4-16. Design Cross Section, from GDM 20, Plate 62

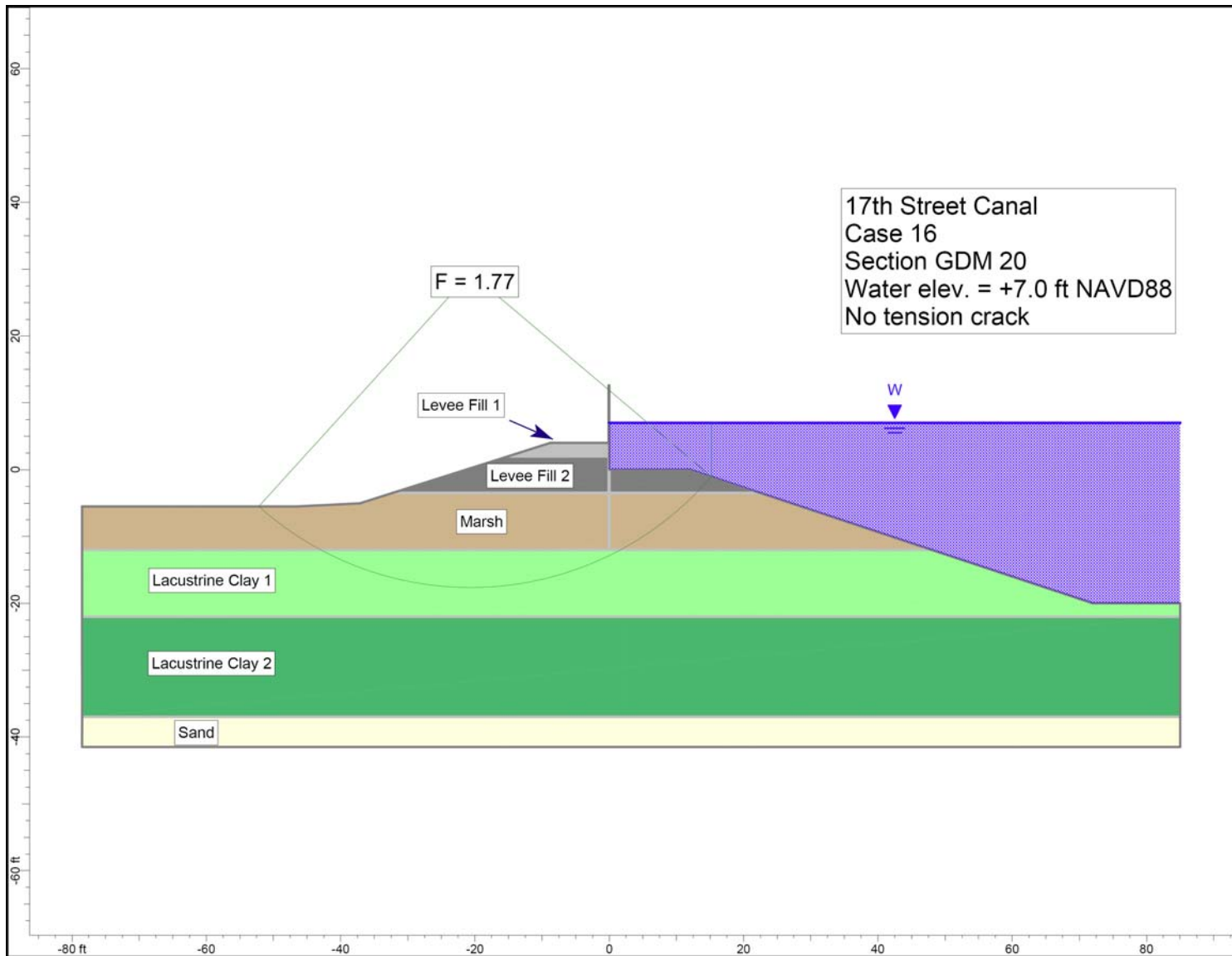


Figure 4-17. Critical Circle for 17th Street Canal Design Cross Section – Water Elevation 7 ft, No Tension Crack

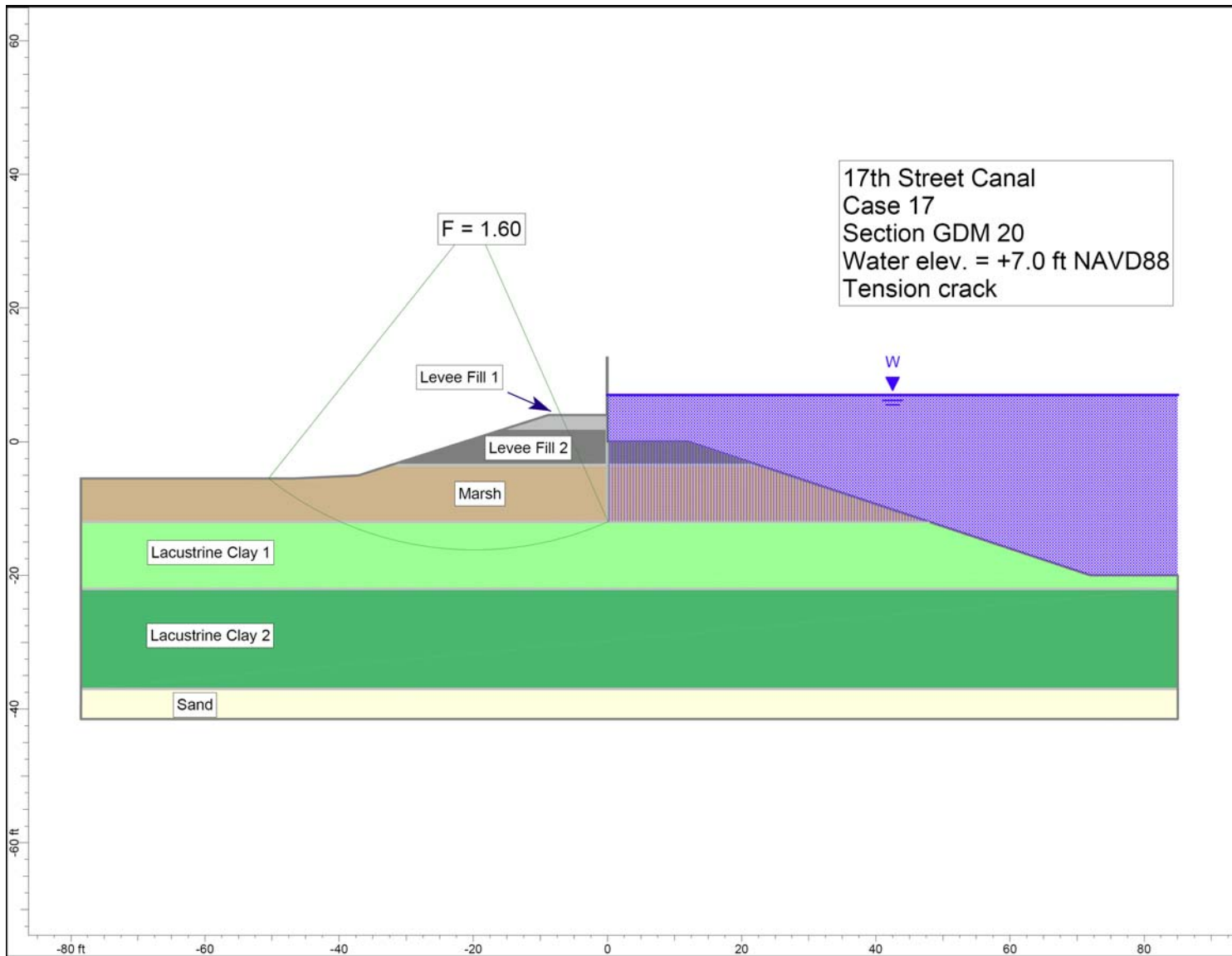


Figure 4-18. Critical Circle for 17th Street Canal Design Cross Section – Water Elevation 7 ft, Tension Crack

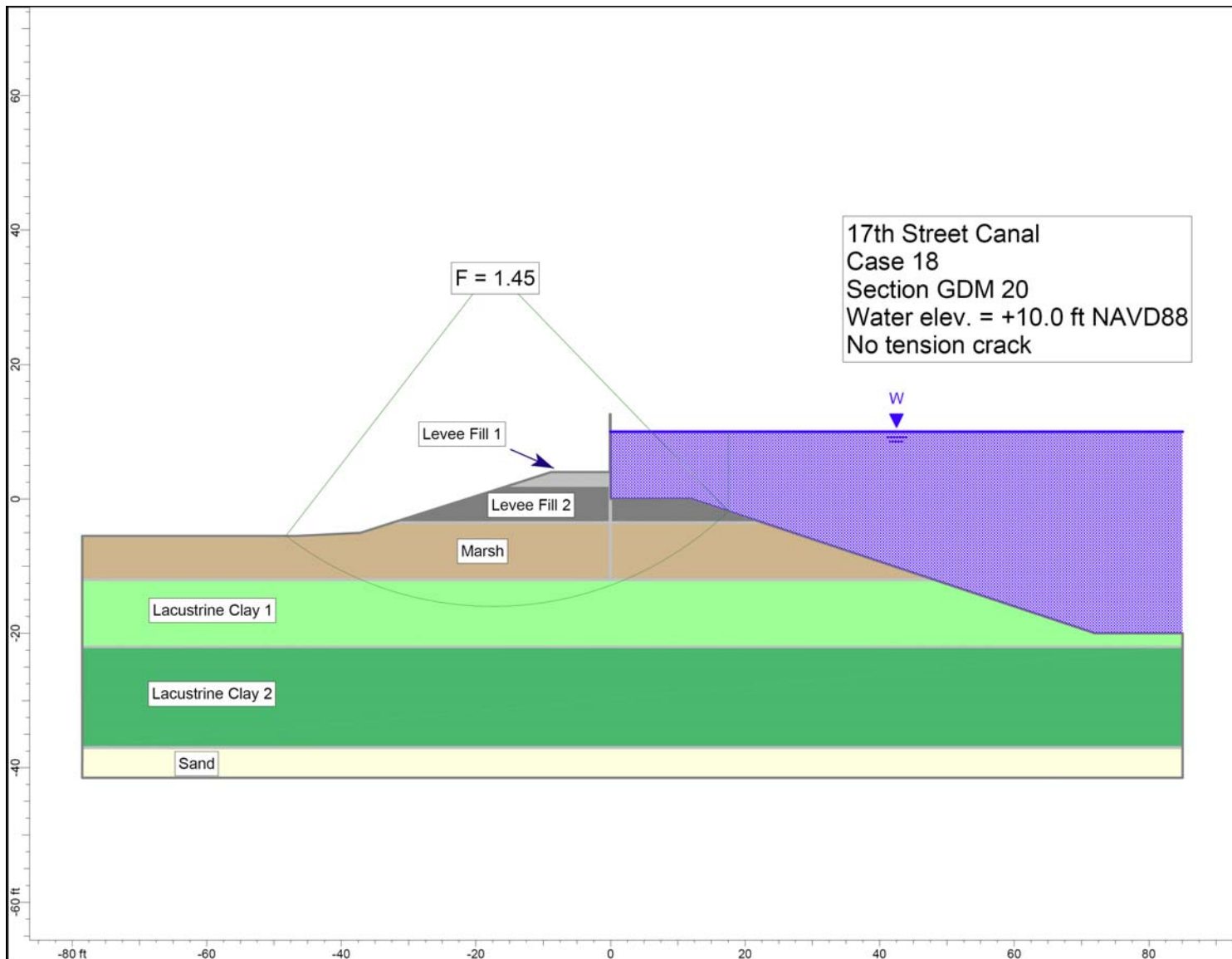


Figure 4-19. Critical Circle for 17th Street Canal Design Cross Section – Water Elevation 10 ft, No Tension Crack

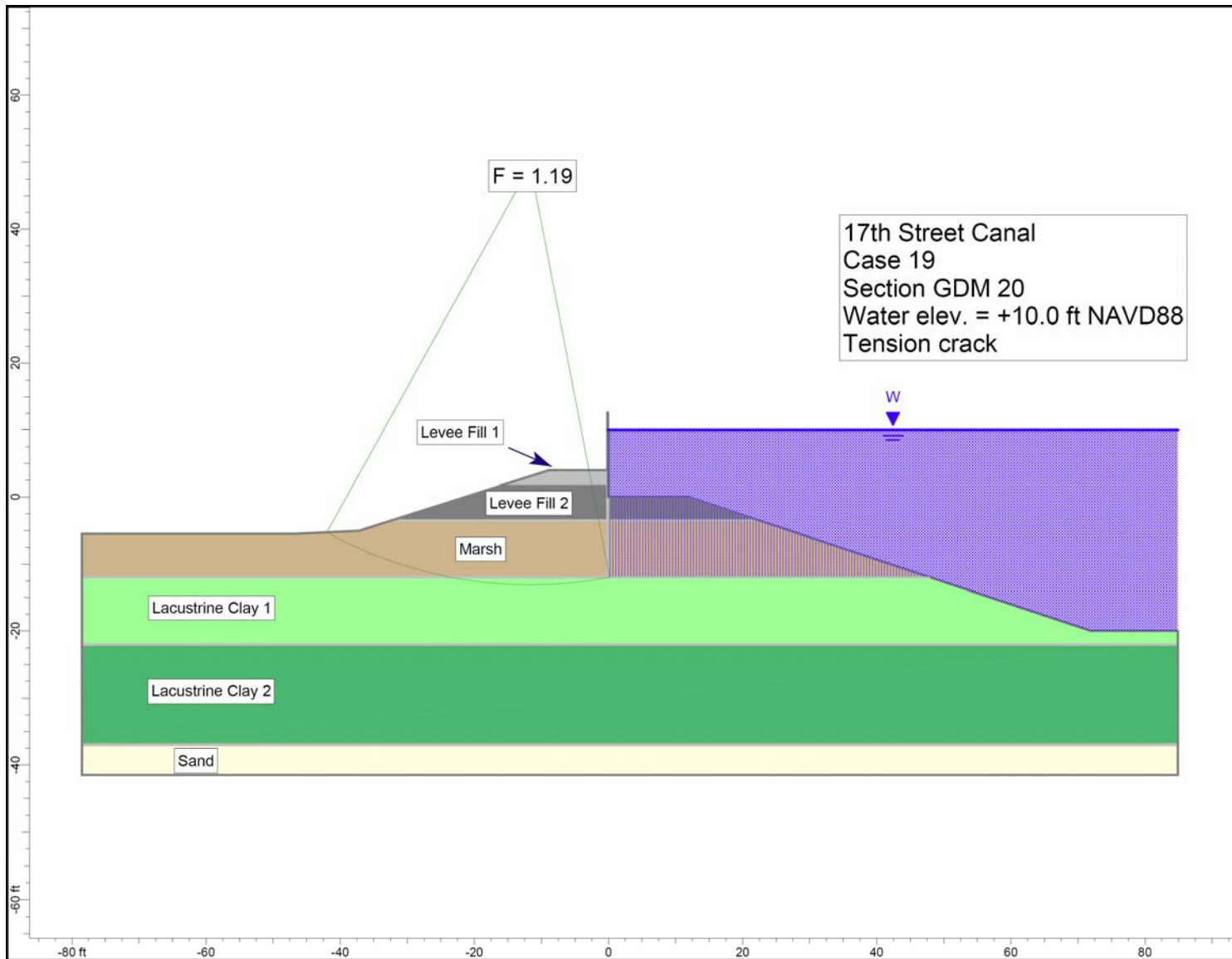


Figure 4-20. Critical Circle for 17th Street Canal Design Cross Section – Water Elevation 10 ft, Tension Crack

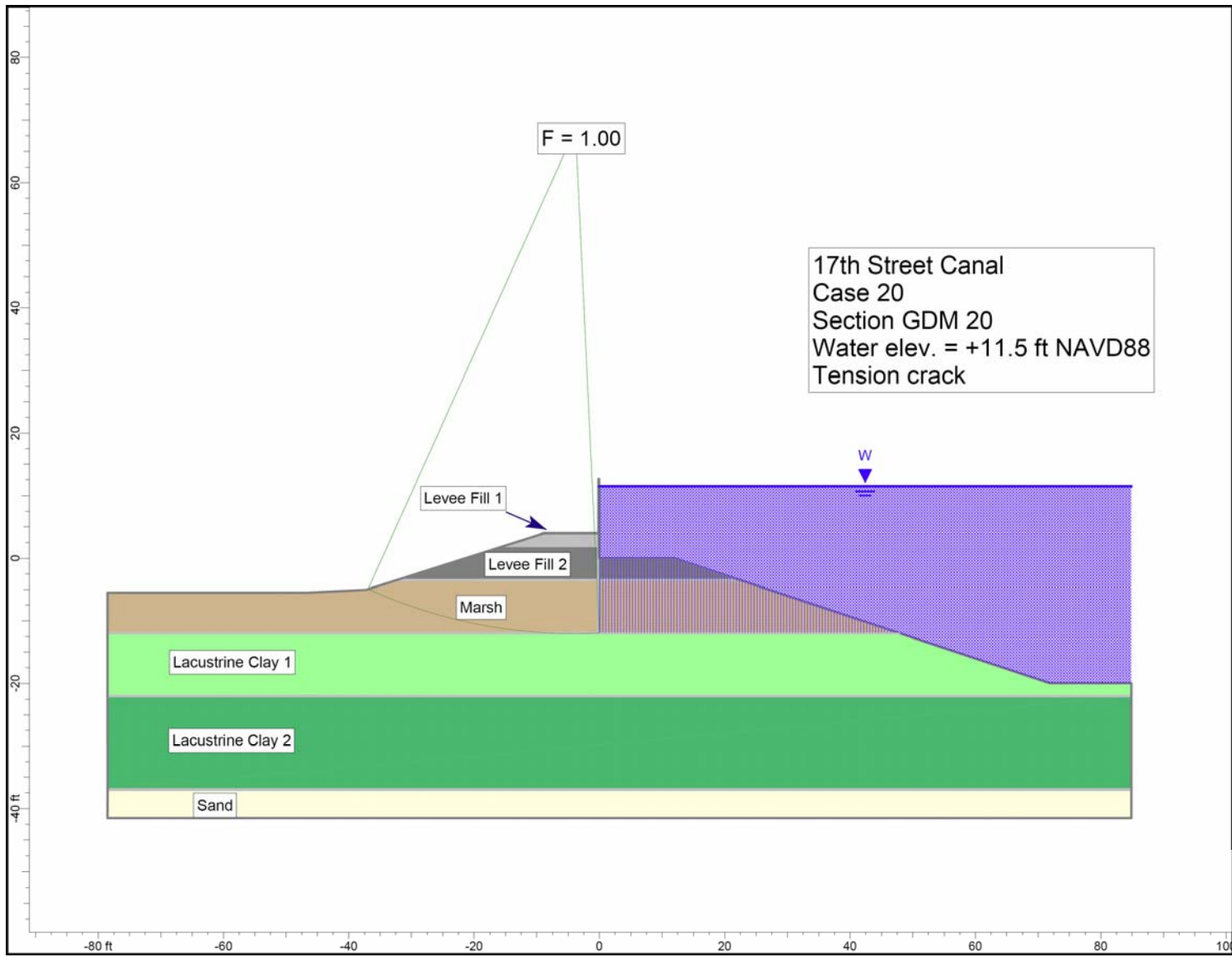


Figure 4-21. Critical Circle for 17th Street Canal Design Cross Section – Water Elevation 11.5 ft, Tension Crack

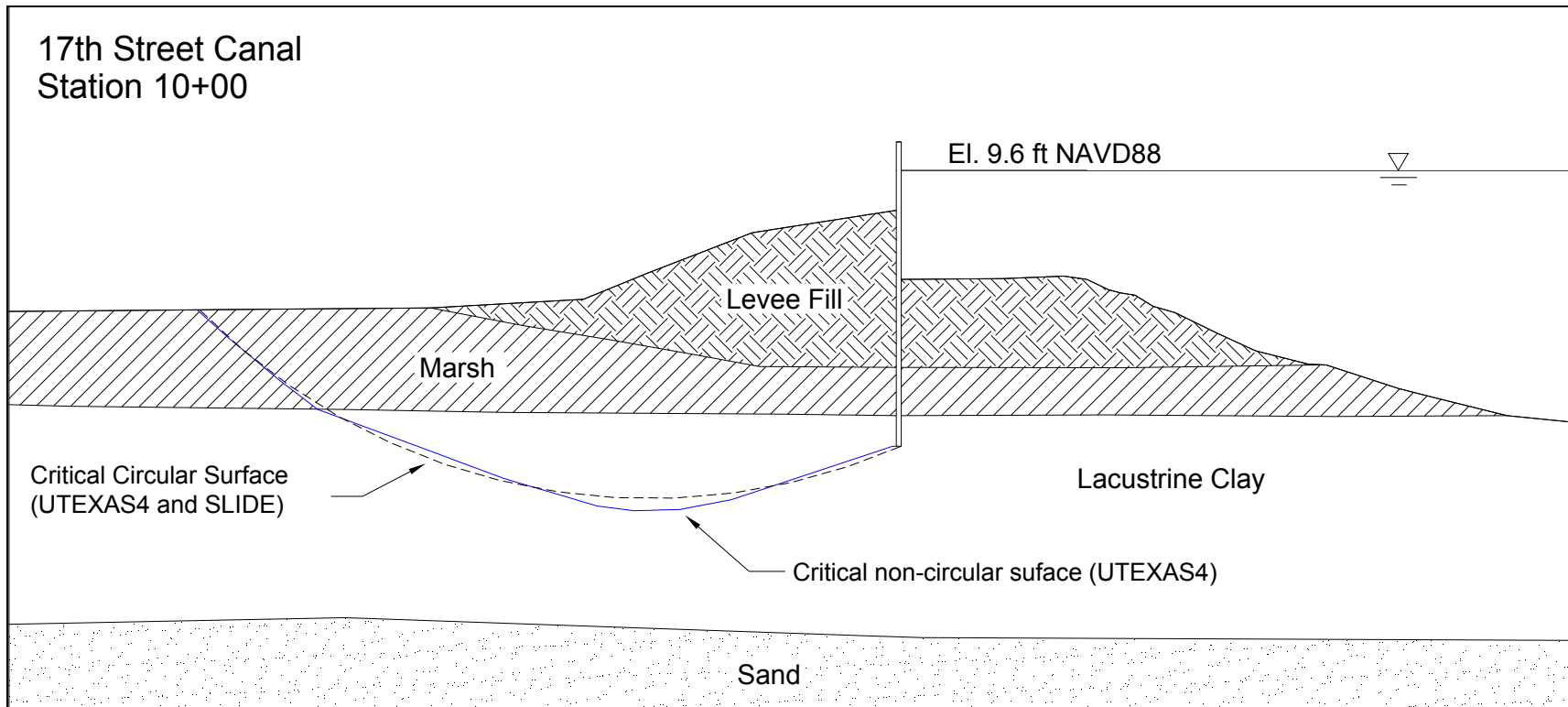


Figure 4-22. Critical Circular and Noncircular Slip Surfaces for 17th Street Canal, Station 10+00, Fully Cracked Condition

Appendix 5

IPET Centrifuge Model Test Report

Executive Summary

The physical (centrifuge) models of the levees on 17th Street, London Avenue, and Orleans canals provided detailed insights into the mechanisms that led to the breaches in the outfall canals in the city. In this section of the report, the contribution of the centrifuge models towards the overall understanding of the performance of the outfall canal levees is presented.

Using a centrifuge is a well-established technique for scale modelling of geotechnical phenomena and many facilities, large and small, exist around the world. The application of centrifuge modelling to the New Orleans levees has been described in detail in earlier reports in this series and will not be repeated here, although a general description is provided to assist the discussion of the results. The centrifuge models were carried out at ERDC, Vicksburg, MS, and at RPI, Troy, NY, with technical support from engineers at GeoDelft in the Netherlands, and from consultants at Steedman & Associates in the UK.

The scale models of the levees relied on the same information used for the numerical modelling of the levee performance, typically the cross sections of the levees at the breach locations and the mechanical properties of the levee material, the floodwall and underlying deposits of sand, swampy marsh and clay. A summary of the scale model tests carried out for this investigation is presented below, together with a summary of relevant material properties and dimensional information.

Two mechanisms were observed in the scale models that could lead to breach, both of which stemmed from a water-filled crack which formed in front of the flood wall as the water in the canal rose above the level of the levee. Depending on the foundation conditions and geometry of the flood wall and levee shoulders, the crack either led to a rotation of the flood wall landward with uplift and sliding on the top of the sand towards the landward toe of the levee, or to a translational (sliding) failure in the clay layer commencing from the bottom or toe of the flood wall. In other circumstances, no failure ensued and comparisons can therefore be drawn between the conditions that led to failure and those that did not.

These mechanisms and the supporting evidence from the scale models are described in the following sections using data from the model tests to explain how the mechanism was initiated and the sequence of events that followed.

Principles of Centrifuge Modeling

The use of a centrifuge is necessary to correct the distortion introduced in a scale model of a geotechnical field problem constructed ‘on the laboratory floor’. As the behaviour of soil is stress dependant, it is crucial in studying the performance of a geotechnical system such as the New Orleans levees to ensure that the correct stresses are applied to each element in the levee and foundation. This is difficult to achieve in a scale model under earth’s gravity alone as the weight of the model is not sufficient to bring the soil to the correct state. In a centrifuge, however, a model such as shown in Figure 5.1 at a scale of $1/N$ can be subjected to a steady acceleration field equivalent to N times earth’s gravity. In this state, the same stress conditions as exist in the field can be effectively reproduced at all points in the model. An event such as rising water leading to the onset of foundation failure in a levee system can then be modelled in a highly realistic manner. Detailed information can be collected during the model test including measurements of water pressure in the ground at different locations, the movement of the flood wall and ground surface, and video imagery of the sequence of events. The history of centrifuge modelling and explanation of scaling principles is available in the literature. A detailed description of the principles of centrifuge modelling and its application to the model tests carried out for this investigation was presented in an earlier report, and is not repeated here.

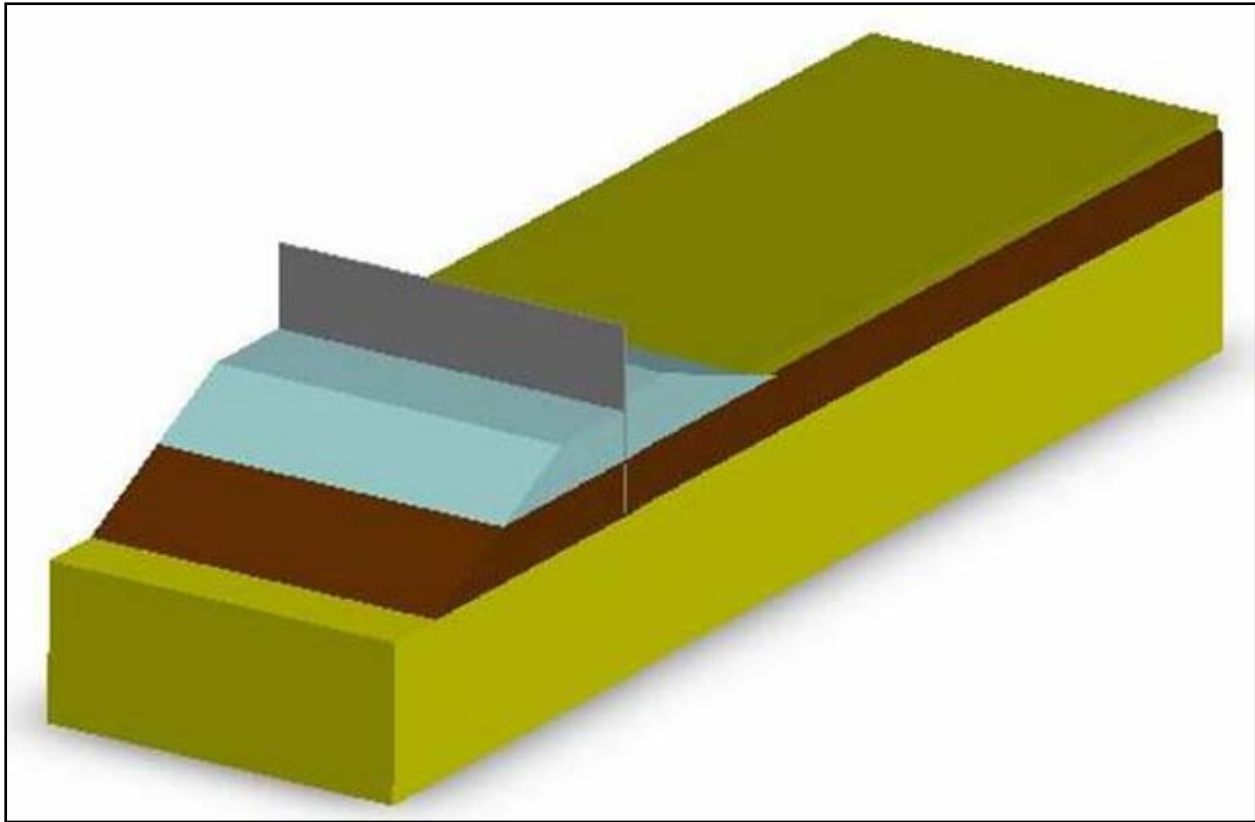


Figure 5-1. Typical geometry of scale model test (canal on the left hand side)

Summary of Model Tests

Model tests were carried out using the Army Centrifuge at ERDC, Vicksburg and at RPI, Troy. Table 5.1 summarises the models completed for this investigation.

Table 5-1 Model Tests completed for IPET			
Levee profile	Research center	Foundation	Mechanism
London North	ERDC	Swampy marsh over sand	Rotational failure of wall
London North	RPI	Swampy marsh over sand	Rotational failure of wall
London South	ERDC	Swampy marsh over sand	Rotational failure of wall
London South	RPI	Swampy marsh over sand	Rotational failure of wall
17th Street	RPI	Swampy marsh over clay	Translational failure in clay layer
17th Street	ERDC	Swampy marsh over clay	Translational failure in clay layer
17th Street	ERDC	Swampy marsh over clay	Translational failure in clay layer
Orleans South	RPI	Swampy marsh over sand	No failure
Orleans North	ERDC	Swampy marsh	No failure

The model tests generated large volumes of data for analysis. It was evident that in all cases failure of the levees was presaged by the opening of a water filled crack on the canal side of the

levee, which allowed full hydrostatic pressure to act on the flood wall over its entire submerged height. The flood water in the centrifuge models was raised steadily, without wave effects, and it was observed that once a crack had opened, then in the cases of London Avenue and 17th Street canal models, a failure soon followed, either by rotation of the flood wall (London Avenue) and uplift (sliding) on the top of the sand layer or by translational failure (sliding) in the clay stratum (17th Street), originating at the bottom (toe) of the sheet pile wall.

In this report, these data are used to illustrate the mechanisms of failure observed in the models, and to draw conclusions concerning the onset of failure in the field. Analysis of the mechanisms of failure provides insights into the Factor of Safety (FoS) as the water levels in the canals rise.

Material Properties

The levee and foundation in all of the models was constructed using three materials: sand, and clay to represent the natural sand, soft lacustrine clay and levee clay and natural material from the field to represent the swampy marsh deposits.

The sand used in all the models was a fine laboratory sand (Nevada sand), which is well characterized as a result of its widespread use by different research laboratories. Nevada sand has a specific gravity of 2.67 and maximum and minimum dry densities of 17.33 kN/m^3 and 13.87 KN/m^3 respectively at corresponding minimum and maximum void ratios of $e_{\min} = 0.511$ and $e_{\max} = 0.887$. The permeability of Nevada sand in a medium dense state is around $5.6 \times 10^{-5} \text{ m/sec}$ and its mean grain size (D_{50}) is 0.15mm.

The material selected to model the soft normally consolidated 'lacustrine' clay stratum and the stiffer clay that forms the levees was a speswhite kaolin clay, widely used in geotechnical research laboratories. Kaolin is coarse grained clay with a Specific Gravity of 2.58. For normally consolidated or lightly overconsolidated clays the ratio of undrained strength S_u to the effective overburden stress S_u/σ'_v has been shown empirically to lie in the range 0.2-0.25, and for kaolin clay a value of 0.22 is typical. For overconsolidated clays, this ratio depends on the overconsolidation ratio and is larger.

The water content, w at the Liquid Limit (LL) and Plastic Limit (PL) of the clay used in these model tests was measured using the Fall cone method (following BS1377) as 70% and 33% respectively, giving a Plasticity Index (PI) of 37%. The Fall cone method was used to determine the LL in preference to the percussion cup method (following ASTM) as, being a strength test, it enables a theoretical relationship between water content and undrained shear strength S_u to be derived directly. This was used in the model testing to help confirm the initial condition of the clay layer and levee.

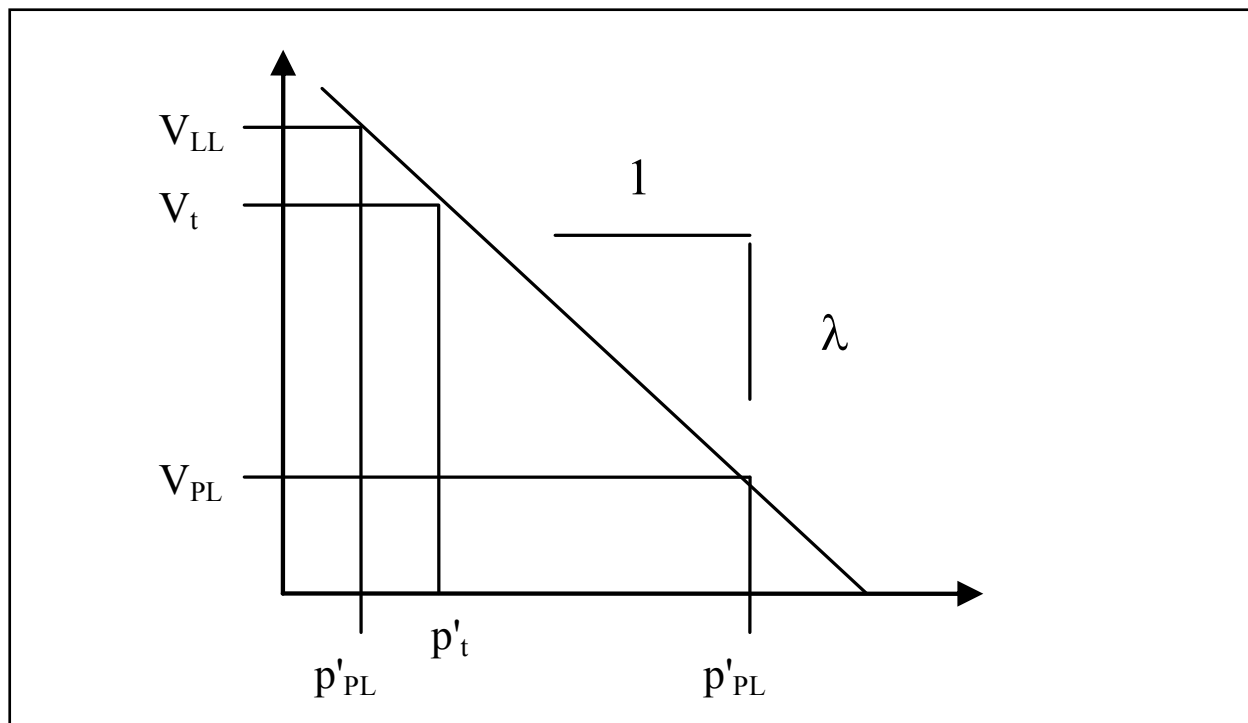


Figure 5.2. Normal consolidation curve in $V - \ln p'$ space

Assuming that the undrained shear strength S_u at a mean effective confining stress, p'_t may be related at the water content w_t via the Specific Volume (V) by a log-linear relation (Figure 5.2) of the form:

$$p'_{PL} / p'_t = (S_u)_{PL} / (S_u) = \exp [(V_t - V_{PL}) / \lambda]$$

where the subscript $_{PL}$ refers to the Plastic Limit, V is the Specific Volume and λ is the slope of the (linear) normal consolidation line in $V - \ln p'$ space, Figure 5.2, then λ may be deduced from the Plasticity Index, noting that

$$V = 1 + e = 1 + wGs$$

and

$$w_{LL} - w_{PL} (\%) = (\lambda / Gs) \ln R = PI / 100$$

where $e (= wGs$ for fully saturated soil) is the void ratio, R is the ratio between the strength of the clay at the plastic limit and the liquid limit and is related to the characteristics of the clay. This provides a relationship between the moisture content of the clay and the undrained shear strength, which is consistent with the empirical approach based on strength ratio S_u / cv' outlined above.

The saturated unit weight of kaolin at a moisture content of around 43% is 109 pcf (17.1 KN/m³).

The model tests used bulk samples of the natural material from the field to represent the swampy marsh stratum in the foundation of all the levee models. Undisturbed samples taken from borings have provided laboratory samples from which compression tests, moisture content and unit weights have been determined. These are reported elsewhere in this report. The saturated unit weight of peat was taken as 80 pcf (12.6 KN/m³), consistent with the slope stability analyses. Site investigation reports show that the unit weight of the swampy marsh is variable, from a low of around 65 pcf (10.2 KN/m³) to a high of around 80 pcf (12.6 KN/m³). The stiffness of the swampy marsh varies but consolidated undrained direct simple shear laboratory tests on samples taken from the 17th Street breach area suggest that a value of Shear Modulus, $G/\sigma_v' \approx 10$, where σ_v' is the initial vertical effective stress may be appropriate for strains up to 2-3%.

In the field, the concrete flood wall is supported by a steel sheet pile wall that passes through the levee, terminating at a variable elevation. In the model tests, this wall element was scaled using an aluminium or steel plate, with a bending stiffness comparable to the bending stiffness of the sheet pile wall. A solid plate was used in the model tests as there was no evidence from the walls in the field that water leakage through the sheet piles was significant in the early stages of wall movement.

Further details of each of these materials, how they were used and placed in the models and the techniques for controlling their strength and stiffness with depth were reported in Report 2 of this series.

Establishing Initial Conditions

All centrifuge models completed for this study fall broadly in one of two categories: those with a clay sub-stratum (e.g 17th Street) and those with a sand layer beneath the swampy marsh (e.g. London Avenue). In each case, it was necessary to confirm that the correct initial conditions had been established prior to the flood stage.

In the sand models, seepage under the levee was driven by a differential head between the water in the canal and the ground water table on the landward side. Over time in the field, a steady state ' flownet ' will develop governing the excess water pressure or head at different locations under the levee. Figure 3 shows a steady state flownet (calculated using the software programme SEEP-W) compared to piezometric head levels measured by pore pressure transducers at different locations under the levee at around the same depth in the sand.

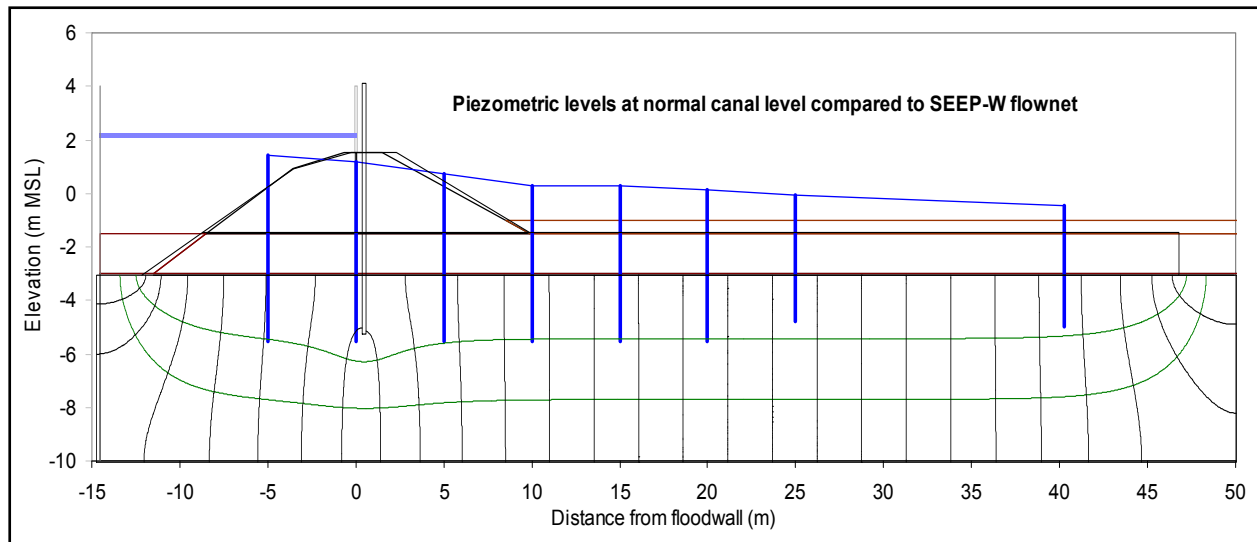


Figure 5.3. London south model, flownet and piezometric levels at different locations, typical canal level

The early stages of water rise in the model tests in all cases were characterised by rising water pressures in the soil layers beneath the levee. This was most apparent in the case of the London Avenue models, where the deep sand layer underlying the swampy marsh was connected hydraulically to the canal, and showed an immediate response as the canal water level changed, Figure 5.4.

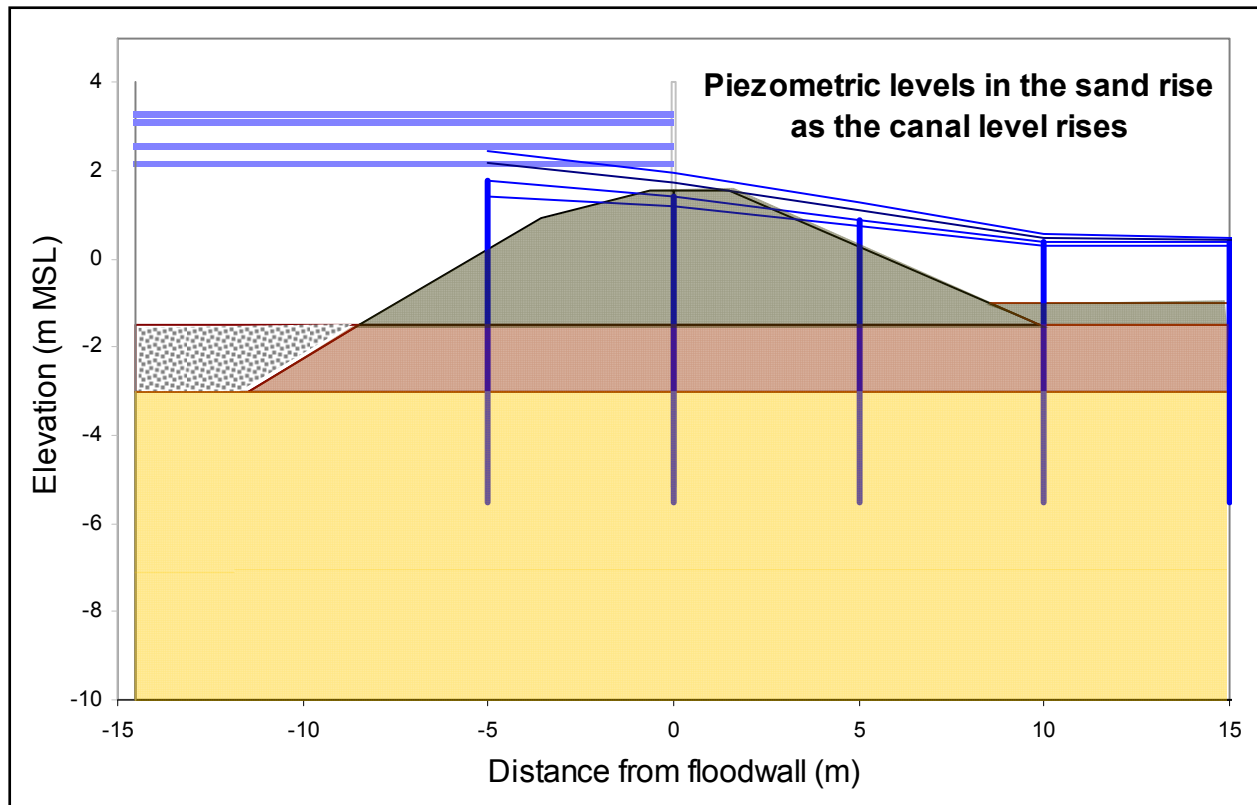


Figure 5.4. Rising canal levels lead to immediate rise in piezometric levels

In the sand layer, the increase of water pressure (head) was largest nearest to the canal and reduced with distance from the canal, landward. This is due to head loss in the sand layer as seepage through the sand layer developed from the flood side towards the land side drain and is seen clearly in the figures above.

The second class of centrifuge model was the clay models, simulating the ground profile below the 17th Street levee. Establishing initial conditions in the peat and clay layers requires confirmation that the swampy marsh and clay layers have reached a stress state comparable to that in the field. This is achieved by a process of consolidation in the centrifuge over time, using self weight and surcharging, to bring the clay forming the levee, the foundation sub-stratum and the shallow swampy marsh deposits into their required condition.

The consolidation process for a layer with vertical (one-way) drainage may be analysed using parabolic isochrones in the standard way. Two stages of consolidation are observed, Stage 1 and Stage 2, as the excess pore water pressures drain over time and a total stress increment is transferred from the pore water to the soil skeleton. The two stages are illustrated in Figure 5.5, which shows how excess pore water pressures at different depths through the layer decay with time, returning to a simple hydrostatic profile towards the end of the consolidation process. The units are at model scale as these are the units used to monitor the progress of the experiment. The length of time required for consolidation is independent of the stress increment.

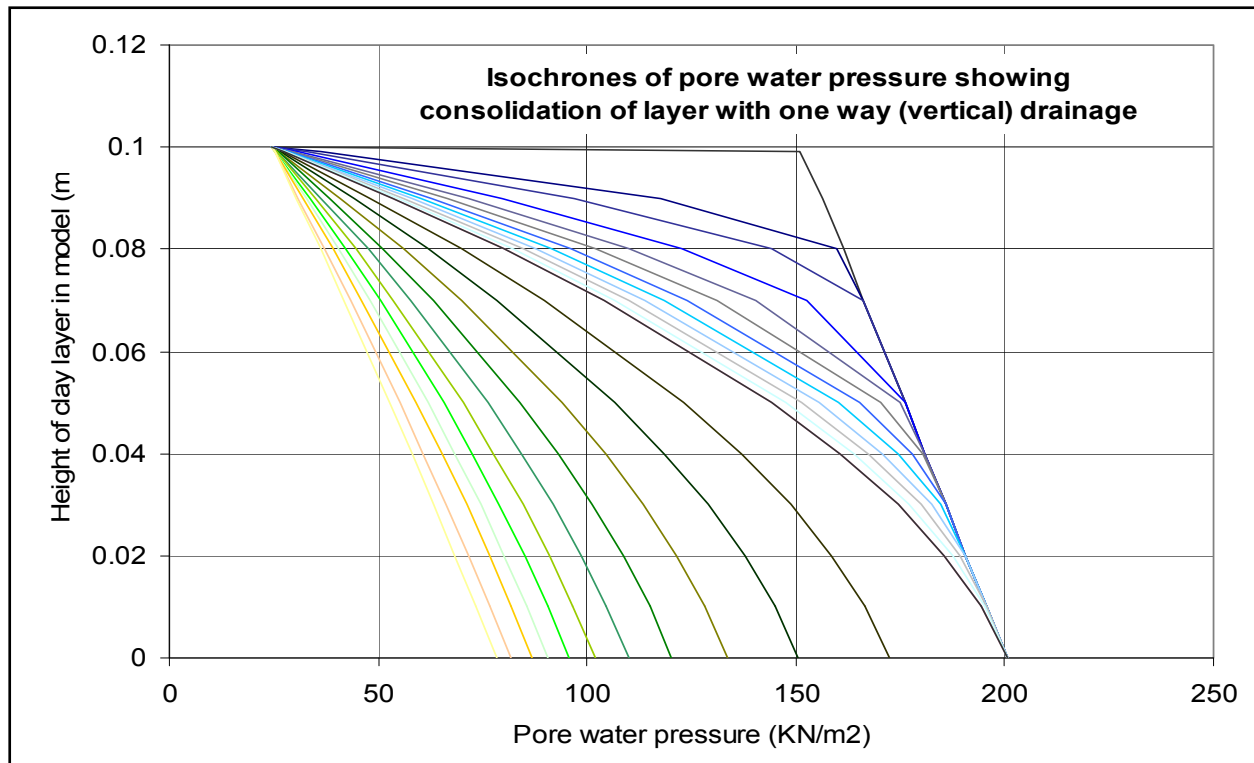


Figure 5.5. Theoretical isochrones for a clay layer in model units, draining upwards

Plotting the pore water pressure at different depths over time gives a prediction of the decay in pore water pressure at different depths which can be used to compare with the experimental data during the initial stage. For the clay layer beneath the levee and for the swamp marsh the actual and predicted time histories of pore water pressure dissipation are shown in Figures 5.6 and 5.7 for two typical models, confirming that consolidation has been achieved and the initial conditions for the soil beneath the levee were established.

In both model and field conditions with a clay substratum layer, the flooding of the canal is too rapid a process to permit drained behaviour of the clay to take place, and hence the process may be considered as an undrained event. As water levels in the canal rise, the pore water pressures in the clay also rise due to the increase in total stress (the weight of the water in the canal) and not due to seepage, as in the sand foundation. Over time, if the canal water levels were held at a high water level then drainage would take place and the original profile of effective stress would ultimately be re-established. In practice, there was no time for drainage to take place and the models reflect this behaviour, exactly as in the field conditions. Figure 5.8 shows the rise in pore water pressure at four locations in the clay layer beneath the levee on the canal side as the canal water level is raised. The exact correspondence confirms that the clay layer is responding in an undrained manner, with the increment of total stress (due to the weight of water in the canal) exactly matched by the increment of pore water pressure, regardless of depth in the foundation, which means that the strength of the underlying clay is fully described by its undrained shear strength. (As the canal level rises higher, the additional load on the canal side of the levee will also alter the elastic stress distribution in the foundation beneath, and this adds a slight additional increment to the transducers under the levee shoulder.)

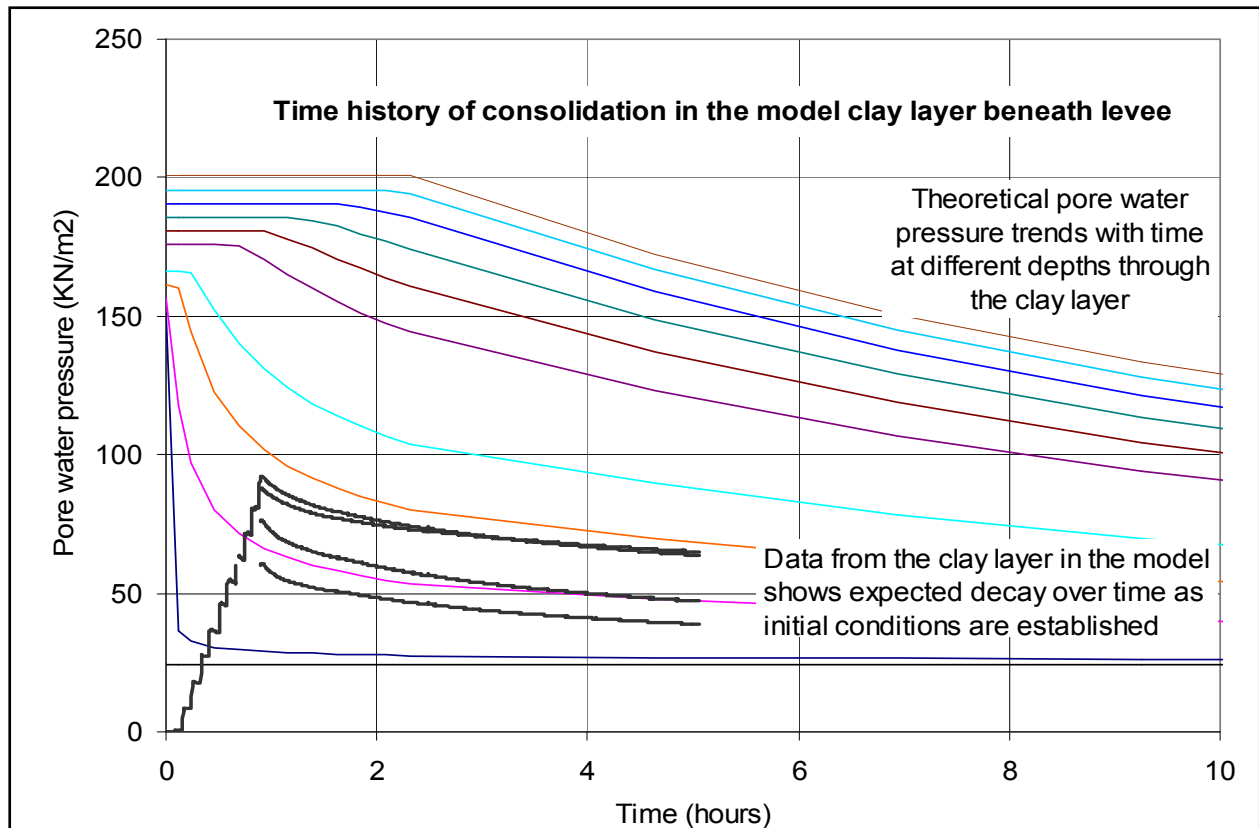


Figure 5.6. Trend of dissipating pore water pressure in the clay layer as initial conditions are established (time in model units)

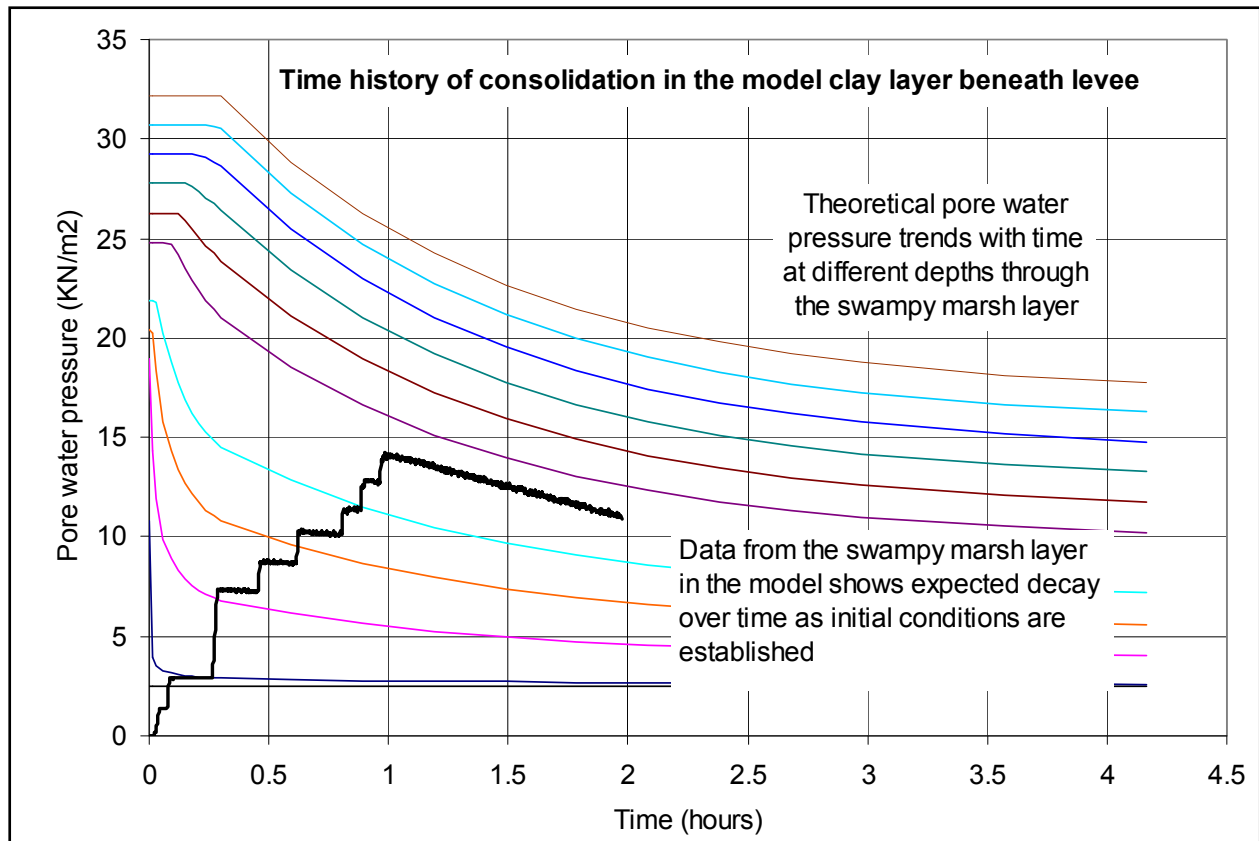


Figure 5.7. Trend of dissipating pore water pressure in the swampy marsh layer as initial conditions are established (time in model units)

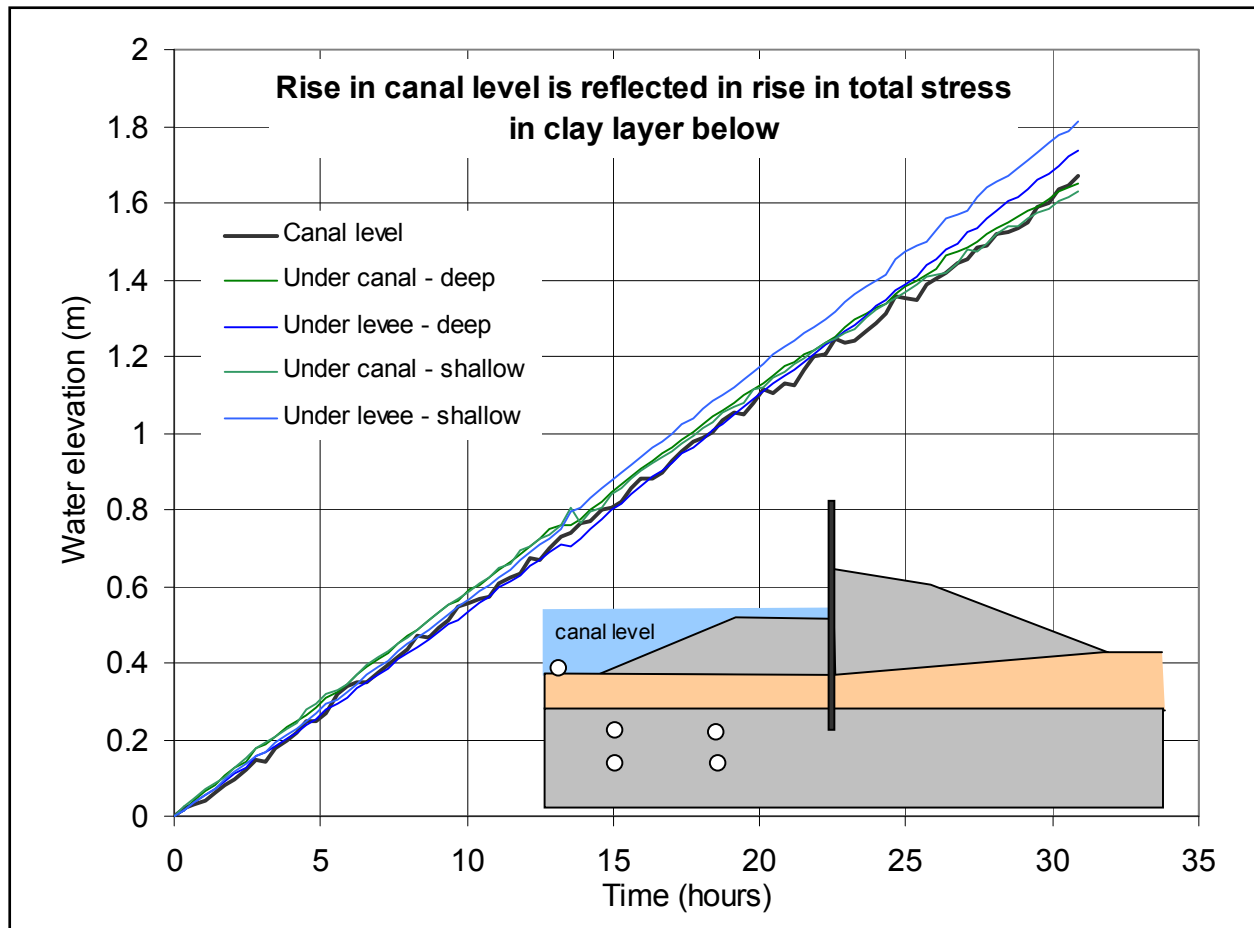


Figure 5.8. Water level in canal compared to incremental pore water pressure rise in clay layer beneath levee

Formation of a Water Filled Crack

In all of the centrifuge model tests on the London Avenue, 17th Street and Orleans levee profiles, with both sand and clay foundations, a crack or gap was observed to form on the flooded side of the flood wall once water had overtopped the canal side crest of the levee and the wall rotated slightly landwards. The gap permitted a full hydrostatic head of water to develop to the bottom of the crack, which in the case of the London South and North profiles, provided a hydraulic connection between the underlying sand layer and the canal above under the centre of the levee. In the case of the 17th Street profile, where the wall penetrated through the swampy marsh into the clay stratum beneath, the crack opened to near the toe of the wall. In the case of the Orleans South profile, where the wall did not penetrate through the swampy marsh layer, the swampy marsh continued to provide a hydraulic barrier to prevent high water pressures reaching the underlying sand.

The formation of the crack followed the rise in water level on the canal side. As the water level rose against the levee, the flood wall did not experience any increase in lateral load. Once the water reached the flood wall, however, a hydrostatic force started to build up on the wall,

pushing it landward. All of the flood walls in this study were un-propped (as in the field), and therefore the rising water on the flood wall is reacted by a small rotation of the wall, resisted by the embedment of the sheet pile wall, and the passive resistance of the levee material on the landward side of the flood wall.

In this condition, an un-propped wall is susceptible to the opening of a tension crack down the canal side of the flood wall which is immediately water filled.

The theoretical depth, z of a dry tension crack for an unpropped smooth wall retaining a cohesive clay material with undrained strength S_u , Figure 5.9, is simply derived following Rankine as:

$$z = (2 S_u - q) / \gamma$$

where q is a surcharge and γ is the unit weight of the clay. A similar depth of crack could occur through desiccation cracking. Where water is able to fill the crack and the clay responds in an undrained manner, the water is able to partially support the clay and the theoretical depth of the crack increases to:

$$z = (2 S_u - q) / (\gamma - \gamma_w)$$

where γ_w is the unit weight of water.

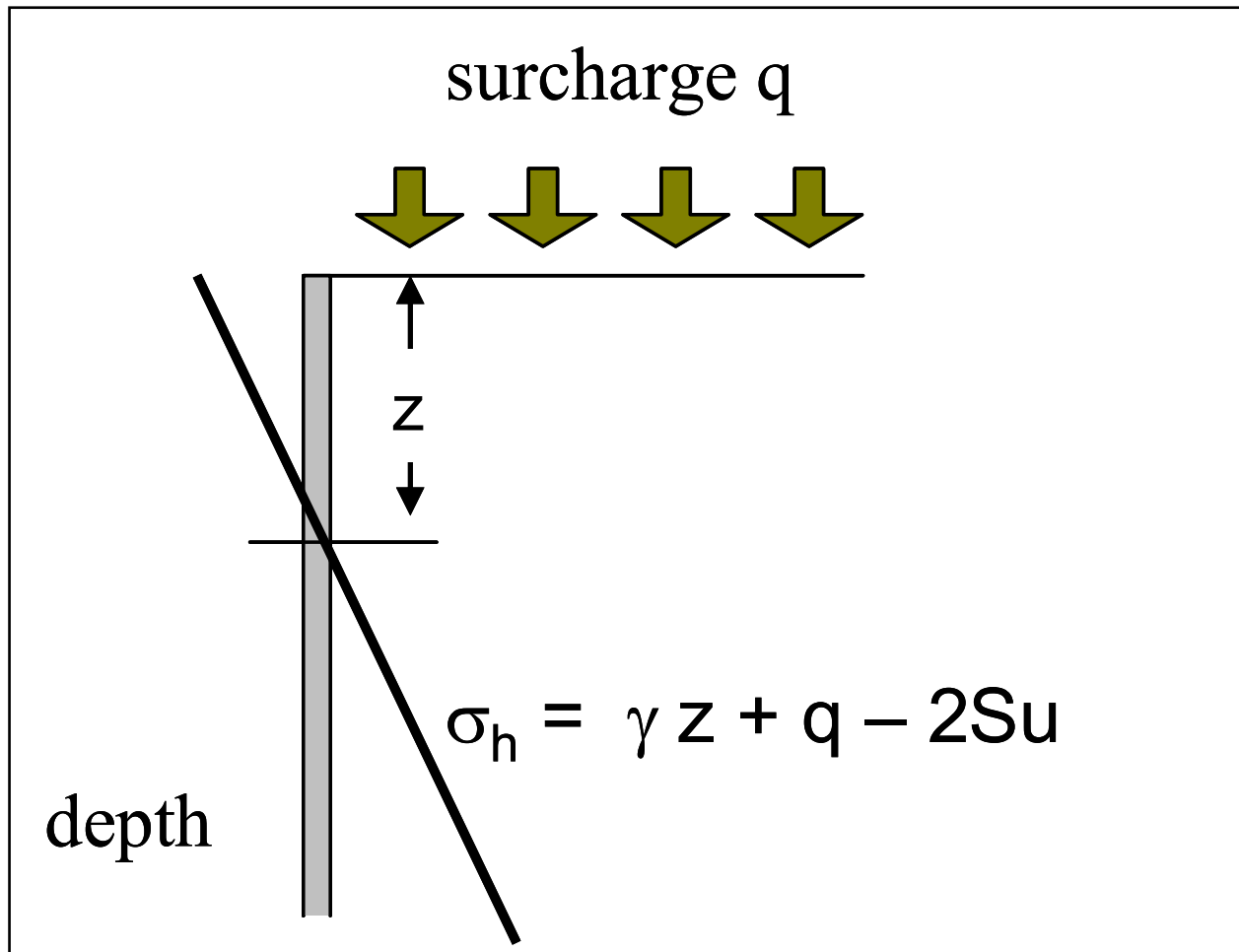


Figure 5.9. Depth z , of a dry crack behind an unpropped smooth retaining wall, limiting active Rankine stress state

The analysis above is relevant to unpropped walls supporting soil in an undrained condition adjacent to an open excavation. In the case of a wall with support on the passive side, however, the theoretical depth of the crack will be less, provided that the strain required to mobilise the passive (or propping) resistance is small.

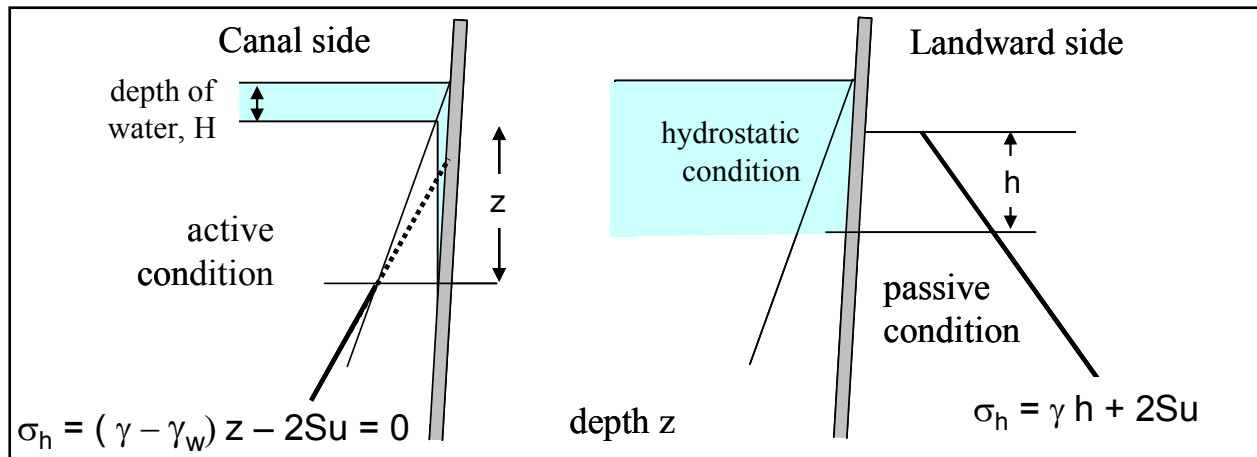


Figure 5.10. Limiting Active and Passive Rankine stress states on either side of a stiff wall with water filled crack

Figure 5.10 shows the canal side and land side conditions similar to those in the models carried out for this study. Water fills a gap between the wall and the clay on the ‘active’ side. The depth of the water filled crack in this active condition (without support) is unchanged from the simple equation above as the increase in total vertical stress is equal to the increase in hydrostatic pressure from the water in the gap. If limiting passive resistance can be mobilised on the landward side of the wall with negligible landward movement, then the theoretical depth of the crack (in almost all cases) will be controlled by the passive propping force that is mobilised to resist the hydrostatic force on the opposite side of the wall. The depth of the crack, z below the crest of the levee on the canal side (if any) would then be given by:

$$\gamma_w (z + H) = \gamma h + 2 S_u$$

Under the conditions of 17th Street or London Avenue, this ‘rigid prop’ approach does not suggest that a crack would form. However, this analysis takes no account of the actual movement required to mobilise passive resistance from the landward side of the levee. In practice, the geometry of the landward shoulder of the levees and the low shear stiffness of the swampy marsh beneath, mean that significant movement of the passive block on the landward side is required to mobilise any resistance to the crack formation.

Rotation of the floodwall under the additional hydrostatic load (and moment) caused by the water rising up the exposed face will therefore negate the potential benefit (in terms of reduced crack depth) of the passive resistance on the landward side opening a gap on the canal side of the wall as if there was no resistance from the landward side. Unlike the case of the rigid prop, which is infinitely stiffer than the soil, the passive soil block is only capable of resisting the lateral load by movement, and any movement landward at all of the wall will open a crack that is immediately water filled.

Figure 5-11 shows a typical example of the relationship between movement $\Delta H/H$ of a stiff retaining wall into or out of the backfill and the mobilisation of active and passive resistance (for a wall translating or rotating about the toe). It is seen that as much as 5% rotation is required to

mobilise full passive resistance, even in a condition where there is an extensive horizontal layer of soil beyond the wall.

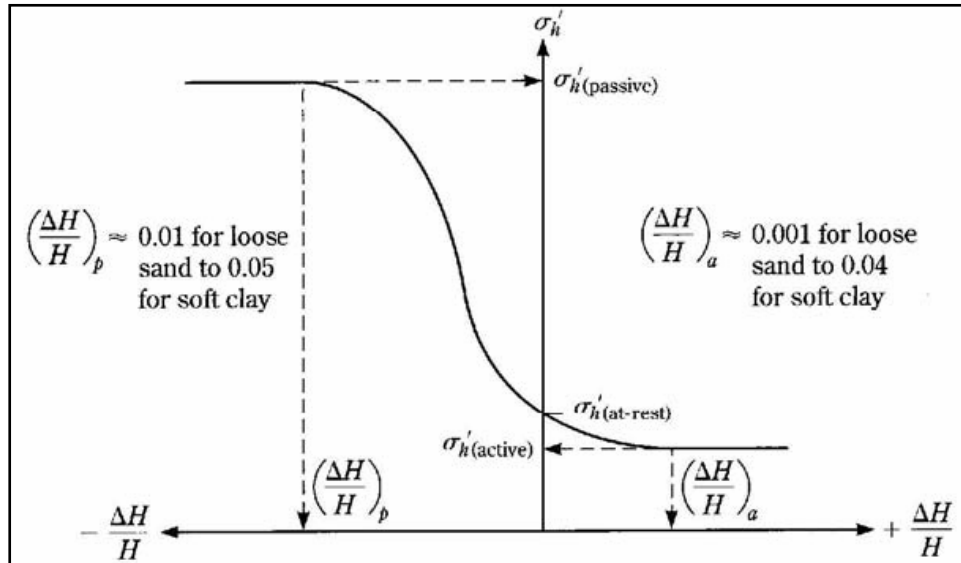


Figure 5-11. Rotation or movement required to mobilize active and passive resistance, from Principles of Foundation Engineering, BM Das

It is concluded that any rotation of the wall landward as it mobilises passive resistance against the flood condition will immediately open a water filled crack on the canal side, as the canal side acts in an undrained active manner, following the approach described above.

As the clay levee is saturated, it is sufficient to ‘break the seal’ on the canal side for full hydrostatic conditions to exist (in the case of the levee profiles considered) either to the base of the wall (where the wall does not reach an underlying sand layer), or to the top of the sand layer (where it does). (Note that following the approach outlined above, for an undrained strength $S_u = 500$ psf, the theoretical depth of a water filled crack will be over 21 feet.)

The evidence for the formation of the crack is clearly seen in the video imagery from the model tests, seen here in Figure 5.12, and also in the record of the pore pressure transducers located near the toe of the flood wall, Figure 5.13, which showed a rapid rise in water pressure to the full canal water level as the wall moved landward slightly.

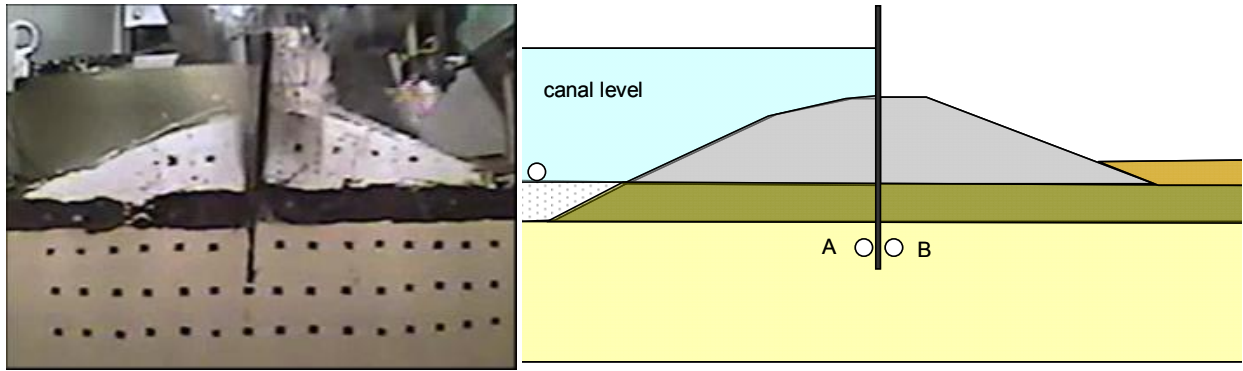


Figure 5.12. Early stage of crack formation in London South model

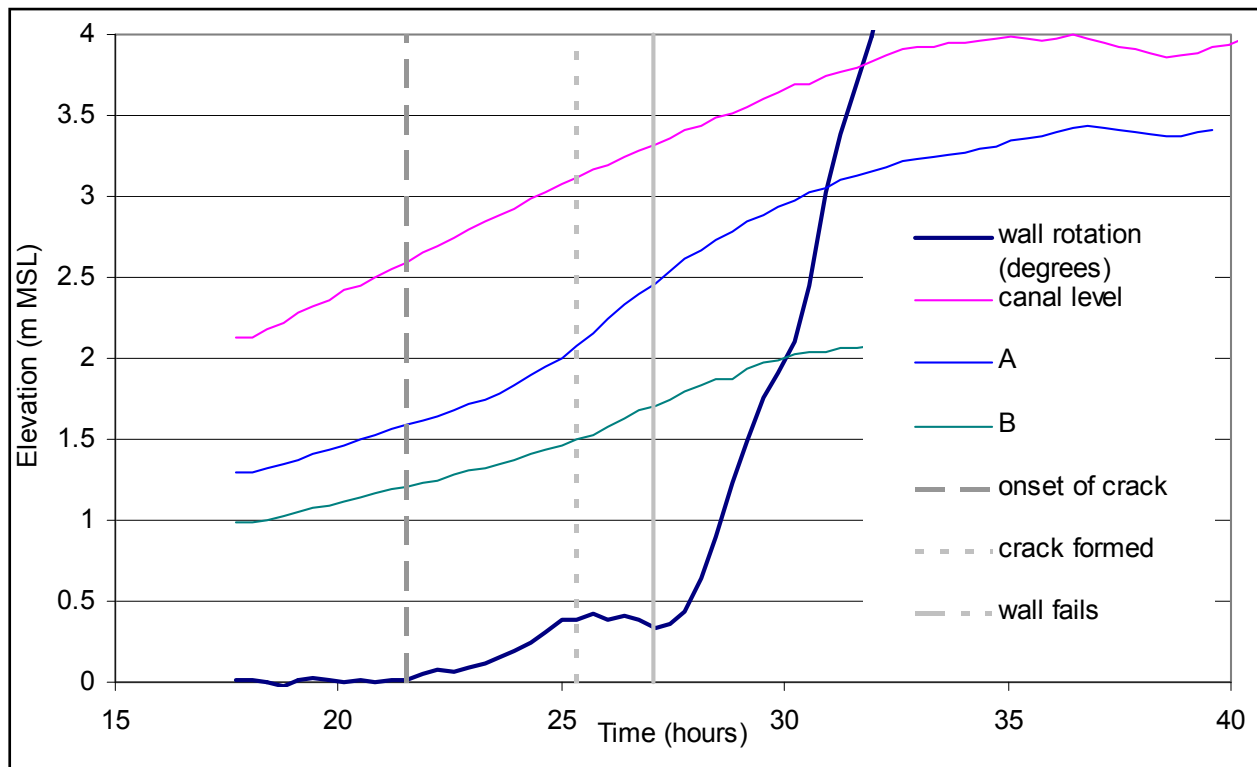


Figure 5.13. Comparison between canal level, water pressure at base of wall and wall rotation, London South Model 1, ERDC

The same sequence of crack formation, wall stabilisation and then wall failure was observed in a repeat model of London South, Model 2, carried out at RPI, Figures 5.14 and 5.15.

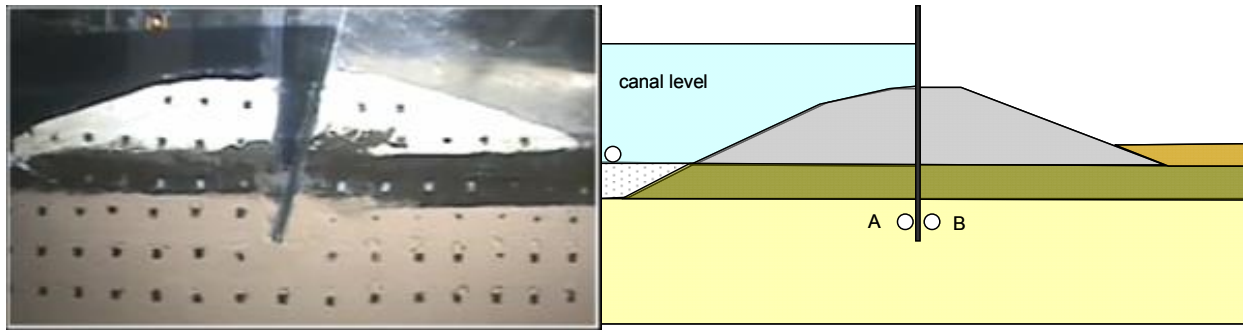


Figure 5.14. Early stage of crack formation in London South Model 2

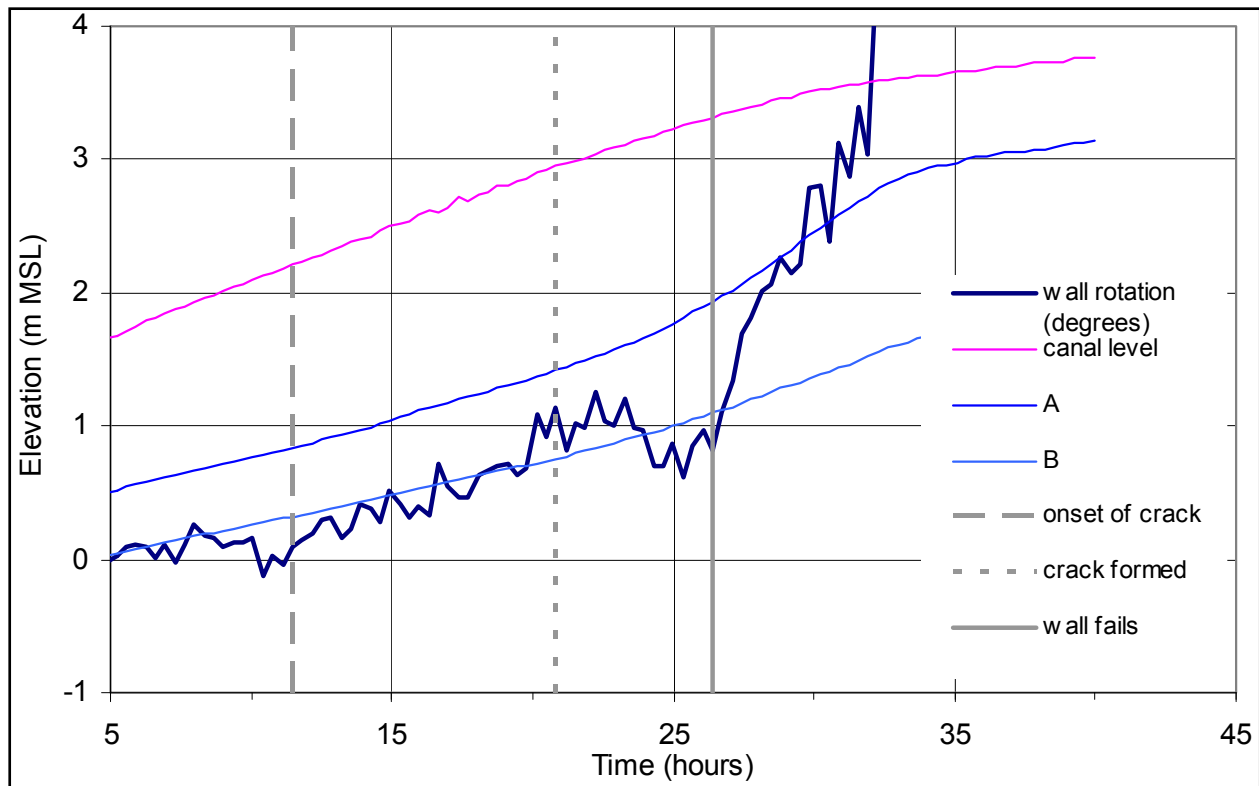


Figure 5.15. Comparison between canal level, water pressure at base of wall and wall rotation, London South Model 2

In the case of levees on clay foundations, a similar phenomenon was observed. Figure 5.16 shows the rotation of the wall followed by a brief period of stabilisation before the main failure ensued.

Model tests carried out on a cross section representative of the Orleans canal (Orleans South), which has a less deep flood wall that does not reach the underlying sand layer showed very small movements of the wall at flood levels up to Katrina. Beyond the Katrina flood level (over 1m higher) movement of the wall was observed indicative of crack formation. This is clearly seen in the video image, Figure 5.17. Plotting canal elevation against wall displacement, Figure 5.18, for Orleans South, shows the early time stiff response of the levee system up to the

Katrina flood level. At higher flood levels, the rate of landward movement of the wall increases sharply as the crack forms. The formation of the crack increased both the load and the moment on the wall. In this model test the flood wall remained in place and did not show the same unstable response to high flood levels as the levee sections on 17th Street and London Avenue though its performance did appear to be close to failure (discussed below).

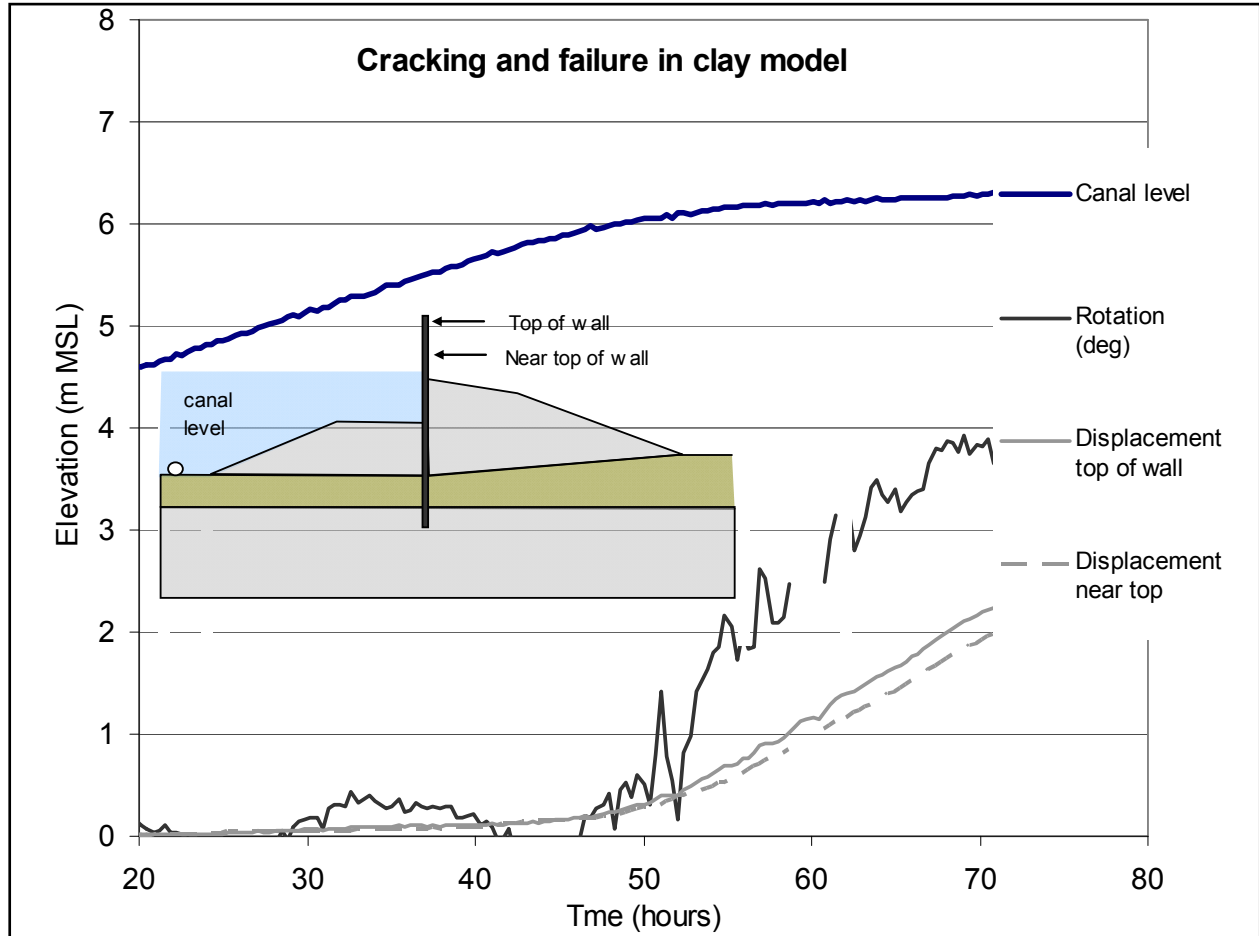


Figure 5.16. Rotation and translation evidence of crack formation prior to failure, 17th Street model

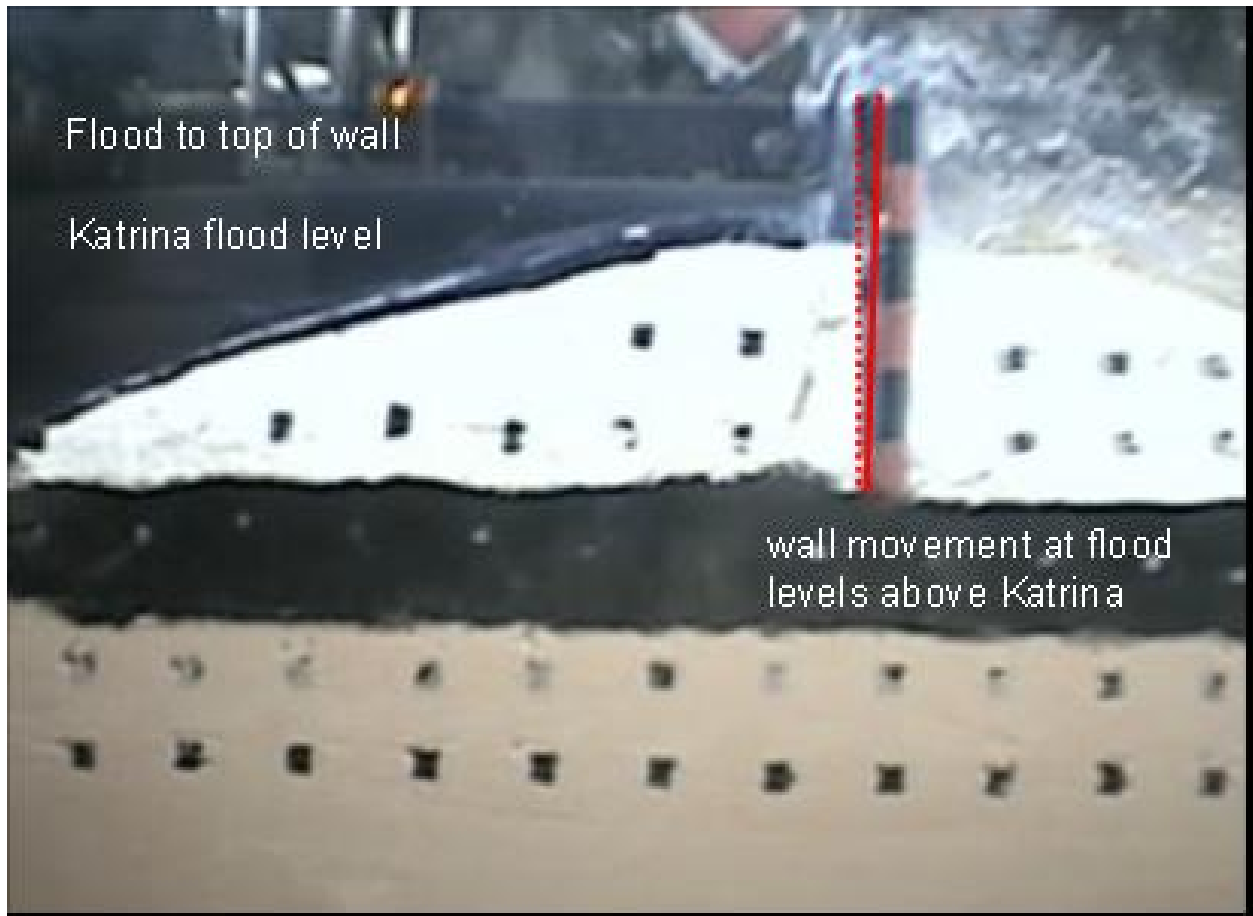


Figure 5.17. Crack forming at Orleans South levee section at flood level above Katrina

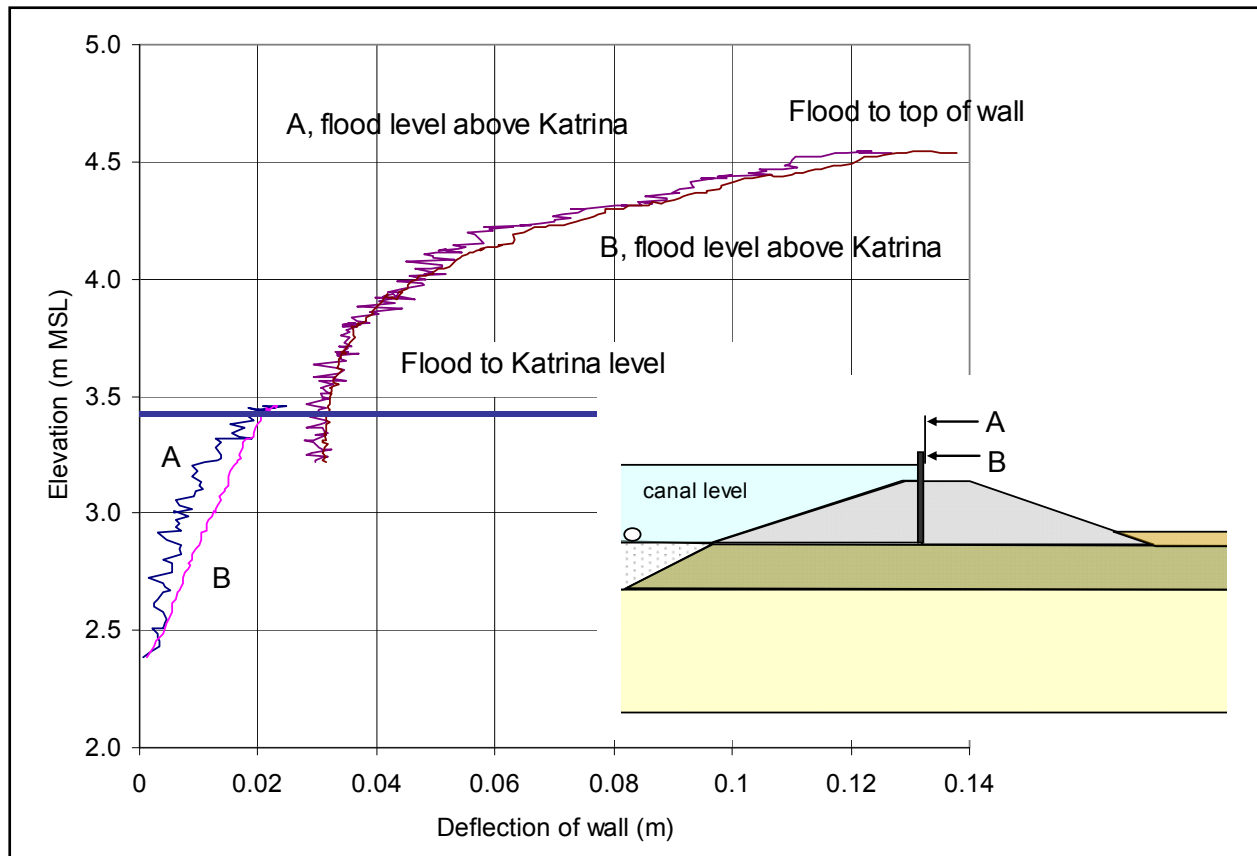


Figure 5.18. Small translation of wall at Orleans South at Katrina flood level, larger movement at higher flood levels indicative of crack formation

Rotation of the Wall

In the model tests where the toe of the sheet pile wall penetrated into the sand and was restrained from lateral movement, the opening of the crack on the canal side of the flood wall was followed by a rotation of the wall landward. Instruments on the wall recorded the horizontal movement, from which it may be seen that the wall rotated, consistent with the video imagery of the failure. In all of the model tests with sand foundations (London South and London North) that showed gross movements indicative of wall failure, the rotational movement was accompanied by a translational sliding of the landward part of the levee with the underlying swampy marsh, on top of the deeper sand layer.

Piezometric levels indicating the pore water pressure in the sand foundation show that the vertical stress on the foundation at the onset of failure was near zero towards the toe of the levee on the landward side.

Figure 5.19 shows rotation of the wall in a London South model and Figure 5.20 shows a sequence of video images of the rotational movement in progress. A similar sequence was found for the repeat model of London South, Model 2, Figure 5.21.

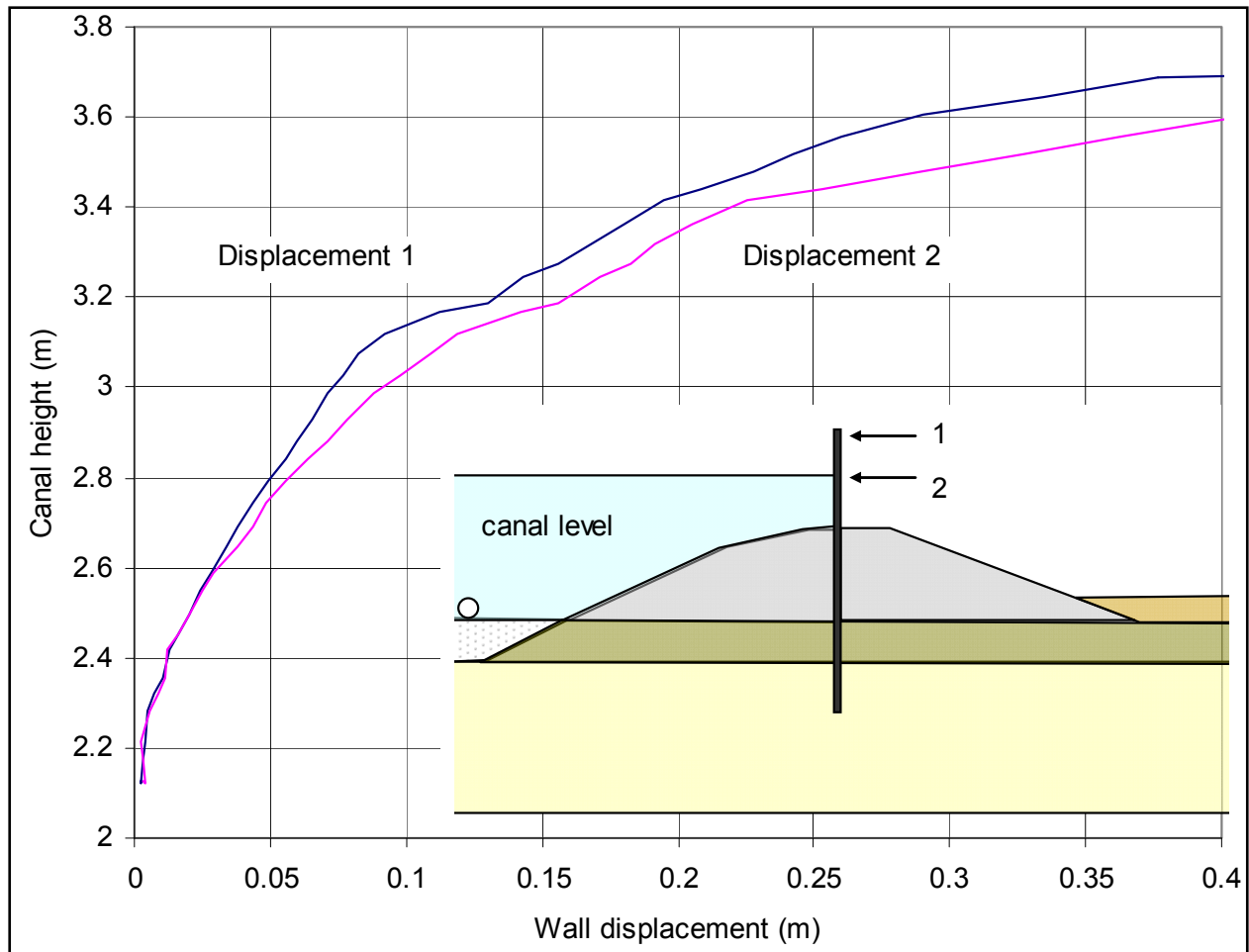


Figure 5.19. Rotation of the wall as canal level increases followed by failure, London South, Model 1



Figure 5.20. Wall failure follows crack formation, London South model, Model 1



Figure 5.21. Crack formation, wall rotation and sliding failure, London South Model 2

The rotation of the wall is linked to the reduction in effective confining stress in the sand layer beneath the landward shoulder of the levee. Once the crack was fully opened pore pressure transducers in the foundation sand layer show that the excess pore pressure in the sand rises to reflect the increase in pressure at the toe of the wall. The increase is seen to reduce linearly with distance from the toe of the wall. The increasing water pressure in the sand layer reduces the vertical effective stress under the swampy marsh.

The reduction in vertical effective stress has two effects: the first is to increase the likelihood of uplift of the swampy marsh (as the increasing water pressure in the foundation balances the weight of the levee and swampy marsh layer above) and the second is to reduce the stiffness of the sand surrounding the toe of the sheet pile wall, providing passive resistance.

The mechanism of failure in the sand models (London South, London North) was analysed as follows. Piezometric levels under the levee on the landward side rise, reducing the vertical effective stress on the swampy marsh – sand interface as the canal level rises, Figure 5.22. Rotation of the wall under the hydrostatic load on the exposed section of floodwall above the crest is resisted by the embedment of the wall in the sand layer, the elastic stiffness of the swampy marsh layer and the clay levee (landward side).

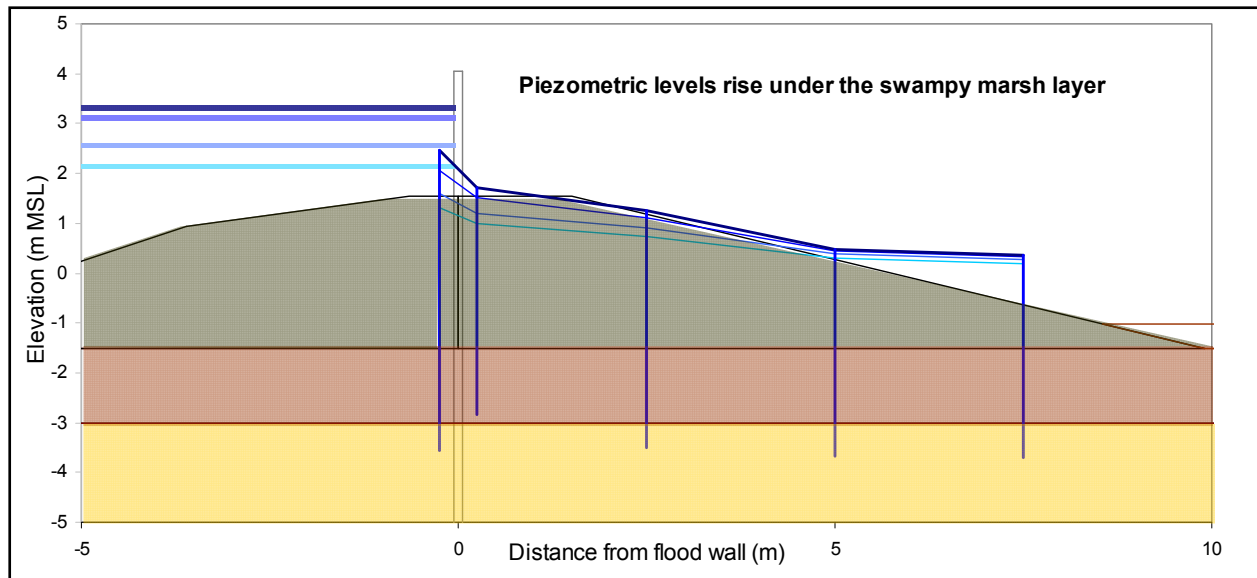


Figure 5.22. Piezometric levels immediately under the swampy marsh show increase under the levee as the wall rotates

Observations of the extent of crack rotation prior to failure show that the rotation reached around 0.5 degrees prior to a brief period of stabilisation, before the rising piezometric levels under the levee coupled with the rising canal level triggered the failure of the wall, Figure 5.13 above. As noted earlier, a passive rotation of less than 1% (around 0.5 degrees) in loose sand or less in dense sand (as at London South) is sufficient to mobilise the limiting passive resistance of sand.

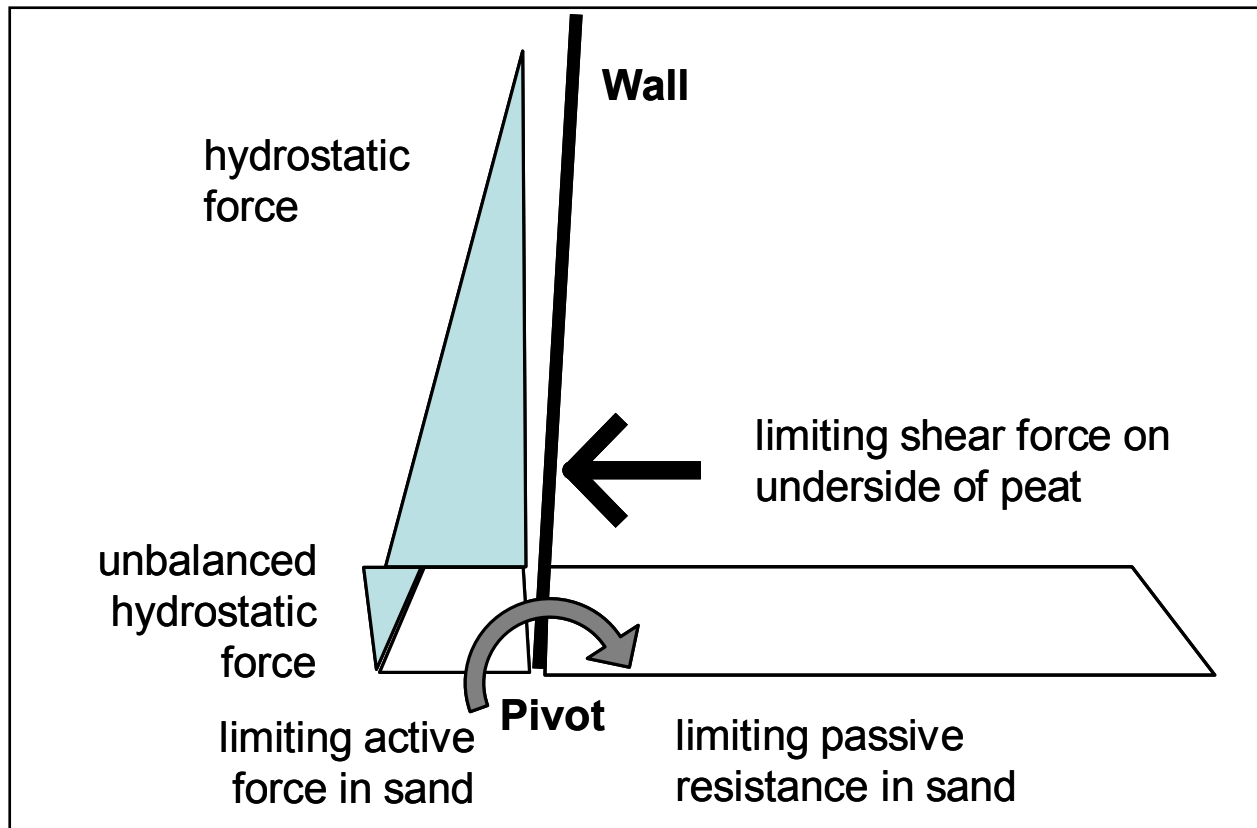


Figure 5.23. Equilibrium stress analysis for the collapse of the wall

Figure 5.23 shows an equilibrium stress analysis for the wall at the onset of failure used for the analysis of the London Avenue models. Hydrostatic pressure from the canal reaches the base of the swampy marsh. Below this level, an active stress condition exists to the base of the wall (for simplicity). Differences in the hydrostatic pressure on either side of the toe of the wall in the sand lead to a small resultant ‘unbalanced’ force landward. On the passive side, full passive pressure is mobilised in the sand, and a limiting shear stress is mobilised along the underside of the swampy marsh beyond the passive zone, where the vertical effective stress is greater than zero. Forces acting on the swampy marsh are discussed further below (Figure 5.25).

Figure 5.24 shows a superposition of three images at different stages of the levee failure, with two marker points highlighted in the passive zone and in the swampy marsh near to the levee toe. It is clear that the swampy marsh is moving laterally while a wedge shaped passive zone develops in the sand showing both a slip surface extending from near the toe of the wall and some heave at the top of the sand layer, below the levee crest.



Figure 5.24. Overlay of video images of the rotational failure of the London South model wall, Model 1

Figure 5.25 shows diagrammatically the forces acting on the swampy marsh towards the landward side of the levee and beyond the passive wedge in the sand layer at the toe of the wall (Figure 5.24). The compressibility of the swampy marsh landward of the levee means that no significant passive resistance from this layer can be mobilised in the ‘crumple zone’. Near the toe of the levee, water pressures in the sand layer are sufficiently high that the vertical effective stress between the swampy marsh and the sand layer is near zero (Figure 5.27), and hence the shear stress that may be carried across this interface in this area is also near zero. Forces acting on the levee from the wall must be transferred through the swampy marsh to the sand below, and therefore the maximum horizontal force that may be applied from the wall is controlled by the maximum shear force that can be mobilised on the underside of the swampy marsh layer.

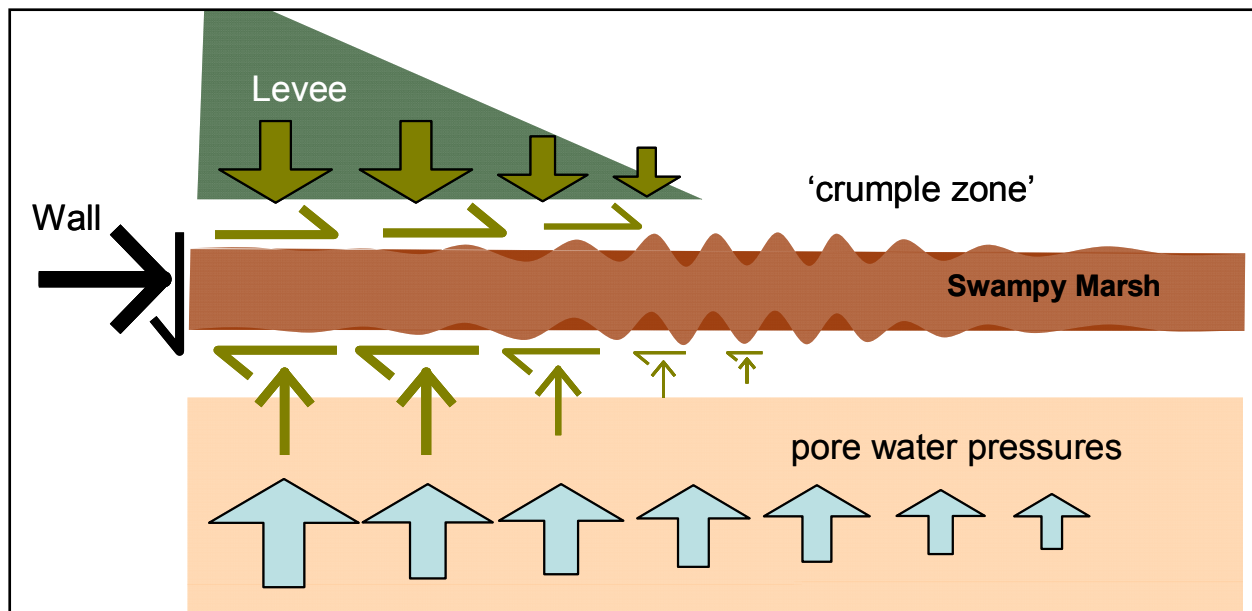


Figure 5.25. Diagram of forces acting on the swampy marsh towards the toe of the levee

The Factor of Safety for the London South models was analysed at a series of discrete instants when the water level in the canal was (a) normal or typical canal level (b) at the onset of crack formation (c) at the completion of crack formation and (d) at the onset of sudden failure. These instants are also shown in Figure 5.13 above entitled, 'Comparison between canal level, water pressure at base of wall and wall rotation, London South model'.

Figure 5.22 showed the piezometric levels under the swampy marsh at different canal levels. Figure 5.26 shows the reduction in vertical effective stress under the swampy marsh as the wall starts to fail. Near the wall, vertical effective stresses are slightly lower on the canal side of the levee, compared to the landward side. Towards the toe of the levee, the vertical effective stress falls to near zero.

The passive and active forces in the sand were calculated on the basis of a limiting angle of shearing resistance of 33 degrees, considered appropriate to the degree of strain that the wall had undergone. The limiting shear force on the underside of the swampy marsh was calculated on the basis of the average vertical effective stress acting over discrete lengths of the interface, outside the passive zone and where the effective stress was greater than zero. The unbalanced hydrostatic force was computed from the measured water pressures in the sand on either side of the wall (this force is due to seepage effects). Saturated unit weights of the levee clay, swampy marsh and sand were taken as 110 pcf, 80 pcf and 120 pcf respectively, appropriate to the unit weight of kaolin and Nevada sand. (The value for the saturated unit weight of the swampy marsh was the same value used for the slope stability analysis.)

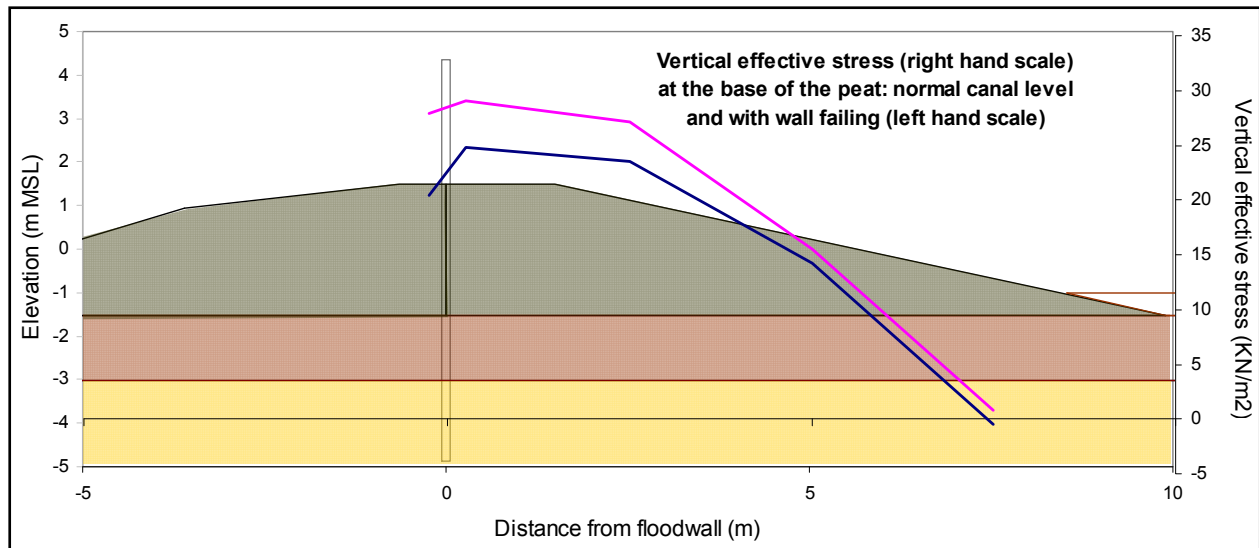


Figure 5.26. Reduction of vertical effective stress on landward side of flood wall at onset of failure

The results of the calculation for two different models were highly consistent, showing that this mechanism of failure was in a limiting condition at the instant of failure, based on the measured data from the model tests. Figure 5.27 shows the Factor of Safety calculated for the two models, at four different stages of normal (typical) canal level, crack opening, crack formed and the onset of wall failure.

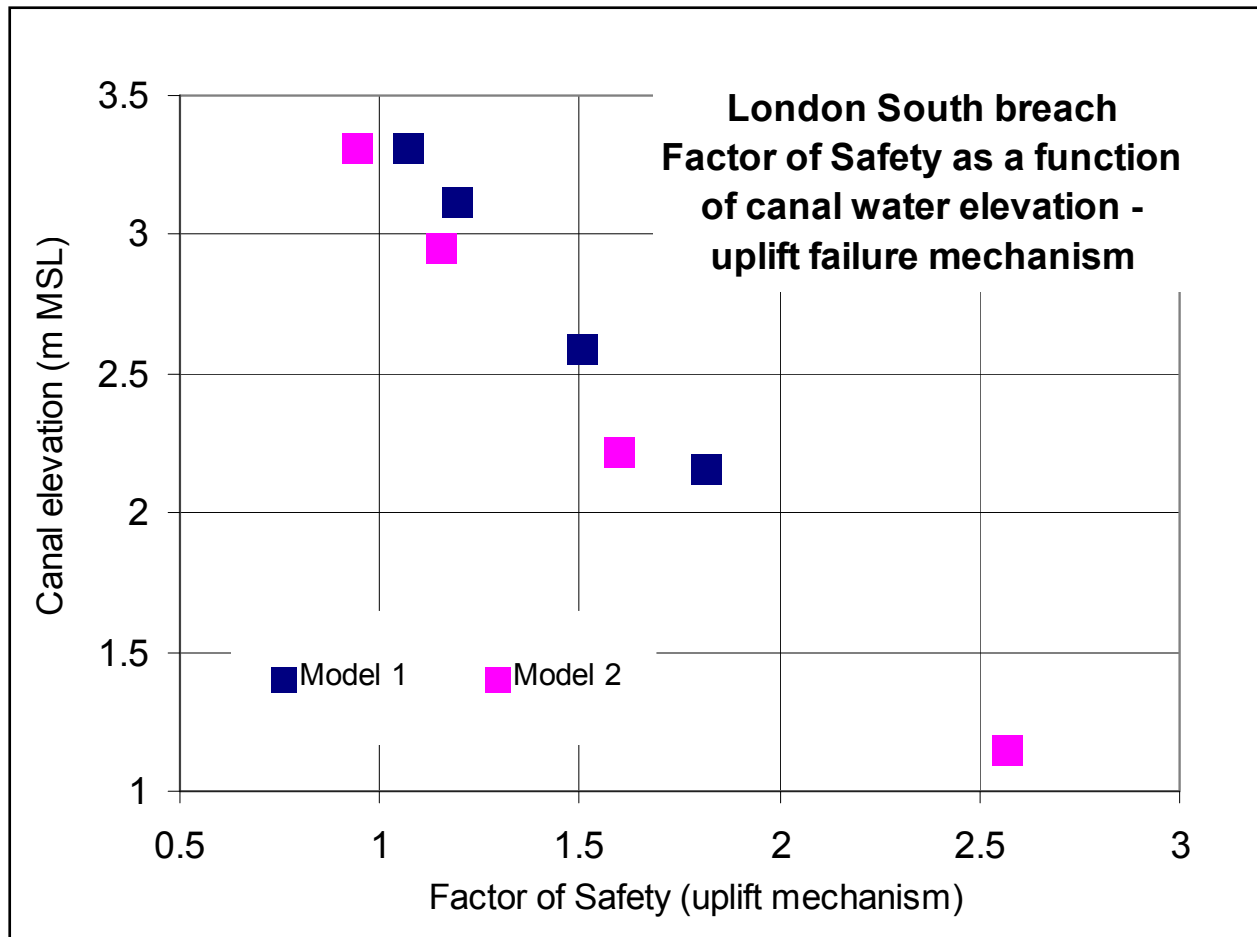


Figure 5.27. Factor of Safety for observed failure mechanism (uplift and rotation) for two London South models carried out at ERDC and RPI

The analysis is consistent with the observation from all the model tests that the formation of the crack and the re-adjustment of the wall to the new hydrostatic loading condition, with increased moment and lateral force, is a separate event from the failure that follows. In both models analysed here, the factor of safety remains above 1 at the completion of the crack formation, and falls to 1 at the onset of failure.

The rotation and uplift mechanism of failure observed in all the sand foundation models (London South and London North) is sensitive to the unit weight of the swampy marsh. In the analysis of the model tests presented above, the unit weight for this material was selected appropriate to the samples used in the experiments. Reducing the unit weight of the swampy marsh by 10 pcf (80 pcf to 70 pcf) reduces the FoS by around 0.1.

Because of the significance of the formation of the crack, the model tests show that shallow penetrations into the sand layer will have particularly low FoS. Following the analysis above, varying the depth of the bottom of the sheet pile wall by 1 ft up or down changes the FoS by +/- 0.15.

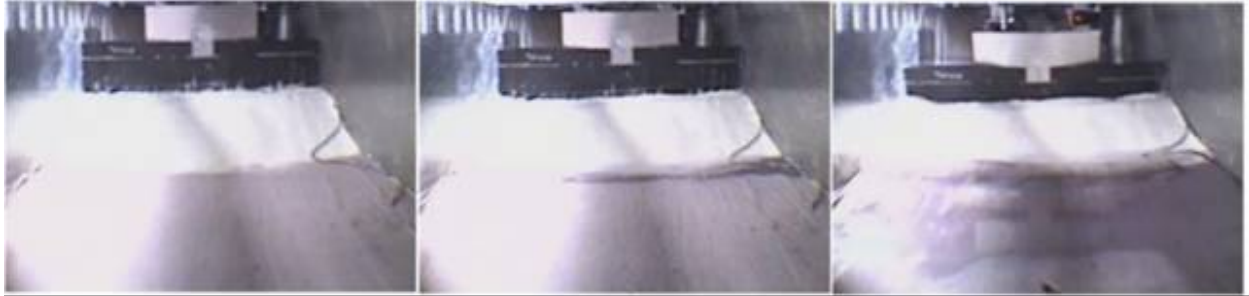


Figure 5.28. Water emerging from toe of levee as failure progresses, London South Model 2

The high pore water pressures under the toe of the levee on the landward side and under the swampy marsh led to water being ejected from the ground at the toe of the levee. This may be deduced from the piezometric heads near the toe of the levee, and may be seen in the video images of the landward toe. Figure 5.28 shows a view of the levee and floodwall as seen from the ‘backyard’ of houses behind the levee showing ‘black’ water emerging from the toe of the levee as the flood wall rotates landward.

Translation of the Wall

In all of the scale models where the toe of the sheet pile wall terminated in the clay layer, then following the opening of the water filled crack a translational failure occurred through the clay, starting at the toe of the wall and progressing landwards. This is clearly seen in the instruments recording movement of the wall and in the video imagery, Figure 5.32.

The observation of crack formation in the 17th Street levee models has been described above and was shown in Figure 5.16 for one case. A second example is shown here, Figure 5.29, from 17th Street Model 1, which shows an early rotation that briefly stabilises before the main failure commences (Scale time 28 to 36). (Note time scales in the centrifuge models are unrelated to the actual time line of the Katrina flooding. Time in the centrifuge models is therefore referred to in the text here as ‘Scale time’ to distinguish the two time lines.) Video imagery of the phase between the initial opening of the crack and the onset of the main failure shows active slumping behind the wall, which may explain the increase in rotation between around Scale time 37 and 42 hours.

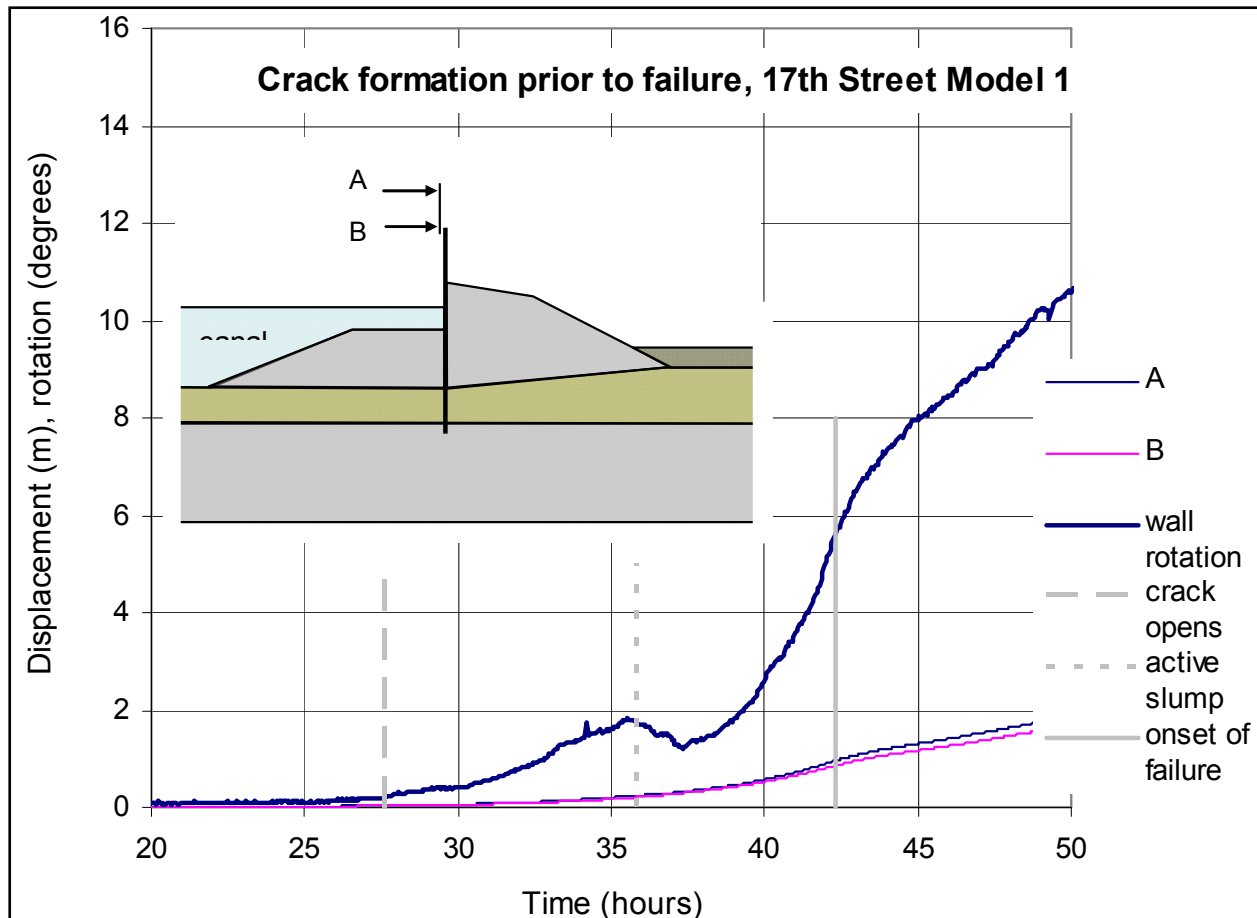


Figure 5.29. Crack formation prior to wall failure, 17th Street Model 1

The sliding surface developed near the top of the clay layer and progressed landwards until it was outside the levee, before it turned upwards to exit through the swampy marsh layer. This mechanism is similar to the observations in the field from 17th Street. The progression of the slip surface landwards can be identified from the pore pressure records, which show a progressively delayed reaction landwards to the translational movement.

Comparing the wall rotation with the pore water pressure measurements at locations in the clay on the canal side of the wall, at the toe of the wall and the canal level (expressed as head in m of water) with the wall rotation gives further insight into the mechanism of failure, Figure 5.30. The crack formation phase is marked by a small rotation, up to 2 degrees movement, following which the wall briefly stabilises. As noted above, active slumping starts towards the end of the crack formation phase, perhaps as early as Scale time 30, indicated by the change of slope and reduction in excess head near the toe of the wall on the canal side. During this period, the pore pressures beneath the levee on the canal side reflect the increase in total stress but show no evidence of the wall movement.

The reduction in excess head near the toe of the wall continues as the wall ceases to rotate but continues to translate (between Scale time 36 – 37.5) before rotation starts again, leading to a sharp transition in performance around Scale time 42 as the wall fails. At this moment, the canal

level drops due to the rapid lateral movement, the water pressure at the bottom of the wall changes slope again and rapidly rises (to reach and exceed the canal level), and the rate of rotation slightly decreases as the main translational movement commences.

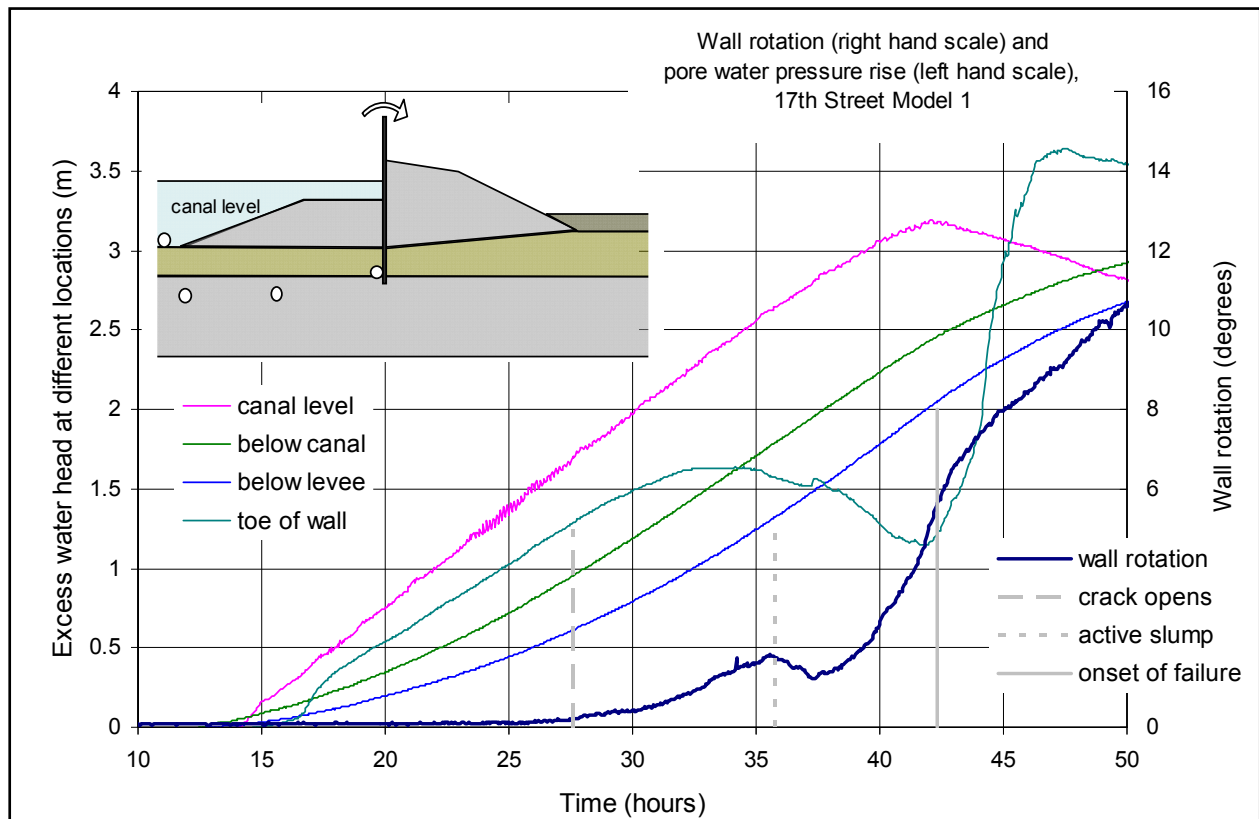


Figure 5.30. Comparison between wall rotation and excess head at onset of failure, 17th Street, Model 1

The sliding failure of the model wall was arrested before a full breach took place to capture the final state of the 17th Street model (Model 1), Figure 5.31. Despite the large lateral movement, there is minimal heave of the swampy marsh layer on the landward side.



Figure 5.31. Final state of 17th Street Model 1 showing lateral translation on sliding surface starting at the toe of the wall and progressing landwards.

All of the clay foundation models failed with a similar mechanism under the flood loading, commencing with a small rotation and crack formation, followed by further rotation and large translation associated with a shear plane the formed from the toe of the sheet pile wall and progressed landwards through the top of the clay layer. This was consistent with the field observations.

Other observations relevant to the site conditions on 17th Street were also noted from the centrifuge model tests. The very soft, normally consolidated clay beneath the levee experienced significant settlements as the weight of the levee was increased to full height. The swampy marsh layer also tended to be compressed below the levee, but predominantly through elastic compression.

In one model of the 17th Street levee, the weight of the levee on the landward side was sufficient to provoke bearing failure in the clay foundation, Figure 5.33, with the formation of inclined slip planes, prior to the flood condition. This is a situation analogous in the field to raising the height of the levee too rapidly, without allowing time for the high excess pore pressures in the foundation to dissipate and the strength of the clay to develop. On the surface, the only evidence is increased settlement. At depth, however, local slip surfaces form in the soft clay and swampy marsh

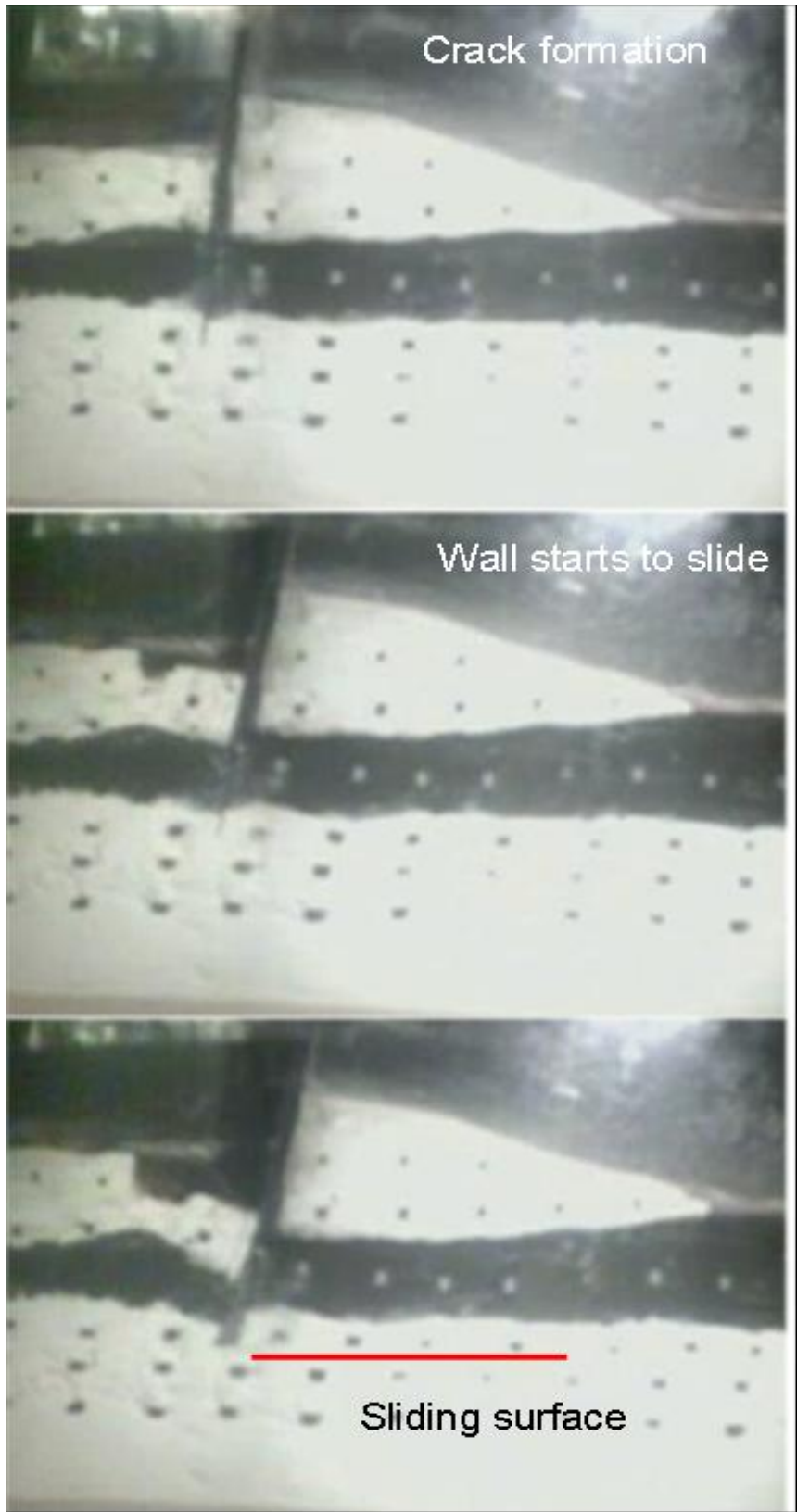


Figure 5.32. Sliding surface forms at top of clay layer in 17th Street Model 1



Figure 5.33. Bearing failure and multiple slip planes in the clay foundation caused by rapid construction on landward side, 17th Street Model 2

On flooding of this model, the same mechanism of translational failure was observed, independent of the initial disturbance in the clay foundation of the levee. The new sliding surface cut ‘horizontally’ through the pre-existing inclined surfaces along the top of the clay layer as in previous models. The new surface exited through the swampy marsh along the pre-existing surface, forming an up thrust on the ground surface. The bearing failure in the foundation had no significant effect on the height of flood water to cause translational failure.

No Failure Condition

Scale model tests were also carried out of levee sections on Orleans Avenue canal which did not fail, as part of a validation process. The cross section chosen to represent the southern portion of the Orleans Avenue levees is similar to the cross section at London Avenue, except that the levee is wider and higher, and the penetration of the flood wall is less (the toe of the wall is at the base of the levee/top of the swampy marsh layer).

As with the other levee sections, the instruments beneath the model levee responded to the rising water in the canal by an increased excess water pressures in the ground, reducing linearly

from a maximum near the canal to a minimum to the landward side of the levee, Figure 5.34. At the water level experienced in Orleans Avenue canal, the floodwall did not show any movement to indicate the opening of a crack, Figure 5.35.

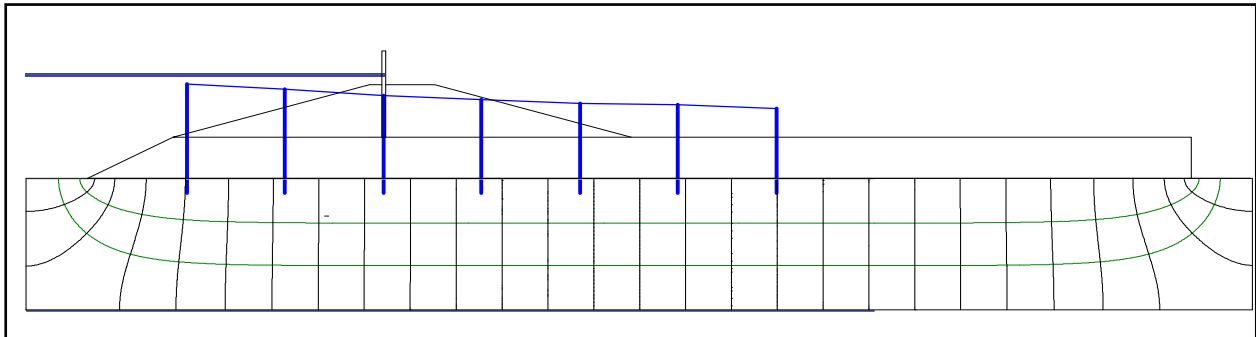


Figure 5.34. Seepage flow net for Orleans Avenue South with piezometric levels under the swampy marsh at Katrina flood level



Figure 5.35. Orleans South model at Katrina flood level

The piezometric levels below the swampy marsh in the Orleans South model showed a declining level from the canal side to the protected side of the levee, Figure 5.36. The additional height and width of the Orleans South levee, seen overplotted in the figure for both Orleans South and London South, significantly increase its capacity to resist the flood levels and no evidence was seen of a crack opening through the swampy marsh and providing a hydraulic

connection to the sand below. The London South piezometric levels, shown in the figure for comparison together with its cross section (aligned at the elevation of the top of the sand layer) show a more critical condition in terms of uplift under the landward side of the levee. Both models however show high piezometric levels near the toe of the levee on the landward side, sufficient to lead to hydraulic fracture.

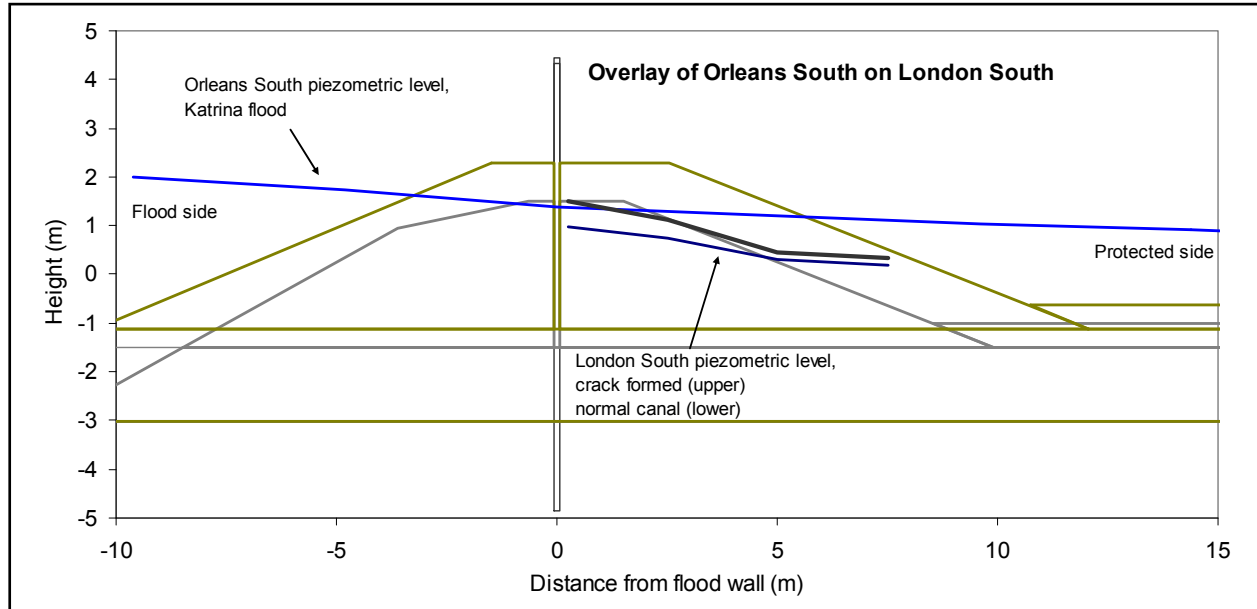


Figure 5.36. Comparison of piezometric levels in Orleans South (Katrina flood) and London South, with the base of the swampy marsh assumed to be at a common elevation

As the water level was increased above the Katrina flood level in the Orleans South model, a crack was seen to open to the toe of the flood wall, associated with small movements of the flood wall landward, as shown in Figure 5.37. Unlike the other models, this crack did not develop into a full failure condition; no unstable movement of the flood wall was observed, despite the water level reaching the top of the flood wall. Translational movements were observed to be controlled by compression of the swampy marsh layer. Relative movement between the top of the sand and the swampy marsh was apparent, in a similar manner to the uplift mechanism in the London Avenue models.



Figure 5.37. Sliding movement of swampy marsh as crack forms, Orleans South model

Comparison between the geometry of Orleans and London Avenue shows that the vertical effective stress in the sand foundation below the levee was considerably higher under the Orleans levee than under the London Avenue levees. The capacity of the flood wall to rotate is reduced by the height and weight of the landward section of the Orleans levee. Figure 5.38 shows the vertical effective stress on the underside of the swampy marsh layer measured in the Orleans South and, for comparison, the London South models. Although the Orleans levee section is higher than London South, the piezometric levels near the landward toe are sufficiently high that a zero vertical effective stress condition is created near the landward toe of the Orleans South levee in both the Katrina flood and full flood condition.

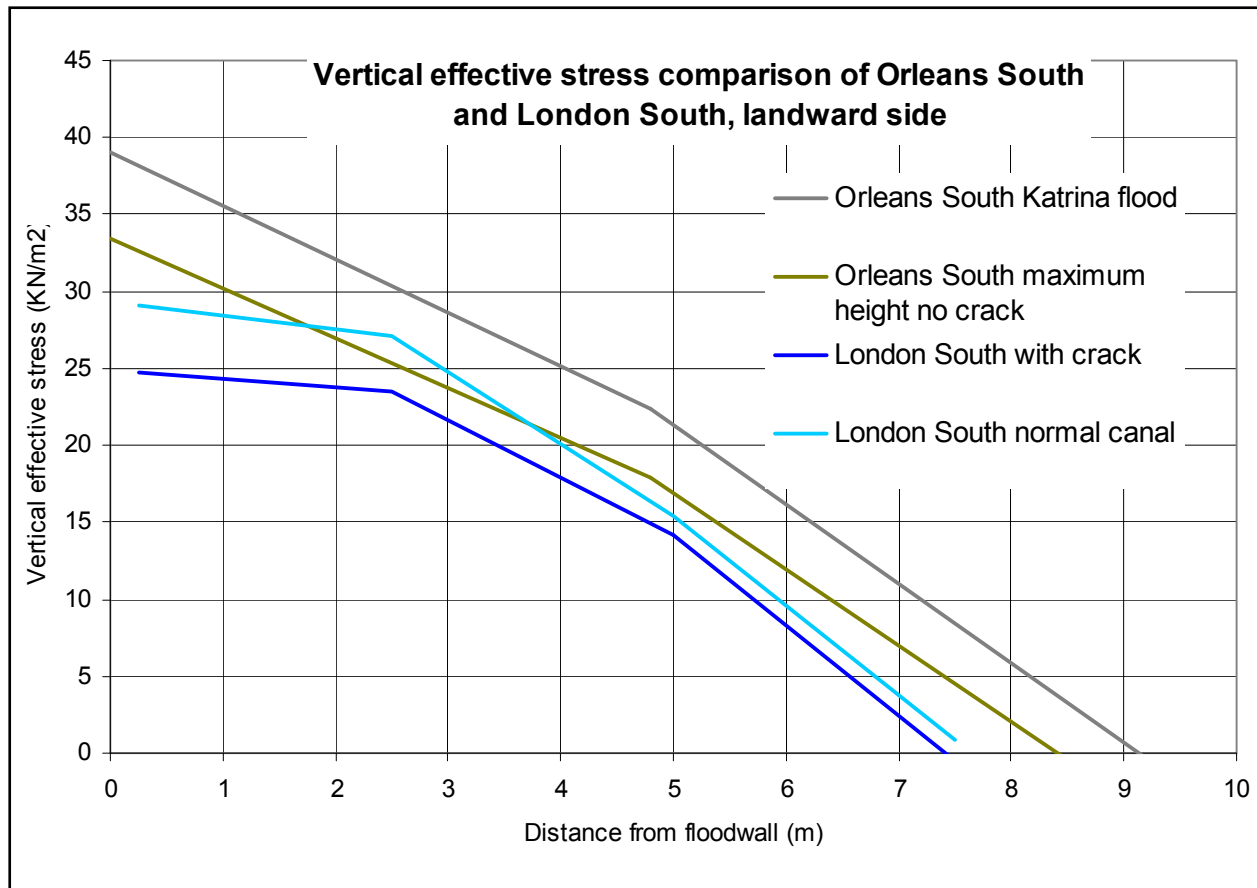


Figure 5.38. Vertical effective stress comparison between Orleans South and London South

Examining the stability of the Orleans South model, Figure 5.37 shows that the formation of the crack during the raising of the water level to the top of the wall was accompanied by lateral sliding or translation of the swampy marsh layer. The landward movement was small but noticeable and appeared uniform under the landward side of the levee, extending close to the canal side of the wall. A shearing zone appears to dip steeply downwards from the canal side toe of the wall landwards.

The stability of the landward section of the Orleans South levee may be analysed using the simple mechanism shown in Figure 5.39. Video imagery show sliding of the swampy marsh on the top of the sand layer. The sliding surfaces through the swampy marsh forming a triangular sliding block ABC are chosen to lie at angles of 60 degrees for simplicity. Assuming the levee block is free to move laterally with the swampy marsh, then work is only done on the lower surface of the swampy marsh, and on the internal sliding surfaces AB, BC and CA.

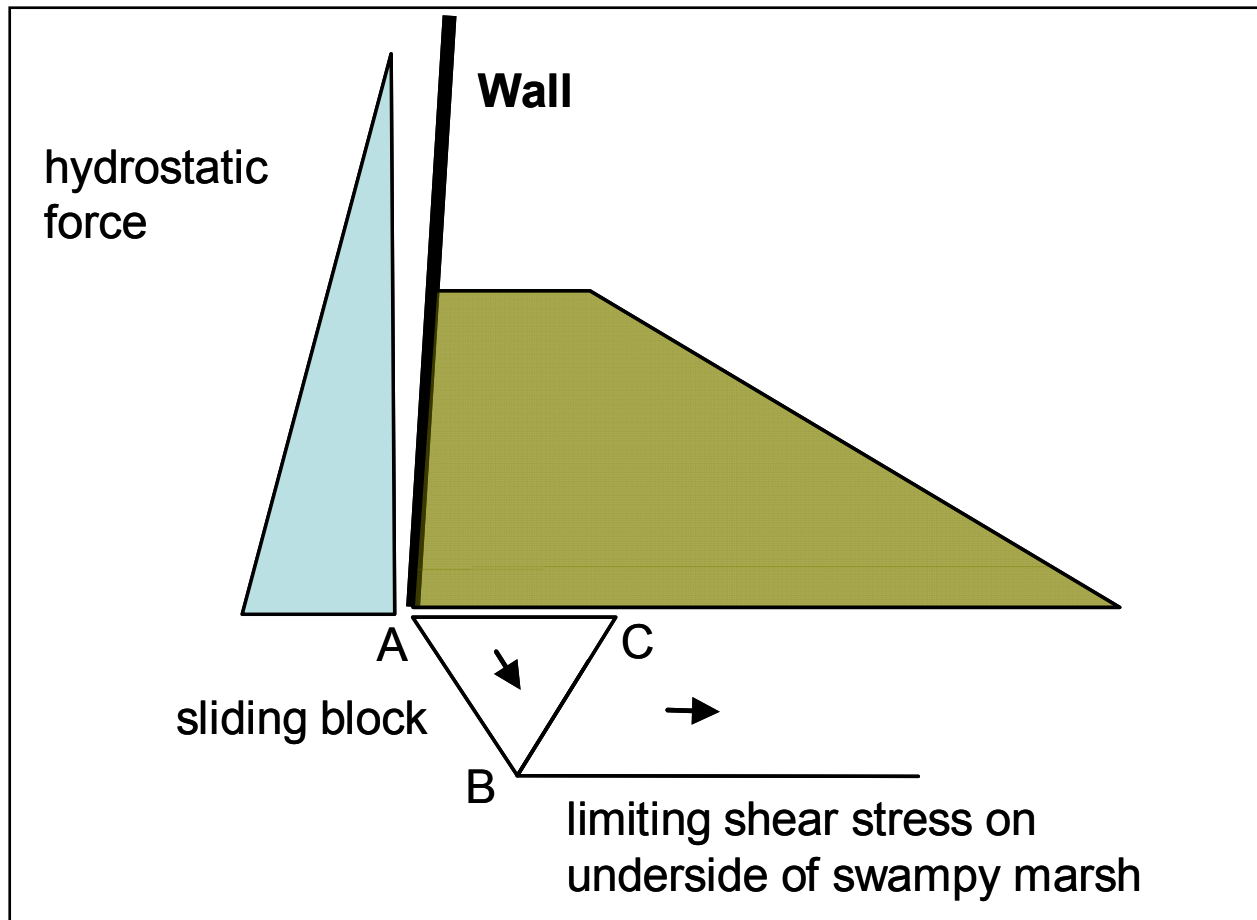


Figure 5.39. Possible upper bound mechanism for Orleans South

For infinitesimal lateral movements, a work balance gives an expression for the limiting height of water, H as a function of the depth of swampy marsh, D , its undrained shear strength S_u and the limiting shear stress mobilised on the top of the sand layer, $\sigma_v' \tan \phi'$.

$$\sigma_v D + \gamma_w H^2 = 6S_u D/\sqrt{3} + \sigma_v' \tan \phi' L$$

where σ_v is the vertical stress on the landward side of the flood wall, D is the depth of the swampy marsh, H is the height of water above the toe of the wall and L is the length of the shear surface along the top of the sand layer offering significant shear resistance.

Solving this equation for H , the critical depth of water in the crack, and using the actual measured excess pore water pressures in the Orleans South model (Figure 5.36) suggests that the Orleans South model was close to failure at full flood level. Using the value of undrained shear strength adopted for the slope stability calculations for the swampy marsh ($S_u = 400$ psf) and a limiting angle of shearing resistance of 33 degrees in the sand, a Factor of Safety may be calculated of 1.50 under Katrina flood conditions (Figure 5.35) and 1.07 under full flood conditions (flood to the top of the wall, as seen in Figure 5.37). This is consistent with the

observations of small but continuing displacements of the wall under full flood conditions, Figure 5.18 above.

Onset of Failure

The transition from an initial condition prior to the rise in water level, through the development of a water filled crack in front of the wall to ultimate failure of the levee by rotation or sliding has been clearly demonstrated in the centrifuge models. The comparison with Orleans South has shown that a water filled crack does not necessarily lead to failure, and therefore the conditions that presage the onset of failure are of particular importance.

The models showed that following the formation of the crack on the canal side of the flood wall, there was a rapid re-adjustment of the levee and its foundation to the new loading conditions. In this state, the residual levee section on the canal side is isolated from the landward section and submerged. In the case of a sand foundation, the hydraulic connection between the sand layer and the canal through the centre of the levee means that water pressures in the ground on the canal side quickly re-establish a hydrostatic state with no landward seepage. The remaining material on the canal side provides some passive restraint to the toe of the flood wall.

Water in the crack creates a hydrostatic force on the floodwall over the height of the crack. One of three conditions was observed to follow. In the Orleans South model, at water levels higher than the Katrina flood level and sufficiently high to lead to the formation of a crack to the toe of the wall, the wall remains stable, though with creeping movements landwards indicative of a near failure condition. The failure mode that is seen to be developing (Figure 5.37 above) closely resembles London South (Figure 5.14, 5.20). Stability analysis confirms that the condition of the floodwall is near failure.

In the London Avenue models, the formation of the crack and resulting hydraulic connection between the canal and the sand layer is followed by an upsurge in the water pressure below the landward section of the levee, which is coincident with an increasing rotation of the flood wall and eventual failure. This is an unstable event, which once initiated, leads to a rapid collapse as the increasing water pressures under the swampy marsh further reduce the shear resistance on the sliding surface along the top of the sand.

In the 17th Street models, the formation of the crack is followed by the immediate development of a slip movement at the toe of the wall, and an increasing rate of landward movement. The absence of a time delay between these observations is notable. This mode of failure is also unstable. As the initial slip surface extends landwards towards the toe of the levee, the weaker clay further from the centreline of the levee is less and less able to resist the driving forces acting on the levee block.

The observations in the physical models have provided detailed insights into the mechanisms that lead to the onset of failure. The profile or geometry of the levee, flood wall and foundation was found to be critical to the development of the shallow failure mechanisms. Pre-existing

water pressures in the ground were seen to be key to the failure in all the sand foundation profiles.

The low shear stiffness of the swampy marsh and large passive strain (movement) required in the landward levee block to mobilise passive resistance controlled the mechanism of the crack formation in all models.

Summary of Physical Model Tests

Introduction

The preliminary observations of levee performance in and around N.O. indicate that foundation soils possibly played a large role in the performance. Evaluation of levee performance including the effects of the foundation in the overall behavior was conducted through scaled physical centrifuge modeling. The physical data collected from the centrifuge models was used for direct observations of levee performance and primarily to improve numerical model predictions. Results from centrifuge modeling of the failed levees in and around New Orleans resulted in a detailed set of well controlled data used to validate numerical models used in analysis, confirmation of the failure mechanisms, and additional insights of factors that may have played a part in the failure as of yet unrecognized.

The objectives of this task were to physically model selected sections of the N.O. levees to determine plausible mechanisms of failure and to provide data for use in validating and verifying the numerical modeling tools. Specifically, typical levee sections along the 17th Street Canal, London Avenue Canal, and Orleans Canal representative of the failed and non-failed sections were modeled. The specific objective for the 17th Street Canal levee models was to explore the foundation peat and clay layers and their role in the failure. For the London Avenue Canal levee models, the specific objective was to explore the role of the fine sand foundation material in the failures (North and South). The specific objective for the Orleans Canal levee models (North and South) was to explore the behavior in a canal where no failures occurred.

Physical Model Plan

A detailed plan for completing the required physical modeling tests was developed by the task research team prior to initiation of any testing. In order to complete the test in a timely manner and to provide redundancy and independence in the modeling effort, it was decided that two centrifuge facilities would perform the work. Those two facilities are the Centrifuge Research Center at ERDC, and the Geotechnical Centrifuge facility at Rensselaer Polytechnic Institute. The physical modeling plan consists of modeling the single breach at 17th Street Canal, the two breaches at London Avenue Canal, and two non-breached sections of the Orleans Canal (one on the north end and one on the south end). Each of these areas would have two models completed, one at ERDC and one at RPI.

The model tests generated large volumes of data for analysis. It was evident that in all cases failure of the levees was presaged by the opening of a water filled crack on the canal side of the

levee, which allowed full hydrostatic pressure to act on the flood wall over its entire submerged height. The flood water in the centrifuge models was raised steadily, without wave effects, and it was observed that once a crack had opened, then in the cases of London Avenue and 17th Street canal models, a failure soon followed, either by rotation of the flood wall (London Avenue) or by translational failure (sliding) in the clay stratum (17th Street), originating at the bottom (toe) of the sheet pile wall. In the following sections, synopsis of the test layout, instrumentation, and results for each test will be presented.

Physical Models of 17th Street Canal

Two models of a section at the breach location were completed. One of the models was performed at RPI and the other one at ERDC. This section of the report will present information relevant to each model. Thorough details of the levee geometry and material in addition to foundation materials were determined from field and laboratory data as highlighted in other sections of the performance evaluation report. Based on careful analysis of all that information a section representative of the breach area was developed and led to the physical models as described following. All of the models were constructed in the same container with dimensions 1.2 m in length and 44 cm in width. The models are a 1/50th scale of the actual 17th Street levee and foundation, therefore all model dimensions should be increased 50 times. Henceforth, all dimensions will be given in prototype scale. In all plots, the time is scaled time not field time.

ERDC 17th Street Canal Model

The model representative of a section through the breach at 17th Street Canal is shown in Figure 5.40. The layers consists of 1.5 m thick sand layer, 5 m thick clay layer, 1.5 m to 2.5 m thick swampy/marsh layer, 0.5 m thick overburden The levee is constructed of kaolin clay and the sheet pile of aluminium.

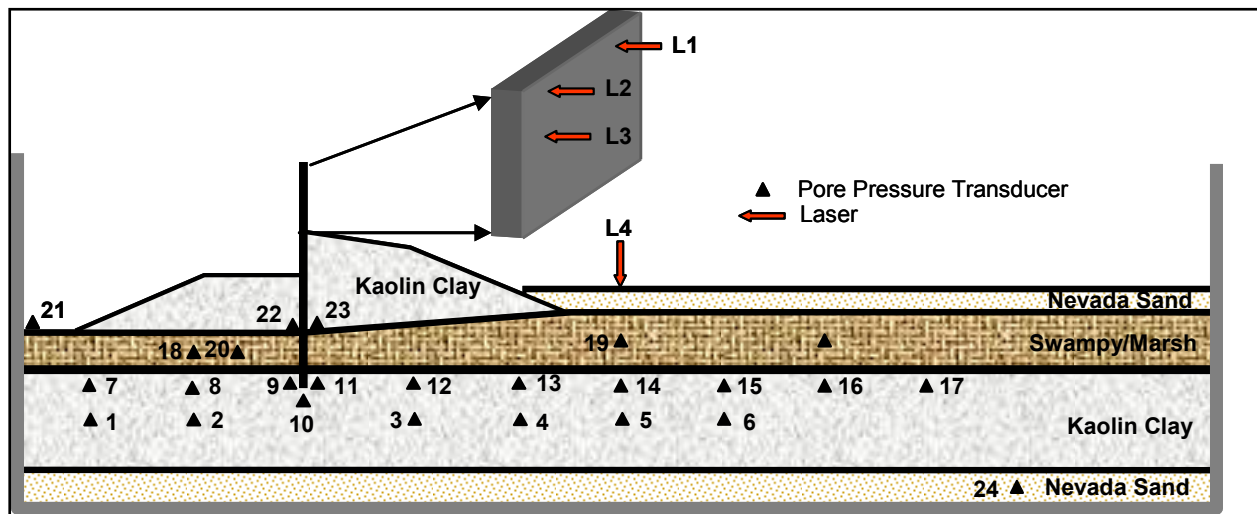


Figure 5.40. Schematic of ERDC 17th Street physical model

The sequence of model construction proceeded as follows. The Nevada sand layer is rained in dry with instrumentation placed at the appropriate location. The model was then sealed, vacuumed, and the sand layer saturated. A view of the model at the end of this step is shown in Figure 5.41. At the conclusion of this step, the mixed kaolin clay was placed on top of the sand with instrumentation placed where appropriate. Figure 5.42 shows a photo of the clay mixing process and Figure 5.43 a view of the finished clay layer with markers clearly visible. The pre-mix water content was targeted to be 100%, with post-mix measurements giving moisture contents of 102%. Based on vane shear measurements the pre-consolidation strength of the clay was 48 psf.

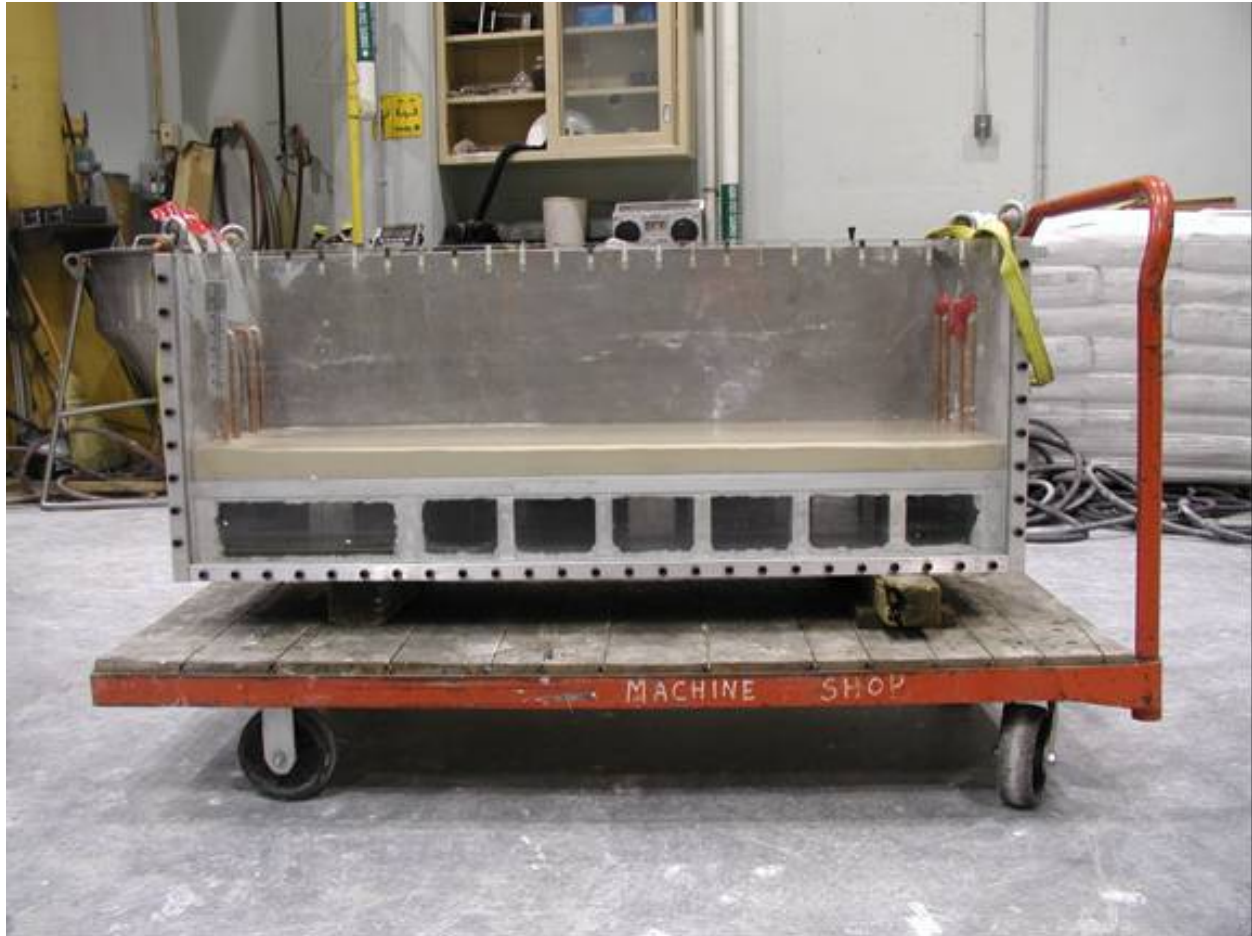


Figure 5.41. View of ERDC 17th Street model at end of sand layer placement and saturation



Figure 5.42. View of the clay mixing process

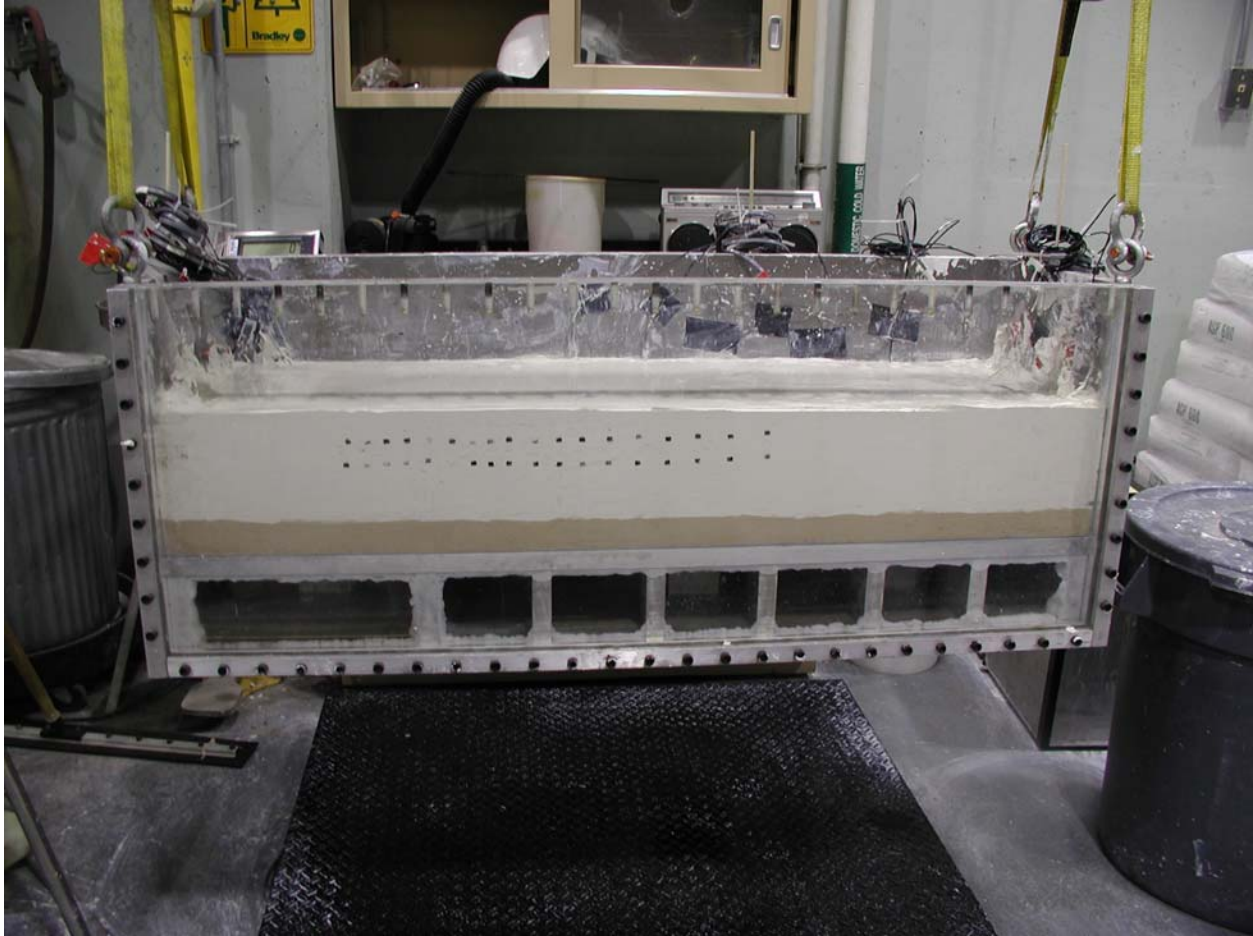


Figure 5.43. View of the completed clay layer for the ERDC 17th Street model

After completion of the clay layer, the swampy/marsh layer was placed. This was material taken directly from the site collected in 40.5 cm cube undisturbed block samples. The material was stored in a humid room prior to use and sliced into segments of the appropriate thickness for use in the model. A view of the model with swampy/marsh layer in place is shown in Figure 5.44.

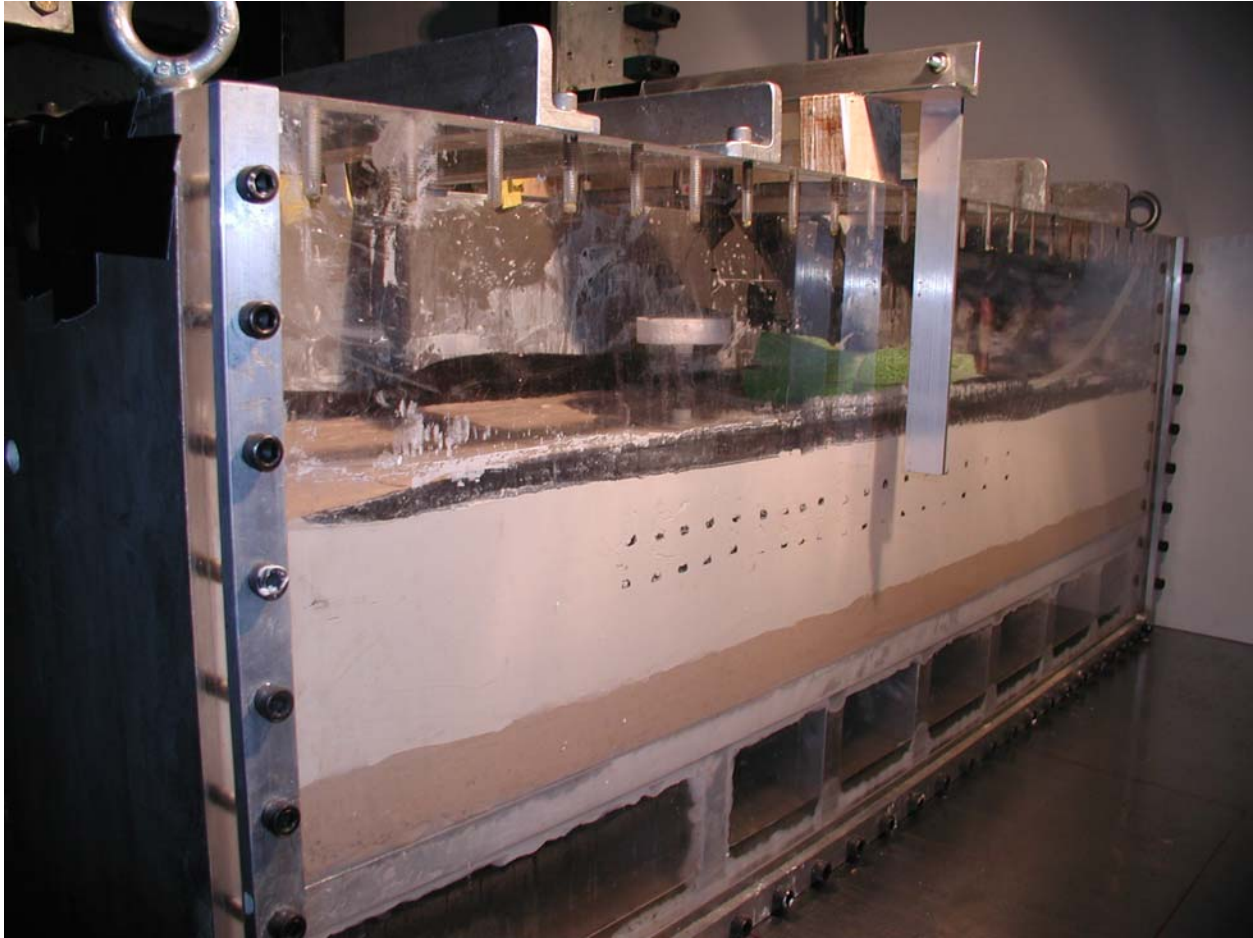


Figure 5.44. View of ERDC 17th Street model with swampy/marsh layer

This layer had markers similar to the clay layer placed for tracking movement and PPT's added for measuring pore pressure. Prior to placement of the swampy/marsh material both vane shear and moisture contents were obtained. Average values for the vane shear readings were 280 psf and the moisture contents 324%.

The clay layer was normally consolidated at 50 g. Additionally, gravel was added of a shape and weight simulating the levee to further consolidate the swampy/marsh layer. This material was removed and the consolidated clay levee added. Vane shear measurements of the clay levee material averaged 325 psf and moisture contents averaged 105%. Lasers to measure displacements were added and the model was placed on the centrifuge for testing at 50 g. The completed model is shown in Figure 5.45. The canal side is on the left of the model in the figure and the protected land side is on the right. The sheet pile wall on the canal side extends 4.6 m above the top of the levee.

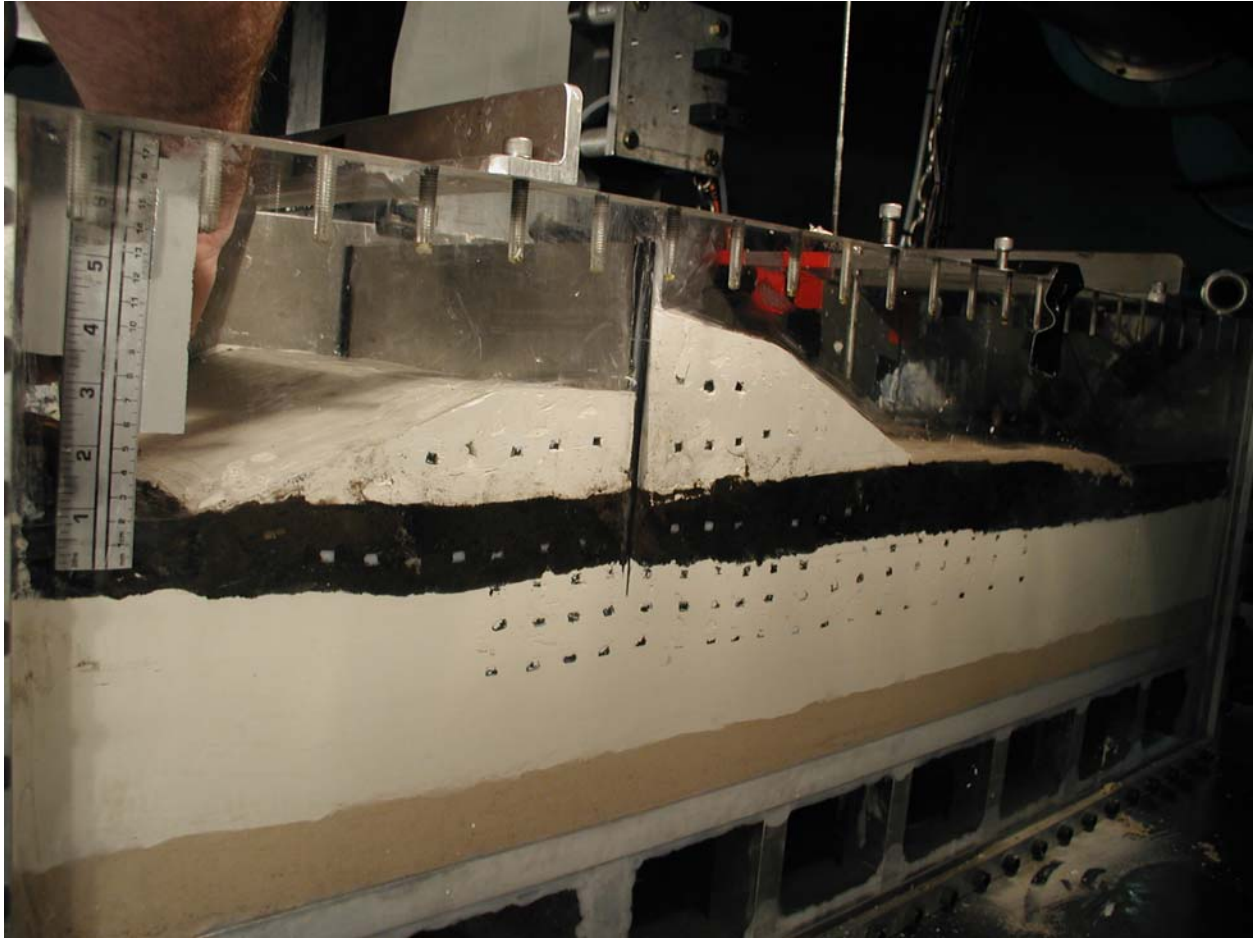


Figure 5.45. Completed ERDC 17th Street model

Once the model is completed and all instrumentation connected and zeroed, the package is slowly spun up to 50 g. Water is maintained in the canal at a depth of approximately 2.5 m until 50 g is reached. At 50 g, the model is properly scaled such that it has the correct weight, and pressure at all points in the model as would be the case in the field. The water level in the canal is increased to what it would be during normal canal operation level. In this case the normal canal level prior to Hurricane Katrina was approximately 30 cm above the canal levee top elevation. The model is allowed to stabilize (pore pressures equalize) at 50 g, with the correct canal water elevation prior to addition of flood load.

The flood load is applied to the model in a steady increment. Figure 5.46 is a sequence of still shots taken from the video recording detailing the flood and failure event. The failure event is as highlighted following.

1. Water level increases to a point on the wall where initial movement of the wall begins to occur. This movement starts out as a rotation of the wall.
2. A crack begins to form between the sheet wall and canal side levee.

3. As the crack reaches the bottom of the sheet pile, hydrostatic pressure increases in the foundation soil. The low shear strength in the clay layer just beneath the swampy/marsh is not enough to resist the driving force of the flood load.
4. A near horizontal shear failure surface forms in the clay layer and the entire wall/land side levee begins to translate toward the land side.
5. As the flood load is maintained the translational failure continues.



Figure 5.46a. ERDC 17th Street model at flood load just prior to development of crack



Figure 5.46b. ERDC 17th Street model just after wall movement and crack formation

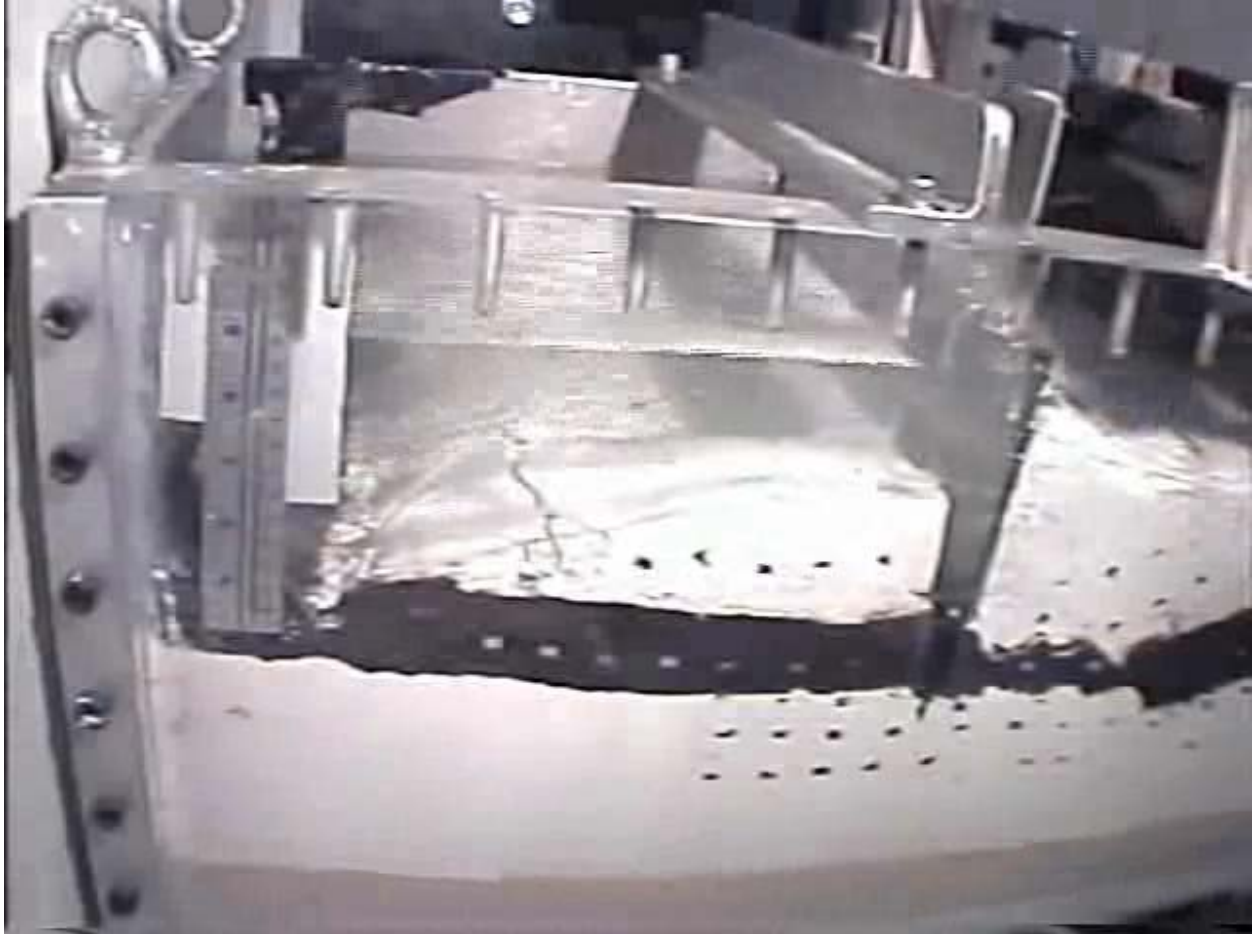


Figure 5.46c. ERDC 17th Street model near end of failure

At completion of the test, sample tubes were pushed through the levee and foundation on the landside for laboratory testing. Average values of the moisture contents for the levee section were 53%, for the swampy/marsh 155%, and for the foundation clay layer 58%.

The next series of plots will show the recorded data during the actual flood event. Recall that the model is at 50 g such that everything is properly scaled to field weights and pressures, the water is held at normal canal operating elevation, and all instruments have equalized under those conditions prior to addition of the flood load. The data is presented in Figures 5.47 through 5.50. Figure 5.47 is a plot of the PPT's located mid-depth of the foundation clay layer. Detailed discussions related to the processes and mechanisms occurring during the flood load and subsequent failure were previously discussed. Figure 5.48 is a plot of the PPT's located near the top of the foundation clay layer, revealing a similar characteristic as the mid-depth PPT's. Figure 5.49 is a plot of the PPT's located in the swampy/marsh layer and the levee both canal and land side. Finally, Figure 5.50 is a plot of the lasers, three on the sheet pile wall and one on the land side surface away from the toe. Notice that there is some heaving of the foundation away from the toe on the land side as the failure occurs.

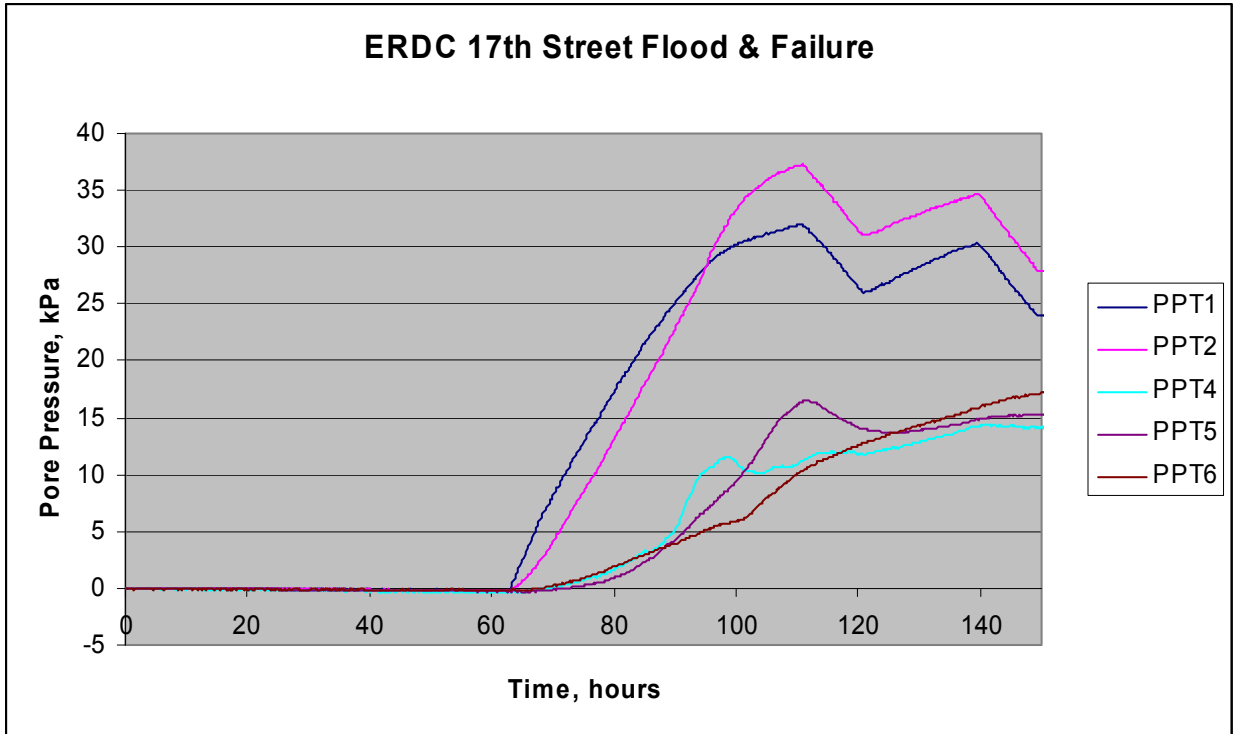


Figure 5.47. Data from mid-depth of foundation clay layer during flood loading

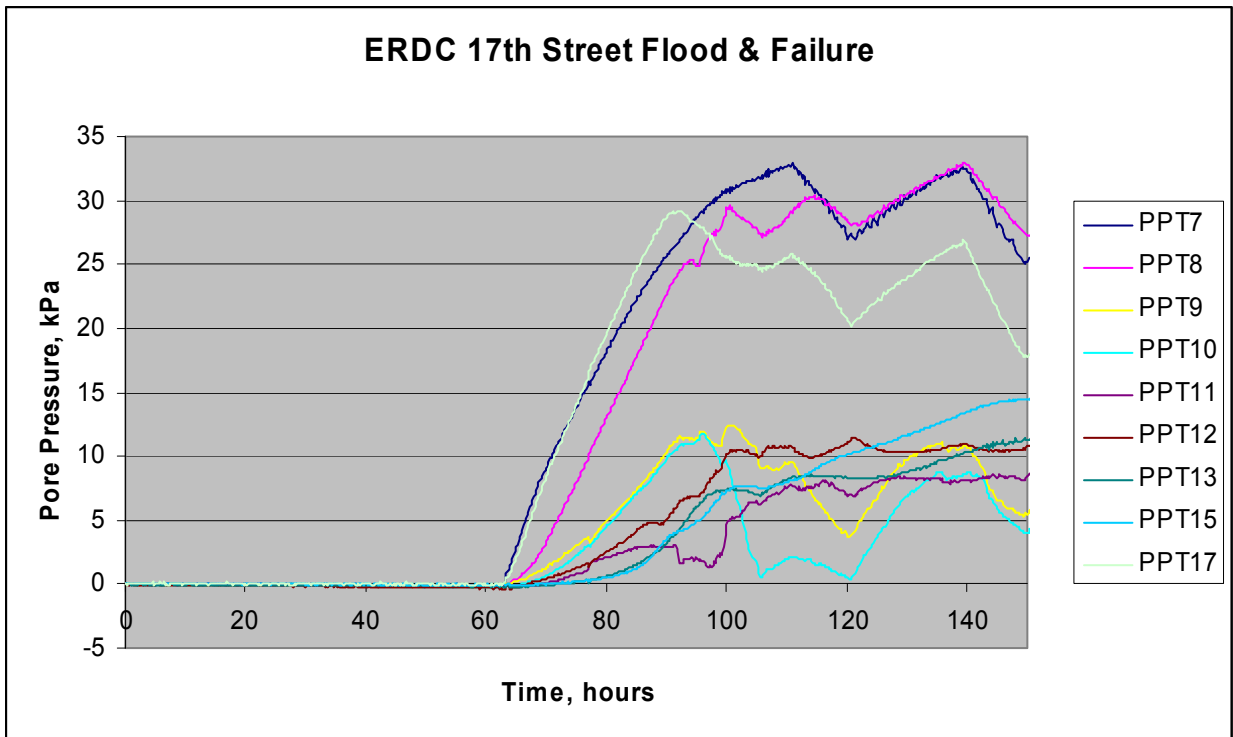


Figure 5.48. Data from top of foundation clay layer during flood loading

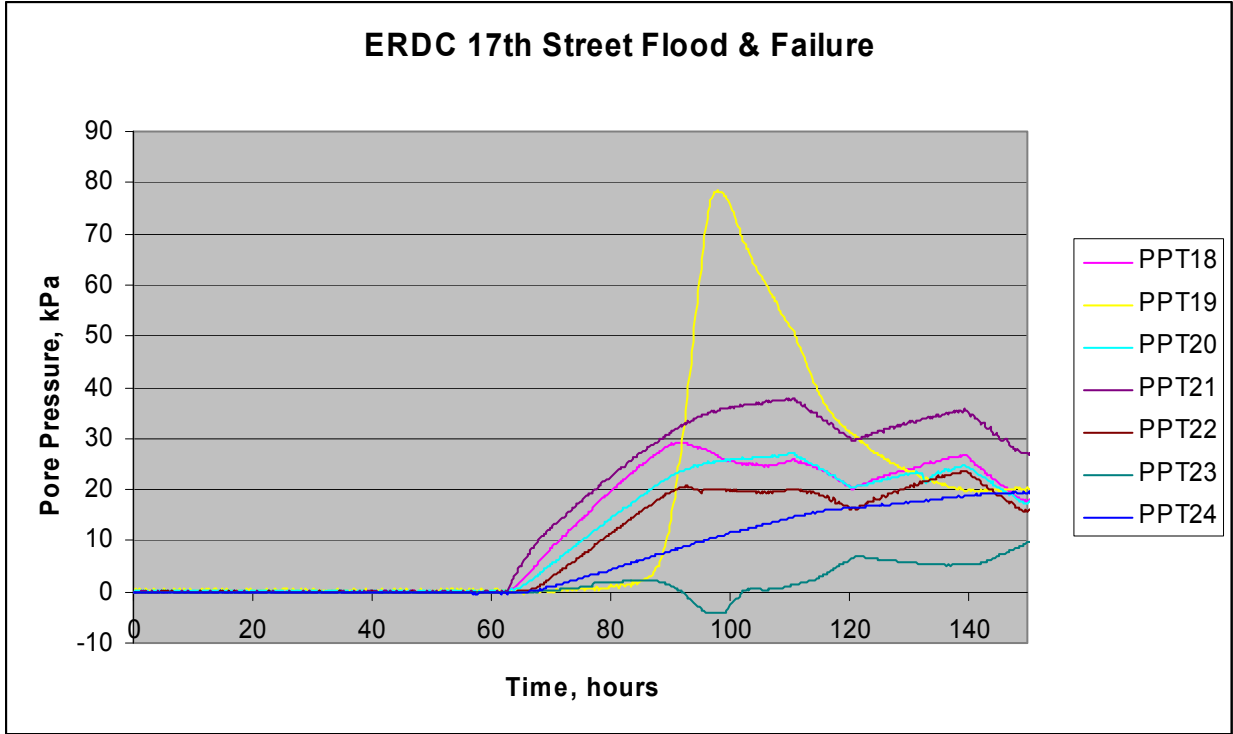


Figure 5.49. Data from levee and swampy/marsh during flood loading

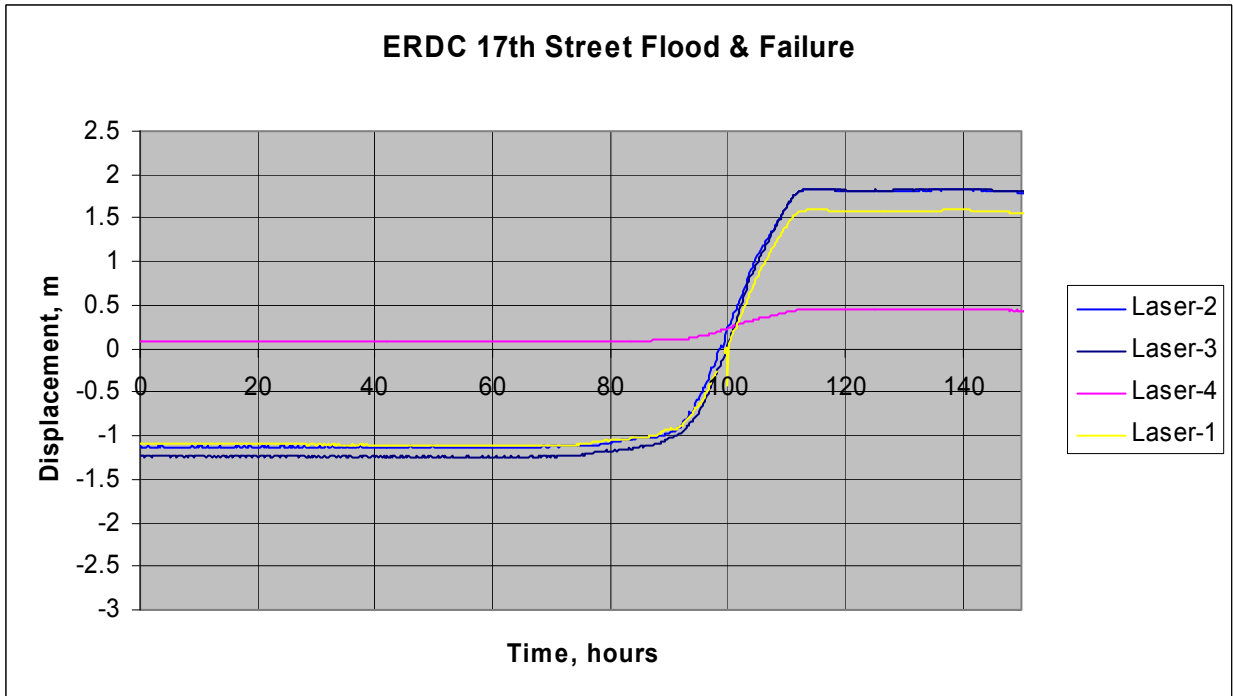


Figure 5.50. Displacement data from lasers during flood loading

RPI 17th Street Canal Model

A second model of the 17th Street canal breach was conducted at RPI. The model is shown in Figure 5.51. Material used in the model and construction sequence was exactly as described for the ERDC model above. Moisture content in the foundation clay layer averaged 61% with strength from the vane shear of 125 psf. For the levee the moisture content was average of 47% with vane shear strength of 355 psf. The swampy/marsh was consistent with the ERDC values since the material all came from the same area and was collected at the same time in the same manner.

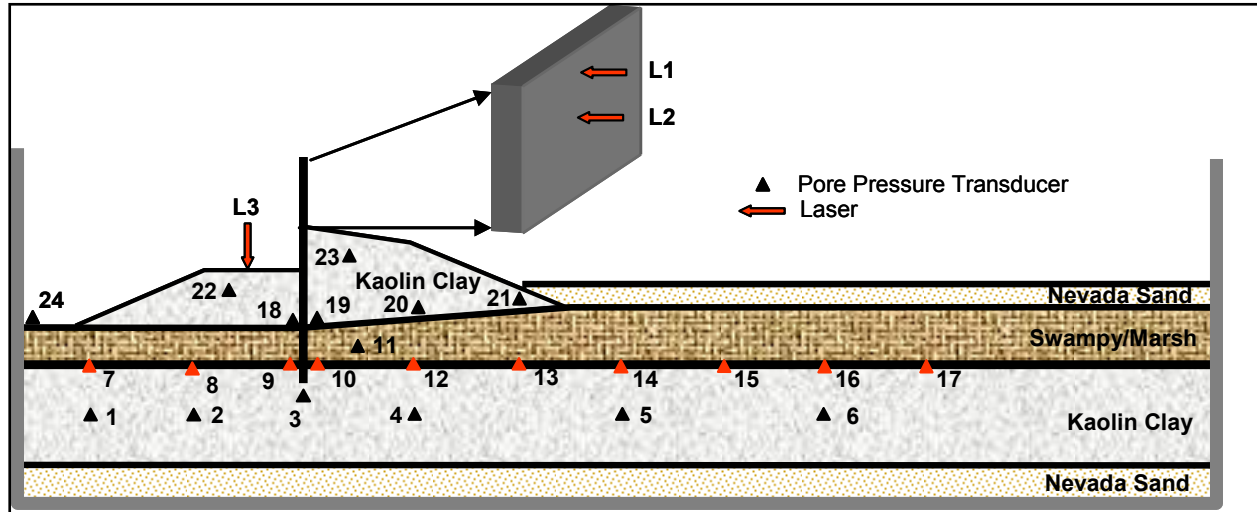


Figure 5.51. RPI 17th Street model

The following discussions and presentations focus on the flood and failure of the model. The model was spun to 50 g with water level held at a depth consistent with canal operating water level, instrumentation allowed to stabilize and ready for application of flood load. Results of the flood loading are presented in Figures 5.52 through 5.55. Figure 5.52 is a plot of the PPT data from series of transducers located in the foundation clay layer. The PPT shown in yellow on Figure 5.52 is attached to the bottom of the sheet pile wall in the clay layer. The sudden decrease and sharp increase in the reading is associated with development of the crack between the sheet pile wall and canal side levee.

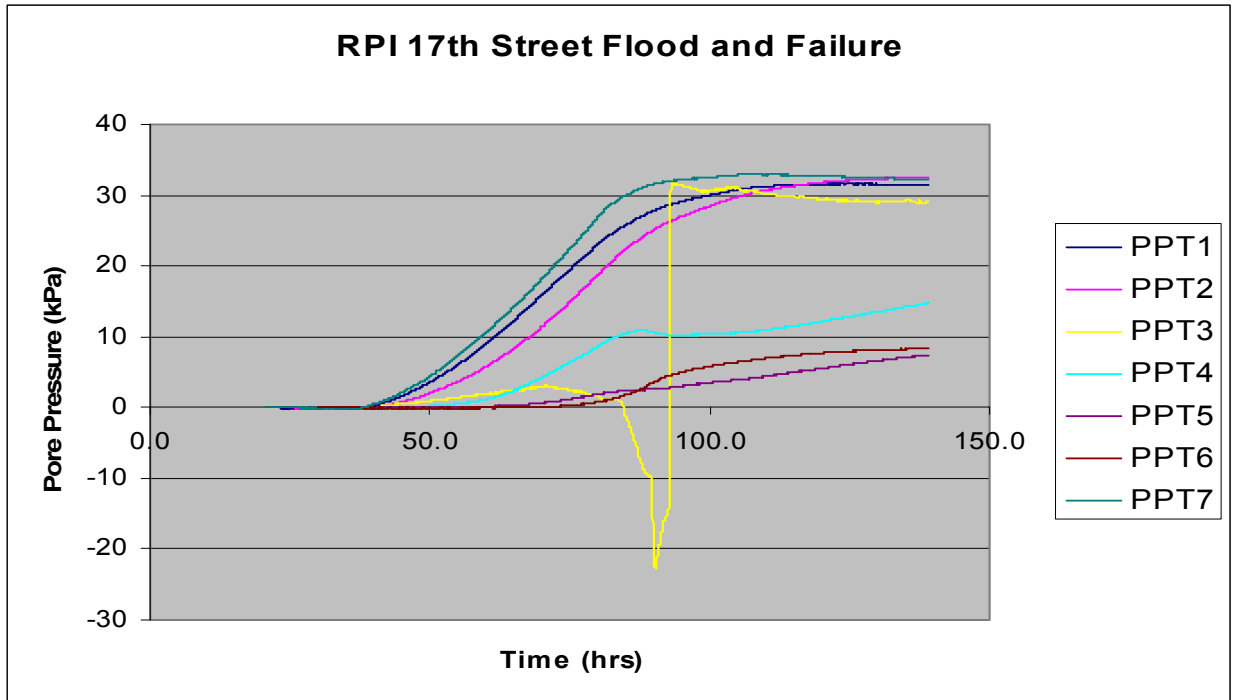


Figure 5.52. PPT data in foundation clay layer during flood and failure

Data from the PPT's located along the foundation clay swampy/marsh interface is shown in Figure 5.53. Notice that some of the PPT's show an initial rise in values followed by a drop in values then a sudden increase in values. These PPT's are located very near the sheet pile and are indicative of development of the crack. A second observation is the value of each PPT reading. The PPT values in Figure 5.53 from highest to lowest represent sensors located in the model moving from the canal side to the land side. So, the highest recorded values are in the material under the canal/land side with decreasing values under the land side levee and out into the free field. This is exactly as would be expected for this type of foundation material. Figure 5.54 is the recorded PPT data in the levee. Behavior is consistent with that previously discussed.

Figure 5.55 shows the recordings of the lasers on the sheet pile wall and top of the levee canal side. In the figure, the green and blue curves show movement of the wall with the two measurements on the same vertical plane of the wall but separated some distance apart. This arrangement allows determination of how the wall moved in terms of rotation, translation, etc. The data show that from start of movement until sometime thereafter, the wall movement was translational and at the very end became more rotational (the lines are diverging). This is an important point in confirming that the failure was translational. The red curve in the plot is the displacement of the canal side levee during the flood and failure.

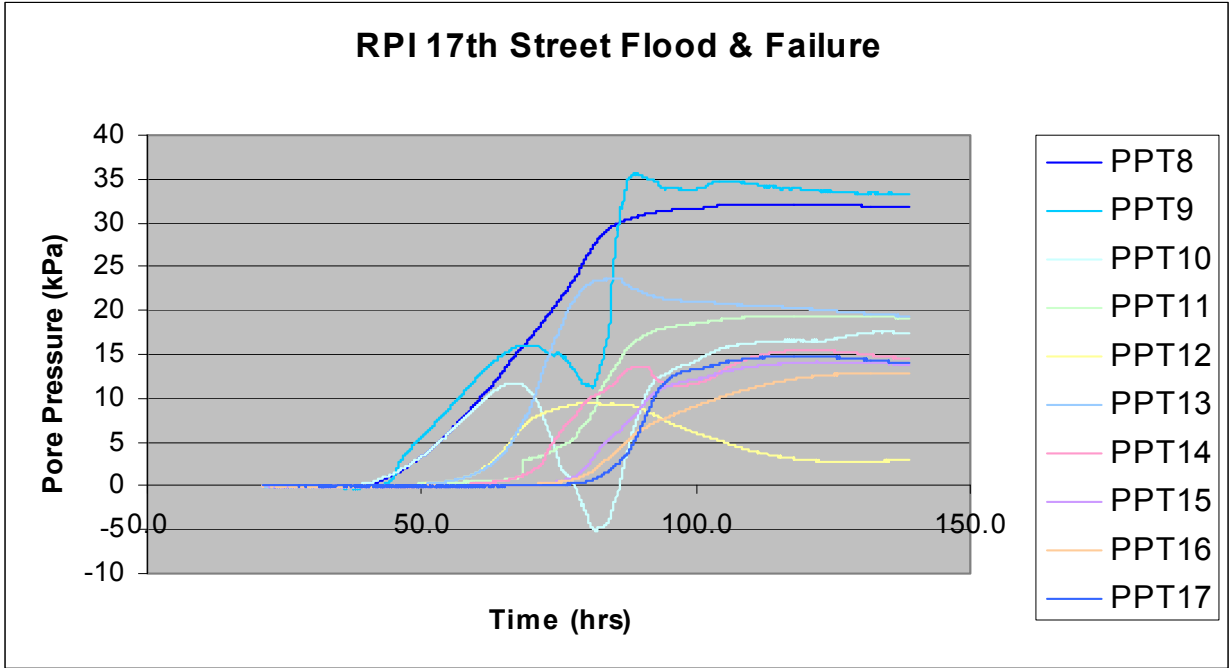


Figure 5.53. PPT data along the foundation clay swampy/marsh interface during flood and failure

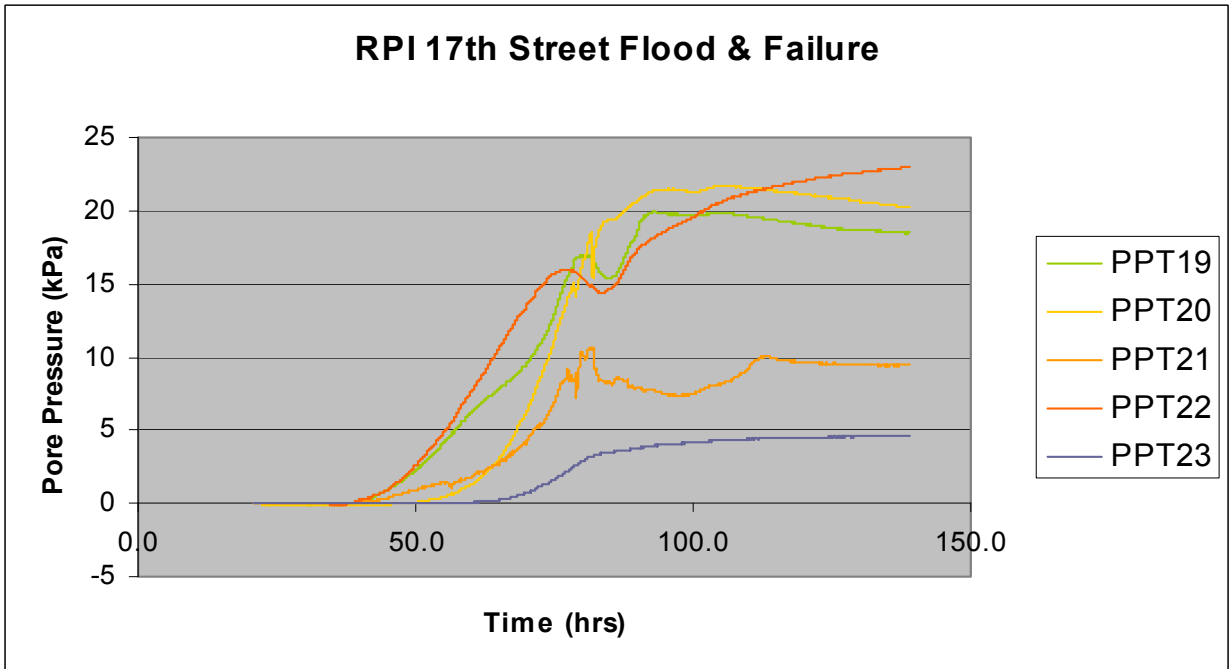


Figure 5.54. PPT data in the levee during flood and failure

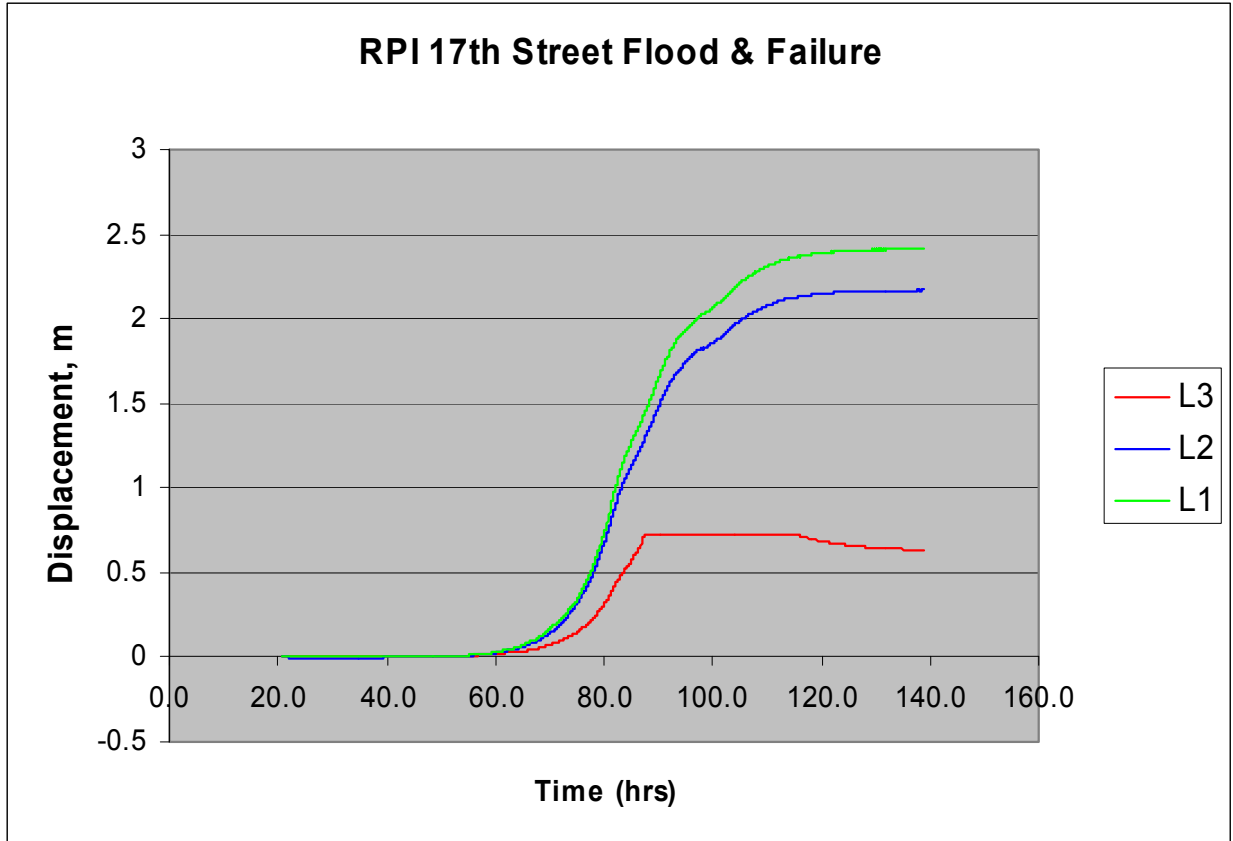


Figure 5.55. Displacement recordings of the sheet pile and canal side levee

The following series of pictures are still captures from the video recorded during flood and failure. Figure 5.56 is a shot captured with the water elevation at maximum level just prior to any wall movement. In the figures, the canal side is on the left and the protected side on the right. The sheet pile can be seen in the middle of the figure with the shorter canal levee on the left and the taller land side levee on the right.



Figure 5.56. RPI 17th Street model during flood load

In Figure 5.57, the wall has moved toward the land side, a crack has formed between the sheet pile wall and canal levee. The crack has penetrated through the levee, through the swampy/marsh and into the top surface of the clay layer.



Figure 5.57. RPI 17th Street model just after movement of wall and crack formation



Figure 5.58. RPI 17th Street model in process of translational failure

Figure 5.58 shows the model at a time where the failure is well in progress. Attention should be given to the row of markers just below the swampy/marsh layer in the clay on the land side of the sheet pile. Notice that the entire row of markers has moved to the right while the row of markers below remains unmoved. Also notice that the wall has remained at a similar angle as in Figure 5.57. All of this information indicates that there is a horizontal failure plane in the clay and that the wall-land side levee-land side swampy/marsh is translating to the right. Figure 5.59 is a view near the end of failure. Notice the row of markers displaced well to the right and the non-rotated nature of the sheet pile wall. Again indications of translational failure along a horizontal failure plane in the foundation clay layer.



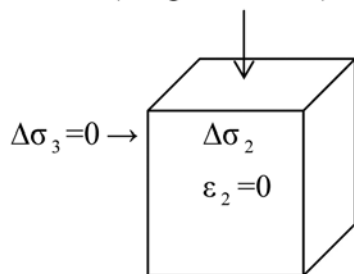
Figure 5.59. RPI 17th Street model near end of flood failure

Discussion presented in the following section will highlight the agreement between the measured data in the foundation clay layer and basic soil mechanics predicted behavior. Focusing on the foundation clay layer material on the canal side before any failure, the following observations can be made.

Measured Δu on the upstream side before levee failure

$$\Delta\sigma_1 = \Delta\sigma_w \text{ (weight of water) - levee weight near the toe}$$

Assuming levee weight near the toe is small,
then $\Delta\sigma_1 = \Delta\sigma_w$



$$\varepsilon_2 = \frac{1}{E} [\Delta\sigma_2 - \mu(\Delta\sigma_1 + \Delta\sigma_3)]$$

$$0 = \frac{1}{E} [\Delta\sigma_2 - \mu\Delta\sigma_1]$$

$$0 = \Delta\sigma_2 - \mu\Delta\sigma_w \rightarrow \text{for undrained condition. } \mu=0.5$$

$$\Delta\sigma_2 = 0.5 \Delta\sigma_w$$

$$\Delta u = A (\Delta\sigma_1 + \Delta\sigma_2 + \Delta\sigma_3) \quad A = \frac{1}{3}$$

$$\Delta u = \frac{1}{3} (\Delta\sigma_1 + \Delta\sigma_2)$$

$$\Delta u = \frac{1}{3} (\Delta\sigma_w + 0.5 \Delta\sigma_w)$$

$$\Delta u = 0.5 \Delta\sigma_w$$

As shown in Figure 5.60, in the early stages of water rise, with the canal level very low, the ratio between the increase in water pressure $\Delta\sigma_w$ (red line) and the increase in measured (blue and green lines) near the toe varies between 0.4-0.55 (comparing the slope of the lines). As the water rises higher, the rate of increase of water pressure Δu increases to match the rate of increase of total vertical stress, $\Delta\sigma_w$, indicating one dimensional loading in the clay layer at higher water levels.

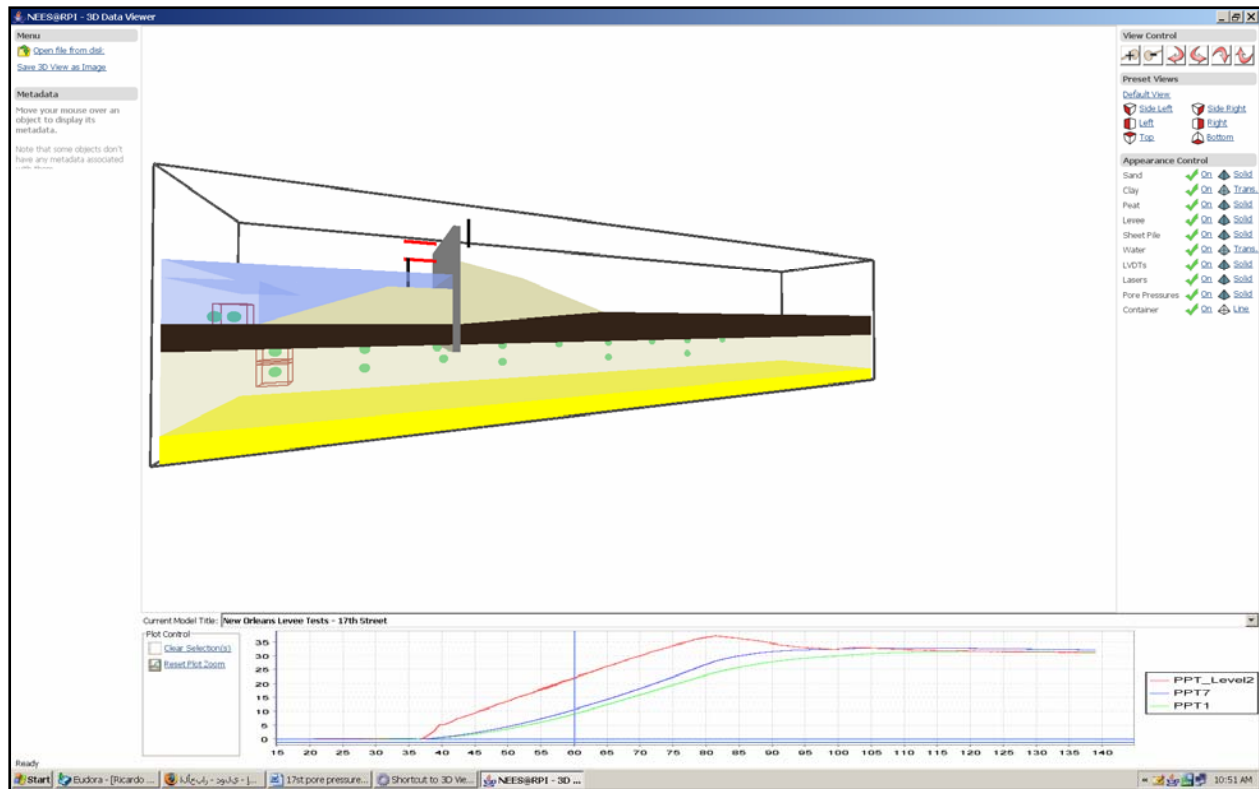


Figure 5.60. PPT data for transducers as indicated in the figure

Measured Δu on the downstream side due to levee failure

It is assumed that the soil outside the failure zone remains elastic (Figure 5.61). A soil element outside the failure zone will be subjected to an increase in the horizontal pressure while the vertical pressure remains constant. Thus $\Delta\sigma_1 = \Delta\sigma_h$ and $\Delta\sigma_3 = \Delta\sigma_v = 0$. For plain strain condition $\epsilon_2 = 0$.



Figure 5.61. View of model after failure

$$\varepsilon_2 = \frac{1}{E} [\Delta\sigma_2 - \mu (\Delta\sigma_1 + \Delta\sigma_3)]$$

$$\Delta\sigma_2 - \mu (\Delta\sigma_1 + \Delta\sigma_3) = 0$$

$$\Delta\sigma_2 - \mu \Delta\sigma_1 = 0$$

$$\Delta\sigma_2 = \mu \Delta\sigma_1 \text{ for undrained condition. } \mu=0.5$$

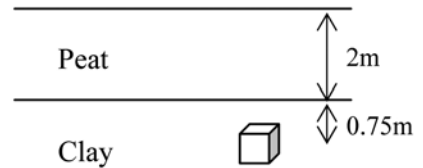
$$\Delta\sigma_2 = 0.5 \Delta\sigma_1$$

$$\Delta\sigma_1 = \sum \gamma_t H (k_p - k_0) + 2 S_u$$

$$\Delta\sigma_1 = (12.5 * 2 * 0.5 + 17.5 * 0.75 * 0.5) + 2 * 5$$

$$\Delta\sigma_1 = 29 \text{ kpa}$$

$$\Delta\sigma_2 = 0.5 \Delta\sigma_1 = 0.5 (29) = 14.5 \text{ kpa}$$



$$\Delta u = A (\Delta\sigma_1 + \Delta\sigma_2 + \Delta\sigma_3) \quad A = \frac{1}{3}$$

$$\Delta u = \frac{1}{3} (\Delta\sigma_1 + \Delta\sigma_2)$$

$$\Delta u = \frac{1}{3} (29 + 14.5) = 14.5 \text{ kpa}$$

As shown in Figure 5.62 the pore pressure measured by the three pore pressure sensors just outside of the failure zone recorded about 14kpa. It is important to note that the measured Δu indicate that it started to increase at the same time the levee started to fail.

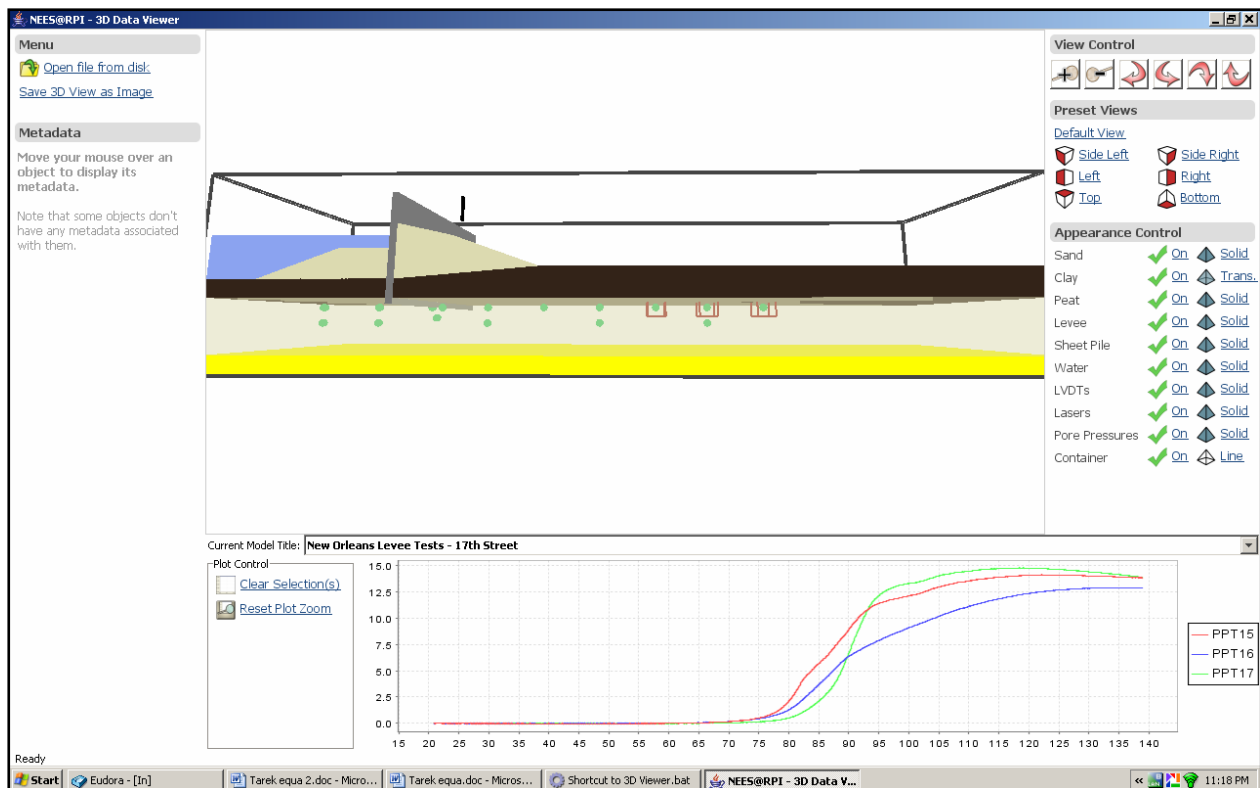


Figure 5.62. PPT data for the transducers as indicated in the figure

All of the information presented and discussed for the RPI 17th Street model enforces the following observations about the model behavior.

1. At a certain time during rise in canal water elevation, the wall moved slightly to the land side and allowed the start of a crack forming.
2. This crack propagated down through the canal side levee, the swampy/marsh layer, and the top portion of the foundation clay layer to the end of the sheet pile.

3. This allowed full hydrostatic pressures to reach the underlying foundation material.
4. A horizontal failure surface forms in the foundation clay layer and the entire land side levee material translates along this surface to the land side.
5. This movement continues as the water load remains constant leading to total failure of the levee.

Physical Models of London Avenue Canal, South Breach

Two models of a section at the south breach location of London Avenue canal were completed. One of the models was performed at RPI and the other at ERDC. This section of the report will present information relevant to each model.

ERDC London Avenue Canal, South Breach Model

The model representative of a section through the south breach at London Avenue canal is shown in Figure 5.63.

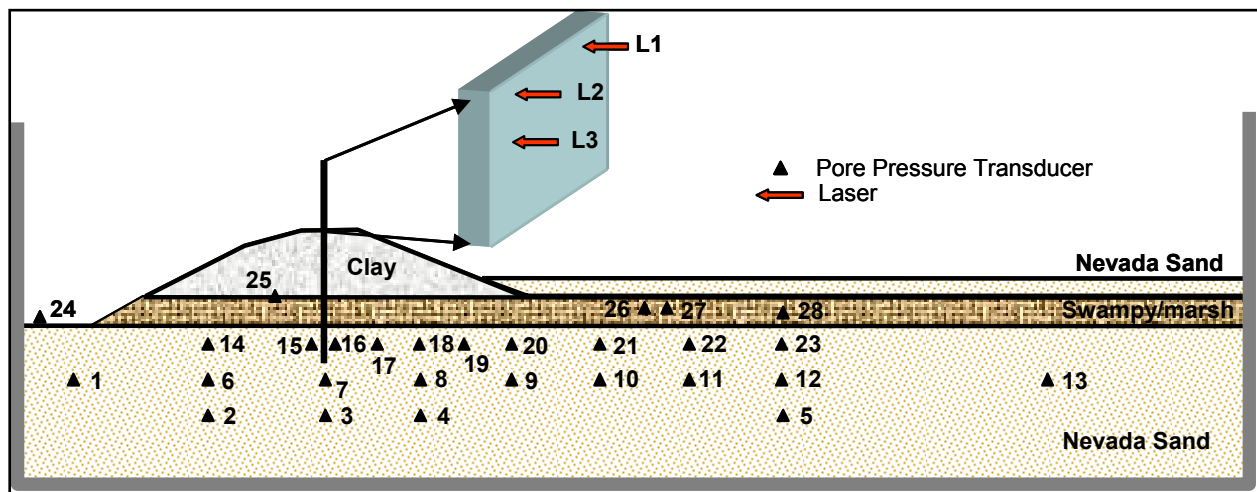


Figure 5.63. Physical model of ERDC London Avenue canal, south breach area

The sequence of model construction and testing were as previously discussed for other models. Prior to placement of the swampy/marsh material both penetrometer and moisture contents were obtained. Average values for the penetration testing were 400 psf and the moisture contents 357%. Penetration measurements of the levee material after consolidation averaged 360 psf and moisture contents averaged 61%. A view of the model with saturated sand layer and swampy/marsh layer in place is shown in Figure 5.64.

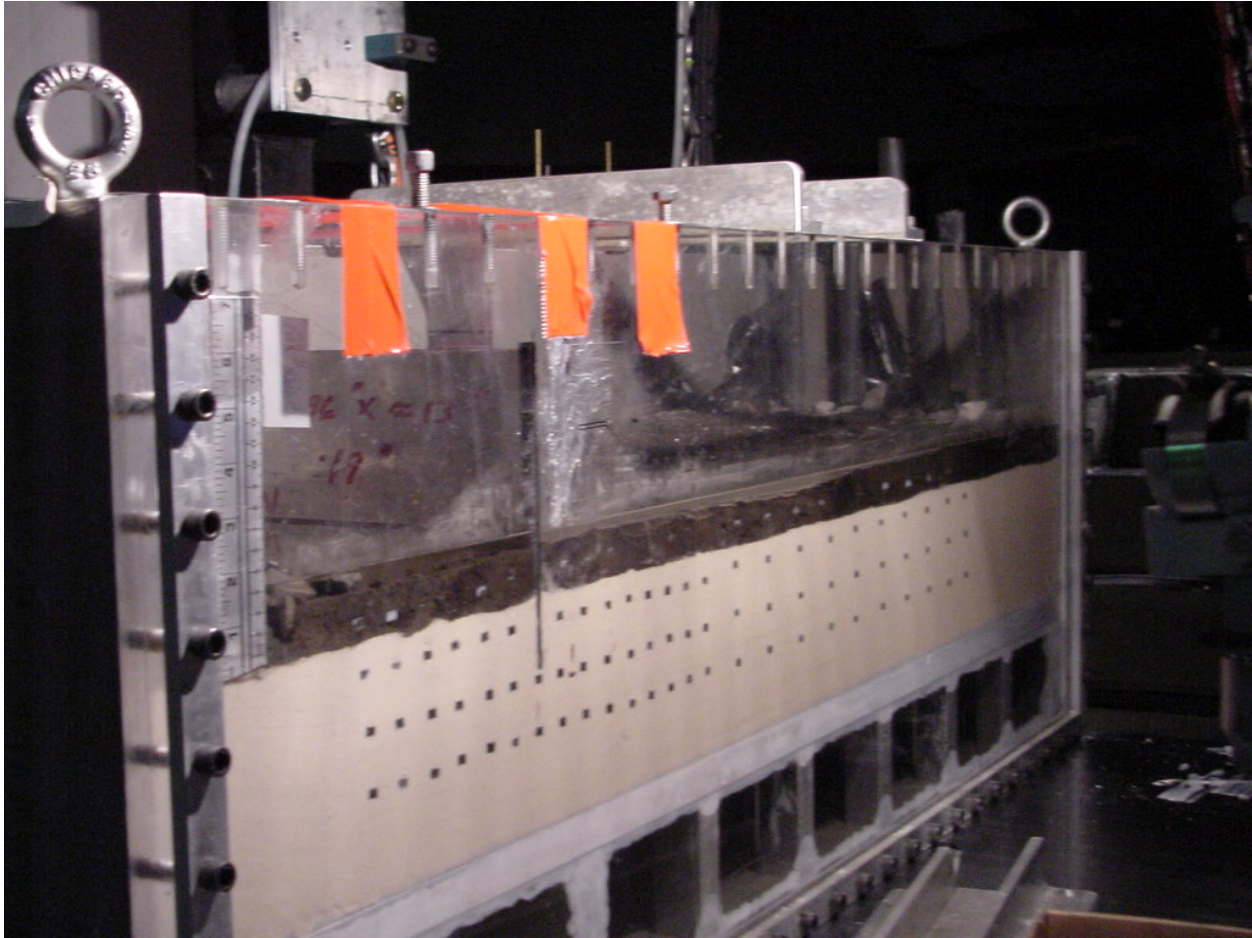


Figure 5.64. View of the ERDC model with sand and swampy/marsh layer

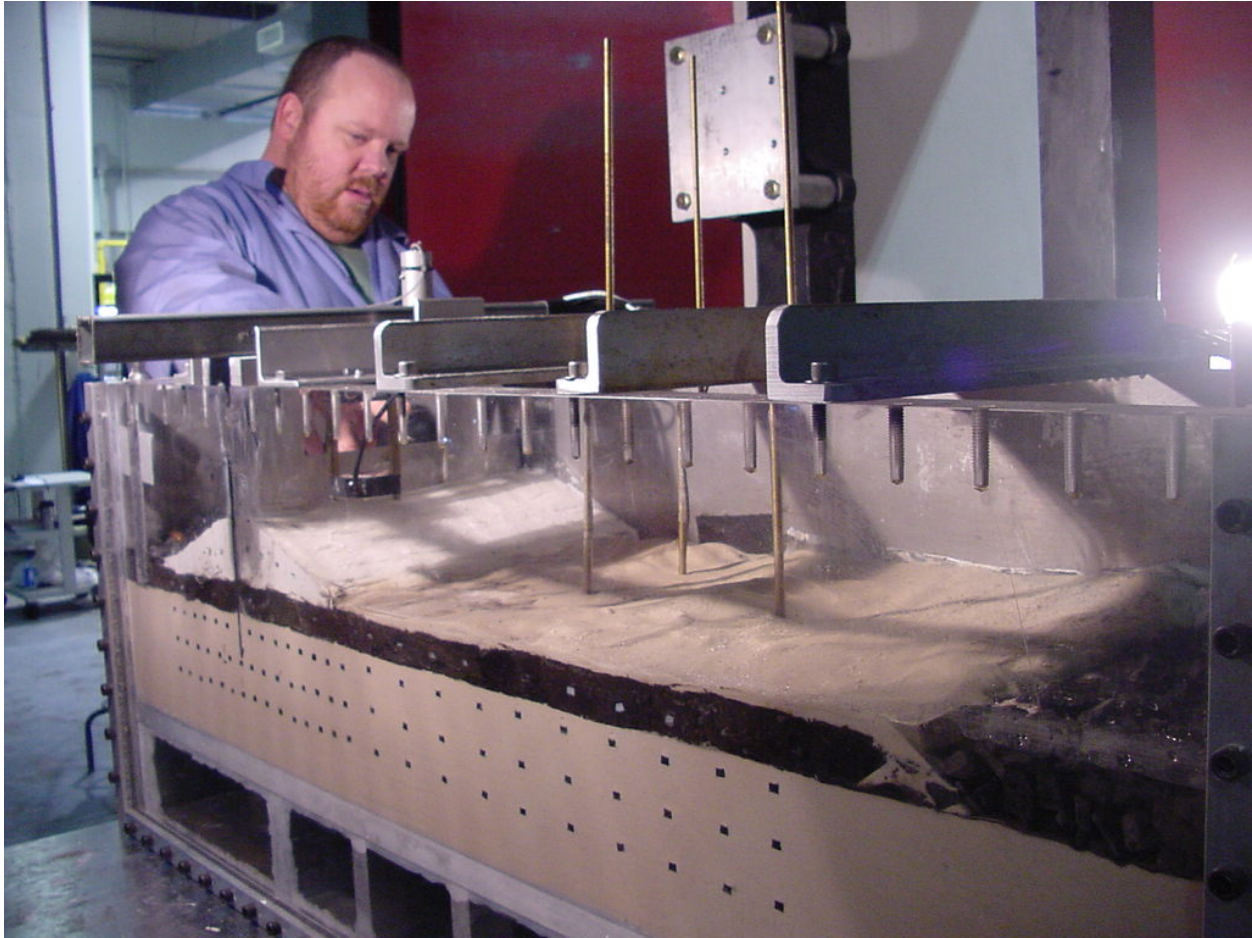


Figure 5.65. Completed ERDC London Avenue south model

The completed model is shown in Figure 5.65. The canal side is on the left of the model in the figure and the protected land side is on the right. The canal side and land side levees were nearly identical in height. The sheet pile wall extends 2.5 m above the top of the levee.

Once the model is completed and all instrumentation connected and zeroed, the package is slowly spun up to 50 g. Water is maintained in the canal at a depth of approximately 1 m until 50 g is reached. At 50 g, the model is properly scaled such that it has the correct weight, and pressure at all points in the model as would be the case in the field. The water level in the canal is increased to what it would be during normal canal operation level. In this case the normal canal level prior to Hurricane Katrina was approximately 30 cm above the canal levee top elevation. The model is allowed to stabilize (pore pressures equalize) at 50 g with the correct canal water elevation prior to addition of flood load.

Figure 5.66 is a sequence of still shots taken from the video recording detailing the flood and failure event. The failure event is as highlighted following.

1. Water level increases to a point on the wall where initial movement of the wall begins to occur. This movement starts out as a rotation of the wall.

2. A crack begins to form between the sheet wall and canal side levee and propagates downward.
3. The crack extends all the way through the levee and the swampy/marsh layer to the top of the sand layer.
4. Full hydrostatic pressure is allowed to reach the foundation sand layer causing a sudden increase in pore water pressure.
5. This increase in pore water pressure reduces the vertical effective stress of the overlying swampy/marsh and levee material. Effectively the land side material approaches zero effective stress and begins to 'float'.
6. Load from the flood pushes the wall over in a rotational manner with no resisting force from the land side material.

This failure mechanism will be shown through the recorded data to be presented and discussed following. Post test measurements of the swampy/marsh and levee material were taken and produced these results. Moisture contents in the swampy/marsh on the canal side were 301% and on the land side 217%. For the clay levee, canal side moisture contents were 64% and land side 61%.

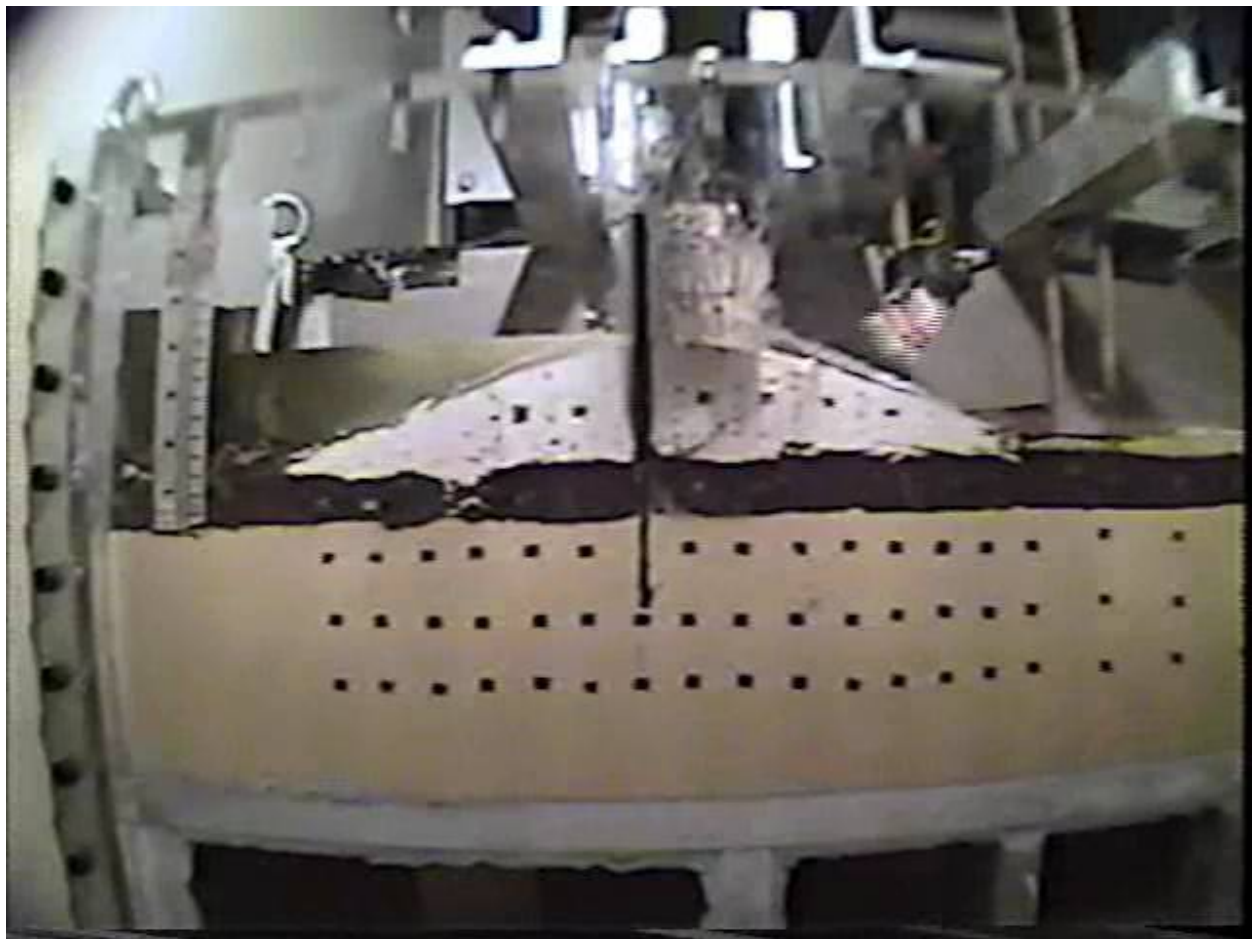


Figure 5.66a. ERDC London Avenue south model at normal canal water level

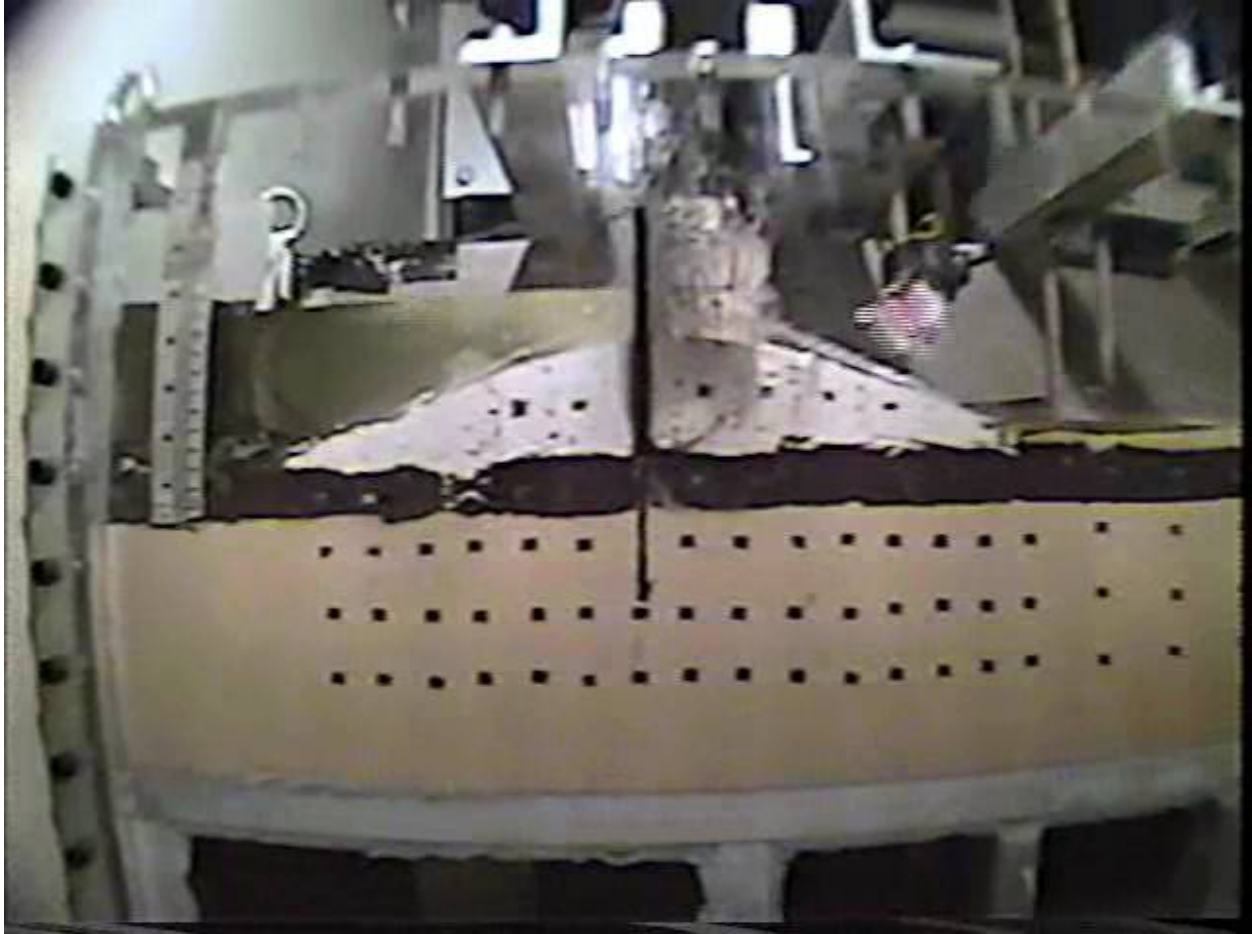


Figure 5.66b. ERDC London Avenue south model at flood level just prior to any wall movement

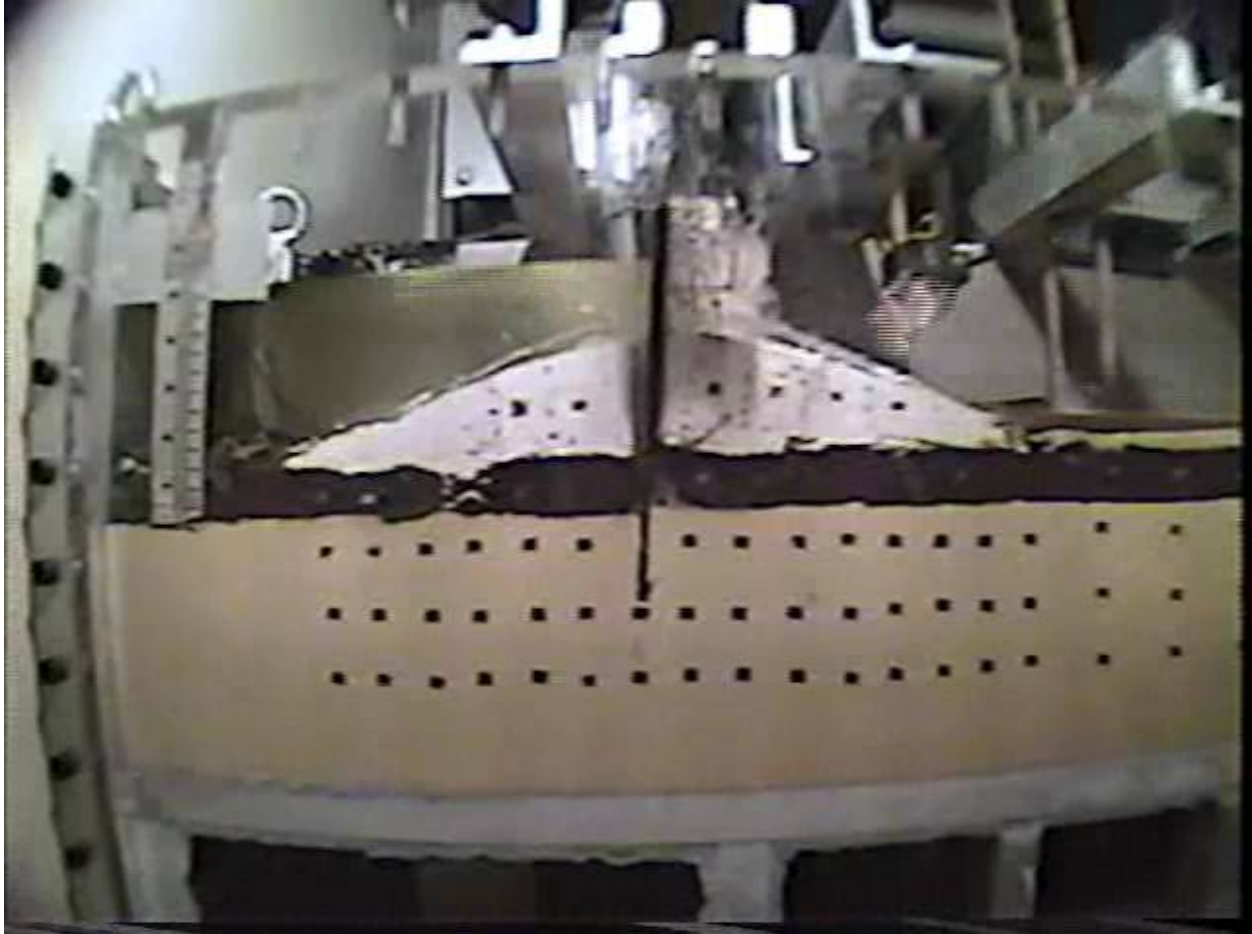


Figure 5.66c. ERDC London Avenue south model after wall movement and crack formation

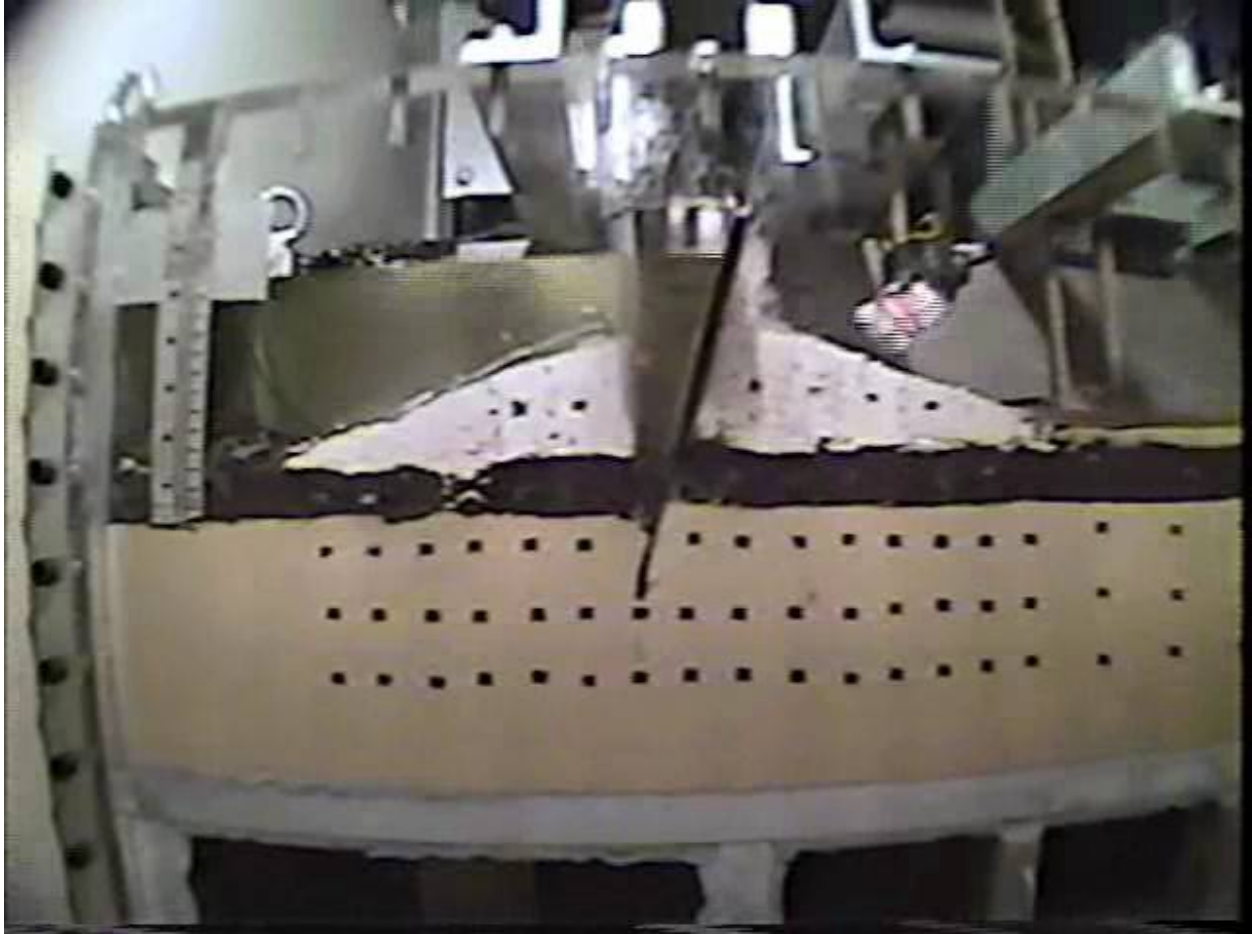


Figure 5.66d. ERDC London Avenue south model well into failure model



Figure 5.66e. ERDC London Avenue south model at end of test

The data recorded during the flood loading are presented in the following figures. The model is at 50 g, water level in the canal is at normal operating levels, and the flood load is steadily applied. Figure 5.67 presents the results of the PPT's at depth in the sand layer. Figure 5.68 is a plot of PPT data from the top of the sand layer with behavior as shown in Figure 5.67. Notice the change in character of the data indicated by a very short plateau, this is the onset of crack formation and the wall really rotating. This is most evident in PPT's 15 and 16 which are located very close to the wall.

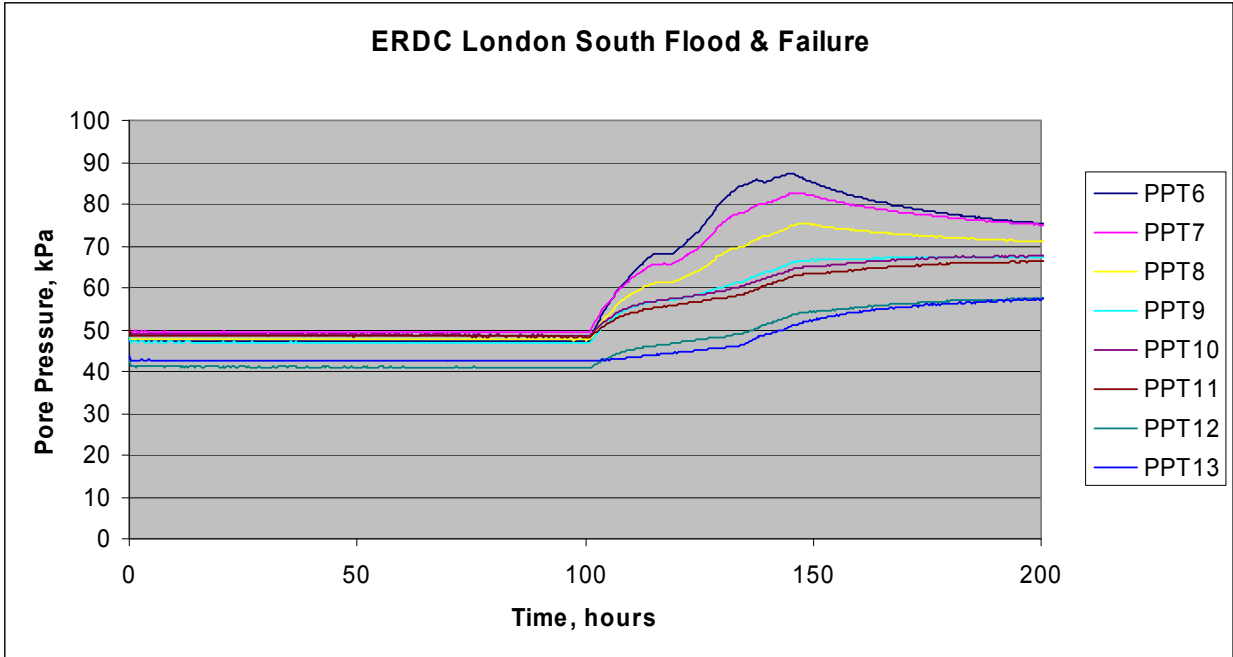


Figure 5.67. PPT data at depth in the sand layer during flood load

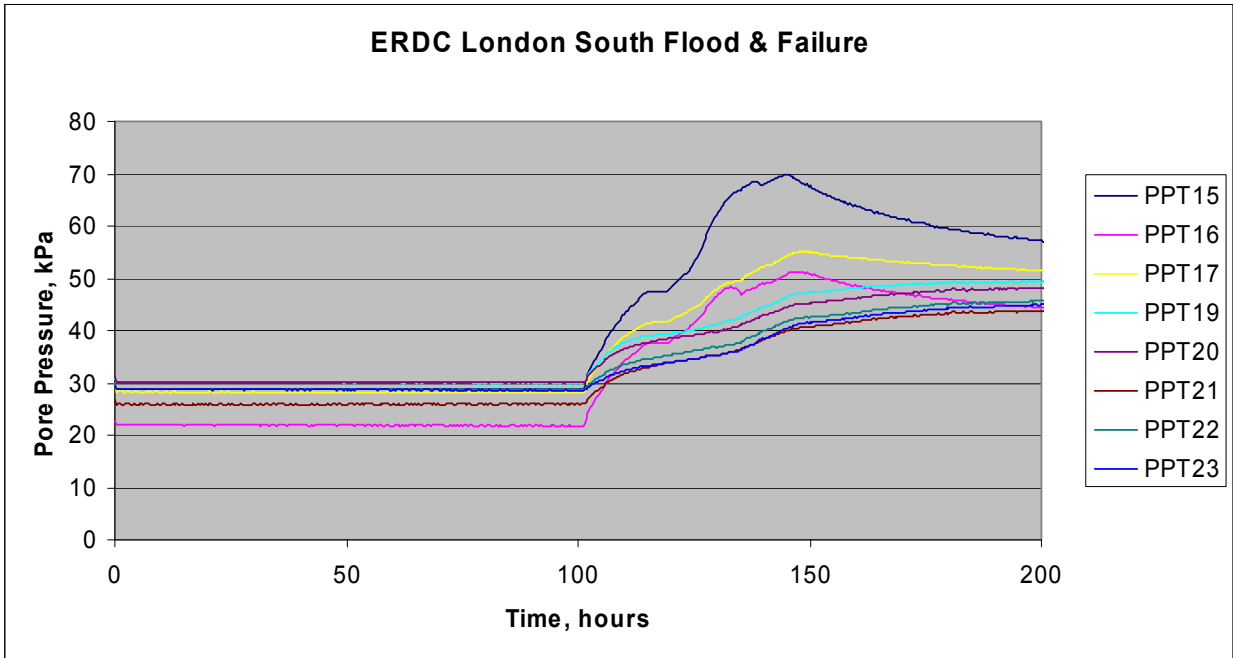


Figure 5.68. PPT data near the top of the sand layer during flood load

Data from the PPT’s located in the levee and swampy/marsh is shown in Figure 5.69. Instrument 24 is located in the canal and tracks the increase in pore pressure associated with increase of water depth in the canal. As can be seen in data from the previous plot, there is a slight delay in reaction of the PPT data in the soil and that in the canal. Figure 5.70 shows the

displacement of the wall during the flood load. Notice that laser one and two are perfectly in sync. These are at the same elevation on the wall and reveal that wall movement remains constant along the plane of the wall (there is no twisting from front side to back side of the model). Secondly, notice that all lasers are moving together until later in time where laser three begins to change slope. This is an indication that the movement is becoming much more rotational in nature as the failure proceeds.

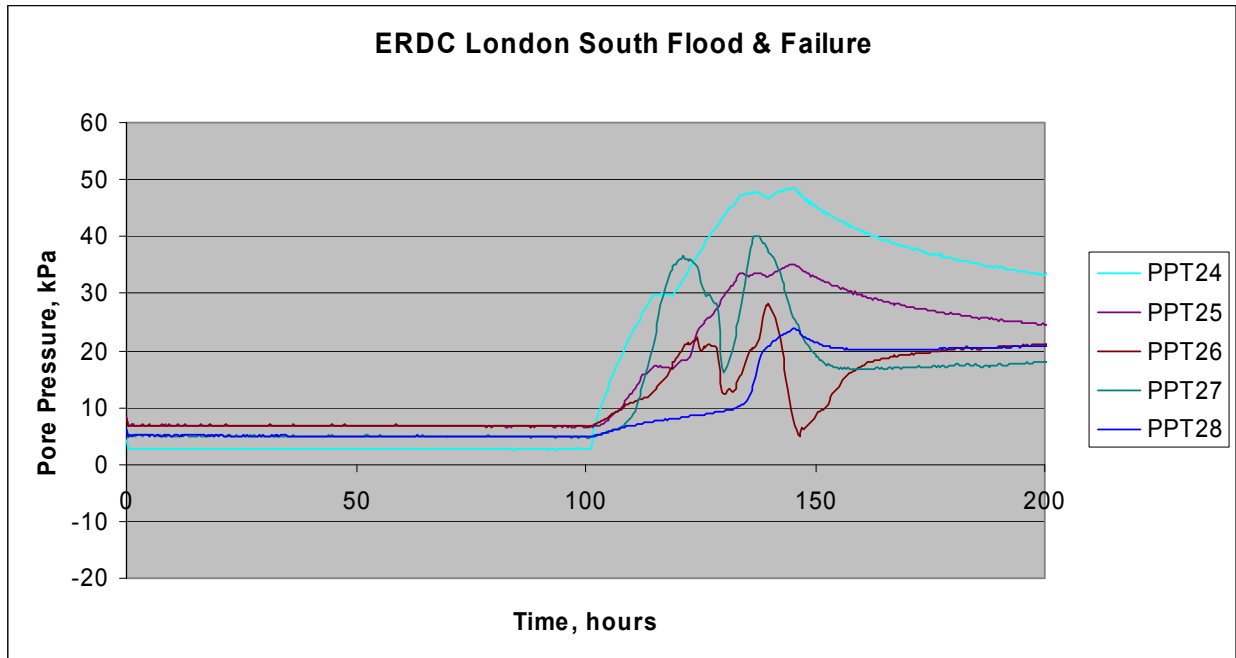


Figure 5.69. PPT data in the levee and swampy/marsh layer during flood load

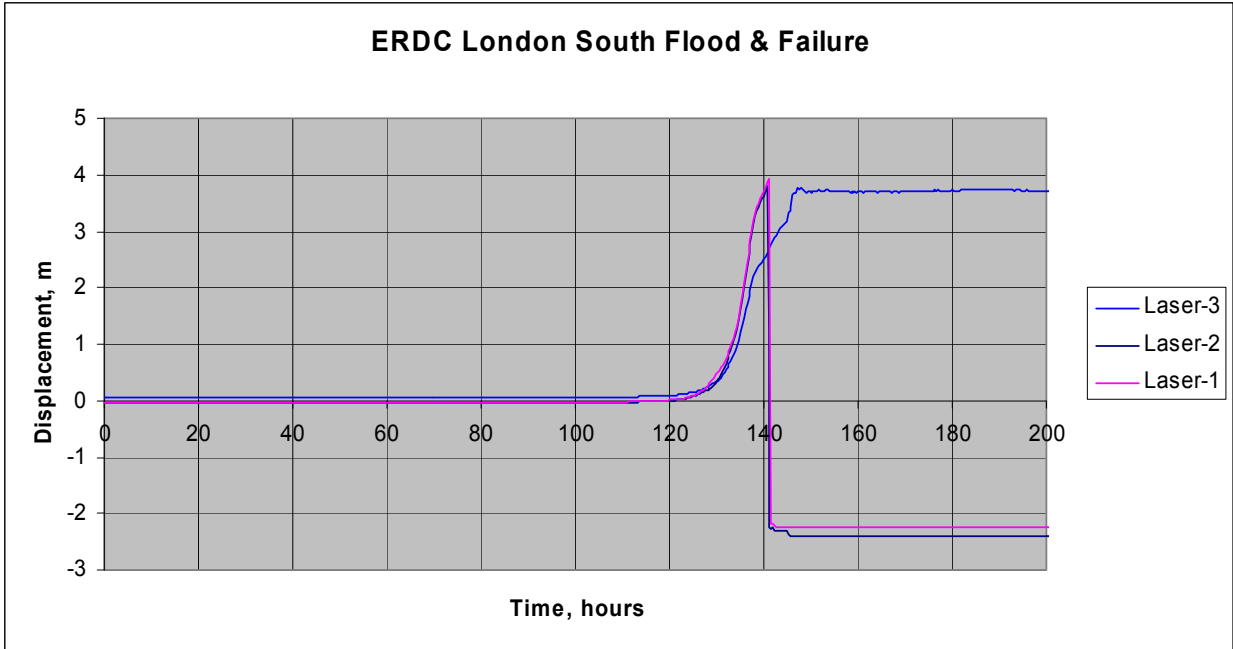


Figure 5.70. Displacement of the wall during flood load

RPI London Avenue Canal, South Breach Model

The second model representative of a section through the south breach at London Avenue canal tested at RPI is shown in Figure 5.71. The model has the same dimensions and makeup as described for the ERDC model.

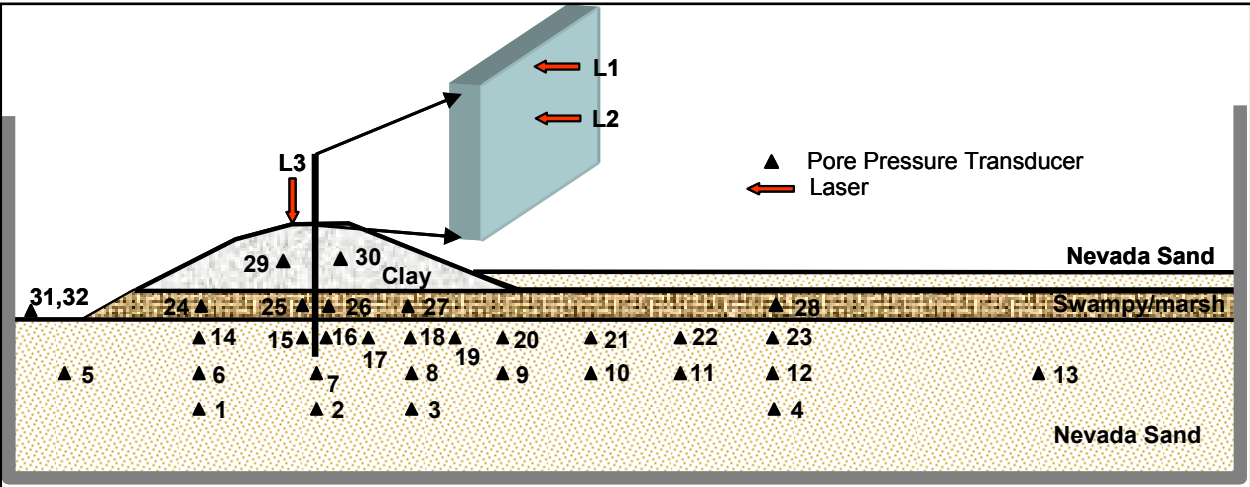


Figure 5.71. RPI London Avenue canal, south breach area model

The sequence of model construction and testing were as previously described for the ERDC model and will be briefly highlighted following. Measurements of water content in the clay

material after consolidation prior to forming the levee averaged 43% and vane shear measurements averaged 525 psf.

The model was slowly spun up to 50 g to prevent any sudden increase in pore pressure. Water elevation was maintained in the canal until reaching 50 g. At this point the water level was brought to normal canal elevation and the instruments allowed to equalize. Once this was accomplished the flood load could be applied. Data recorded during the flood and failure event will be presented in Figures 5.72 through 5.75. Figure 5.72 is a plot of PPT data recorded in the sand layer at approximated mid-depth.

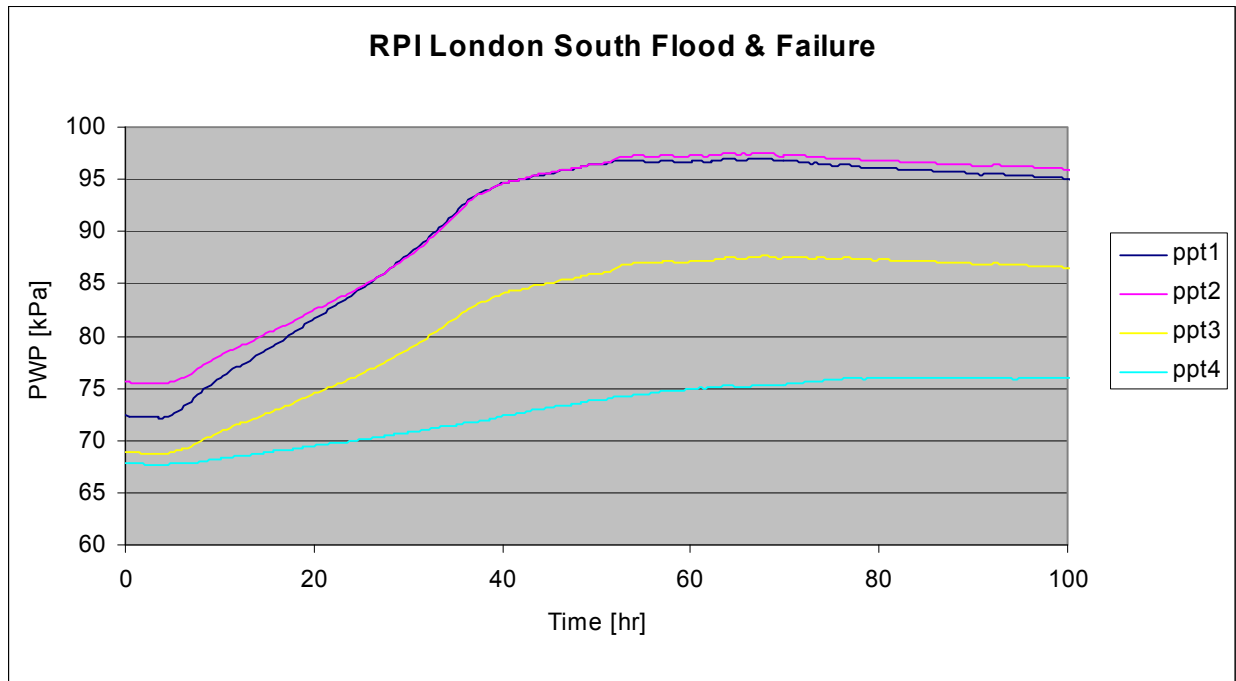


Figure 5.72. PPT data in the sand layer, mid-depth during flood.

It is seen in the data of Figure 5.72 that water pressure is highest closer to the canal (source of water) and reduces through the sand layer moving away from the canal. This is indicative of the transient flow situation that was created in the model by allowing water to move through the sand layer from the canal under the levee and then be collected and disposed of on the land side at the far end of the levee. Figure 5.73 shows data for the PPT's located in the sand layer at a higher elevation. PPT's 5, 6, and 7 are responding to more hydrostatic pressure than are any of the other instruments. This is also a consequence of the fact that after the crack forms, this material now has two sources for water, the canal and the crack.

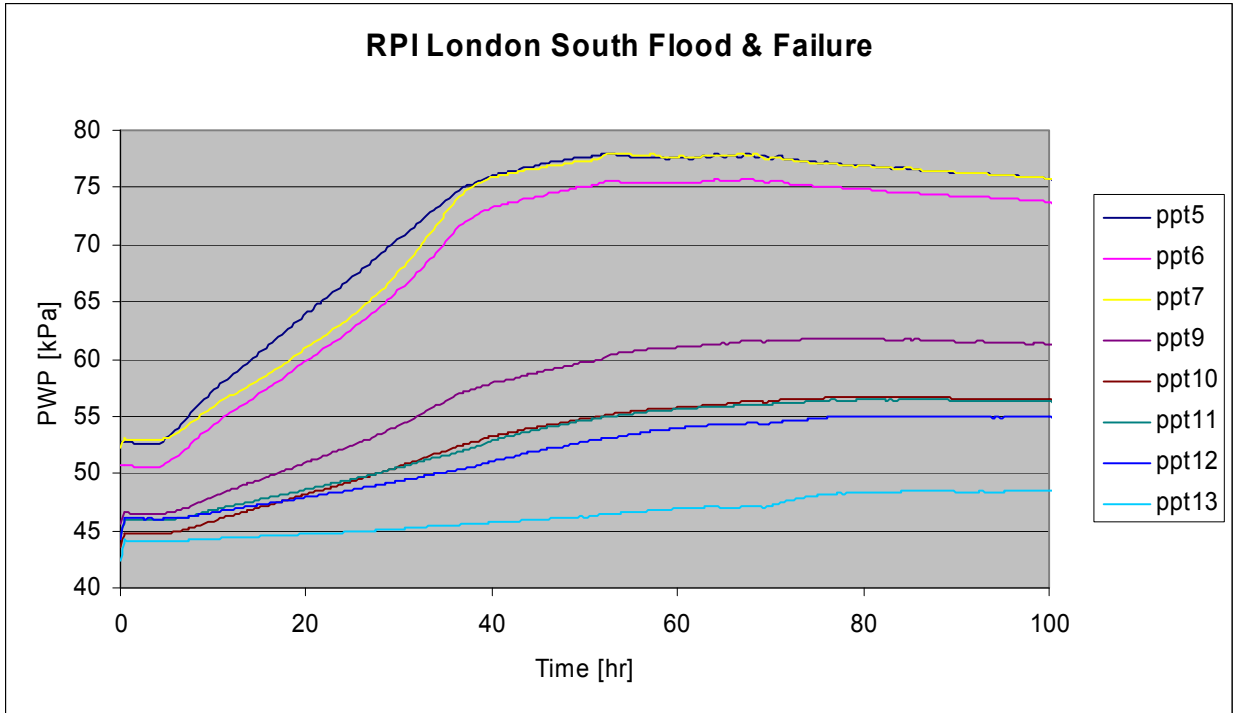


Figure 5.73. PPT data at higher elevation in the sand layer during flood

Figure 5.74 is a plot of the PPT data in the sand layer just at the interface of the sand layer and the swampy/marsh layer. Notice that PPT 15 has nearly reached full hydrostatic pressure as the crack has formed all the way to this elevation. This is true for PPT 7 in Figure 5.73 also. Figure 5.75 is a plot of the PPT data in the levee and swampy/marsh layer during the flood event. Measurement of displacement data of the sheet pile wall is presented in Figure 5.76.

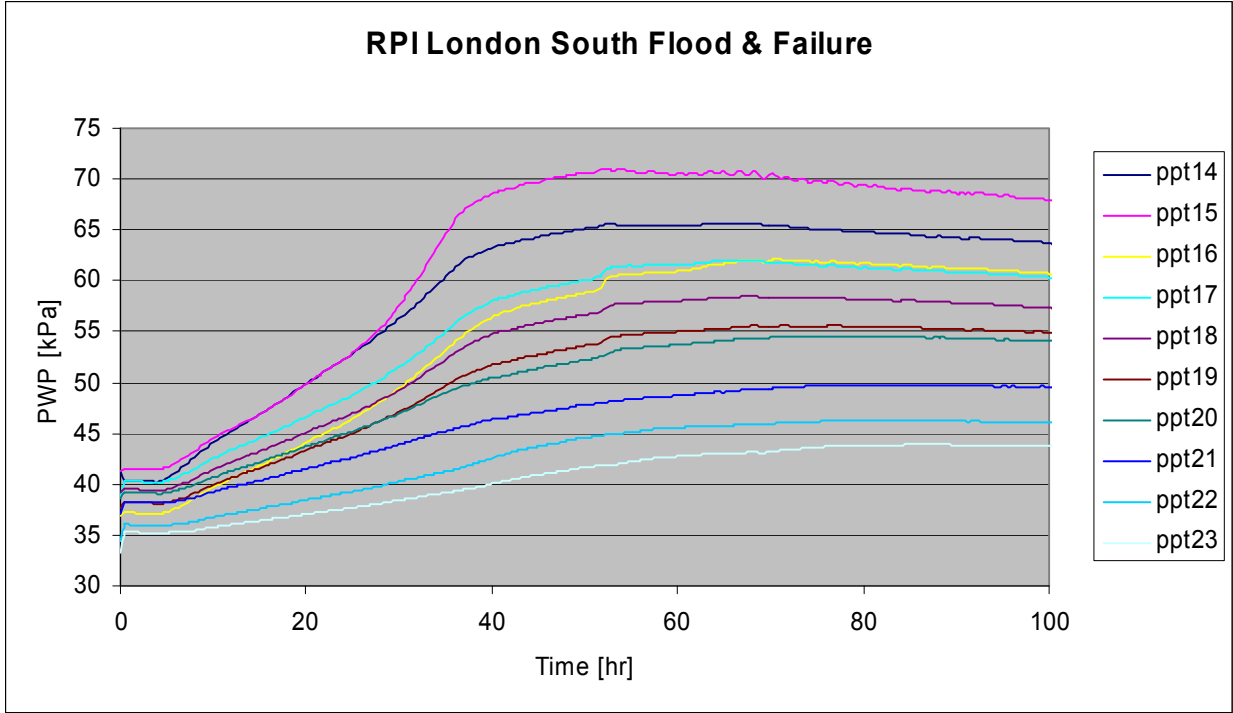


Figure 5.74. PPT data at the interface of the sand layer and the swampy/marsh layer during flood

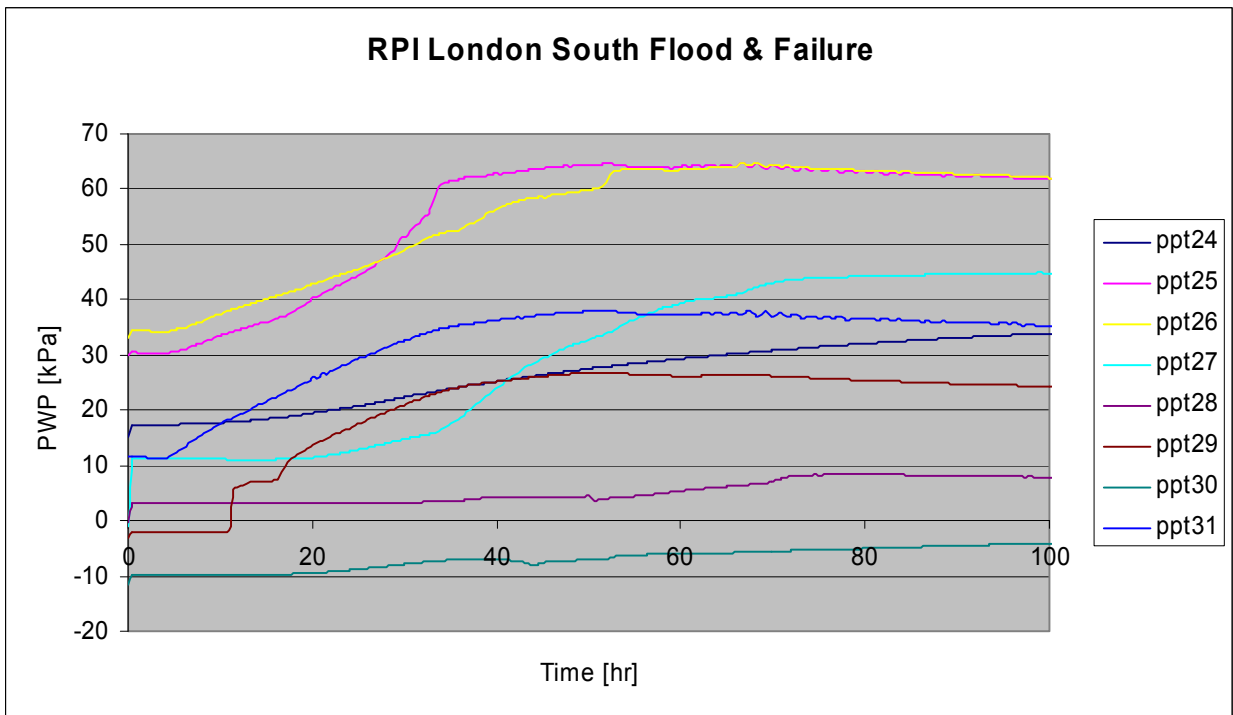


Figure 5.75. PPT data in the levee and swampy/marsh layer during flood

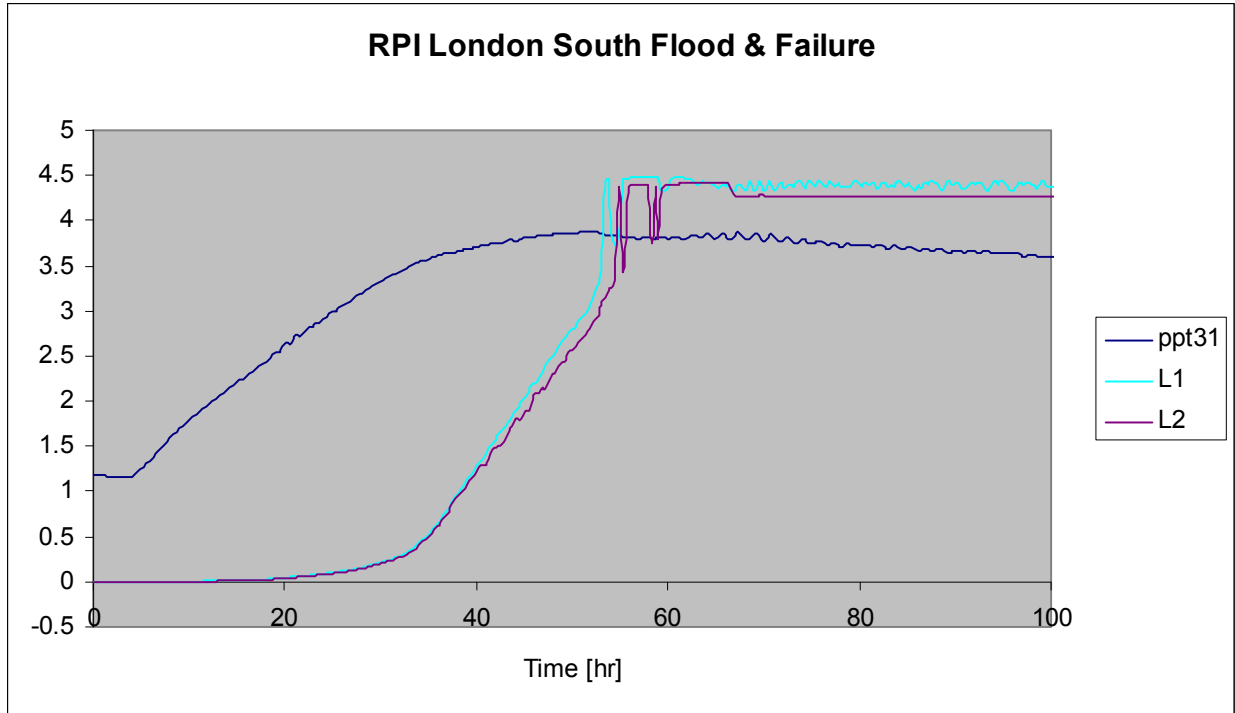


Figure 5.76. Displacement of the sheet pile wall during flood load

The increase in water level is shown to occur at time five hours and steadily increase to a depth of around 4 m (y-axis is water depth, m and displacement, m). The movement of the wall begins at around time ten hours with a small initial movement that is associated with the crack. At time 30 hours, the wall movement is seen to greatly increase, which is associated with failure of the wall. The two readings are parallel for most of the recorded time indicating that the wall is failing in a rotational manner. The following sequence of images shown in Figure 5.77 are stills taken from the video recording during the flood event. In the sequence the entire flood and failure event is shown.

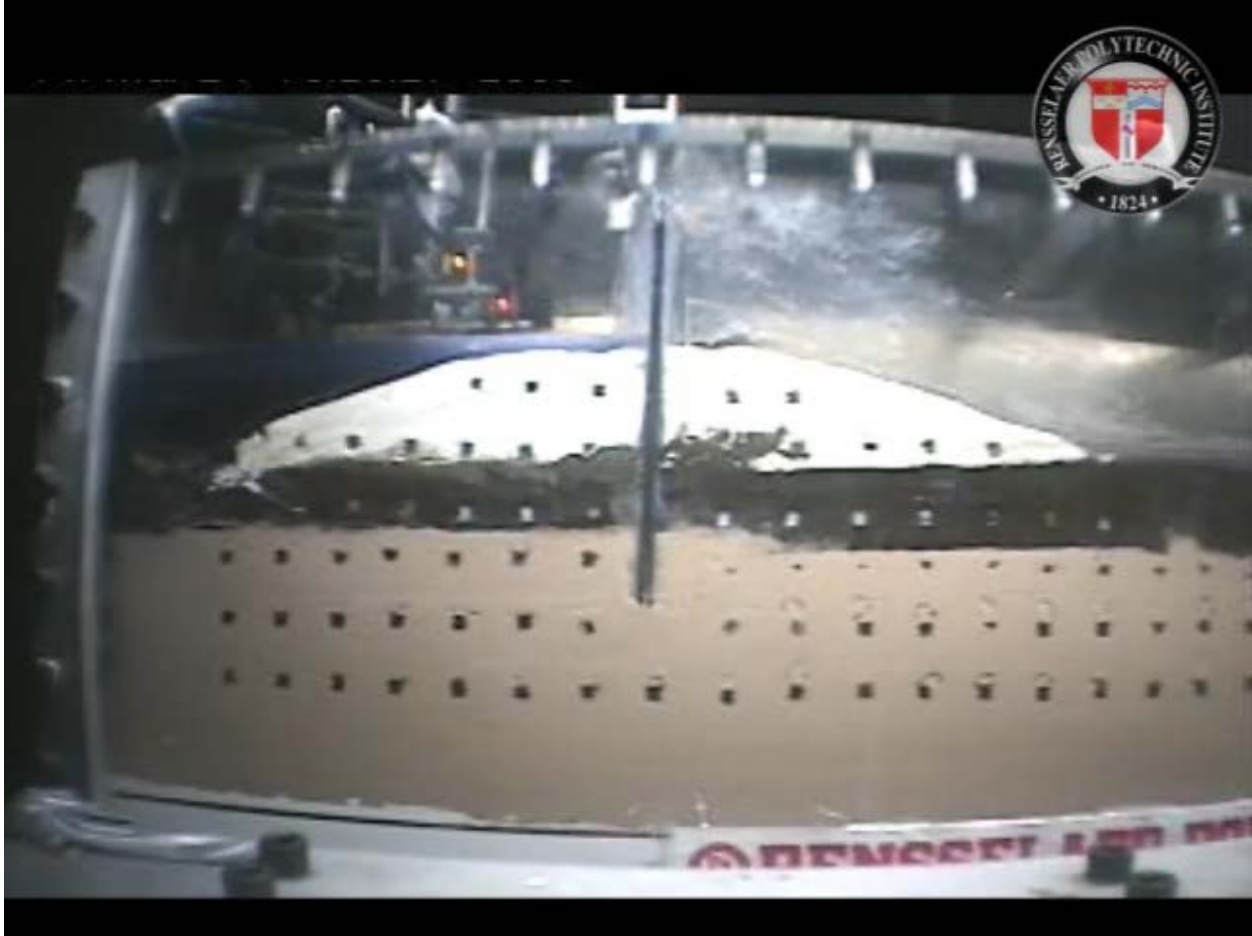


Figure 5.77a. RPI London south model at normal canal water elevation

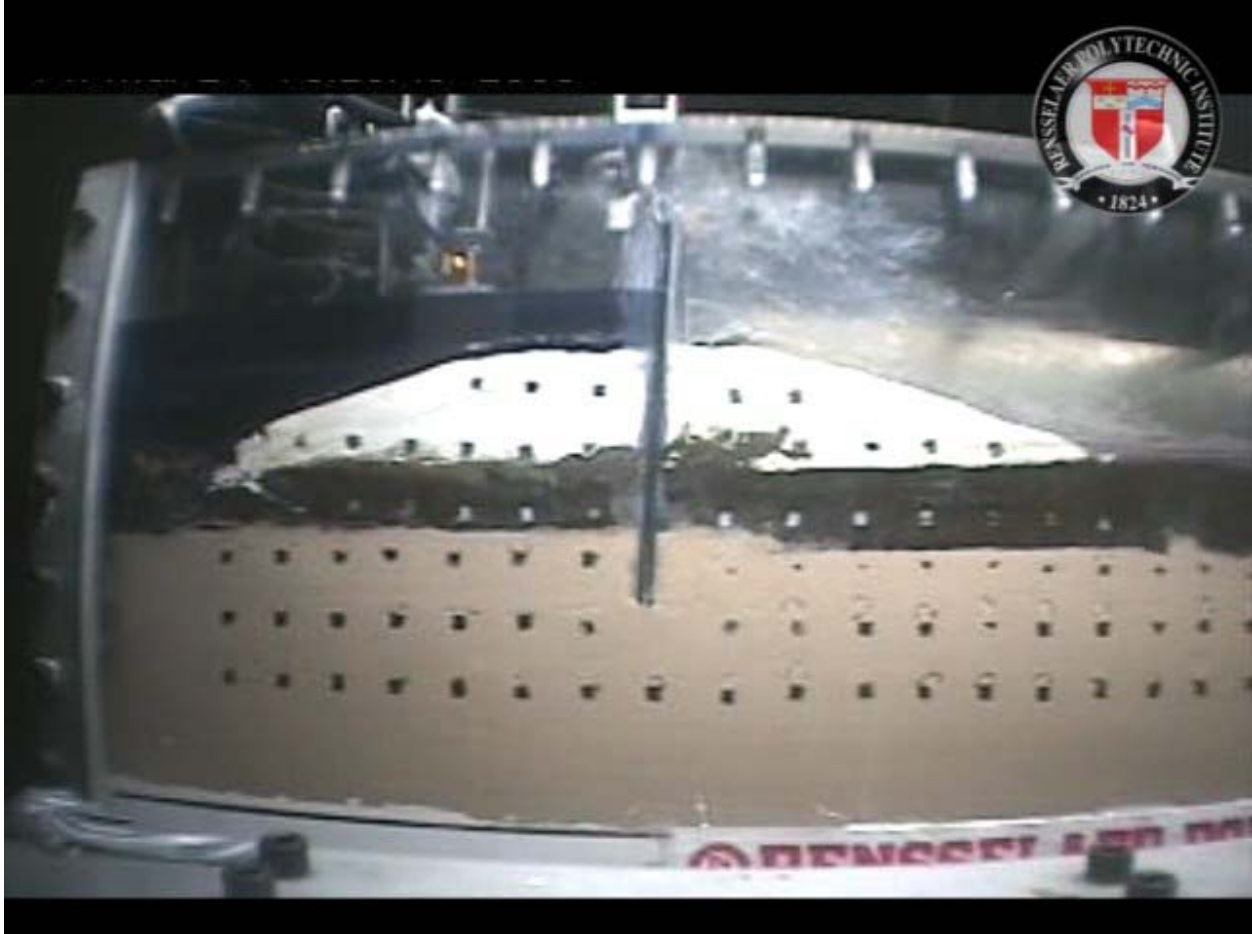


Figure 5.77b. RPI London south model flood level prior to any wall movement

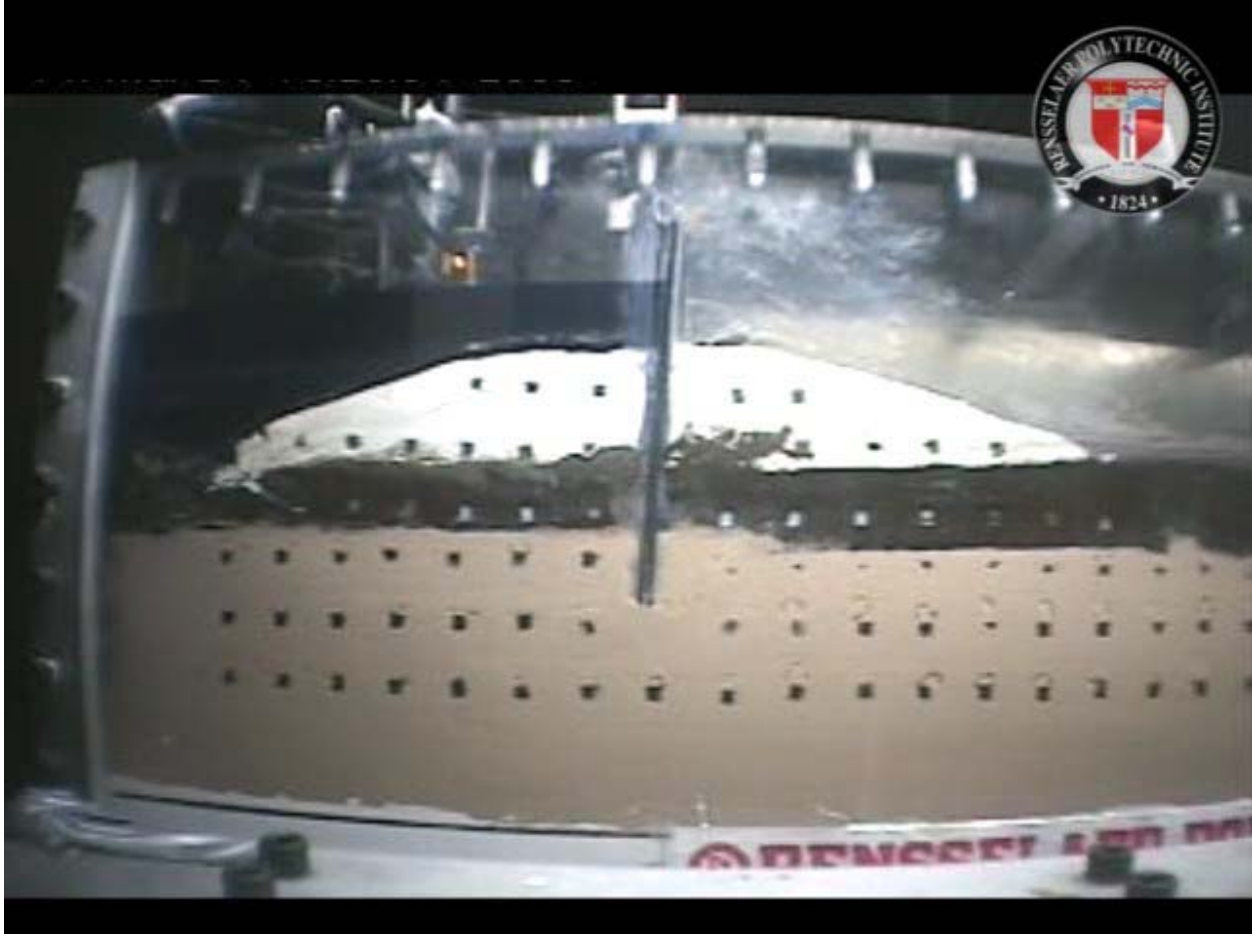


Figure 5.77c. RPI London south model just after wall movement and crack formation



Figure 5.77d. RPI London south model in process of failure



Figure 5.77e. RPI London south model in failure showing rotation of wall

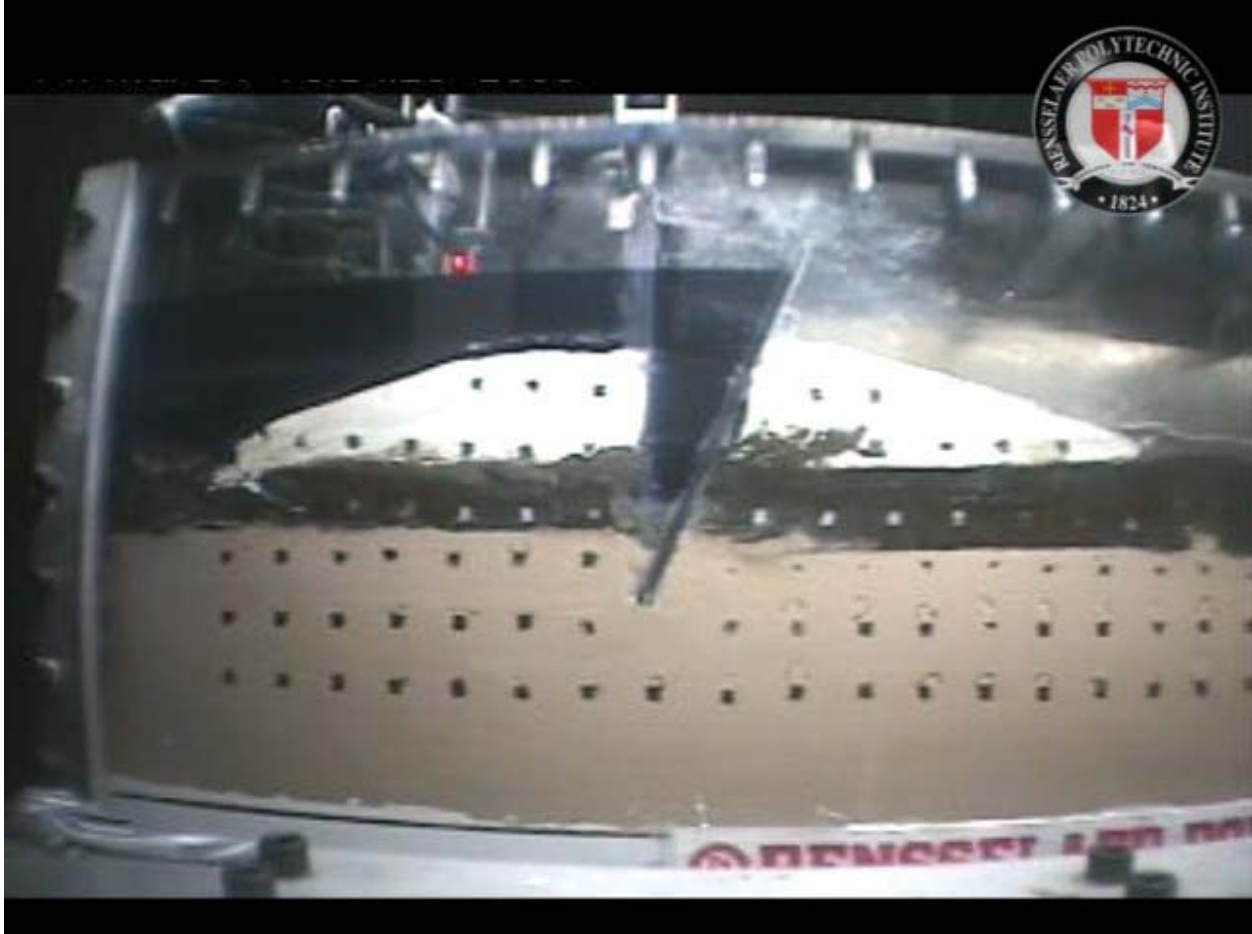


Figure 5.77f. RPI London south model during failure, note how the swampy/marsh layer is moving as evidenced by the white markers



Figure 5.77g. RPI London south model at end of failure

A synopsis of the failure event that occurred in the RPI London south model is as highlighted following. This is exactly the same failure event as was observed in the ERDC London south model and confirms the event.

1. Water level increases to a point on the wall where initial movement of the wall begins to occur. This movement starts out as a rotation of the wall.
2. A crack begins to form between the sheet wall and canal side levee and propagates downward.
3. The crack extends all the way through the levee and the swampy/marsh layer to the top of the sand layer.
4. Full hydrostatic pressure is allowed to reach the foundation sand layer causing a sudden increase in pore water pressure.
5. This increase in pore water pressure reduces the vertical effective stress of the overlying swampy/marsh and levee material. Effectively the land side material approaches zero effective stress and begins to ‘float.’
6. Load from the flood pushes the wall over in a rotational manner with no resisting force from the land side material.

Physical Models of London Avenue Canal, North Breach

Two models of a section at the north breach location of London Avenue canal were completed. One of the models was performed at RPI and the other at ERDC. This section of the report will present information relevant to each model.

ERDC London Avenue Canal, North Breach Model

The model representative of a section through the north breach at London Avenue canal is shown in Figure 5.78. The main difference between the London south model previously discussed and the north model to be discussed following is the levee geometry and depth of sheet pile embedment in the sand layer, also the density of the sand deposit. In London south the sheet pile is into the sand seven feet while in London north it extends into the sand four feet. Density of the sand at the London south area was 75% while at London north 60%.

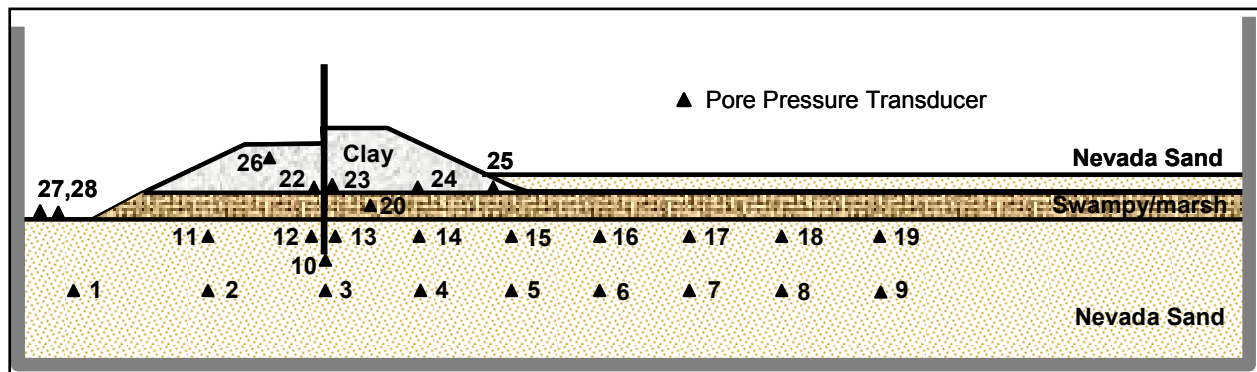


Figure 5.78. ERDC London north breach area model

Prior to placement of the swampy/marsh layer into the model vane shear measurements were made and averaged 275 psf. A view of the swampy/marsh layer and vane shear testing is shown in Figure 5.79. A view of placement of the swampy/marsh layer into the model is shown in Figure 5.80. Great care is taken to insure that the material remains intact during placement and that there is a good tight seal along the edges where the material contacts the container.



Figure 5.79. Swampy/marsh layer and taking vane shear measurements



Figure 5.80. View of placement of swampy/marsh layer

A view of the completed model ready for testing is shown in Figure 5.81. The model was slowly spun up to 50 g. As mentioned in the previous models, this slow spin up prevents any pre-failure associated with sudden increase in pore pressure but it also serves to allow the clay levee

to further consolidate and mold itself against the container side walls and the aluminum plate. Evidence of the effectiveness of this lies in the fact that no water was seen to move between the levee and container side walls nor between the aluminum plate and side walls. All movement of water was confined to the foundation material. Once the model had reached 50 g, water was raised to the level of normal canal operating elevation (just over the canal side levee crest) and time was given to allow the model and instrumentation to stabilize. When all recordings from PPT's indicated that the pore pressures were stable (not increasing or decreasing) then the actual flood event was initiated. The results of the recorded data will be presented and discussed in the next section. Typically the water was maintained on the wall until full movement had concluded.

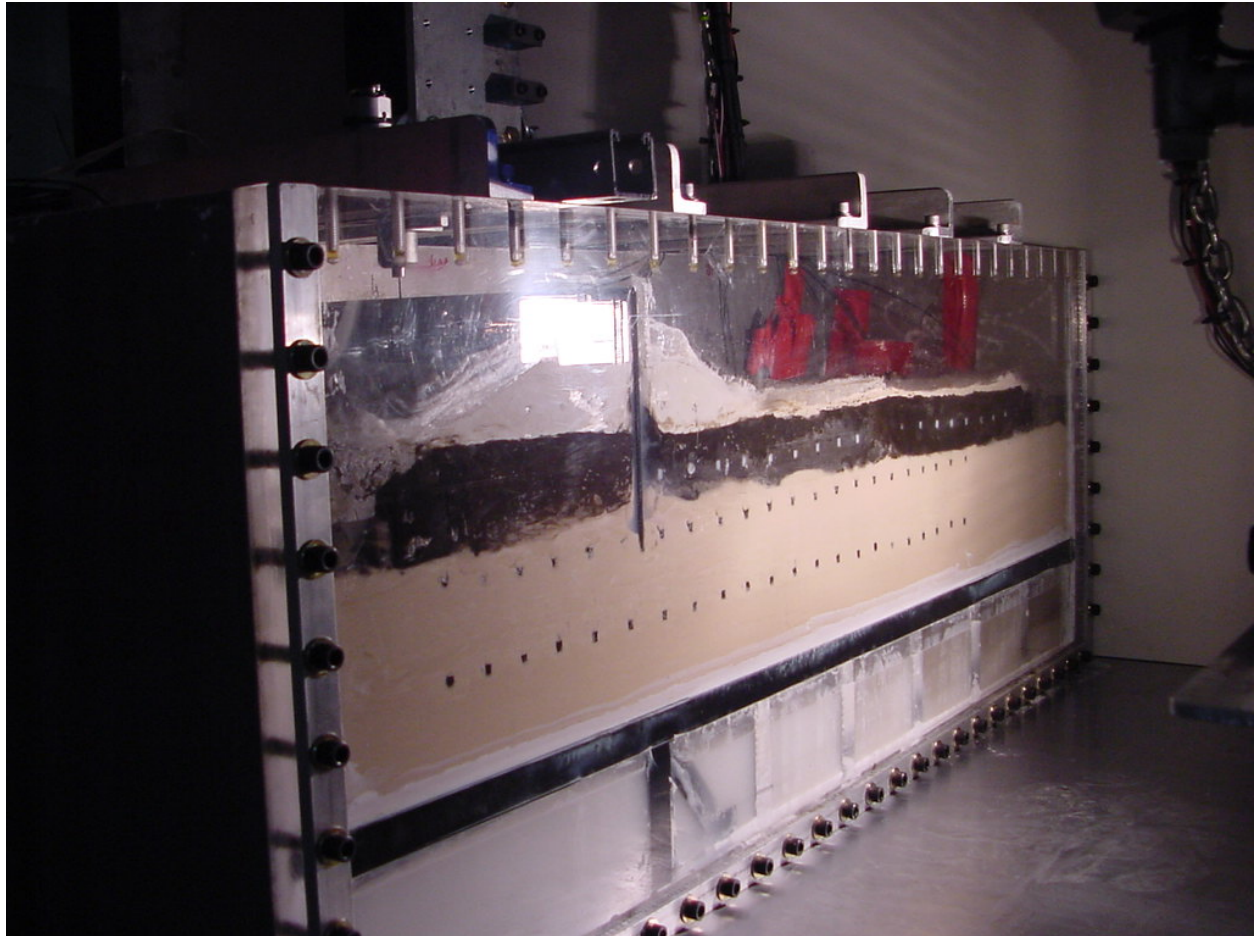


Figure 5.81. View of completed model prior to testing

This section will present the data recorded during the flood and failure event. As mentioned previously the displacement transducers on the wall failed to operate, therefore only PPT data will be shown. That data is given in Figures 5.82 through 5.84. Figure 5.82 is the PPT data in the sand layer about mid-depth. The small short plateau is associated with wall movement forming a crack that leads to eventual failure.

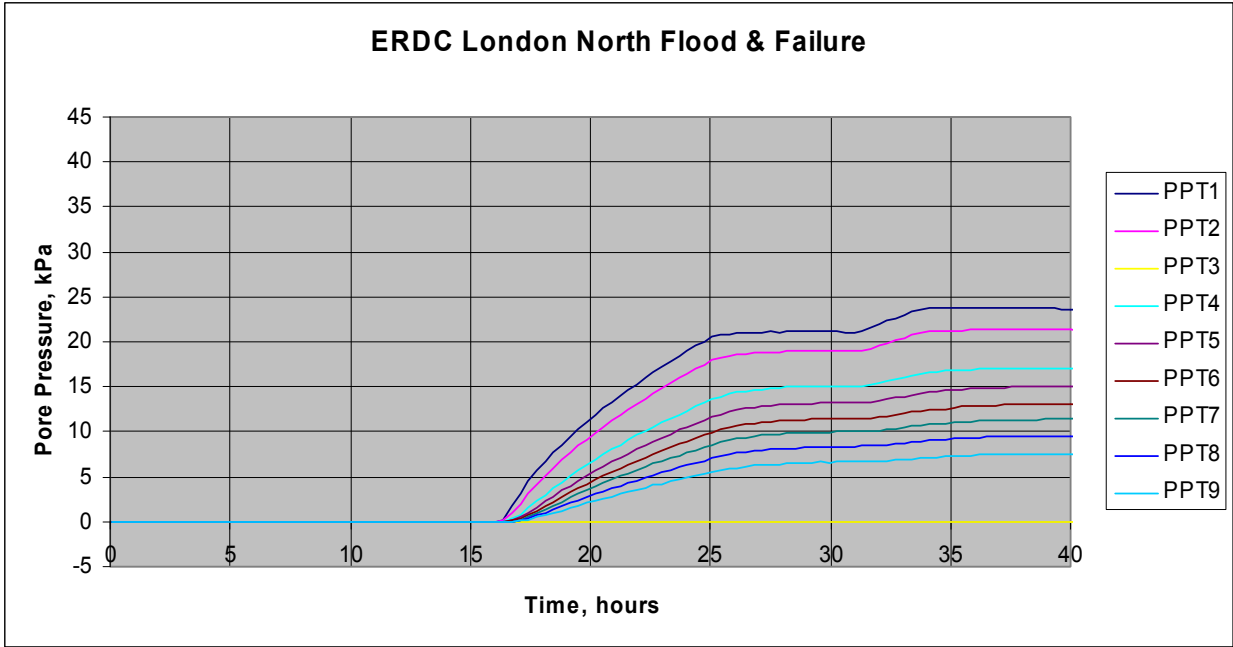


Figure 5.82. PPT data in the sand layer, mid-depth during flood event

Figure 5.83 is a plot of PPT data in the sand layer just near the top of that layer. The behavior is exactly as described above. Finally, the PPT data from the levee and swampy/marsh recorded during the flood are shown in Figure 5.84. The PPT's in the clay are very erratic. This response is attributed to a combination of the clay material drying out during the long spin time and to changes in the clay geometry as the failure is occurring.

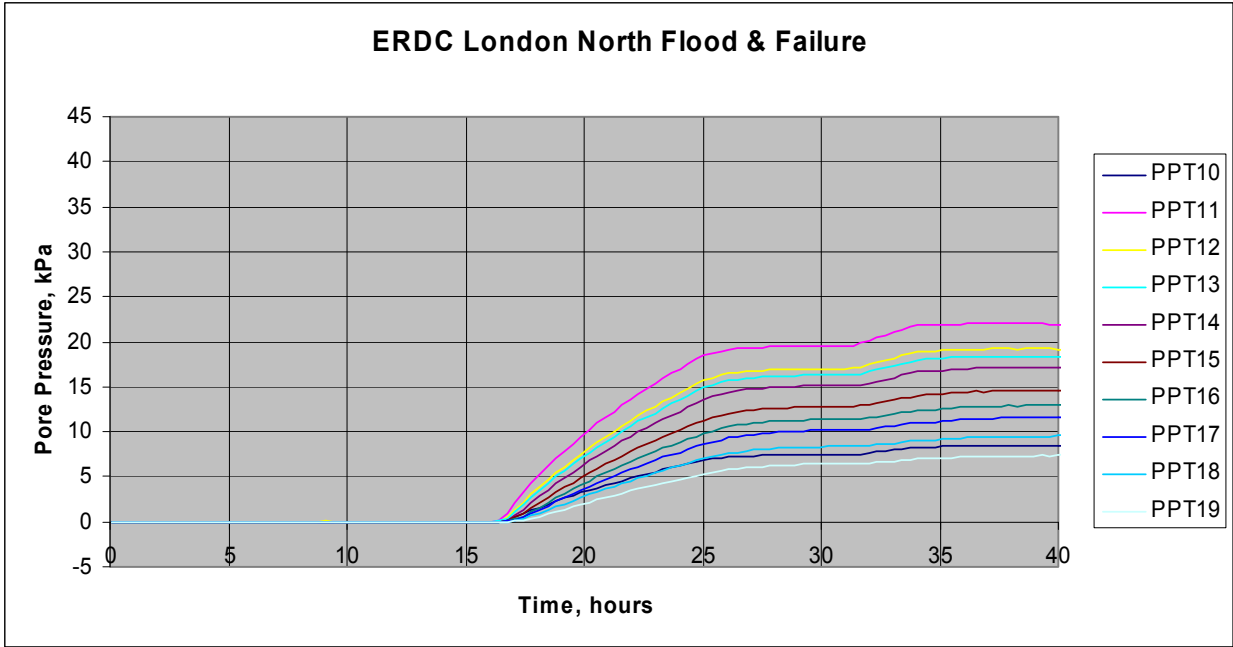


Figure 5.83. PPT data in the sand layer, near top, during flood

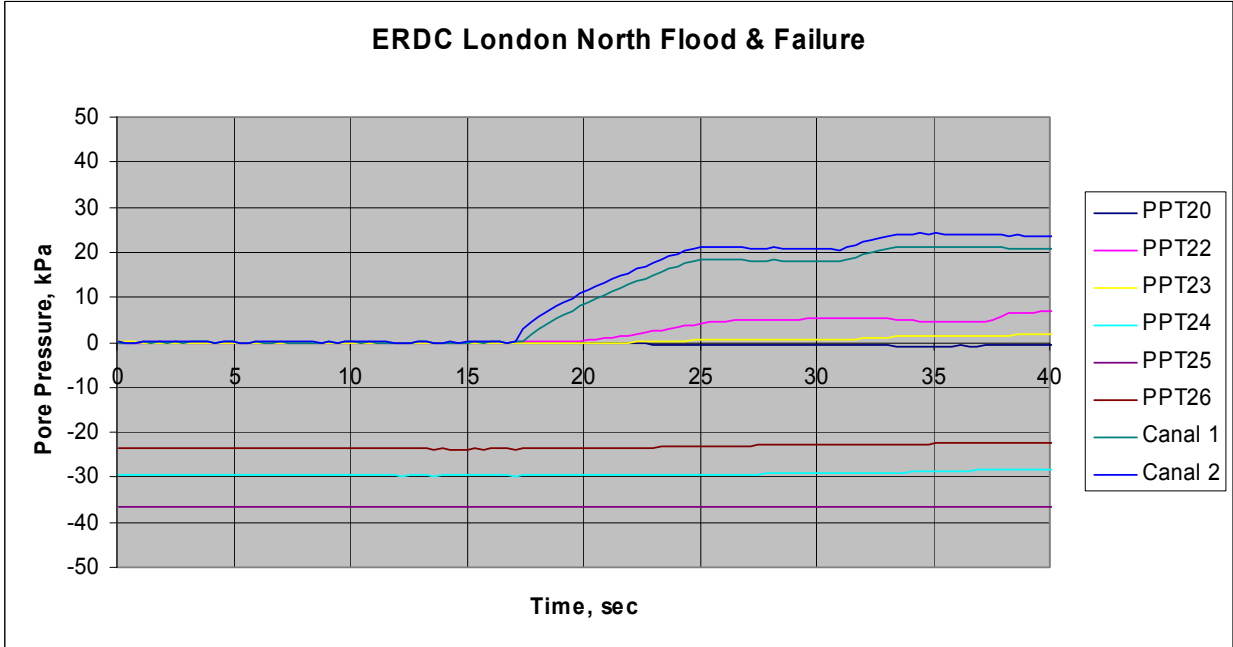


Figure 5.84. PPT data in the levee and swampy/marsh layer during flood

Finally, this section will present still shots taken from the video during flood and failure to highlight the event. Those views are shown in Figure 5.85, and clearly indicate the failure mechanism.



Figure 5.85a. View of ERDC London north model at normal canal water elevation



Figure 5.85b. View of ERDC London north model at flood level prior to wall movement



Figure 5.85c. View of ERDC London north model at flood level just after wall movement and opening of crack between wall and canal side levee



Figure 5.85d. View of ERDC London north model at flood level well into failure



Figure 5.85e. View of ERDC London north model at flood level end of failure

In a manner very similar to what was revealed in the two London south models, the description of failure mechanism for this London north model follows.

1. Water level increases to a point on the wall where initial movement of the wall begins to occur. This movement starts out as a rotation of the wall.
2. A crack begins to form between the sheet wall and canal side levee and propagates downward.
3. The crack extends all the way through the levee and the swampy/marsh layer to the top of the sand layer.
4. Full hydrostatic pressure is allowed to reach the foundation sand layer causing a sudden increase in pore water pressure.
5. This increase in pore water pressure reduces the vertical effective stress of the overlying swampy/marsh and levee material. Effectively the land side material approaches zero effective stress and begins to 'float'.
6. Load from the flood pushes the wall over in a rotational manner with no resisting force from the land side material.

RPI London Avenue Canal, North Breach Model

A second model representative of a section through the north breach at London Avenue canal was conducted at RPI and shown in Figure 5.86. The model was exactly as previously described for the ERDC London north model.

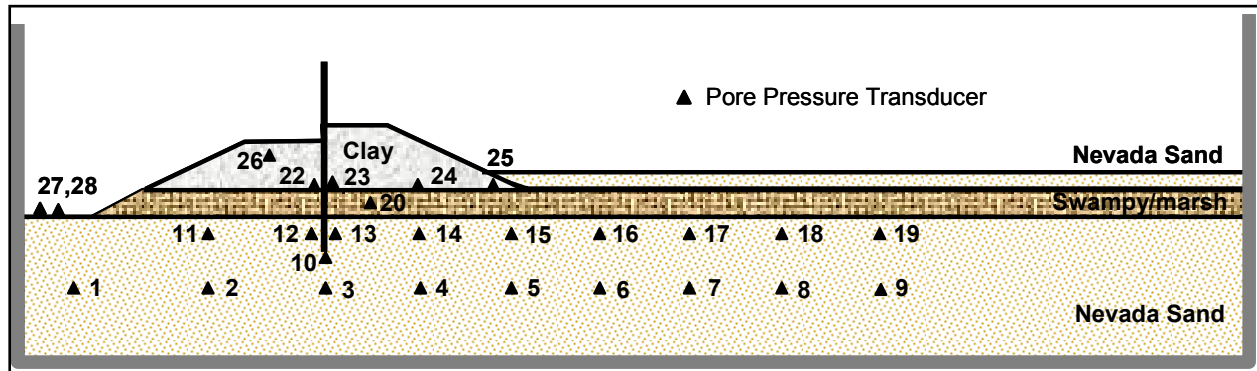


Figure 5.86. RPI London north model

The sequence of construction and testing has already been described for the ERDC model. At the conclusion of the consolidation process, moisture contents and shear strengths of the levee material were taken. Average moisture contents 47% and vane shear 375 psf.

The model was slowly spun up to 50 g in a manner previously described. At 50 g the water in the canal was brought to an elevation consistent with normal canal operating levels. All instrumentation was allowed to stabilize prior to the addition of any flood loading. The next section will present data recorded during the flood and failure event.

Results of the flood event are shown in Figures 5.87 through 5.90. Figure 5.87 is a plot of the rise in water during the flood event. Figure 5.88 is a plot of the PPT data in the sand layer mid-depth during the flood event. The data has a character as described for the ERDC model. The curves show a steady increase in pressure then a marked change in slope. This is associated with the crack formation and ultimate failure of the levee. Also, the pressure are higher under the canal and canal side levee reducing as you move through the foundation to the land side, as would be expected for the flow conditions of the model. Figure 5.89 is a plot of the PPT data in the sand layer near the top of that layer during the flood event. Finally, Figure 5.90 shows the PPT data in the levee and swampy/marsh during the flood. The data are erratic as discussed in the ERDC model but do show a change in character of the curves at a time near 50 hours.

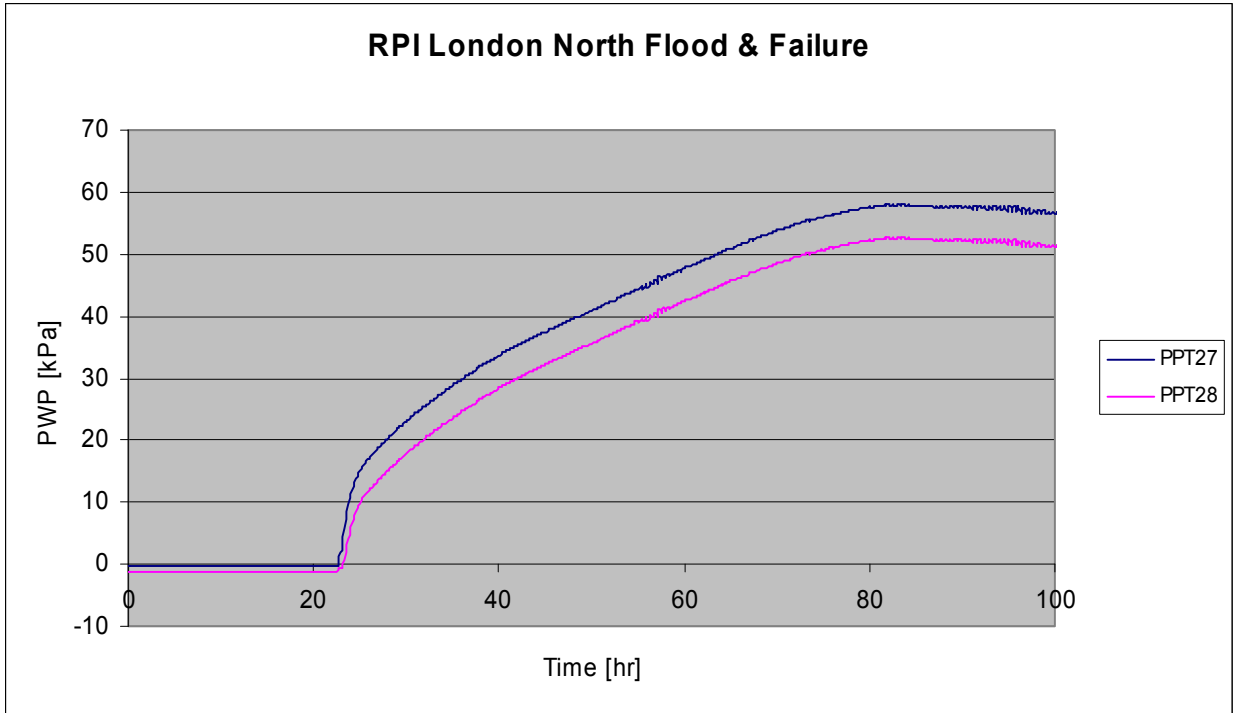


Figure 5.87. PPT data showing the rise in canal water elevation

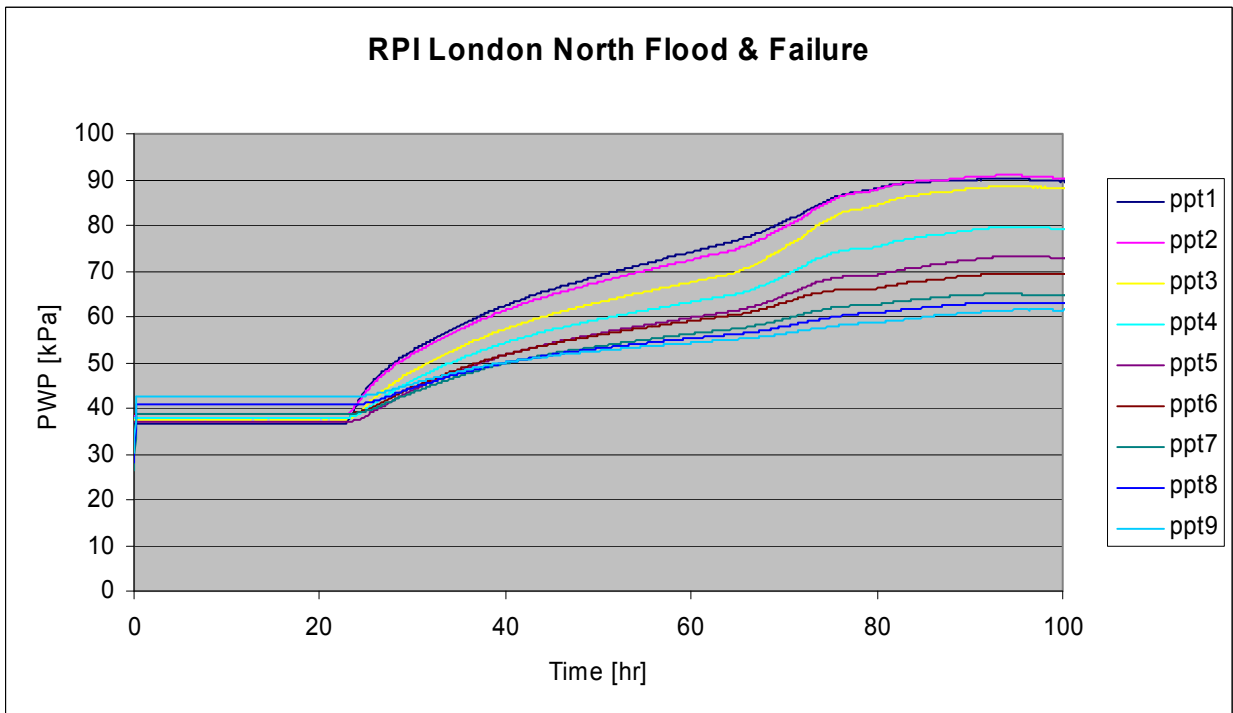


Figure 5.88. PPT data in the sand layer mid-depth during flood

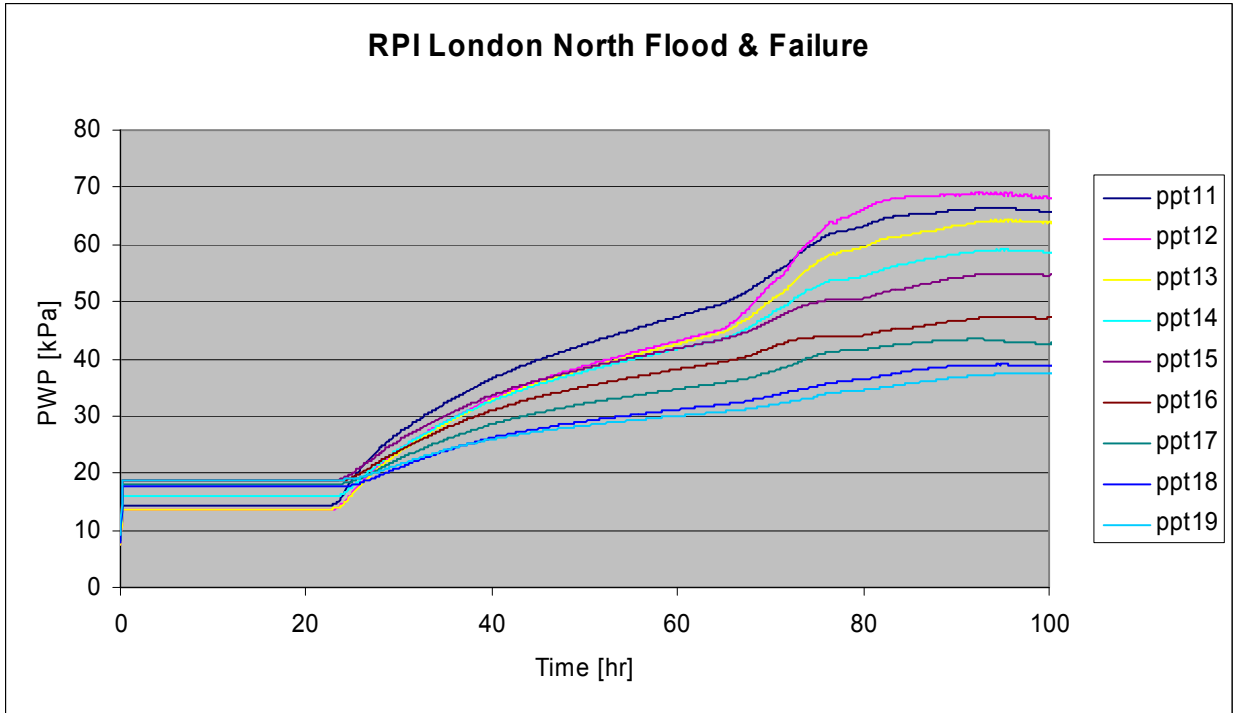


Figure 5.89. PPT data in the sand layer near top during flood

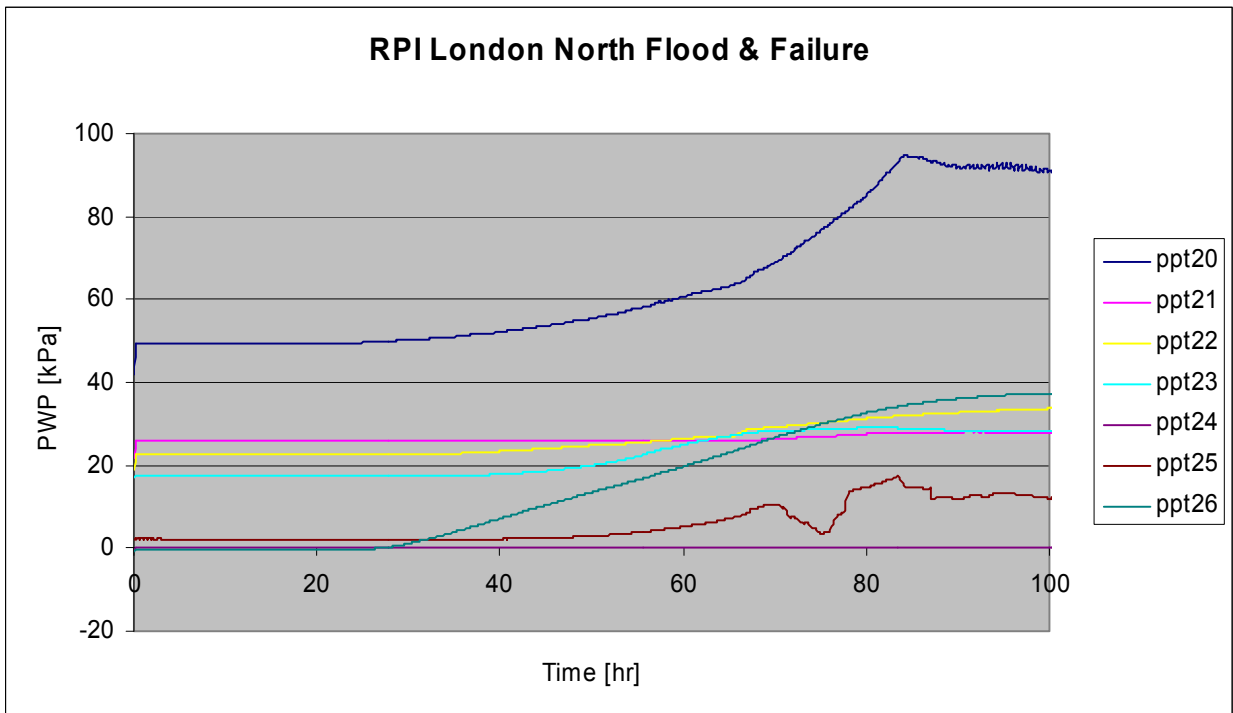


Figure 5.90. PPT data in the levee and swampy/marsh during flood

The following sequence of views, shown in Figure 5.91, are stills taken from the video recording of the flood and failure event. These shots clearly show the mechanism of failure. The vertical striations in the model are markers placed to determine deformations in the clay levee and foundation (this is similar to the “dots” used in previous models).



Figure 5.91a. RPI London north model at normal canal water elevation



Figure 5.91b. RPI London north model at flood level just prior to any wall movement



Figure 5.91c. RPI London north model at flood level just after wall movement when crack has opened



Figure 5.91d. RPI London north model at flood level well into failure



Figure 5.91e. RPI London north model at flood level end of failure

A synopsis of the failure event that occurred in the RPI London north model is as highlighted following. This is exactly the same failure event as was observed in the ERDC London north model and confirms the event.

1. Water level increases to a point on the wall where initial movement of the wall begins to occur. This movement starts out as a rotation of the wall.
2. A crack begins to form between the sheet wall and canal side levee and propagates downward.
3. The crack extends all the way through the levee and the swampy/marsh layer to the top of the sand layer.
4. Full hydrostatic pressure is allowed to reach the foundation sand layer causing a sudden increase in pore water pressure.
5. This increase in pore water pressure reduces the vertical effective stress of the overlying swampy/marsh and levee material. Effectively the land side material approaches zero effective stress and begins to 'float'.
6. Load from the flood pushes the wall over in a rotational manner with no resisting force from the land side material.

Physical Models of Orleans Avenue Canal

Two models of sections of the Orleans Avenue canal were completed. One of the models was performed at RPI representing a section at the south end of the canal and the other at ERDC representing a section at the north end of the canal. There were no failures of any of the walls in the Orleans canal and the two sections were selected to be representative of the canal in general. Only sections of the east levee were modeled since this levee contains I-walls while the west levees have T-walls. The south section of the canal is similar in foundation material to that of the London Avenue canal south breach area. The north section of the canal has foundation conditions similar to those of the 17th Street canal breach area. This section of the report will present information relevant to each model.

ERDC Orleans Avenue Canal, North Area Model

The model representative of a section through the north end of the Orleans Avenue canal is shown in Figure 5.92. The sheet pile extends through the swampy/marsh layer almost to the bottom. The height of the wall above the levee crest on the canal side is approximately 1.5 m, and the normal canal elevation does not reach the top of the levee.

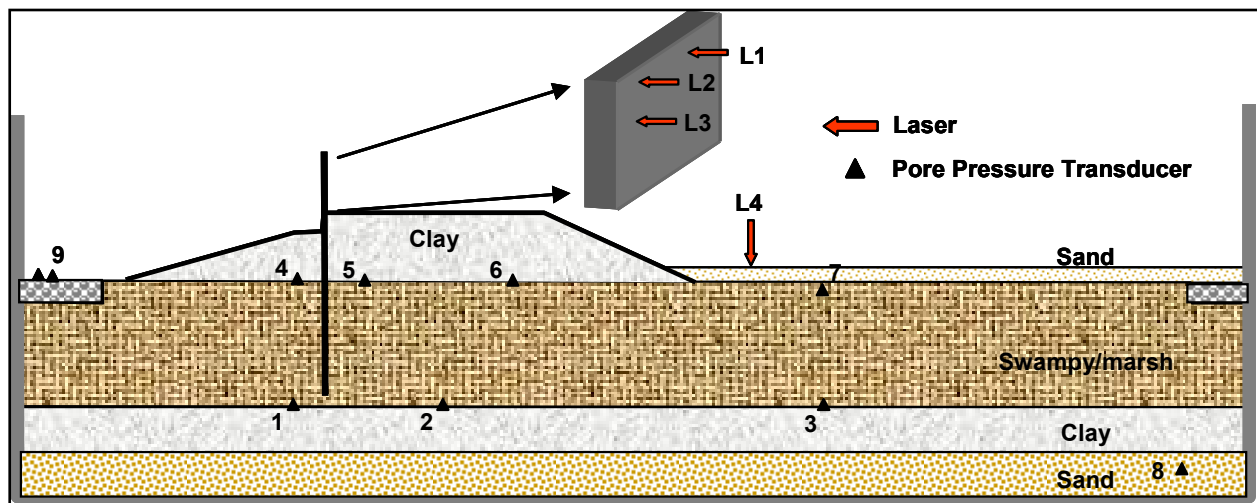


Figure 5.92. ERDC model of Orleans Avenue canal, north area

Post consolidation moisture content of the levee was 54%. The swampy/marsh layer had an average vane shear of 350 psf. The model was slowly spun up to 50 g and readied for testing. Water was maintained in the canal during spin up to 50 g, where it was increased to normal canal water elevation. The model and instrumentation were allowed to stabilize prior to increasing the water level from normal canal level to flood level. The following section will present data and discussions recorded during the flood and failure process.

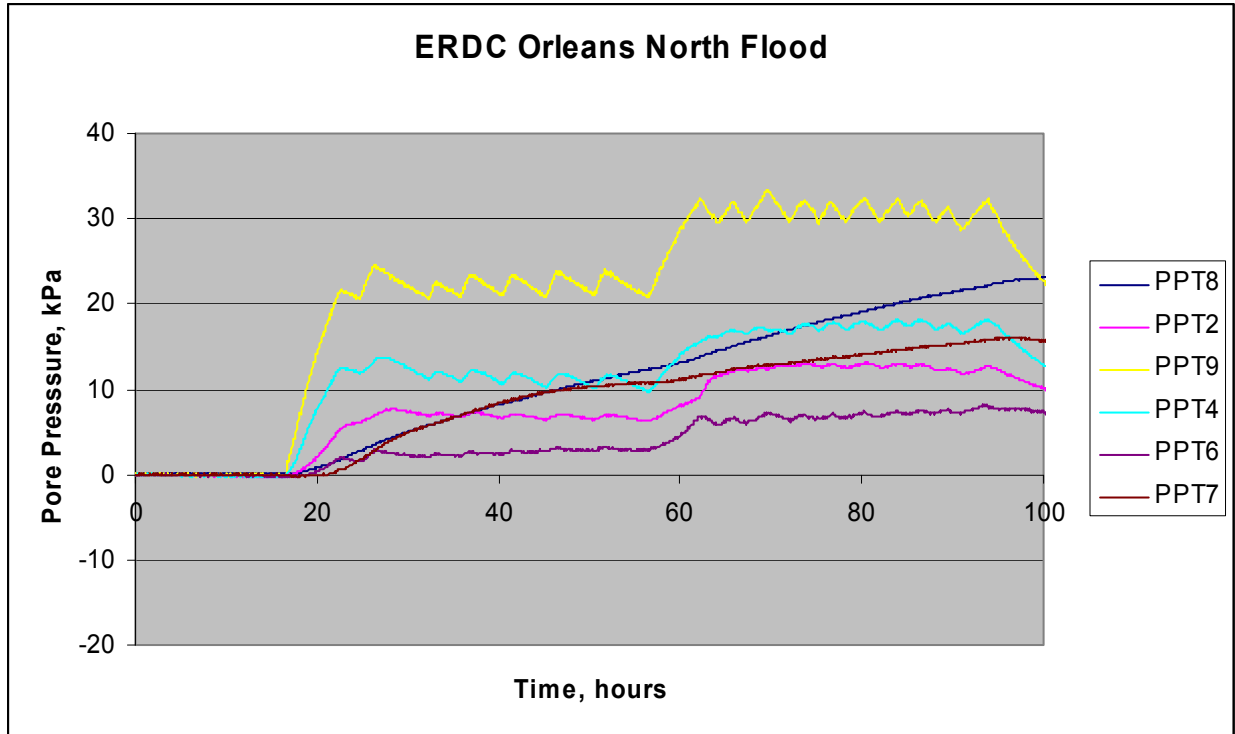


Figure 5.93. PPT data recorded in the ERDC Orleans North model during the flood

There is a step in the PPT data from shortly after the flood event associated with the rise in water level from the normal canal elevation to that at Hurricane Katrina. Starting at time 20 hours until approximately 55 hours is the water level being held at the Katrina flood level. A second increase in pressure that is associated with increase in water level to the top of the wall occurs between time 60 hours and 95 hours. This was done to explore the behavior of the wall should the water elevation have gone up to a higher level.

Displacement of the wall as recorded during the flood event is shown in Figure 5.94. As the water level increases there is a point where the wall moves slightly, this is seen as a movement of less than 0.1 m that quickly stops and remains constant for the period of water being held at flood level. At a time of approximately 25 hours the water level was increased to the top of the wall. The displacement data shows that the wall moved an additional 0.2 m. At this point the wall continued a slow movement of an additional 0.1 m. In the video to be shown following, there was a clear formation of a crack at the increased water elevation but this did not develop into a failure of any type.

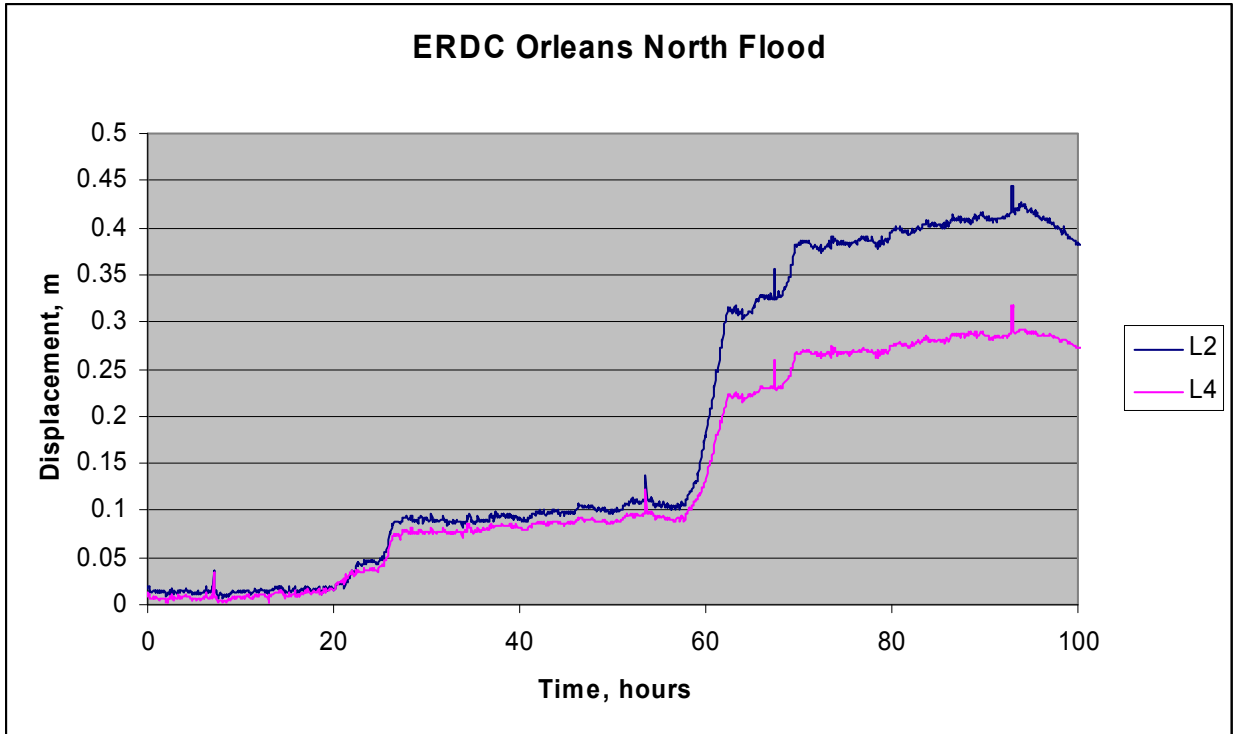


Figure 5.94. Displacement of wall during flood event, Katrina level and additional flood to top of wall

The following sequence of images shown in Figure 5.95 are stills taken from the video recording of the flood and failure event.



Figure 5.95a. View of model at normal canal elevation prior to flood



Figure 5.95b. View of model at Hurricane Katrina flood level



Figure 5.95c. View of model at Hurricane Katrina flood level, extended time at flood



Figure 5.95d. View of model where water has been increased above Hurricane Katrina level to explore wall behavior



Figure 5.95e. View of model at flood level greater than Hurricane Katrina, wall has moved

A synopsis of the model results is presented following for both conditions of Hurricane Katrina flood level and the increased flood level.

1. The canal water elevation was increased from normal elevations to those of Hurricane Katrina where a very small movement in the wall occurred.
2. Water was held at this level for a long period of time and no further movement of the wall occurred, and the levee was completely stable.
3. Water level was increased from Hurricane Katrina level to near top of wall. The wall had an additional movement that formed a crack between the wall and canal side levee.
4. The wall continued to move a very small amount toward the land side but did not lead to failure of any kind in the levee.

RPI Orleans Avenue Canal, South Area Model

The model representative of a section through the south end of the Orleans Avenue canal is shown in Figure 5.96. The sheet pile extends through the levee to the top of the swampy/marsh

layer. The height of the wall above the levee crest on the canal side is approximately 1.5 m, and the normal canal elevation does not reach the top of the levee.

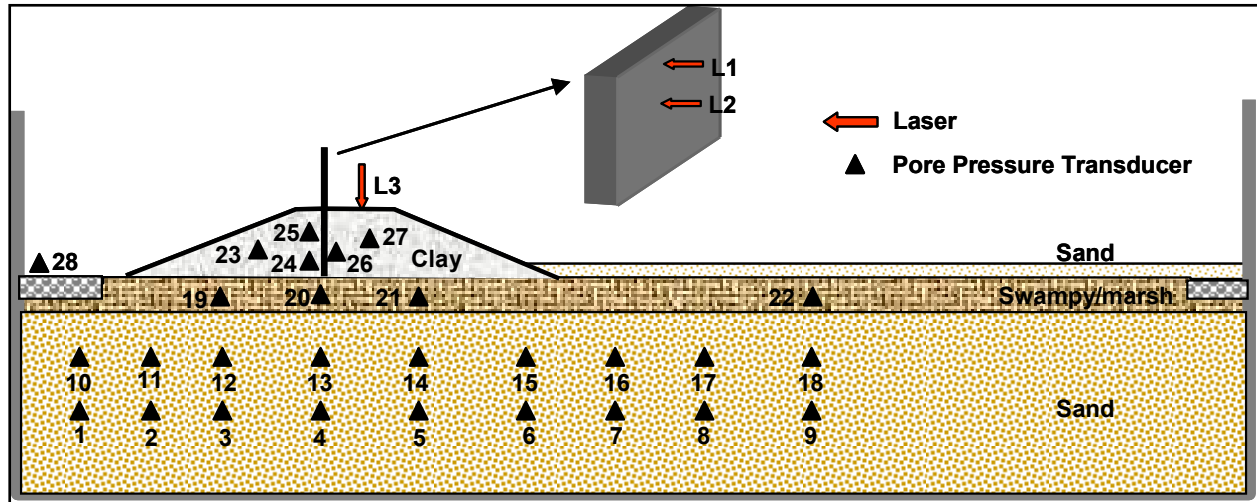


Figure 5.96. RPI model of the Orleans Avenue canal, south area

At the conclusion of consolidation moisture content and vane shear measurements of the levee were taken. Those values indicate moisture contents of 47% and vane shear readings of 505 psf.

The model was slowly spun to 50 g, water level increased to that at normal canal operation and all instrumentation allowed to stabilize. Once this was accomplished, the flood load was applied. Results of the flood loading are presented in Figures 5.97 through 5.100. Figure 5.97 is a plot of the PPT data recorded in the sand layer at mid-depth. Notice that there is a steady increase in the pore pressures reaching a level where they remain constant through the flood load.

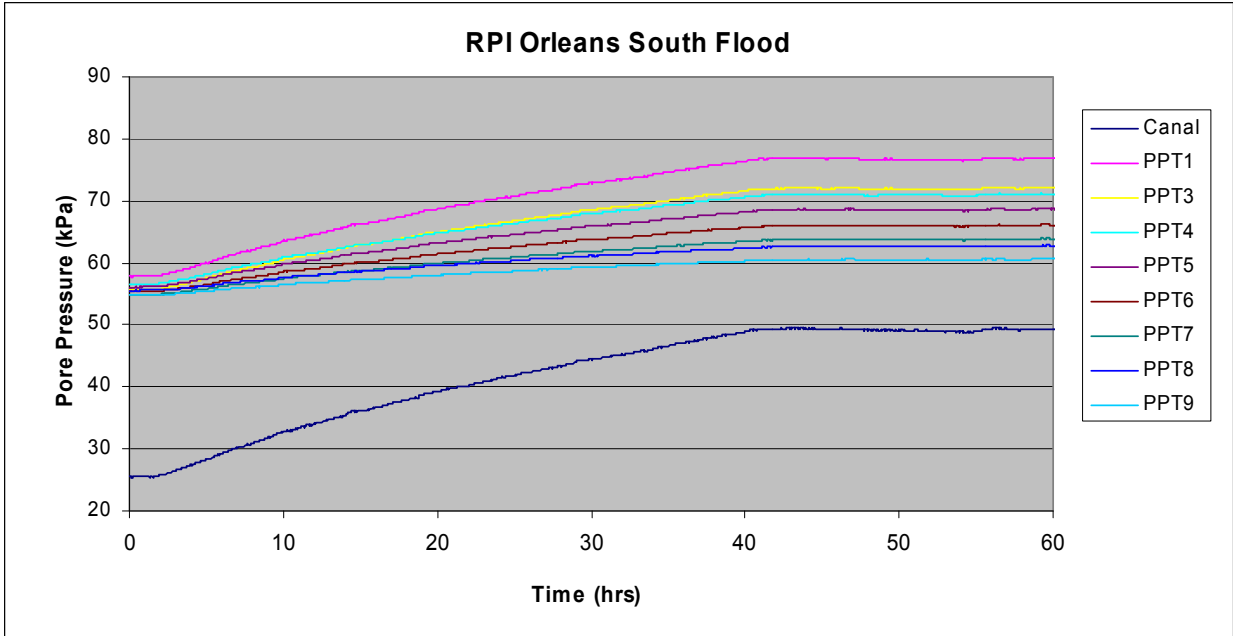


Figure 5.97. PPT data recorded in the sand layer, mid-depth during flood

Figure 5.98 is a plot of the PPT data in the sand layer near top during flood event. The character is very much like that of the data in Figure 5.97. Figure 5.99 is the PPT data recorded in the levee and swampy/marsh layer during the flood. There is very little to no response from any of the PPT's located in the swampy/marsh layer. This is not an unexpected event since increase in canal water level would have little effect on these readings over the relatively short duration of the flood event. Notice that there is an increase in PPT's 24, 25 and 26. Instruments 24 and 25 are located near the wall on the canal side and are feeling the load of the increased water level. There is a delayed response in the rise of pressure recorded by PPT 26 which would be expected.

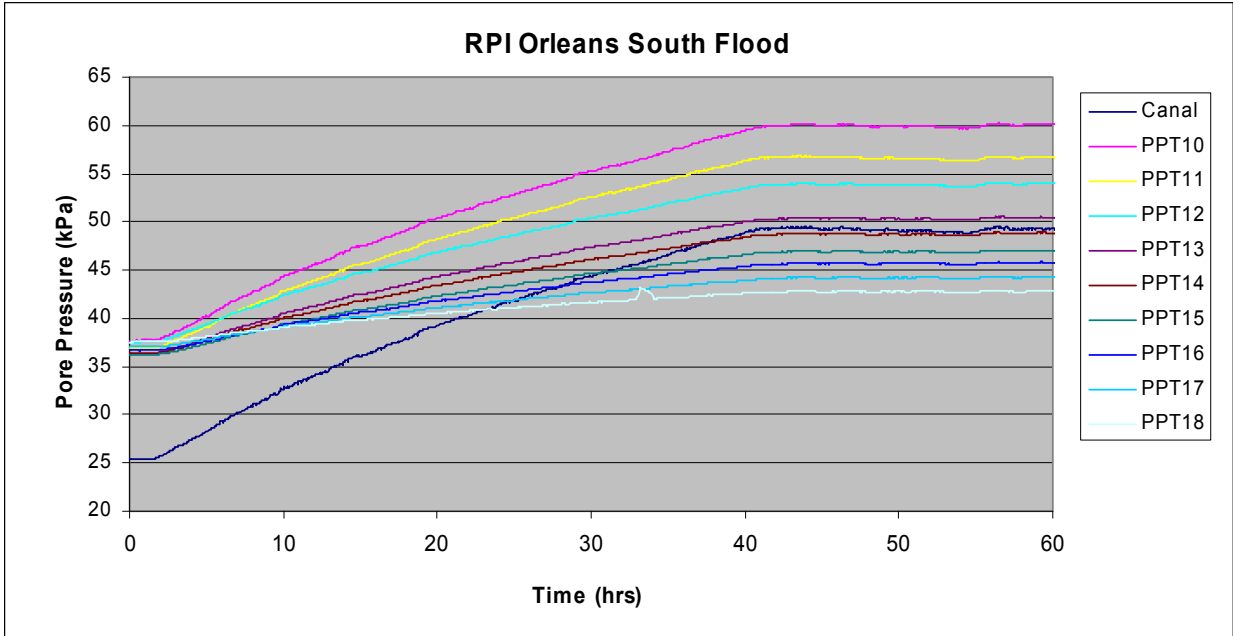


Figure 5.98. PPT data in the sand layer, near top during flood event

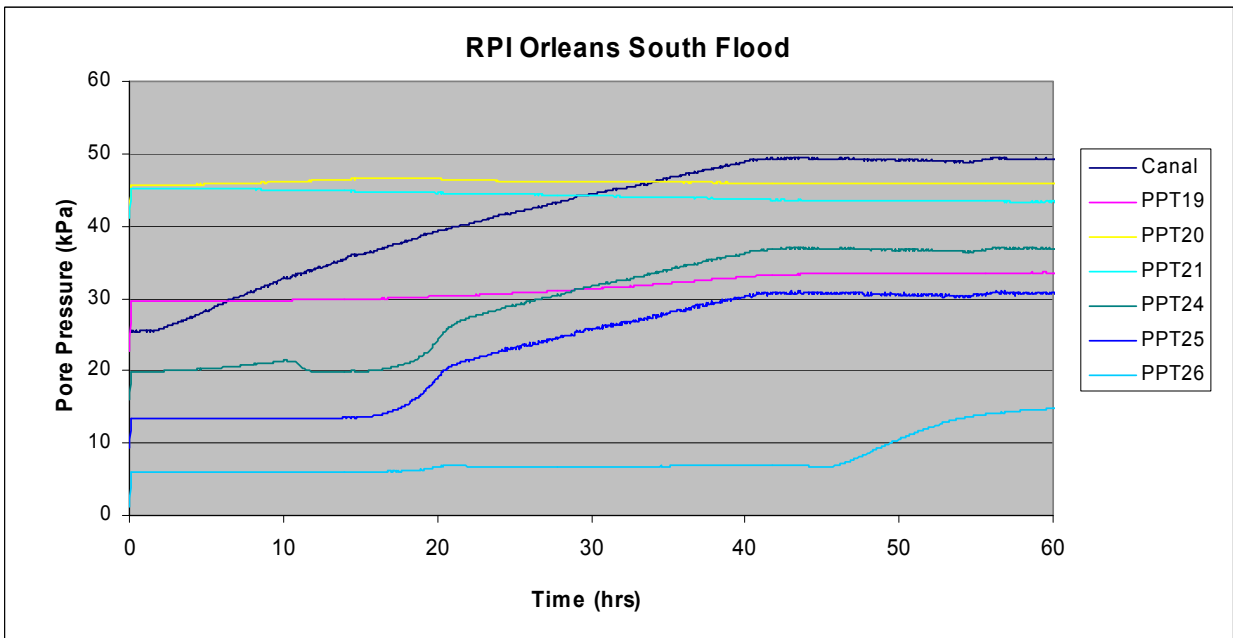


Figure 5.99. PPT data in the levee and swampy/marsh layer during flood

Measurement of wall movement is shown in Figure 5.100. There is a very small movement in the wall of only 0.03 m but the wall remains constant with no movement thereafter. Although this movement may have opened a very small crack behind the wall, this did not lead to any further movement of the wall or failure of the levee.

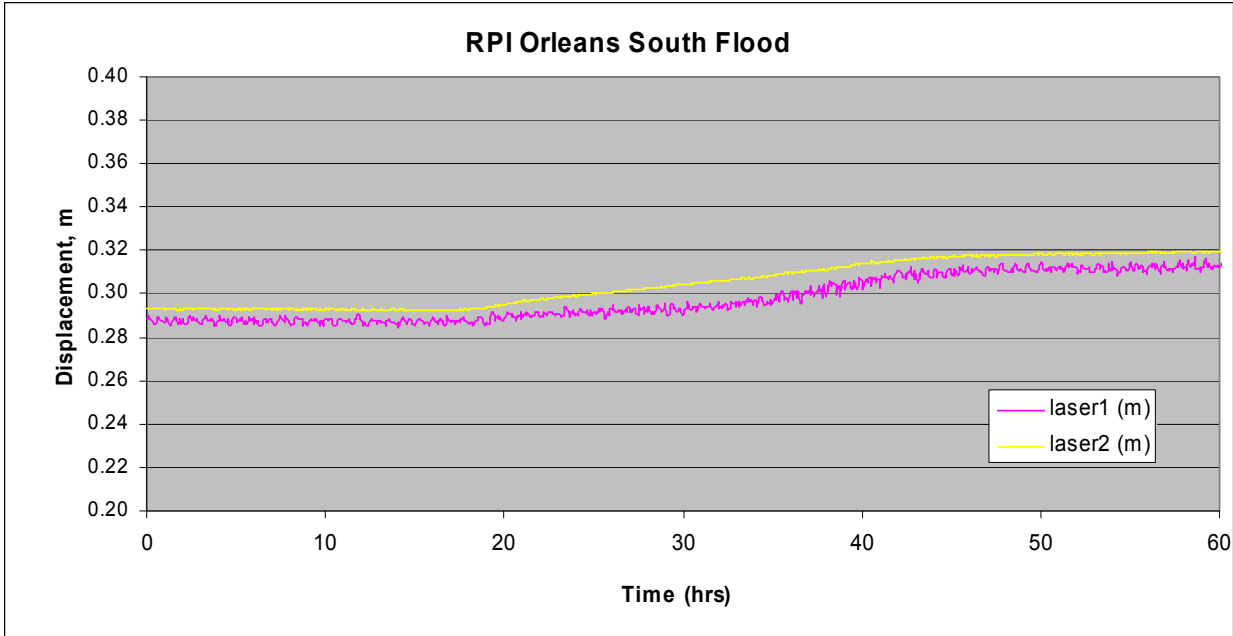


Figure 5.100. Displacement of the wall during flood loading

After the model was held at the Hurricane Katrina level for a period sufficient to show that no failure of the levee would occur, the water elevation was increased to near the top of the wall to explore the behavior of the levee. This was done simply as an exercise to determine what would have happened had the flood level actually reached that high. Just showing the movement of the wall, Figure 101, is enough to show the behavior. The zero time on the plot corresponds to the time when the water elevation is at Hurricane Katrina level and risen to the top of the wall. Therefore, all wall movements were as a result of the increased water load above Hurricane Katrina level. Notice that the wall starts to move immediately and continues on a fixed slope until about 50 hours. This movement is associated with opening of a crack behind the wall. From this point on, there is a slow steady movement of the wall amounting to about 0.2 m total. This movement would have been enough to cause concern about future stability of the wall.

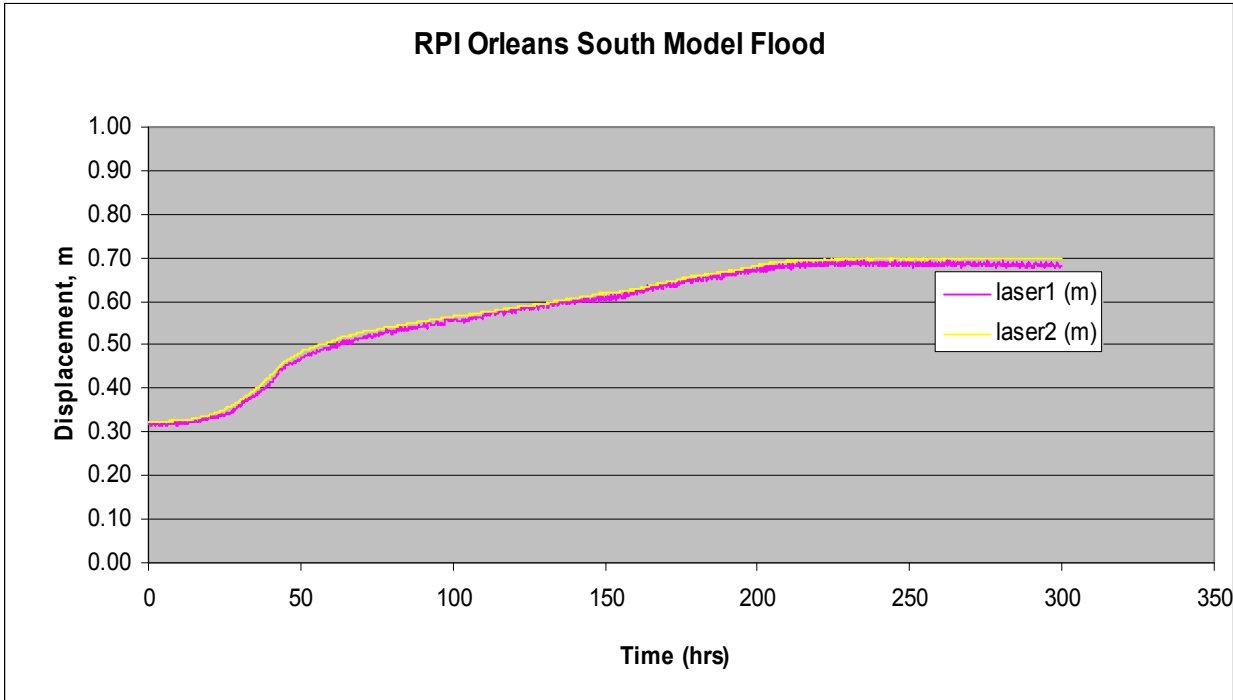


Figure 5.101. Displacement of wall during increased flood load above Hurricane Katrina level

The sequence of images shown in Figure 5.102 are stills taken from the video recording of the flood event. The images clearly show the behavior of the levee during the flood load.



Figure 5.102a. View of RPI Orleans south model at normal canal elevation



Figure 5.102b. View of RPI Orleans south model at Hurricane Katrina flood level



Figure 5.102c. View of RPI Orleans south model at Hurricane Katrina flood level, held here for long period



Figure 5.102d. View of RPI Orleans south model with water elevation raised above Hurricane Katrina level to near top of wall



Figure 5.102e. View of RPI Orleans south model with water elevation raised above Hurricane Katrina level showing movement of wall

The sequence of events in the Orleans south model are as highlighted following. These events are very similar to those as described for the north section of the levee.

1. Water was raised to the level of Hurricane Katrina and allowed to remain there for an extended period of time
2. The wall moved slightly but did not lead to any failure of the levee or subsequent movement in the wall.
3. Water elevation was then taken to the top of the wall, above Hurricane Katrina level. The wall moved an additional amount forming a crack behind the wall as was observed in the other canal walls.
4. This crack opening was preceded by slow steady movement of the wall that did not lead to catastrophic failure, but would have placed the stability of the levee in jeopardy.

Appendix 6

Soil-Structure Interaction Analysis of the Floodwall at 17th Street

Introduction

This section describes a complete soil-structure interaction (SSI) analysis of an existing floodwall within 17th Street Canal using the PC-based finite-element program, Plaxis (2004). A two-dimensional (2-D) cross section within the section of the east side of the 17th Street Canal that failed during hurricane Katrina is the subject of this evaluation. Results of a complete nonlinear finite-element analysis of a 2-D cross section at Station 10+00 during simulated flood loading are described.

Plaxis is a complete nonlinear finite-element package geared towards geotechnical engineering applications that include SSI issues such as those that occur between a sheet pile and the soils in which it is embedded. It allows for the nonlinear response of soils to flood loading as occurred at the 17th Street Canal with an I-wall along the centerline of the soil-founded levee. The Plaxis PC-based software comprises a visual pre-processor, a nonlinear finite-element engineering analysis module, and a visual post-processor. All software components are combined into a single package. Computed results include not only soil stresses, but also structural (e.g. sheet pile and I-wall) bending moments, interaction stresses between sheet piling, the soil in which it is embedded, as well as soil (e.g., levee) and structural deformations. A complete SSI analysis is considered to provide the most reasonable estimate for deformation response of a soil-structural system involving nonlinear material behavior. In a complete SSI analysis, loads exerted by the canal water acting on the soils of the levee and then onto the sheet pile wall (below the I-wall) by means of a load transfer through the levee and foundation soils are generated automatically during the analysis (i.e., predetermined earth pressure force distributions between the soil and the embedded sheet pile are not specified).

Section Analyzed

The 2-D cross section within the failed section of the east side of the 17th Street Canal at Station 10+00 analyzed for flood loading is shown in Figure 6-1.¹ The 2-D section is 247-ft wide and extends from x-coordinate equal to -27 ft to the centerline of the canal at x equal to 220 ft. The top of the I-wall is at El 12.5. The crest of the earthen levee on the protected (east) side of the I-wall is at El 5, with a crest width of approximately 15 ft. Note that the I-wall extends above the crest of the soil-founded levee. The protected side of the levee has a 1 on 3 side slope to approximately El -4.5. The protected side ground surface is assigned El -5 for this section. A bench exists at El -2.5 on the canal side of the I-wall. This bench is submerged for the normal water level in the canal, El 1. In the canal and beyond the end of the bench, the submerged levee face has a 1 on 3 side slope to approximately El -11.5. Between El -11.5 and El -16.5, the face of the peat soil layer is exposed to canal water. Below El -16.5, the Lacustrine clay soil layer is exposed to water in the canal. The deepest point in the canal is at the canal centerline (i.e., x = 220 ft in Figure 6-1), with a top of Lacustrine clay at El -18.5 at this location.

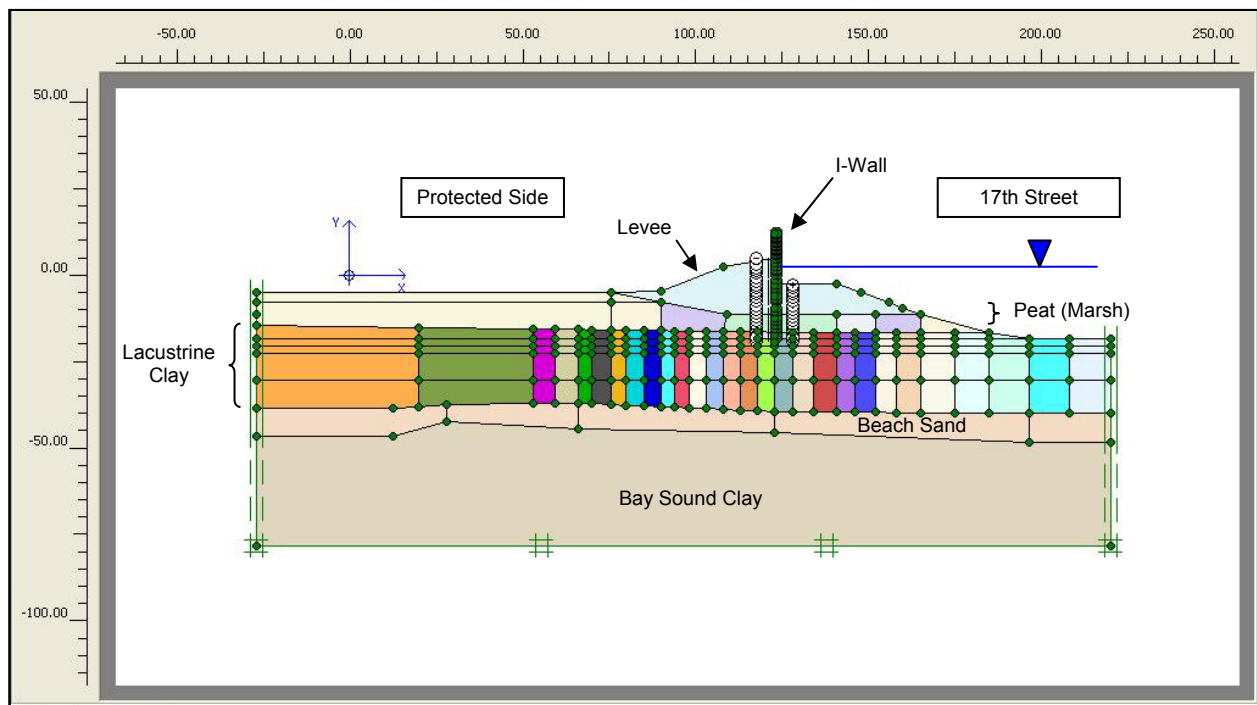


Figure 6-1. Two-Dimensional Cross-Section Model used in the Complete SSI Analysis of Station 10+00 at the 17th Street Canal – East Side

Proceeding from top to bottom in Figure 6-1, this cross section contains layers of levee fill (clay), peat (also referred to as marsh), lacustrine clay, beach sand, and Bay Sound clay. The top of the I-wall is at El 12.5, and the base of the Figure 6-1 cross section is assigned to El -78.5. El -78.5 corresponds (approximately) to the bottom of the Bay Sound clay at Station 10+00. The soil layering is consistent with that used in the slope stability evaluations made for this cross

¹ All elevations cited are according to NAD88.

section. The regions of uniform color in Figure 6-1 reflect the Plaxis “soil clusters” used to define the mesh and to assign soil regions with common properties.

Finite-Element Mesh

Key Plaxis modeling features used in the plane strain analysis of the 17th Street include the use of 15-node triangular elements to model the soil, plates (i.e., special beam elements) to model the bending of the I-wall and the sheet pile wall, and interface elements to model SSI between the sheet pile wall and the adjacent soil elements. A total of 26,858 nodes and 3,374 elements, containing 39,492 stress points, were used to define the Figure 6-2 mesh. Details regarding the quantity of each of the three types of plane strain elements used in the finite-element model, as well as select characteristics of each type of element, are summarized in Table 6-1.

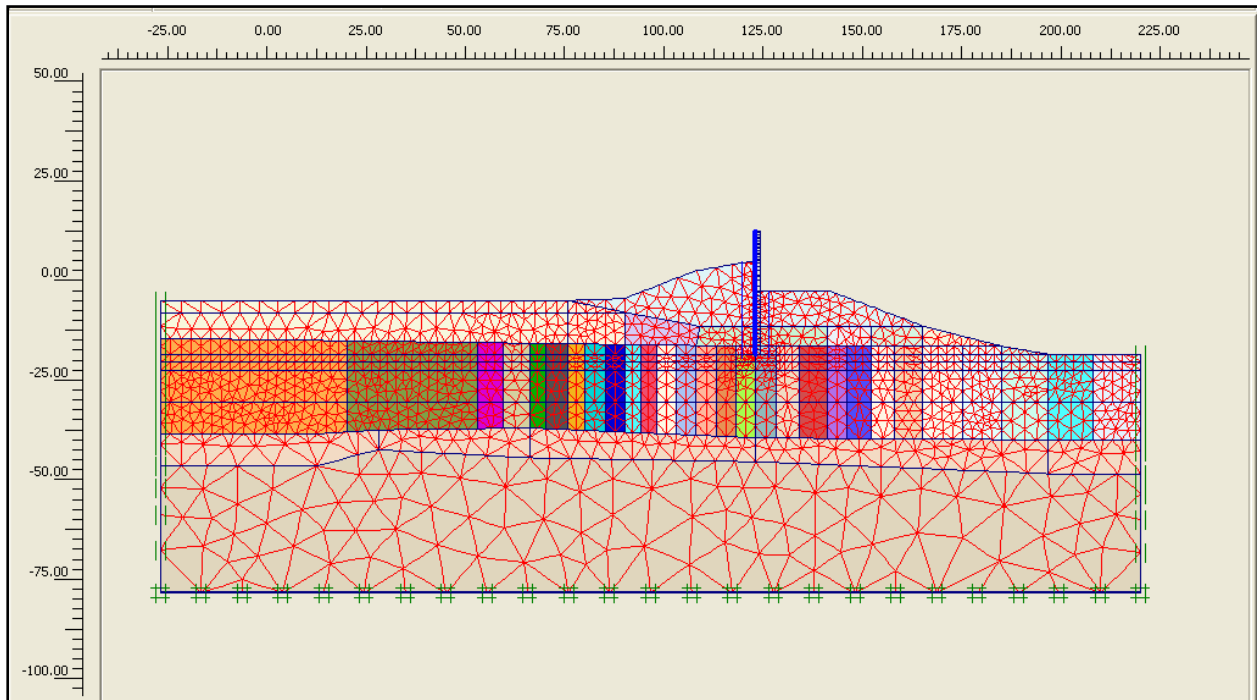


Figure 6-2. Finite-Element Mesh used in the Complete SSI Analysis of Station 10+00 at 17th Street Canal – East Side

Table 6-1 Mesh Data Summary of Elements Used			
Type	Type of element	Type of integration	Total No.
Soil	15-noded	12-point Gauss	3291
Plate	5-node line	4-point Gauss	39
Interface	5-node line	4-point Newton-Cotes	44

A zero horizontal displacement is specified along the left- and right-hand side vertical boundaries of the Figure 6-2 finite-element mesh. However, these nodes are free to displace in the vertical direction. Along the bottom boundary of the mesh, zero horizontal and vertical displacements are specified at these nodes.

Material Properties for the Soils and Floodwall in the Complete Soil-Structure Interaction Analysis

The soil material properties used in this complete SSI analysis are the same as those used in the slope stability analyses of this cross section. Figure 6-3 shows the 219 soil clusters used to define the regions of common soil properties for the five categories of soil within the mesh (i.e., the levee clay, peat (or marsh), lacustrine clay, beach sand, Bay Sound clay). Note that each soil layer comprises many clusters, each of which is designated by a different color. Spatially varying soil properties are assigned in the slope stability analyses. Accordingly, multiple soil clusters are used in the nonlinear finite-element mesh to assign material properties within each soil layer to accommodate the spatially varying (i.e., vertically as well as horizontally) soil properties. Table 6-2 summarizes the engineering material properties and, for some layers, the range in assigned engineering soil properties used in the complete SSI analysis.

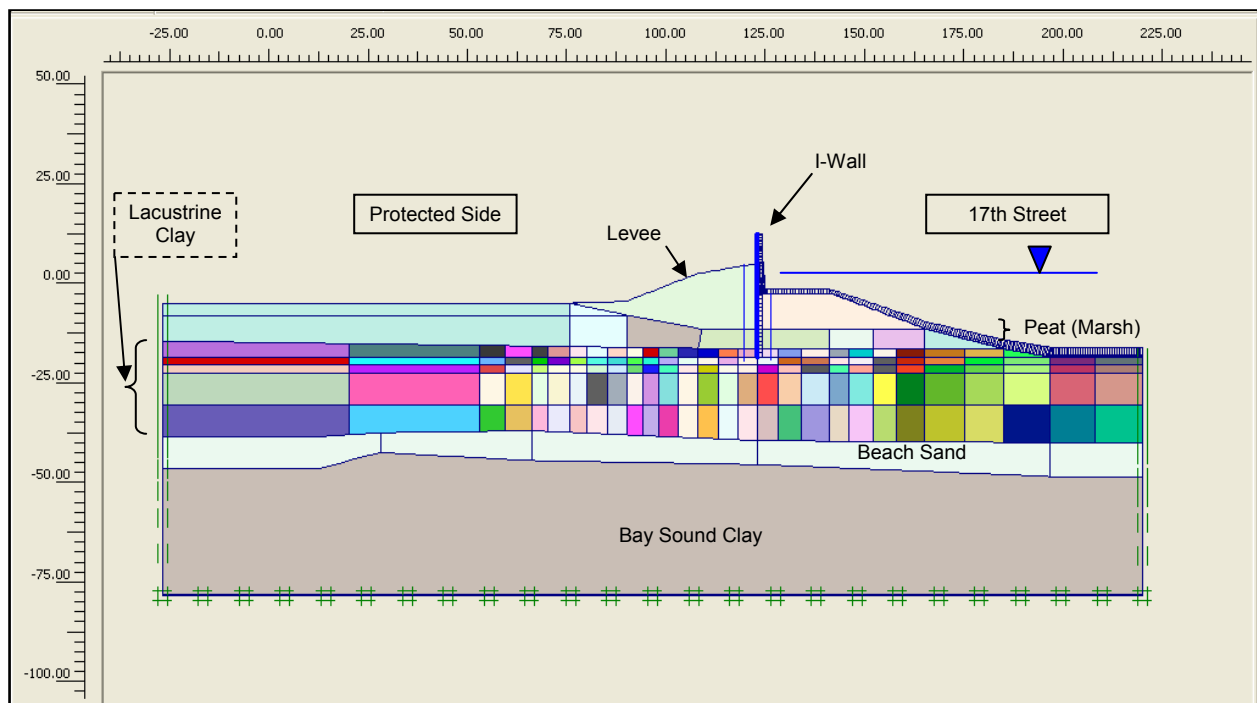


Figure 6-3. The 219 Soil Clusters used in the SSI Analysis of Station 10+00 at 17th Street Canal – East Side

**Table 6-2
Material Characterization for Soils**

Soil type	Total unit weight (pcf)	S_u			ϕ' (deg)	Young's Modulus		m	$R_{interface}$
		Constant value in soil cluster (psf)	S_u @ top of soil layer (psf)	ΔS_u per ft of depth (psf)		E^{ref}/S_u	E^{ref} (psf)		
Levee clay	110	900	-	-	-	48	-	0.5	0.8
Peat (marsh)	80	300 to 400	-	-	-	48	-	0.5	0.8
Lacustrine clay	109	-	45 to 300	11	-	92	-	1.0	0.8/1.0
Beach sand	120	-	-	-	36	-	477,725	0.5	-
Bay Sound clay	102	779	-	-	-	68	-	1.0	-

Note: $(E^{ref})_{50} = (E^{ref})_{oed} = E^{ref}$; $(E^{ref})_{ur} = 3 * E^{ref}$; $\psi = 0$ deg; $p_{ref} = 2116$ psf; $v_{ur} = 0.2$; $R_f = 0.9$

Levee clay: A total unit weight of 110 pcf is assigned to the levee clay soil clusters. Stress-strain data for levee clay specimens tested in an undrained shearing (mode) to failure in laboratory triaxial tests leads to the assignment of a value for Young's modulus, E^{ref} , expressed in terms of (E^{ref}) normalized by S_u and equal to 48. A value for E^{ref}/S_u of 48 corresponds to the mean value from the stress-strain results of 15 triaxial tests conducted on levee clay. Note that a secant value definition for Young's modulus (for a secant line originating at a strain of zero and passing through the point on the nonlinear stress-strain curve corresponding to 50% of the principal stress difference for the soil specimen) is used to assign a value for E^{ref} . Based on this and other shear strength test data, the undrained shear strength (S_u) is set equal to 900 psf for the levee clay (average value).

For the Plaxis nonlinear Hardening Soil (HS) model, the parameters $(E^{ref})_{50}$ and $(E^{ref})_{oed}$ are set equal to $[E^{ref}/S_u \text{ times } S_u]$. Additional HS parameters assigned are reference stress for stiffness, p_{ref} , equal to 2,116 psf, failure ratio $R_f = 0.9$, and the exponent $m = 0.5$. For unload reload HS parameters, $(E^{ref})_{ur}$ is set equal to 3 times $(E^{ref})_{50}$ and v_{ur} equals 0.2. For Hoesch 12 steel sheet piles to levee clay, the interface strength parameter, $R_{interface}$, is set equal to 0.8 for levee clay-to-steel interfaces (by the Potyondy, 1961, data).

Peat (or marsh): A total unit weight of 80 pcf is assigned to the peat (or marsh) soil clusters. Stress-strain data for peat specimens tested in an undrained shearing (mode) to failure in laboratory triaxial tests leads to the assignment of a value for Young's modulus (E^{ref}) normalized by S_u equal to 48. A value for E^{ref}/S_u of 48 corresponds to the mean value for 27 triaxial tests conducted on peat/marsh, with a 50% stress level secant value definition being used for E^{ref} . Based on this and other test data, the undrained shear strength (S_u) is set equal to between 300 and 400 psf for the peat, depending on overburden and/or location. Strength test results indicate that peat regions located below overburden, such as below the levee, have higher shear strengths. The region of peat immediately below the centerline region of the levee, the location of greatest overburden, is assigned $S_u = 400$ psf. The peat on the protected side and immediately beyond the toe of the levee (i.e., $x < 75$ ft) is assigned $S_u = 300$ psf, as is the peat at the toe of the canal side ($x = 185$ ft). A shear strength value is assigned to each peat cluster based on the magnitude of the

overburden for the center position of each peat cluster below the levee. There is an approximate linear variation in S_u with position between the centerline and the toe on the protected side and the centerline and the toe on the canal side. There is no vertical variation in undrained shear strength for the peat layer.

For the Plaxis nonlinear Hardening Soil (HS) model, the parameters $(E^{ref})_{50}$ and $(E^{ref})_{oed}$ are set equal to $[E^{ref}/S_u \text{ times } S_u]$. Additional HS parameters assigned are reference stress for stiffness, p_{ref} , equal to 2,116 psf, failure ratio $R_f = 0.9$, and the exponent $m = 0.5$. For unload reload HS parameters, $(E^{ref})_{ur}$ is set equal to 3 times $(E^{ref})_{50}$, and v_{ur} equals 0.2. For Hoesch 12 steel sheet piles to peat/marsh interface, $R_{interface}$ is set equal to 0.8.

Lacustrine clay: A total unit weight of 109 pcf is assigned to lacustrine clay soil clusters. Stress-strain data for Lacustrine clay specimens tested in an undrained shearing (mode) to failure in laboratory triaxial tests leads to the assignment of a value for Young's modulus (E^{ref}) normalized by S_u equal to 92. A value for E^{ref}/S_u of 92 corresponds to the mean value for 57 triaxial tests conducted on lacustrine clay, with a 50% stress level secant value definition being used for E^{ref} . Consolidation test data results show the lacustrine clay to be normally consolidated below the protected side and below the levee. Based on this data, as well as other laboratory and field test data, including interpreted cone data results, the undrained shear strength at the top of the lacustrine clay layer is defined in terms of an S_u/σ_v' equal to 0.24. The value of S_u at any point along the top of the lacustrine clay layer is equal to 0.24 times the effective overburden pressure. At the top of the lacustrine clay layer on the protected side, S_u ranges in value from 44 psf beyond the toe of the levee, to 53 psf below the toe of the levee. The value for S_u at the top of the lacustrine clay increases from 53 psf below the toe of the levee (on the protected side) to a maximum value of 300 psf below the I-wall, with a distribution for S_u that approximately mirrors the shape of the ground surface between these two points (refer to Figure 6-3). The value for S_u at the top of the lacustrine clay decreases from a maximum value of 300 psf below the I-wall to a value of 76 psf below the toe of the submerged peat layer on the canal side, with a distribution for S_u that mirrors the shape of the ground surface between these two points. At the top of the lacustrine clay layer below the canal, S_u is set equal to a value of between 82 and 96 psf. This zone of levee clay is overconsolidated as a result of the removal of overburden during the canal excavation process that has taken place over the years.

There are five rows of soil clusters used to define the lacustrine clay layer (refer to Figure 6-3). Shear strengths for the top row of soil clusters are assigned undrained shear strength values using the data discussed in the previous paragraph and based on its center x-coordinate. Interpretation of cone test results shows an increase in undrained shear strength with depth equal to 11 psf per ft depth. Undrained shear strengths for the lower four rows of lacustrine clay are assigned based on the value for S_u at the top of the lacustrine clay, plus the product of 11 psf per ft depth times the vertical distance between cluster center and the top of the lacustrine clay layer.

For the Plaxis nonlinear Hardening Soil (HS) model, the parameters $(E^{ref})_{50}$ and $(E^{ref})_{oed}$ are set equal to $[E^{ref}/S_u \text{ times } S_u]$ for each soil cluster. Additional HS parameters assigned are reference stress for stiffness, p_{ref} , equal to 2,116 psf, failure ratio $R_f = 0.9$, and the exponent $m = 1$. For unload reload HS parameters, $(E^{ref})_{ur}$ is set equal to 3 times $(E^{ref})_{50}$ and v_{ur} equals 0.2.

For Hoesch 12 steel sheet piles to lacustrine clay interface, $R_{\text{interface}}$ is set equal to 0.8. $R_{\text{interface}}$ is set equal to 1.0 for all soil-to-soil interfaces.

Beach sand: A total unit weight of 120 pcf is assigned to the beach sand soil clusters. Standard Penetration Test results in this layer indicate an average value of 21 blows per ft depth for 60% of free-fall energy (i.e., $N_{60} = 21$). Correcting these results to an effective overburden pressure of 1 ton/ft² results in $(N_1)_{60}$ equal to 25 blows per ft depth. For a fine sand with $(N_1)_{60} = 25$, the relative density (D_r) is 63% by Skempton's (1986) correlation. For fine sand with a D_r of 63%, the effective angle of internal friction is equal to 36 degrees by Schmertman's (1978) correlation. For $N_{60} = 21$ and using the Kulhawy and Mayne (1990) equation, 5-26b, the value of Young's modulus E^{ref} is set equal to 477,725 psf.

For the Plaxis nonlinear Hardening Soil (HS) model, the parameters $(E^{\text{ref}})_{50}$ and $(E^{\text{ref}})_{\text{oad}}$ are set equal to 477,725 psf. Additional HS parameters assigned are reference stress for stiffness, p_{ref} , equal to 2,116 psf, failure ratio $R_f = 0.9$, and the exponent $m = 0.5$. For unload reload HS parameters, $(E^{\text{ref}})_{\text{ur}}$ is set equal to 3 times $(E^{\text{ref}})_{50}$, and v_{ur} equals 0.2. For Hoesch 12 steel sheet piles to beach sand, the interface strength parameter, $R_{\text{interface}}$, is set equal to 0.8.

Bay Sound clay: A total unit weight of 102 pcf is assigned to the Bay Sound clay soil cluster. Stress-strain data for Bay Sound clay specimens tested in an undrained shearing (mode) to failure in laboratory triaxial tests leads to the assignment of a value for Young's modulus, E^{ref} , expressed in terms of (E^{ref}) normalized by S_u and equal to 68. A value for E^{ref}/S_u of 68 corresponds to the mean value for 54 triaxial tests conducted on Bay Sound clay, with a 50% stress level secant value definition being used for E^{ref} . Based on this and other shear strength test data, the undrained shear strength (S_u) is set equal to 779 psf for the Bay Sound clay (average value).

For the Plaxis nonlinear Hardening Soil (HS) model, the parameters $(E^{\text{ref}})_{50}$ and $(E^{\text{ref}})_{\text{oad}}$ are set equal to $[E^{\text{ref}}/S_u \text{ times } S_u]$. Additional HS parameters assigned are reference stress for stiffness, p_{ref} , equal to 2,116 psf, failure ratio $R_f = 0.9$, and the exponent $m = 1.0$. For unload reload HS parameters, $(E^{\text{ref}})_{\text{ur}}$ is set equal to 3 times $(E^{\text{ref}})_{50}$, and v_{ur} equals 0.2.

Floodwall: The floodwall comprises an exposed reinforced concrete I-wall, a reinforced concrete cap, and Hoesch 12 hot-rolled sheet pile. The 12-in.-thick reinforced concrete I-wall extends from the top of protected levee (El 5) to El 12.5. At Station 10+00, the sheet pile tip is at El -18.5. The upper reach of pile is encased in a 2-ft-thick reinforced concrete cap, extending below the surface of the protected side of the levee. Linear-elastic material response was assumed in the complete SSI analysis. Engineering properties for the I-wall, cap, and sheet pile are summarized in Table 6-3 for the zero thickness plate elements used in the finite-element model.

**Table 6-3
Material Characterization for the Floodwall**

Identification	EA [lb/ft]	EI [lbft ² /ft]	Weight [lb/ft/ft]	v [-]
Reinforced Concrete I-wall	4.32E8	3.6E7	150.00	0.20
Reinforced Concrete Cap	8.64E8	2.88E8	190.00	0.20
Sheet Pile (Hoesch 12)	1.88E8	1.83E7	17.64	0.30

Complete Soil-Structure Interaction Analysis

Introduction: A complete SSI analysis of the Figure 6-1 2-D cross section of Station 10+00 at the 17th Street Canal from canal water at El 1.0, on through a series of incremental 0.5- to 1-ft raises in canal elevation to model flood loading is conducted in a staged analysis using Plaxis. Table 6-4 summarizes the calculation phases of the analysis. More than 25 phases of calculations are used in the complete SSI analysis.

**Table 6-4
Calculation Phases of the Nonlinear Finite-Element Analysis**

Phase	Phase No.	Calculation type	Load input
Initial Phase	0		-
Place Wall & Interface	1	Plastic analysis	Staged construction
Gravity (0.15)	2	Plastic analysis	Total multipliers
Water Table El -11.5	3	Plastic analysis	Staged construction
Gravity (0.3)	4	Plastic analysis	Total multipliers
Water Table El -8	5	Plastic analysis	Staged construction
Gravity (0.45)	6	Plastic analysis	Total multipliers
Water Table El -5.0	7	Plastic analysis	Staged construction
Gravity (0.60)	8	Plastic analysis	Total multipliers
Water Table El -2.5	9	Plastic analysis	Staged construction
Gravity (0.75)	10	Plastic analysis	Total multipliers
Water Table 0.0	11	Plastic analysis	Staged construction
Gravity (1.0)	12	Plastic analysis	Total multipliers
Water Table El +1	13	Plastic analysis	Staged construction
Canal Water El +1.5	14	Plastic analysis	Staged construction
Canal Water El +2.5	15	Plastic analysis	Staged construction
Canal Water El +3.5	16	Plastic analysis	Staged construction
Canal Water El +4.5	17	Plastic analysis	Staged construction
Canal Water El +5.5	18	Plastic analysis	Staged construction
Canal Water El +6.5	19	Plastic analysis	Staged construction
Crack to El -16.5	20	Plastic analysis	Staged construction
Crack to El -18.5	21	Plastic analysis	Staged construction
Canal Water El +7.5	22	Plastic analysis	Staged construction
Canal Water El +8.5	23	Plastic analysis	Staged construction
Canal Water El +9	24	Plastic analysis	Staged construction
Phi-C Reductions	25*	Phi/c reduction	Incremental multipliers

Loading phases 0 through 13 are used in the complete SSI analysis to establish the initial total stress state condition existing prior to flooding. Loading phase 13 concludes with canal water at El 1, a steady state water elevation in the canal.

Loading phases 14 through 24 are used in the complete SSI analysis to perform an incremental raise in the canal water to El 9, modeling the flood loading of the levee/I-wall system and the introduction of a crack along the canal-side face of the sheet pile in the levee clay, the peat/marsh, and the 2 ft of lacustrine clay.

The last of the loading phases is used to compute the reserve capacity of the levee/I-wall system for different canal water elevations. This reserve capacity is expressed in terms of a factor of safety and is computed in a series of Plaxis phi/c reduction loading phases.

Initial steady state condition for canal water at EL 1: Loading phases 0 through 13 are used in the complete SSI analysis to establish the initial total stress state within the finite-element mesh with a steady state canal water elevation at El 1. An alternating series of incremental applications of gravity loading followed by incremental raises of the water table is conducted. In the beach sand layer, the water table is established at El -6.33 by analysis phase 5 and is maintained at this elevation in all subsequent computation phases. This elevation is established by piezometric readings taken in the beach sand layer. Load input for gravity loading is specified in Plaxis by means of the total multiplier method, and changes in water table are accomplished by staged construction.

The initial steady-state, total stress condition for the usual canal water elevation of 1 is established by adjusting modulus values for the Mohr-Coulomb soil model until a suitable total stress regime is obtained within the mesh for loading phases 0 through 13. The results from the IPET Task 7 slope stability analyses for this usual canal elevation indicate a stable cross section with an ample factor of safety, i.e., above 1.5. Consequently, an important aspect of the total stress regime achieved within the Figure 6-2 finite-element mesh is that the mobilized shear stress at the strain integration points within the finite-elements contained in the soil clusters shown in this figure be less than the shear strength of the soil. The resulting computed fraction of mobilized shear strength (referred to as relative shear stress in Plaxis output) from the resulting initial total stress condition is shown in Figure 6-4. The fraction of mobilized shear strength is less than or equal to 0.95 at the stress integration points for the five soil types.

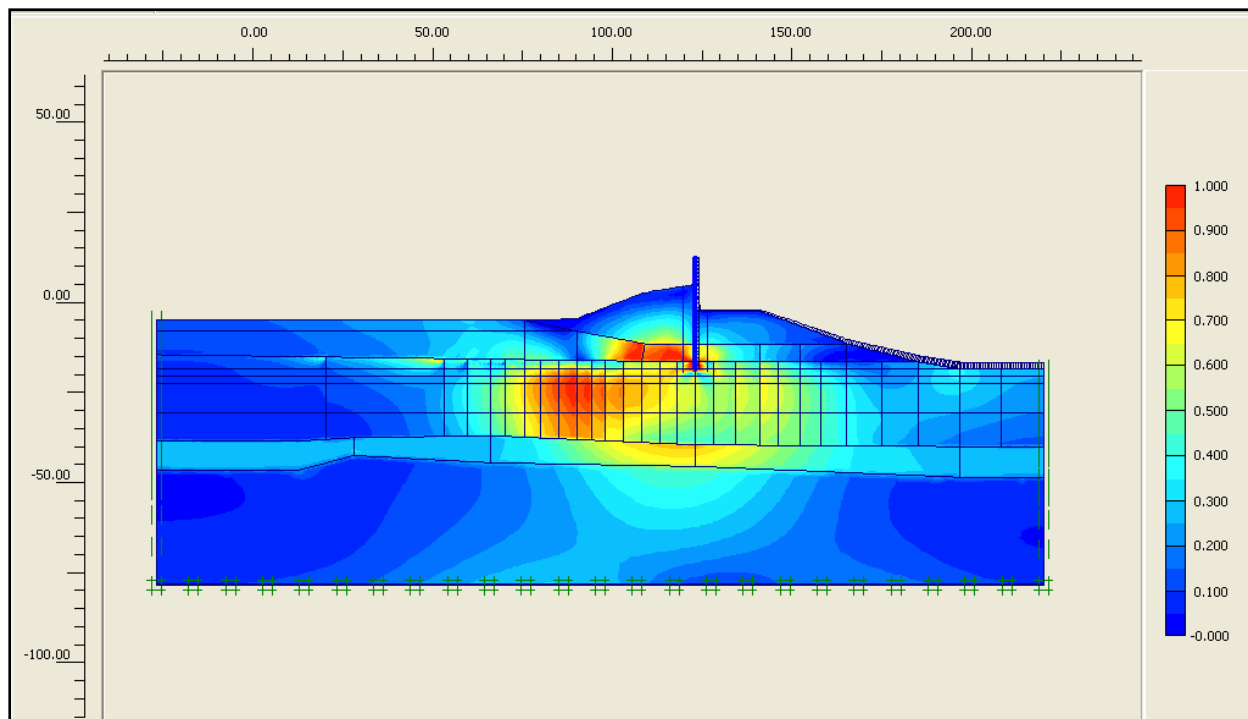


Figure 6-4. Fraction of Mobilized Shear Strength for Canal El 1

Flood loading: Modeling of flood loading commenced in the complete SSI analysis after the total initial stress state is established within the finite element mesh for steady state canal elevation (i.e., El 1). The hardening soil model with the Table 6-2 material property values is assigned to each of the five types of soil regimes. Loading phases 14 through 24 are used in the complete SSI analysis to perform an incremental raise in the canal water to El 9, modeling the flood loading of the levee/I-wall system. Load input for changes in canal water elevation is specified by staged construction.

Canal El 1.5: The first increment in flood loading, designated loading phase 14, corresponds to a 0.5-ft increase in canal water, i.e., from canal steady state El 1 to El 1.5. Hydrostatic canal water pressures are applied as boundary water pressures normal to the wetted side of the I-wall and normal to the wetted exposed face of the levee and clays below the canal. The deformed mesh is shown in Figure 6-5. Note that the nodal deformations are increased by a factor of 100 in order to show the deformed mesh relative to its position at a canal water elevation of 1.0 (shown as a blue outline in this figure). The general trend of deformations is downward and towards the protected side due to the boundary water pressure loading applied within the canal. The maximum (relative) displacement within the mesh is 0.028 ft (< 3/8 in.). There is no indication of a fully developed failure mechanism occurring at this flood stage.

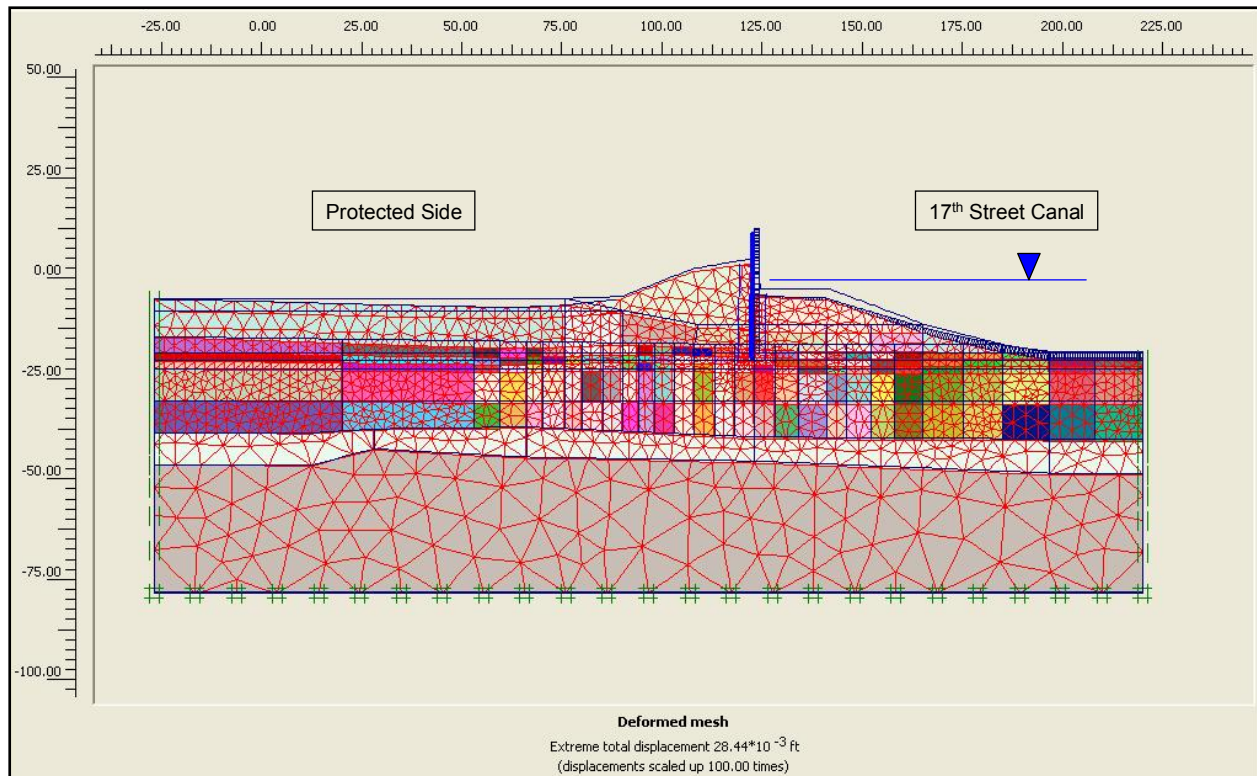


Figure 6-5. Deformed Mesh, Exaggerated by a Factor of 100, for Canal EI 1.5 (Note: Canal EI not to scale in figure)

The mobilized shear stress at the strain integration points within the finite elements contained in the soil clusters is shown in Figure 6-6 to be less than the shear strength of the soil. The resulting computed fraction of mobilized shear strength is less than or equal to 0.96 at the stress integration points for the five soil types. The horizontal total stress state at the top of the submerged levee berm on the canal side and adjacent to the sheet pile does not indicate that a crack will open at this canal water elevation.

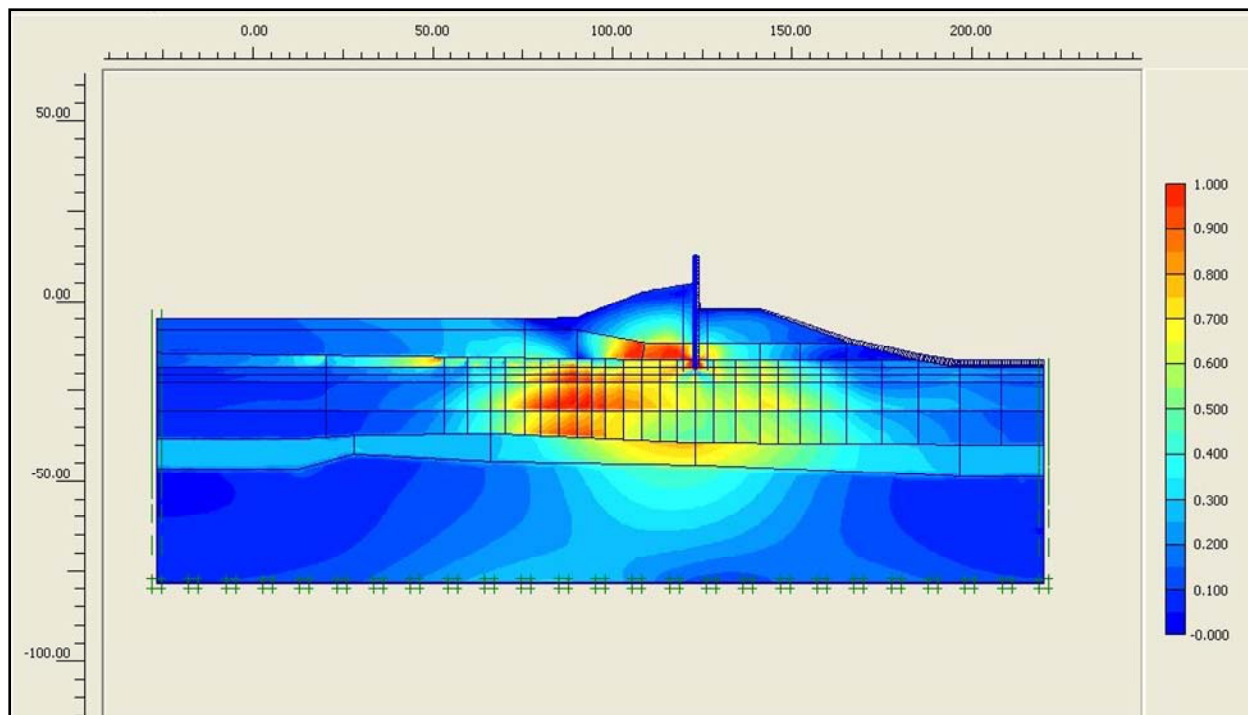


Figure 6-6. Fraction of Mobilized Shear Strength for Canal El 1.5

Canal El 2.5: The second increment in flood loading, designated loading phase 15, raises the canal water to El 2.5. This is a 1.5-ft increase in canal water relative to canal steady state El 1 or, equivalently, a 1-ft increase in canal flood water elevation from canal El 1.5 of loading phase 14. The loading applied to the mesh is again solely due to hydrostatic canal water pressures applied as boundary water pressures normal to the wetted side of the I-wall and normal to the wetted exposed face of the levee and clays forming the sides and base of the canal. The deformed mesh is shown in Figure 6-7. Note that the nodal deformations are increased by a factor of 50 in order to show the deformed mesh relative to its position at a canal water elevation of 1.0 (shown as a blue outline in this figure). The general trend of deformations is downward and towards the protected side due to the boundary water pressure loading applied within the canal. The maximum (relative) displacement within the mesh is 0.093 ft (< 1-1/8 in.). There is no indication of a fully developed failure mechanism occurring at this flood stage.

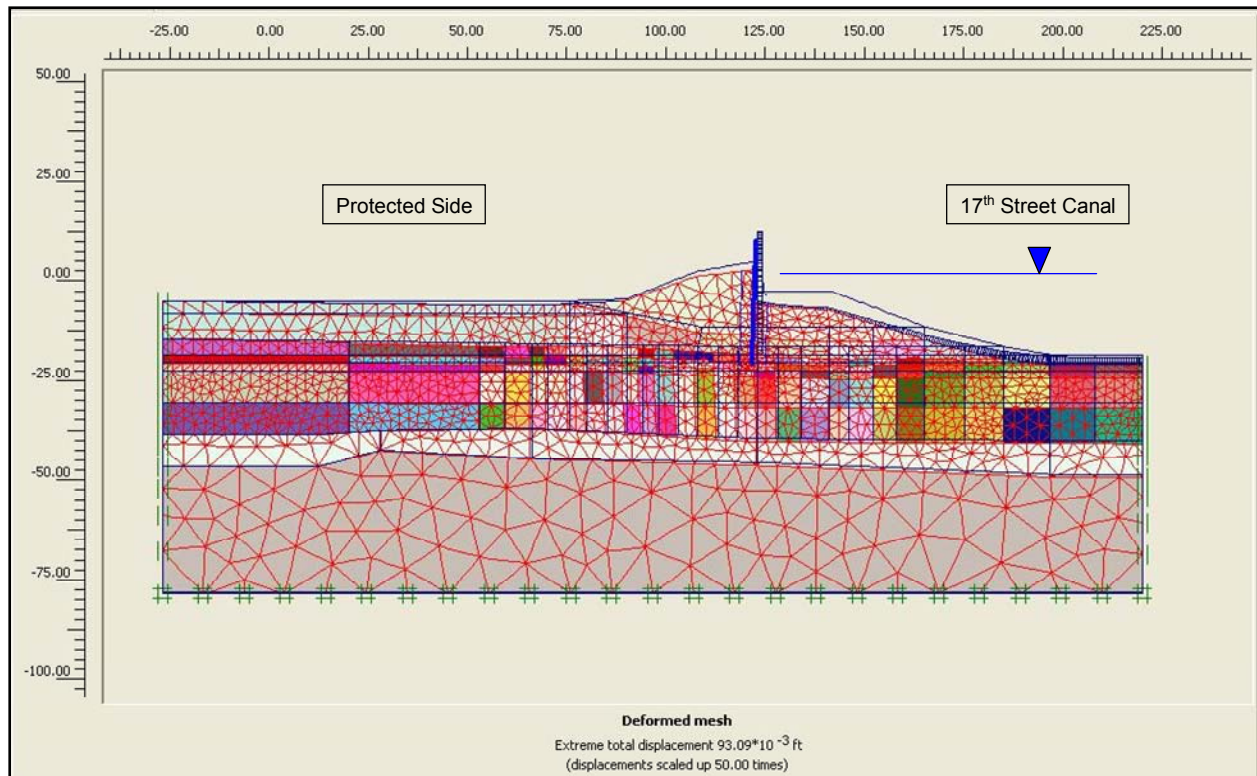


Figure 6-7. Deformed Mesh, Exaggerated by a Factor of 50, for Canal EI 2.5 (Note: Canal EI not to scale in figure)

The mobilized shear stress at the strain integration points within the finite elements contained in the soil clusters is shown in Figure 6-8 to be less than the shear strength of the soil. The resulting computed fraction of mobilized shear strength is less than or equal to 0.96 at the stress integration points for the five soil types. The horizontal total stress state at the top of the submerged levee berm on the canal side and adjacent to the sheet pile does not indicate that a crack will open at this canal water elevation.

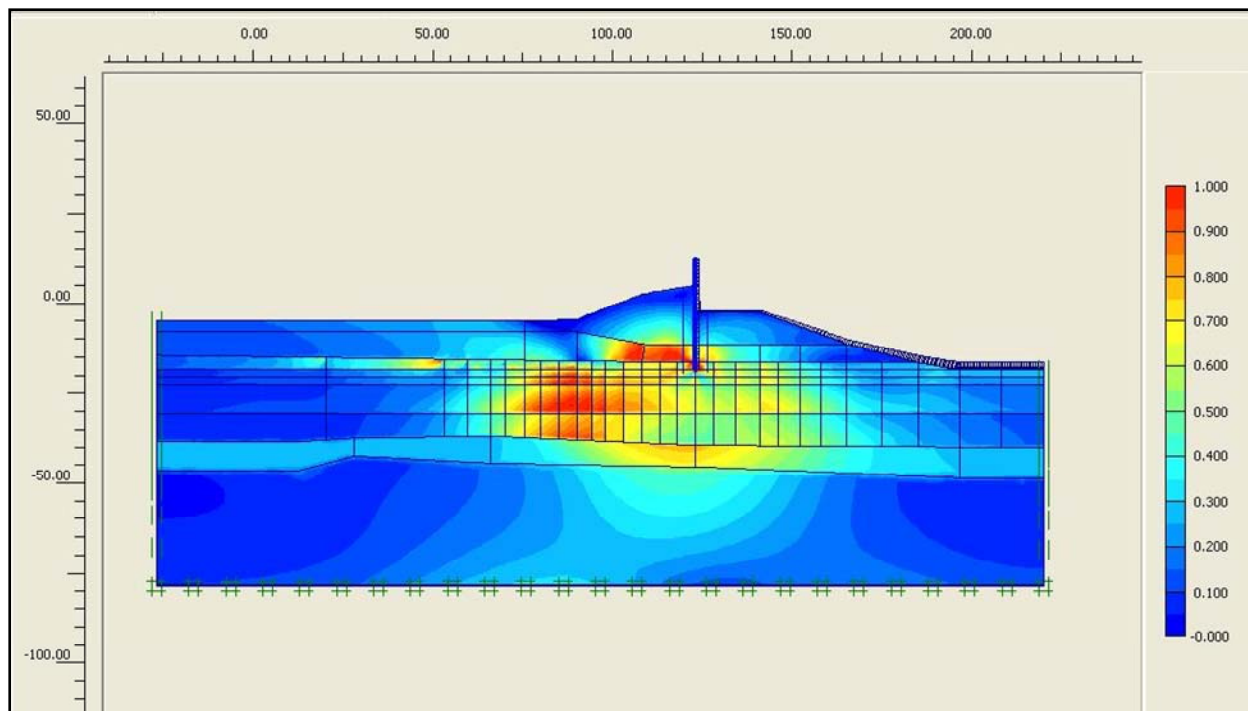


Figure 6-8. Fraction of Mobilized Shear Strength for Canal El 2.5

Canal El 3.5: The third increment in flood loading, designated loading phase 16, raises the canal water to El 3.5. This is a 2.5-ft increase in canal water relative to canal steady state El 1 or, equivalently, a 1-ft increase in canal flood water elevation from canal El 2.5 of loading phase 15. The loading applied to the mesh is again solely due to hydrostatic canal water pressures applied as boundary water pressures normal to the wetted side of the I-wall and normal to the wetted exposed face of the levee and clays forming the sides and base of the canal. The deformed mesh is shown in Figure 6-9. Note that the nodal deformations are increased by a factor of 25 in order to show the deformed mesh relative to its position at a canal water elevation of 1.0 (shown as a blue outline in this figure). The general trend of deformations is downward and towards the protected side due to the boundary water pressure loading applied within the canal. The maximum (relative) displacement within the mesh is 0.176 ft ($< 2\text{-}1/8$ in.). There is no indication of a fully developed failure mechanism occurring at this flood stage.

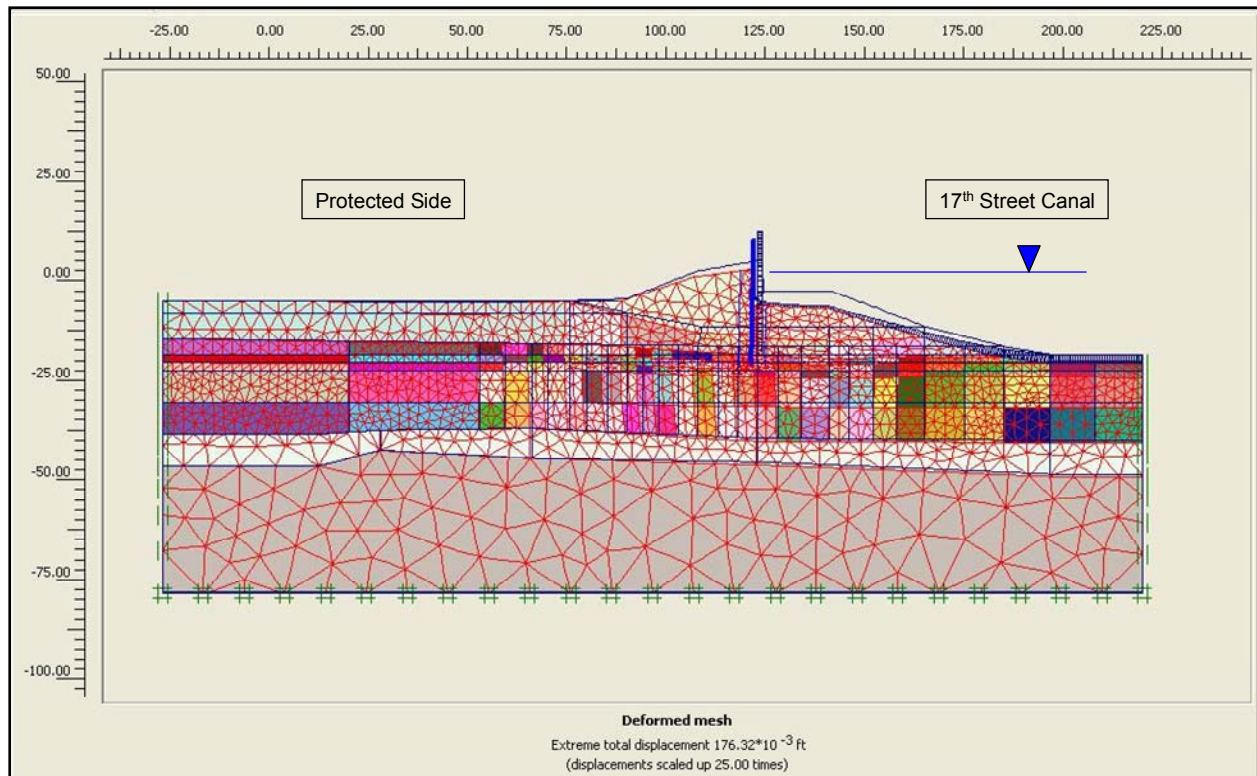


Figure 6-9. Deformed Mesh, Exaggerated by a Factor of 25, for Canal EI 3.5 (Note: Canal EI not to scale in figure)

The mobilized shear stress at the strain integration points within the finite elements contained in the soil clusters is shown in Figure 6-10 to be less than the shear strength of the soil. The resulting computed fraction of mobilized shear strength is less than or equal to 0.96 at the stress integration points for the five soil types. The horizontal total stress state at the top of the submerged levee berm on the canal side and adjacent to the sheet pile does not indicate that a crack will open at this canal water elevation.

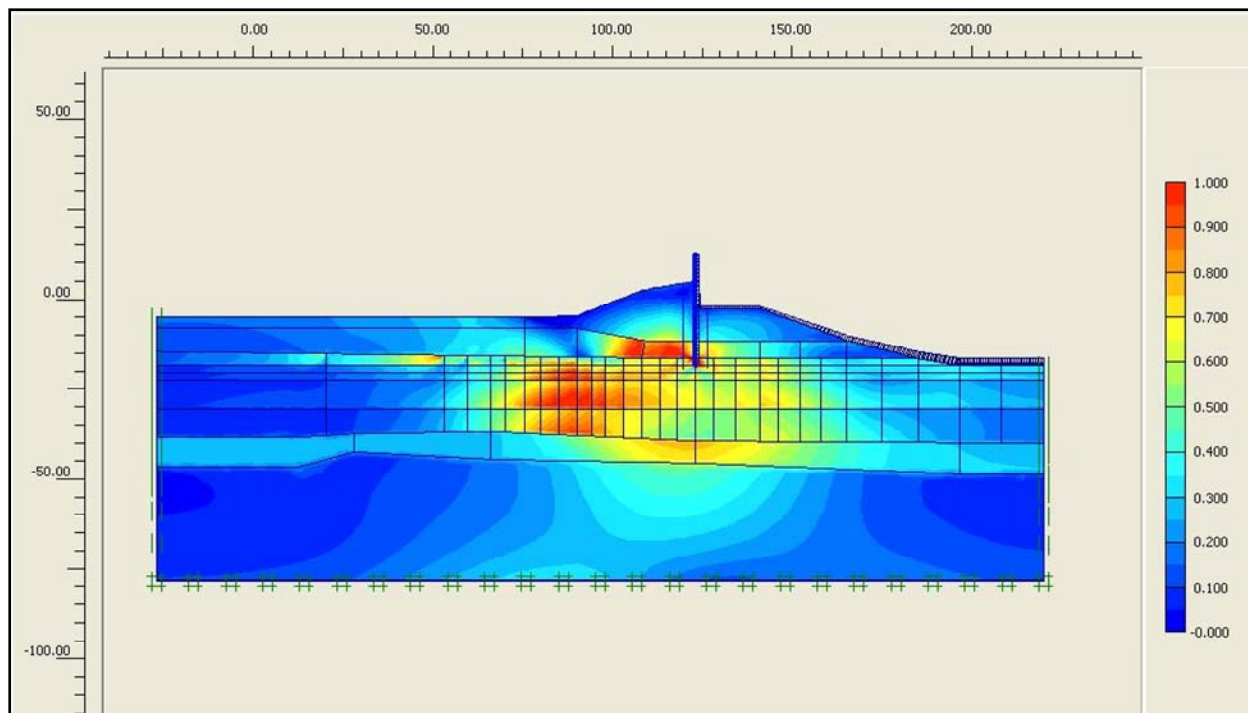


Figure 6-10. Fraction of Mobilized Shear Strength for Canal El 3.5

Canal El 4.5: The fourth increment in flood loading, designated loading phase 17, raises the canal water to El 4.5. This is a 3.5-ft increase in canal water relative to canal steady state El 1 or, equivalently, a 1-ft increase in canal flood water elevation from canal El 3.5 of loading phase 16. The loading applied to the mesh is again solely due to hydrostatic canal water pressures applied as boundary water pressures normal to the wetted side of the I-wall and normal to the wetted exposed face of the levee and clays forming the sides and base of the canal. The deformed mesh is shown in Figure 6-11. Note that the nodal deformations are increased by a factor of 20 in order to show the deformed mesh relative to its position at a canal water elevation of 1.0 (shown as a blue outline in this figure). The general trend of deformations is downward and towards the protected side due to the boundary water pressure loading applied within the canal. The maximum (relative) displacement within the mesh is 0.273 ft (approximately 3-1/4 in.). There is no indication of a fully developed failure mechanism occurring at this flood stage.

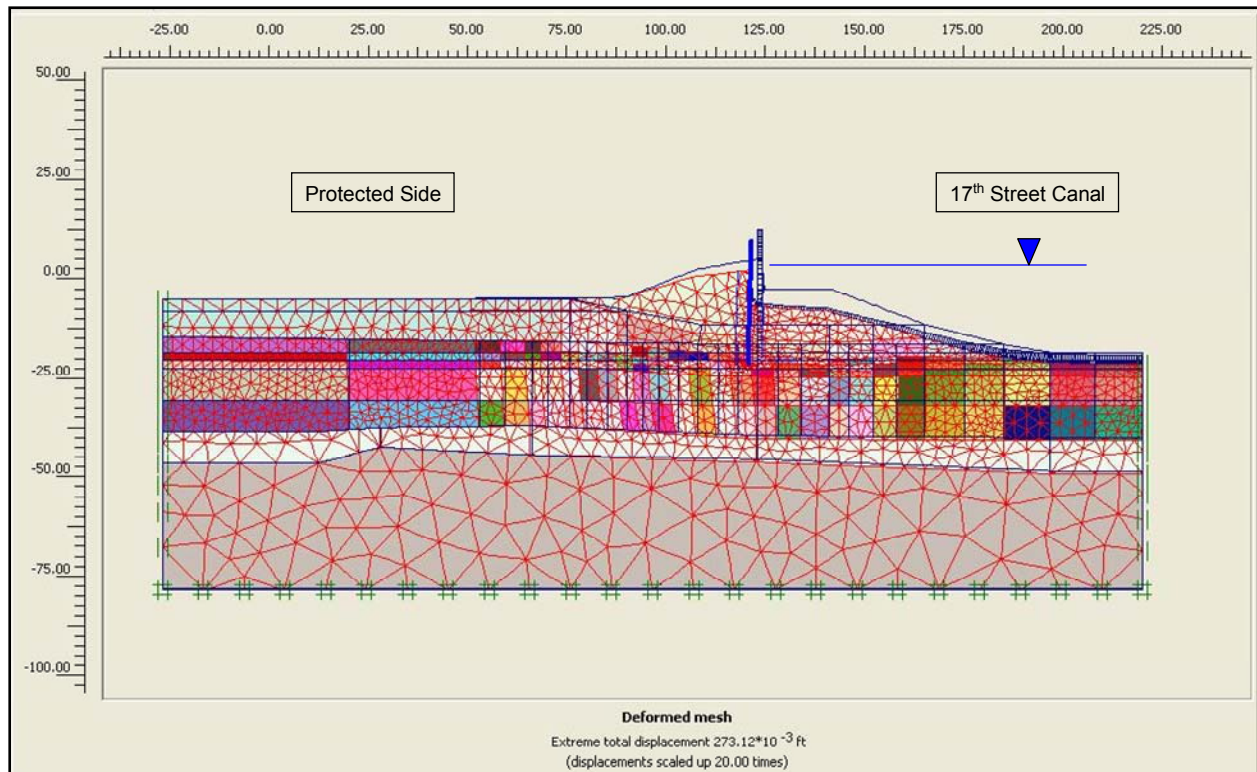


Figure 6-11. Deformed Mesh, Exaggerated by a Factor of 20, for Canal EI 4.5 (Note: Canal EI not to scale in figure)

The mobilized shear stress at the strain integration points within the finite elements contained in the soil clusters is shown in Figure 6-12 to be less than the shear strength of the soil. The resulting computed fraction of mobilized shear strength is less than or equal to 0.96 at the stress integration points for the five soil types. The horizontal total stress state at the top of the submerged levee berm on the canal side and adjacent to the sheet pile does not indicate that a crack will open at this canal water elevation.

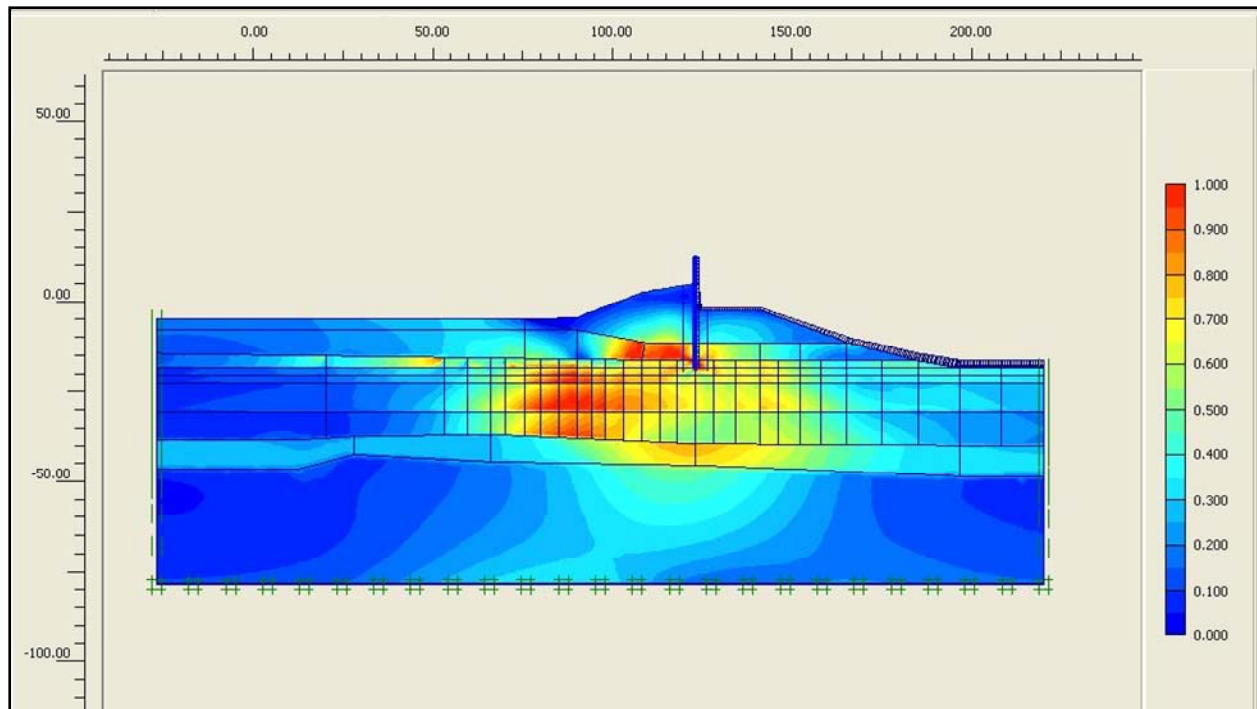


Figure 6-12. Fraction of Mobilized Shear Strength for Canal El 4.5

Canal El 5.5: The fifth increment in flood loading, designated loading phase 18, raises the canal water to El 5.5. This is a 4.5-ft increase in canal water relative to canal steady state El 1 or, equivalently, a 1-ft increase in canal flood water elevation from canal El 4.5 of loading phase 17. The loading applied to the mesh is again solely due to hydrostatic canal water pressures applied as boundary water pressures normal to the wetted side of the I-wall and normal to the wetted exposed face of the levee and clays, forming the sides and base of the canal. The deformed mesh is shown in Figure 6-13. Note that the nodal deformations are increased by a factor of 13 in order to show the deformed mesh relative to its position at a canal water elevation of 1.0 (shown as a blue outline in this figure). The general trend of deformations is downward and towards the protected side due to the boundary water pressure loading applied within the canal. The maximum (relative) displacement within the mesh is 0.383 ft ($< 4\text{-}5/8$ in.). There is no indication of a fully developed failure mechanism occurring at this flood stage.

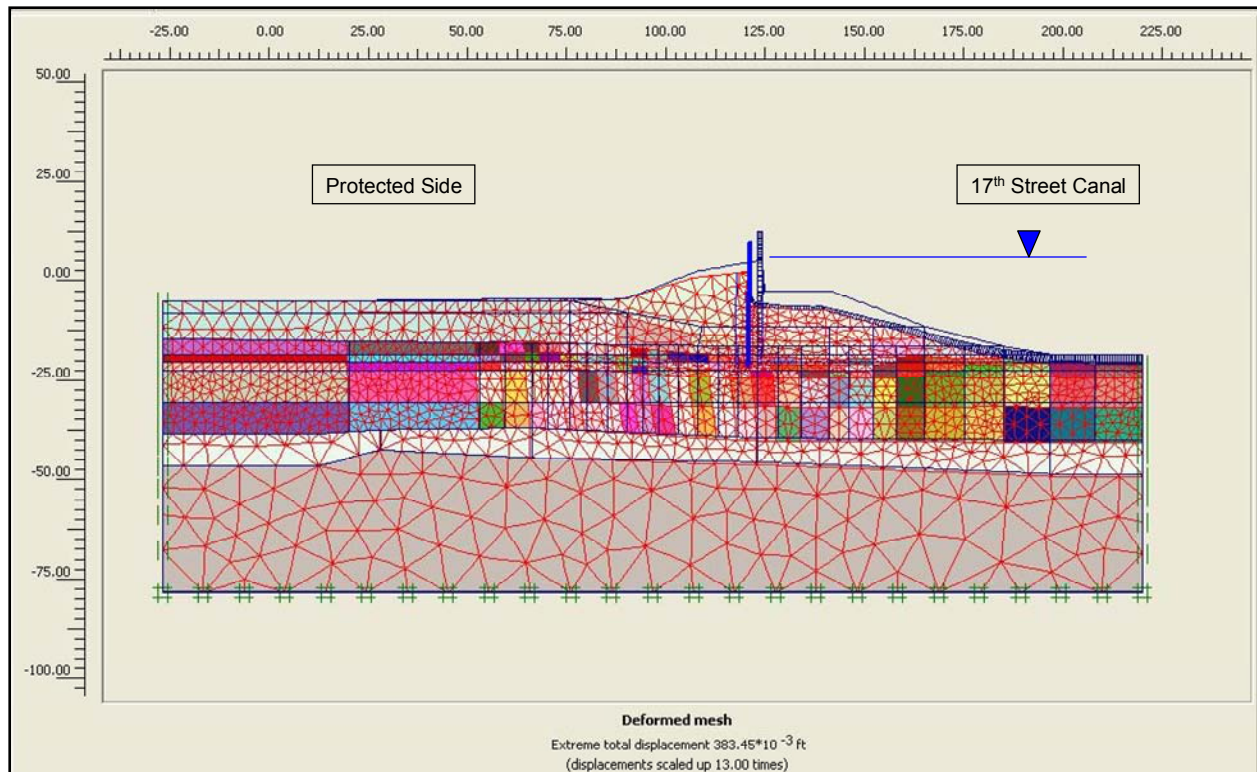


Figure 6-13. Deformed Mesh, Exaggerated by a Factor of 13, for Canal EI 5.5 (Note: Canal EI not to scale in figure)

The mobilized shear stress at the strain integration points within the finite elements contained in the soil clusters is shown in Figure 6-14 to be less than the shear strength of the soil. The resulting computed fraction of mobilized shear strength is less than or equal to 0.96 at the stress integration points for the five soil types. The horizontal total stress state at the top of the submerged levee berm on the canal side and adjacent to the sheet pile does not indicate that a crack will open at this canal water elevation.

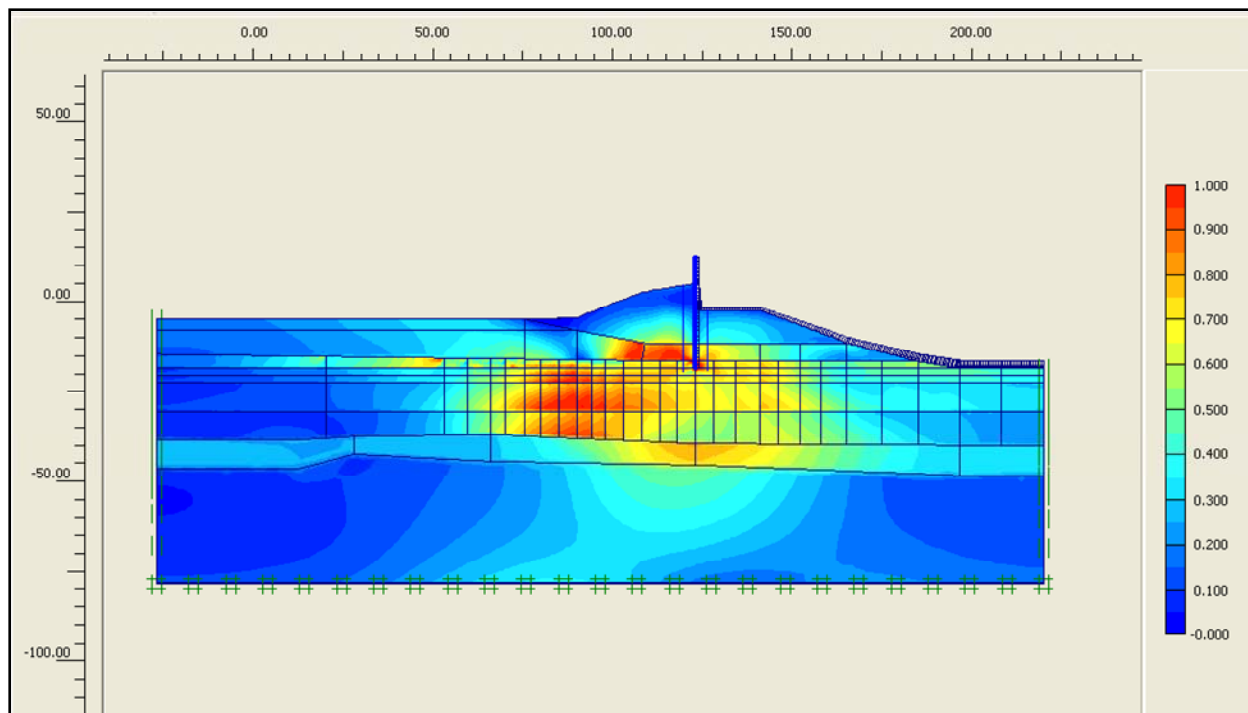


Figure 6-14. Fraction of Mobilized Shear Strength for Canal El 5.5

Canal El 6.5: The sixth increment in flood loading, designated loading phase 19, raises the canal water to El 6.5. This is a 5.5-ft increase in canal water relative to canal steady state El 1 or, equivalently, a 1-ft increase in canal flood water elevation from canal El 5.5 of loading phase 18. The loading applied to the mesh is again solely due to hydrostatic canal water pressures applied as boundary water pressures normal to the wetted side of the I-wall and normal to the wetted exposed face of the levee and clays forming the sides and base of the canal. The deformed mesh is shown in Figure 6-15. Note that the nodal deformations are increased by a factor of 10 in order to show the deformed mesh relative to its position at a canal water elevation of 1.0 (shown as a blue outline in this figure). The general trend of deformations is downward and towards the protected side due to the boundary water pressure loading applied within the canal. The maximum (relative) displacement within the mesh is 0.479 ft (approximately 5-3/4 in.). There is no indication of a fully developed failure mechanism occurring at this flood stage.

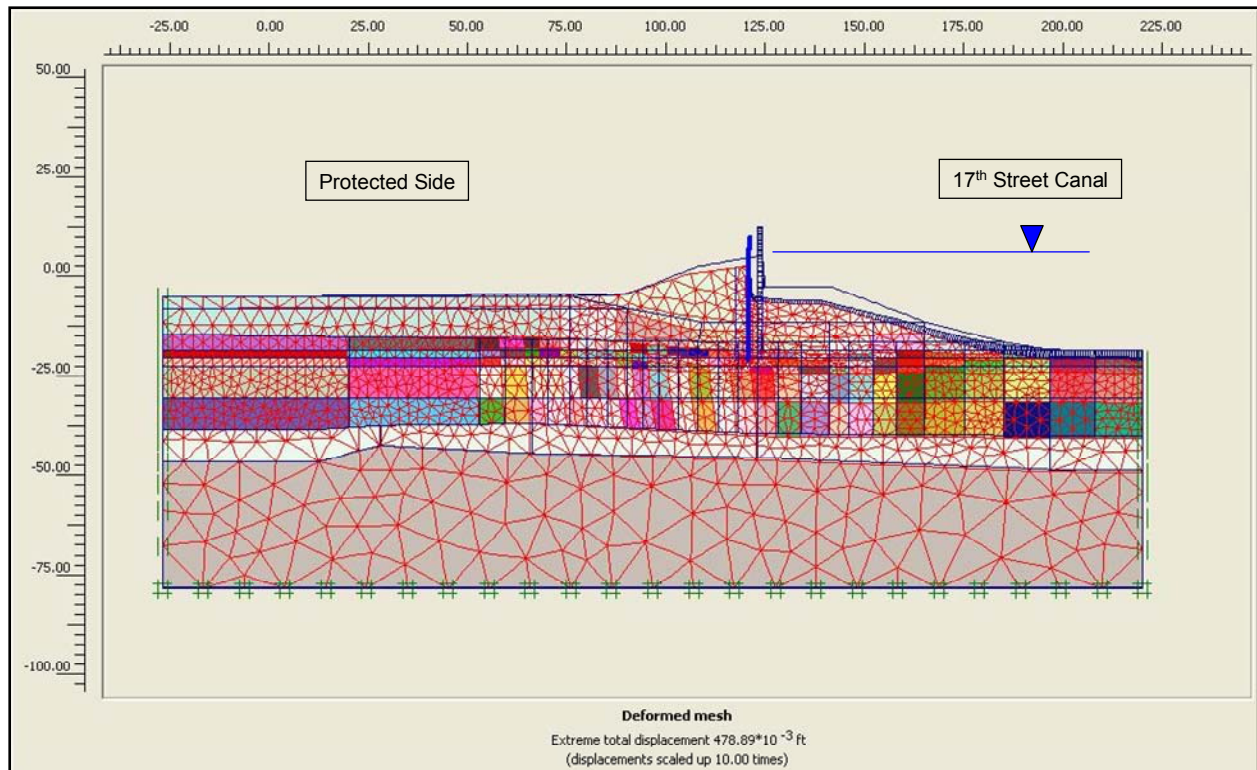


Figure 6-15. Deformed Mesh, Exaggerated by a Factor of 10, for Canal EI 6.5 (Note: Canal EI not to scale in figure)

The mobilized shear stress at the strain integration points within the finite elements contained in the soil clusters is shown in Figure 6-16 to be less than the shear strength of the soil. The resulting computed fraction of mobilized shear strength is less than or equal to 0.96 at the stress integration points for the five soil types. The horizontal total stress state at the top of the submerged levee berm on the canal side and adjacent to the sheet pile indicates that a crack will open at this canal water elevation.

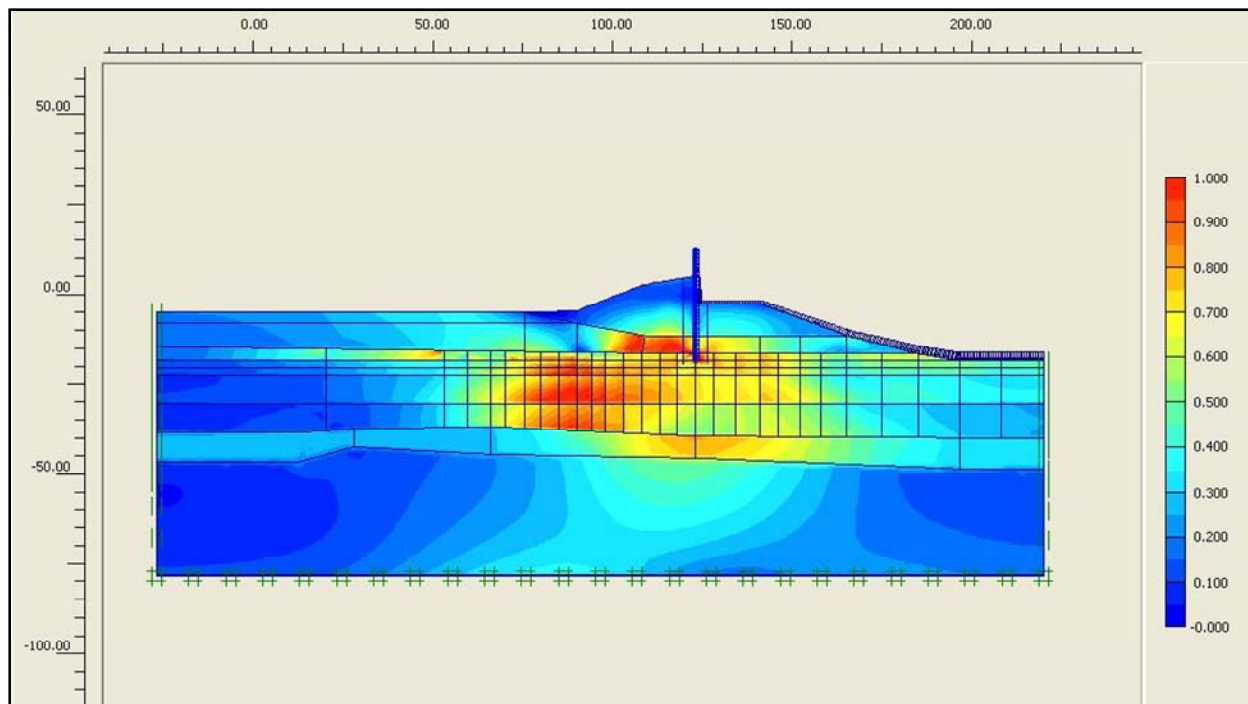


Figure 6-16. Fraction of Mobilized Shear Strength for Canal El 6.5

Crack initiation occurs at the top of the levee clay, on the canal side (at El -2.5) of the sheet pile wall when the total horizontal stress in the clay is less than the value for hydrostatic water pressure (i.e., γ_{water} times depth below canal water surface). This first occurs after raising canal water to El 6.5 (i.e., loading phase 19). Comparisons of values for hydrostatic water pressure, generated by hand computation, with the total horizontal stresses computed in the complete SSI analysis, indicate a crack will extend from El -2.5 down to EL -16.5, the elevation of the peat (or marsh) to lacustrine clay interface. For reference, the levee clay to peat (or marsh) interface is at EL -11.5. A 14-ft-long crack is introduced along the canal side interface of the sheet pile wall in the next loading phase.

Canal El 6.5: In the seventh increment in loading, designated loading phase 20, a crack is introduced at the top of the levee soil (El -2.5) on the canal-side face of the sheet pile. This crack extends from the top of the canal side submerged levee to El -16.5. For reference, the sheet pile tip is at El -18.5. The development of the crack in loading phase 20 is accomplished by means of staged excavation of a narrow (i.e., 1-ft-wide) column of vertical clusters of levee and peat soils along this canal side face of the sheet pile wall to El -16.5. Additionally, loading phase 20 differs from loading phase 19 in that hydrostatic water pressures, corresponding to canal water at El 6.5, are applied to the now exposed canal-side sheet pile face, as well as the now exposed levee clay face that form the sides of the crack in these 1-ft-wide (excavated) vertical soil clusters. The deformed mesh is shown in Figure 6-17. Note that the nodal deformations are increased by a factor of 10 in order to show the deformed mesh relative to its position at a canal water elevation of 1.0 (shown as a blue outline in this figure). The general trend of deformations is downward and towards the protected side due to the boundary water pressure loading applied within the

canal and the crack. The maximum (relative) displacement within the mesh is 0.88 ft (approximately 10.5 in.).

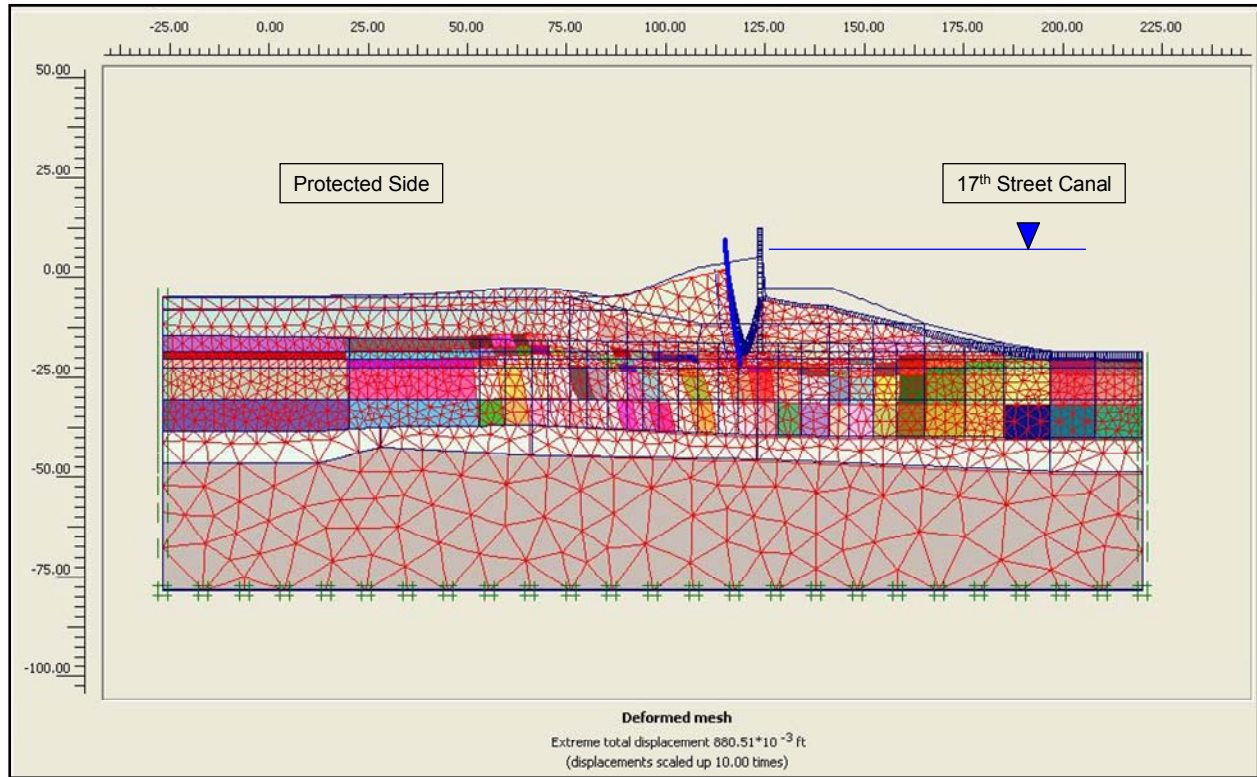


Figure 6-17. Deformed Mesh, Exaggerated by a Factor of 10, for Canal El 6.5 and Crack to El -16.5 (Note: Canal El not to scale in figure)

The mobilized shear stress at the strain integration points within the finite elements contained in the soil clusters is shown in Figure 6-18 to be less than the shear strength of the soil. The resulting computed fraction of mobilized shear strength is less than or equal to 0.96 at the stress integration points for the five soil types. Introduction of the crack to El -16.5, as well as application of hydrostatic water pressures within the crack, results in more of the lacustrine clay being loaded, as indicated by comparison of Figure 6-18 fraction of mobilized shear strength results to the Figure 6-16 pre-crack results.

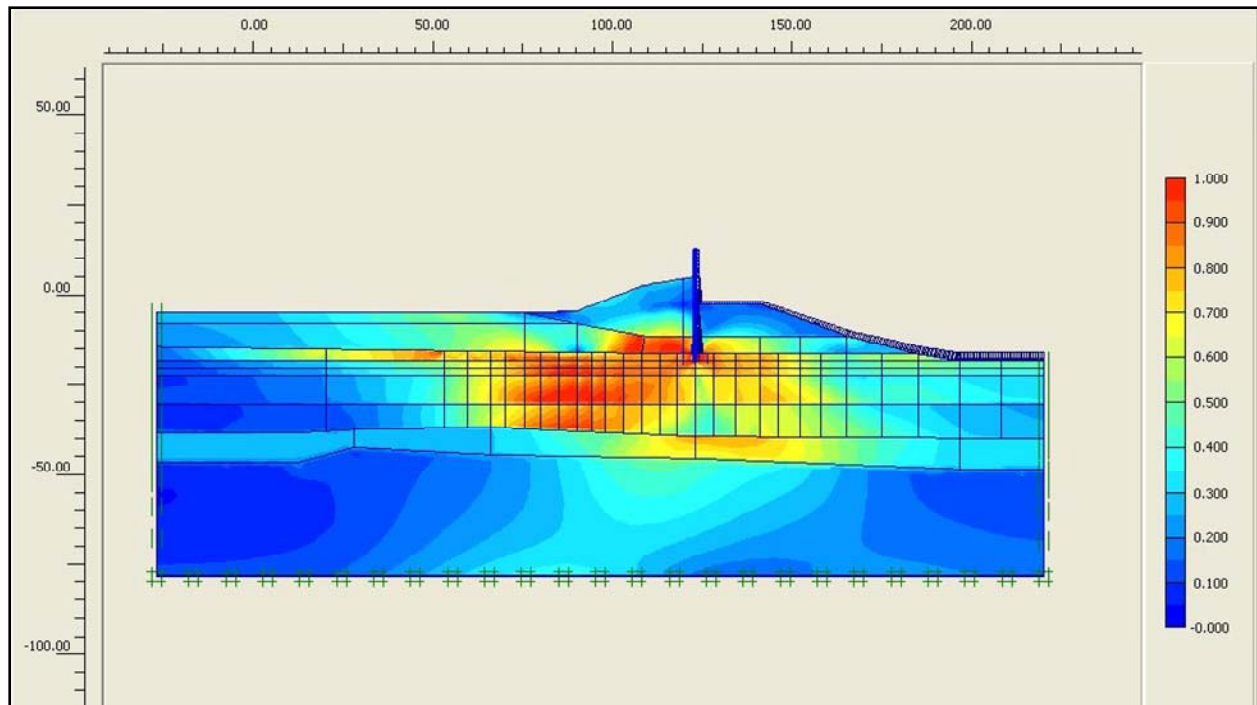


Figure 6-18. Fraction of Mobilized Shear Strength for Canal El 6.5 and Crack to El -16.5

There is no indication of a fully developed failure mechanism at this flood stage for a crack to El -16.5. However, Figure 6-19 shows four distinct reaches of high shear strains (that may, with additional applied loadings, develop into a complete failure mechanism). Evaluation of the computed horizontal total stress state immediately below the El -16.5 crack tip region on the canal side of the sheet pile indicates that this crack will extend to the sheet pile tip, El -18.5. Consequently, in the next loading phase (21), the crack is extended by means of staged excavation of a narrow cluster of lacustrine clay from El -16.5 to El -18.5 and with hydrostatic water pressures applied along the exposed sheet pile and clay faces that form the sides of the crack.

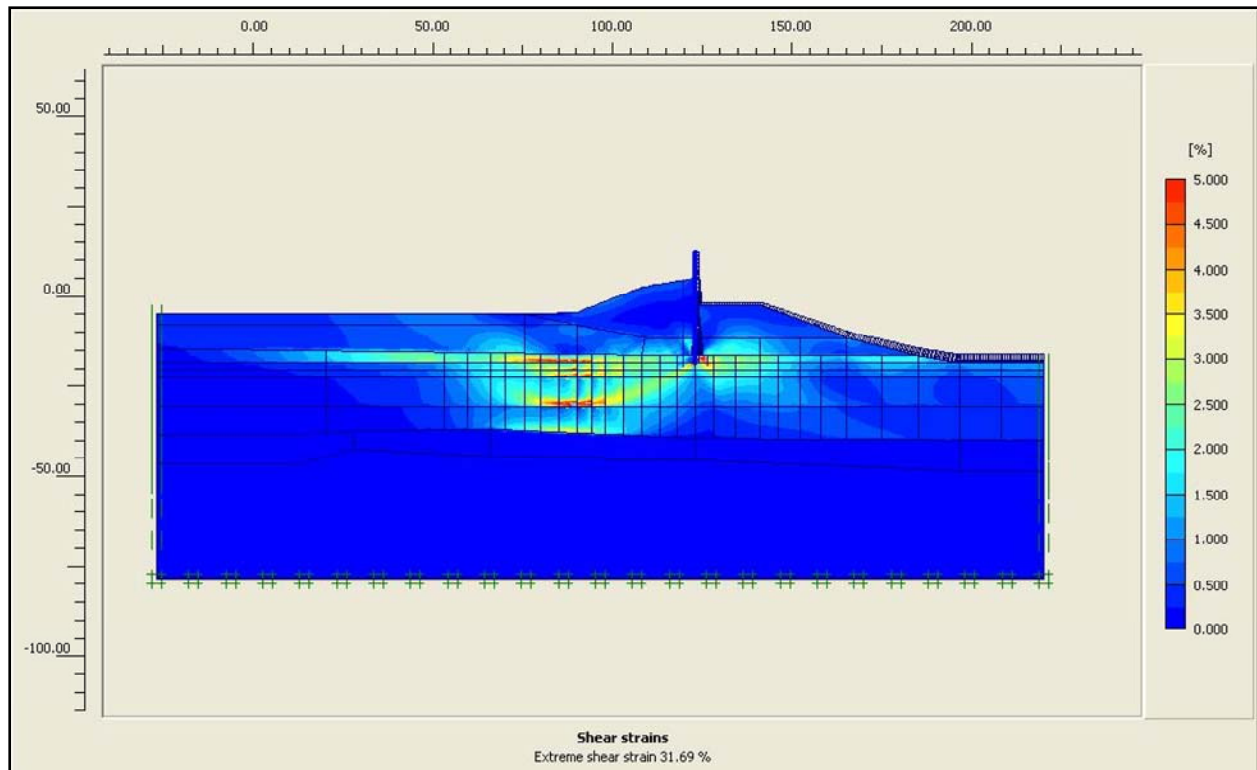


Figure 6-19. Reaches of Large Shear Strains for Canal El 6.5 and Crack to El -16.5

Canal El 6.5: In the eighth increment in loading, designated loading phase 21, the crack is extended to the sheet pile tip (El -18.5) on the canal-side face of the sheet pile. The development of the crack in loading phase 20 is accomplished by means of 2 ft of additional staged excavation of a narrow (i.e., 1-ft wide) column of vertical clusters of lacustrine clay soil along this canal-side face of the sheet pile wall. Additionally, loading phase 21 differs from loading phase 20 in that hydrostatic water pressures, corresponding to canal water at El 6.5, are applied along this additional 2 ft of newly exposed canal-side face of sheet pile, as well as the now exposed 2-ft-high lacustrine clay face that form the sides of this last segment of crack. The deformed mesh is shown in Figure 6-20. Note that the nodal deformations are increased by a factor of 10 in order to show the deformed mesh relative to its position at a canal water elevation of 1.0 (shown as a blue outline in this figure). The general trend of deformations is downward and towards the protected side due to the boundary water pressure loading applied within the canal and the 14-ft-deep crack. The maximum (relative) displacement within the mesh is 0.888 ft (approximately 10-5/8 in.).

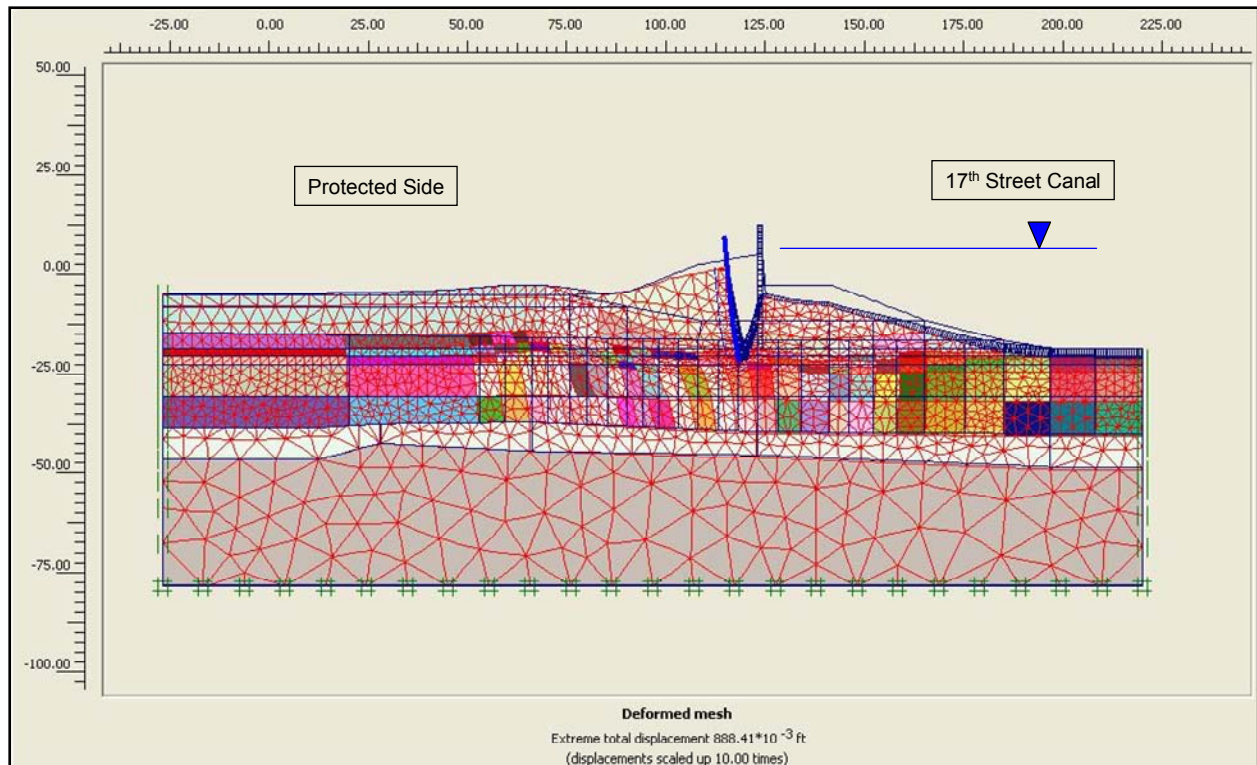


Figure 6-20. Deformed Mesh, Exaggerated by a Factor of 10, for Canal EI 6.5 and Crack to EI -18.5 (Note: Canal EI not to scale in figure)

The mobilized shear stress at the strain integration points within the finite elements contained in the soil clusters is shown in Figure 6-18 to be less than the shear strength of the soil. The resulting computed fraction of mobilized shear strength is less than or equal to 0.96 at the stress integration points for the five soil types.

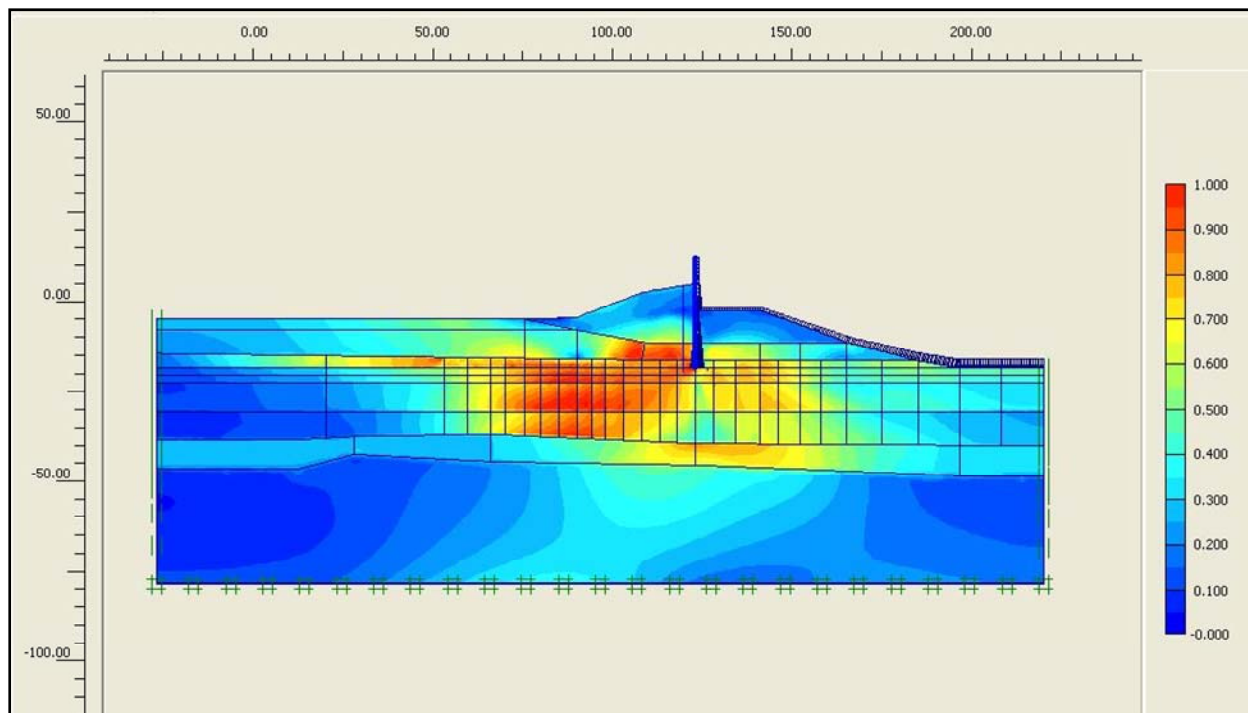


Figure 6-21. Fraction of Mobilized Shear Strength for Canal El 6.5 and Crack to El -18.5

There is no indication of a fully developed failure mechanism at this flood stage for a crack to El -16.5. However, Figure 6-19 shows that at this stage of flood loading, there are four distinct reaches of high shear strains (that may, with additional applied loadings, develop into a complete failure mechanism).

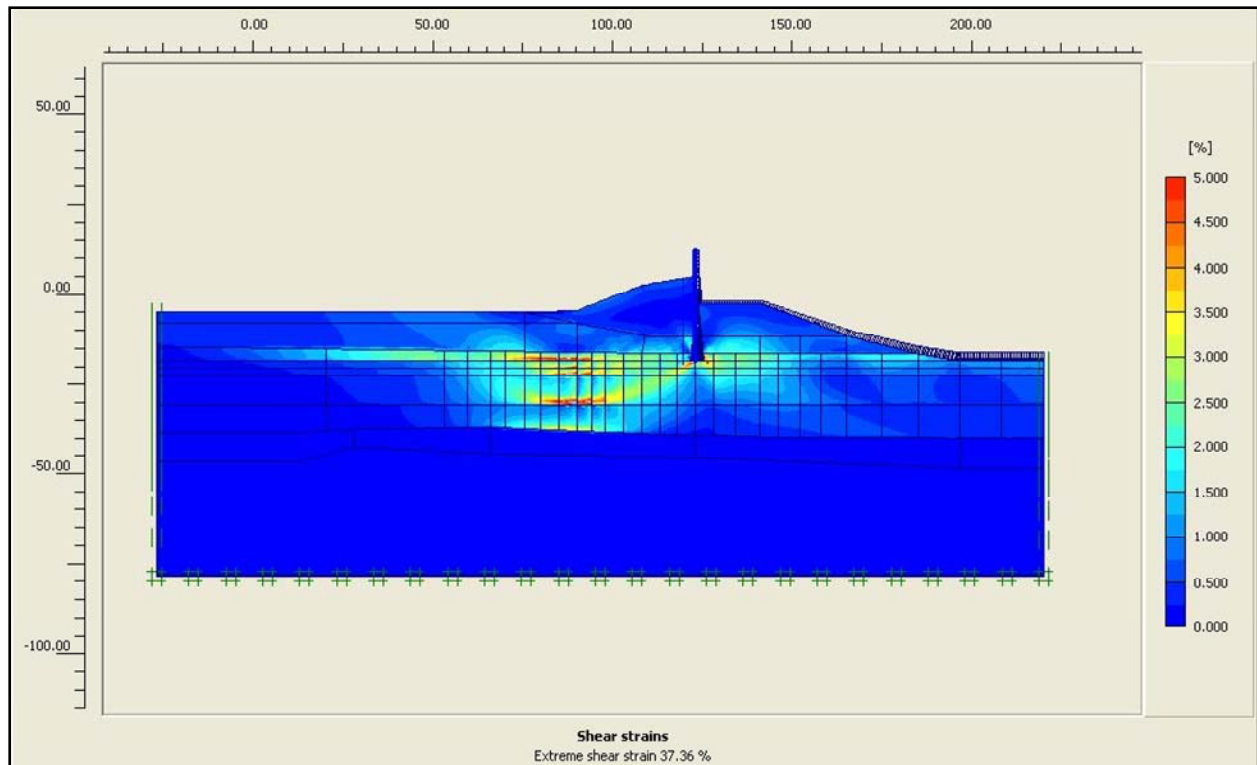


Figure 6-22. Reaches of Large Shear Strains for Canal El 6.5 and Crack to El -18.5

Figure 6-23 shows the horizontal displacements of the soil regions within the mesh, relative to their position at a canal water elevation of 1.0. This figure shows the deformation of the protected side levee, the peat below the levee, and the top layer of the lacustrine clay, all to be moving away from the canal with a displacement of between -0.6 to -0.8 ft under an El 6.5 flood loading and including a full crack. (Note negative Ux values denote movement towards the protected side.)

Figure 6-24 shows the horizontal displacements of three points within the flood wall, relative to its position at a canal water elevation of 1.0. The points monitored through the analyses are at the top of the I-wall, at El 5 (top of levee), and at sheet pile tip (El -18.5). This figure shows that prior to the crack opening at canal water El 6.5, the deformation of the sheet pile is uniformly translational. At canal water El 6.5 and prior to cracking, the flood wall translates towards the protected side by 0.21 ft (2.5 in.). After the crack opens to sheet pile tip and with the flood loading maintained at El -6.5, the horizontal deformation at the top of the I-wall and at the base of the I-wall (El 5) is identical, implying uniform translation of the I-wall by 0.79 ft (9.5 in.). However, the tip of the sheet pile undergoes less than half as much horizontal deformation as the I-wall, 0.44 ft (5-¼ in.).

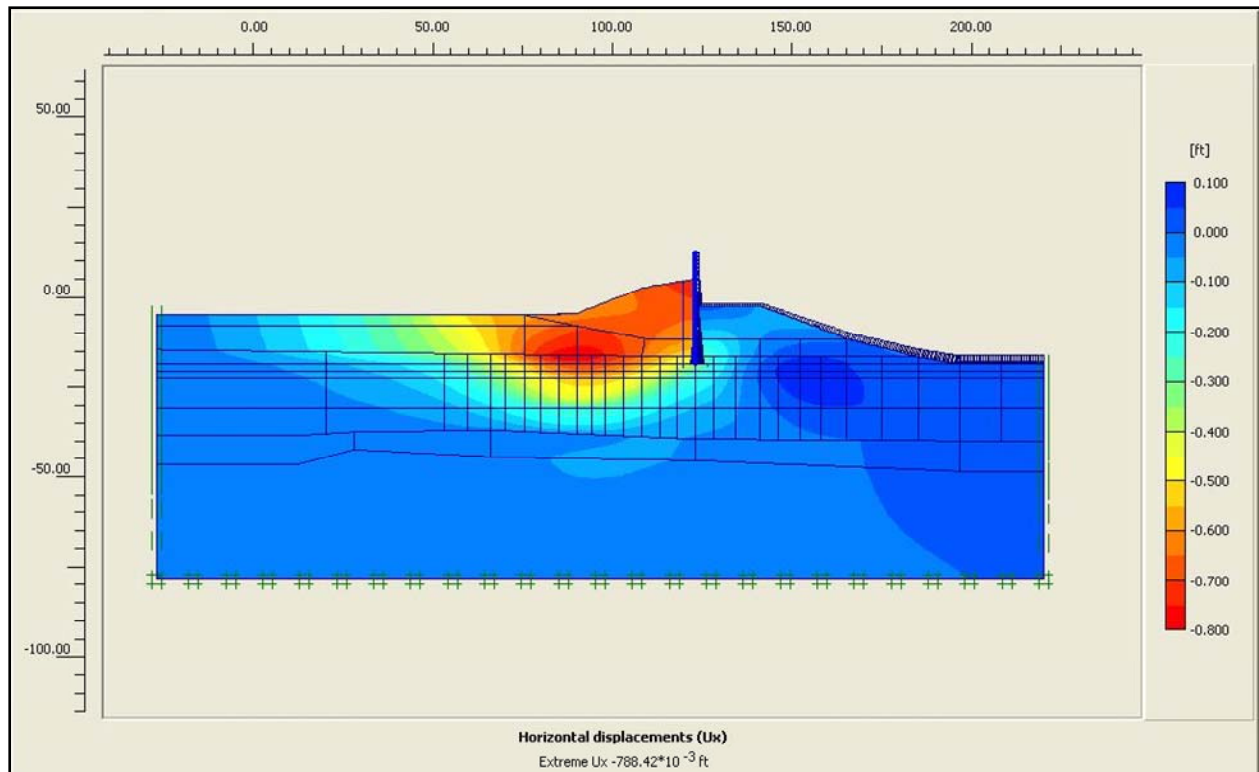


Figure 6-23. Horizontal Deformation Shadings for Canal EI 6.5 and Crack to EI -18.5

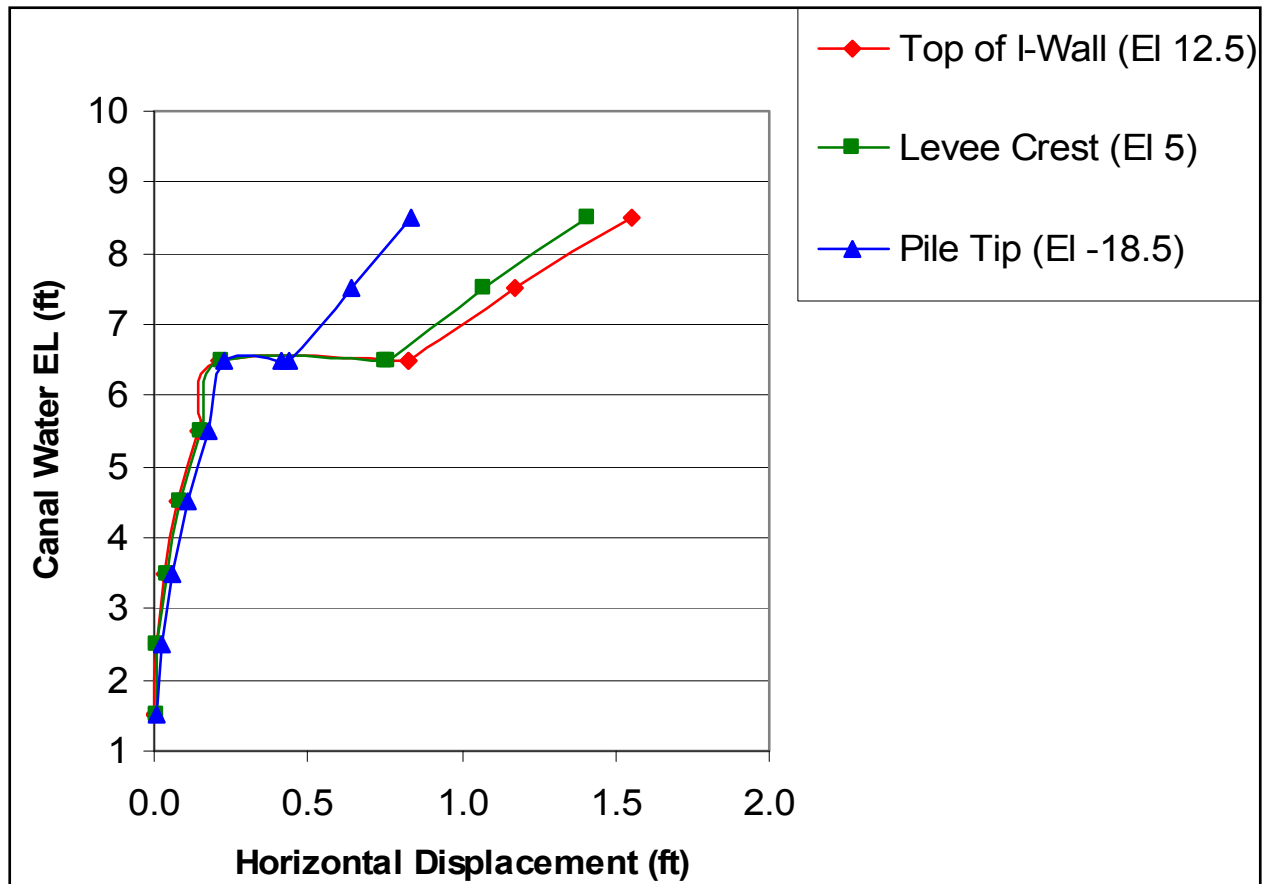


Figure 6-24. Horizontal Sheet Pile Deflections versus Canal Water EI

Figure 6-25 shows the vertical displacements of the soil regions within the mesh for canal El 6.5 and with full crack, relative to its position at a canal water elevation of 1.0. This figure shows the deformation tendency of the peat to rise up (i.e., positive displacements) just beyond the toe of the levee on the protected side, and the levee berm to move downwards (i.e., negative displacements).

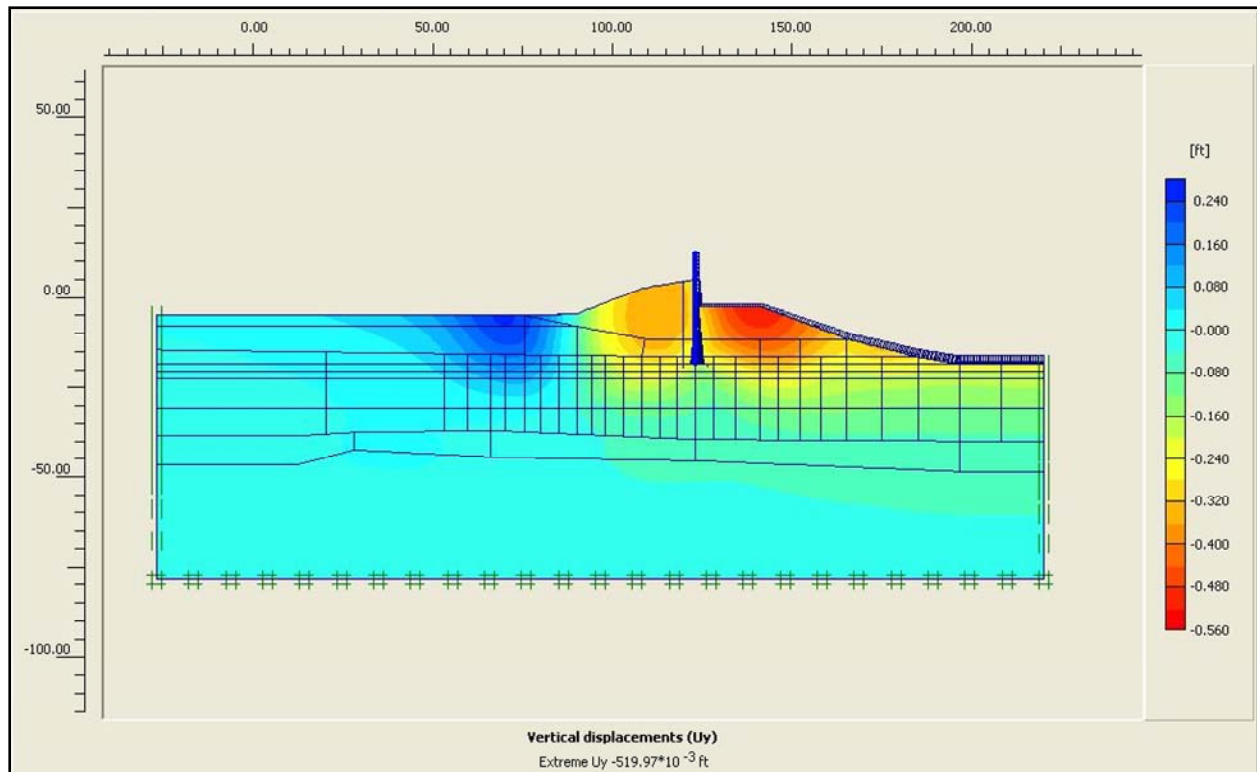


Figure 6-25. Vertical Deformation Shadings for Canal El 6.5 and Crack to El -18.5

Crack propagation concludes with a 16-ft-deep crack extending from the top of the submerged levee berm at El -2.5 to the sheet pile tip. This crack is maintained with subsequent rises in canal water, with water pressures within the crack increased accordingly.

Canal El 7.5: The ninth increment in loading, designated loading phase 22, raises the canal water to El 7.5. This is a 6.5-ft increase in canal water relative to canal steady state El 1 or, equivalently, a 1-ft increase in canal flood water elevation from canal El 6.5 of loading phases 19, 20, and 21. The loading applied to the mesh is again solely due to hydrostatic canal water pressures applied as boundary water pressures normal to the wetted side of the I-wall, normal to the wetted exposed face of the levee and clays forming the sides and base of the canal, and normal to the sheet pile and soil that form the crack. The deformed mesh is shown in Figure 6-26. Note that the nodal deformations are increased by a factor of 8 in order to show the deformed mesh relative to its position at a canal water elevation of 1.0 (shown as a blue outline in this figure). The general trend of deformations is downward and towards the protected side due to the boundary water pressure loading applied within the canal. The maximum (relative) displacement within the mesh is 1.22 ft (approximately 14-5/8 in.). There is no indication of a fully developed failure mechanism occurring at this flood stage.

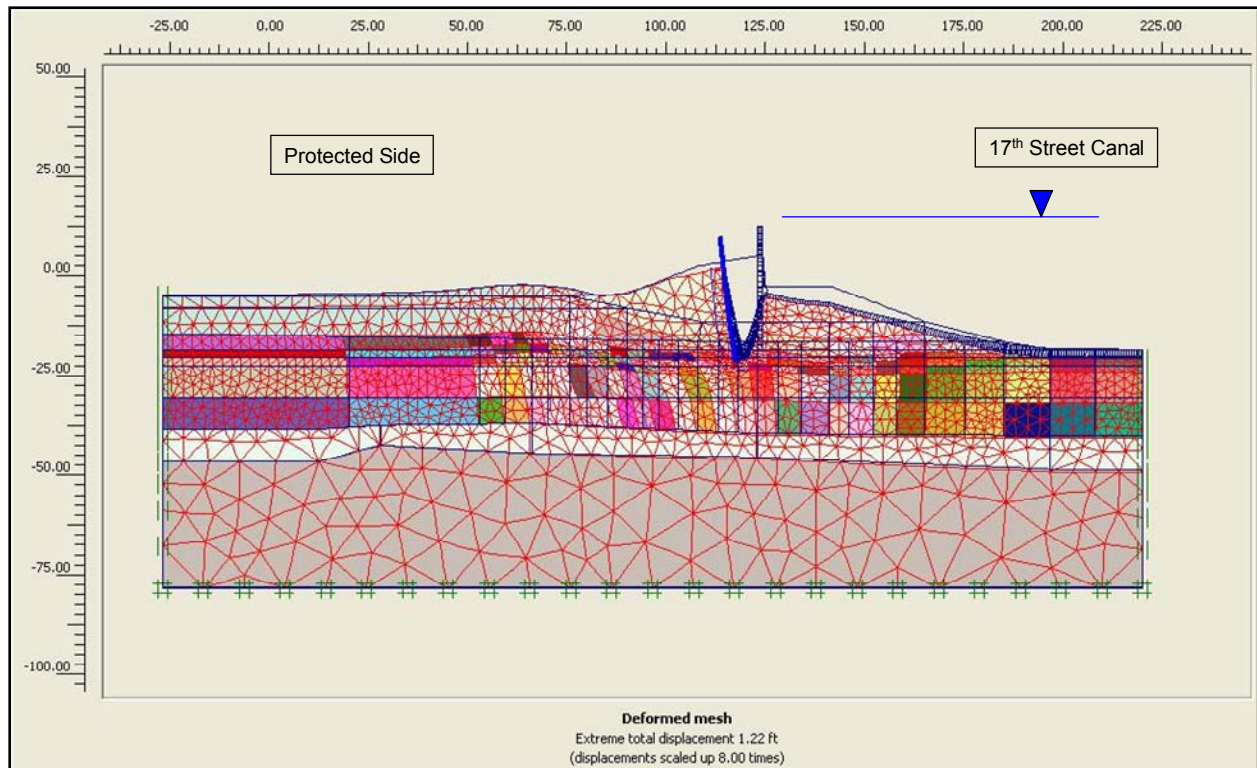


Figure 6-26. Deformed Mesh, Exaggerated by a Factor of 8, for Canal El 7.5 and Crack to El -18.5
 (Note: Canal El not to scale in figure)

The mobilized shear stress at the strain integration points within the finite elements contained in the soil clusters is shown in Figure 6-27 to be less than the shear strength of the soil. The resulting computed fraction of mobilized shear strength is less than or equal to 0.96 at the stress integration points for the five soil types.

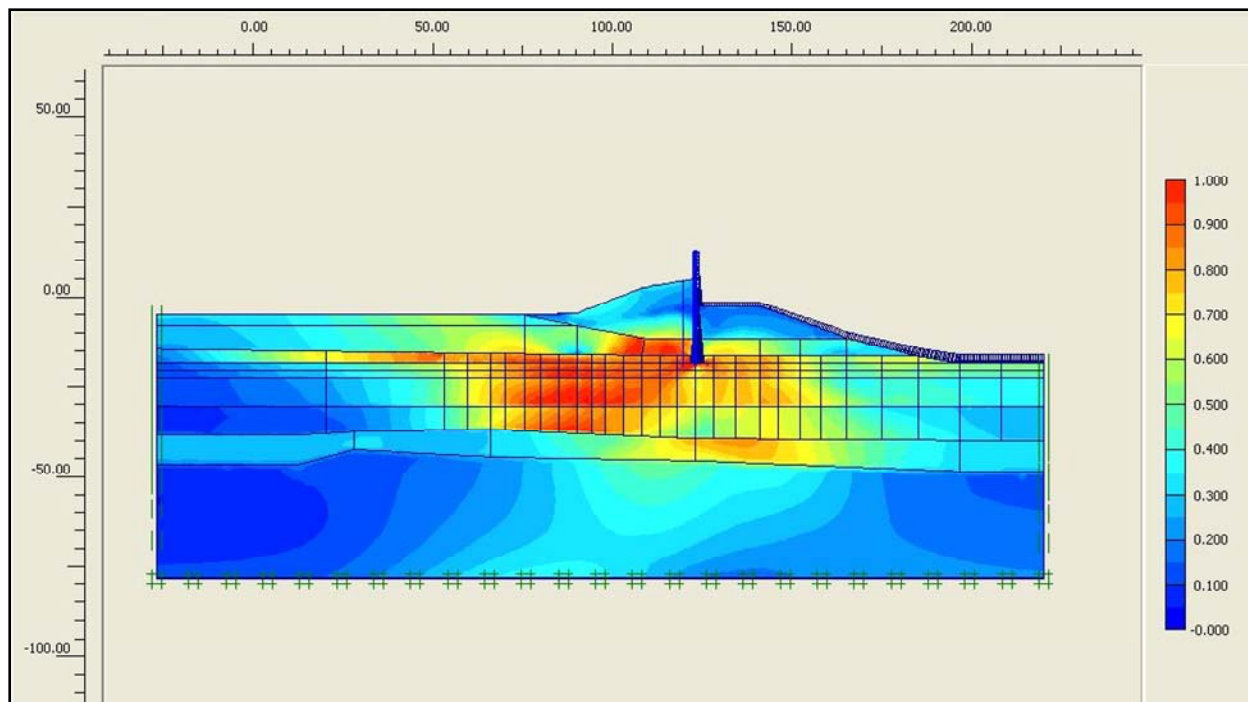


Figure 6-27. Fraction of Mobilized Shear Strength for Canal El 7.5 and Crack to El -18.5

There is no indication of a fully developed failure mechanism at this flood stage for a crack to El -16.5. However, Figure 6-28 shows that at this stage of flood loading, there are four distinct reaches of high shear strains (that may, with additional applied loadings, develop into a complete failure mechanism).

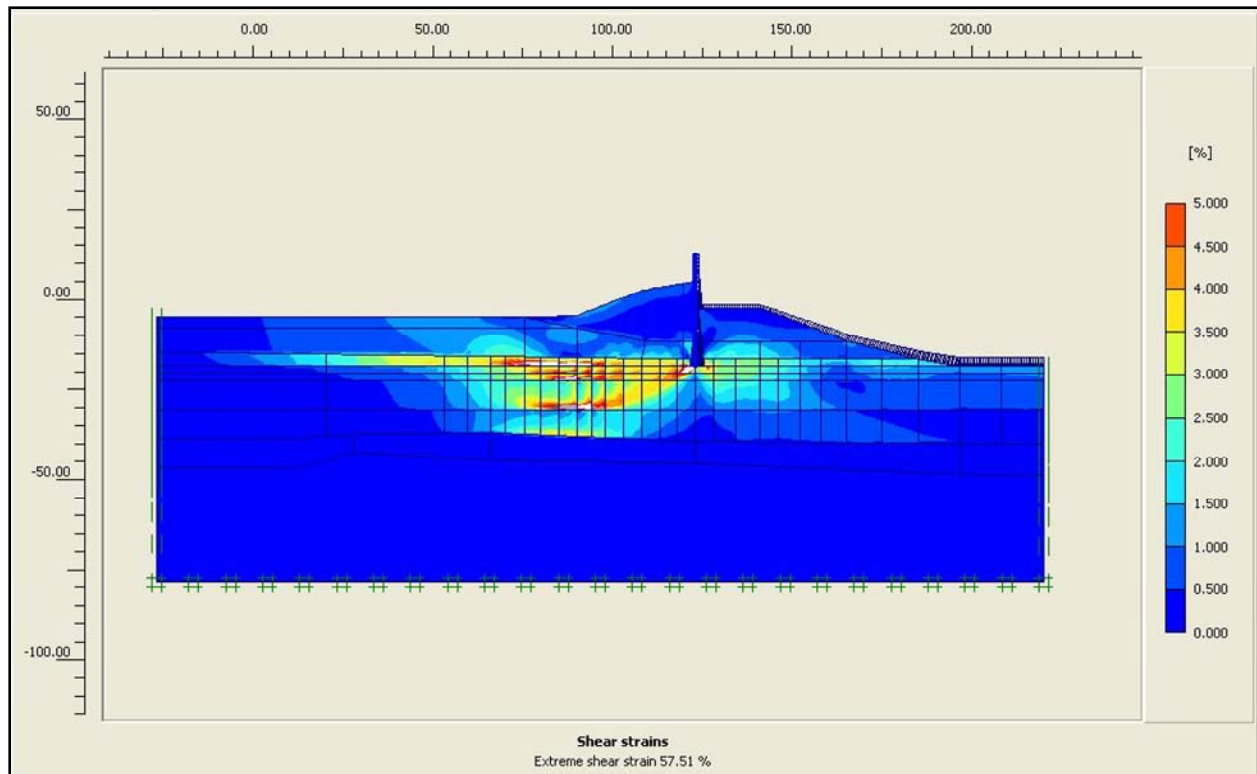


Figure 6-28. Reaches of Large Shear Strains for Canal El 7.5 and Crack to El -18.5

Figure 6-29 shows the horizontal displacements of the soil regions within the mesh, relative to their position at a canal water elevation of 1.0. This figure shows the deformation of the protected side levee, the peat below the levee, and the top layer of the lacustrine clay, all to be moving away from the canal with a displacement of between -0.7 to -1.1 ft under an El 7.5 flood loading and including a full crack.

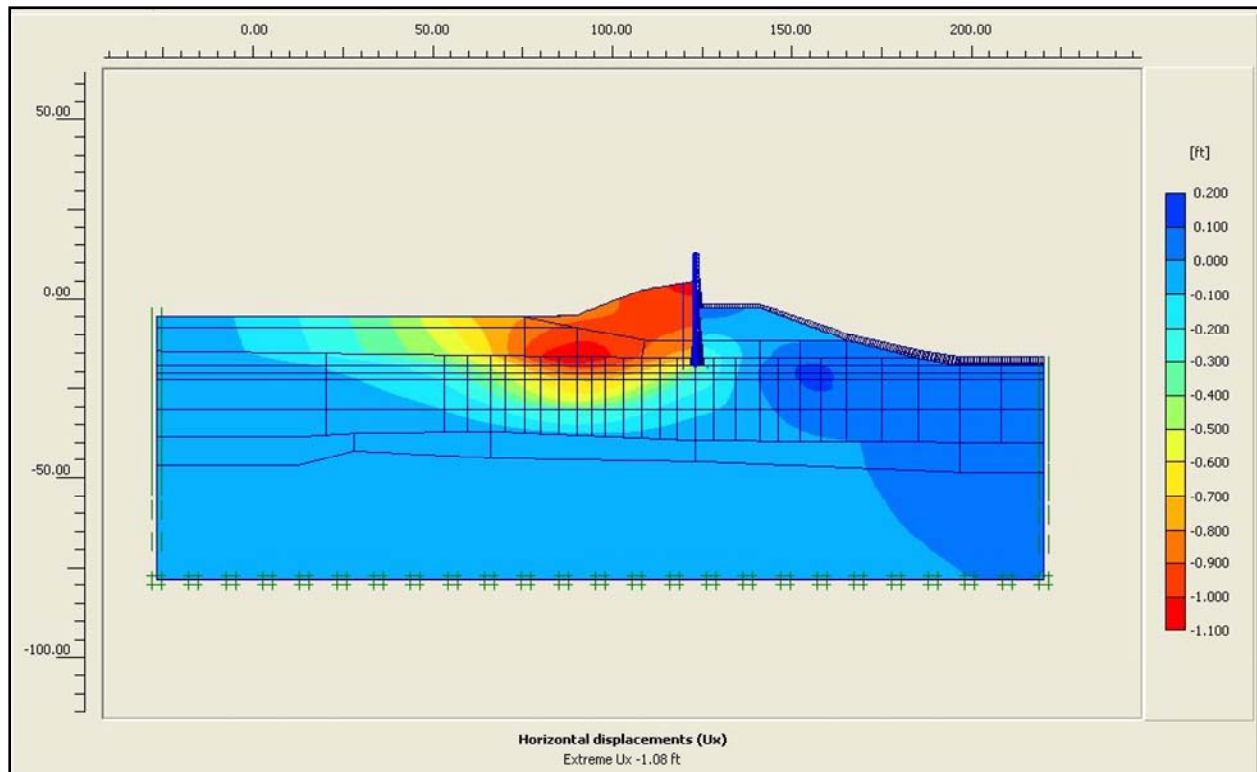


Figure 6-29. Horizontal Deformation Shadings for Canal EI 7.5 and Crack to EI -18.5

Figure 6-24 shows the horizontal displacements of three points within the floodwall, relative to its position at a canal water elevation of 1.0. The points monitored through the analyses are at the top of the I-wall, at EI 5 (top of levee) and at sheet pile tip (EI -18.5). With an open crack to sheet pile tip and with the flood loading maintained at EI -7.5, the horizontal deformations at the top of the I-wall and at the base of the I-wall (EI 5) are nearly identical, 1.17 ft and 1.07 ft. This implies uniform translation of the I-wall. However, the tip of the sheet pile undergoes less than half as much horizontal deformation as the I-wall, 0.64 ft.

Figure 6-30 shows the vertical displacements of the soil regions within the mesh for canal EI 7.5 and with full crack, relative to its position at a canal water elevation of 1.0. This figure shows the deformation tendency of the peat to rise up (i.e., positive displacements) just beyond the toe of the levee on the protected side and the levee berm to move downwards (i.e., negative displacements).

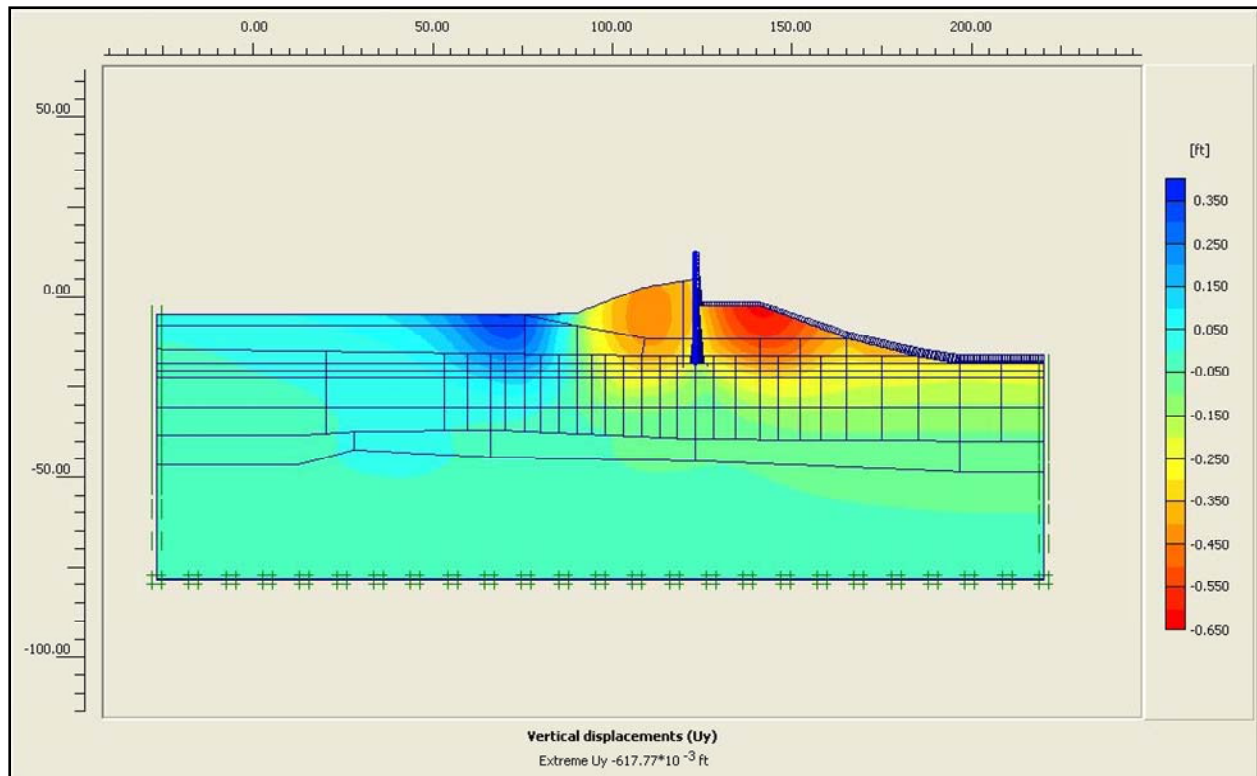


Figure 6-30. Vertical Deformation Shadings for Canal El 7.5 and Crack to El -18.5

Canal El 8.5: The tenth increment in loading, designated loading phase 23, raises the canal water to El 8.5. This is a 7.5-ft increase in canal water relative to canal steady state El 1 or, equivalently, a 1-ft increase in canal flood water elevation from canal El 7.5 of loading phase 22. The loading applied to the mesh is again solely due to hydrostatic canal water pressures applied as boundary water pressures normal to the wetted side of the I-wall, normal to the wetted exposed face of the levee and clays forming the sides and base of the canal, and normal to the sheet pile and soil that form the crack. The deformed mesh is shown in Figure 6-31. Note that the nodal deformations are increased by a factor of 7 in order to show the deformed mesh relative to its position at a canal water elevation of 1.0 (shown as a blue outline in this figure). The general trend of deformations is downward and towards the protected side due to the boundary water pressure loading applied within the canal. The maximum (relative) displacement within the mesh is 1.6 ft (19.5 in.). There is no indication of a fully developed failure mechanism occurring at this flood stage.

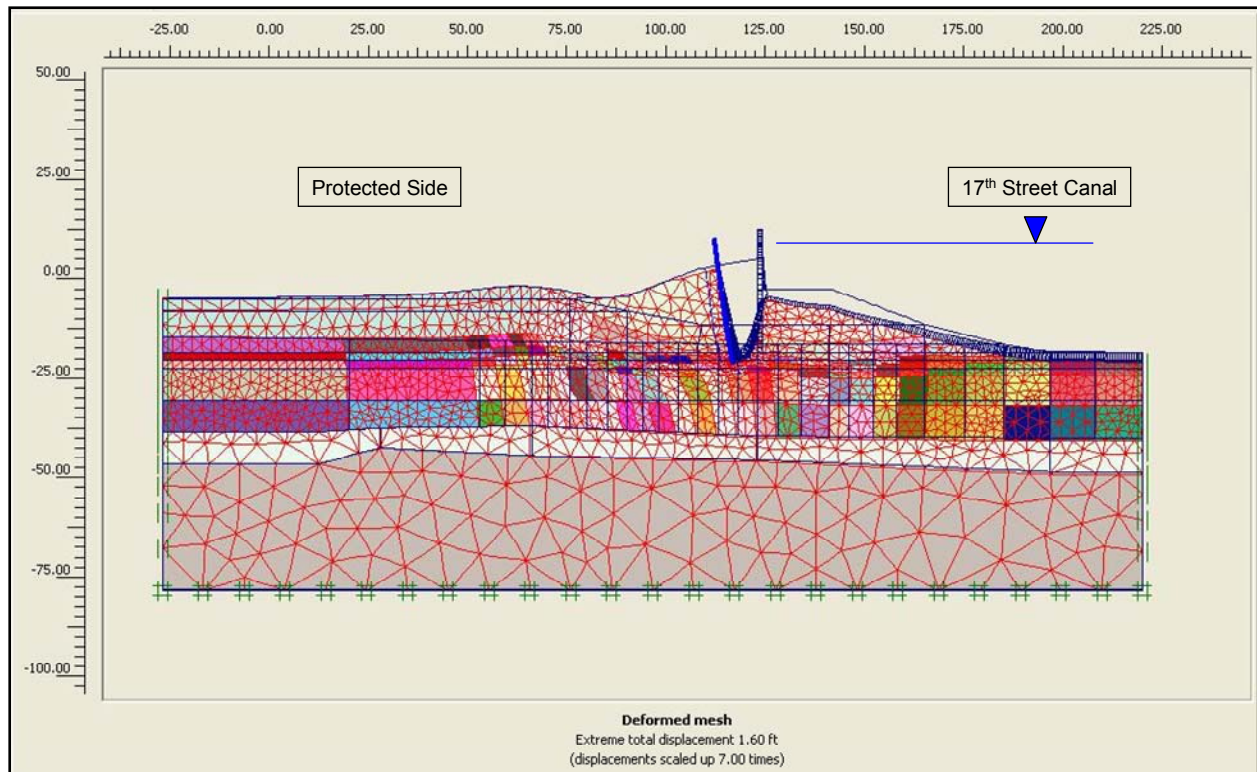


Figure 6-31. Deformed Mesh, Exaggerated by a Factor of 7, for Canal El 8.5 and Crack to El -18.5 (Note: Canal El not to scale in figure)

The mobilized shear stress at the strain integration points within the finite elements contained in the soil clusters is shown in Figure 6-32 to be less than the shear strength of the soil. The resulting computed fraction of mobilized shear strength is less than or equal to 0.96 at the stress integration points for the five soil types. Raising of canal water El 8.5 (as well as application of hydrostatic water pressures within the crack) results in more of the upper portion of the lacustrine clay layer being loaded, as indicated by comparison of Figure 6-32 fraction of mobilized shear strength results to the Figure 6-27 El 7.5 results.

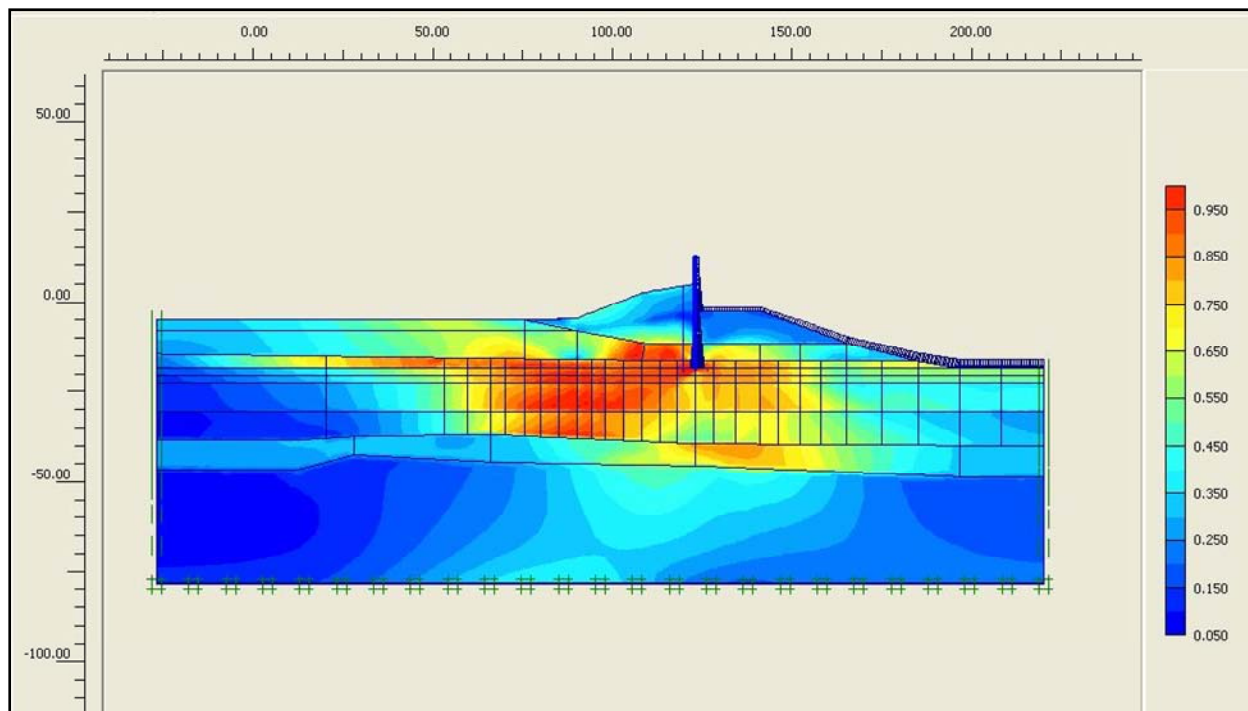


Figure 6-32. Fraction of Mobilized Shear Strength for Canal EI 8.5 and Crack to EI -18.5

Figure 6-33 shows at this stage of flood loading the upper zone of high shear strains (beyond the toe of the levee), indicating a failure mechanism is developing.

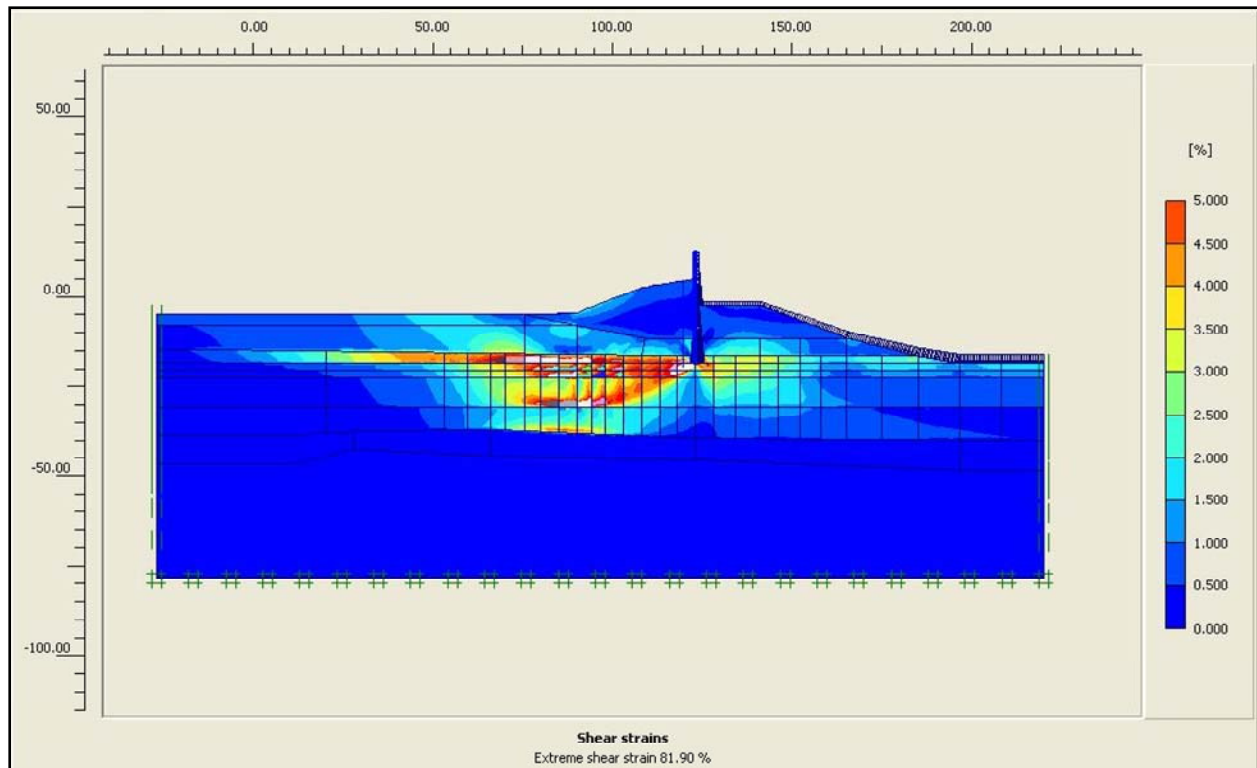


Figure 6-33. Reaches of Large Shear Strains for Canal El 8.5 and Crack to El -18.5

Figure 6-34 shows the horizontal displacements of the soil regions within the mesh, relative to their position at a canal water elevation of 1.0. This figure shows the deformation of the protected side levee, the peat below the levee, and the top layer of the lacustrine clay, all to be moving away from the canal, with a displacement of between -1.0 to -1.4 ft under an El 8.5 flood loading and including a full crack.

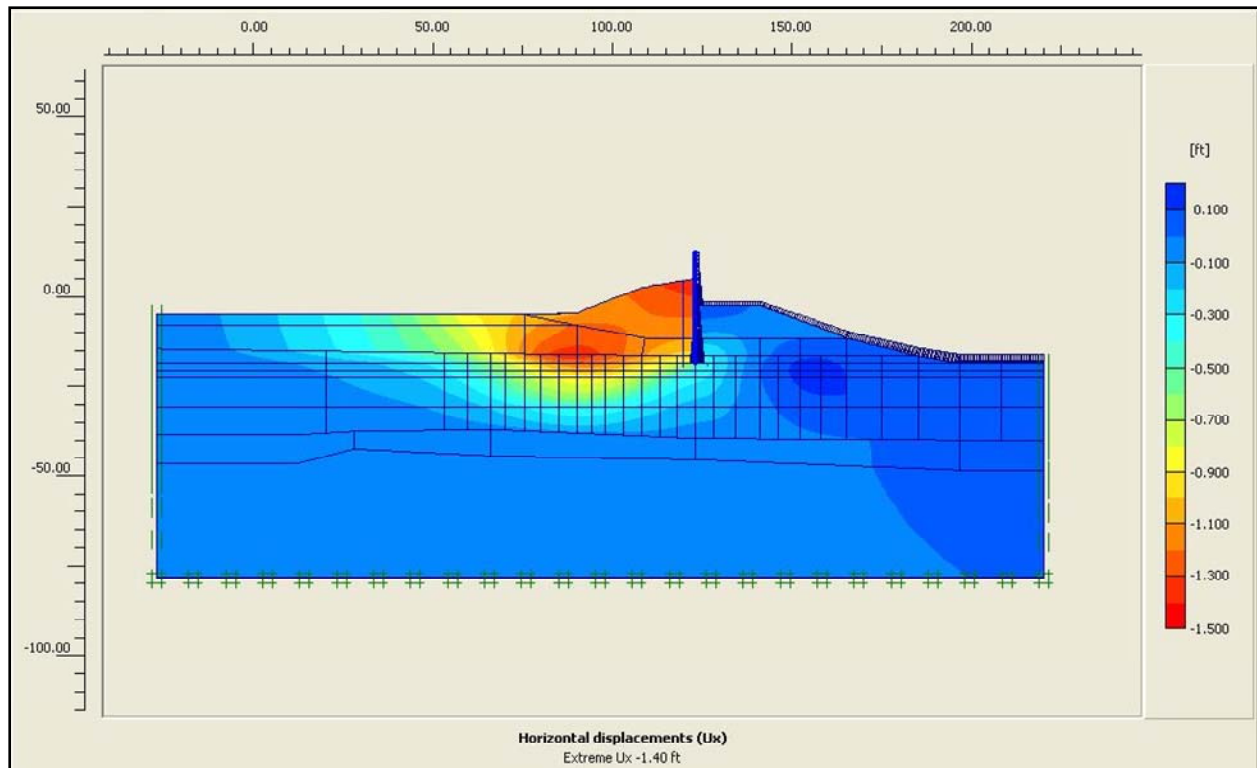


Figure 6-34. Horizontal Deformation Shadings for Canal El 8.5 and Crack to El -18.5

Figure 6-24 shows the horizontal displacements of three points within the floodwall, relative to its position at a canal water elevation of 1.0. The points monitored through the analyses are at the top of the I-wall, at El 5 (top of levee), and at sheet pile tip (El -18.5). With an open crack to sheet pile tip and with the flood loading maintained at El -8.5, the horizontal deformations at the top of the I-wall and at the base of the I-wall (El 5) are nearly identical, 1.55 ft and 1.41 ft. This implies uniform translation of the I-wall. However, the tip of the sheet pile undergoes less than half as much horizontal deformation as the I-wall, 0.84 ft.

Figure 6-35 shows the vertical displacements of the soil regions within the mesh for canal El 8.5 and with full crack, relative to its position at a canal water elevation of 1.0. This figure shows the deformation tendency of the peat to rise up (i.e., positive displacements) just beyond the toe of the levee on the protected side, and the levee berm to move downwards (i.e., negative displacements).

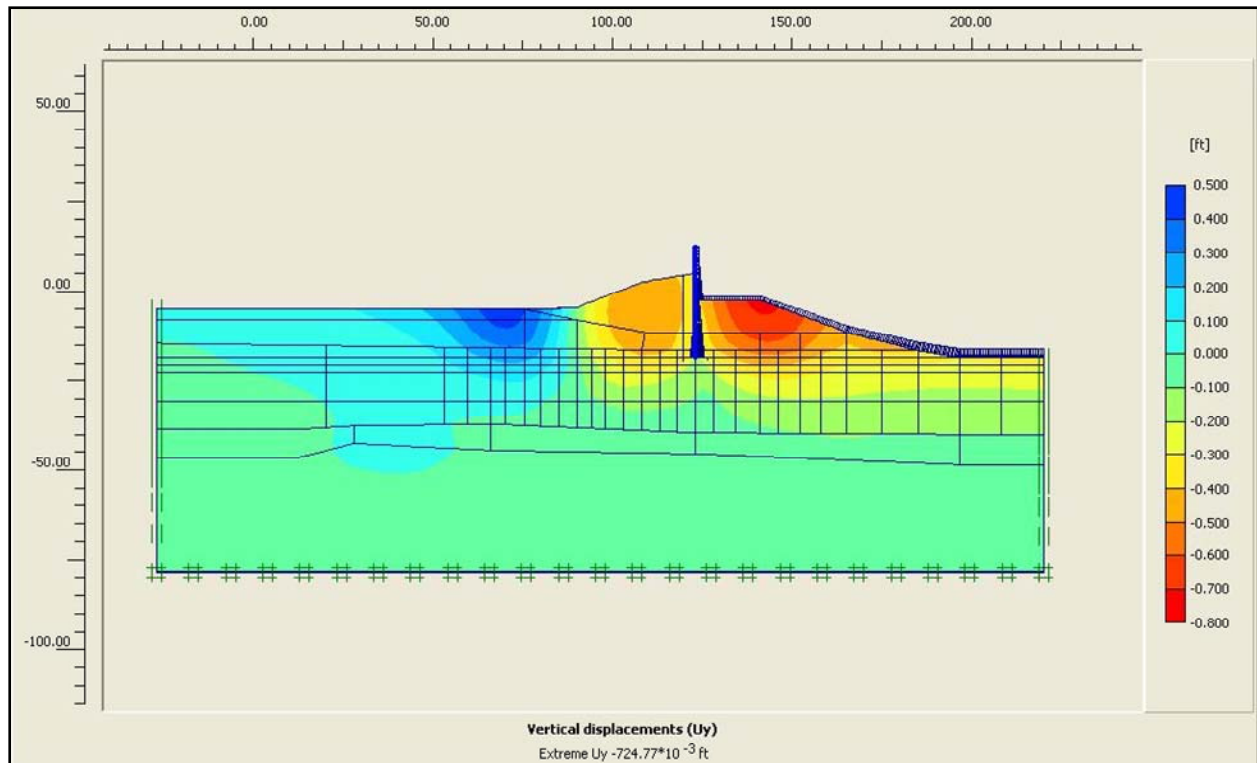


Figure 6-35. Vertical Deformation Shadings for Canal EI 8.5 and Crack to EI -18.5

Canal EI 9: The eleventh increment in loading, designated loading phase 24, raises the canal water to EI 9. This is an 8.5-ft increase in canal water relative to canal steady state EI 1 or, equivalently, a 1-ft increase in canal flood water elevation from canal EI 8.5 of loading phase 23. The loading applied to the mesh is again solely due to hydrostatic canal water pressures applied as boundary water pressures normal to the wetted side of the I-wall, normal to the wetted exposed face of the levee and clays forming the sides and base of the canal, and normal to the sheet pile and soil that form the crack. The deformed mesh is shown in Figure 6-36. Note that the nodal deformations are increased by a factor of 2 in order to show the deformed mesh relative to its position at a canal water elevation of 1.0 (shown as a blue outline in this figure). The general trend of deformations is downward and towards the protected side due to the boundary water pressure loading applied within the canal. The computed maximum (relative) displacement within the mesh is excessive, more than 5 ft. Note the upward bulge in the surface of the peat/marsh layer beyond the toe of the levee.

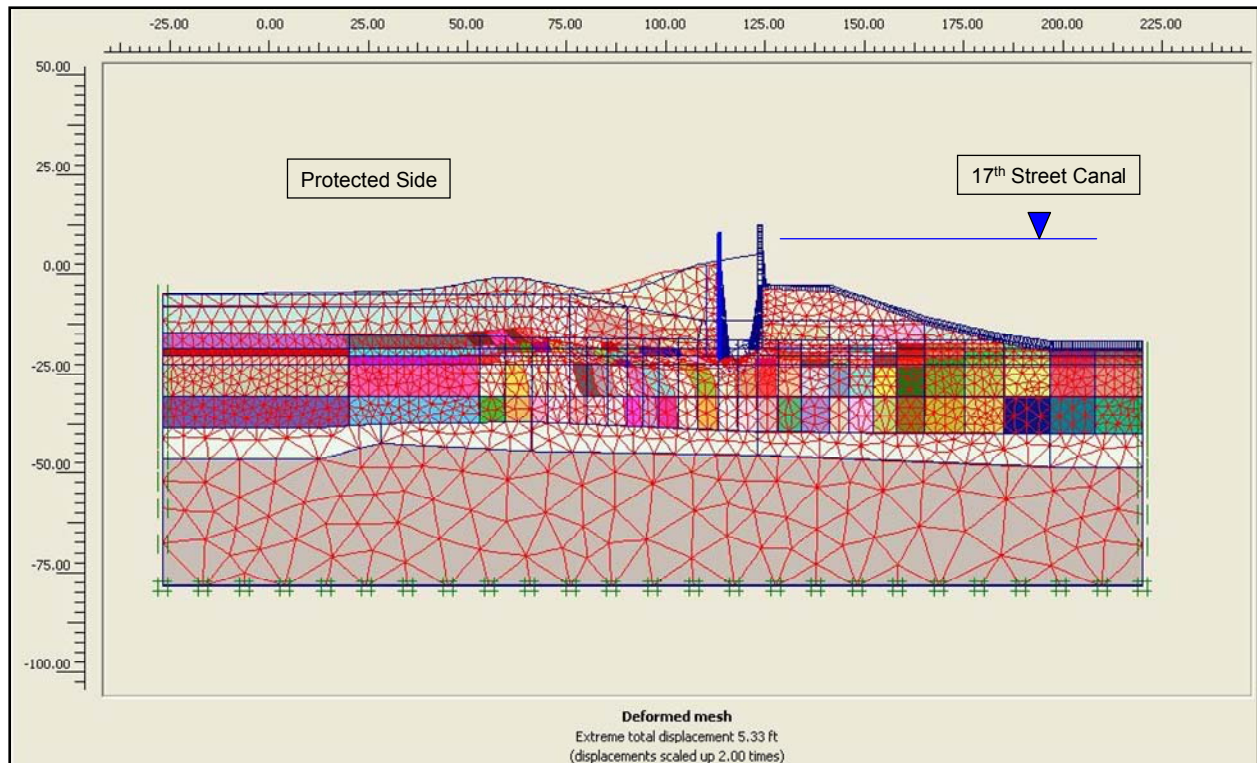


Figure 6-36. Deformed Mesh, Exaggerated by a Factor of 2, for Canal EI 9 and Crack to EI -18.5 (Note: Canal EI not to scale in figure)

The mobilized shear stress at the strain integration points within the finite elements contained in the soil clusters is shown in Figure 6-37. Note that the zone of high values for the computed fraction of mobilized shear strength now extends to the peat/marsh region beyond the toe of the levee. These and the Figure 6-36 results indicate the formation of a failure mechanism that “daylights” beyond the toe of the levee.

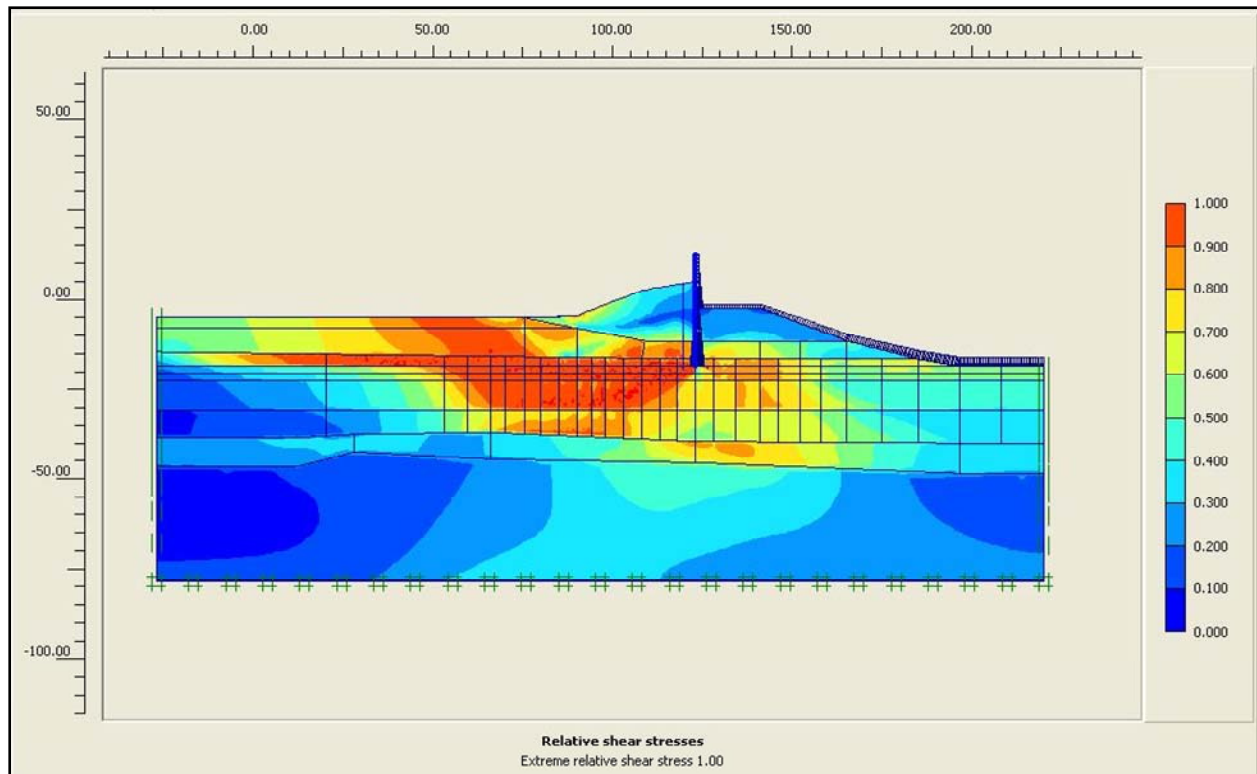


Figure 6-37. Fraction of Mobilized Shear Strength for Canal EI 9 and Crack to EI -18.5

Figure 6-38 shows that at this stage of flood loading, the upper reach of high shear strains also now indicate the formation of a failure mechanism up through the peat/marsh region beyond the toe of the levee.

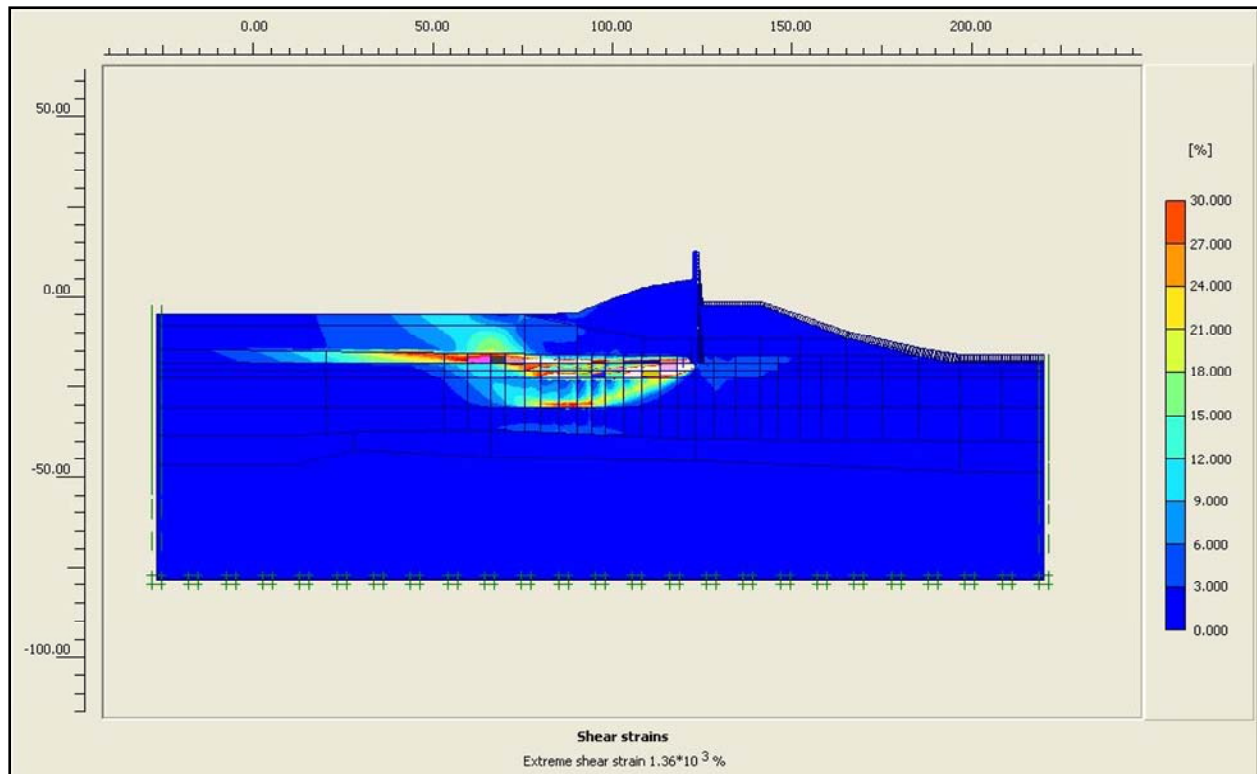


Figure 6-38. Reaches of Large Shear Strains for Canal El 9 and Crack to El -18.5

Figure 6-39 shows the failure mechanism based on a Plaxis Phi/C reduction procedure resulting in a computed factor of safety against shear failure of 0.98, while the corresponding Figure 6-40 shear strains show that the zone of higher shear strains extend to the upper layer of the lacustrine clay. Note the mechanism “daylighting” beyond the toe of the levee. This result is consistent with the Figure 6-36 displacements, showing the bulging upwards of the peat/marsh layer beyond levee toe; the zone of high values for the computed fraction of mobilized shear strength within this region in Figure 6-37; and the Figure 6-38 high shear strains also computed within this region.

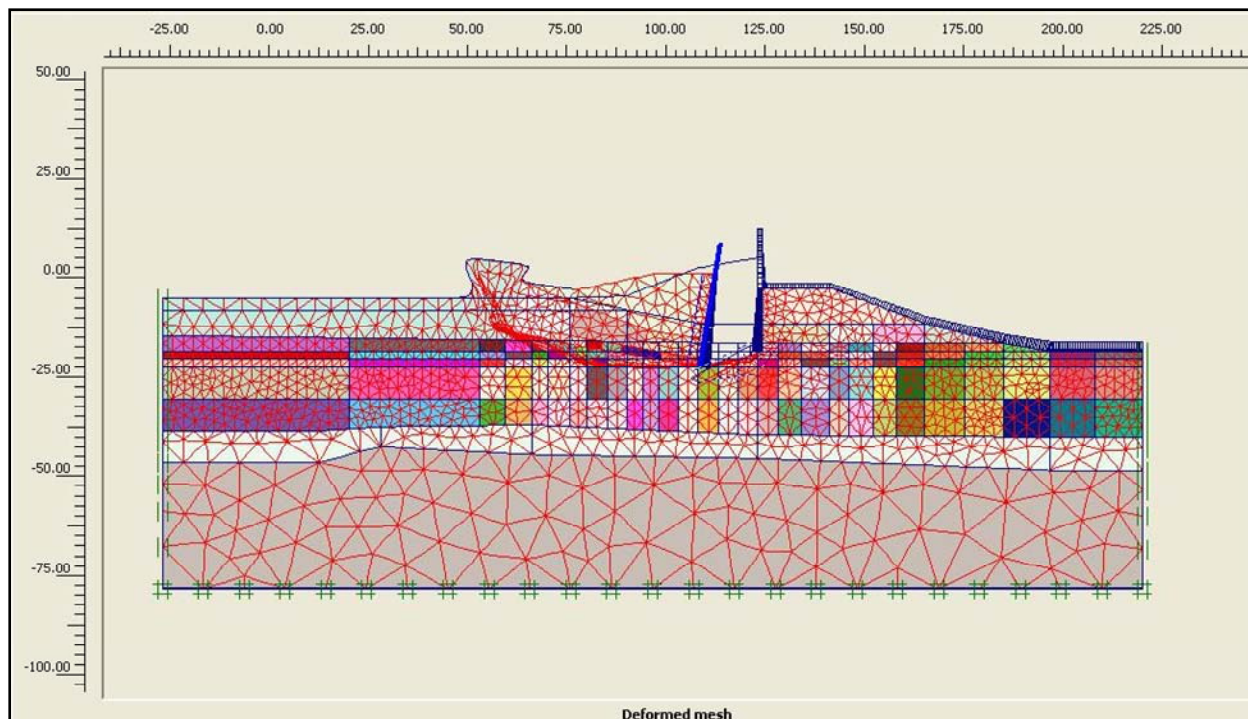


Figure 6-39. Failure Mechanism from Phi/C Reduction for Canal EI 9 and Crack to EI -18.5

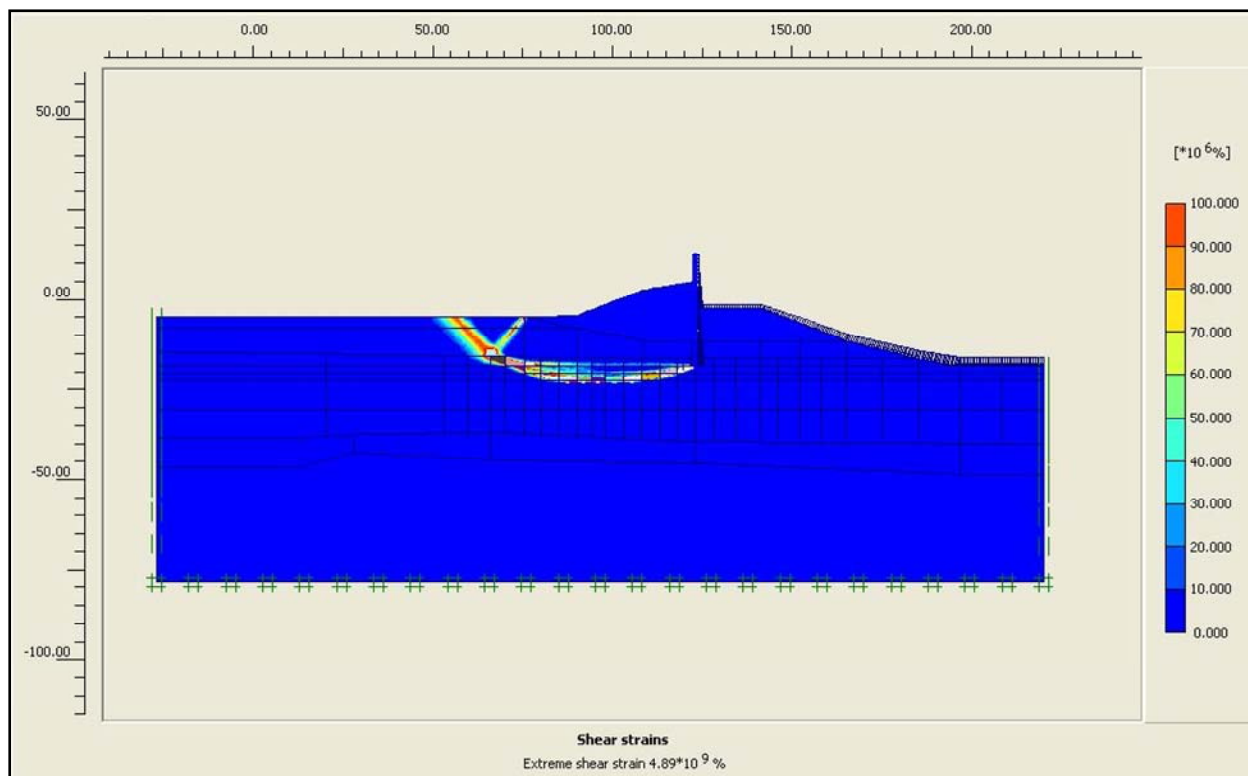


Figure 6-40. Reaches of Large Shear Strains from Phi/C Reduction for Canal EI 9 and Crack to EI -18.5

Subsequent complete SSI analyses are made to compute the factors of safety against shear failure for canal water less than El 9. The results summarized in Figure 6-41 indicate that the factor of safety is equal to unity for canal water El 8.8. These results demonstrate the reserve capacity of the levee/I-wall system for canal water less than El 8.8. For example, Figure 6-41 shows that at El 6.5, the factor of safety against shear failure is 1.46 prior to cracking. Figure 6-42 shows that the failure mechanism based on a Plaxis Phi/C reduction procedure, if allowed to develop, would also be “daylighting” beyond the toe of the levee, while the corresponding Figure 6-43 shear strains show that the zone of higher shear strains extend to mid-layer in the lacustrine clay. After the full crack is introduced to the sheet pile tip for canal water El 6.5, the factor of safety reduces to 1.17.

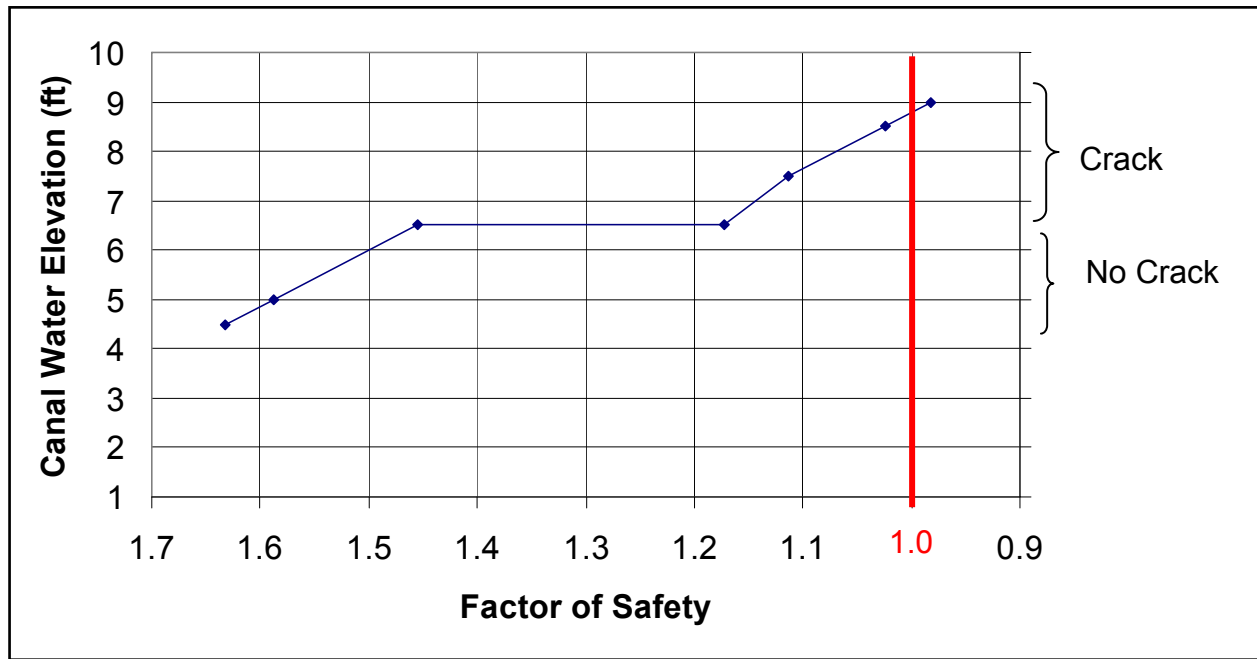


Figure 6-41. Factor of Safety Versus Canal Water El (Complete SSI results)

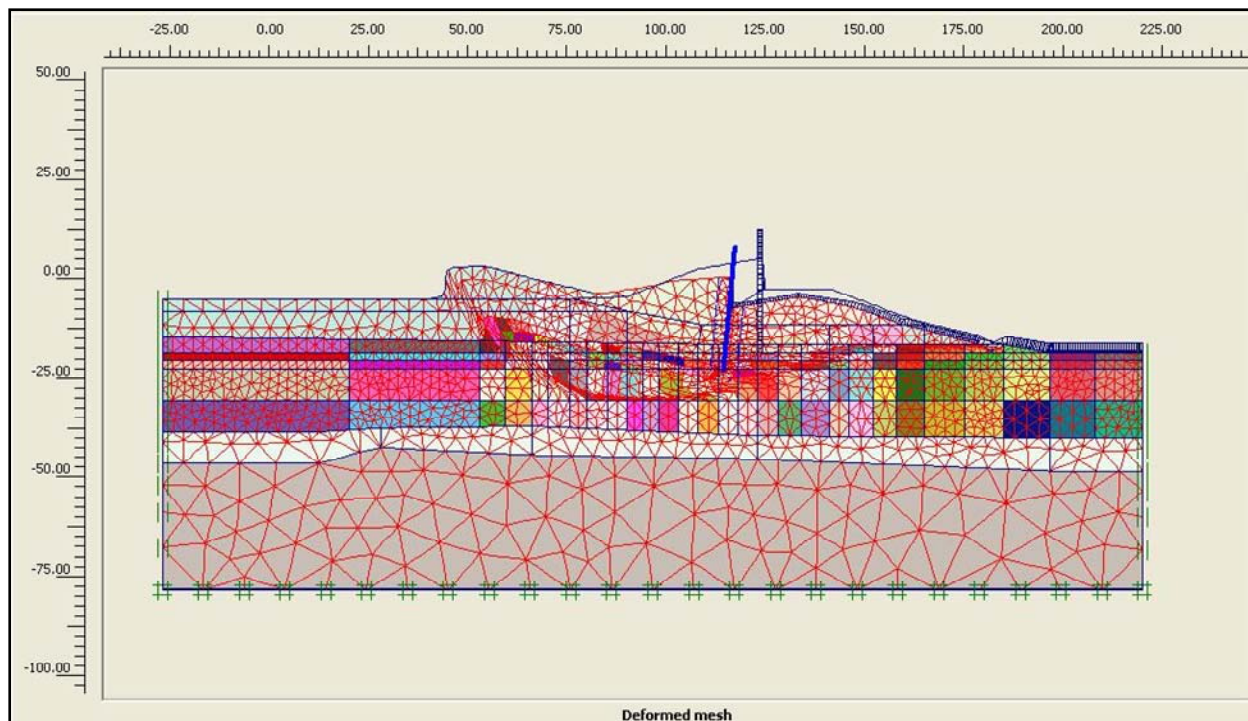


Figure 6-42. Failure Mechanism from Phi/C Reduction for Canal EI 6.5 and No Crack

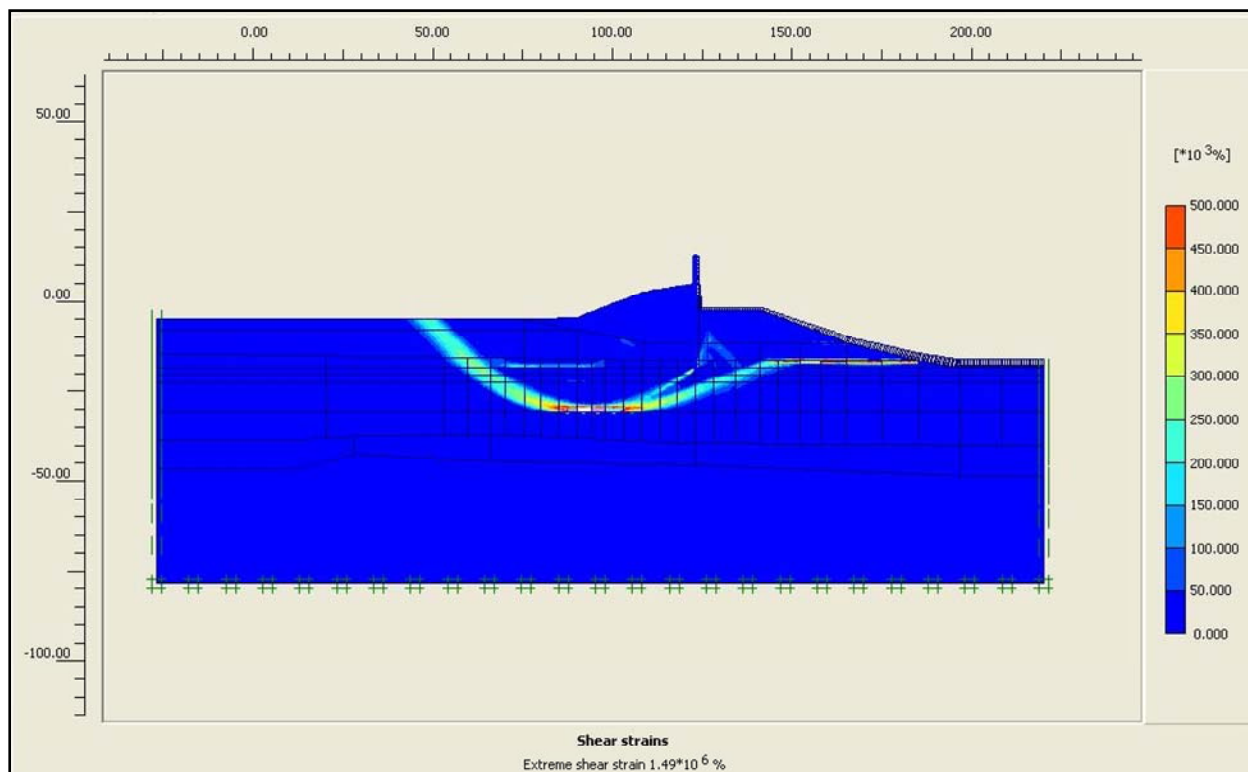


Figure 6-43. Reaches of Large Shear Strains from Phi/C Reduction for Canal EI 6.5 and No Crack

References

Brinkgreve, R. B. J., Broere, W., and Waterman, D., ed. 2004. *Plaxis 2D – Version 8*. Plaxis B.V. The Netherlands: Delft University of Technology.

Kulhawy, F. H., and Mayne, P. W. 1990 (Aug). Manual on Estimating Soil Properties for Foundation Design, Research Report EL-6800, prepared for Electric Power Research Institute, Palo Alto, CA.

Potyondy, J. G. 1961. Skin Friction Between Various Soils and Construction Materials, *Geotechnique*, Vol. II, pp. 339-353.

Schmertmann, J. H. 1978. Guidelines for Cone Penetration Test, Performance and Design, Report FHWA-TS-78-209, U.S. Department of Transportation, Washington, DC, 145 p.

Skempton, A. W. 1986. Standard Penetration Test Procedures and the Effects in Sands of Overburden Pressure, Relative Density, Particle Size, Ageing and Overconsolidation, *Geotechnique*, Vol. 36, No. 3, pp. 425-447.

Appendix 7

Interim Data Report, London Avenue Outfall Canal

Introduction

This is an interim report that documents data collected to date for the analysis of the failure of the I-wall sections at the London Avenue Outfall Canal (north and south failures) as a result of Hurricane Katrina on August 29, 2005. London Avenue Outfall Canal and the location of the levee breaches are shown on Figure 7-1. The north is located on the west bank of the canal, south of the Robert E. Lee Blvd. Bridge and about one mile south of the outlet of the London Ave. canal. Opposite the north breach, the east I-wall experienced extreme levee distress, including landward deflection of the I-wall, cracked concrete, and the presence of several sink holes at the levee crown, and a sand boil at the levee toe. The south London or Mirabeau breach is located on the east bank, north of and adjacent to the Mirabeau Bridge.

Key data obtained for the breach sites and presented in this report include:

- a.* Description of geology and soil stratigraphy
- b.* Representative pre-Katrina cross section through the breach area
- c.* Undrained shear strength soil profiles
- d.* Piezometer data

Engineering and geologic data were obtained from a variety of sources, including the project General Design Memorandum, design documents, and surveys prepared prior to Katrina. In addition, this report contains information obtained from field and laboratory investigations and surveys conducted after the Hurricane Katrina event. This report was prepared to provide numerical and physical modelers with the information needed to build models for analyses of levee stability.

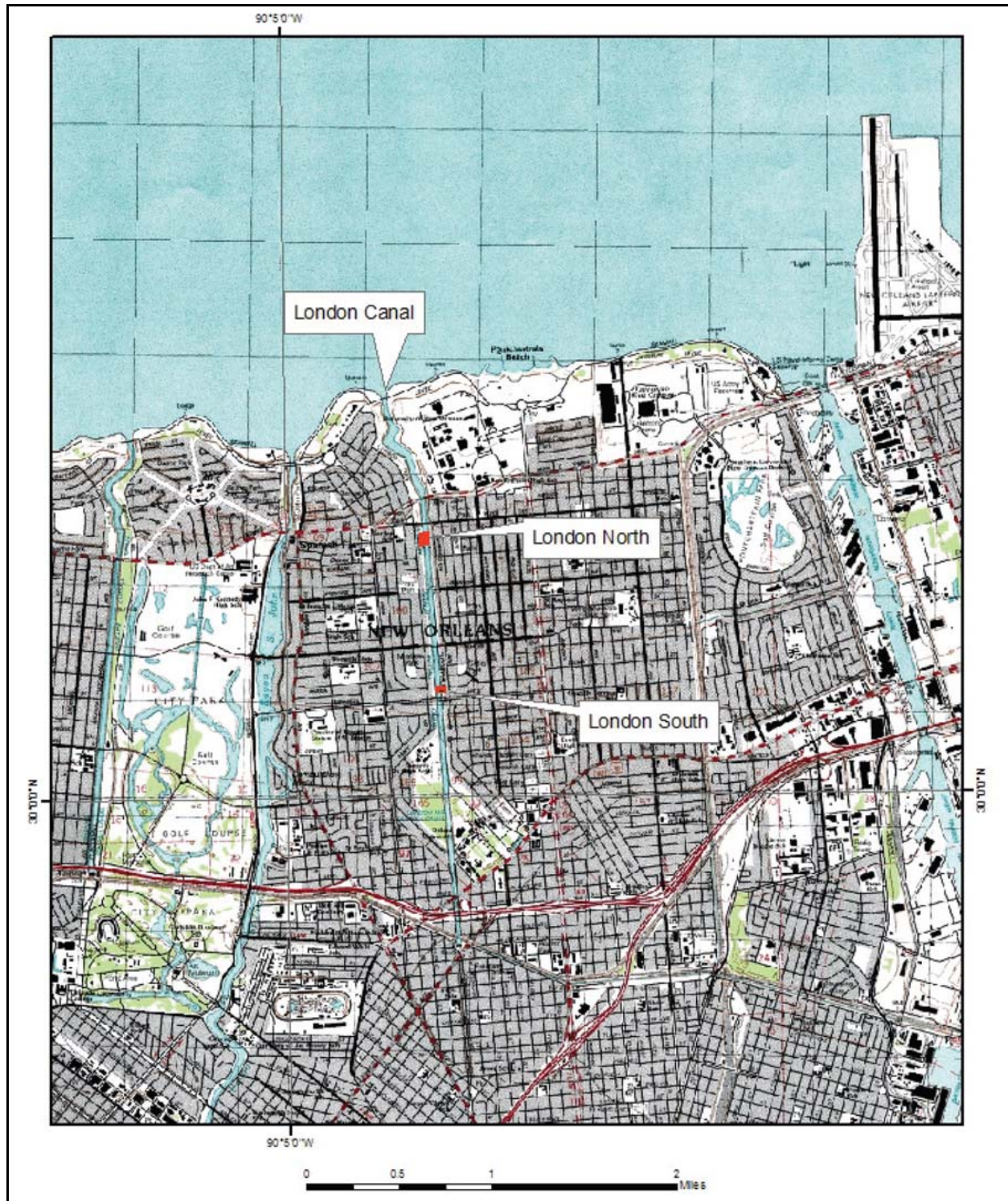


Figure 7-1. Location of the London Canal and Levee Breaches at Robert E. Lee and Mirabeau (North and South Breaches, Respectively)

Geology

Introduction

Before examining the individual failure areas at London Canal, a review of the geology is presented to familiarize the reader with the broader context of the geology of the delta plain, its stratigraphy, and the soils comprising the foundations at the different failure areas. For comparison purposes, the general geology of both the 17th Street and London Canal levee breaches is reviewed. The geology of the New Orleans area has been determined from detailed mapping studies of the Louisiana Coastal Plain (LCP), a review of the published literature, from data collection activities at each of the failure sites by an ERDC study team, and from an evaluation of preexisting and recently drilled engineering borings from each of the failure areas.

Previous Studies

A review of the past geologic literature from the New Orleans area identifies the US Army Corps of Engineers (USACE) as being actively involved with much of the regional and focused geologic studies that have been performed in the eastern LCP or deltaic plain (Dunbar and others, 1994 and 1995; Dunbar, Torrey, and Wakeley, 1999; Fisk, 1944; Kemp and Michel, 1967; Kolb, Smith, and Silva, 1975; Kolb, 1964; Kolb and Van Lopik, 1958a and 1958b; Kolb and Schultz, 1954; Kolb and Saucier, 1982; May and others, 1984; Michel, 1967; Saucier, 1963, 1984, and 1994; and Schultz and Kolb, 1950). Many of these studies and associated geologic maps are available from a USACE-sponsored website on the geology of the Lower Mississippi Valley that is accessible to the public at lmvmapping.erd.c.usace.army.mil.

Geologic History and Principal Physiographic Features of the New Orleans Area

To better understand the soils beneath the 17th Street and London Canals, and the engineering properties of these soils, a brief summary of the geologic history of the New Orleans area is presented. Detailed descriptions of the geologic history are presented in Saucier (1964 and 1994), Kolb, Smith, and Silva (1975), Kolb and Saucier (1982); and Kolb and Van Lopik (1958).

The geology and stratigraphy of the New Orleans area are young in terms of its age. Generally, sediments comprising the New Orleans area are less than 7,000 years old. Formation of the present day New Orleans began with the rise in global sea level, beginning about 12,000 to 15,000 years before present. The rise in sea level was caused by melting of continental glaciers in the Northern Hemisphere and the release of ice-bound water to the oceans. At the maximum extent of continental glaciation, the eustatic sea level was approximately 300 ft (~100 m) lower than the present level. In addition, the ancestral coastal shoreline was much farther south of its current location, probably near the edge of the continental shelf.

The underlying Pleistocene surface throughout much of coastal Louisiana was subaerial, and exposed to oxidation, weathering, and erosion. These conditions led to the development of a well-developed drainage network across its surface, and created a distinct soil horizon in terms

of its engineering properties. The Pleistocene horizon is easily recognizable in borings because of its distinct physical properties as compared to the overlying Holocene fill (i.e., oxidized color, stiffer consistency, higher shear strength, lower water content, and other physical properties.). The axis of the main valley or entrenchment of the Mississippi River was located west of New Orleans, in the vicinity of present day Morgan City, LA (Figure 7-2). Consequently, development of the early Holocene deltas was concentrated near the axis of Mississippi entrenchment when sea-level rise began to stabilize sometime between 5,000 to 7,000 years before the present. New Orleans is located on the eastern edge of this buried entrenchment or alluvial valley.

The Pleistocene surface in the New Orleans area is variable, but generally ranges between 50 and 75 ft below sea level, as determined from detailed mapping and examination of boring data (Kolb and Van Lopik, 1958; Kolb, Smith, and Silva, 1974; Saucier, 1994; and Dunbar and others, 1994 and 1995). Various sea level curves for the Louisiana coast are presented and discussed in Kolb, Smith, and Silva (1975) and Tornquist and Gonzalez (2002). These curves generally indicate that sea level transgression in the New Orleans area generally occurred between 6,000 to 9,000 years before the present, based on the mapped depths to the top of the Pleistocene surface.

As the rate of sea level rise declined and stabilized, it led to the development of five, short-lived delta complexes across the Louisiana coast by deposition of Mississippi River sediments (Figure 7-2). Individual delta complexes are composed of numerous, branching distributary channels. These channels transport and deposit fluvial sediments along the margin of the delta and build land seaward into shallow coastal water. Distributary channels from the St. Bernard delta are responsible for filling the shallow Gulf waters in the greater New Orleans area (Frazier, 1967).

Bayou Sauvage is a major distributary involved in the filling of the shallow Gulf waters in the New Orleans area (Figure 7-3). This channel extends eastward from the Mississippi River and is composed of Bayous Metairie, Gentilly (or Gentilly Ridge), and Sauvage. Natural levees of this distributary channel form a pronounced physiographic feature in the northern New Orleans area (Figure 7-3). Similarly, Mississippi River natural levees are some of the highest land elevations found in New Orleans, and these were the first areas to be settled by the early inhabitants in the 1700s. Distributary channels in New Orleans are pronounced physiographic features, and are associated with the St. Bernard delta complex as determined from radiocarbon dating of organic sediments (Frazier, 1967; Kolb and Van Lopik, 1958, McFarlan, 1961; Britsch and Dunbar, 1999; and Smith, Dunbar, and Britsch, 1986).

Equally important to the development and filling history of the New Orleans area is the presence of a buried, barrier beach ridge which formed approximately 4,500 to 5,000 years before the present. This beach extends northeast in the subsurface along the southern shore of Lake Pontchartrain (Figure 7-4). Sea level was 10 to 15 ft lower than the current level when the beach ridge formed. A stable sea level permitted sandy sediments from the Pearl River to the east to be concentrated by longshore drift, and formed a sandy spit or barrier beach complex in the New Orleans area as shown by Figure 7-3 (Saucier, 1994).

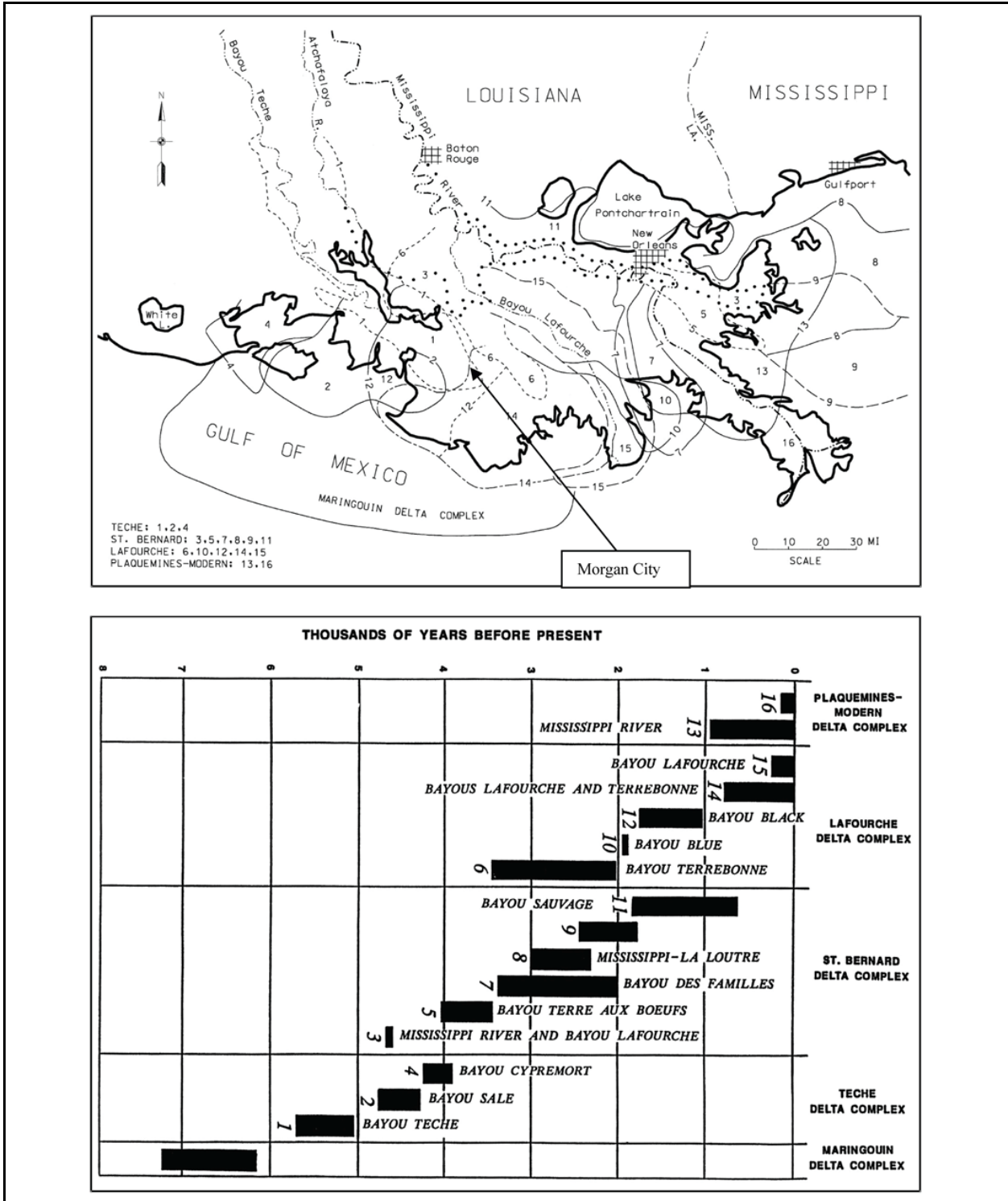


Figure 7-2. Location and Approximate Chronology of the Mississippi River Deltas, Major Distributary Channels are Numbered, Note Bayou Sauvage (No. 11) which Extends across the New Orleans Area and Forms the Bayou Metairie/Gentilly Ridge (after Frazier, 1967). Morgan City, LA, Located along Axis of Maximum Mississippi River Entrenchment.

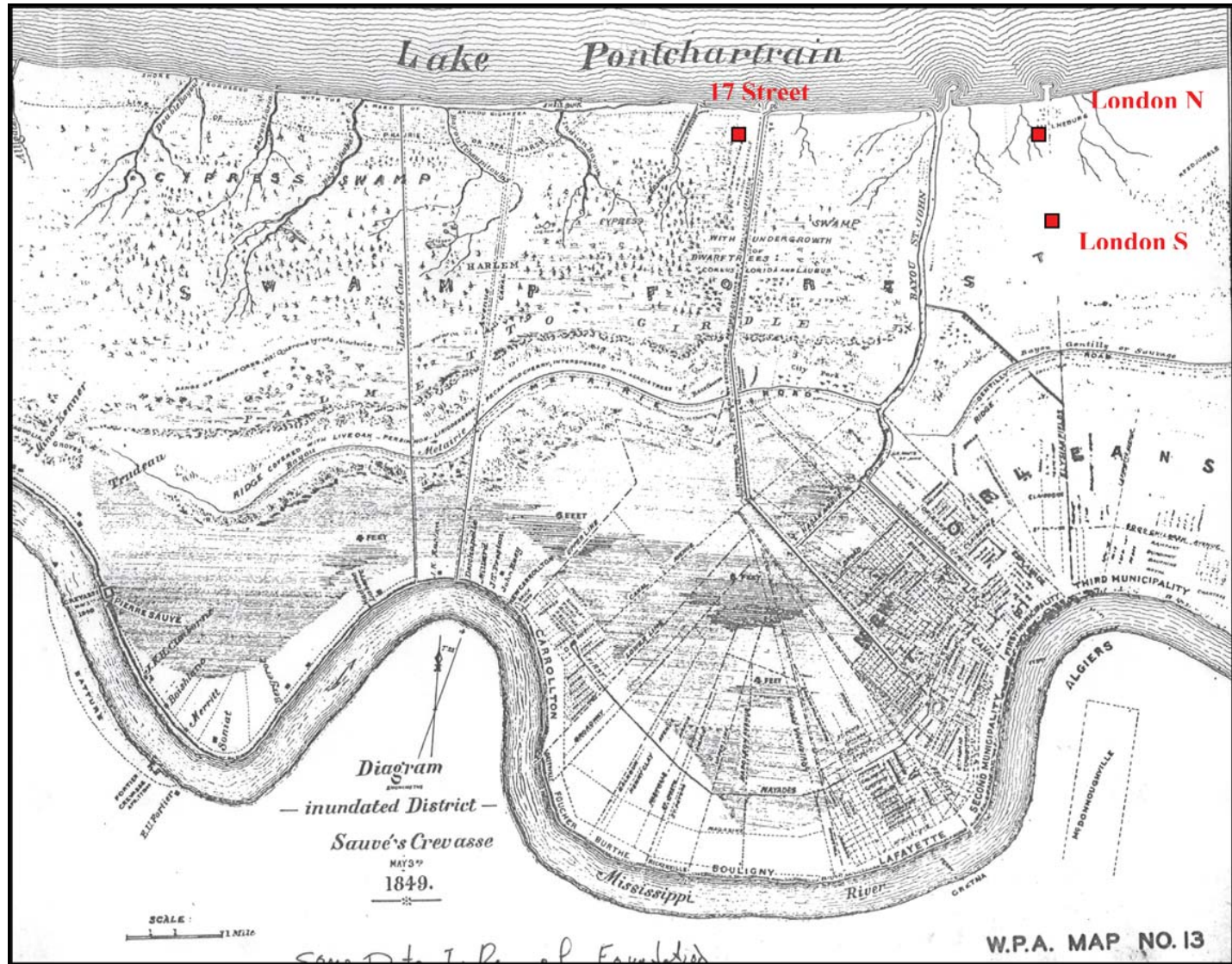


Figure 7-3. New Orleans Area Map from 1849 Showing City Limits and Topography. Note the Location of Bayous Metairie and Gentilly (i.e., Bayou Sauvage) and the Identified Cypress Swamp North of the City at this Time (Work Projects Administration, 1943).

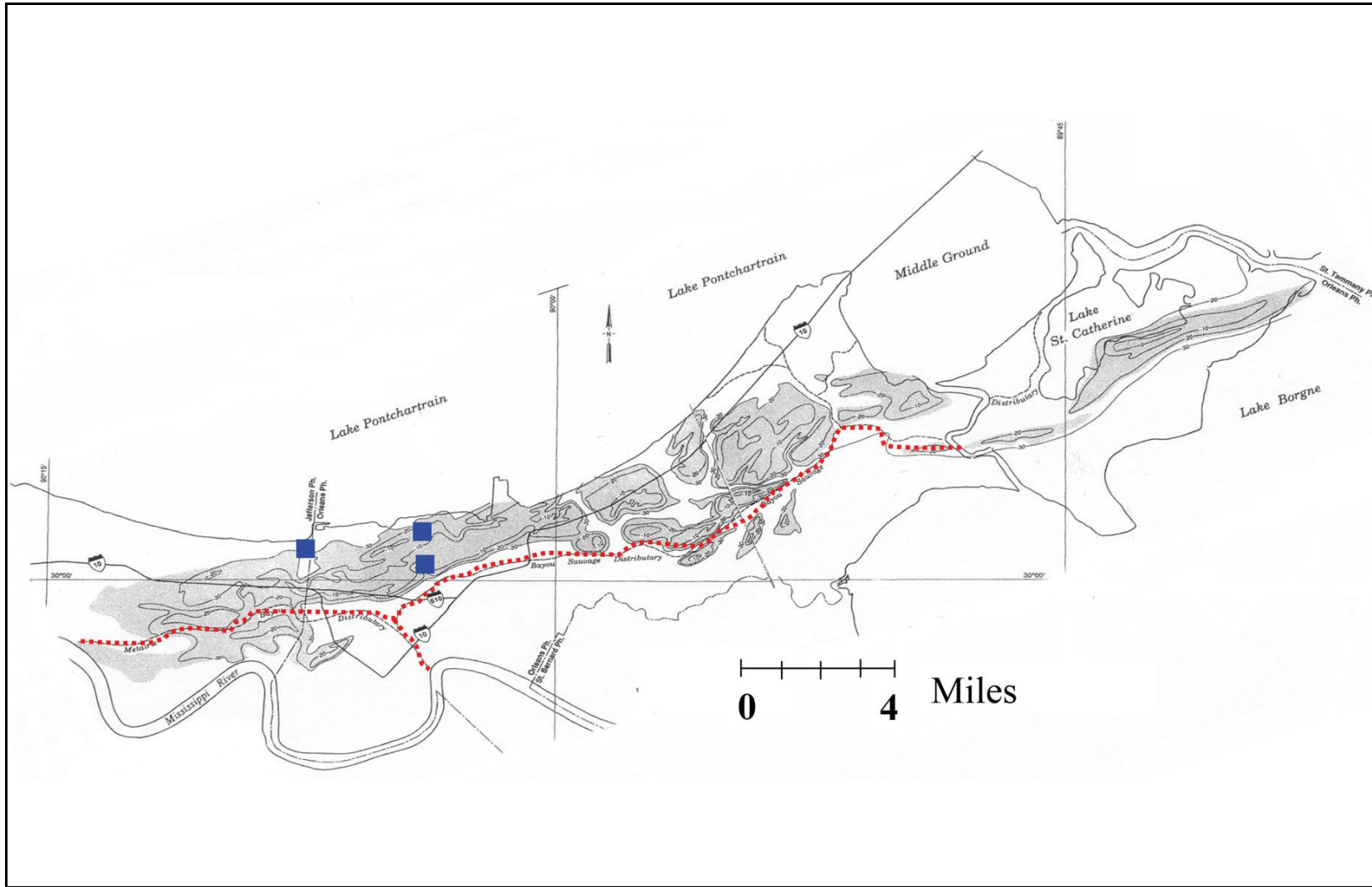


Figure 7-4a. Pine Island Buried Beach Complex in the New Orleans Area (from Saucier 1994). Course of Bayou Sauvage (I.E., Bayous Metairie and Gentilly) Identified in Red. Note the Presence of the Barrier Beach Prevented this Distributary Course from Extending Northward into Present Day Lake Pontchartrain and Filling the Lake. Canal Breaches are Identified in Blue, with 17th Street Breach Behind the Thickest Part of the Beach Ridge, while Both the London North and South Breaches are on the Axis of the Barrier. See Figure 7-4b for Close-up of Canal Areas.

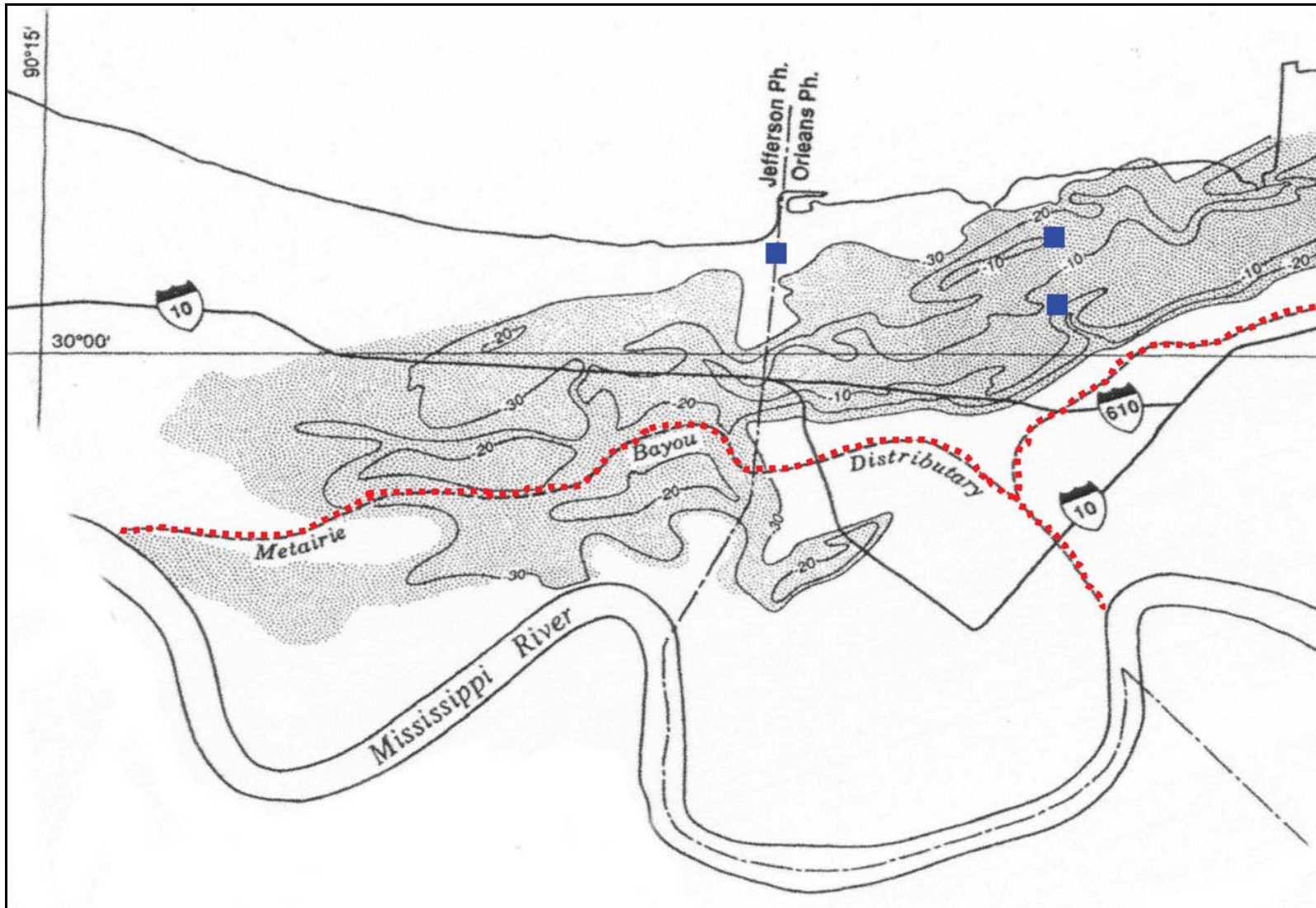


Figure 7-4b. Close-up View of the Buried Beach Ridge and the Locations of the Canal Breaches to the Buried Beach (After Saucier 1994). The 17th Street Breach is Located Behind the Axis of the Beach Ridge, while the London Canal Breaches are Located on the Axis of the Ridge. Bayou Metairie is Identified in Red and Forms the Bayou Sauvage Distributary Course (No. 11) in Figure 7-2.

The presence of the barrier beach affected sedimentation patterns and the subsequent locations for advancing distributary channels in the New Orleans area. The beach complex likely prevented the Mississippi River and later St. Bernard distributaries from completely filling Lake Pontchartrain with sediment. Consequently, foundation soils beneath the 17th and London Canal breaches are affected by their proximity to the buried beach complex. As shown by Figure 7-4, the breach at the 17th Street Canal is located on the protected or land side of the beach ridge, while both of the London Canal breaches are located over the thickest part or axis of this ridge complex.

Surface and Subsurface Geology of the New Orleans Area

A geologic map of the New Orleans area is presented in Figure 7-5 and identifies the major environments of deposition at the surface in the vicinity of the 17th Street and London Canals. Located on the surface of the New Orleans area are natural levee and point bar deposits adjacent to the Mississippi River, abandoned distributary courses (Bayou Sauvage-Metairie north of the Mississippi River and Bayou des Familles south of the Mississippi River, respectively), and extensive marsh-swamp deposits at the surface (see also Figure 7-3). Land reclamation occurred in the 1920's along the shore of Lake Pontchartrain by dredging, and this area is identified as spoil deposits.

A portion of cross-section C-C from the Spanish Fort Quadrangle is presented as Figure 7-6 to identify the general subsurface stratigraphy beneath the 17th Street and London Canal breaches. Boring data from this section identify distinct depositional environments in the subsurface that are stacked vertically and form a stratigraphic record of the filling history during the Holocene. Major stratigraphic units in the subsurface, beginning with the oldest, include the Pleistocene (older fluvial and deltaic deposits), bay sound/estuarine, relic beach (Pine Island beach ridge) lacustrine/interdistributary, and marsh/swamp deposits. A summary description of the different depositional environments in the New Orleans area is presented in Appendix 2 (from Dunbar, Torrey, and Wakeley, 1999). Additionally, detailed descriptions of the different depositional environments are contained in Saucier (1994), Kolb (1962), and Kolb and Van Lopik (1958).

Besides mapping the horizontal and vertical limits of the various environments of deposition, relationships between these environments and key engineering properties of the respective soils have been developed. These relationships have been tabulated and are published in Kolb (1962), Montgomery (1974), and Saucier (1994). A summary of these engineering relationships is presented in Appendix 2. Similarly, relationships have been developed from the engineering properties and laboratory soil test data from 17th Street and London Canals. These data are presented in later sections of this summary as related to discussion of their engineering significance.

Geologic information from the New Orleans area helped focus the ERDC investigation and collection of data by the study team at the 17th Street and London canal failures. An understanding of the geology was an important first step to systematically collecting and evaluating stratigraphic and engineering data from these failures areas.

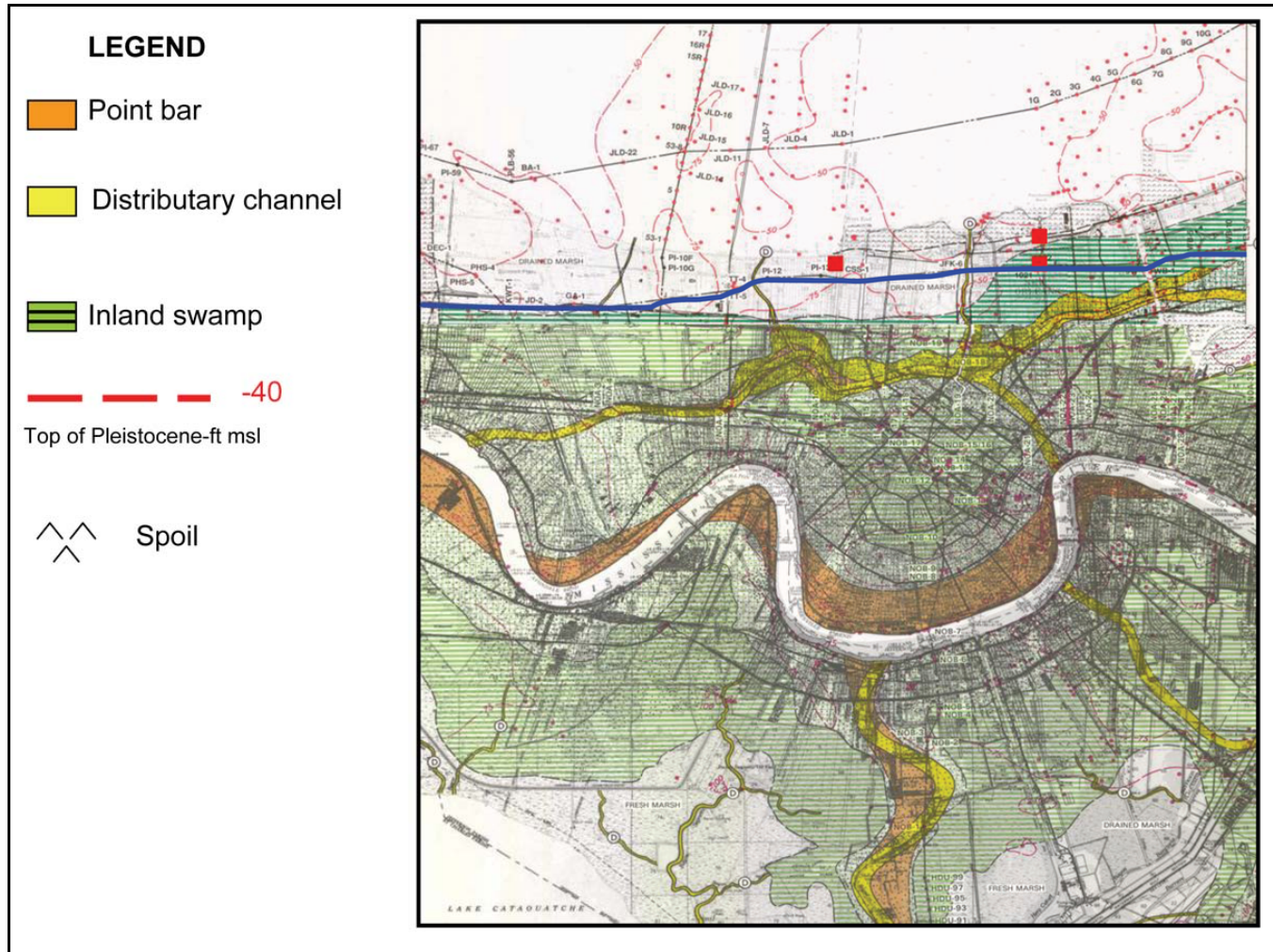


Figure 7-5. Geology Map of the New Orleans and Spanish Fort Quadrangles Showing the Distribution of Depositional Environments at Surface. Elevation of the Pleistocene Surface Shown in Red, along with Borings Used to Map this Surface. Cross-section C-C' in Blue Extends Through 17th Street and London Canal Areas (Areas Identified in Red). See Website lmvmapping.erd.c.usace.army.mil for Nearby Maps and Other Cross Sections Identified. Portion of Cross-section C-C' Above is Presented as Figure 7-6 (from Dunbar and Others, 1994 and 1995).

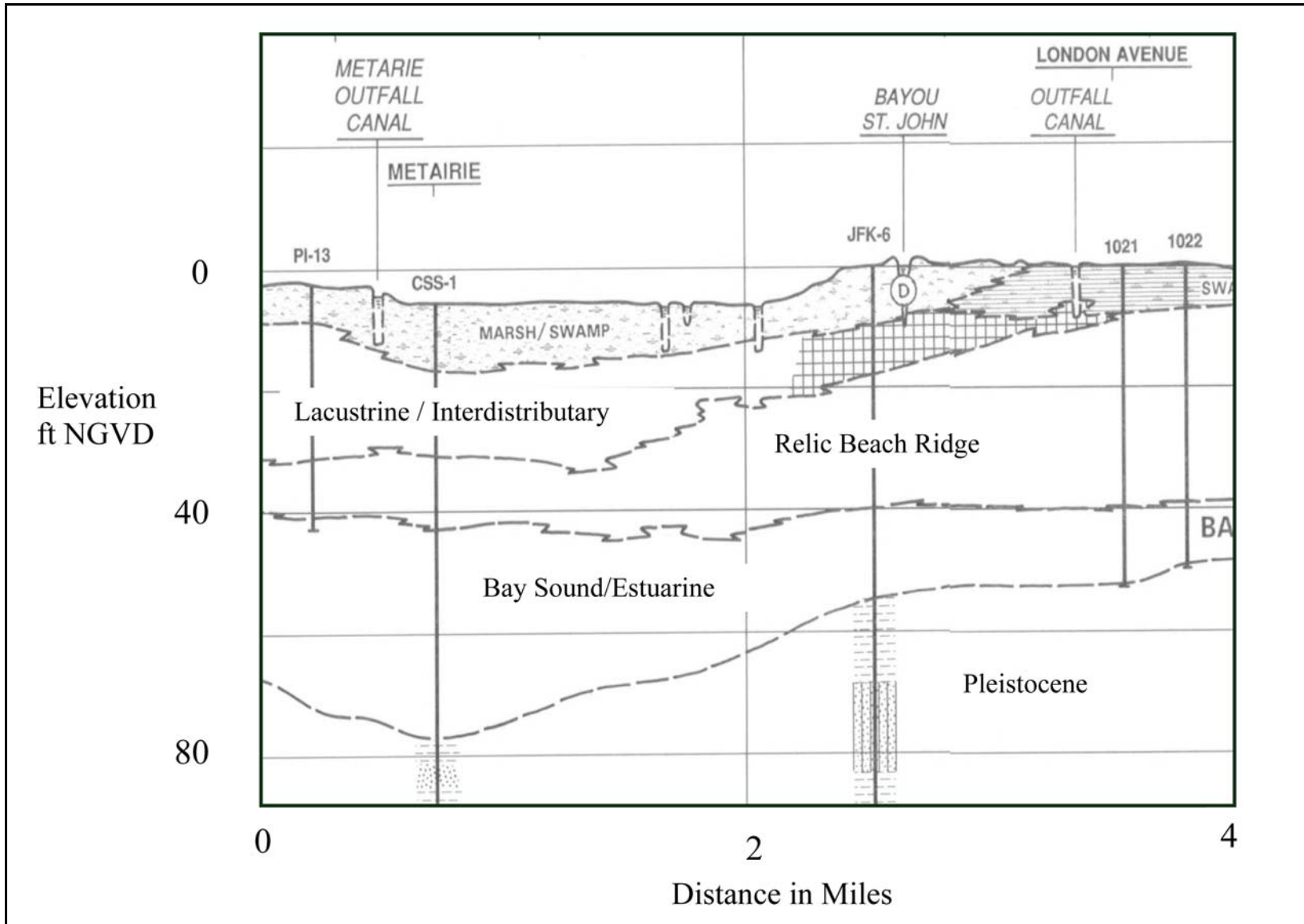


Figure 7-6. Portion of Cross-section C-C" from the Spanish Fort Quadrangle, which Extends Through the 17th and London Canal Breaches and Identifies the Stratigraphic Environments in the Subsurface (from Dunbar and Others, 1995).

Development of Cross Sections

Pre-Katrina Data

A significant amount of information was obtained from General Design Memorandum No. 19A – London Avenue Outfall Canal – Volumes I and II (USACE, 1989). This document was completed in January 1989 in preparation for upgrading the New Orleans levee system to provide increased flood protection against a stronger revised design hurricane and contains stratigraphic sections along the levee centerline. Longitudinal or centerline profiles of the west and east bank levees of the London Avenue Outfall Canal are presented as Figures 7-7 and 7-8, respectively (USACE, 1989, p. 134 and 137, respectively). These longitudinal profiles show boring locations and the USCS soil types identified during the exploration program for the project upgrade. Individual boring logs are presented in Volume II of the GDM (USACE, 1989). Foundation borings were drilled on approximately 500 ft spacing, and it is noted that odd-numbered borings are located on the west bank, and even numbered borings are located on the east bank.

Levee breach sites at London North and South have been noted on these respective sections. The northern breach is situated on the west bank of the canal according to the new levee station between Stations 8+25 and 14+00 (Figure 7-7). Opposite of this location on the east bank, between Stations 8+60 and 12+00, is an area of I-wall distress as previously noted (Figure 7-8). The southern breach (Mirabeau) is situated on the east bank of the canal between Stations 53+24 and 55+45.

Post-Katrina Data

ERDC acquired additional soil borings and cone penetrometer (CPT) borings to supplement the above cross-section data and engineering data in the London Canal breach areas (Figures 7-9 and 7-10). New borings were acquired using the U.S. Army Corps of Engineers, Vicksburg District, soil boring and CPT crews in the post-Katrina study of the New Orleans breaches during September through October 2005. Levee centerline and transverse cross sections for the London north and south areas are presented in Figures 7-11 through 7-15 (sections are in DRAFT form) and are representative of conditions before Katrina. All available elevation and geotechnical data were incorporated into the geological profiles to accurately determine the conditions at each failure site.

In the north breach area, continuous, undisturbed 5-in. soil samples were taken in borings NL-1-05U and NL-2-05U (Figure 7-9). In addition, seven CPT borings were pushed along the west side of the canal at locations NLON-1.05C, NLON-2.05C, NLON-11.05C, NLON-12.05C, NLON-13.05C, NLON-14A.05C, and NLON-15.05C (Figure 7-9). These additional borings and CPTs were needed because only two pre-Katrina borings (B26 and B27 from GDM #19A) were in the immediate vicinity of the north breach. The new borings extended the depth of the investigation in this area from an approximate elevation of -45 ft to -60 ft NGVD. Data from CPTs were used to supplement the existing soils data and better refine the stratigraphy in the breach area. Along the east wall, borings NL3-05U and 4 CPTs (CP-1, CP-2, CP-3, and CP-4)

were used to help define the stratigraphy in the area where the I-wall was in distress. Revised post-Katrina sections for the London north area are presented in Figures 7-11 through 7-13.

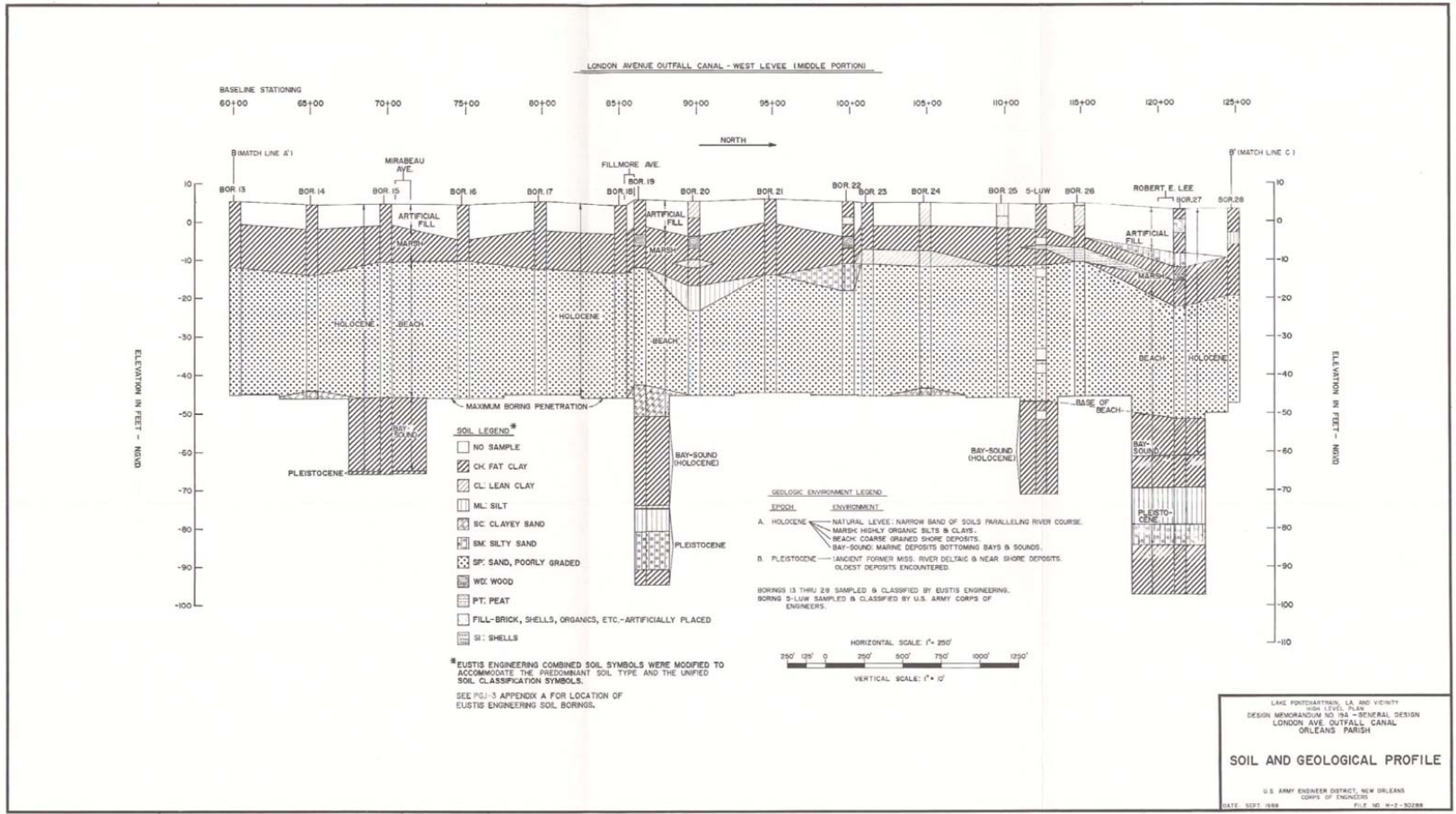


Figure 7-7. Geological Profile, along West Levee at London Canal. North London breach is South of Robert E. Lee Bridge as Shown (USACE, 1989, p. 134)

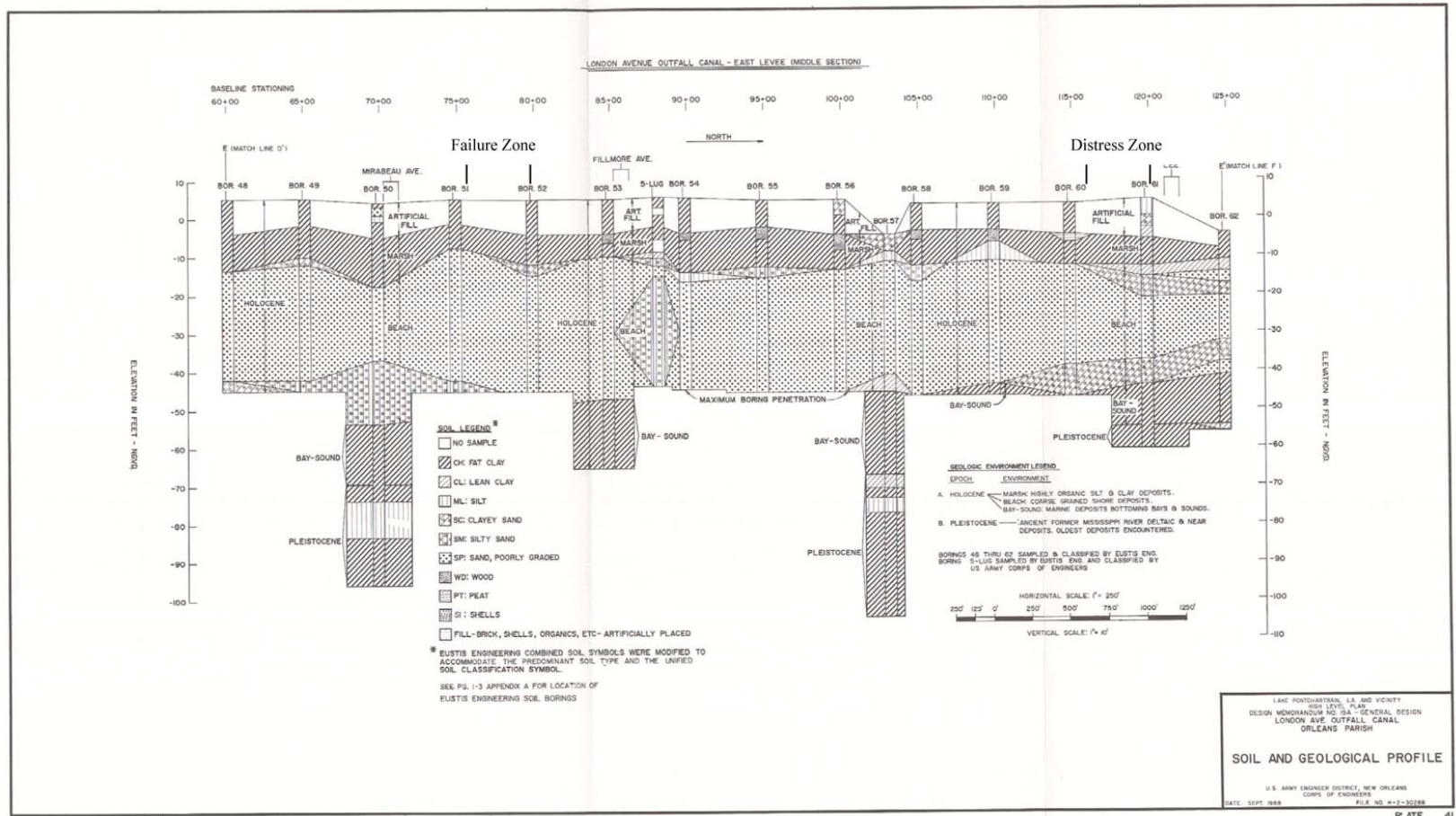


Figure 7-8. Geological Profile Along East Levee at London Canal. North London Area of Levee Distress is South of Robert E. Lee Bridge as Shown, and South London Breach Area is North of Mirabeau Bridge (USACE, 1989, p. 137).

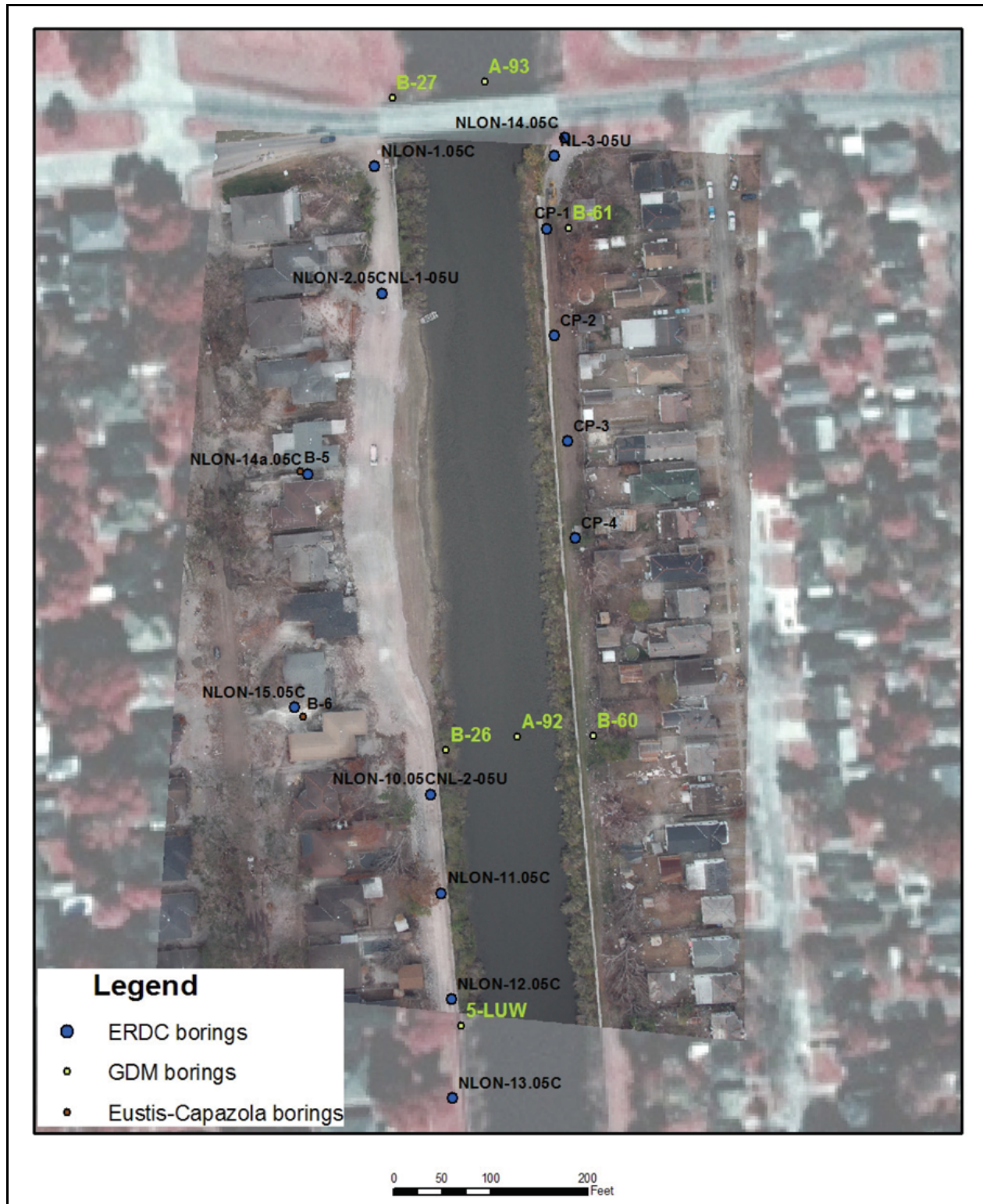


Figure 7-9. Location of all London North Borings and CPTs

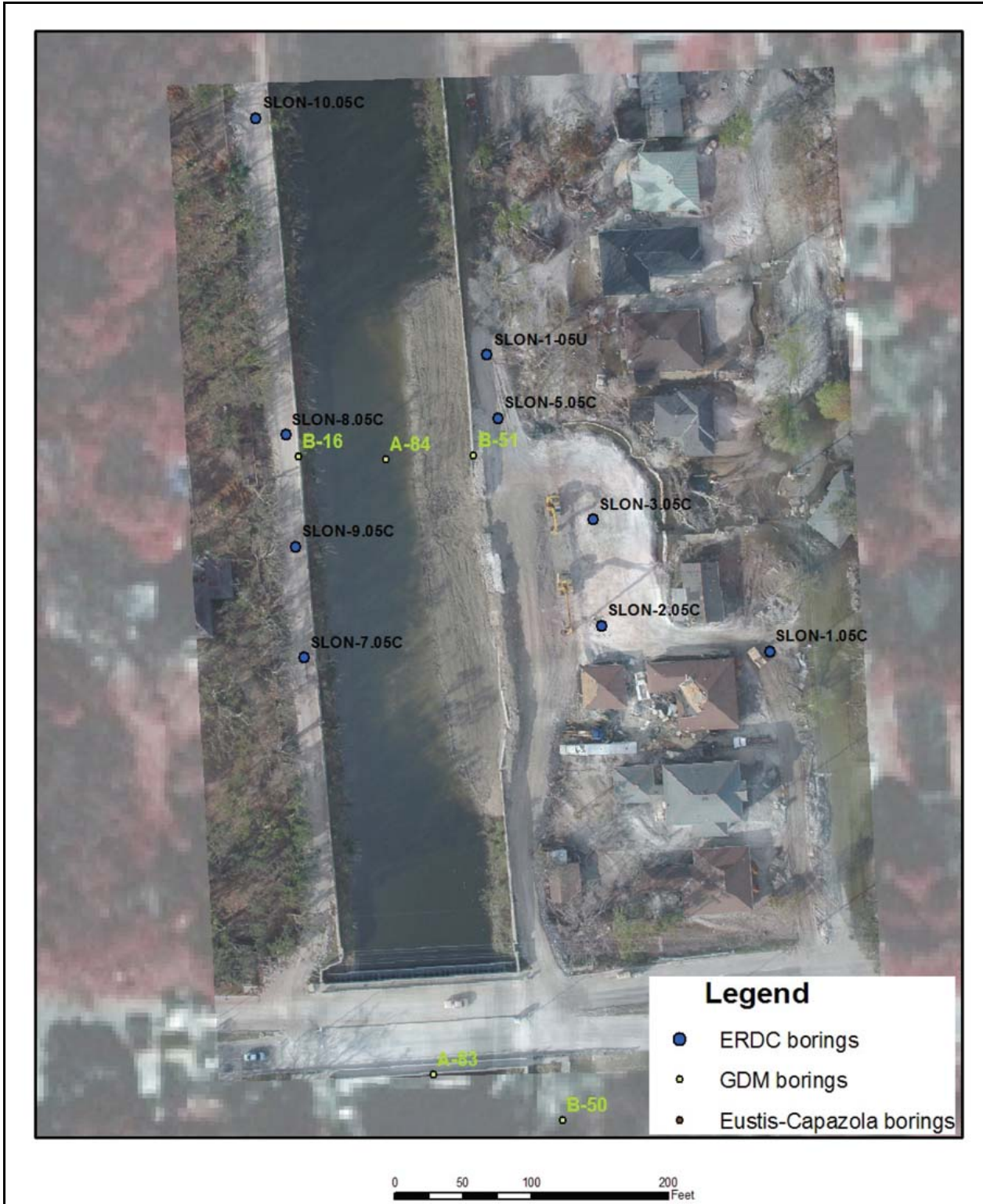


Figure 7-10. Location of all London South Borings and CPTs

Additional soil borings for the south breach included borings SL-1-05U and CPTs SLON-02/2A.05C, SLON-03.05C, and SLON-05.05C (Figure 7-10). Only one existing boring (i.e., B50, GDM #19A) was in the immediate vicinity of the south breach, and additional borings were drilled as shown by Figure 7-10. Two cross sections of the south breach were prepared from these data (Figures 7-14 and 7-15).

Information from all of the soil borings and CPTs was classified into five depositional units in the cross sections in Figures 7-11 through 7-15 over the depth of the investigation (Tables 7-1 and 7-2). Classification of the subsurface into depositional environments is based on previous studies by the USACE for geotechnical purposes (see Appendix 2 for general descriptions of these environments). A summary of these different units is presented in Tables 7-1 and 7-2 for the north and south London breaches, respectively.

Table 7-1 Major Soil Groups at London Ave. Outfall Canal North Breach Site						
Layer	Approximate Elevation of Top of Layer, ft		Approximate Elevation of Bottom of Layer		Soil Type	Consistency
	NGVD	NAVD 88	NGVD	NAVD 88		
Embankment (Spoil)	4	2.5	-4	-5.5	Clayey (CL's and CH)	Stiff
Swamp-Marsh	-4	-5.5	-13	-14.5	Organic/Peat	Very Soft
Beach Sand	-13	-14.5	-45	-46.5	Sand (SP, SM)	
Bay Sound/Estuarine	-45	-46.5	-60	-61.5	Clayey (CH)	Stiff to V. Stiff
Pleistocene (Undifferentiated) Prairie Formation	-60	-61.5			Clays – Generally CH with some sand	V. Stiff

Table 7-2 Major Soil Groups at London Ave. Outfall Canal South Breach Site						
Layer	Approximate Elevation of Top of Layer, ft		Approximate Elevation of Bottom of Layer		Soil Type	Consistency
	NGVD	NAVD 88	NGVD	NAVD88		
Embankment (Spoil)	5	3.5	-2	-3.5	Clayey (CL's and CH)	Stiff
Swamp-Marsh	-2	-3.5	-14	-15.5	Organic/Peat	Very Soft
Beach Sand	-14	-15.5	-50	-51.5	Sand (SP, SM)	
Bay Sound/Estuarine	-50	-51.5	-78	-79.5	Clayey (CH)	Stiff to V. Stiff
Pleistocene (Undifferentiated) Prairie Formation	-78	-79.5			Clays – Generally CH with some sand	V. Stiff

In the New Orleans area, the top of the Pleistocene is an important surface for engineering purposes with foundation borings often terminating in this unit. The Pleistocene is considered to be the base of the section, and the sediments above this surface representing the Holocene fill. At the top of this Holocene fill sequence is a Swamp-Marsh unit. This unit is represented in borings as organic clay (usually CH) and a peat. Examination of the drilling logs indicates that wood is usually encountered at the top of this unit, and organic clay at the base.

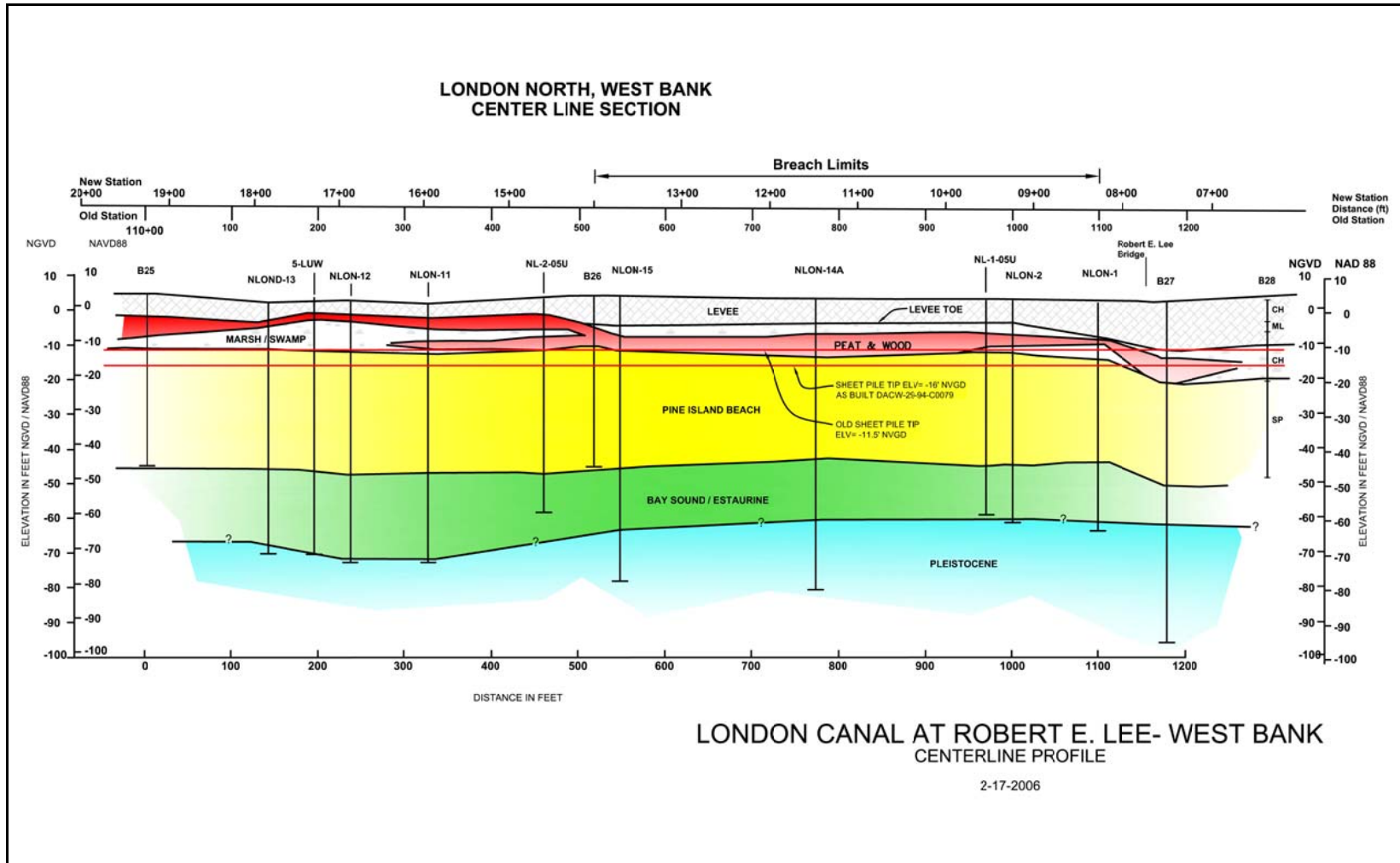


Figure 7-11. Centerline profile along West Bank London North

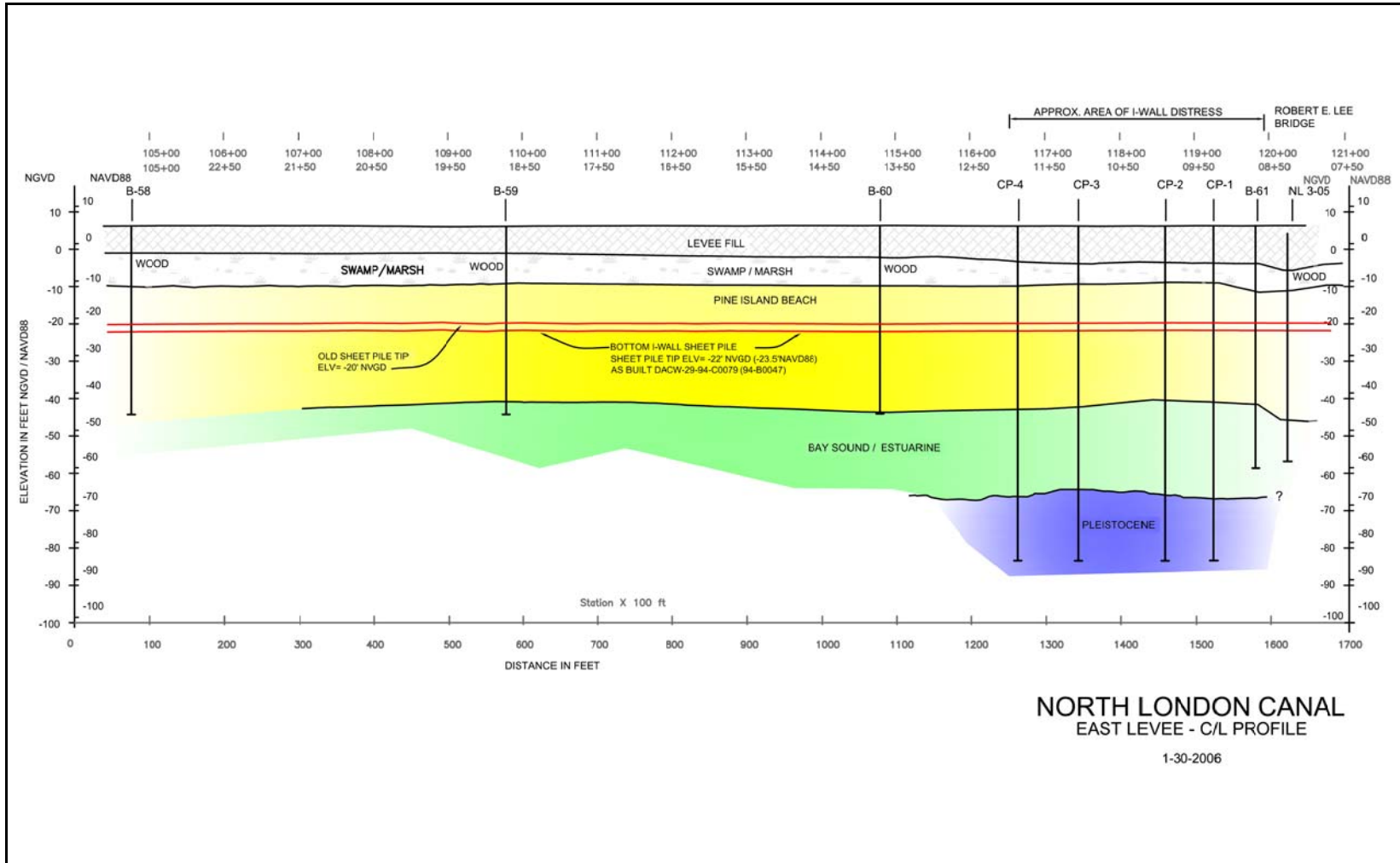


Figure 7-12. Centerline profile along East Bank London North

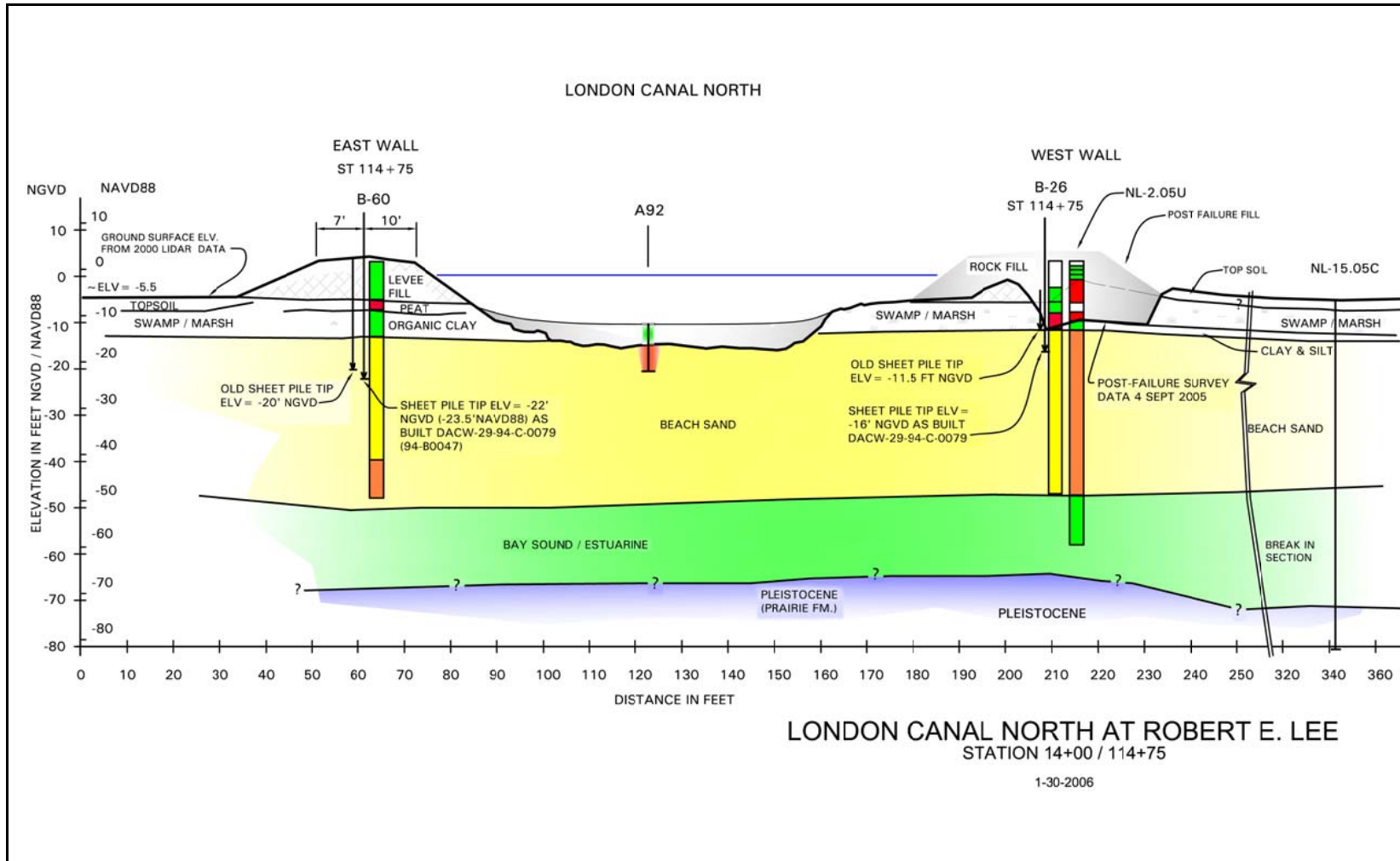


Figure 7-13. Transverse profile at Station 14+00 (Old Station 114+75) London North

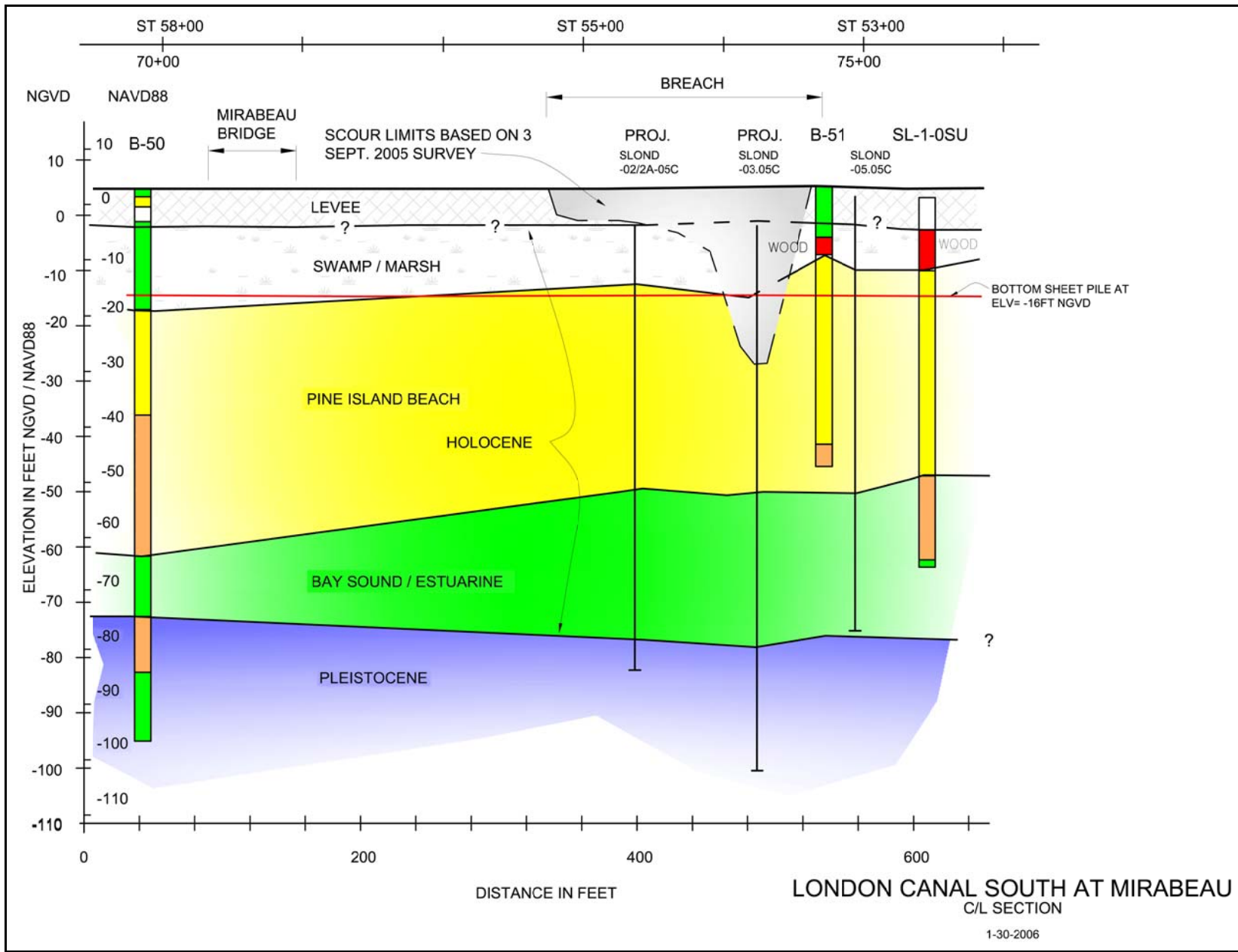


Figure 7-14. Centerline profile along East Bank London South

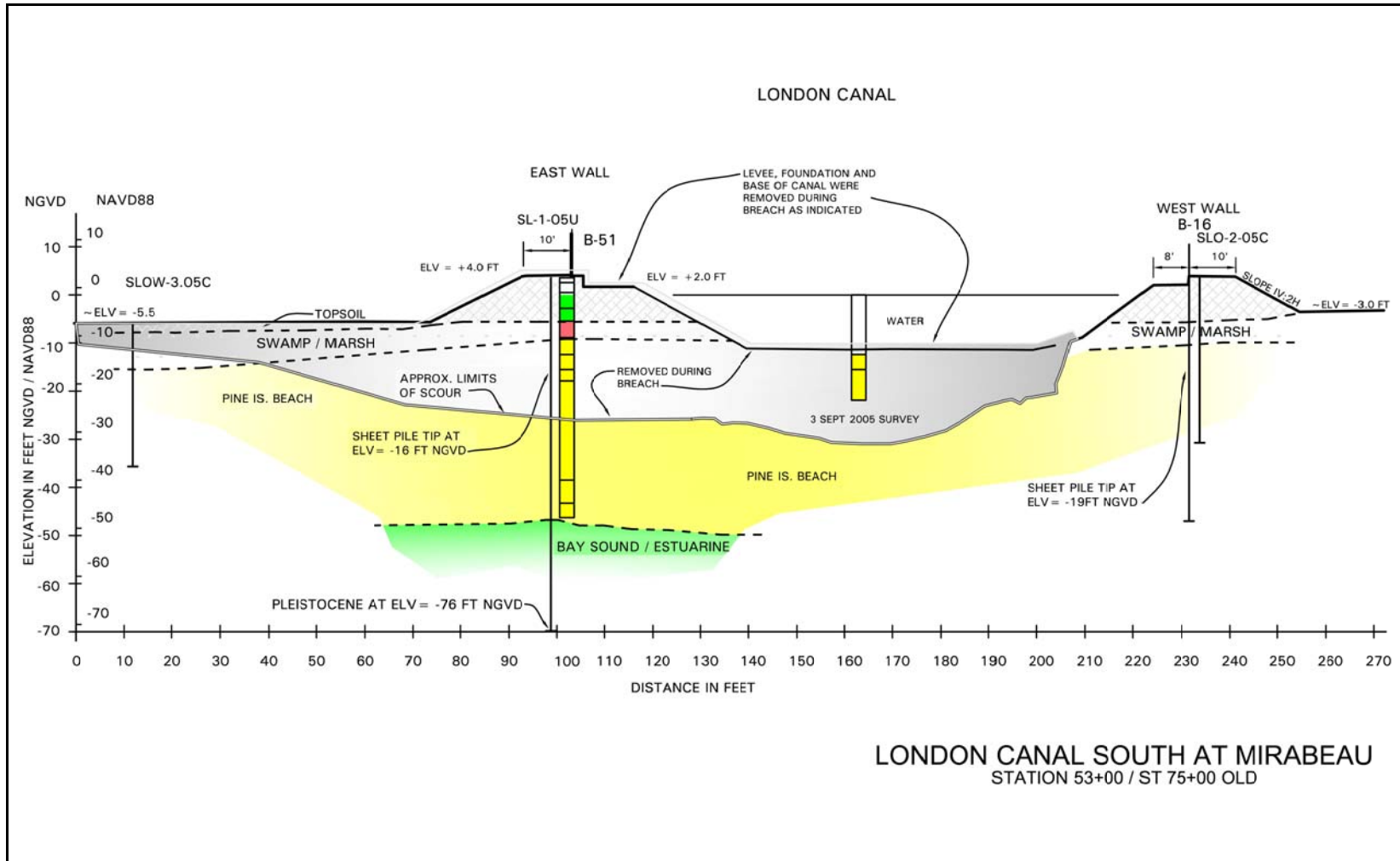


Figure 7-15. Transverse profile at Station 53+00 (Old Station 75+00) London South

This observation is supported from a survey of the displaced peat blocks at the 17th Street area as part of the ERDC investigation of the failures. Relatively intact sections of the swamp-marsh unit were observed along the street where these blocks were eventually displaced by the flood. The swamp (woody) part of the section was at the top, graded towards a peat (fibrous) section in the middle, and an organic clay section at the base. In several instances, the displaced “peat blocks” contained the intact, underlying shallow water unit, or the entire transition representing the shallow water to a terrestrial fill sequence that occurred during the Holocene. This same environmental transition is observed at London, except the underlying unit is not cohesive. Instead, the underlying unit is sand that was easily displaced from the buried beach unit as evidenced by the volume of sand at London north and south in the nearby neighborhood.

In addition, old sheet pile that was put in before or right after Hurricane Betsy (1965) exists at the north and south London breaches. At the north breach, on the west bank, the old sheet pile is canal side of the floodwall, and the tip elevation is unknown at this time. On the east bank at the distressed area, the old sheet pile is on the protected side of the floodwall. At the south London breach, on the east bank, the old sheet pile is on the canal side of the floodwall. The tip elevations of the old sheet pile are shown on the transverse cross sections.

Transverse Cross Sections through the Breach Sites

Transverse cross sections through the London north and south breach sites (Figures 7-13 and 7-15) incorporate remotely sensed elevation and bathymetry data from in the canals. Data from a pre-Katrina airborne LIDAR (Light Detection and Ranging) survey along the New Orleans Levee System that was flown in 2000 was incorporated into the cross sections to improve the surface topography in the breach area. This 2000 LIDAR survey is the best data available for establishing the pre-Katrina surface topography of the levee embankment. LIDAR surveys generate points of X, Y, and Z data that are accurate to the nearest foot. Additionally, this LIDAR data identifies tree locations along the levee and approximate size of these trees based on the diameter of the canopies. Profiles of the levee embankments were evaluated using ArcView software to determine the elevation profiles between the vegetated areas.

Post-Katrina Bathymetric survey data were incorporated into the transverse sections to determine the canal depths and slopes in relation to the embankment geometry and stratigraphy. Survey data from September 4 and 29, 2005, were evaluated to determine the elevations of the canal bottom between the floodwalls. This early Bathymetric survey data is reflected in the cross sections. Bathymetric survey data for London South show massive scouring in the channel and are reflected by the transverse cross section in Figure 7-15, and the volume of sand deposited in the neighborhood.

Uncertainties

Many uncertainties pertaining to the subsurface in the breach area will be difficult, if not impossible, to resolve because the levee in the London north and south breach areas was destroyed and drastically changed by emergency repair efforts. Furthermore, there was a lack of subsurface information on the protected side of the levee during the 1990 levee raising project

described in GDM#20. ERDC is obtaining additional information in the vicinity of the breach areas with field vane shear tests, cone penetrometer tests, and laboratory testing of samples retrieved from existing borings to obtain data pertaining to the strength and the thickness of these layers.

Soil Properties

Introduction

The following is a summary of the current geotechnical data available in the breach areas on the London Canal. These breach areas include the north breach site, the south breach site, and the distressed area across from the north breach site. Engineering soil data from each site will include all boring, laboratory, and cone penetrometer tests (CPT) in the breach area.

North Breach Site – West Levee

New borings were taken at the centerline and toe of the levee. Centerline borings include two new borings, two borings from the GDM, and four CPTs. New borings include NL-1-05U and NL-2-05U, consisting of 5-in. undisturbed samples. The GDM borings included 5-LUW (5-in. undisturbed samples) and B-26 (3-in. undisturbed samples). The CPTs include NLON-2.05C, NLON-10.05C, NLON-11.05C, and NLON-12.05C. CPTs NLON-2.05C and NLON-10.05C were the only ones taken with pore pressure measurements.

Borings at the toe of the levee include two new borings, one boring from the GDM, and two CPTs. The new borings include B-5 and B-6, with both borings consisting of 3-in. undisturbed samples. The GDM boring includes B-27 (3-in. undisturbed samples). The CPTs include NLON-14a.05C and NLON-15.05C. NLON-14a.05c was the only CPT taken with pore pressure measurements.

Moisture Content and Unit Weights

The moisture content (%w) versus elevation (NAVD 88) for samples taken from the levee centerline and above the beach sand is shown in Figure 7-16. Generally, the borings from the levee centerline show levee fill on top of a marsh layer (which consists of peat or organic clay) and a 2-ft clay (CH) layer below the marsh layer. Boring NL-2-05 shows a 2-ft clay (CL) seam in the marsh layer from about elevation -5 to -8 (NAVD 88). However, GDM boring B-26 does not show the 2-ft clay layer at the bottom of the marsh layer.

Table 7-3 summarizes laboratory test data, showing the wet unit weights for samples taken from the levee centerline in the breach area.

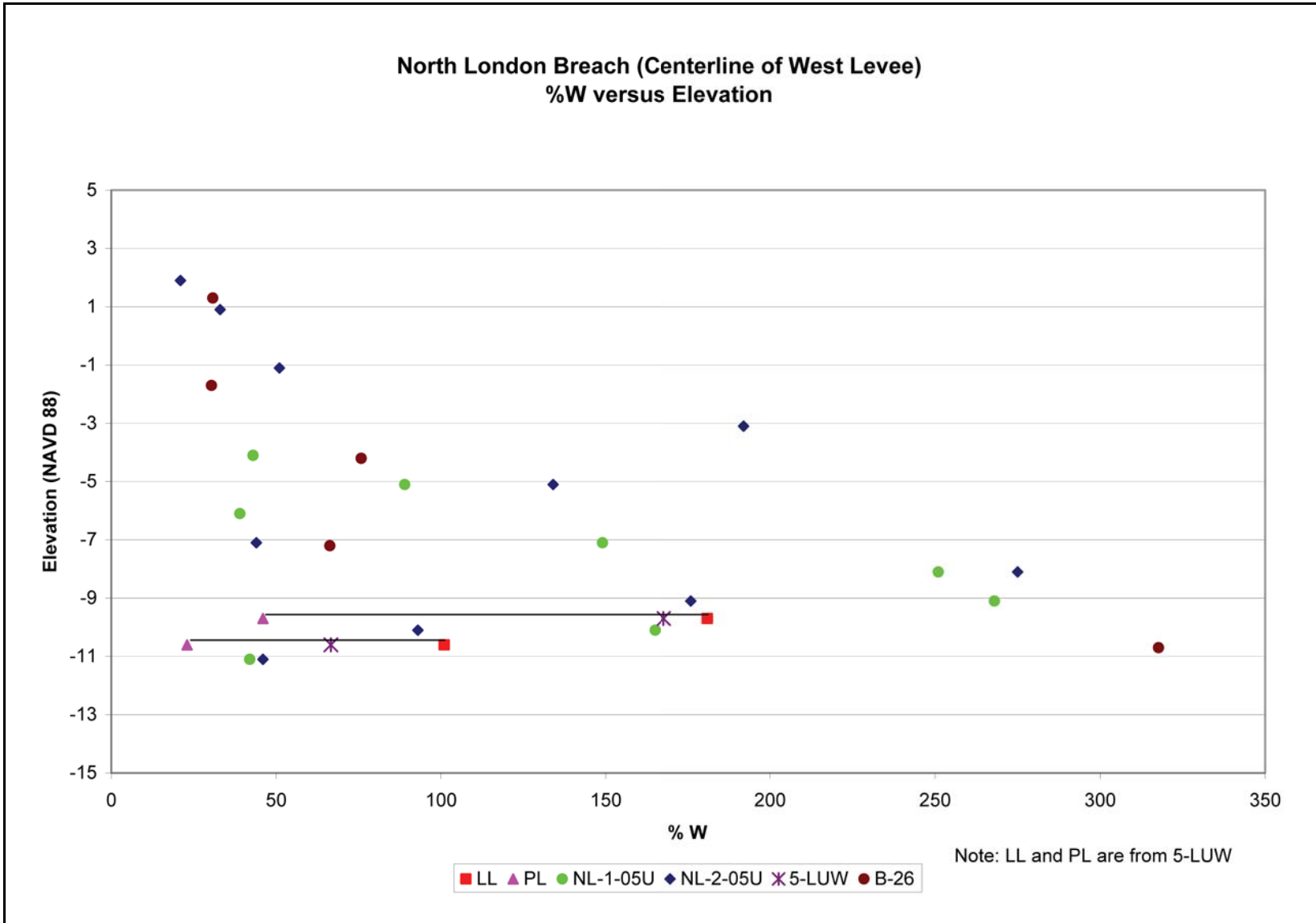


Figure 7-16. North London Breach (Centerline of West Levee), %w versus Elevation

**Table 7-3
Wet Unit Weights from Levee Centerline**

Boring	Elevation (NAVD 88)	Soil Type	%w	Dry Unit Weight (pcf)	Wet Unit Weight (pcf)	Average Wet Unit Weight
Levee Embankment						
B-26	1.30	Silty Clay	30.8	79	103.4	108.1
B-26	-1.70	Silty Clay	30.4	86.5	112.8	
Marsh Layer						
B-26	-7.20	Clay	66.3	54.3	90.3	
5LUW	-9.7	CH	167.7	29	80	
5LUW	-10.6	CH	66.6	60	100	

The geologic environment for the breach area is similar to the geologic environment for the west levee between GDM Stationing 39+60 to 121+35. Therefore, the moisture content (%w) versus elevation (NAVD 88) and the wet unit weight versus elevation (NAVD 88) were plotted in Figures 7-17 through 7-20.

The moisture content (%w) versus elevation (NAVD 88) for samples taken from the levee toe and above the beach sand is shown in Figure 7-21. Generally, borings from the levee toe show a top soil layer on top of a marsh layer (which consists of peat or organic clay) and a 2-ft clay and silt layer below the marsh layer.

Below is a table showing the wet unit weights for samples taken from the levee toe in the breach area.

Boring	Elevation (NAVD 88)	Soil Type	%w	Dry Unit Weight (pcf)	Wet Unit Weight (pcf)
B-6	-4.28	CH	40	71.4	99.9
B-6	-6.78	CH	239	23.6	79.7
B-5	-6.97	CH	204	21.7	65.8
B-6	-9.28	CH	67	57.1	95.2
B-5	-9.47	CH	67	56.7	94.7
B-6	-11.78	CL	36	84.1	114.6
B-27	-14.50	Clay	70	57.8	98.2
B-27	-18.00	Organic Clay	193.4	24.5	71.8
B-27	-22.00	Organic Clay	149.2	31.3	78

Shear Strength

Shear strengths from laboratory tests of the levee embankment and marsh unit (under the centerline) are fairly sparse. Figure 7-22 shows a plot of the four shear strength data points. However, two CPTs with pore pressure measurements were taken in the breach area through the centerline. Shear strength plots of CPT NLON-2.05C using the bearing capacity method ($N_k=15$)

and Mayne's method are shown in Figure 7-23. Also shown in Figure 7-23 is boring NL-1-05U, which was drilled next to the CPT. From the plot on Figure 7-23, a clay layer between elevations -9 and -11, which is at the top of the beach sand, is clearly detected by the CPT. The CPT shows that this clay layer has an Su/P ratio of 0.26 to 0.28.

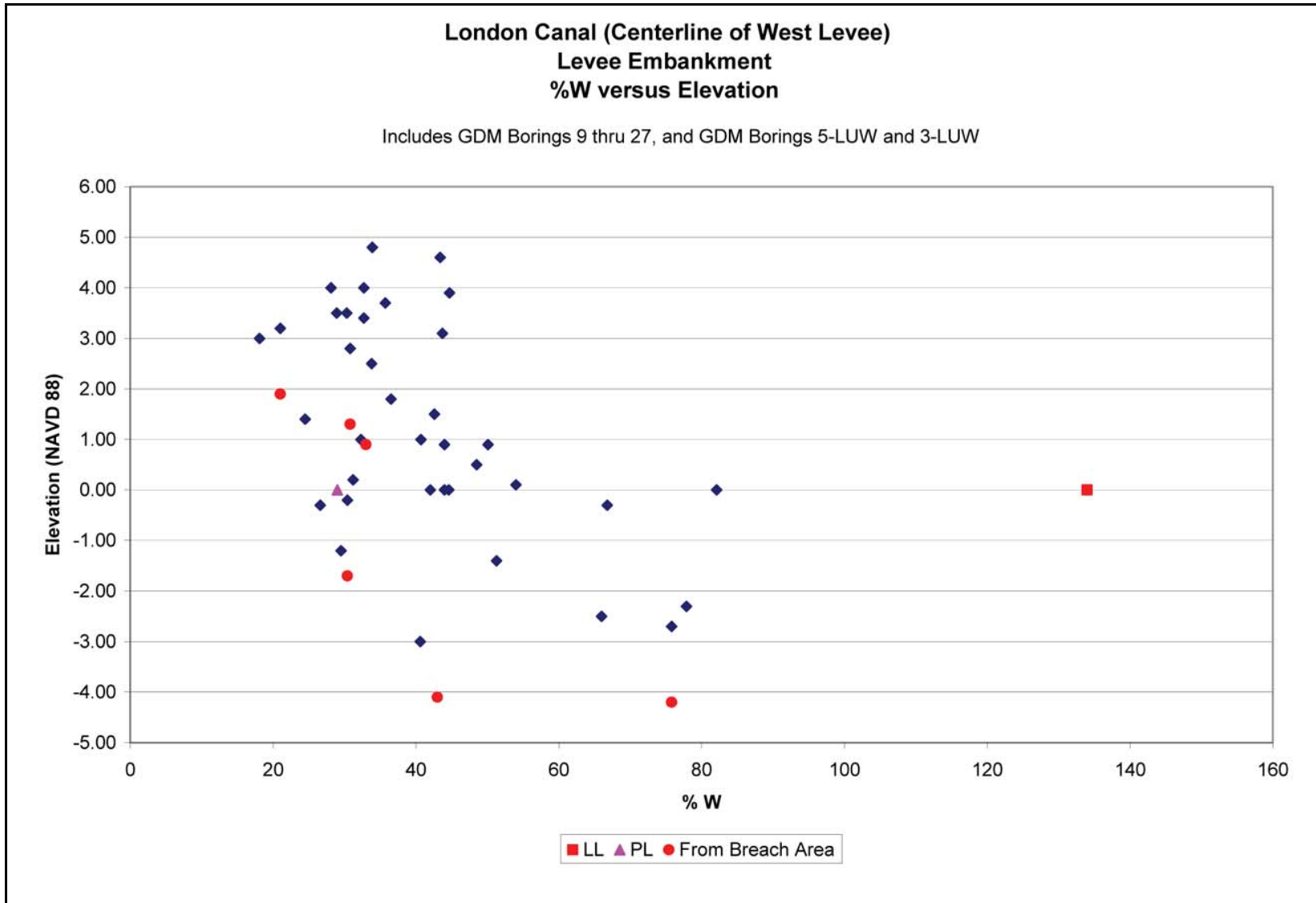


Figure 7-17. London Canal (Centerline of West Levee), Levee Embankment, %w versus Elevation

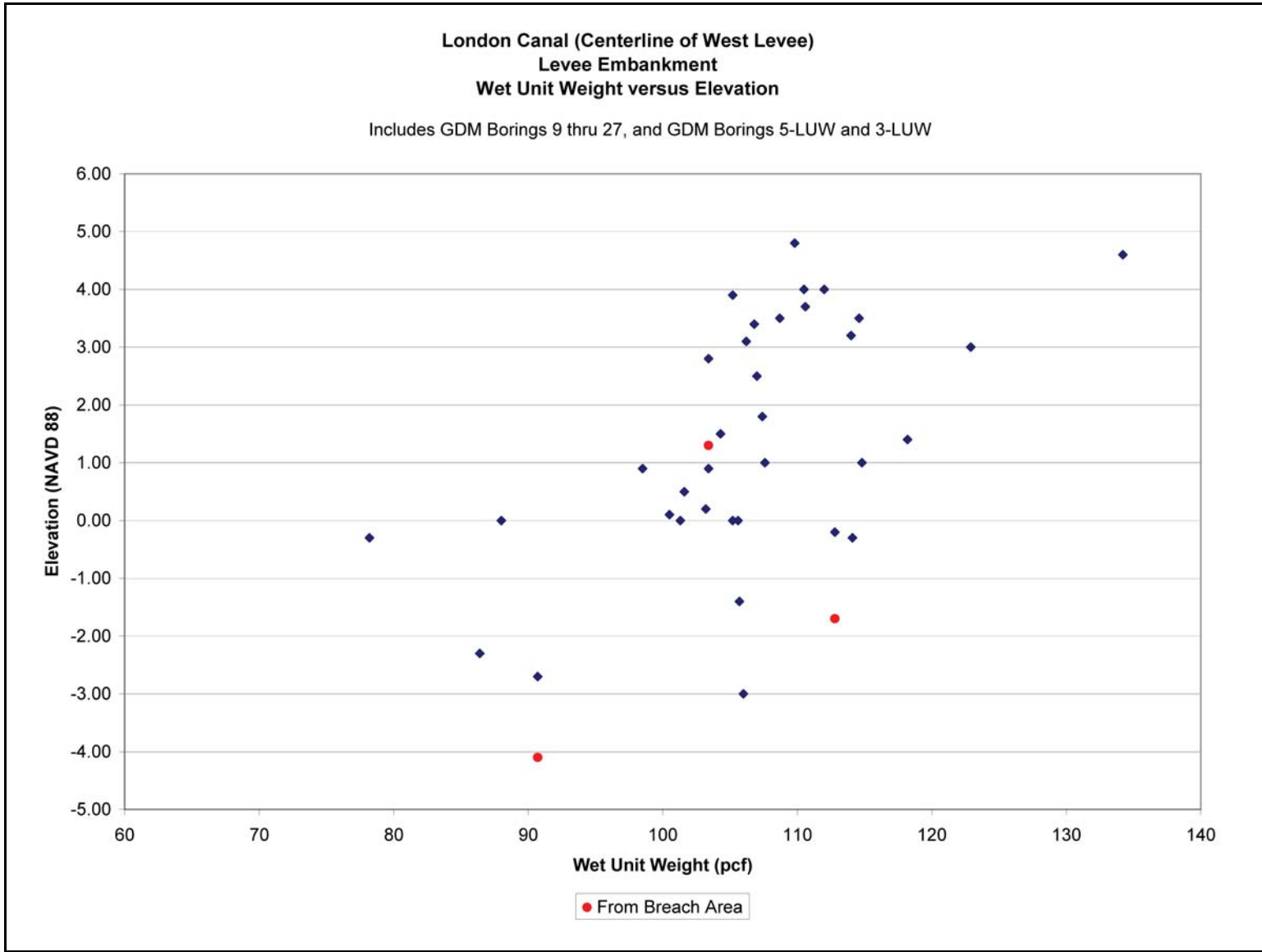


Figure 7-18. London Canal (Centerline of West Levee), Levee Embankment, Wet Unit Weight versus Elevation

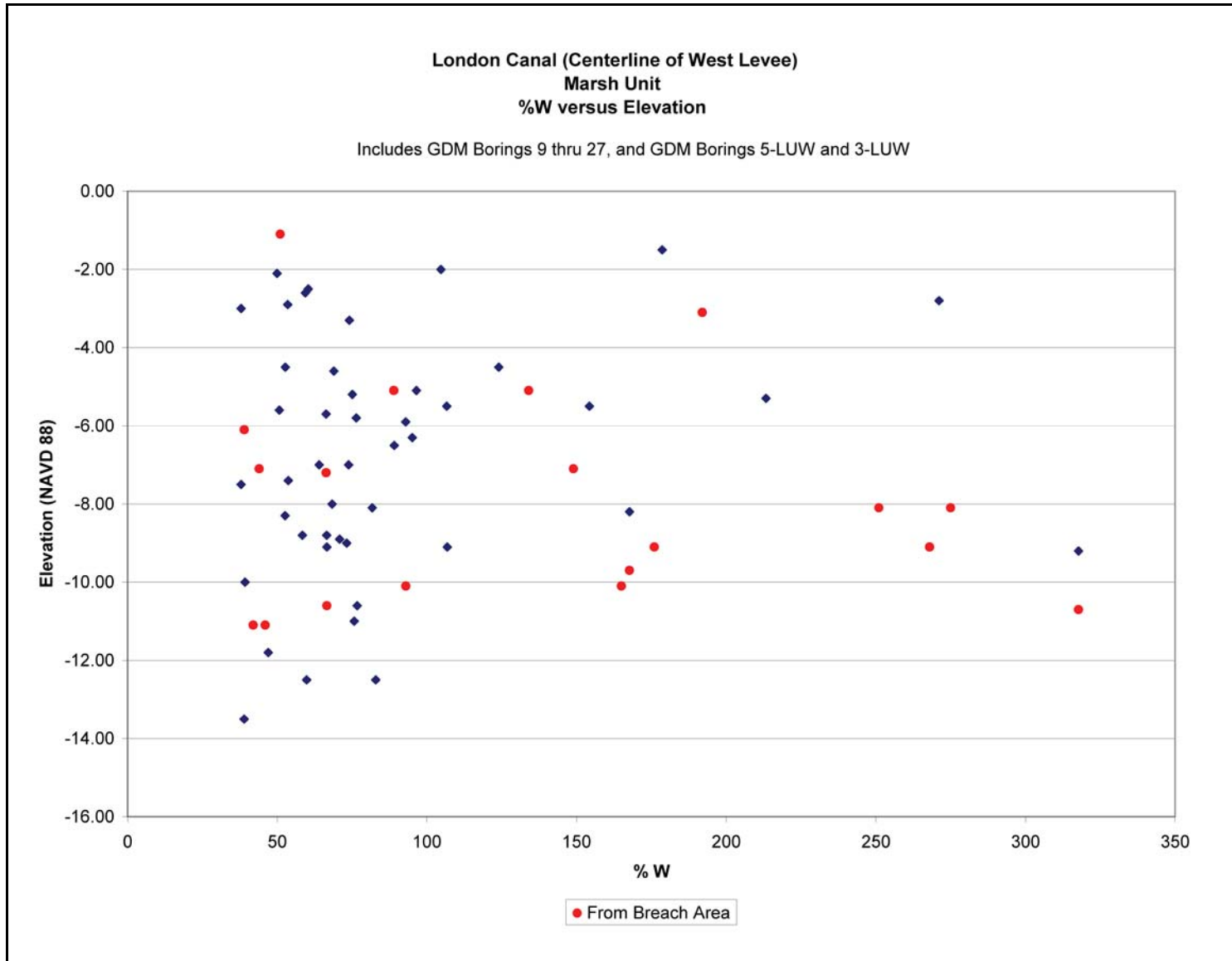


Figure 7-19. London Canal (Centerline of West Levee), Marsh Unit, %w versus Elevation

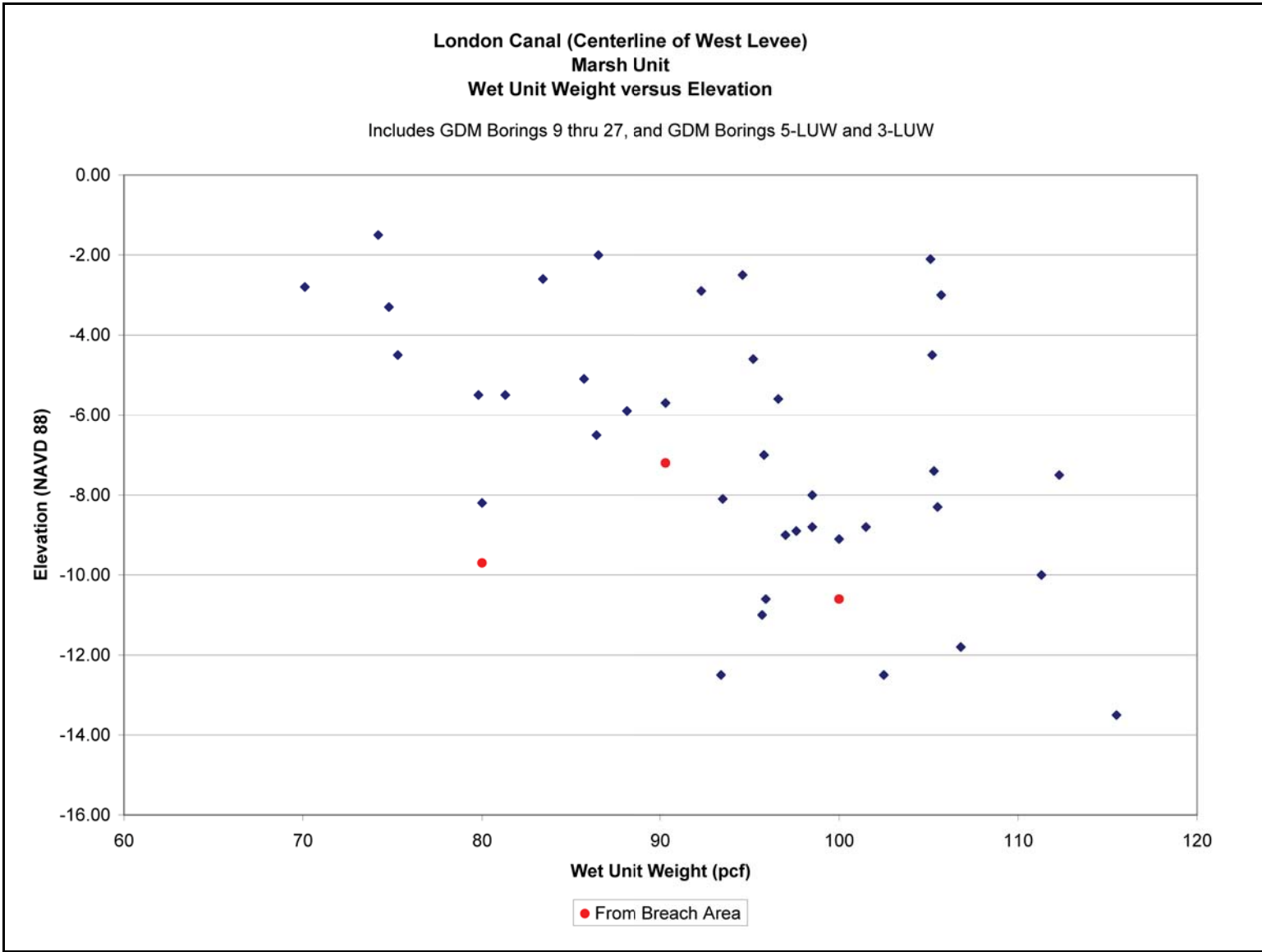


Figure 7-20. London Canal (Centerline of West Levee), Marsh Unit, Wet Unit Weight versus Elevation

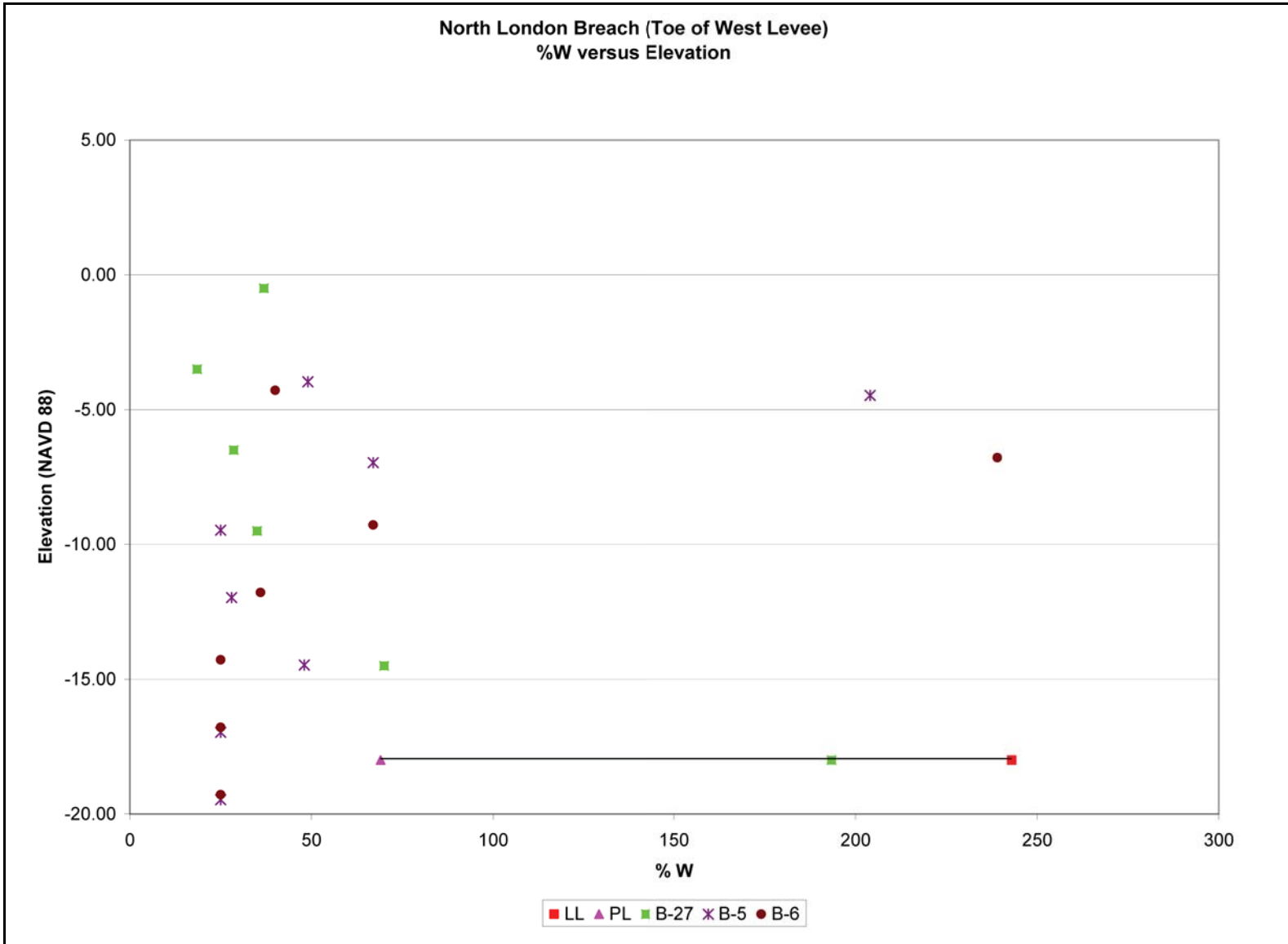


Figure 7-21. North London Breach (Toe of West Levee), %w versus Elevation

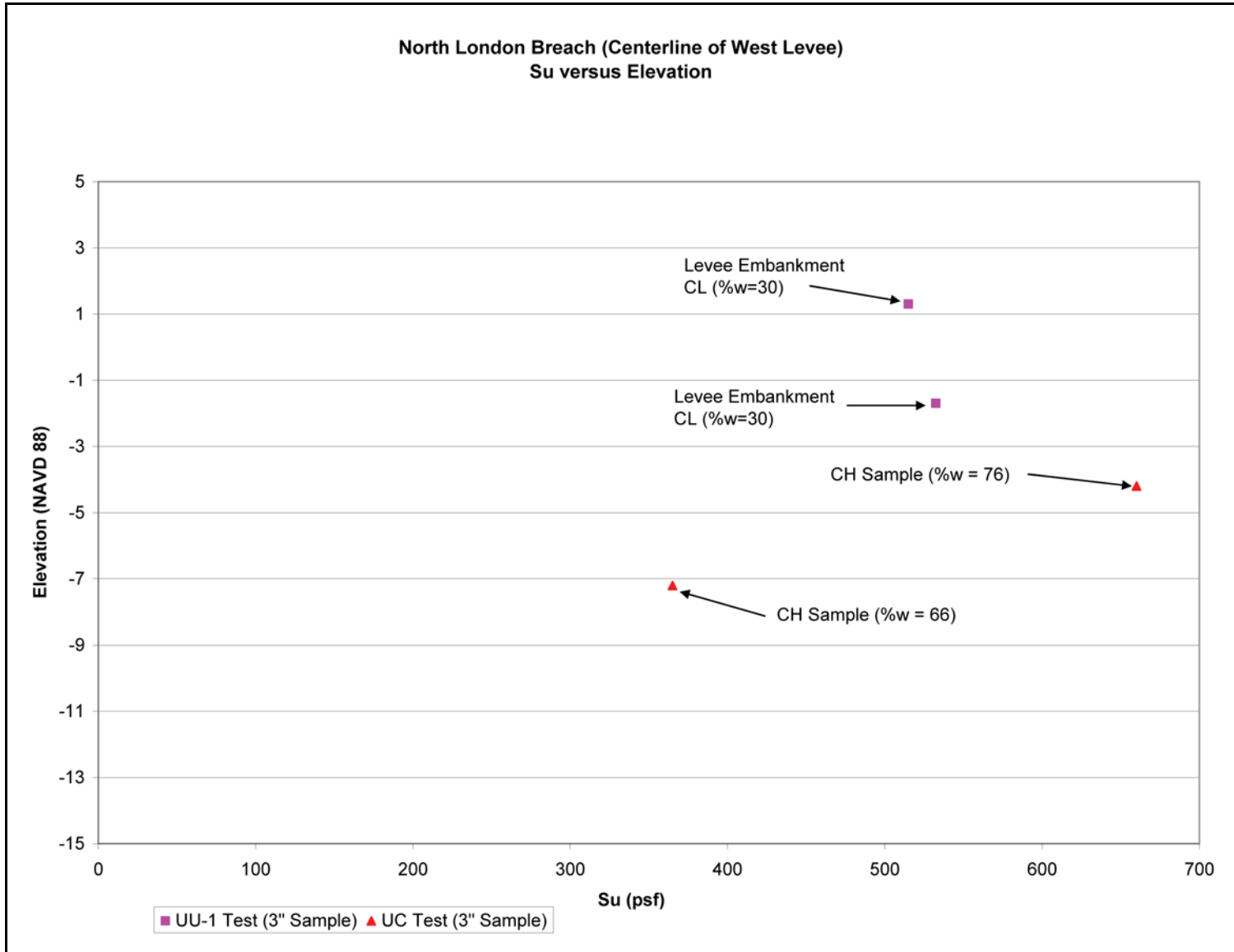


Figure 7-22. North London Breach (Centerline of West Levee), Su versus Elevation

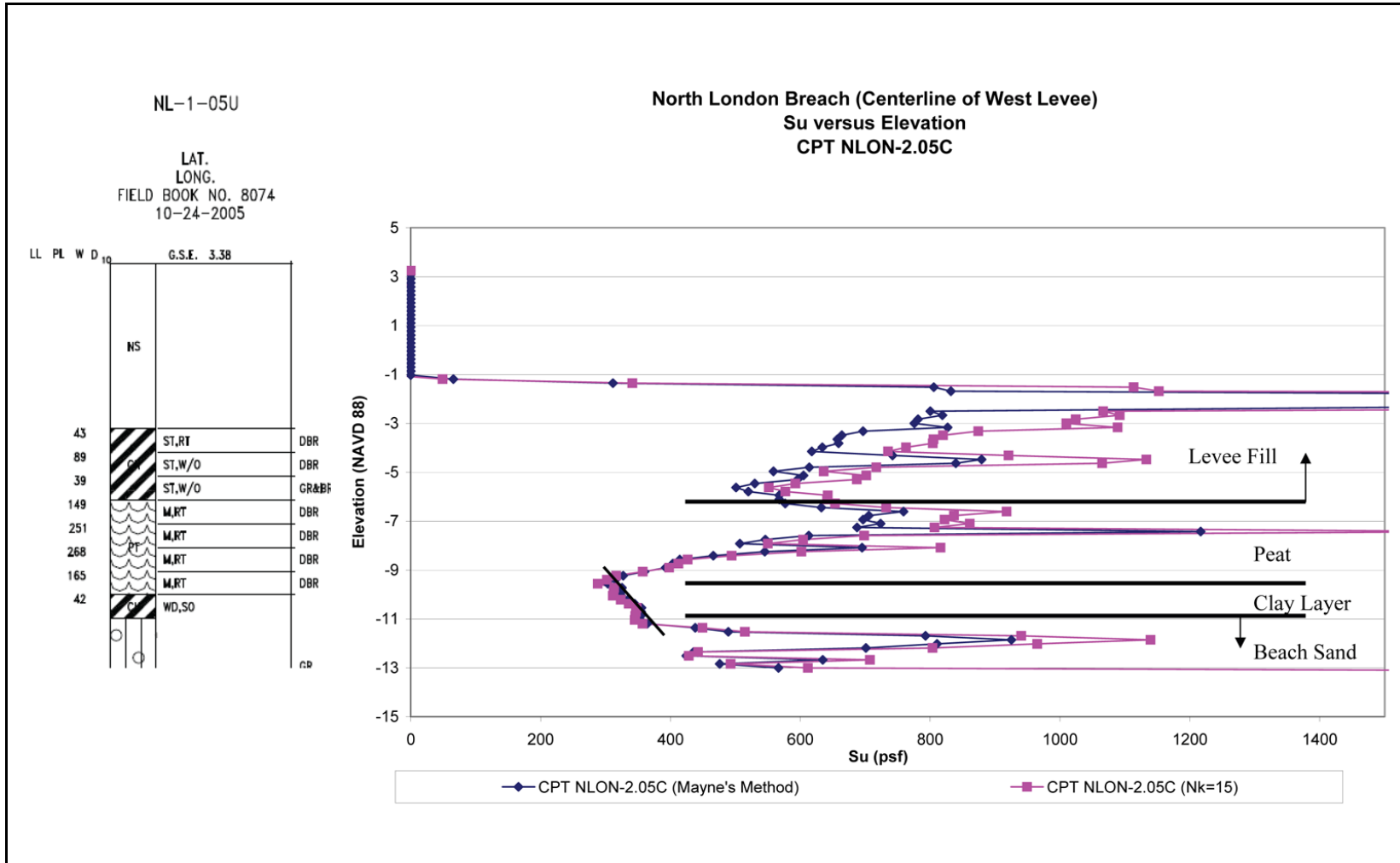


Figure 7-23. North London Breach (Centerline of West Levee), Su versus Elevation for CPT NLON-2.05C

Shear strength plots of CPT N10N-10.05C, using the bearing capacity method ($N_k=15$) and Mayne's method, are shown in Figure 7-24. However, an increase in strength per depth was not detected in the clay layer at the top of the beach sand. The shear strength versus elevation for both CPTs and laboratory test data is shown in Figure 7-25. Mayne's method was used to compute the shear strengths in this figure.

Shear strengths from laboratory tests of the marsh unit at the toe of the levee are shown in Figure 7-26. In addition, shear strength plots of laboratory tests and CPT data are shown in Figure 7-27. Because of equipment difficulties, CPT N14a-14a.05C was only pushed to a depth of 28 ft with pore pressure measurements. The CPT was pushed again to a depth of 80 ft, but no pore measurements were taken. Below is a table summarizing the available laboratory shear strength data from the toe.

Boring	Elevation (NAVD 88)	Soil Type	%w	UC Test (psf)	UU Test (psf)
6	-4.28	CH	40	540	
6	-6.78	CH	239	700	
5	-6.97	CH	204	220	
6	-9.28	CH	67	200	
5	-9.47	CH	67	110	
6	-11.78	CL	36		220
27	-14.50	Clay	70	517.5	
27	-18.00	Organic Clay	193.4	470	
27	-22.00	Organic Clay	149.2	230	

Gradation and Standard Penetration Number for Beach Sand Unit

A plot of the D_{10} , D_{30} , and D_{60} values for the Beach Sand Unit is shown on Figure 7-28. These values consist of gradation tests conducted on samples from borings B-5 and B-6. A summary of these values are presented in the table below.

Boring	Elevation (NAVD 88)	Soil Type	D_{60} (mm)	D_{30} (mm)	D_{10} (mm)
5	-14.47	SM	0.21	0.175	
6	-16.78	SM	0.22	0.18	0.16
5	-19.47	SM	0.205	0.175	0.12
6	-21.78	SM	0.225	0.18	0.125
5	-24.47	SM	0.185	0.15	0.085
6	-26.78	SM	0.18	0.125	0.08
5	-29.47	SM	0.2	0.18	0.125
6	-32.78	SM	0.145	0.096	0.075
5	-34.47	SM	0.205	0.18	0.17
6	-36.78	SM	0.18	0.105	
6	-41.78	SM	0.2	0.175	0.095

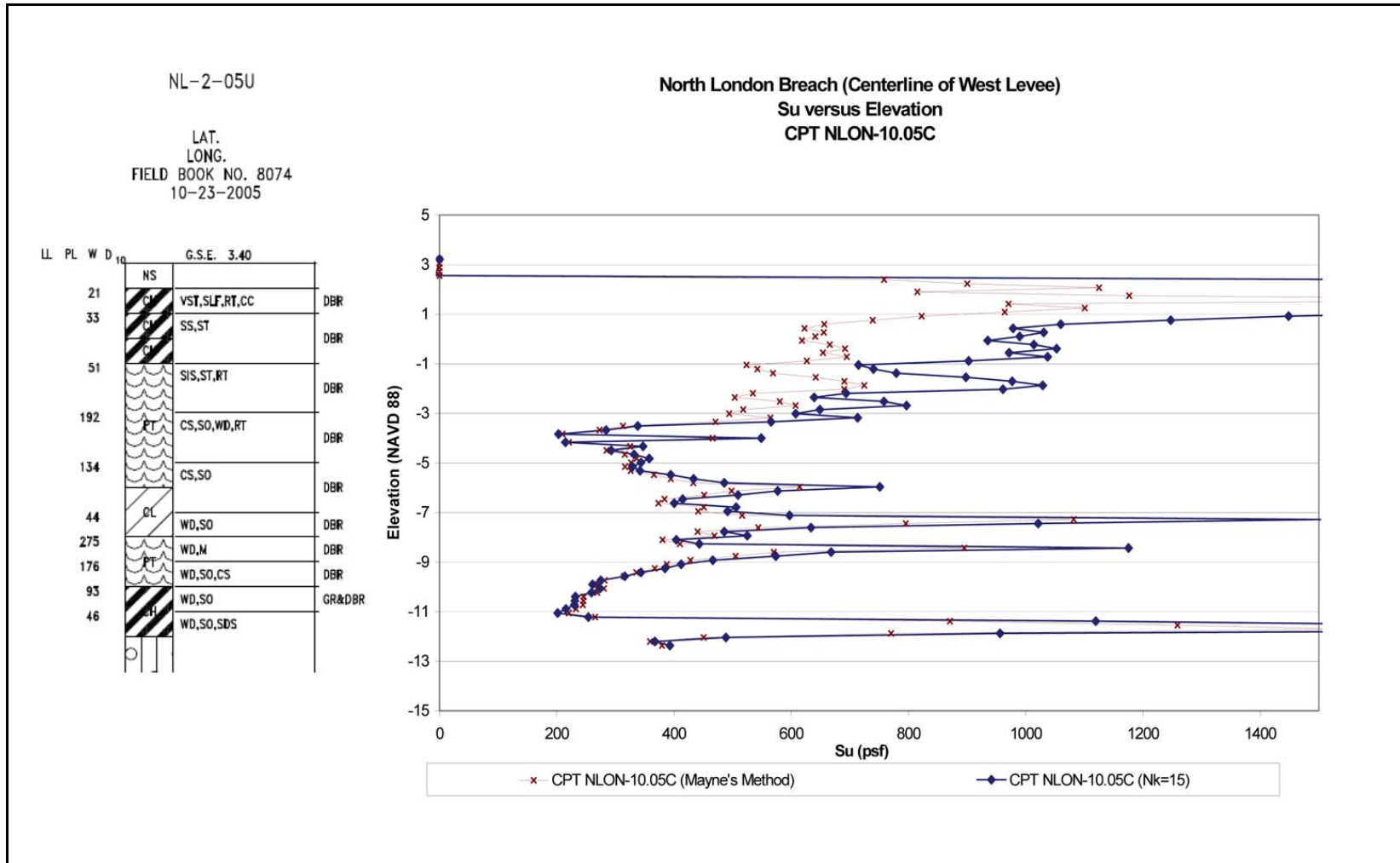


Figure 7-24. North London Breach (Centerline of West Levee), Su versus Elevation for CPT NLON-10.05C

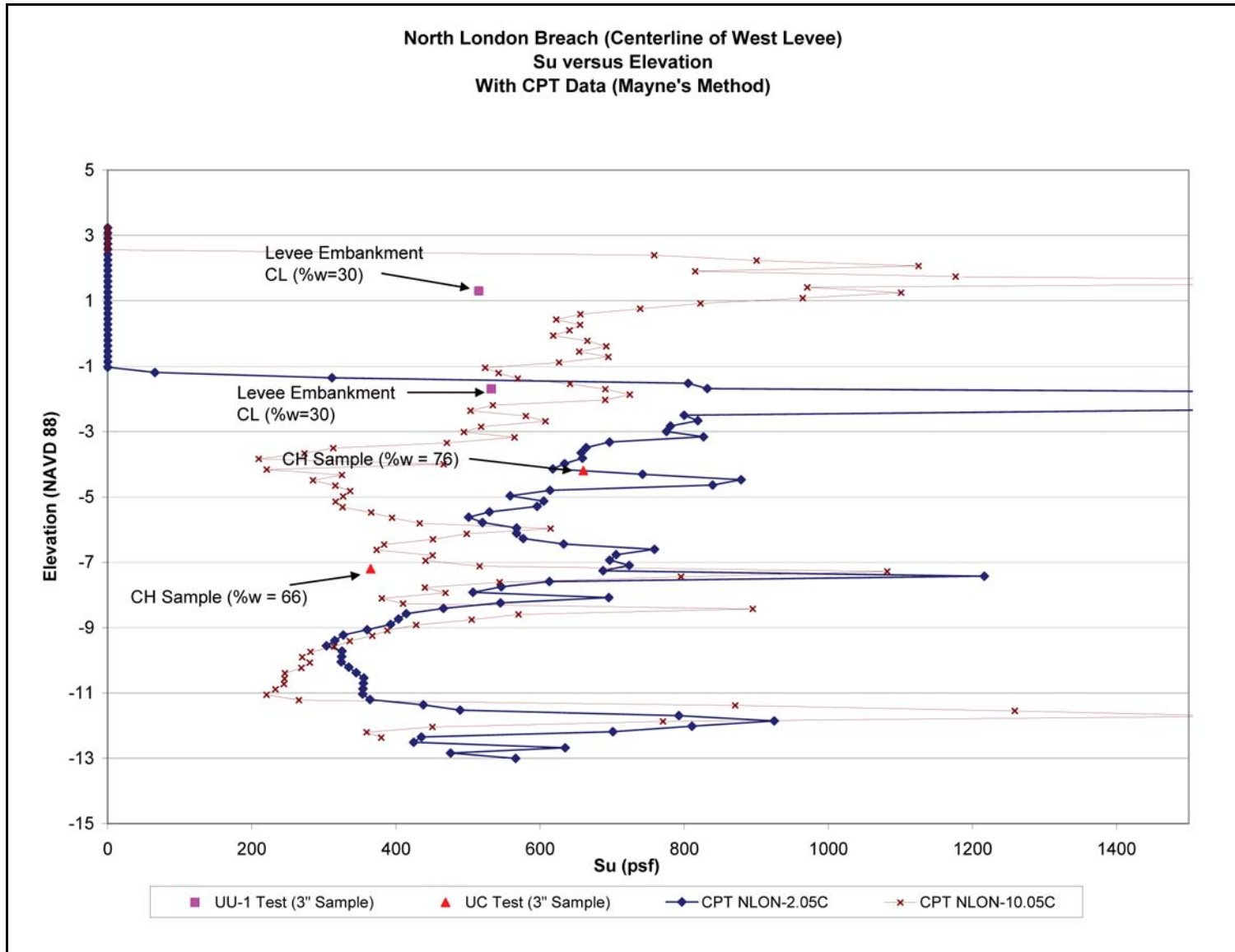


Figure 7-25. North London Breach (Centerline of West Levee), Su versus Elevation with CPT Data

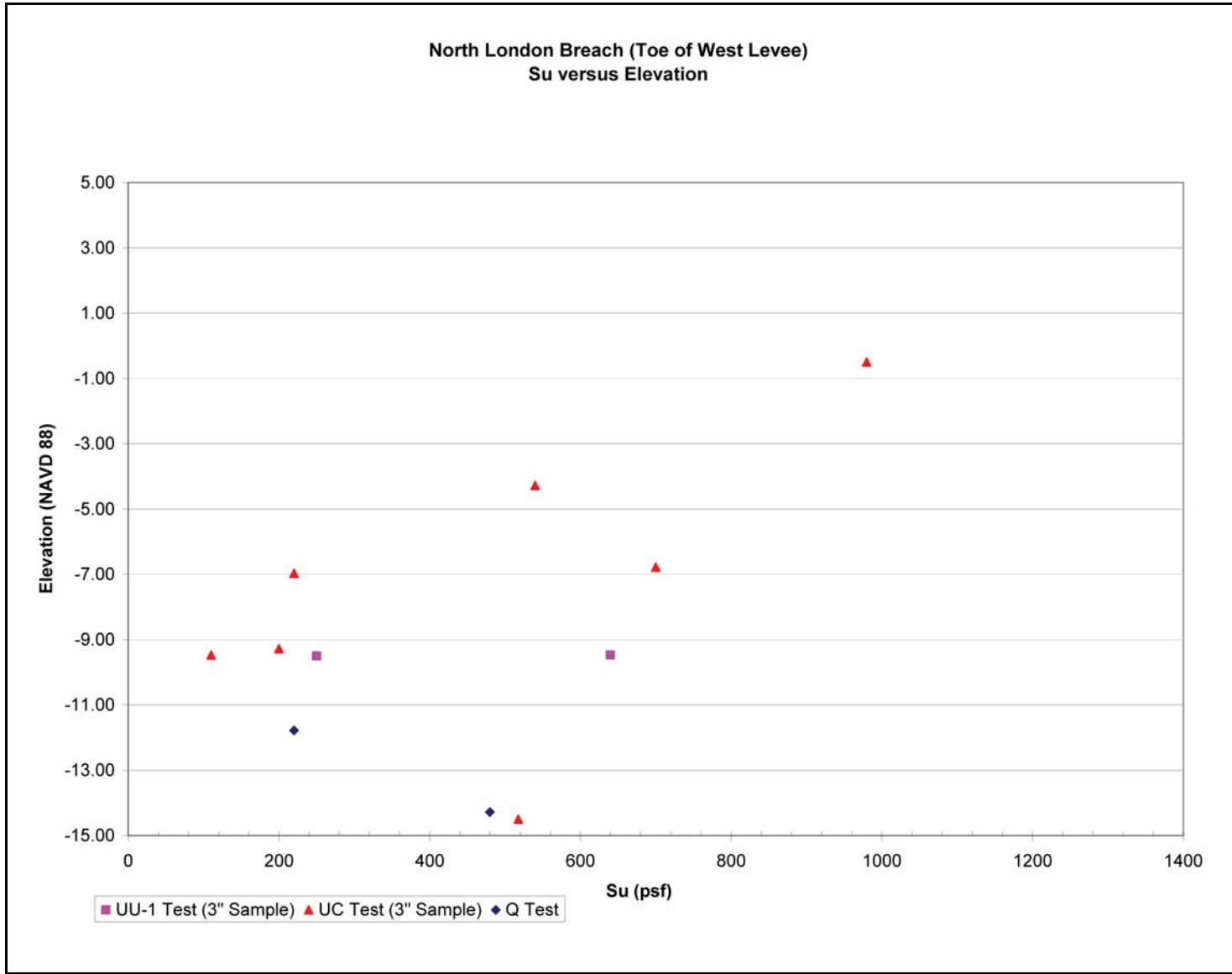


Figure 7-26. North London Breach (Toe of West Levee), Su versus Elevation

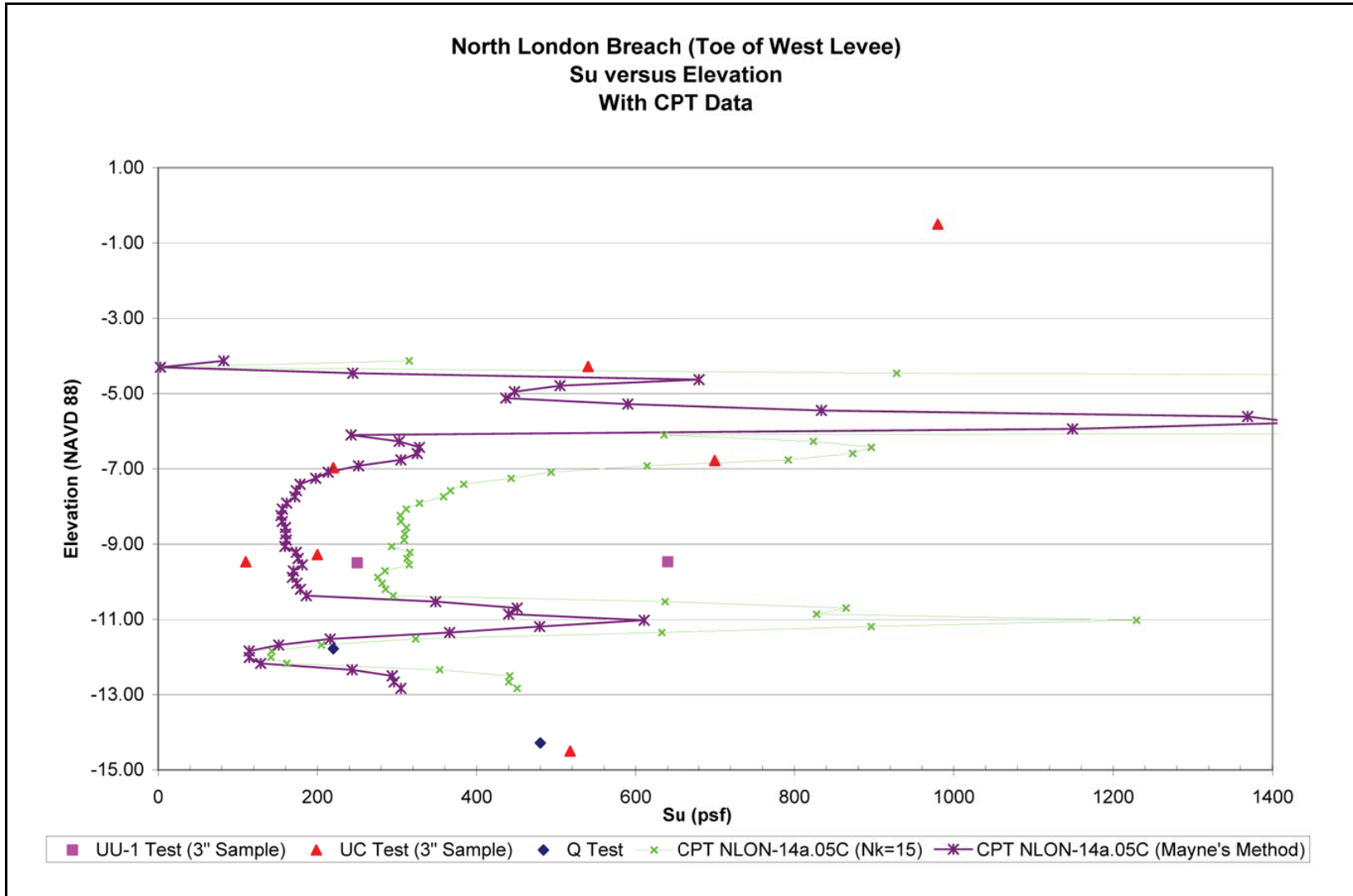


Figure 7-27. North London Breach (Toe of West Levee), S_u versus Elevation with CPT Data

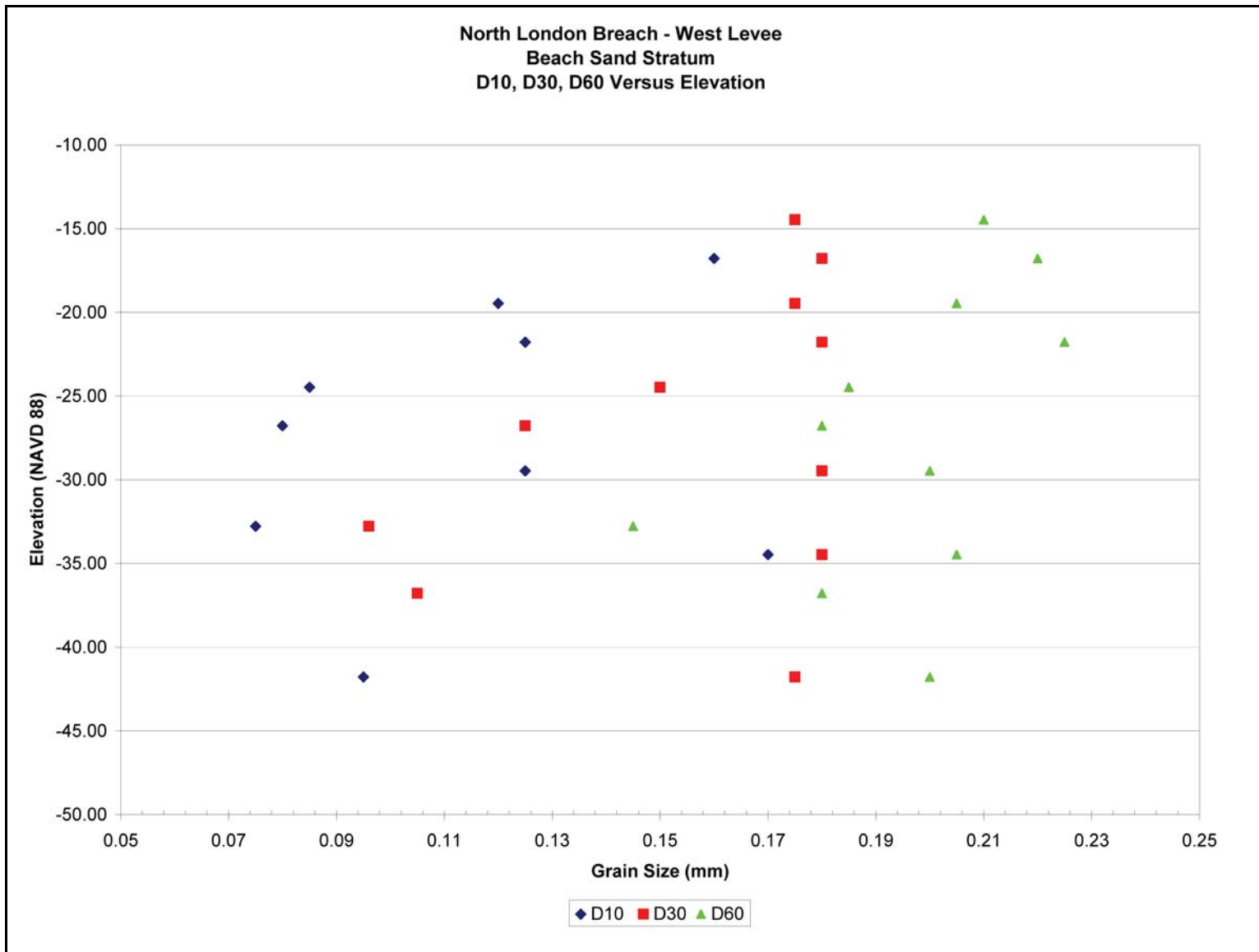


Figure 7-28. North London Breach (Beach Sand Stratum), D10, D30, and D60 versus Elevation

Figure 7-29 shows the $N_{1(60)}$ values of the beach sand under the levee determined from the CPTs. Figure 7-30 shows the $N_{(60)}$ values of the beach sand under the levee determined from the CPTs. In addition, standard penetration tests (SPT) were conducted for GDM borings B-26 and 5-LUW. However, the hammer efficiency is unknown for these borings. The blow counts are shown on Figure 7-30, and they are a fairly good comparison to the CPTs.

Figure 7-31 shows the $N_{1(60)}$ values of the beach sand at the toe of the levee determined from the CPTs. Figure 7-32 shows the $N_{(60)}$ values of the beach sand at the toe of the levee determined from the CPTs. In addition, SPTs were conducted for borings B-5 and B-6. Furthermore, the hammer efficiency is unknown for these borings, but the blow counts are also shown on Figure 7-32, and they are a fairly good comparison to the CPTs.

Pore Pressure Dissipation Tests

Pore pressure dissipation tests were conducted in the beach sand unit at CPTs NLON-2.05C, NLON-10.05c, and NLON-14a.05C. The dissipation tests with the CPTs basically consist of recording the pore pressures at a depth until the pore pressure stabilize to a constant pressure. With pervious materials such as sand, these pressures stabilize fairly quickly. The stabilized values can be assumed to be the actual pore pressure in the sand at the particular depth of the test. Below is a table summarizing the results of the dissipation tests.

CPT	London Canal Staff Gauge Reading (NAVD 88)	Dissipation Test Elevation (NAVD 88)	Stabilized Pressure (psi)	Computed Head (ft) (Stab. Pressure x 2.31 ft/psi)	Head Elevation (NAVD 88)
NLON-2.05c	1.04	-27.93	10	23.1	-4.83
NLON-10.05c	1.04	-25.98	9.1	21.02	-4.96
NLON-14.05c	-0.36	-32.02	13.2	30.49	-1.529

Distressed Area – Opposite of North Breach Site on East Levee

Borings in the distressed area consist of only two GDM borings (B-60, and B-61), one new boring (NL-3-05U), and four CPTUs (CP-1 through CP-4). All data are from the centerline of the levee. The boring profiles, NL-3-05U, B-60, and B-61, are shown in Figures 7-33 thru 7-35, respectively. Some of the New Orleans District personnel have stated that a slide on the canal side of the levee in this area had occurred in the past. Repairs of the area may have caused the area to have different soil conditions than adjacent levee sections. However, the exact date of this occurrence is unknown at this time, but there are efforts to obtain more information about the incident and how it was reported. For reference, the GDM borings were taken in December 1985.

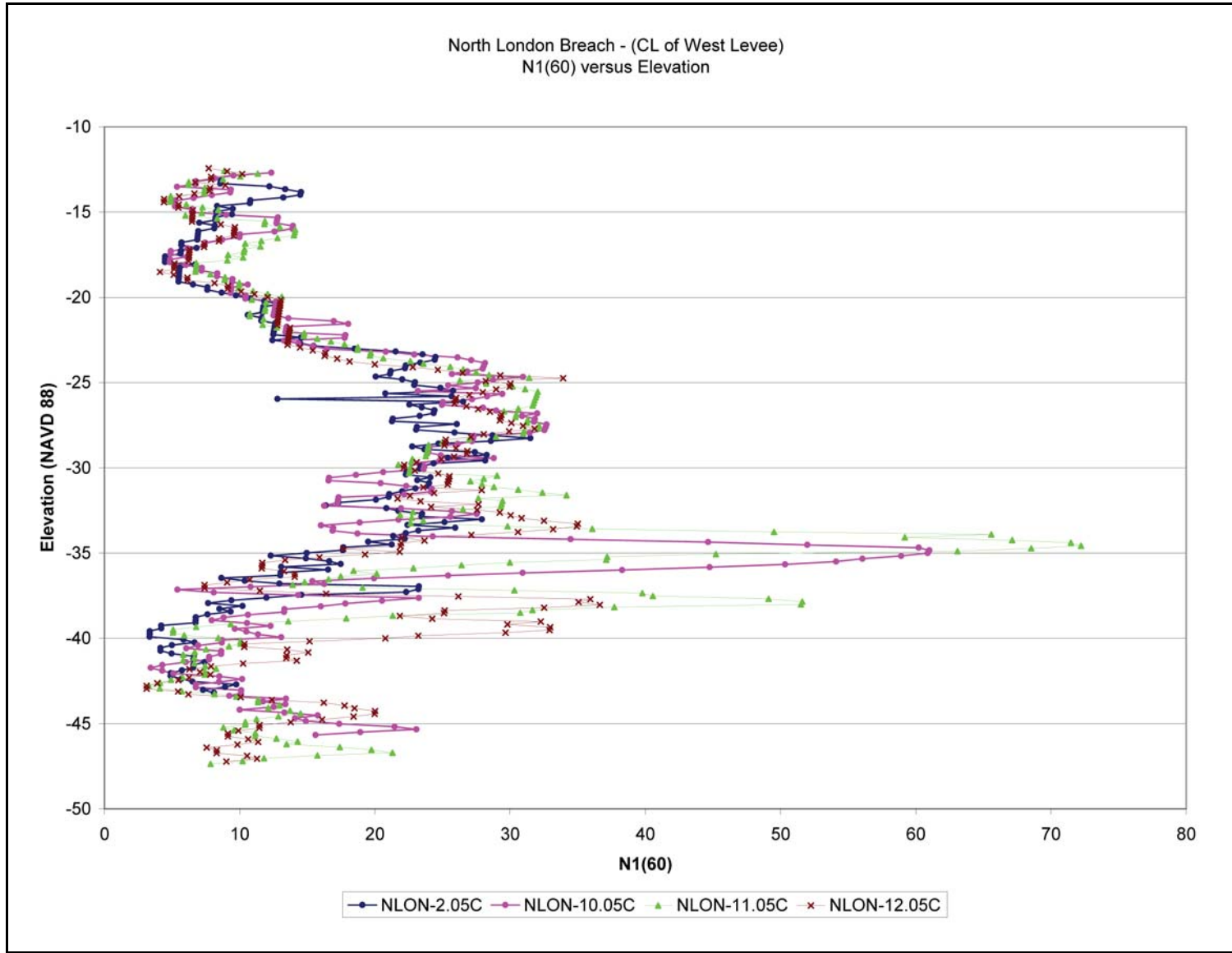


Figure 7-29. North London Breach – Beach Sand Stratum (Centerline of West Levee), N1(60) versus Elevation

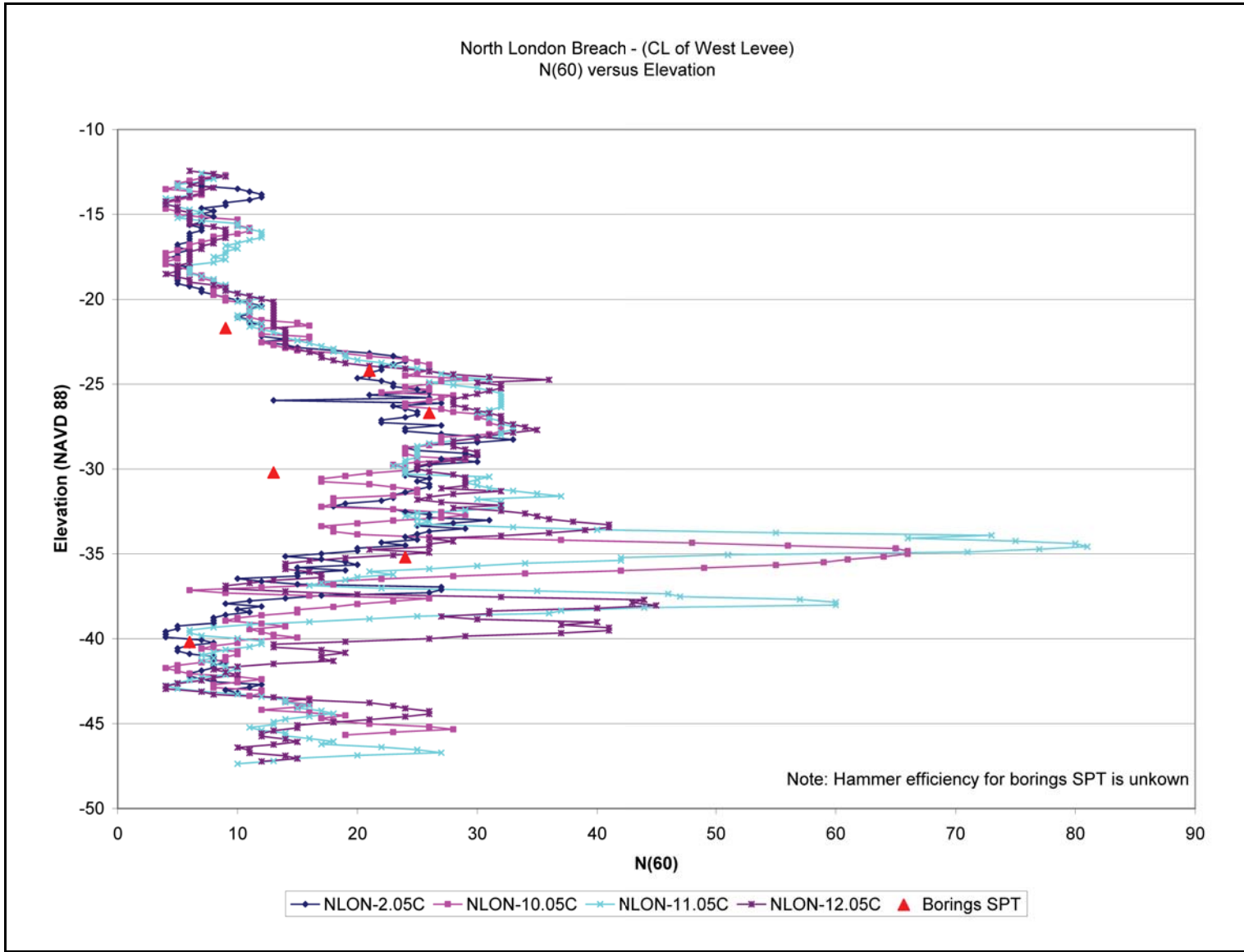


Figure 7-30. North London Breach – Beach Sand Stratum (Centerline of West Levee), N(60) versus Elevation

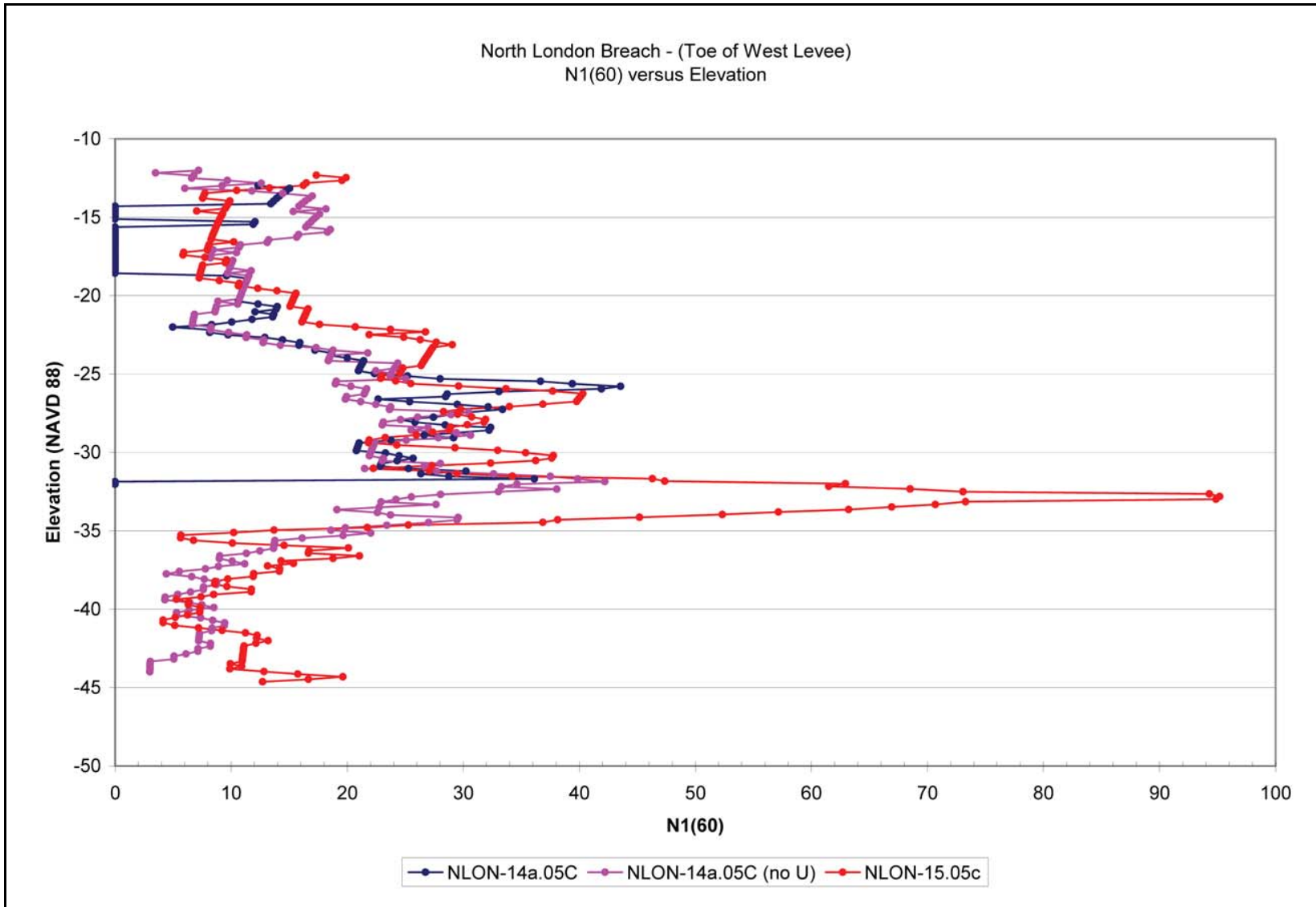


Figure 7-31. North London Breach – Beach Sand Stratum (Toe of West Levee), N1(60) versus Elevation

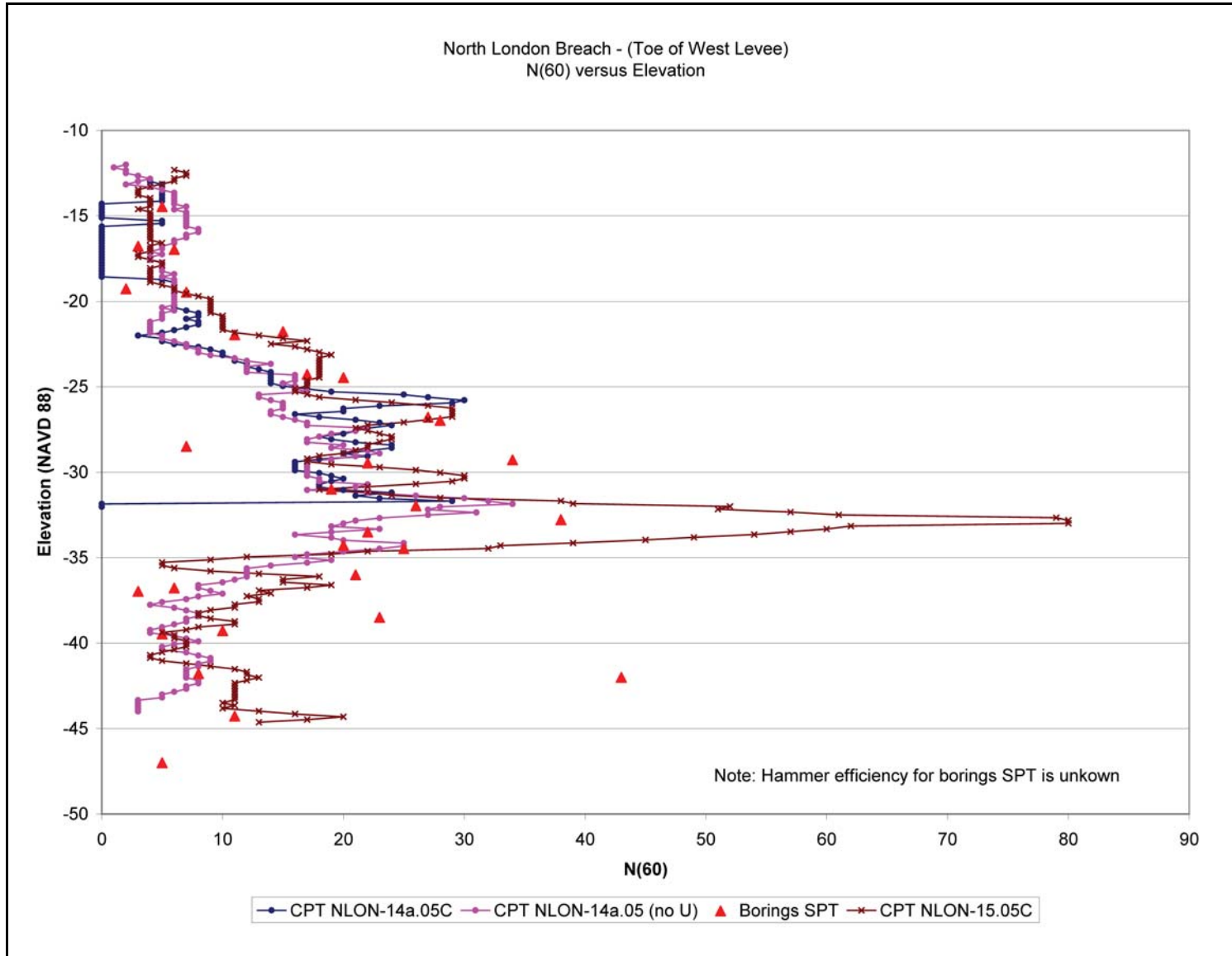


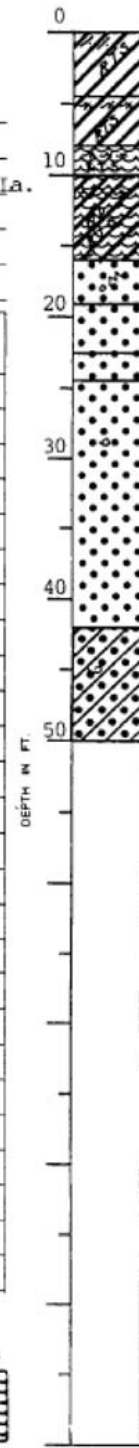
Figure 7-32. North London Breach – Beach Sand Stratum (Toe of West Levee), N(60) versus Elevation

LOG OF BORING
EUSTIS ENGINEERING COMPANY
 SOIL AND FOUNDATION CONSULTANTS
 METAIRIE, LA.

Name of Project: London Avenue Canal, Levee and Floodwall Improvements
Orleans Levee Board Project No. 2049-0269, New Orleans, Louisiana
 For: The Board of Levee Commissioners of the Orleans Levee District, New Orleans, La.
Burk & Associates, Inc., New Orleans, Louisiana

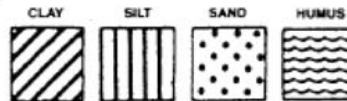
Boring No. 60 Soil Technician A. J. Maveux Date 7 December 1985
 Ground Elev. 3.50 Datum NGVD Gr. Water Depth See Text

Sample No.	SAMPLE Depth - Feet		DEPTH STRATUM Feet		VISUAL CLASSIFICATION	STANDARD PENETRATION TEST	
	From	To	From	To			
1	2.0	2.5	0.0	4.5	Stiff brown & gray clay w/clayey sand pockets & roots		
2	5.0	5.5	4.5	8.0	Soft gray & tan clay w/organic clay layers & roots		
3	8.0	8.5	8.0	10.0	Extremely soft brown humus w/organic clay layers & roots		
4	11.0	11.5	10.0	16.0	Soft brown organic clay w/humus layers, wood & roots		
5	17.0	17.5	16.0	19.0	Very loose gray sand w/organic matter		
6	20.0	21.5	19.0	22.5	Very loose gray sand	1	2
7	22.5	24.0	22.5	24.5	Loose gray sand	1	6
8	25.0	26.5	24.5		Medium dense gray sand w/shell fragments	2	11
9	28.5	30.0			Ditto	2	14
10	33.5	35.0			Ditto	2	11
11	38.5	40.0		42.0	Ditto	5	13
12	43.5	45.0	42.0		Very loose gray clayey sand w/shell fragments	0	2
13	49.0	49.5		50.0	Ditto		



*Number in first column indicates number of blows of 140-lb. hammer dropped 30 in. required to seat 2-in. O. D. split spoon sampler 6 in. Number in second column indicates number of blows of 140-lb. hammer dropped 30 in. required to drive 2-in. O. D. split spoon sampler 1 ft. after seating 6 in.
 WHILE THIS LOG OF BORING IS CONSIDERED TO BE REPRESENTATIVE OF SUBSURFACE CONDITIONS AT ITS RESPECTIVE LOCATION ON THE DATE SHOWN, IT IS NOT WARRANTED THAT IT IS REPRESENTATIVE OF SUBSURFACE CONDITIONS AT OTHER LOCATIONS AND TIMES.

Remarks: _____



Predominant type shown heavy. Modifying type shown light.

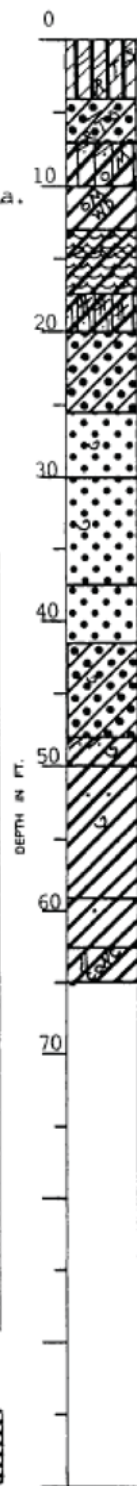
Figure 7-34. Boring B-60 – Boring Log

LOG OF BORING
EUSTIS ENGINEERING COMPANY Sheet 1 of 2
 SOIL AND FOUNDATION CONSULTANTS
 METAIRIE, LA.

Name of Project: London Avenue Canal, Levee and Floodwall Improvements
Orleans Levee Board Project No. 2049-0269, New Orleans, Louisiana
 For: The Board of Levee Commissioners of the Orleans Levee District, New Orleans, La.
Burk & Associates, Inc., New Orleans, Louisiana

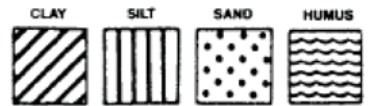
Boring No. 61 Soil Technician A. J. Mayeux Date 10 December 1985
 Ground Elev. 3.50 Datum NGVD Gr. Water Depth See Text

Sample No.	SAMPLE Depth - Feet		DEPTH STRATUM Feet		VISUAL CLASSIFICATION	STANDARD PENETRATION TEST	
	From	To	From	To			
1	2.0	2.5	0.0	4.0	Very compact tan & gray clayey silt w/clay pockets & roots		
2	5.0	5.5	4.0	7.0	Dense tan & gray clayey sand w/clay lenses & roots		
3	8.0	8.5	7.0	10.0	Soft gray silty clay w/clayey sand pockets & trace of organic matter		
4	11.0	11.5	10.0	13.0	Medium stiff dark gray clay w/organic matter & wood		
5	14.0	14.5	13.0	17.5	Stiff brown organic clay w/humus layers		
6	19.0	19.5	17.5	20.0	Soft gray silty clay w/alternating clayey silt & sandy silt layers		
7	20.0	21.5	20.0		Very loose gray clayey sand	1	4
8	22.5	24.0		25.5	Ditto	0	2
9	25.0	26.5	25.5		Loose gray sand w/shell fragments	1	7
10	28.5	30.0		30.0	Ditto	2	10
11	33.5	35.0	30.0	37.5	Medium dense gray sand w/shell fragments	4	15
12	38.5	40.0	37.5	41.5	Dense gray sand	6	34
13	43.5	45.0	41.5	48.0	Loose gray clayey sand w/shell fragments	1	4
14	49.0	49.5	48.0	50.0	Soft gray clay w/clayey sand pockets & shell fragments		
15	54.0	54.5	50.0	59.0	Medium stiff gray clay w/sand pockets & & shell fragments		
16	59.0	59.5	59.0	62.5	Stiff greenish-gray & tan clay w/trace of sand		



*Number in first column indicates number of blows of 140-lb. hammer dropped 30 in. required to seat 2-in. O. D. split spoon sampler 6 in. Number in second column indicates number of blows of 140-lb. hammer dropped 30 in. required to drive 2-in. O. D. split spoon sampler 1 ft. after seating 6 in.
 WHILE THIS LOG OF BORING IS CONSIDERED TO BE REPRESENTATIVE OF SUBSURFACE CONDITIONS AT ITS RESPECTIVE LOCATION ON THE DATE SHOWN, IT IS NOT WARRANTED THAT IT IS REPRESENTATIVE OF SUBSURFACE CONDITIONS AT OTHER LOCATIONS AND TIMES.

Remarks: _____



Predominant type shown heavy. Modifying type shown light.

Figure 7-35. Boring B-61 – Boring Log

Moisture Content and Unit Weights

Moisture contents (%w) and wet unit weights for samples taken from the levee centerline above the beach sand are shown in the table below.

Boring	Elevation (NAVD 88)	Soil Type	%w	Dry Unit Weight (pcf)	Wet Unit Weight (pcf)
B-60	1.50	Clay	34	86.1	115.4
B-61	1.5	Clayey Silt	17.5	104.9	123.2
B-60	-1.50	Clay	62.9	59.6	97.1
B-61	-1.5	Clayey Sand	17	101.5	118.7
B-60	-4.50	Humus	296.4	18	71.5
B-61	-4.5	Silty Clay	39.6	79.3	110.7
B-61	-7.5	Clay	78.5	52.4	93.5
B-61	-10.5	Organic Clay	240.1	20	68.2
B-61	-15.5	Silty Clay	26.7	98.5	124.8

Shear Strength

Shear strengths from laboratory tests of the levee embankment from the GDM borings are shown in the table below.

Boring	Elevation (NAVD 88)	Soil Type	%w	S_u UC Test (psf)	S_u UU-1 Test (psf)
B-60	1.5	Clay	34	1080	
B-60	-1.5	Clay	62.9	455	
B-60	-4.5	Humus	296.4	97.5	
B-61	1.5	Clayey Silt	17.5		1595
B-61	-1.5	Clayey Sand	17		1012.5
B-61	-4.5	Silty Clay	39.6	337.5	
B-61	-7.5	Clay	78.5	587.5	
B-61	-10.5	Organic Clay	240.1	1860	
B-61	-15.5	Silty Clay	26.7	277.5	

Interpretation of the undrained shear strengths (using Mayne's method) of the material above the beach sand unit for CPTs CP-1 and CP-2 is shown in Figure 7-36. Also, plotted in Figure 7-36 is the shear strengths shown in Table 7-9. The shear strength plot for CP-1 shows a potential void at elevation -9 (NAVD 88). However, this void was not detected in CP-2.

Furthermore, interpretation of the undrained shear strengths for CPTs CP-3 and CP-4 is shown in Figure 7-37. CPT CP-3 shows a potential sand pocket at elevation -6.5 (NAVD 88) and CPT CP-4 also shows a potential sand pocket at elevation -4.5. Similar to CP-2, a potential void was detected in CP-4 at elevation -5.

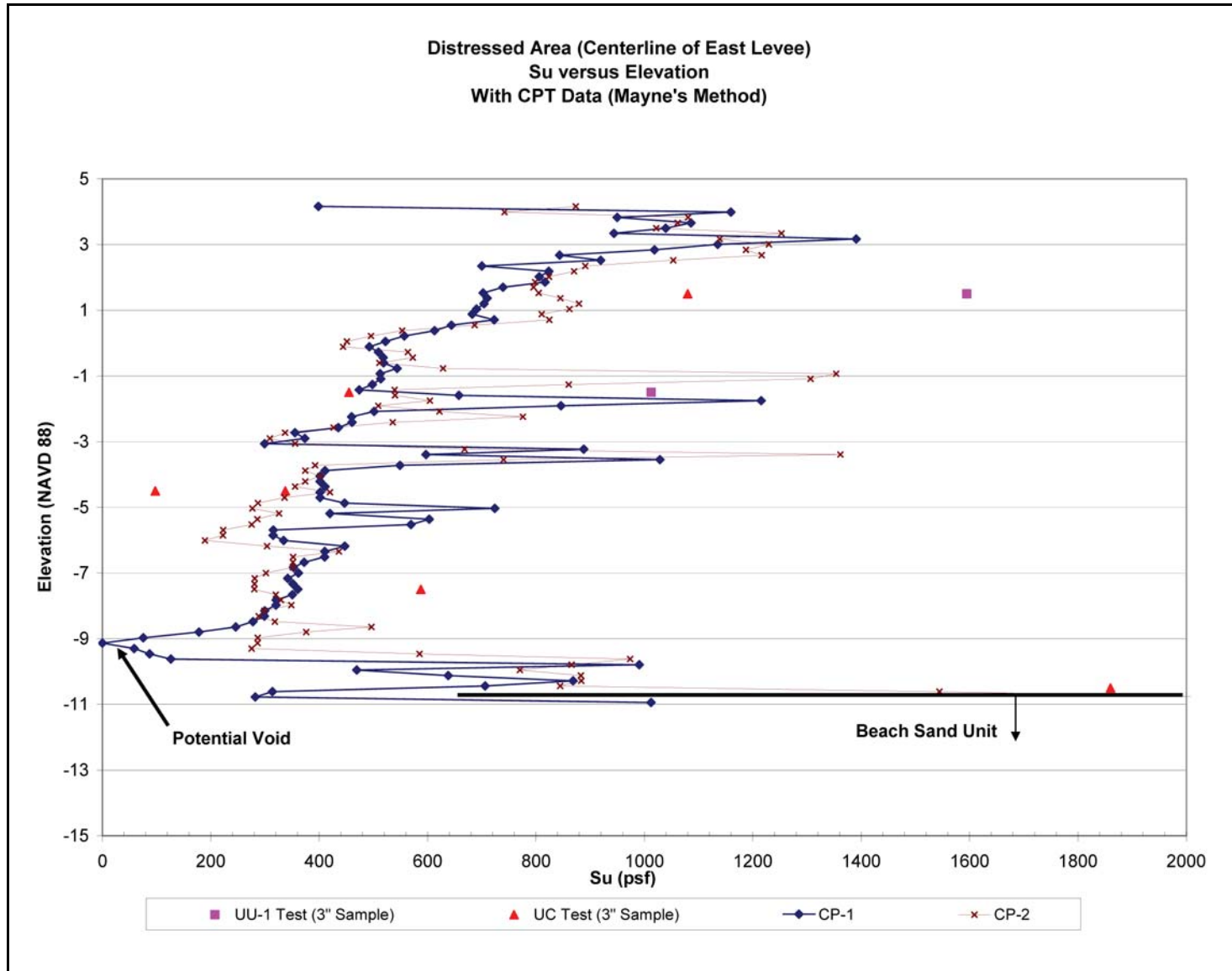


Figure 7-36. Distressed Area (Centerline of East Levee), Su versus Elevation with CPTs CP-1 and CP-2

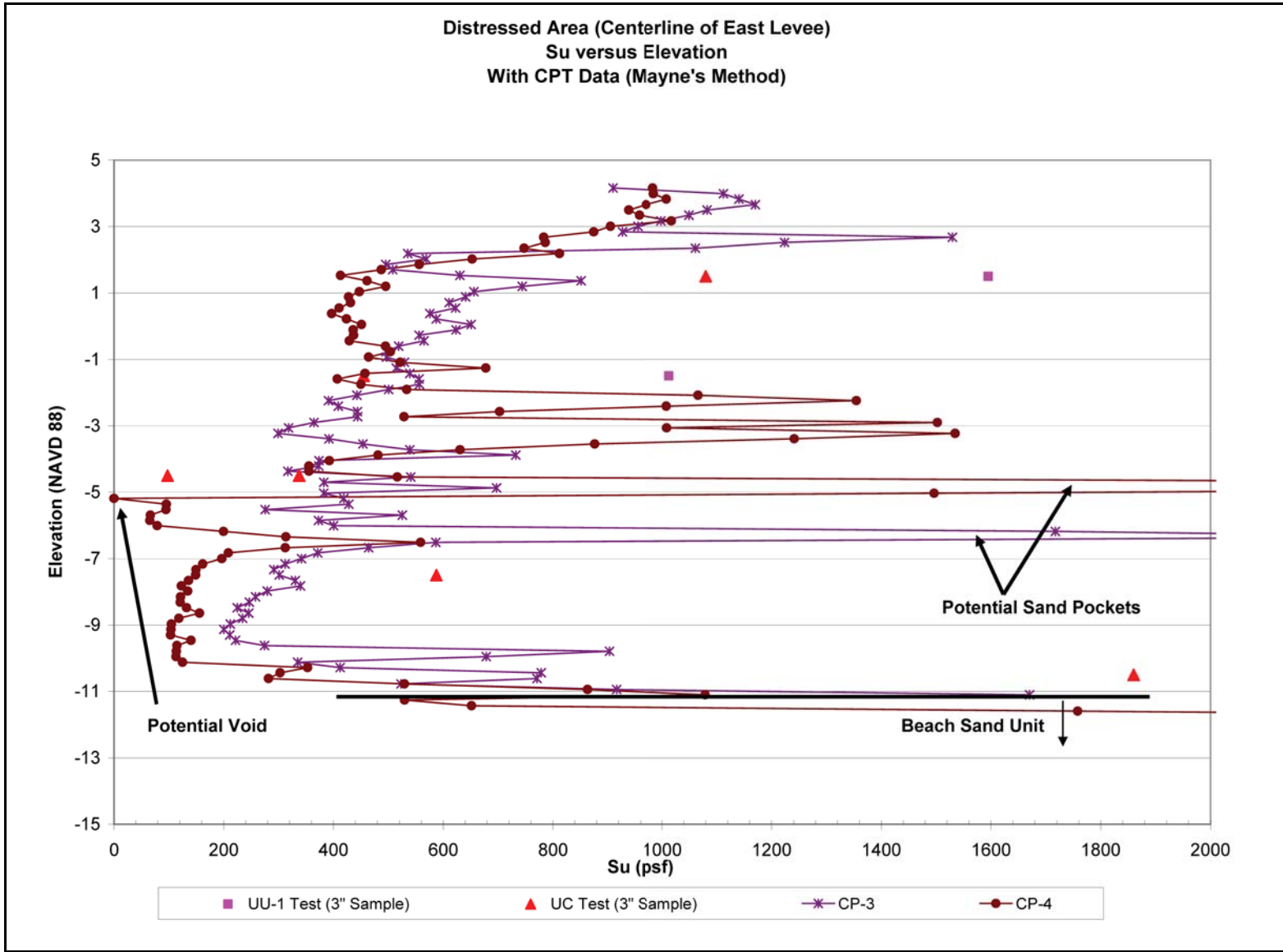


Figure 7-37. Distressed Area (Centerline of East Levee), Su versus Elevation with CPTs CP-1 and CP-2

Gradation and Standard Penetration Number for Beach Sand Unit

No gradation tests have been conducted in this area. However, SPTs were conducted in borings B-60 and B-61. The hammer efficiency is unknown for these borings, but the blow counts were also shown in Figures 7-39 and 7-40. Furthermore, $N_{1(60)}$ and $N_{(60)}$ values can be determined from the CPTs. The $N_{1(60)}$ values for CP-1 and CP-2 are shown on Figure 7-38. In addition, the $N_{(60)}$ values for CP-1 and CP-2 are plotted with the SPTs from the borings in Figure 7-39. This was repeated for CP-3 and CP-4, and Figures 7-40 and 7-41 were produced. The borings' SPT did not correlate well with the $N_{(60)}$ from the CPTs.

The SPTs on the east side show a similar trend as those on the west side.

South Breach Site – East Levee

The data is divided data from the centerline of the levee and from the toe of the levee. Borings from the centerline of the levee include three borings from the GDM (B-50, B-51, and B-52). GDM borings used 3-in.-diameter undisturbed samples. GDM boring B-51 was taken closest to the breach area. The boring log for this boring is shown in Figure 7-42.

Data from the toe of the levee include two new borings, and five CPTs. The new borings include LAC-1G (3-in.-diameter undisturbed samples), LAC-2G (3-in.-diameter undisturbed samples), and SL-1-05U (5-in.-diameter undisturbed samples). The CPTs include SLON-1.05C, SLON-2.05C, SLON-3.05C, and SLON-5.05C. CPT NLON-2.05c was the only CPT taken with pore pressure measurements.

Moisture Content and Unit Weights

Moisture contents (%w) and wet unit weights for samples taken from the levee centerline above the beach sand are shown in the table below.

Boring	Elevation (NAVD 88)	Soil Type	%w	Dry Unit Weight (pcf)	Wet Unit Weight (pcf)
51	3.00	Clay	22.6	90.4	110.8
52	3.00	Clay	35.9	84.3	114.5
51	0.00	Clay	42.6	72.4	103.2
52	0.00	Clay	65.2	59.8	98.7
50	-4.20	Clay	51.6	64.1	97.2
51	-3.00	Clay	52.7	68	103.8
51	-6.00	Clay	75	55.2	96.6
52	-6.00	Clay	164.2	29.1	76.8
50	-6.70	Clay	104.2	41.7	85.2
52	-9.00	Clay	91.2	48.2	92.2
52	-14.00	Clayey Sand	48.1	68.6	101.6
50	-14.20	Clay	84.3	50.6	93.2

Not many data points exist for the marsh unit at the toe of the levee. Table 7-11 shows the moisture contents and the wet unit weights for samples taken from the levee toe in the breach area.

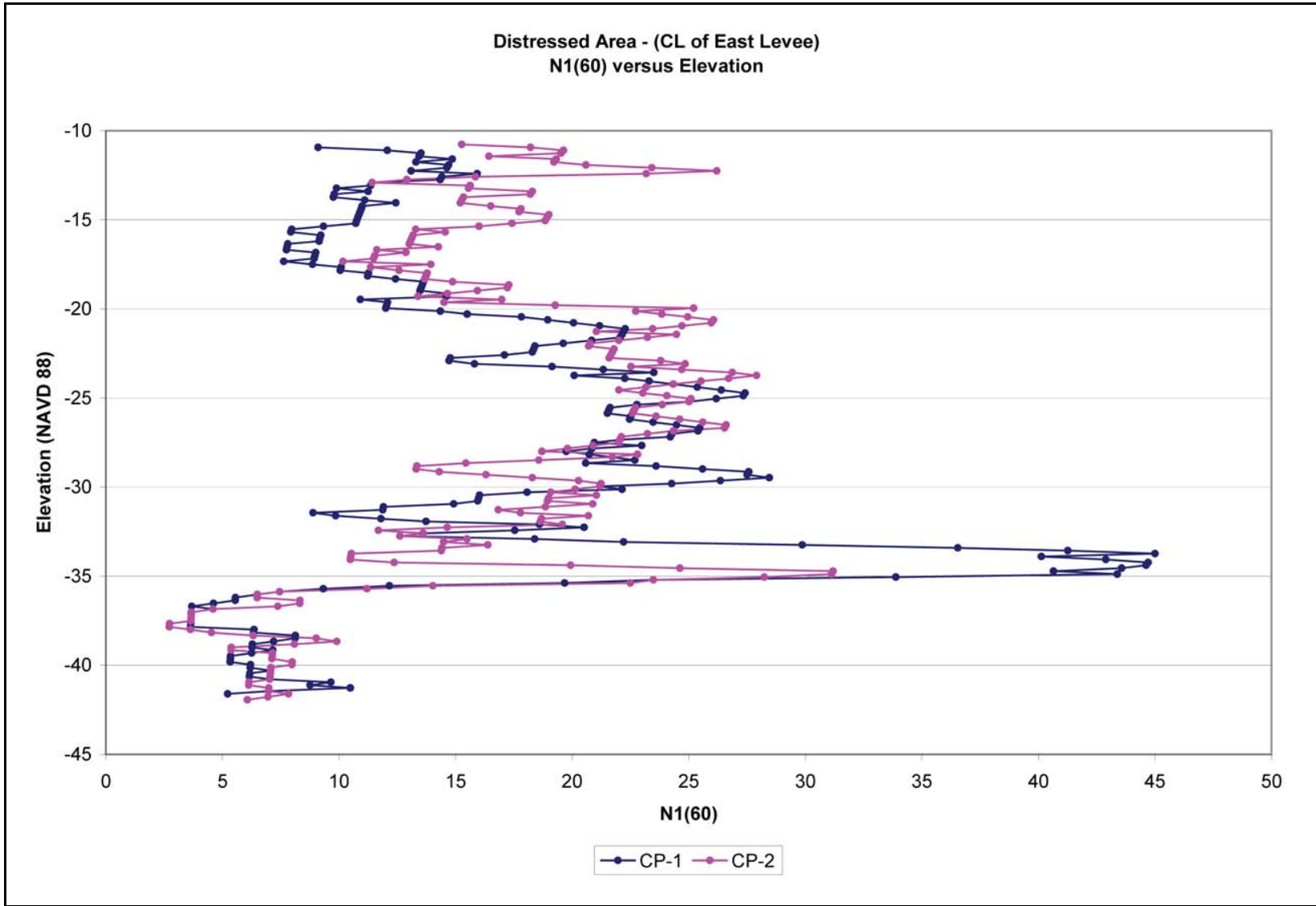


Figure 7-38. Distressed Area – Beach Sand Stratum (Centerline of East Levee), N1(60) versus Elevation for CPTs CP-1 and CP-2

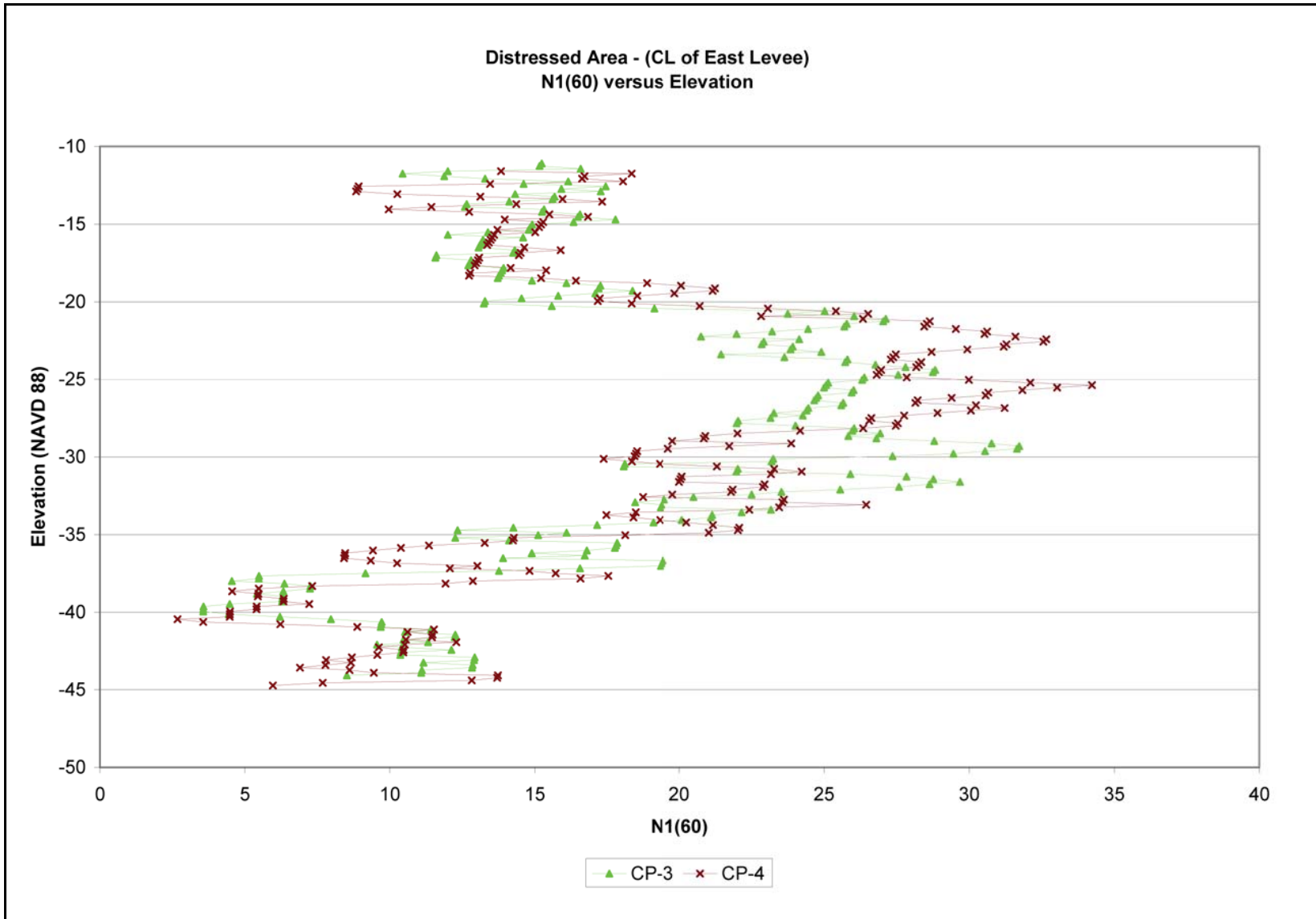


Figure 7-39. Distressed Area – Beach Sand Stratum (Centerline of East Levee), N1(60) versus Elevation for CPTs CP-3 and CP-4

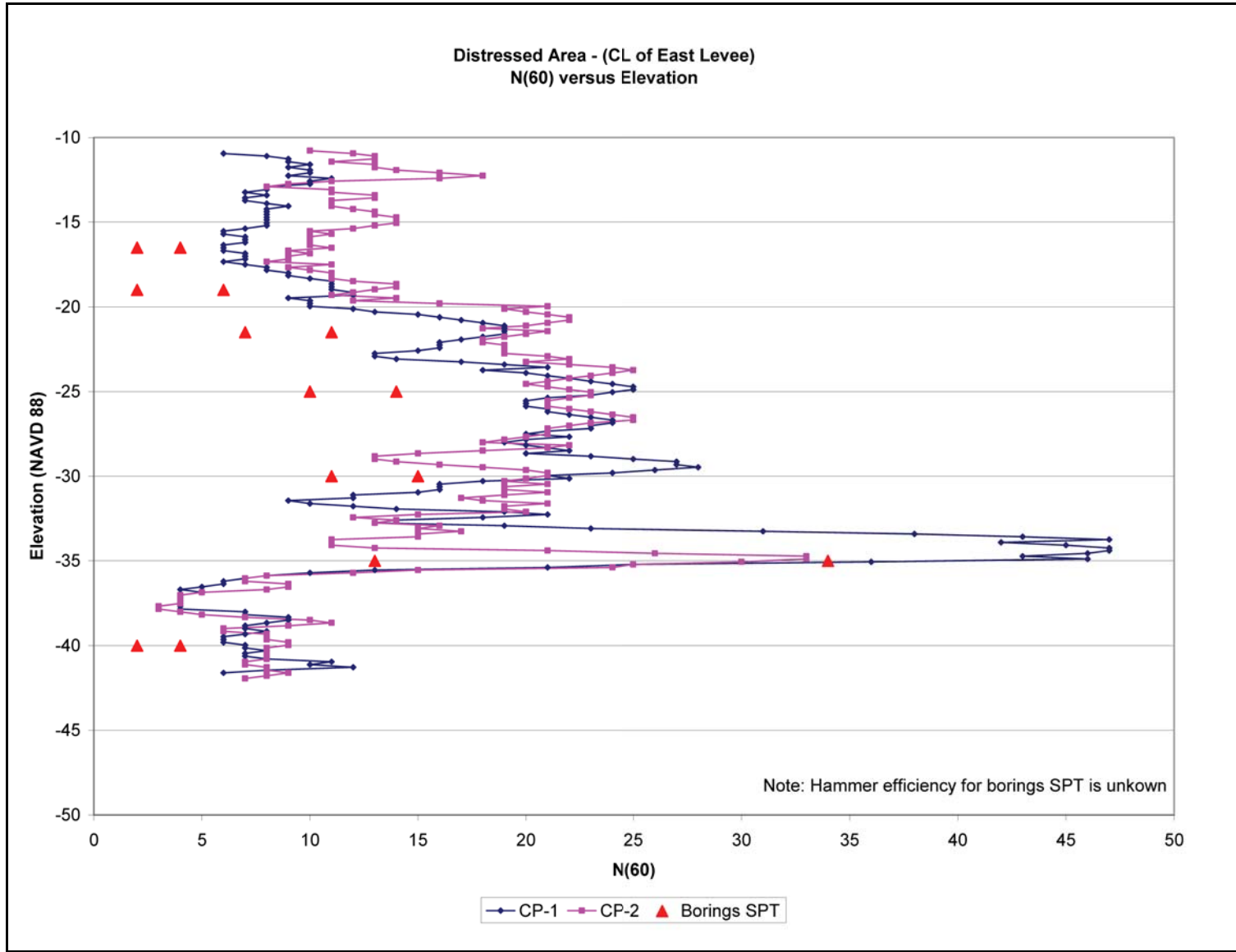


Figure 7-40. Distressed Area – Beach Sand Stratum (Centerline of East Levee), N(60) versus Elevation for CPTs CP-1 and CP-2

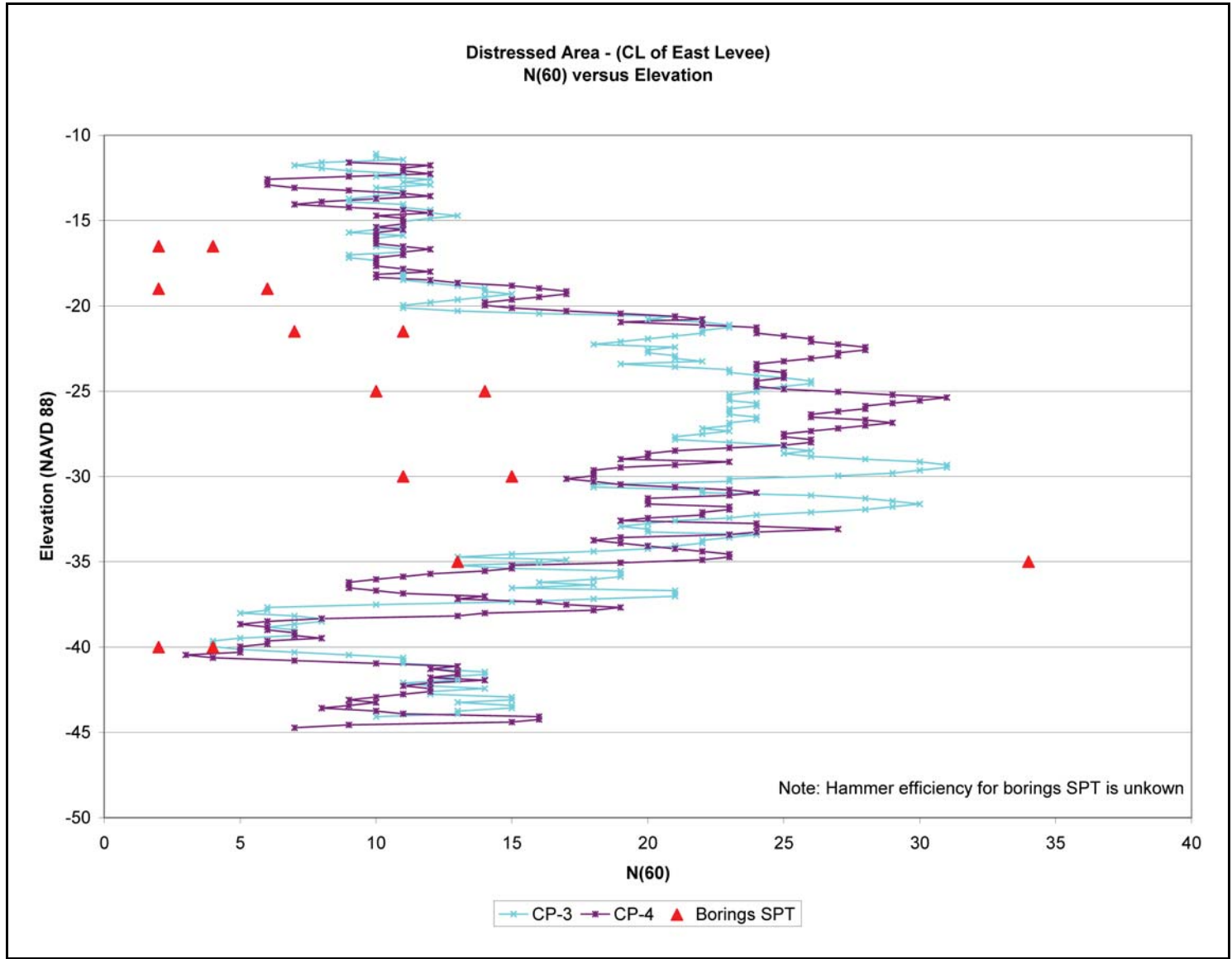


Figure 7-41. Distressed Area – Beach Sand Stratum (Centerline of East Levee), N(60) versus Elevation for CPTs CP-3 and CP-4

LOG OF BORING
EUSTIS ENGINEERING COMPANY
 SOIL AND FOUNDATION CONSULTANTS
 METAIRIE, LA.

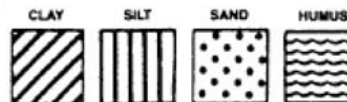
Name of Project: London Avenue Canal, Levee and Floodwall Improvements
Orleans Levee Board Project No. 2049-0269, New Orleans, Louisiana
 For: The Board of Levee Commissioners of the Orleans Levee District, New Orleans, La.
Burk & Associates, Inc., New Orleans, Louisiana

Boring No. 51 Soil Technician A. Croal, Jr. Date 12 November 1985
 Ground Elev. 4.70 Datum NGVD Gr. Water Depth See Text

Sample No.	SAMPLE Depth—Feet		DEPTH STRATUM Feet		VISUAL CLASSIFICATION	STANDARD PENETRATION TEST	
	From	To	From	To			
1	0.0	0.5	0.0	1.0	Stiff brown & gray clay w/shell fragments & grass roots		
2	1.7	2.5	1.0	3.0	Medium stiff tan & gray clay w/fine sand & clayey sand pockets		
3	4.7	5.5	3.0	6.5	Medium stiff black & gray clay w/roots & organic matter		
4	7.7	8.5	6.5	9.0	Medium stiff tan & gray clay w/sand layers & trace of organic matter		
5	10.7	11.5	9.0	12.5	Soft gray clay w/roots & organic matter		
6	13.7	14.5	12.5	16.0	Loose gray fine sand w/clayey sand layers, trace of organic matter & few roots		
7	16.0	17.5	16.0	19.0	Medium dense gray fine sand	2	28
8	18.5	20.0	19.0	21.5	Dense gray fine sand	4	36
9	21.0	22.5	21.5		Very dense gray fine sand	8	50=10"
10	23.5	25.0			Ditto	10	50=10"
11	26.0	27.5			Ditto	15	50=9"
12	28.5	30.0			Very dense gray fine sand w/few shell fragments	11	50=8"
13	33.5	35.0			Very dense gray fine sand	9	50=9"
14	38.5	40.0		42.0	Ditto	12	50=9"
15	43.5	45.0	42.0	47.0	Dense gray fine sand	14	41
16	48.5	50.0	47.0	50.0	Loose gray silty sand w/few clay pockets & trace of clay	2	10

*Number in first column indicates number of blows of 140-lb. hammer dropped 30 in. required to seat 2-in. O. D. splitpoon sampler 6 in. Number in second column indicates number of blows of 140-lb. hammer dropped 30 in. required to drive 2-in. O. D. splitpoon sampler 1 ft. after seating 6 in.
 WHILE THIS LOG OF BORING IS CONSIDERED TO BE REPRESENTATIVE OF SUBSURFACE CONDITIONS AT ITS RESPECTIVE LOCATION ON THE DATE SHOWN, IT IS NOT WARRANTED THAT IT IS REPRESENTATIVE OF SUBSURFACE CONDITIONS AT OTHER LOCATIONS AND TIMES.

Remarks: _____



Predominant type shown heavy. Modifying type shown light.



Figure 7-42. GDM Boring B-51 – Boring Log

**Table 7-11
Moisture Content and Wet Unit Weights from Levee Toe**

Boring	Elevation (NAVD 88)	Soil Type	%w	Dry Unit Weight (pcf)	Wet Unit Weight (pcf)
LAC05-2G	-1.65	CL	28.7	85.3	109.8
SL-1-05U	-2.85	CH	37		
SL-1-05U	-3.85	CH	32		
LAC05-2G	-4.15	CH	148.3	30.3	75.2
SL-1-05U	-4.85	CH	43		
SL-1-05U	-5.85	CH	90		
SL-1-05U	-6.85	CH	70		
SL-1-05U	-7.85	CH	61		
SL-1-05U	-8.85	CH	43		
LAC05-2G	-9.15	CH	47.2	70.5	103.8

Shear Strength

Shear strengths from laboratory tests of the levee embankment and marsh unit (under the centerline) are fairly sparse. The table below shows the shear strength data available from the centerline of the levee.

**Table 7-12
Laboratory Shear Strength Test Data for Samples taken from the Centerline of the Levee**

Boring	Elevation (NAVD 88)	Soil Type	%w	UC Test (psf)	UU-1 Test (psf)
51	3.00	Clay	22.6		535
52	3.00	Clay	35.9	1127.5	
51	0.00	Clay	42.6	637.5	
52	0.00	Clay	65.2	510	
50	-4.20	Clay	51.6	402.5	
51	-3.00	Clay	52.7	605	
51	-6.00	Clay	75	360	
52	-6.00	Clay	164.2	175	
50	-6.70	Clay	104.2	350	
52	-9.00	Clay	91.2	275	
52	-14.00	Clayey Sand	48.1		172.5

Shear strengths from laboratory tests (three unconfined compression tests) taken at the toe of the levee are plotted with interpretation of the undrained shear strengths from CPT SLON-2.05c in Figure 7-43. The unconfined compression tests are from boring LAC-2G.

Gradation and Standard Penetration Number for Beach Sand Unit

A plot of the D_{10} , D_{30} , and D_{60} values of the beach sand unit are shown on Figure 7-44. These values consist of gradation tests conducted on samples from borings LAC-1G and LAC-2G. A summary of these values are presented in the table below.

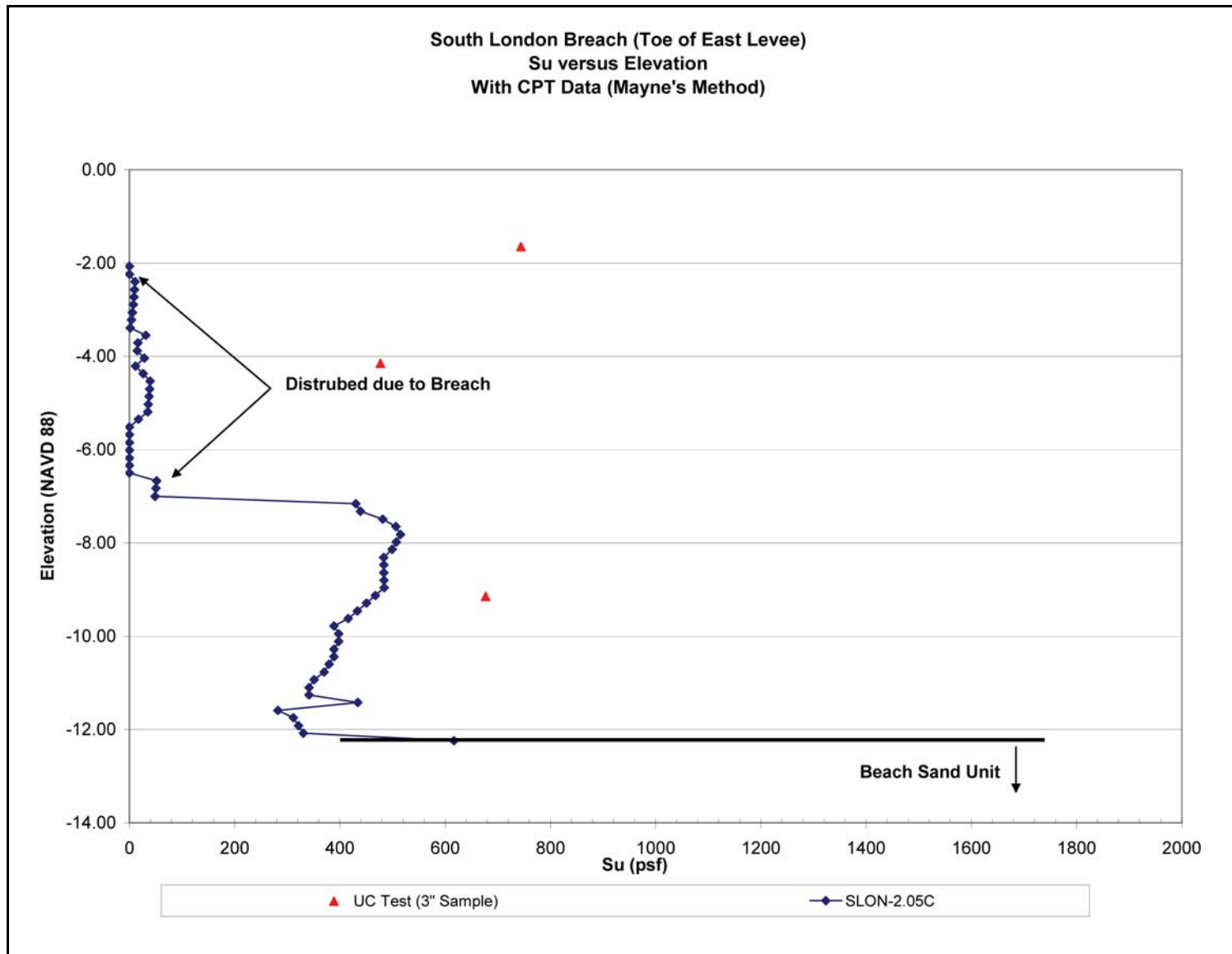


Figure 7-43. South London Breach, Su versus Elevation with CPT Data

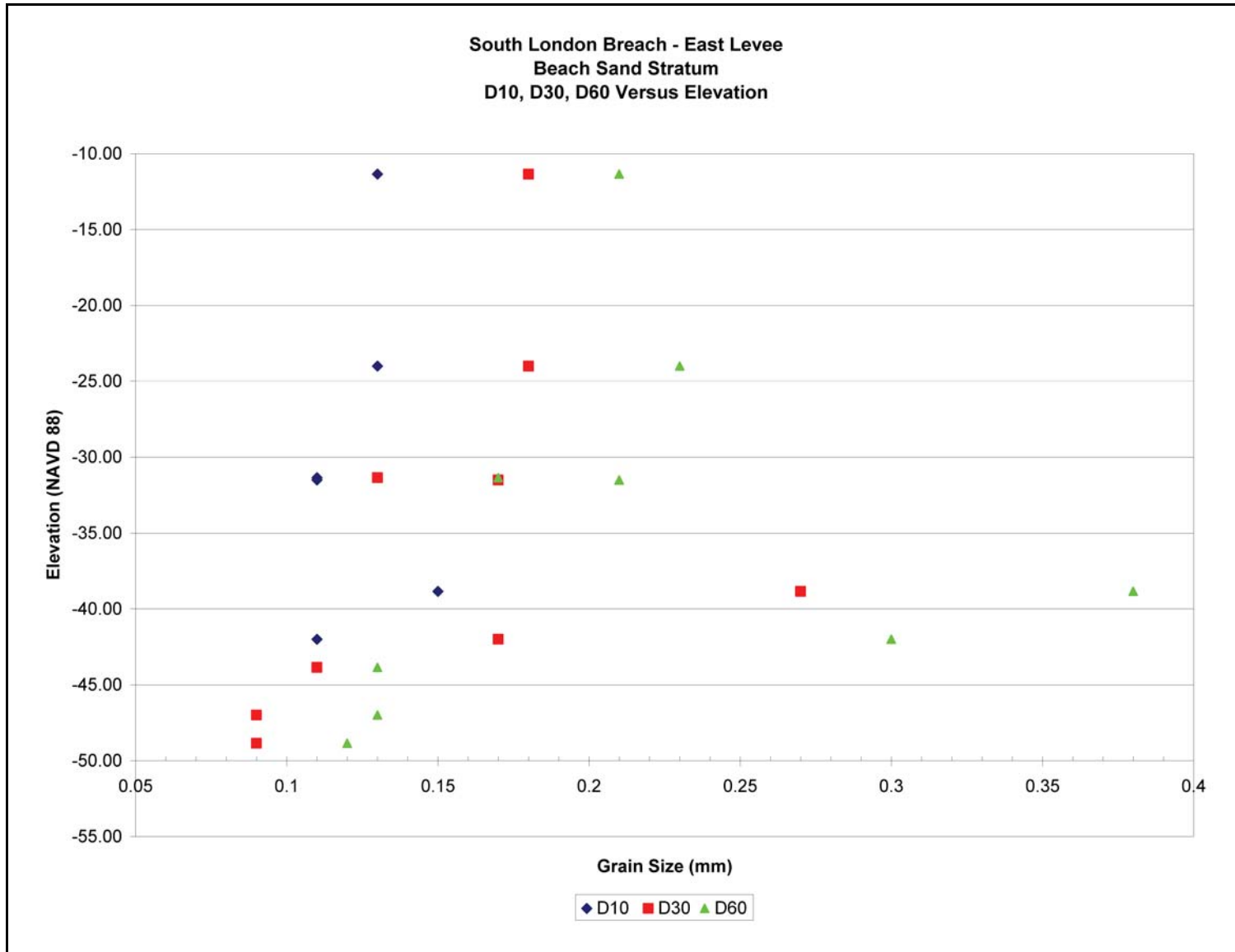


Figure 7-44. South London Breach – Beach Sand Unit, D10, D30, D60 versus Elevation

**Table 7-13
D10, D30, and D60 Values for the Beach Sand Unit**

Boring	Elevation (NAVD 88)	Soil Type	D ₆₀ (mm)	D ₃₀ (mm)	D ₁₀ (mm)
LAC05-2G	-11.35	SP	0.21	0.18	0.13
LAC05-1G	-24.00	SP	0.23	0.18	0.13
LAC05-2G	-31.35	SP	0.17	0.13	0.11
LAC05-1G	-31.50	SM1-s	0.21	0.17	0.11
LAC05-2G	-38.85	SP	0.38	0.27	0.15
LAC05-1G	-42.00	SP	0.3	0.17	0.11
LAC05-2G	-43.85	SM-1	0.13	0.11	
LAC05-1G	-47.00	SC3-s	0.13	0.09	
LAC05-2G	-48.85	SC1	0.12	0.09	

Figure 7-45 shows the SPT values obtained from the GDM borings at the breach. The hammer efficiency is unknown for these borings. Refusal was reached in some dense layers of sand between elevations -15 to -35 (NAVD 88).

Figures 7-46 and 7-47 show the N₁₍₆₀₎ values of the beach sand unit as determined from the CPTs. CPT NLON-2.05C was first pushed with a 5-ton cone penetrometer, but because the tip loads were nearing the capacity of the device at about elevation -31, a 10-ton cone penetrometer was used. On Figure 7-46, NLON-3.05c shows a dense sand layer (N₁₍₆₀₎ values ranging from 50 to 90) from elevations -17 to -23, and elevations -30 to -37. NLON-2.05c shows a dense sand layer (N₁₍₆₀₎ values range from 50 to 90) from elevations -27 to -37.

On Figure 7-47, NLON-5.05c also shows a dense sand layer N₁₍₆₀₎ values range from 50 to over 100) from elevations -15 to -35. Both NLON-5.05c and NLON-1.05c show N₁₍₆₀₎ values over 100. This occurs because of the process in which the N₁₍₆₀₎ values are determined. Because of shallow depths and low overburden pressures, the C_n correction factor is greater than 1; and when multiplied to the N₍₆₀₎ values, will often produce an N₁₍₆₀₎ over 100. Liao and Whitman's (1986) relationship between C_n and vertical effective stress was used to convert the field blowcounts to their N₁₍₆₀₎ values. However, in some cases, the N₍₆₀₎ values are already near or at 100 at overburden pressures less than 1 tsf. Usually, N values greater than 50 are accepted as refusal. NLON-1.05c shows that dense sand layer N₁₍₆₀₎ values range from 50 to over 100) from elevations -13 to -35.

Pore Pressure Dissipation Test

A pore pressure dissipation test was conducted in the beach sand unit at CPT SLON-2.05C. Below is a table summarizing the results of the dissipation tests.

Table 7-14 CPTU Pore Pressure Dissipation Tests in Beach Sand Unit					
CPT	London Canal Staff Gauge Reading (NAVD 88)	Dissipation Test Elevation (NAVD 88)	Stabilized Pressure (psi)	Computed Head (ft) (Stab. Pressure x 2.31 ft/psi)	Head Elevation (NAVD 88)
SLON- 2.05C	0.82	-20.45	5.5	12.70	-7.7

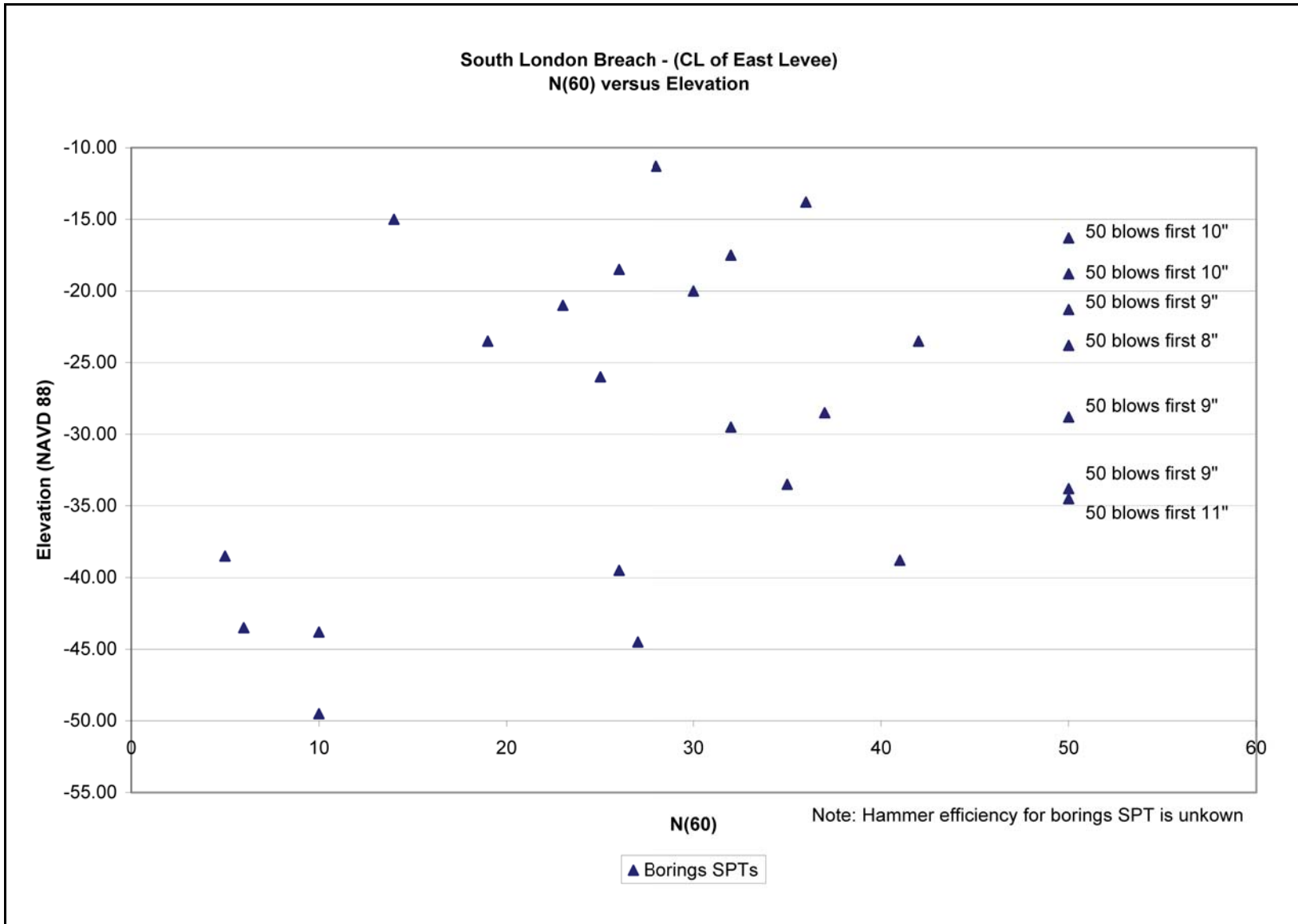


Figure 7-45. South London Breach – Beach Sand Unit (CL of East Levee), SPT versus Elevation

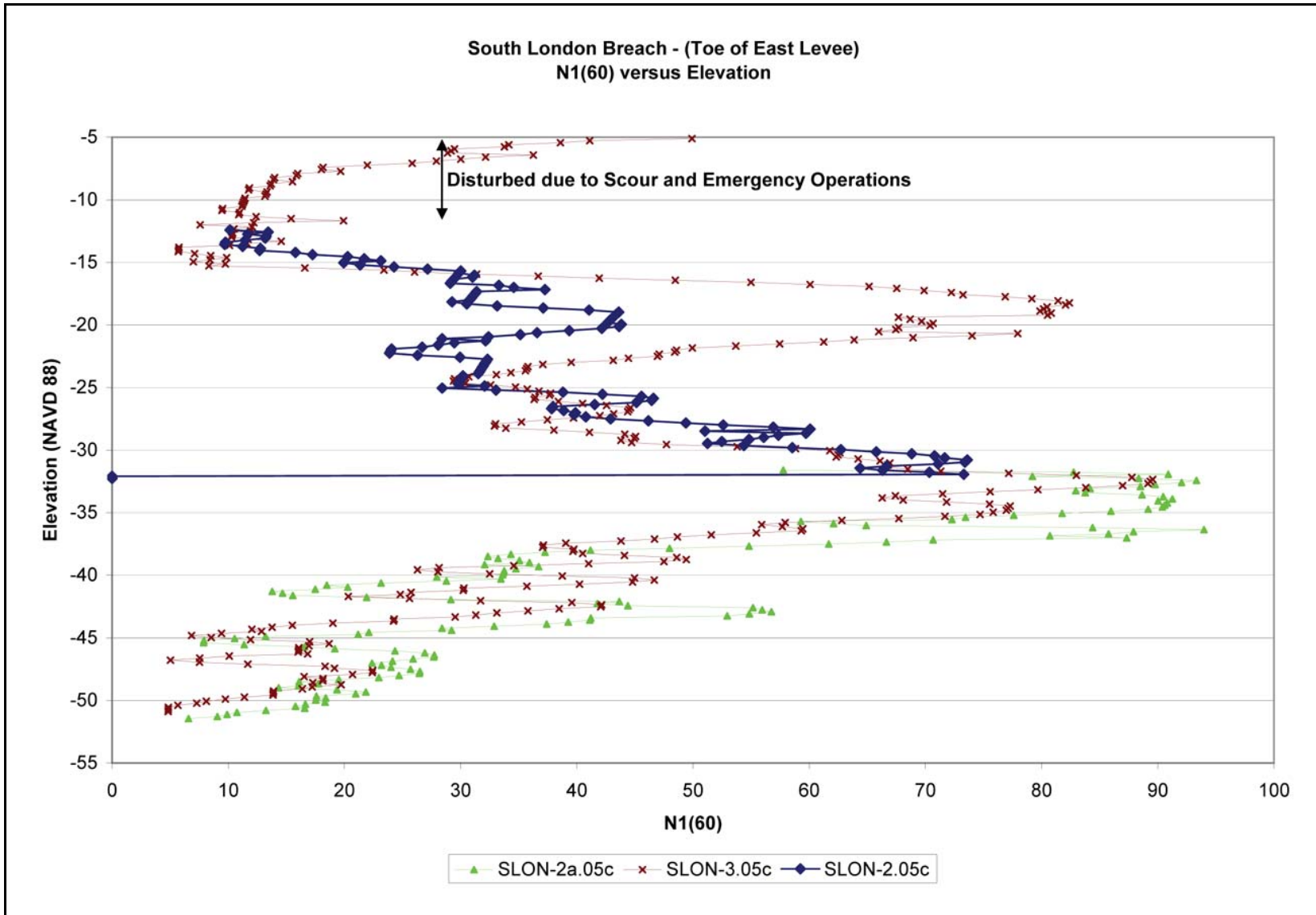


Figure 7-46. South London Breach – Beach Sand Stratum (Toe of East Levee), N1(60) versus Elevation for CPTs SLON-2.05c and SLON-3.05c

South London Breach - (Toe of East Levee)
 N1(60) versus Elevation

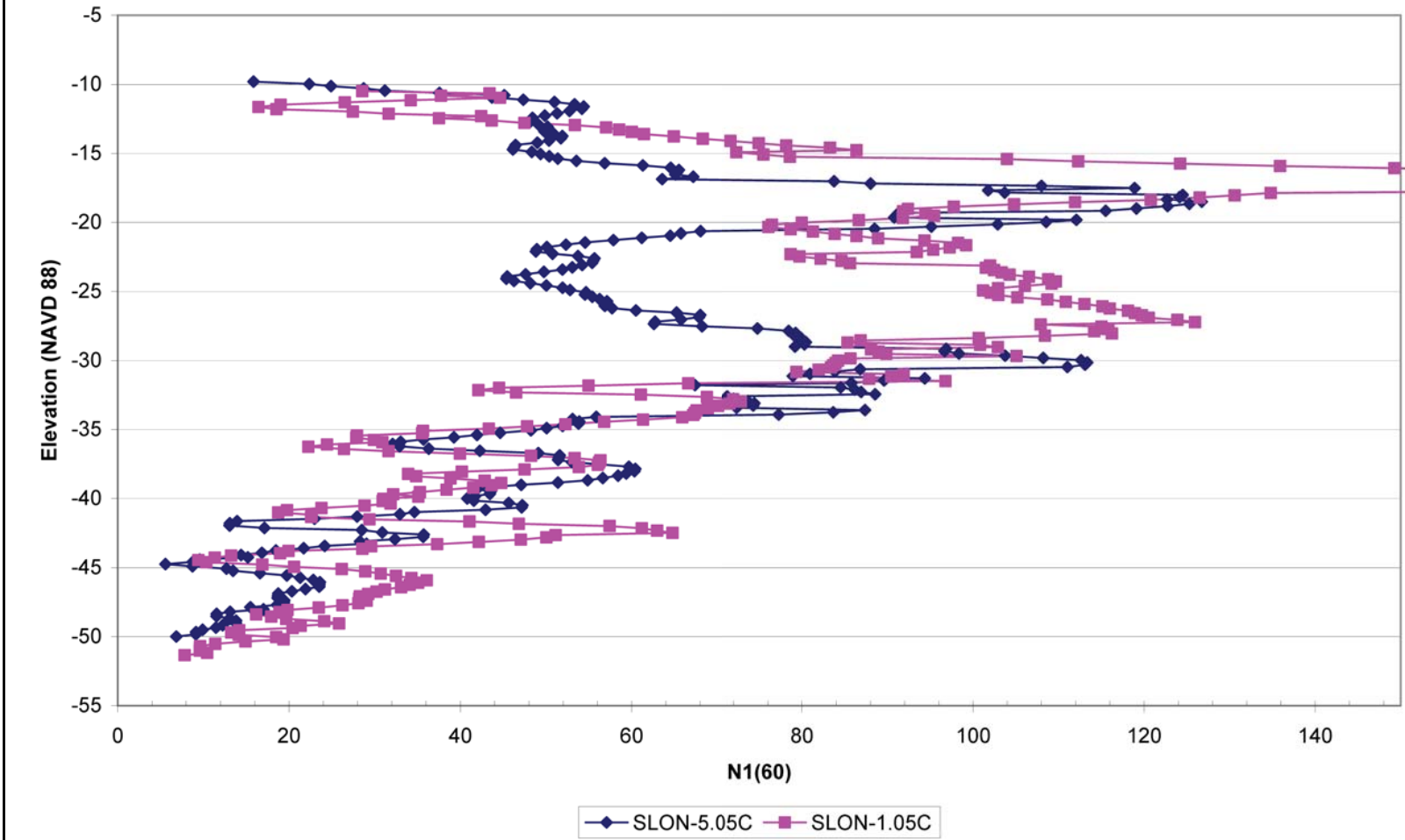


Figure 7-47. South London Breach – Beach Sand Stratum (Toe of East Levee), N1(60) versus Elevation for CPTs SLON-5.05c and SLON-1.05c

Piezometers at London Canal

Piezometer Locations

Nineteen borings with piezometers were installed along London Canal for the purpose of monitoring the piezometric response of the beach sands to changes in the water level in the canal. Figure 7-48 shows the location of these piezometers along the canal. A total of 30 piezometers are in these borings. The piezometers are located and labeled into three basic groups, depending on their location. The first group included four borings, labeled LRP1 through 4, each with two piezometers and is located near the north London Canal breach site on the west bank of the canal just south of Robert E. Lee Boulevard. The second group includes five borings, each containing two piezometers, labeled LMP1 through 5, located on the east bank of the canal in the vicinity of the South London Canal breach site near Mirabeau Avenue. The third group represents secondary borings, labeled LP, and contains a total of 13 piezometers at miscellaneous locations of interest along the canal. All piezometers were put in service by the New Orleans District after Katrina.

Tables 7-15 through 7-17 list the information pertaining to the locations of the piezometer boreholes. Identified for each borehole are the Station, offset distance from the floodwall, the ground surface elevation immediately adjacent to the hole, and an indication of which side of the canal the borehole is located on. Table 7-15 represents this data for the North London breach site; Table 7-16, the data for the South London breach site; and Table 7-17, the data for the miscellaneous group of borings.

Tables 7-18 through 7-20 give information about where the piezometers are located in each boring for the north London breach site, the south London breach site, and the miscellaneous locations, respectively. Each table lists the boring and piezometer label, ground surface elevation immediately adjacent to each boring, and the elevation that each piezometer tip is set at.

Boring	Station	Offset Distance from Wall, ft	Ground Elevation, ft, NGVD88	Description of Location	Bank
LRP1	-----	-----	-4.06	Toe	West
LRP2	-----	-----	+3.54	On Levee near floodwall	West
LRP3	-----	-----	-1.55	Toe	West
LRP4	-----	-----	-5.26	Near street in neutral ground	West

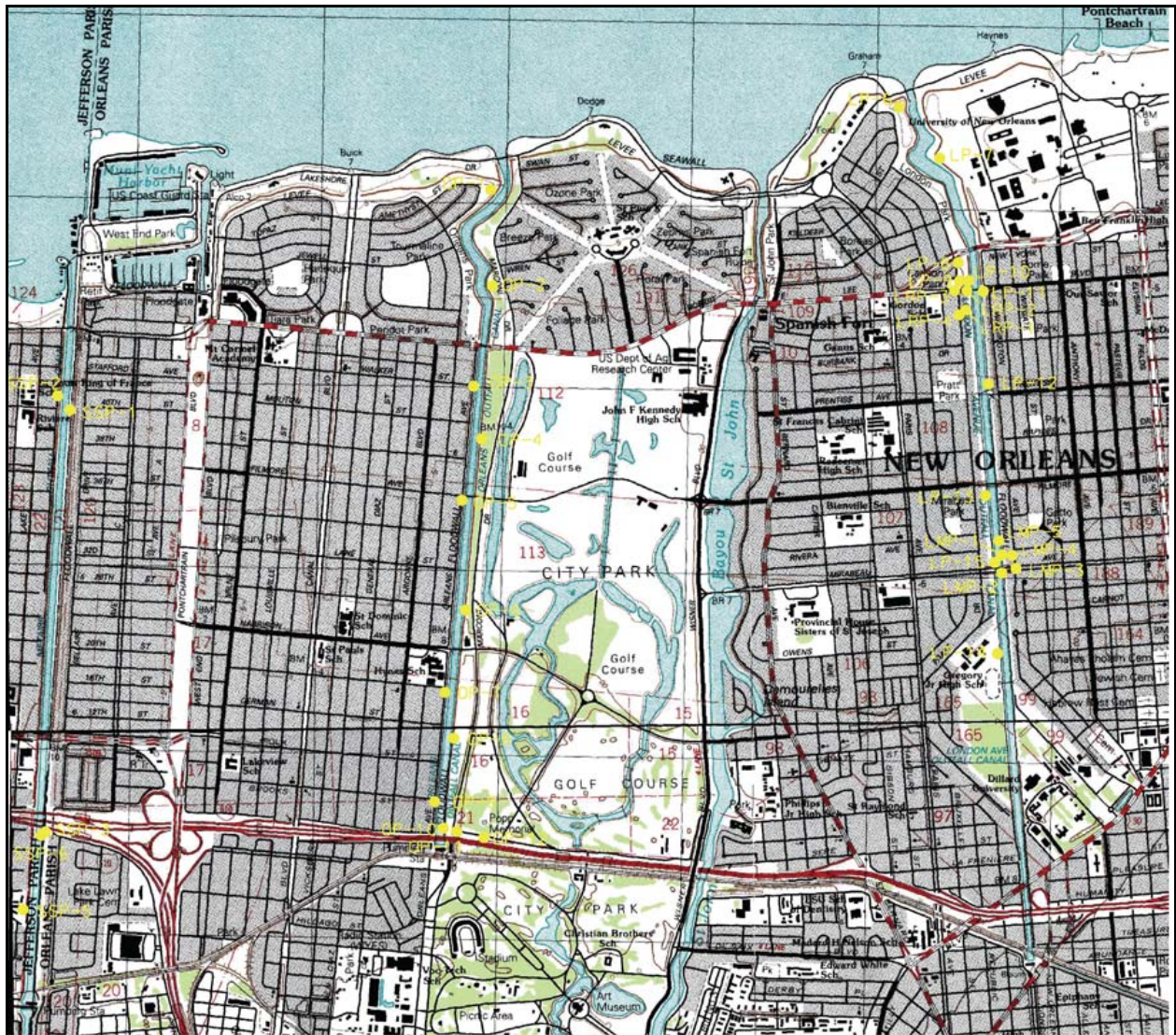


Figure 7-48. Plan View Showing Locations of the Piezometer Boreholes at London Canal

Boring	Station	Offset Distance from Wall, ft	Ground Elevation, ft, NGVD88	Description of Location	Bank
LMP1	----	----	-1.56	In breach	West
LMP2	----	----	-2.16	In breach near toe	West
LMP3	----	----	-3.16	Toe near curb at Warrington Ave	West
LMP4	----	----	-4.86	At breach in the neighborhood backyard	West
LMP5	52+00	----	+0.16	At floodwall north of breach site	West

**Table 7-17
Secondary Piezometer Borings at the London Canal (Miscellaneous Locations)**

Boring	Station	Offset Distance from Wall, ft	Ground Elevation, ft, NGVD88	Description of Location	Bank
LP6	-----	-----	????	At the lakefront on the canal's west bank	West
LP7	-----	-----	-2.62	Near the University of New Orleans on the canal's east bank at the toe	East
LP8	-----	-----	Peat	At Leon C. Simon on the West side of the canal at the toe	
LP9	-----	-----	-0.22	Just north of Robert E. Lee Blvd bridge over canal on west bank	West
LP10	-----	-----	---	Just north of Robert E. Lee Blvd bridge over canal on flood side	West
LP11	-----	-----	-4.27	At bridge abutment at Robert E. Lee Blvd.	East
LP12	-----	-----	----	At Prentiss Ave. mid-way between Mirabeau and north Mirabeau breach sites on toe of levee	East
LP13	-----	-----	0.2	Just south of Fillmore Ave at toe of levee	West
LP14	-----	-----	0.66	Four blocks south of Mirabeau Ave. near Dillard University	West
LP15	-----	-----	----	Directly across from the Mirabeau Ave. breach site	West

**Table 7-18
Piezometer Tip Elevations in the Vicinity of North London Breach Area near Robert E. Lee Boulevard**

Boring	Piezometer	Ground Surface Elevation, ft NGVD88	Tip Elevation, ft NGVD88
LRP1	A	-4.06	-38.7
	B	-4.06	-23.7
LRP2	A	+3.54	-38.1
	B	+3.54	-16.1
LRP3	A	-1.55	-36.19
	B	-1.55	-18.19
LRP4	A	-5.26	-39.9
	B	-5.26	-20.9

**Table 7-19
Piezometer Tip Elevations in the Vicinity of South London Breach Area near Mirabeau Avenue**

Boring	Piezometer	Ground Surface Elevation, ft NGVD88	Tip Elevation, ft NGVD88
LMP1	A	-1.56	-43.2
	B	-1.56	-19.2
LMP2	A	-2.16	-43.8
	B	-2.16	-19.8
LMP3	A	-1.55	-37.8
	B	-1.55	-17.8
LMP4	A	-4.86	-46.5
	B	-4.86	-18.5
LMP5	A	+0.16	-13.48

**Table 7-20
Piezometer Tip Elevations at the London Canal (Miscellaneous Locations)**

Boring	Piezometer	Ground Surface Elevation, ft NGVD88	Tip Elevation, ft NGVD88
LP6	A	Not Reported (NR)	-36.36
	B	NR	-17.52
LP7	A	+2.62	-37.58
	B	NR	-8.65
LP8	A	NR	-21.95
	B	NR	-13.05
LP9	A	-0.22	-18.9
LP10	A	NR	-17.15
LP11	A	-4.27	-15.79
LP12	A	NR	-25.36
LP13	A	0.2	-15.36
LP14	A	0.66	-11.09
LP15	A	NR	-21.46

Piezometer Data

The data collected represent readings taken between the time of installation and early February 2006. Figures 7-49 through 7-67 show piezometer data for each borehole. Each plot shows the response of the piezometers to changing water levels in the canal. The location of the London Avenue staff gauge is unknown at this time. Significant events such as construction and repair activities might have an effect on the piezometer responses and are noted on these plots. In addition, placement of a clay blanket on the canal side of the repair section at Mirabeau Avenue took place between the time periods of mid-October to early November 2005. This clay blanket was placed to reduce seepage through the repair section and a significant amount of clay was also dumped into the canal.

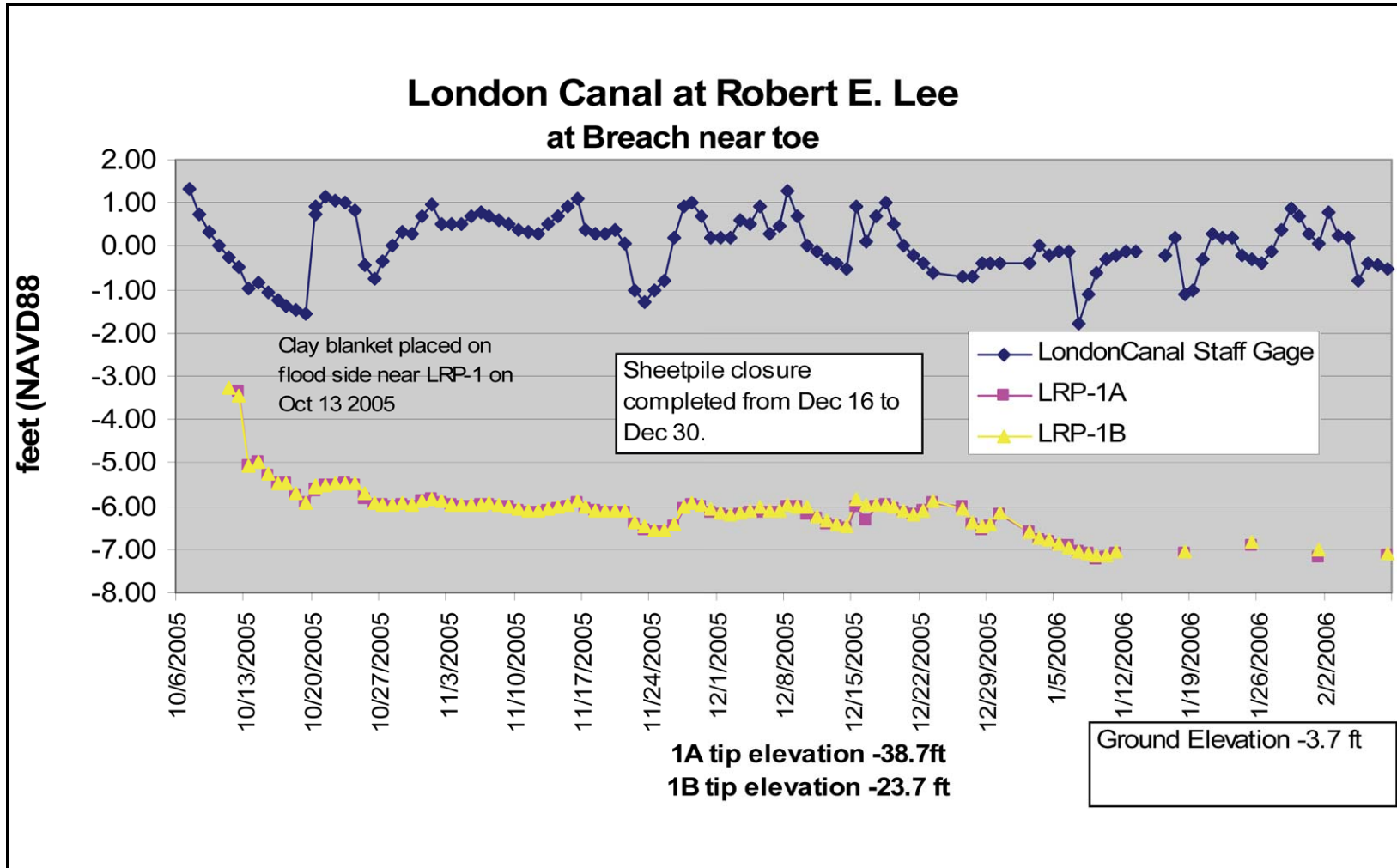


Figure 7-49. Response of Piezometers LRP-1a and LRP-1-B in the Vicinity of the North London Breach Site

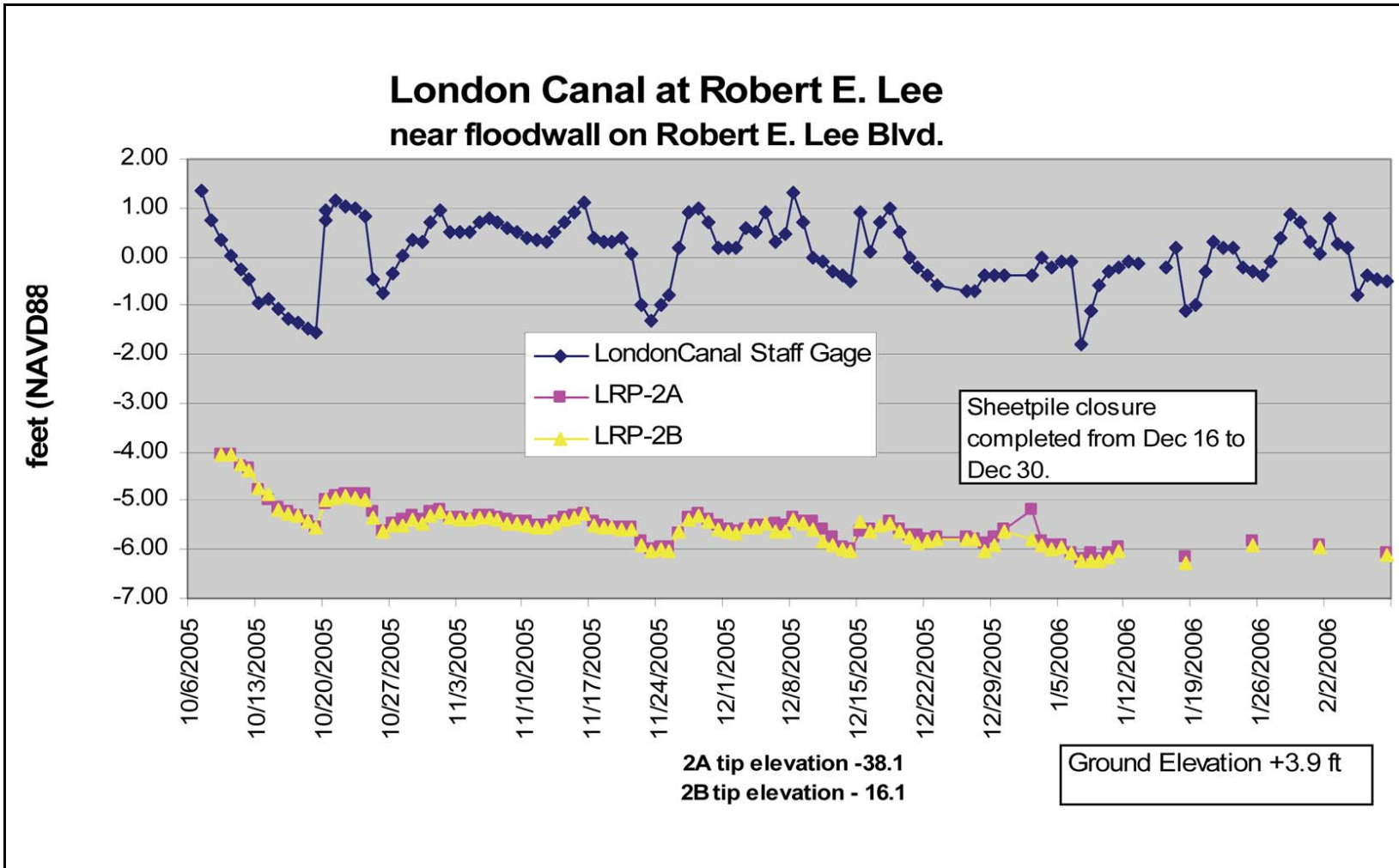


Figure 7-50. Response of Piezometers LRP-2A and LRP-2B in the Vicinity of the North London Breach Site

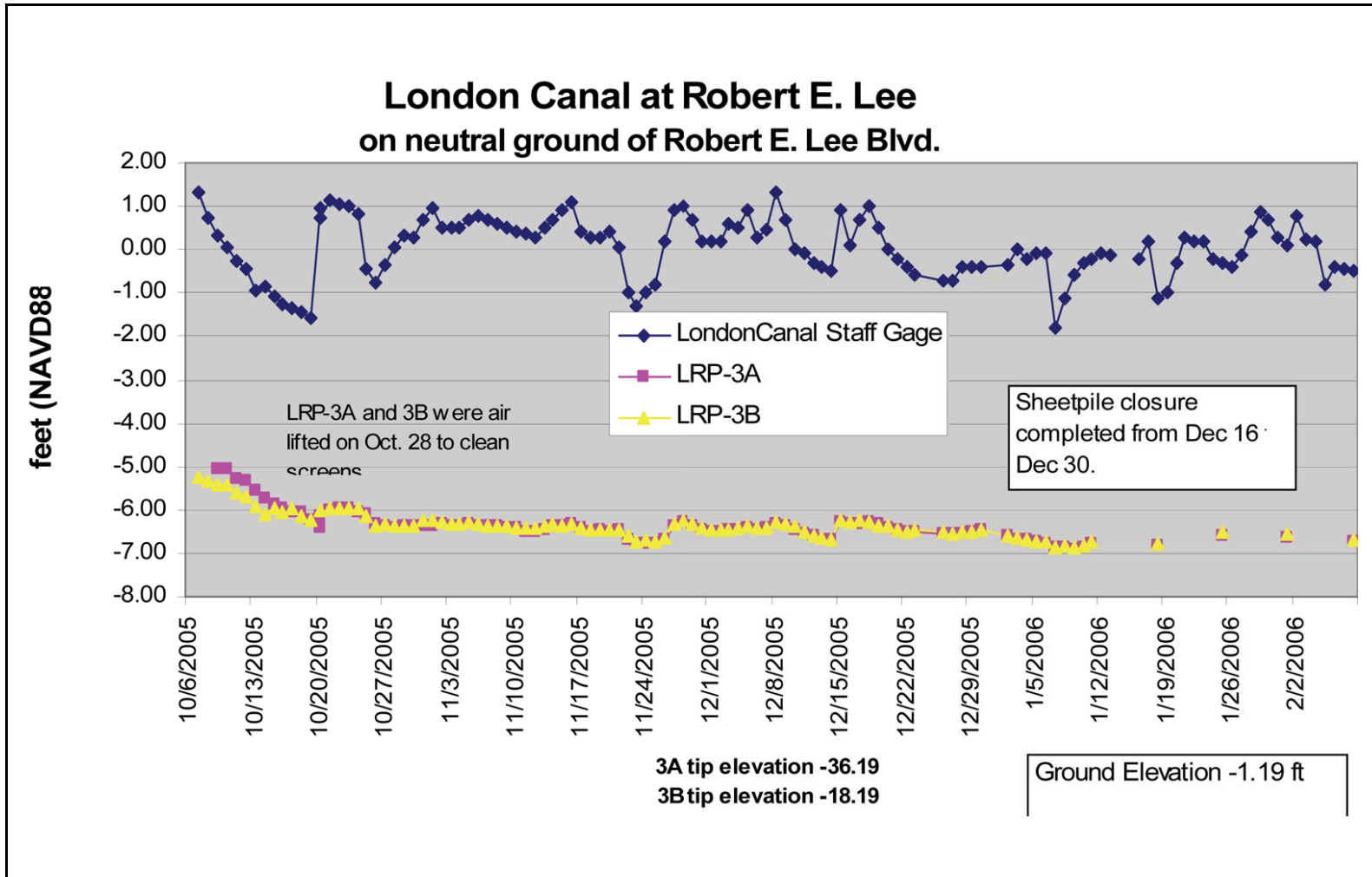


Figure 7-51. Response of Piezometers LRP-3A and LRP-3B in the Vicinity of the North London Breach Site

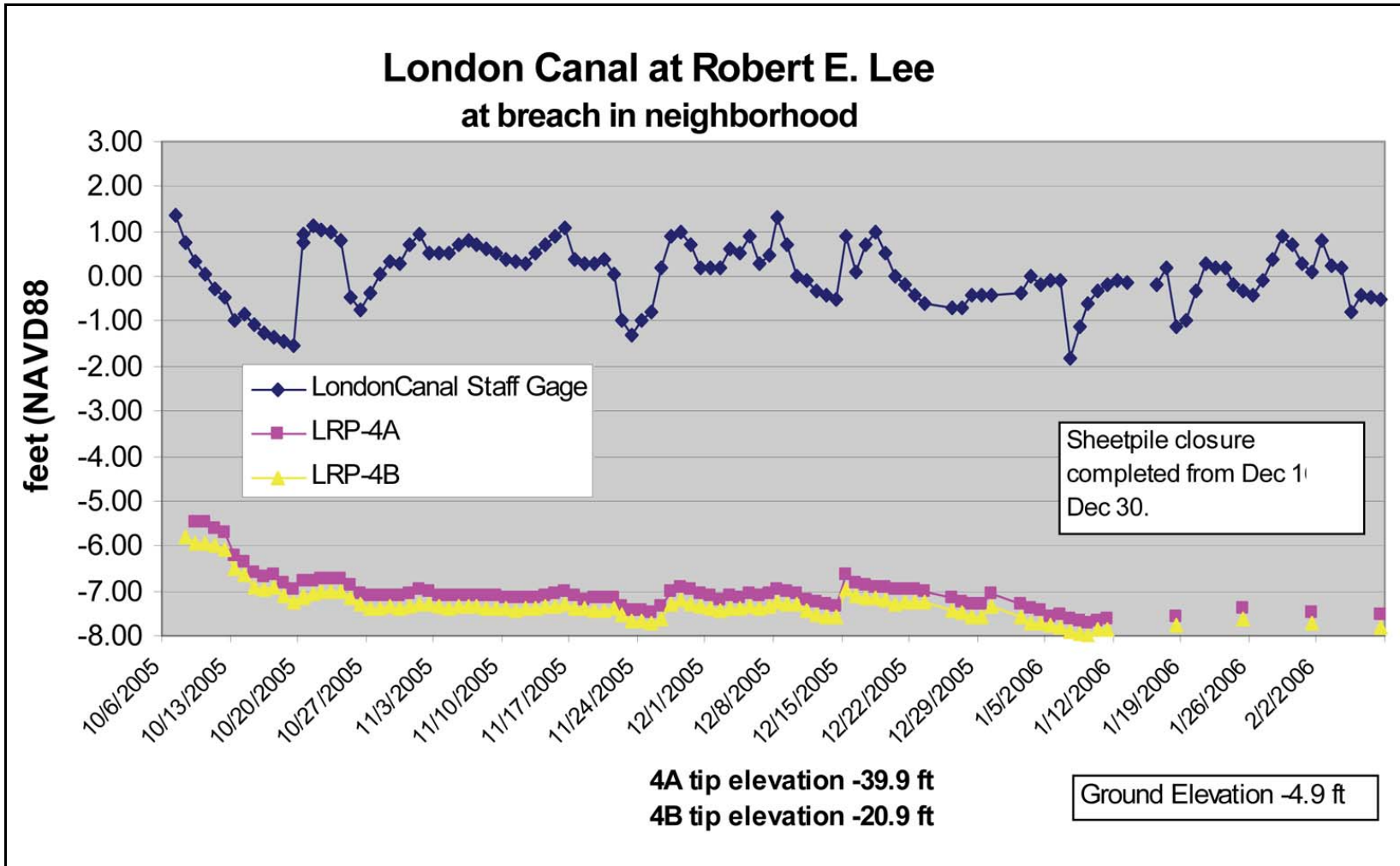


Figure 7-52. Response of Piezometers LRP-4A and LRP-4B in the Vicinity of the North London Breach Site

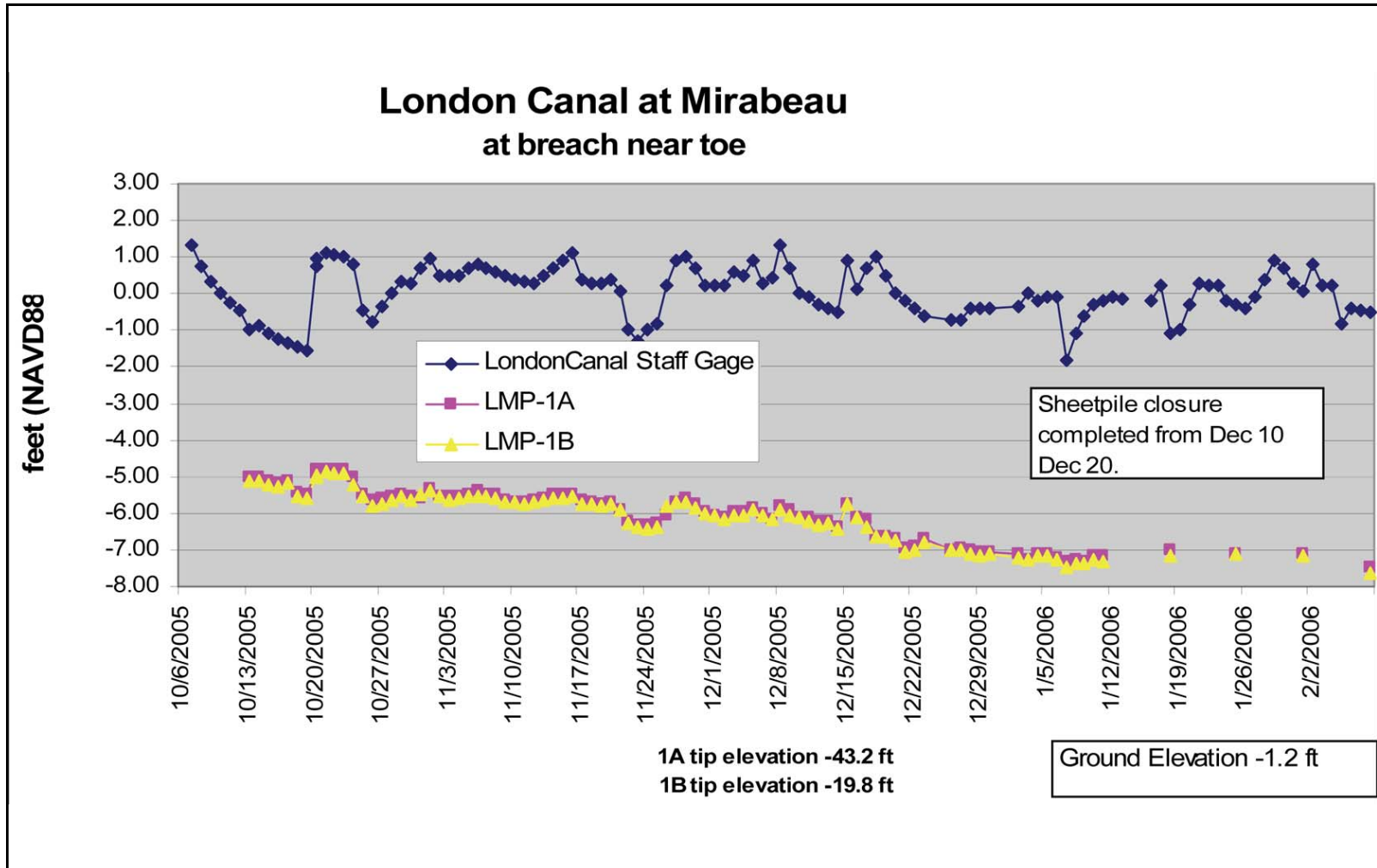


Figure 7-53. Response of Piezometers LMP-1A and LMP-1B in the Vicinity of the South London Breach Site near Mirabeau Avenue

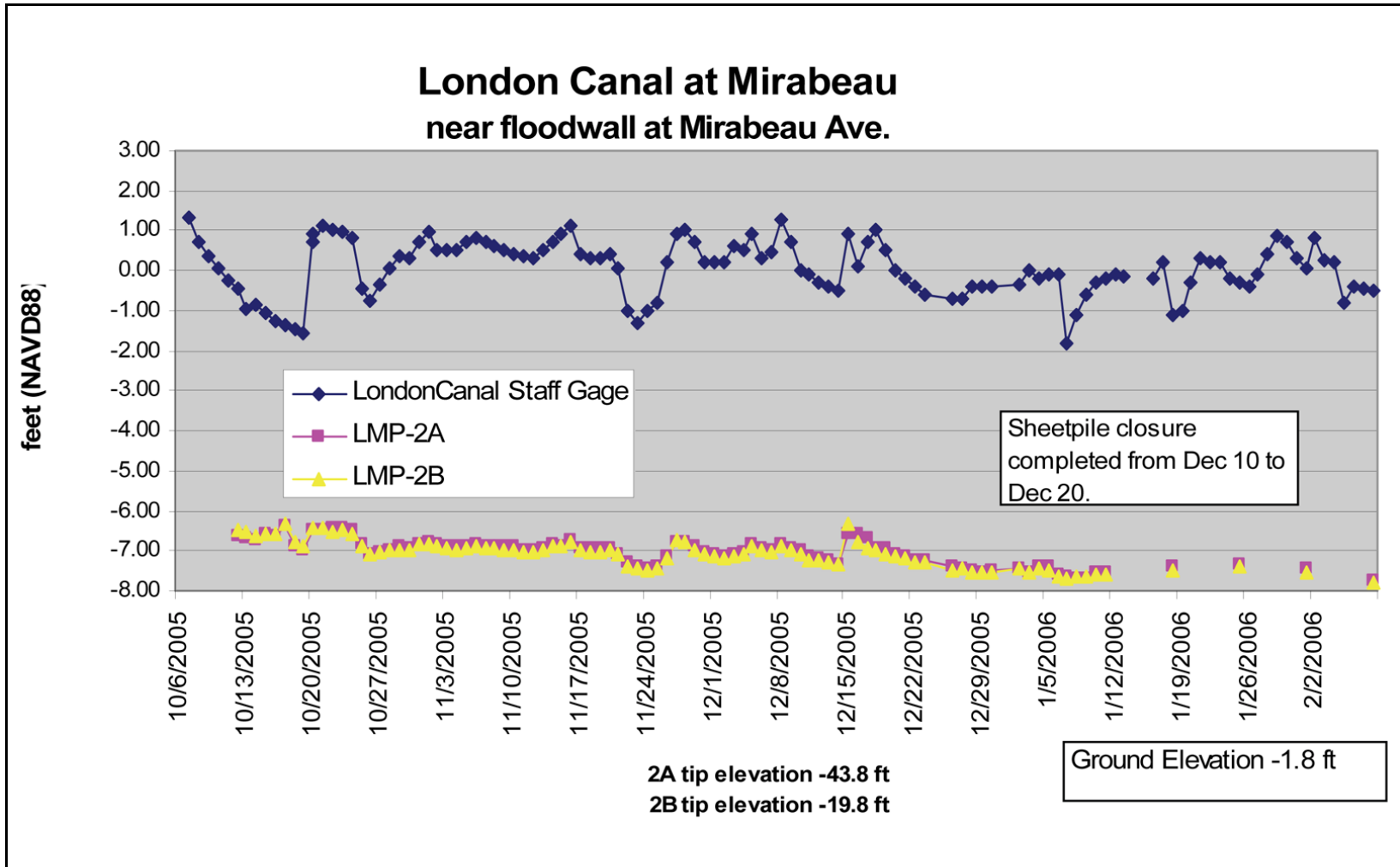


Figure 7-54. Response of Piezometers LMP-2A and LMP-2B in the Vicinity of the South London Breach Site near Mirabeau Avenue

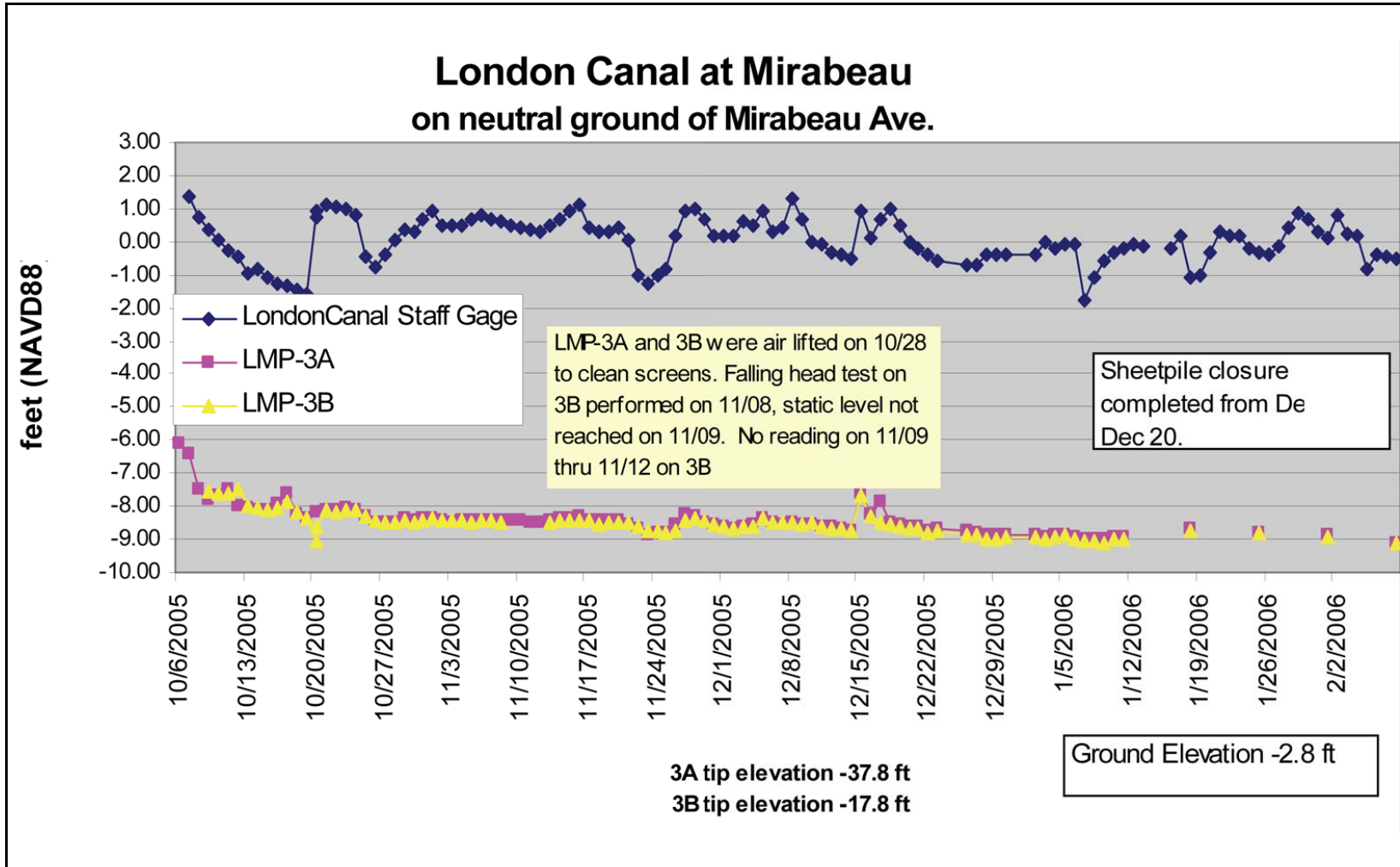


Figure 7-55. Response of Piezometers LMP-3A and LMP-3B in the Vicinity of the South London Breach Site near Mirabeau Avenue

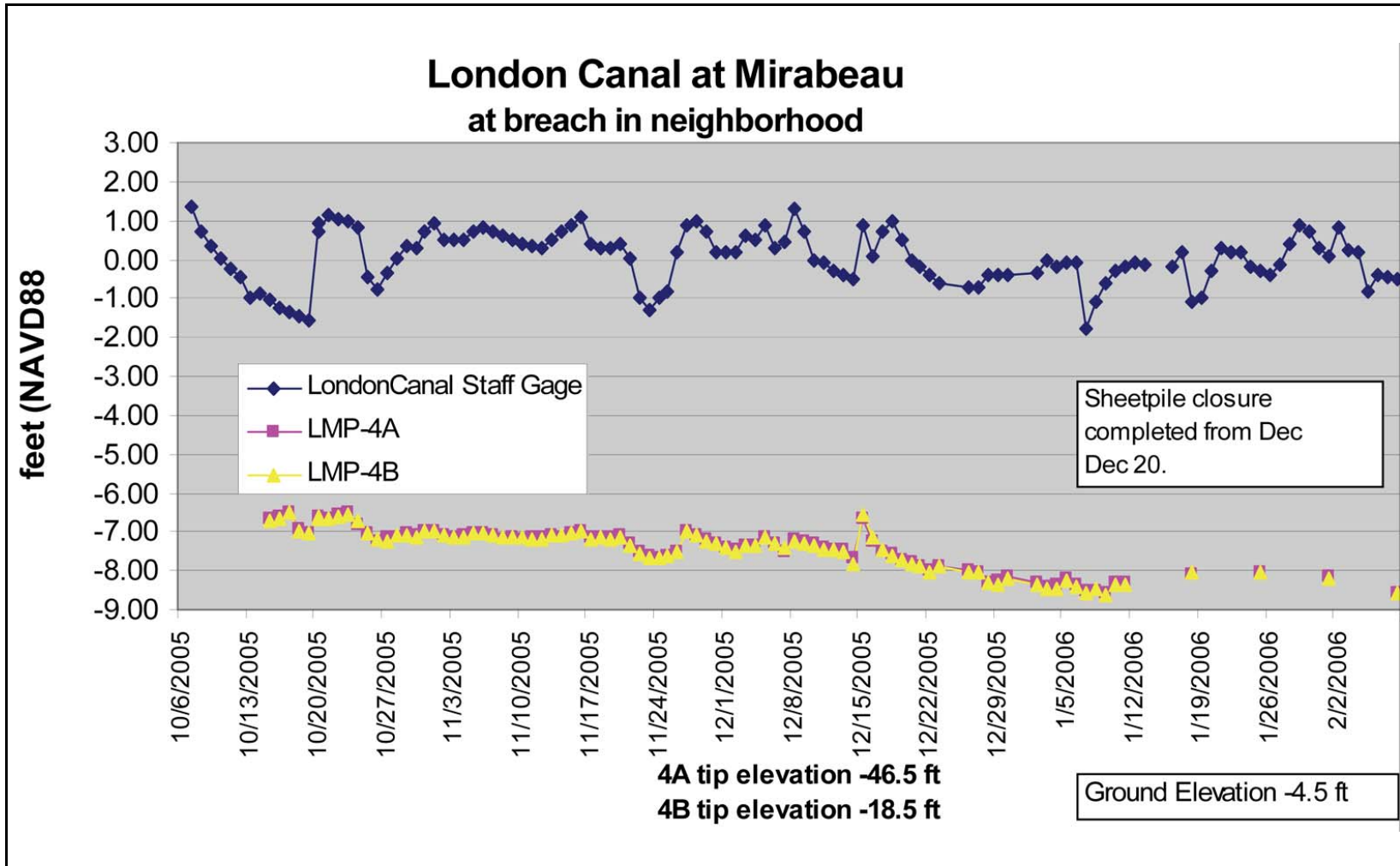


Figure 7-56. Response of Piezometers LMP-4A and LMP-4B in the Vicinity of the South London Breach Site near Mirabeau Avenue

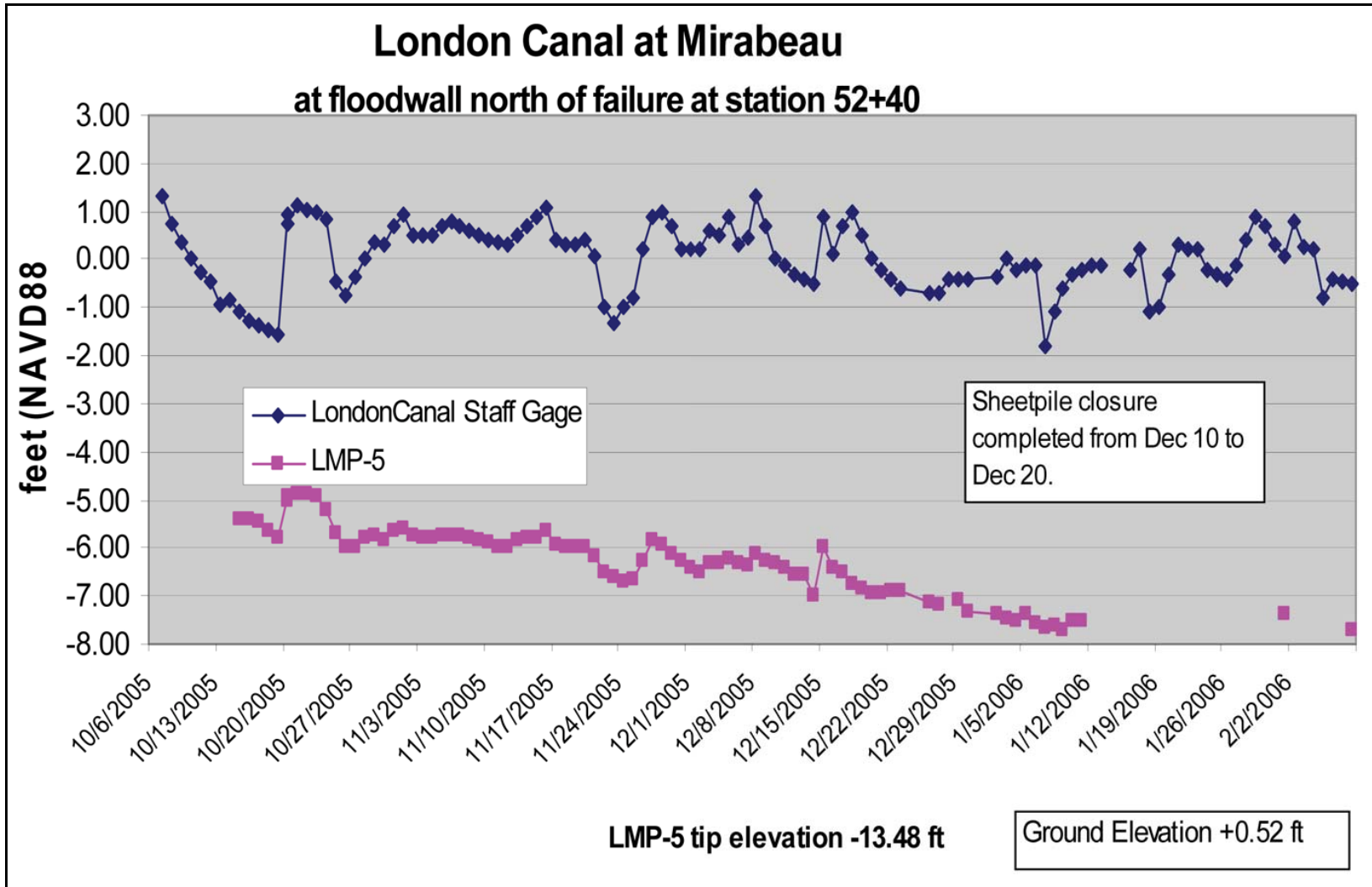


Figure 7-57. Response of Piezometer LMP5 at the South London Breach Site near Mirabeau Avenue at the Floodwall North of Breach Site at Station 52+00

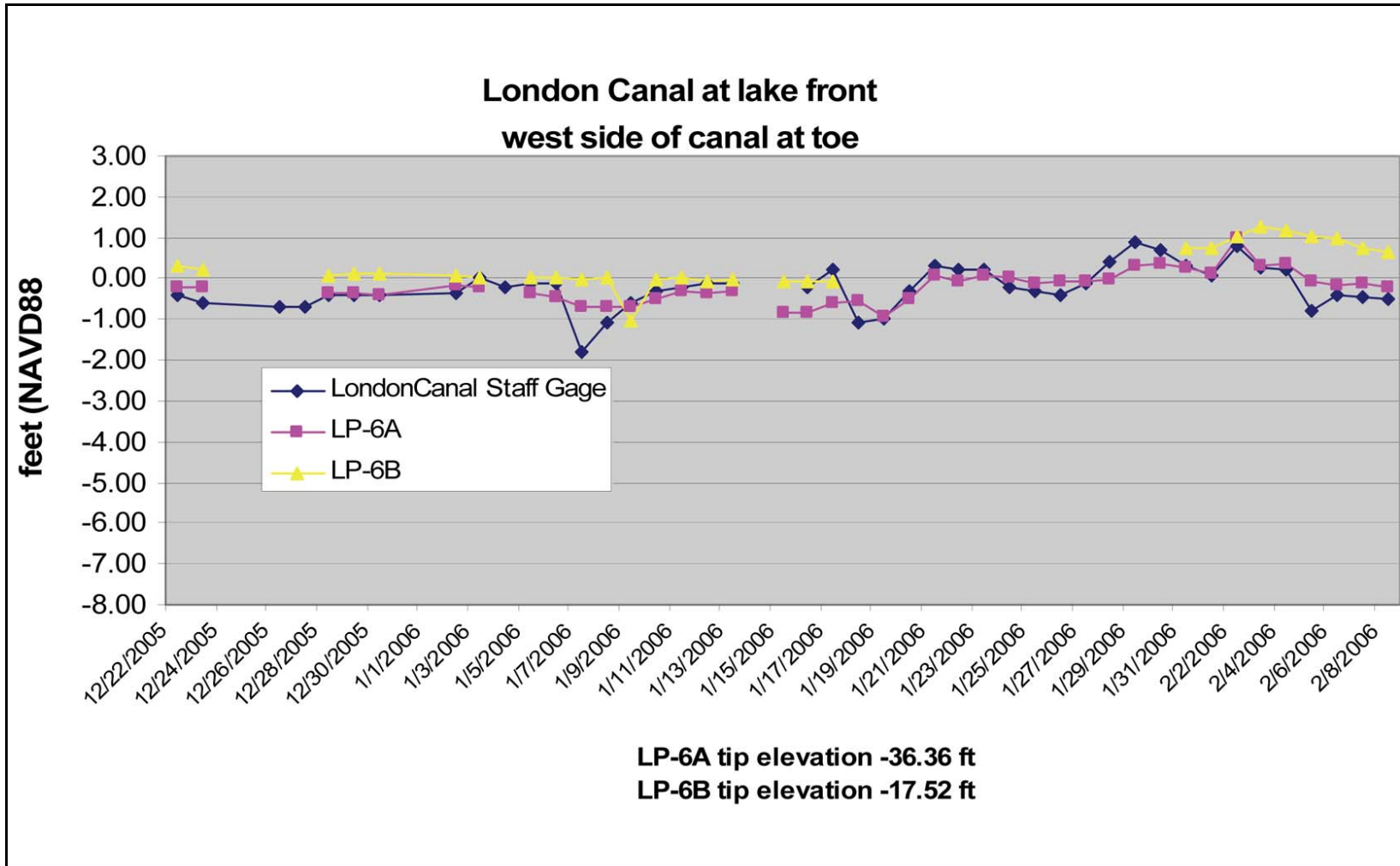


Figure 7-58. Response of Piezometer LP6A and 6B Located on the London Canal at the Lakefront at the Toe on the West Bank of the Canal

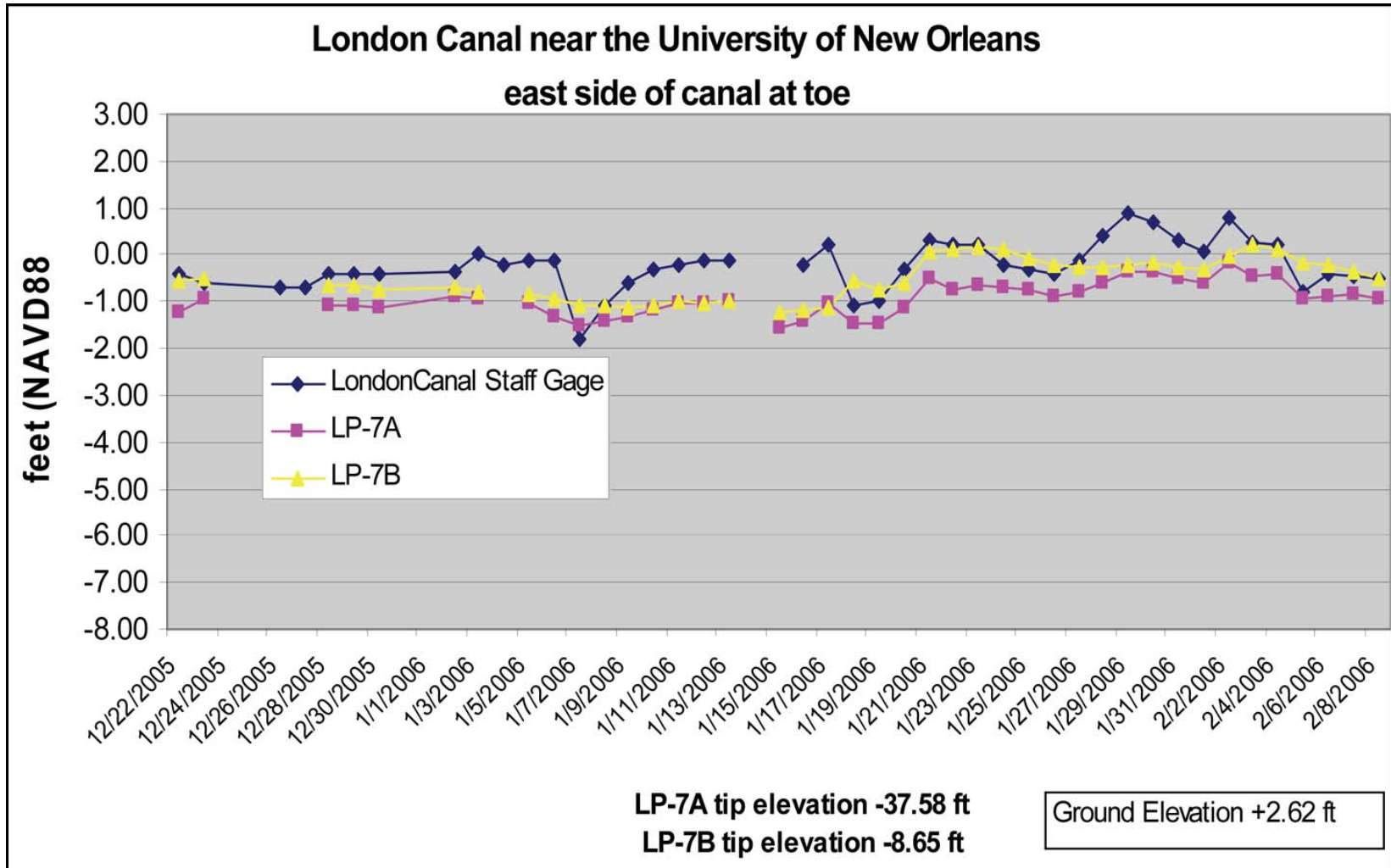


Figure 7-59. Response of Piezometers LP7A and 7B Located on the London Canal near the University of New Orleans on the East Bank of the Canal

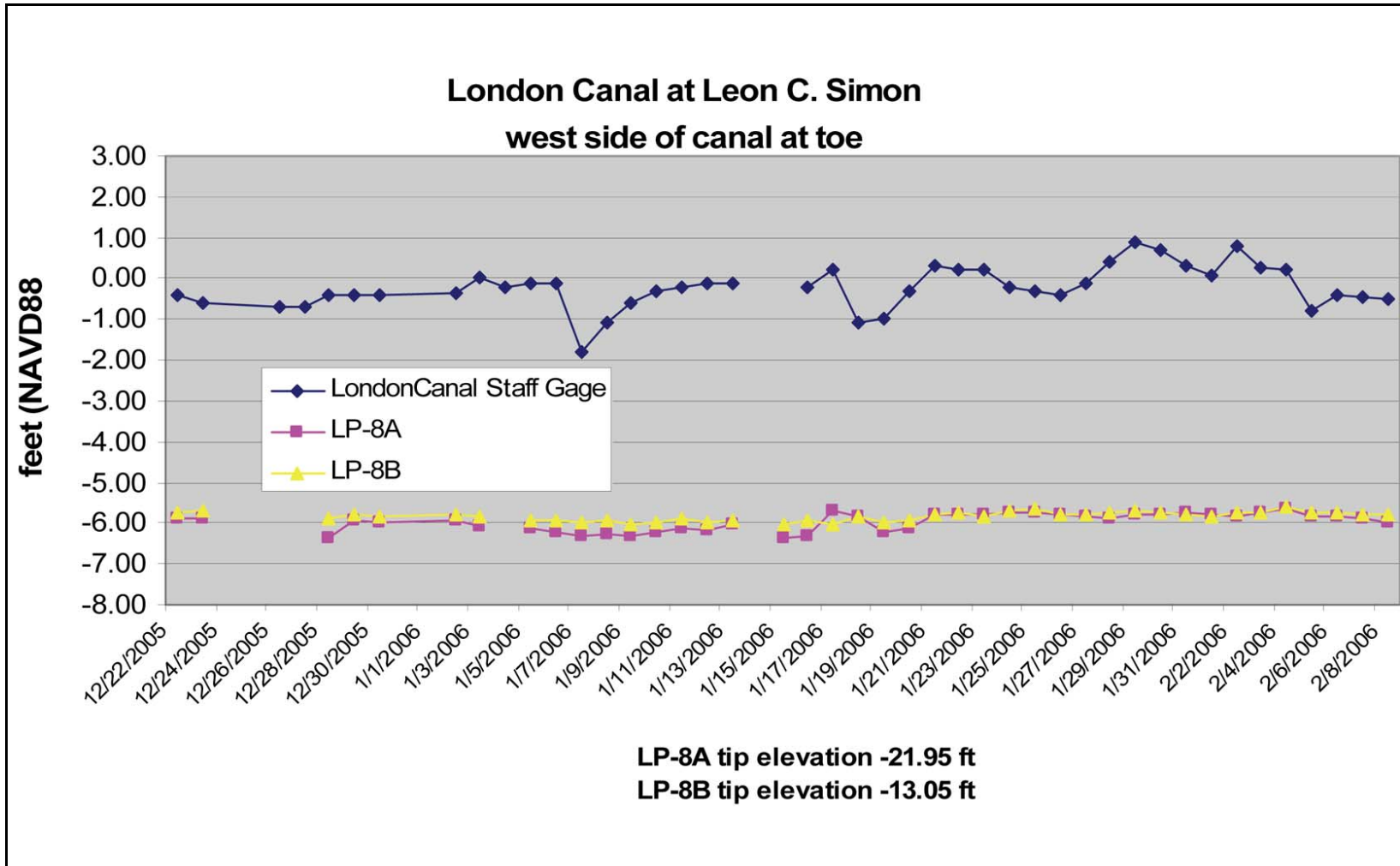


Figure 7-60. Response of Piezometers LP8A and 8B Located on the London Canal at Leon C. Simon on the Canal's West Bank

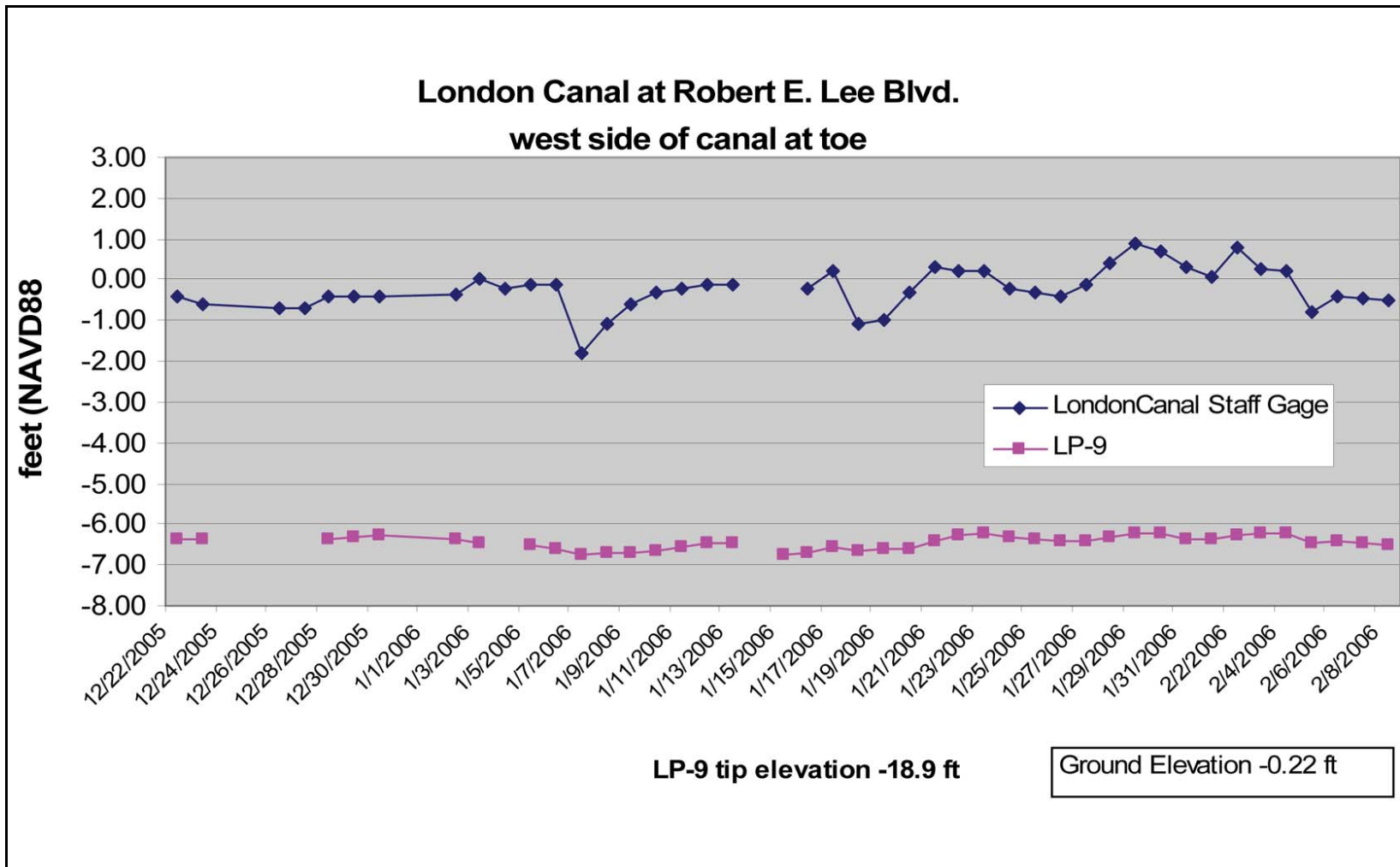


Figure 7-61. Response of Piezometer LP-9 Located on the London Canal at Robert E. Lee Boulevard on the Canal's West Bank

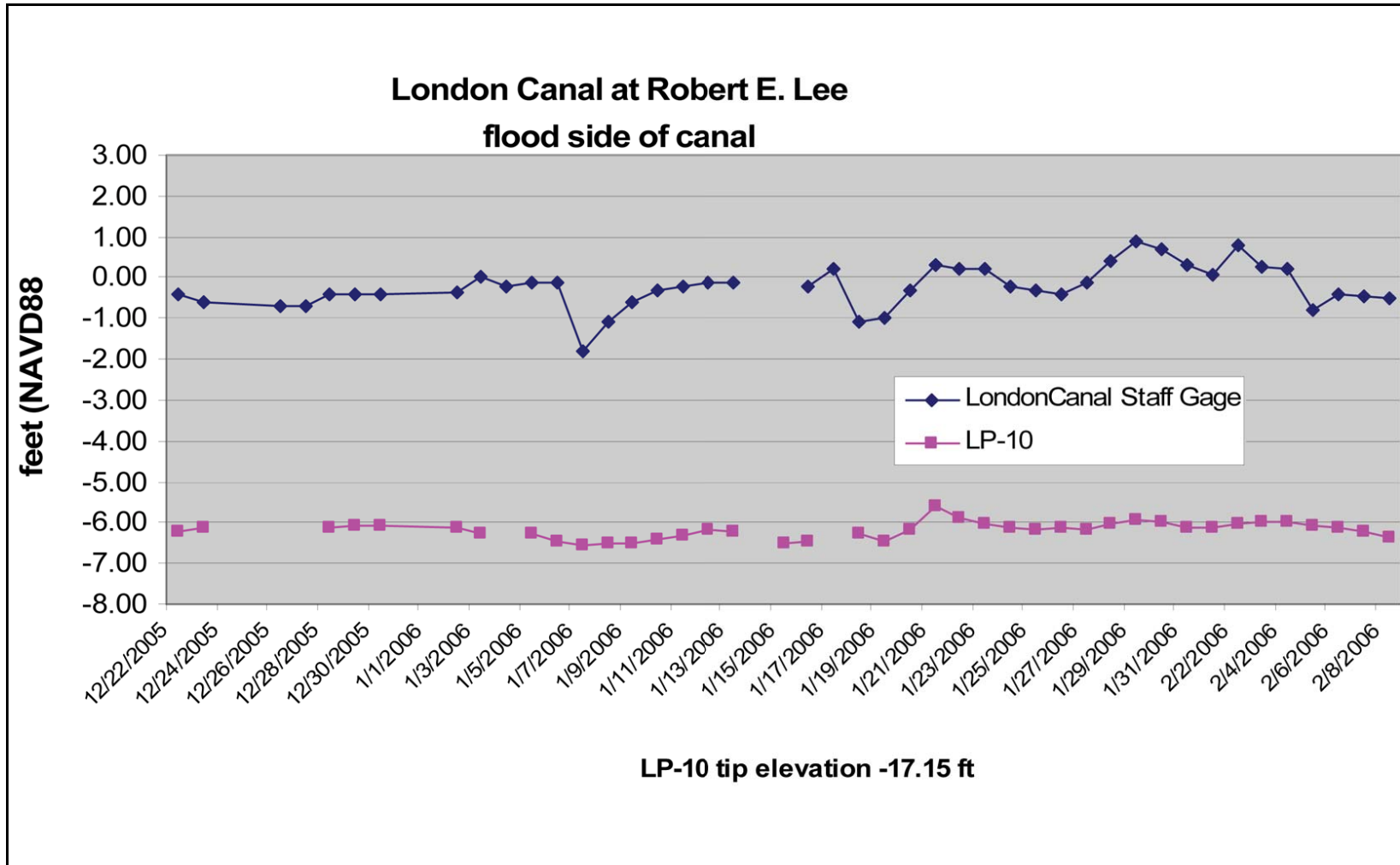


Figure 7-62. Response of Piezometer LP-10 Located on the London Canal at Robert E. Lee Boulevard on the Canal's Flood Side

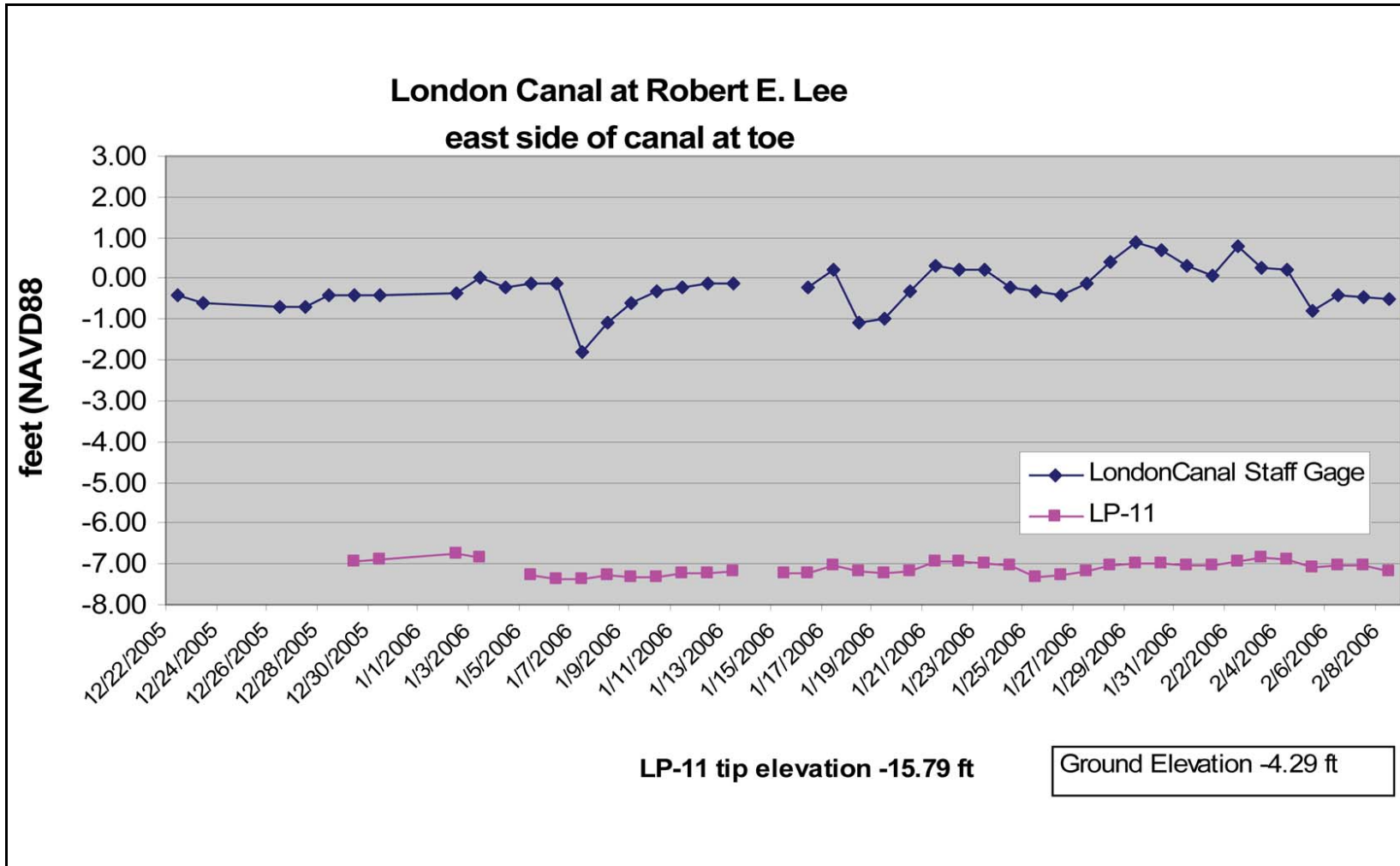


Figure 7-63. Response of Piezometer LP-11 Located on the London Canal at Robert E. Lee Boulevard on the Canal's East Side at the Toe

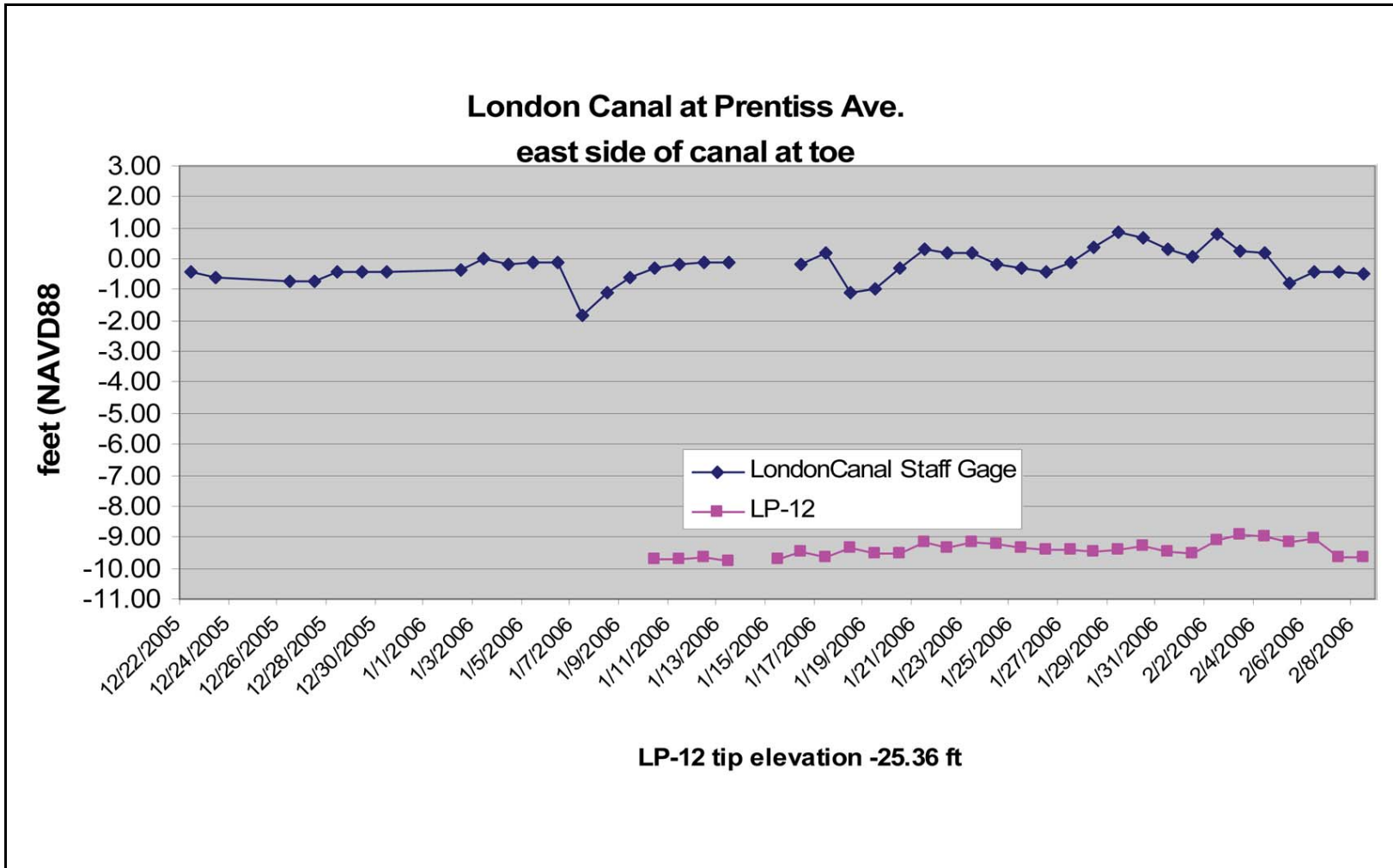


Figure 7-64. Response of Piezometer LP-12 Located at Prentiss Avenue on the Canal’s East Side at the Toe

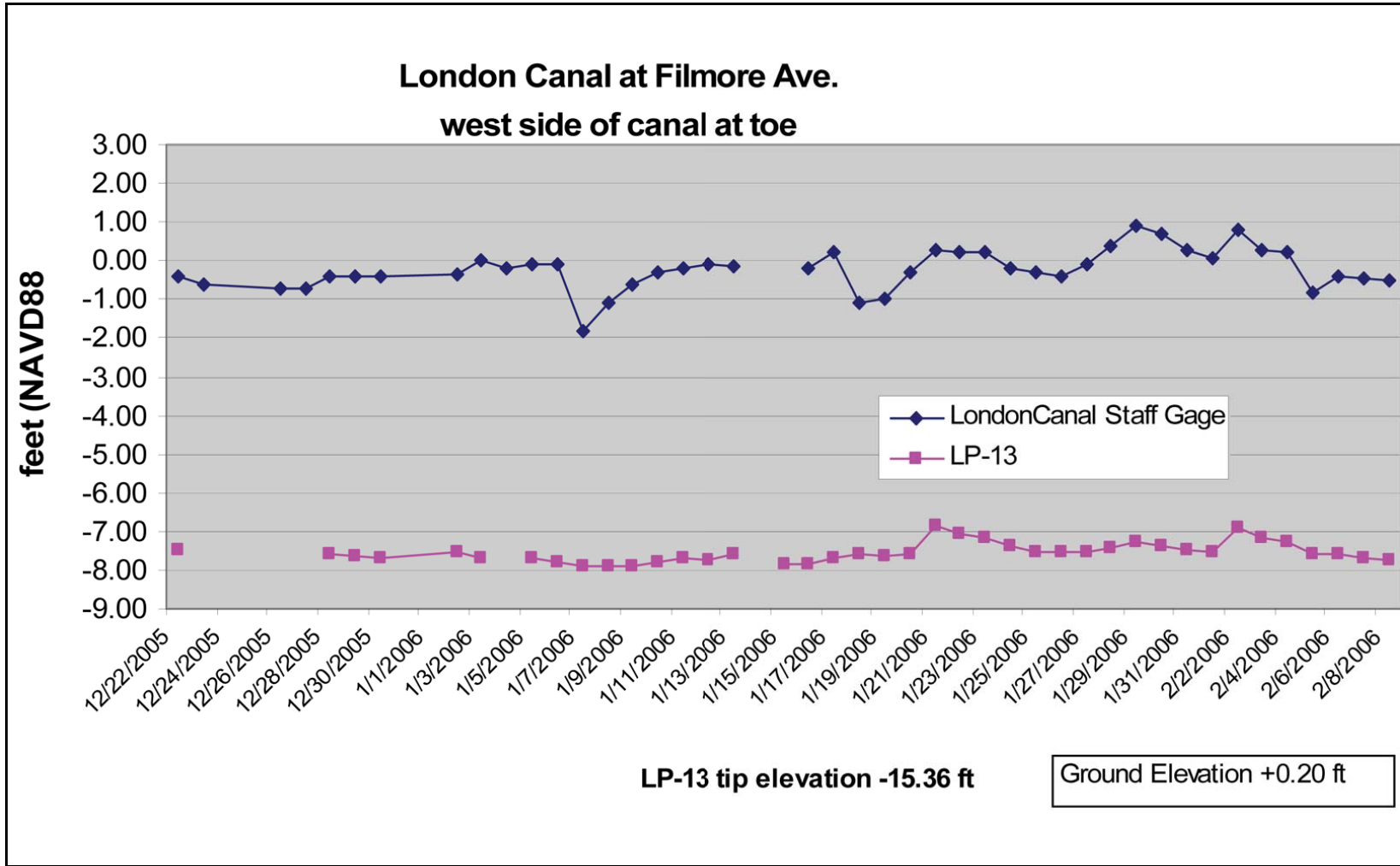


Figure 7-65. Response of Piezometers LP-13 Located at Filmore Avenue on the Canal's West Side at the Toe

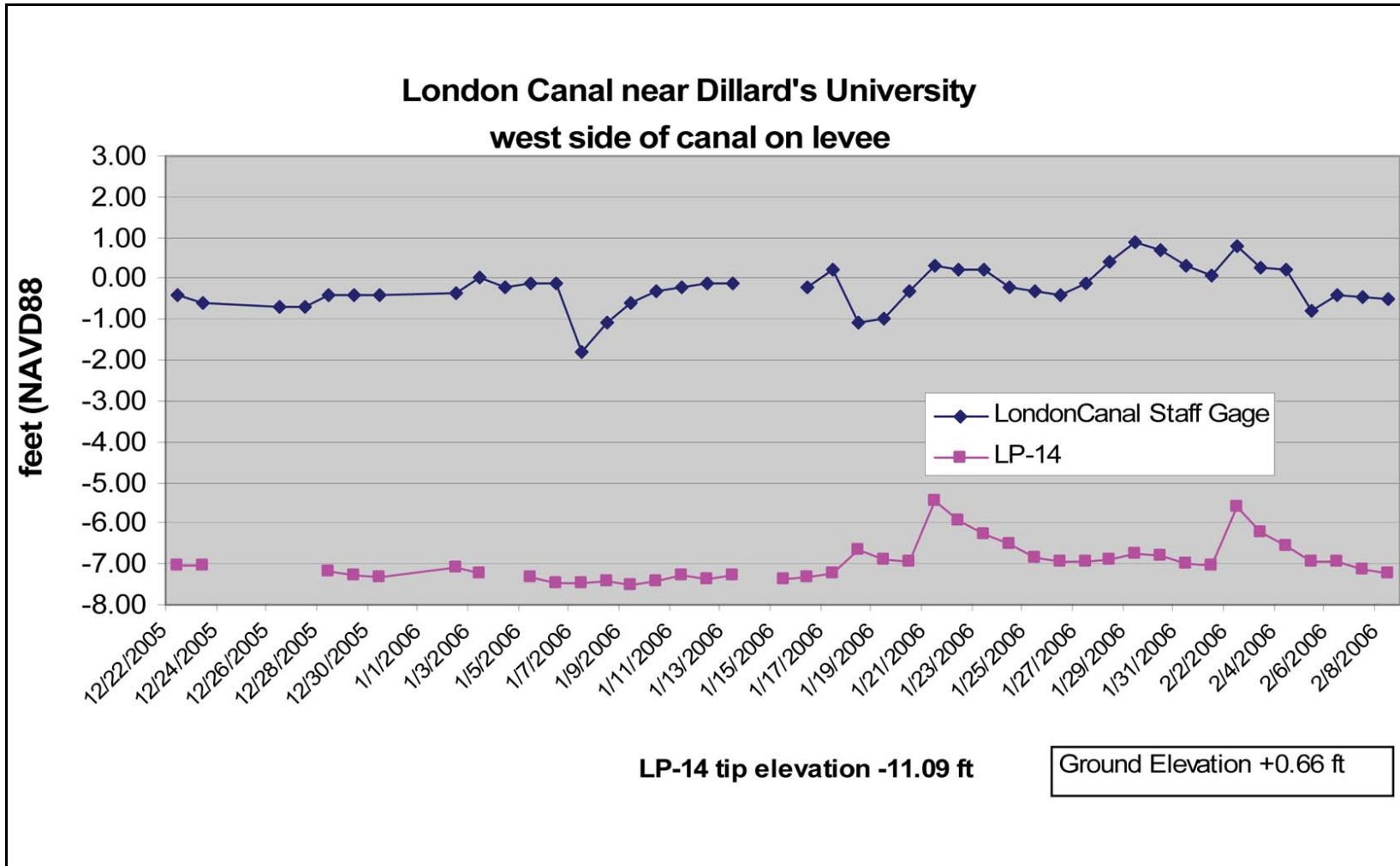


Figure 7-66. Response of Piezometer LP-14 Located near Dillard University on the Canal's West Side on the Levee

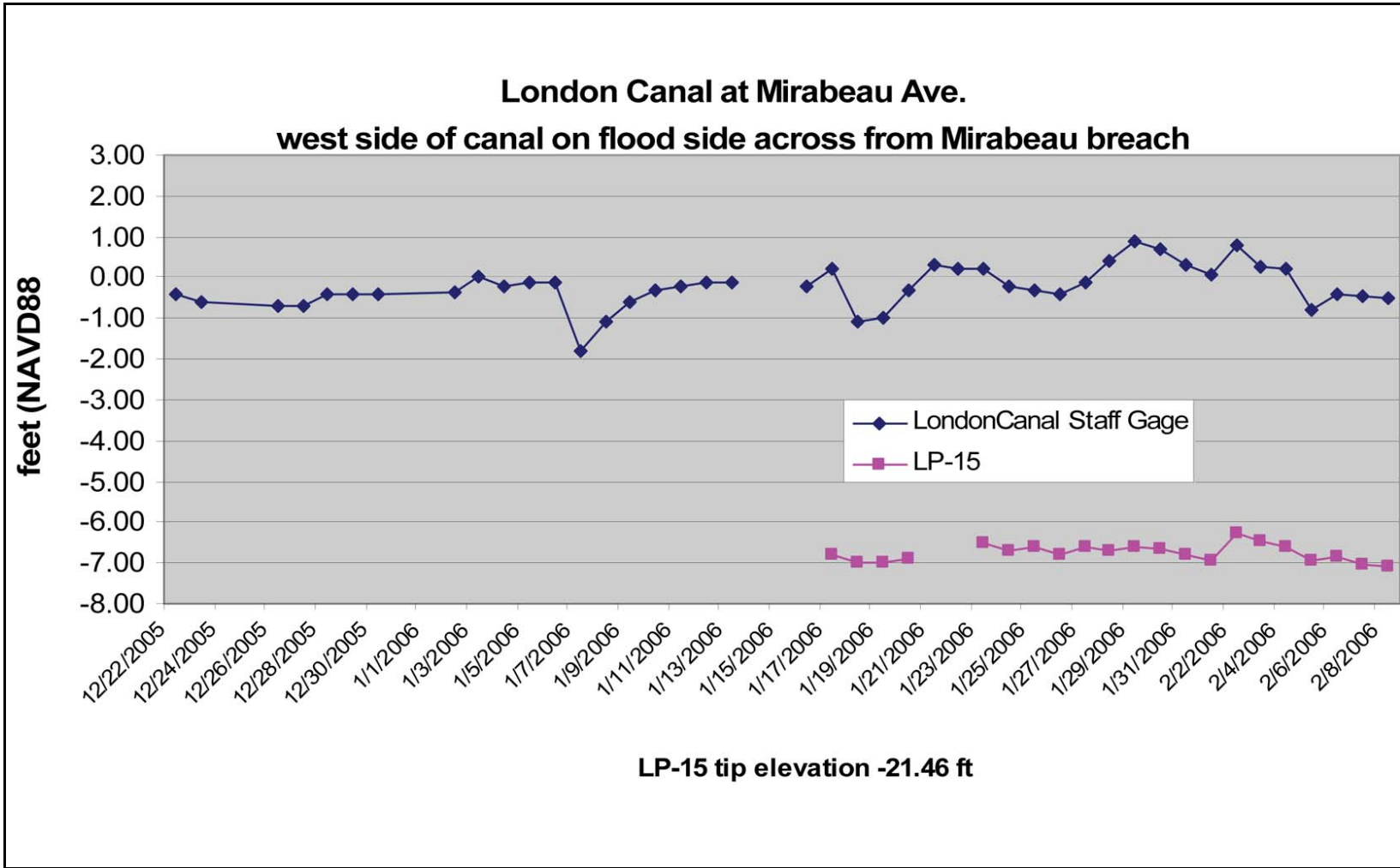


Figure 7-67. Response of Piezometers LP-15 at Mirabeau Avenue on the Canal's West Bank on the Flood Side, Directly Across from the Breach

References

- Britsch, L. D., and Dunbar, J. B. 1990. "Geomorphic Investigation of Davis Pond, Louisiana," Technical Report GL-90-12, USAE Waterways Experiment Station, Vicksburg, MS.
- Dunbar, J. B., Blaes, M. R., Dueitt, S. E., May, J. R., and Stroud, K. W., 1994. "Geological Investigation of the Mississippi River Deltaic Plain," Technical Report GL-84-15, *Report 2 of a Series*, USAE Waterways Experiment Station, Vicksburg, MS.
- Dunbar, J. B., Blaes, M. R., Dueitt, S. E., and May, J. R., 1995. "Geological Investigation of the Mississippi River Deltaic Plain," Technical Report GL-84-15, *Report 3 of a Series*, USAE Waterways Experiment Station, Vicksburg, MS.
- Dunbar, J. B., Torrey, V. H., and Wakeley, L. D., 1999. "A Case History of Embankment Failure: Geological and Geotechnical Aspects of the Celotex Levee Failure, New Orleans, Louisiana," Technical Report GL-99-11, USAE Waterways Experiment Station, Vicksburg, MS.
- Fisk, H. N., 1944. "Geological Investigation of the Alluvial Valley of the Lower Mississippi River," Mississippi River Commission, Vicksburg, MS.
- Frazier, D. E., 1967. "Recent Deltaic Deposits of the Mississippi River: Their Development and Chronology," *Transactions of the Gulf Coast Association of Geological Societies*, Vol. 17, p. 287-315.
- Kemp, E. B., and Michel, U. J., Jr. 1967. *Guidebook New Orleans, LA, and Vicinity Field Trip*, The Geological Society of America and Associated Societies, 1967 Annual Meeting, Geological Society of America.
- Kolb, C. R. 1962. "Distribution of Soils Bordering the Mississippi River from Donaldsonville to Head of Passes," Technical Report No. 3-601, USAE Waterways Experiment Station, Vicksburg, MS.
- Kolb, C. R., and Saucier R. T. 1982. *Engineering Geology of New Orleans. Reviews in Engineering Geology*, Vol. V, Geological Society of America, p. 75-93.
- Kolb, C. R., Smith, F. L., and Silva, R. C. 1975. "Pleistocene Sediments of the New Orleans-Lake Pontchartrain Area," Technical Report S-75-6, USAE Waterways Experiment Station, Vicksburg, MS.
- Kolb, C. R., and Schultz, J. R. 1954. "Geological Investigation of the New Orleans Harbor Area," Technical Memorandum 3-391, USAE Waterways Experiment Station, Vicksburg, MS.
- Kolb, C. R., and Van Lopik, J. R. 1958a. "Geology of the Mississippi River Deltaic Plain, Southeastern Louisiana," Technical Report 3-483, two volumes, USAE Waterways Experiment Station, Vicksburg, MS.

- Kolb, C. R., and Van Lopik, J. R. 1958b. "Geologic Investigation of the Mississippi River Gulf Outlet Channel," Miscellaneous Paper 3-259, USAE Waterways Experiment Station, Vicksburg, MS.
- Liao, S. S., and Whitman, R. V. 1986. "Overburden Correction Factor for SPT in Sand, Journal of Geotechnical Engineering, ASCE 112(3): 373-377.
- May, J. R., Britsch, L. D., Dunbar, J. B., Rodriguez, J. P., and Wlosinski, L. B. 1984. "Geological Investigation of the Mississippi River Deltaic Plain," Technical Report GL-84-15, USAE Waterways Experiment Station, Vicksburg, MS.
- McFarlan, E. 1961. "Radiocarbon Dating of Late Quaternary Deposits, South Louisiana," Geological Society of America Bulletin, Vols. 8, 72, p. 129-158.
- Saucier, R. T. 1963. "Recent Geomorphic History of the Pontchartrain Basin," Coastal Studies Series Number 9, Louisiana State University Studies, Baton Rouge, LA.
- Saucier, R. T. 1994. "Geomorphology and Quaternary Geologic History of the Lower Mississippi Valley," In Two Volumes, Mississippi River Commission, Vicksburg, MS.
- Schultz, J. R., and Kolb, C. R. 1950. "Geological Investigation of the New Orleans Harbor Area," Technical Memorandum No. 3-319, USAE Waterways Experiment Station, Vicksburg, MS.
- Self, R. P., and Davis, D. W. 1983. "Geology of the New Orleans Area," The Compass of Sigma Gamma Epsilon, p. 29-38.
- Smith, L. M., Dunbar, J. B., and Britsch, L. D. 1986. "Geomorphological Investigation of the Atchafalaya Basin, Area West, Atchafalaya Delta, and Terrebonne Marsh," Technical Report GL-86-3, Volumes I and II, USAE Waterways Experiment Station, Vicksburg, MS.
- Tornquist, T. E., and Gonzalez, J. L. 2002. "Reconstructing Background Rates of Sea Level Rise as a Tool for Forecasting Coastal Wetland Loss, Mississippi Delta," EOS, Transactions, American Geophysical Union, Vol. 83, No. 46, p. 525, 530-531.
- U.S. Army Corps of Engineers. 1989. "General Design Memorandum No. 19A, General Design, London Avenue Outfall Canal," Volumes I and II, Department of the Army, New Orleans District, Corps of Engineers, New Orleans, LA.
- U.S. Army Corps of Engineers. 1990. "General Design Memorandum No. 20, General Design, Orleans Parish, Jefferson Parish, 17th St. Outfall Canal (Metairie Relief)," Volumes I and II, Department of the Army, New Orleans District, Corps of Engineers, New Orleans, LA.

Work Projects Administration. 1943. *Foundations in New Orleans and Vicinity, Addendum*, Work Projects Administration, Louisiana Department of Public Works of the Mississippi River Deltas, major distributary channels are numbered, note Bayou Sauvage (No. 11) which extends across the New Orleans area and forms the Bayou Metairie/Gentilly Ridge (after Frazier, 1967). Morgan City, LA, located along axis of maximum Mississippi River entrenchment.

Appendix 8

Analysis of the London Avenue Canal I-Wall Breaches

Executive Summary

This report describes detailed assessments of the two breaches that occurred at the London Avenue Canal. The investigation of these breaches is an important step in IPET's system-wide investigation of floodwall and levee performance, and the findings illuminate a possible mechanism of failure that will be investigated system-wide for locations where sand underlies levees and floodwalls.

The breach on the London Avenue Canal near Mirabeau Avenue (the south breach) occurred at 6:00 AM to 7:00 AM on Monday, 29 August 2005. The breach on the London Avenue Canal near Robert E. Lee Boulevard (the north breach) occurred about an hour later. Field evidence, analyses, and physical model tests show that the breaches were due to the effects of high water pressures within the sand layer beneath the levee, and high water loads on the walls. The London Avenue Canal breaches had a key factor in common with the 17th Street Canal breach – formation of a gap between the wall and the levee fill on the canal side of the wall. At both the 17th Street Canal and the London Avenue Canal, formation of a gap allowed high water pressures to act on the wall below the surface of the levee, severely loading the wall. At the London Avenue Canal, an additional effect of the gap was that water flowed down through the gap into the underlying sand. High water pressures in the sand uplifted the marsh layer on the landside of the levee, resulting in concentrated flow and erosion, removing material and reducing support for the floodwall.

Analyses of the south breach showed that erosion is the most likely principal mode of failure, with sliding instability occurring after significant volumes of sand and marsh had been removed by erosion and piping. Without alteration of the south breach cross section by erosion and piping on the landside of the levee, the calculated factors of safety with respect to sliding instability are greater than 1.0, indicating that alteration of the cross section by erosion and piping probably played an essential role in the failure at this location.

Field observations at the north breach indicate that the canal-side levee crest remained intact after the breach, and a playhouse on the property adjacent to the breach was heaved upward

during the breach. The analyses presented in this report show that conditions for erosion and piping were present at the north breach, but the more likely cause of the failure was sliding instability. High uplift pressures likely resulted in a rupture through the marsh layer and the underlying thin layer of clay. At this location, however, the high pore pressures within the sand would reduce passive resistance sufficiently to result in sliding instability without significant alteration of the cross section.

Observations

Two I-wall failures resulting in breaches occurred at the London Avenue Canal during Hurricane Katrina, one on the east side of the canal at Mirabeau Avenue (the south breach), and the other on the west side of the canal at Robert E. Lee Boulevard (the north breach). At both locations the levees and I-walls were founded on a layer of marsh (peat) overlying sand. In addition, the I-wall on the east side, across the canal from the north breach, moved and tilted, but did not breach.

The south breach, shown in Figure 8-1, occurred about 6:00 AM to 7:00 AM on August 29th, when the water level in the canal was 7.1 ft to 8.2 ft NAVD88. The time sequence for the breach was updated after this work had been completed. The new time for the breach is between 7:00 AM to 8:00 AM, when the water level in the Canal was 8.2 ft to 9.5 ft. Because of the overlap of the times and water level was not necessary to redo the analyses in this breach. The breach was narrower than the breach at 17th Street and the London Avenue north breach. A deep scour hole formed due to the inrush of water, and a large amount of eroded sand was deposited in the neighborhood inland of the breach. It appears that the breach was quite narrow when it formed, and subsequently widened to about 60 ft as wall panels adjacent to the initial breach were undermined by scour, and tilted into the scour hole.

The north breach, shown in Figure 8-2, occurred about 7:00 AM to 8:00 AM on August 29th, about an hour after the south breach, when the canal water level was 8.2 ft to 9.5 ft NAVD88. The time sequence for the breach was updated after this work had been completed. The new time for the breach is between 7:00 AM to 7:30 AM, when the water level in the Canal was 8.2 ft to 8.9 ft. Because of the overlap of the times and water level was not necessary to redo the analyses in this breach. The breach was about 410 ft wide, approximately the same width as the breach at 17th Street. A playhouse on the property adjacent to the breach was heaved upward when the breach occurred, indicating upward movement of the ground inboard of the levee toe. The I-wall opposite the north breach (on the east side of the canal) moved and tilted significantly, presumably at about the same time as the breach occurred on the west side, but the east I-wall did not breach. A line of sinkholes was observed at the inland side of the distressed east I-wall, and a sand boil at the inboard embankment toe indicate that erosive seepage and piping had occurred beneath the levee.

Possible Modes of Failure

At both the south and north breach locations, it seems likely that underseepage and internal erosion caused or contributed to the failures.

It is not possible to establish the cause of the south breach with certainty based on the field observations made after the failure. The failed sections of the I-wall were not found, and large volumes of sand were moved by the inflow of water through the breach, covering the landscape. The failure might have resulted from underseepage erosion and piping, or from sliding instability aggravated by seepage and uplift pressures. Analyses have been performed to examine both of these possibilities.

It has been reported that cold-rolled sheetpiles were used for the I-wall in the area of the south breach. Cold-rolled sheetpiles have lower interlock strengths than hot-rolled sheetpiles. Consequently, use of cold-rolled sheetpiles increases the likelihood that interlocks could have failed during driving, particularly because the sand in the south breach area was dense, and driving was hard. Interlock failure would result in gaps between adjacent sheets in the sheetpile wall, making it possible for water to seep through the wall as well as under the wall. Such through-flow would result in more severe seepage conditions than those reflected in the seepage analyses described here, and would make erosion and piping an even more likely mode of failure at the south breach.

Field observations at the north breach indicate that sliding instability was likely the primary mode of failure, with seepage and high pore pressures in the sand as a significant contributing factor. It seems likely that the failure and breach were the result of insufficient passive resistance to counteract the water pressure forces to which the wall was subjected. The passive resistance was likely reduced by the effects of water seeping through the foundation soils beneath the levee and the marsh layer inland, inducing uplift pressures and reducing shear strengths. Analyses have been performed to examine the likelihood of erosion and piping, and instability due to uplift and reduced shear resistance.

London South Breach Seepage and Stability Analyses

Erosion and Piping

Finite element analyses of seepage beneath the I-wall were performed using the computer program SLIDE¹. The characteristics of the cross section analyzed are shown in Figure 8-3. The relevant materials are the sand at the base of the section, the overlying marsh (peat) layer, and the clayey levee fill. The permeability of the sand, based on field pumping tests, was 1.5×10^{-2} cm/sec. The permeability of the marsh layer was estimated as 1×10^{-5} cm/sec, and the permeability of the levee fill and the Bay Sound clay was estimated as 1×10^{-6} cm/sec. Thorough analyses of transient and steady seepage, described in a separate report, indicated that (a) steady seepage through the sand was established quickly, and (b) the pore pressures within the sand and

¹ Available from Rocscience Inc., 31 Balsam Avenue, Toronto, Ontario, Canada M4E 3B5

the uplift pressures on the base of the marsh layer are not affected by the permeability values assigned to the marsh layer and the levee fill, provided that those materials are at least two orders of magnitude less permeable than the sand. The values of permeability of the marsh layer and the levee fill used in the seepage analyses described here were selected in accordance with these findings, and are considered to be reasonable estimates of the permeabilities of these materials.

The hydraulic boundary conditions used in these analyses are shown in Figure 8-3. The canal water level was either 7.1 ft or 8.2 ft NAVD88, a range consistent with the estimated canal water levels at the time of failure. A constant-head boundary condition was imposed at the location of the drain beneath Warrington Drive. This head value was either -8.4 ft (the normal ground water level with pumps operating), or -5.1 ft NAVD88 (a higher level equal to the ground surface elevation, which might have occurred with pumps not operating). Reports indicate that the pumps stopped operating when the wall failed, severing the power line. In all, four different seepage cases were analyzed, as shown in Table 8-1.

Based on the study of the 17th Street Canal breach, it seems likely that a crack or gap would form between the I-wall and the levee fill on the canal side of the wall. The type of gap assumed to have formed behind the 17th Street Canal I-wall, shown in Figure 8-4, does not seem feasible for the London Avenue foundation conditions, where the I-wall is driven into sand, because cohesionless sand would be unable to support a gap. A more likely condition for a wall driven into sand is shown in Figure 8-5. This “half-cracked” condition involves a crack or gap through the levee fill and the marsh layer, down to the top of the sand. Water would fill this gap, loading the wall and introducing the canal head at the top of the sand. The part of the wall embedded in the sand would be loaded by water pressures that are somewhat lower than hydrostatic pressures, plus active earth pressures, as shown in Figure 8-5. The lower-than-hydrostatic water pressures were determined from the finite element seepage analyses. All of the seepage and stability analyses were performed based on this half-cracked condition.

Six-node triangular elements were used for the seepage analyses. The finite element mesh is shown in Figure 8-6. Computed total head contours for Case 1 are shown in Figure 8-7. It can be seen that the flow through the sand is predominantly horizontal, and that the total head on the landward side of the levee is above the ground surface, which is at elevation -5.1 ft. The head contours for the other three cases shown in Table 8-1 had similar shapes, although the values varied somewhat depending on the canal water level and the Warrington Drive water level.

Computed pore pressures, or uplift pressures, at the base of the marsh layer are shown in Figure 8-8 for the four cases analyzed, together with the total overburden pressure at the base of the marsh layer. It can be seen that in all four cases the computed pore pressures exceed the total overburden pressure at the base of the marsh layer. This result indicates that the marsh layer would be heaved off the underlying sand by the high uplift water pressures. A likely result of this heave would be rupture of the marsh layer at one or more weak points, and upward flow of water through the rupture in the marsh material. This flow would relieve the high water pressure locally, and create a new hydraulic boundary condition at the point of rupture.

Additional seepage analyses were performed to determine if the hydraulic gradients within the sand after rupture of the marsh layer would be large enough to cause erosion of the sand and

begin a piping failure. The seepage boundary conditions used in these analyses are shown in Figure 8-9, where a rupture extends upward through the marsh layer, from the top of the sand to the ground surface. The hydraulic gradients computed in these analyses were found to depend on the assumed width of the rupture in the marsh layer. While it seems clear that the marsh layer would rupture when the uplift pressures exceeded the overburden pressures, the width of the rupture would depend on factors that cannot be evaluated, and it is thus necessary to assign a width to the rupture zone based on judgment. Even so, we believe that the analytical results that follow reflect the essential aspects of the situation. The results support the view that the London south breach developed as a result of erosion and piping.

The narrower the assumed rupture zone, the higher the computed hydraulic gradient at the top of the sand below the rupture, because flow converges toward the rupture, and the flow velocities increase near the rupture. This converging flow is shown by the total head contours in the sand near the rupture in Figure 8-10. A rupture zone width equal to 1.6 ft was used in the analyses, based on a judgment of what seemed a reasonable and possible rupture zone size. Doubling the width of the rupture zone was found to reduce the computed hydraulic gradient by 23%, and cutting the width in half increased the hydraulic gradient by 33%. In the real case, flow would converge in three dimensions rather than two dimensions, as represented in these two-dimensional seepage analyses. It therefore seems likely that the actual hydraulic gradients would be higher than the values discussed in the following sections, but the magnitude of this three-dimensional effect cannot be quantified.

The changed hydraulic boundary conditions caused by the rupture through the marsh layer were computed by imposing a head at the base of the rupture that was equal to the elevation of the ground surface, simulating a condition where the water level within the ruptured zone rises to the ground surface. Values of vertical hydraulic gradient at the top of the sand for this condition are shown in Table 8-2 for the four cases analyzed. It can be seen that they range from 1.03 to 1.24.

The value of hydraulic gradient that would cause erosion of the sand is

$$i_{critical} = \frac{\gamma_b}{\gamma_w} = \frac{\gamma_s - \gamma_w}{\gamma_w}$$

where $i_{critical}$ = hydraulic gradient that would cause erosion of the sand, γ_b = buoyant unit weight of sand, γ_w = unit weight of water, and γ_s = saturated unit weight of sand. With γ_s for the sand assumed to be 120 pcf, the critical hydraulic gradient is 0.92. Thus the values of hydraulic gradient for all four cases analyzed would be large enough to cause erosion and to begin piping, as shown by the values of $F_{erosion}$ listed in Table 8-2.

Considering the variation in factor of safety caused by the uncertain landside water level, the probability of erosion was calculated as shown in Table 8-3. A simple method based on the

Taylor series² was used for these calculations. It can be seen that the probability of erosion approaches 100% for both canal water levels, indicating a high likelihood that erosion occurred and that erosion was the cause of the failure, or an exacerbating factor in the failure.

Considering that three-dimensional concentration of flow would result in even larger hydraulic gradients, it appears that erosion and piping of the sand would be likely at the south breach. With high hydraulic gradients, backward erosion could occur rapidly, extending back to the I-wall, and leading to a catastrophic failure of the type that was observed. The analyses described here consider only the beginning of this process. Once erosion of the sand into the rupture in the marsh layer began, the situation would deteriorate quickly as seepage converged to the zone of erosion, and the rate of erosion increased. Eventually, after enough sand, marsh and possibly levee fill had been eroded away, an unstable condition would develop, with the passive resistance of the materials landward of the wall becoming too small to resist the forces of the water and earth pressures pushing from the canal side of the wall.

Slope Instability

While this erosion and piping failure mechanism appears plausible based on the results of the analyses described above, it is of interest also to examine the possibility that the failure could have occurred by sliding, through a slope instability failure mechanism. To examine this possibility, slope stability analyses were performed using the computer program SLIDE¹.

The stability analyses were performed for the cross section shown in Figures 8-11, 8-12, 8-13, and 8-14. This is the same cross section as used in the seepage analyses, and the same canal water levels and landside water levels were used.

Standard Penetration Tests performed in the breach area before the breach showed that the sand had Standard Penetration Test blow counts (N_{SPT}) greater than 50, which would correspond to values of ϕ' in the range of 40 degrees to 46 degrees. Cone penetration tests performed after the breach showed high tip resistance in the sand adjacent to the breach, which correspond to similar values of ϕ' . In order not to overestimate the strength of the sand, a value of $\phi' = 40$ degrees was used in the stability analyses.

The marsh was treated as undrained, with $s_u = 300$ psf, and $\phi_u = 0$, based on the available test results. A value of $s_u = 300$ psf is considered appropriate for the areas beneath the canal-side levee slope and beyond the levee toe, where the slip circles pass through the marsh. The unit weight of the marsh was assumed to be 80 pcf.

The levee fill was also treated as undrained, with $s_u = 900$ psf, and $\phi_u = 0$. The slip circles do not intersect the levee fill, however, and the levee strength therefore has no influence on the calculated values of factor of safety. The unit weight of the levee fill was assumed to be 109 pcf.

² Wolff, T. F. (1994). "Evaluating the reliability of existing levees." Report, Research Project: Reliability of Existing Levees, prepared for U.S. Army Engineer Waterways Experiment Station Geotechnical Laboratory, Vicksburg, Miss.

Analyses were performed with canal water levels at 7.1 ft and 8.2 ft NAVD88, using pore pressures in the sand from the finite element seepage analyses without a rupture through the marsh layer. The non-ruptured seepage analyses were used to determine pore pressures because the rupture is conceived as a feature of very limited size, not appropriate for inclusion in a two-dimensional cross section. At the bases of the slices where the pore pressures exceeded the overburden pressures near the top of the sand on the inboard side, zero shear strength was assigned for the sand.

As discussed earlier, it was assumed in all analyses that deflection of the wall toward the land side would result in formation of a gap through the levee fill and the marsh in back of the wall, down to the top of the sand. It was assumed that the gap would not extend into the sand, because the sand is cohesionless, and would be expected to slump and fill any gap. This “half-cracked” condition was used in all stability analyses. It can be seen in Figures 8-11, 8-12, 8-13, and 8-14 that the slip circles extend to the bottom of the sheetpile wall furthest from the canal.

The factors of safety calculated in these analyses are shown in Figures 8-11 through 8-14, and in Table 8-4. For the canal water levels estimated at the time of the breach (7.1 ft to 8.2 ft) the calculated factors of safety range from a low value of $F = 1.19$ to a high value of $F = 1.56$. Thus, with this interpretation of the available data, and consistent assumptions for the seepage and stability analyses, a mechanism of failure involving erosion and piping is plausible at the south breach, but a slope stability failure mechanism is not.

An analysis was performed, with the landside water level at -8.4 ft, to determine the canal water level corresponding to a calculated factor of safety equal to 1.00. As shown in Figure 8-15, a canal water level equal to 9.7 ft would be required for a factor of safety equal to 1.00. This is 1.5 ft higher than the highest estimated water level at the time the breach occurred, indicating that instability without removal of material by erosion and piping is unlikely at the south breach.

Additional stability analyses were performed, varying the friction angle of the sand and the strength of the marsh layer, to compute the probability of slope instability. The results of these cases are shown in Table 8-5. The Taylor series approach² was used to compute the standard deviation of the factor of safety and the probability of failure. The most likely value of factor of safety was taken as the average of the values for the high and low inland water levels. The probability of instability was estimated assuming a log-normal distribution of factor of safety, with the results shown in Table 8-5. It can be seen that the estimated probability of instability is 1% for the lower canal water level, and 10% for the higher canal water level. Thus, while there is a small probability that failure might have occurred due to instability without erosion and piping, this mode of failure is much less likely than failure by erosion and piping.

London North Breach Seepage and Stability Analyses

The possibilities of failure due to erosion and piping, and due to instability, were also examined for the London Avenue north breach. The differences between the London south breach analyses and the London north breach analyses were:

1. The seepage boundary conditions were different. The canal water level at the time of the north breach was 8.2 ft to 9.5 ft, higher than at the south breach because the north breach occurred later. The inland seepage boundary condition ranged from -8.4 ft to -3.9 ft because Pratt Drive is at a slightly higher elevation than Warrington Drive. Four cases were analyzed, using the seepage boundary conditions shown in Figure 8-16, and summarized Table 8-6. An additional analysis was performed to determine the canal water level required for a calculated factor of safety equal to 1.00.
2. The cross sections are somewhat different. On the inland side of the wall at the north breach, there is a thin layer of lacustrine clay between the marsh layer and the sand.
3. The sand is less dense in the north breach area. Standard Penetration Test blow counts (N_{SPT}) in this area range from 2 to 14, with an average of about 10. This range of values of N_{SPT} corresponds to values of ϕ' in the range of 30 degrees to 34 degrees. Cone penetration tests performed after the breach, in the area adjacent to the breach, showed tip resistances that correspond to about the same values of ϕ' . A value of $\phi' = 32$ degrees was used in the stability analyses for the north breach area.

Erosion and Piping

Six-node triangular elements were used for the seepage analyses, as for the south breach. The finite element mesh for the north breach is shown in Figure 8-17. The same values of permeability were used as for the south breach. The lacustrine clay between the sand and the marsh layer was assumed to have a permeability of 1×10^{-6} cm/sec.

Computed total head contours for Case 1 are shown in Figure 8-18. As for the south breach, the flow through the sand is predominantly horizontal, and the total head on the landward side of the levee is above the ground surface, which is at elevation - 3.9 ft. The head contours for the other three cases that were analyzed had similar shapes, although the values varied somewhat depending on the canal water level and the Pratt Drive water level.

Water pressures at the base of the marsh layer for the north breach area are shown in Figure 8-19. As in the case of the south breach area, the uplift water pressures exceed the overburden pressures due to the weight of the marsh layer at the landside of the levee, and it would be expected that the marsh layer would be heaved upward and would rupture.

Additional seepage analyses were performed with revised boundary conditions, as was done in the south breach analyses, using the conditions shown in Figure 8-20. A rupture 1.6 ft wide, extending through the marsh layer and the lacustrine clay layer was assumed, and a hydraulic boundary condition with the water level at the ground surface was applied in the area of the rupture. Total head contours for the area around the assumed rupture through the lacustrine clay and peat are shown in Figure 8-21. The hydraulic gradients calculated for these conditions are shown in Table 8-7.

With γ_s for the sand equal to 115 pcf (5 pcf less than at the south breach where the sand was more dense), the critical hydraulic gradient is 0.84. The values of hydraulic gradient all four

cases analyzed would be large enough to cause erosion and begin piping of the sand. Thus erosion and piping appears to be a plausible mode of failure for the London north breach, as well as the south breach.

Probabilities of erosion for the high and low canal water levels were calculated using the same procedure as for the south breach², with the results shown in Table 8-8. It can be seen that the probability of erosion exceeds 90% for both the low and the high canal water levels, and approaches 100% for the higher level. These probabilities are slightly smaller than for the south breach, where the probability of erosion approached 100% for both high and low canal water levels.

Slope Instability

While erosion and piping appears possible based on the results of the analyses described above, it is also of interest to examine the factor of safety against slope instability. To examine the possibility that the failure mechanism involved sliding, slope stability analyses were performed using the same procedures as used for the south breach. The stability analyses were performed for the cross section shown in Figures 8-22, 8-23, 8-24, and 8-25. This is the same cross section as used in the seepage analyses.

Analyses were performed for four cases, using the canal water levels and inland water levels shown in Table 8-6, and pore pressures in the sand from the same finite element seepage analyses used to compute the uplift pressures shown in Figure 8-19. As noted previously, a value of $\phi' = 32$ degrees was used for the sand. The strengths and unit weights of the marsh and the levee fill were the same as used in the south breach stability analyses described previously. The undrained strength of the lacustrine clay was assumed to be equal to 42 psf. The strength of this thin layer has a very small influence on the calculated factors of safety. At the bases of slices where the pore pressures exceeded the overburden pressures at the top of the sand on the inland side, zero shear strength was assigned for the sand.

The same half-cracked condition was used in these analyses as was used for stability analyses at the south breach. It can be seen in Figures 8-22, 8-23, 8-24, and 8-25 that the slip circles extend to the bottom of the sheetpiles. Full hydrostatic water pressure force acts on the sheetpile down to the top of the sand. From the top of the sand to the bottom of the sheetpile, the sheetpile is acted on by water pressures determined from the seepage analyses and active earth pressures.

The factors of safety for Cases 1 through 4 are shown in Figures 8-22 through 8-25, and are listed in Table 8-9. They range from a low value of $F = 0.67$ to a high value of $F = 0.99$. Thus, because the sand is considerably less dense in the north breach area, and would have a smaller friction angle, a mechanism of failure involving slope instability is plausible.

An additional analysis was performed, with the landside water level at -8.4 ft, to determine the canal water level corresponding to a calculated factor of safety equal to 1.00. As shown in Figure 8-26 and Table 8-9, a canal water level equal to 8.1 ft corresponds to a factor of safety

equal to 1.00. This is very nearly equal to the lowest estimated water level at the time the breach occurred, indicating that instability is a highly likely mode of failure at the north breach.

Further analyses were performed, varying the friction angle of the sand and the strength of the marsh layer, to compute the probability of slope instability, using the Taylor series method.² The results of these cases are shown in Table 8-10. The most likely value of factor of safety was taken as the average of the values for the high and low inland water levels. The results of these calculations are shown in Table 8-10. It can be seen that the estimated probability of instability is 70% for the lower canal water level, and 97% for the higher canal water level. Thus, there is a very significant probability that instability could have occurred without erosion and piping. However, given the very high probability of erosion, it seems likely that both mechanisms were involved in the failure.

Design analyses

The design was divided into five reaches, designated as Reaches I, II, III, IV, and V. The south and north breaches both occurred in Reach III, which encompassed Stations 37+00 to 120+00. Seepage analyses described in paragraphs 44, 45, 47, and 52 of the geotechnical investigation report³ were performed to evaluate the potential for erosion and piping in areas where the London Avenue Canal levee and I-wall were underlain by sand, as at the south and north breach locations. The analyses were performed using flow nets, Lane's Weighted Creep Ratio method⁴, and Harr's Method.⁵

Flow net analyses were performed for the levees in Reach IV and Reach V, based on levee base width of 80 ft, 60 ft depth of pervious foundation soil, and canal water level at 10.2 ft NAVD88. The calculated values of exit gradient were found to be about 0.25. These were judged to provide a factor of safety of approximately 4.0 against erosion and piping. This factor of safety was considered acceptable, and not to require measures to cut off underseepage.

Lane's Weighted Creep Ratio values were computed for the I-walls in Reaches I, II, III, IV, and V. The results indicated that the calculated creep ratios were not acceptable for parts of Reach V where the levee and I-wall would be underlain by sand, according to Lane's empirical criteria. The required cutoff depths within this reach were subsequently evaluated using Harr's Method, and were found to require sheetpile wall penetration to elevation -14.4 ft NAVD88.

None of the seepage analyses considered the possibility that a gap might develop due to water pressures on the I-wall, resulting in flow down the canal side of the wall and into the foundation at that location.

³ Geotechnical Investigation, Orleans Levee District, London Avenue Outfall Canal, OLB Project No. 2049-0269, New Orleans, Louisiana, Volume 1, for The Board of Levee Commissioners of the Orleans Levee District, New Orleans, Louisiana, by Eustis Engineering Company, Metairie, Louisiana, 4 March, 1986, contained in GDM86, Volume 1, Part 1, U. S. Army Corps of Engineers, New Orleans District.

⁴ Lane, E. W. (1935), "Security from under-seepage – masonry dams on earth foundations," ASCE Transactions, Vol. 100, pp. 1235-1251.

⁵ Harr, M. E. (1966), *Groundwater and Seepage*, McGraw-Hill, New York, 381 pp.

Paragraph 45 of the design report³ discussed the likelihood that the canal bottom would be covered with silt, which would impede seepage into the foundation in areas where the foundation soils were permeable sand. The relatively short duration of the design high water was also discussed. Based on data from field piezometer studies, it was judged that head levels on the land side of the levee would not be above the ground surface. Paragraph 46 of the report recommended that piezometers be installed and monitored periodically to provide a basis for estimating piezometric levels during floods more accurately, and for evaluating the need for landside pressure relief measures. Paragraph 47 of the report discussed the possible consequences of dredging the canal, exposing more pervious materials in the canal bottom, which could result in more adverse seepage conditions, and requested notification if dredging was planned.

Stability analyses performed for Reach III did not show the failure surface entering the sand layer. All of the analyses were performed using slip surfaces within the clay layer beneath the levee and the I-wall. A minimum factor of safety of 1.30 computed by the Method of Planes⁶ was required. Required depths of penetration and bending moment capacity for the I-wall were determined by cantilever analyses, as described in paragraphs 48 and 49 of the report.³

Summary

The analyses described in the preceding sections indicate a strong likelihood that high uplift pressure on the base of the levee and the marsh layer was a key factor in the failures at both the south and the north breaches on the London Avenue Canal. At both locations these high uplift pressures probably resulted in development of a rupture through the marsh layer, and hydraulic gradients large enough to cause erosion of the sand.

At the south breach area this erosion may have been the principal mode of failure, with gross instability occurring after considerable volumes of sand, marsh and levee fill had been removed by erosion and piping. Without alteration of the south breach cross section by erosion and piping, the calculated factors of safety with respect to instability are greater than 1.0, indicating that alteration of the profile by erosion and piping probably played an essential role in the failure at this location where the sand was dense, and the sand friction angle would have been high. An additional important factor is that cold-rolled sheetpiles, with weak interlocks, were reported to have been used at this location. Loss of interlocks during driving in the dense sand would have resulted in even more severe seepage conditions than are reflected in the analyses described here, which modeled the sheetpiles as an intact seepage barrier. The south breach failure appears to have been caused principally by erosion and piping in a localized area focused in a relatively small zone where hydraulic gradients were increased by a rupture through the marsh layer overlying the sand, or by a gap in the sheetpiles due to interlock failure during driving, or both. The conclusion that the failure probably started in a small zone of intense seepage is consistent with the narrow breach that eventually developed.

⁶ A study of the Method of Planes, undertaken by IPET at the request of the New Orleans District Task Force Guardian, indicates that the Method of Planes gives lower factors of safety than more accurate methods of analysis, such as Spencer's method. The magnitude of the difference between the two varies from case to case.

At the north breach area the probability of erosion and piping is slightly less than at the south breach, although still very high. The probability of instability is higher than the probability of erosion, due to the fact that the sand was loose, and would have had a low friction angle. High uplift pressures likely resulted in a rupture through the marsh layer and the underlying thick layer of lacustrine clay. At this location, however, the high pore pressures within the sand would be sufficient to cause instability without significant alteration of the cross section by erosion. The failure at the north affected a much wider zone than the failure at the south, indicating that intense localized erosion and piping did not play a key role in the failure at the north breach. It appears that high uplift pressures and lower friction angle of the less-dense sand were key elements in the failure at the north breach.

Table 8-1 Hydraulic Boundary Conditions for Seepage Analyses – London Avenue South Breach		
Case	Canal water level – CWL (NAVD88)	Warrington Drive water level – LWL (NAVD88)
1	7.1 ft	-8.4 ft
2	8.2 ft	-8.4 ft
3	7.1 ft	-5.1 ft
4	8.2 ft	-5.1 ft

Table 8-2 Calculated Hydraulic Gradients and Factors of Safety Against Erosion – London Avenue South Breach				
Case	CWL	LWL	i = vertical hydraulic gradient	F _{erosion} = i _{crit} /i
1	7.1 ft	-8.4 ft	1.03	0.89
2	8.2 ft	-8.4 ft	1.14	0.81
3	7.1 ft	-5.1 ft	1.13	0.81
4	8.2 ft	-5.1 ft	1.24	0.74

Note: with $\gamma_{sat} = 120$ pcf, $i_{crit} = 0.92$

Table 8-3 Calculated Probabilities of Erosion – London Avenue South Breach								
Case	CWL	LWL	F _{erosion}	ΔF	σ_F	F _{MLV}	COV _F	p _{erosion}
1	7.1 ft	-8.4 ft	0.89	0.08	0.04	0.85	5%	> 99%
3	7.1 ft	-5.1 ft	0.81					
2	8.2 ft	-8.4 ft	0.81	0.07	0.04	0.78	4%	> 99%
4	8.2 ft	-5.1 ft	0.74					

Notes:
 ΔF = change in F due to variation in parameter values
 σ_F = standard deviation of factor of safety for the variations considered
F_{MLV} = most likely value of factor of safety
COV_F = coefficient of variation of factor of safety
p_{erosion} = probability of erosion

Table 8-4 Factor of Safety Against Instability – London South Breach			
Case	CWL	LWL	F _{stability}
1	7.1 ft	-8.4 ft	1.56
2	8.2 ft	-8.4 ft	1.29
3	7.1 ft	-5.1 ft	1.44
4	8.2 ft	-5.1 ft	1.19
5	9.7 ft	-8.4 ft	1.00

Table 8-5 Probability of Instability – London South Breach										
Case	CWL (ft)	LWL (ft)	ϕ' (deg)	S _u (psf)	F	ΔF	σ_F	F _{MLV}	COV _F	P _{instability}
1	7.1	-8.4	40	300	1.56	0.12	0.25	1.50	17%	1%
3	7.1	-5.1	40	300	1.44					
1a	7.1	-8.4	44	300	1.78	0.40	0.25	1.50	17%	1%
1b	7.1	-8.4	36	300	1.38					
1c	7.1	-8.4	40	200	1.42	0.28	0.25	1.50	17%	1%
1d	7.1	-8.4	40	400	1.70					
2	8.2	-8.4	40	300	1.29	0.10	0.20	1.24	16%	10%
4	8.2	-5.1	40	300	1.19					
2a	8.2	-8.4	44	300	1.47	0.30	0.20	1.24	16%	10%
2b	8.2	-8.4	36	300	1.17					
2c	8.2	-8.4	40	200	1.17	0.24	0.20	1.24	16%	10%
2d	8.2	-8.4	40	400	1.41					

Notes:
 ΔF = change in F due to variation in parameters for the two conditions
 σ_F = standard deviation of factor of safety for the variations considered
F_{MLV} = most likely value of factor of safety
COV_F = coefficient of variation of factor of safety
P_{instability} = probability of instability

Table 8-6 Hydraulic Boundary Conditions for Seepage Analyses – London Avenue North Breach		
Case	Canal water level – (CWL) NAVD88	Pratt Drive water level – (LWL) NAVD88
1	8.2 ft	-8.4 ft
2	9.5 ft	-8.4 ft
3	8.2 ft	-3.9 ft
4	9.5 ft	-3.9 ft

Table 8-7 Calculated Hydraulic Gradients and Factors of Safety Against Erosion – London Avenue North Breach				
Case	CWL	LWL	i = vertical hydraulic gradient	$F_{\text{erosion}} = i_{\text{crit}}/i$
1	8.2 ft	-8.4 ft	0.95	0.88
2	9.5 ft	-8.4 ft	1.08	0.78
3	8.2 ft	-3.9 ft	1.12	0.75
4	9.5 ft	-3.9 ft	1.25	0.67

Note: with $\gamma_{\text{sat}} = 115 \text{ pcf}$, $i_{\text{crit}} = 0.84$

Table 8-8 Calculated Probabilities of Erosion – London Avenue North Breach								
Case	CWL	LWL	F_{erosion}	ΔF	σ_F	F_{MLV}	COV_F	p_{erosion}
1	8.2ft	-8.4 ft	0.88	0.13	0.07	0.82	16%	91%
3	8.2 ft	-3.9 ft	0.75					
2	9.5 ft	-8.4 ft	0.78	0.11	0.06	0.73	15%	99%
4	9.5 ft	-3.9 ft	0.67					

Notes:
 ΔF = change in F due to variation in parameters for the two conditions
 σ_F = standard deviation of factor of safety for the variations considered
 F_{MLV} = most likely value of factor of safety
 COV_F = coefficient of variation of factor of safety
 p_{erosion} = probability of erosion

Table 8-9 Factor of Safety Against Instability – London North Breach			
Case	CWL	LWL	$F_{\text{stability}}$
1	8.2 ft	-8.4 ft	0.99
2	9.5 ft	-8.4 ft	0.77
3	8.2 ft	-3.9 ft	0.84
4	9.5 ft	-3.9 ft	0.67
5	8.1 ft	-8.4 ft	1.00

**Table 8-10
Probability of Instability – North Breach**

Case	CWL (ft)	LWL (ft)	ϕ' (deg)	S_u (psf)	F	ΔF	σ_F	F_{MLV}	COV_F	$p_{instability}$
1	8.2	-8.4	32	300	0.99	0.15	0.17	0.92	19%	70%
3	8.2	-3.9	32	300	0.84					
1a	8.2	-8.4	36	300	1.11	0.24	0.17	0.92	19%	70%
1b	8.2	-8.4	28	300	0.87					
1c	8.2	-8.4	32	200	0.89	0.20	0.17	0.92	19%	70%
1d	8.2	-8.4	32	400	1.09					
2	9.5	-8.4	32	300	0.77	0.10	0.14	0.72	19%	97%
4	9.5	-3.9	32	300	0.67					
2a	9.5	-8.4	36	300	0.87	0.18	0.14	0.72	19%	97%
2b	9.5	-8.4	28	300	0.69					
2c	9.5	-8.4	32	200	0.68	0.18	0.14	0.72	19%	97%
2d	9.5	-8.4	32	400	0.86					

Notes:

ΔF = change in F due to variation in parameters
 σ_F = standard deviation of factor of safety for the variations considered
 F_{MLV} = most likely value of factor of safety
 COV_F = coefficient of variation of factor of safety
 $p_{instability}$ = probability of instability



Figure 8-1. The South Breach at the London Avenue Canal Occurred at 6:00 AM to 7:00 AM on August 29, 2005. The breach, on the east side of the canal, was approximately 60 feet wide.



Figure 8-2. The North Breach at the London Avenue Canal Occurred at 7:00 AM to 8:00 AM on August 29, 2005. The breach, on the west side of the canal, is approximately 410 feet wide.

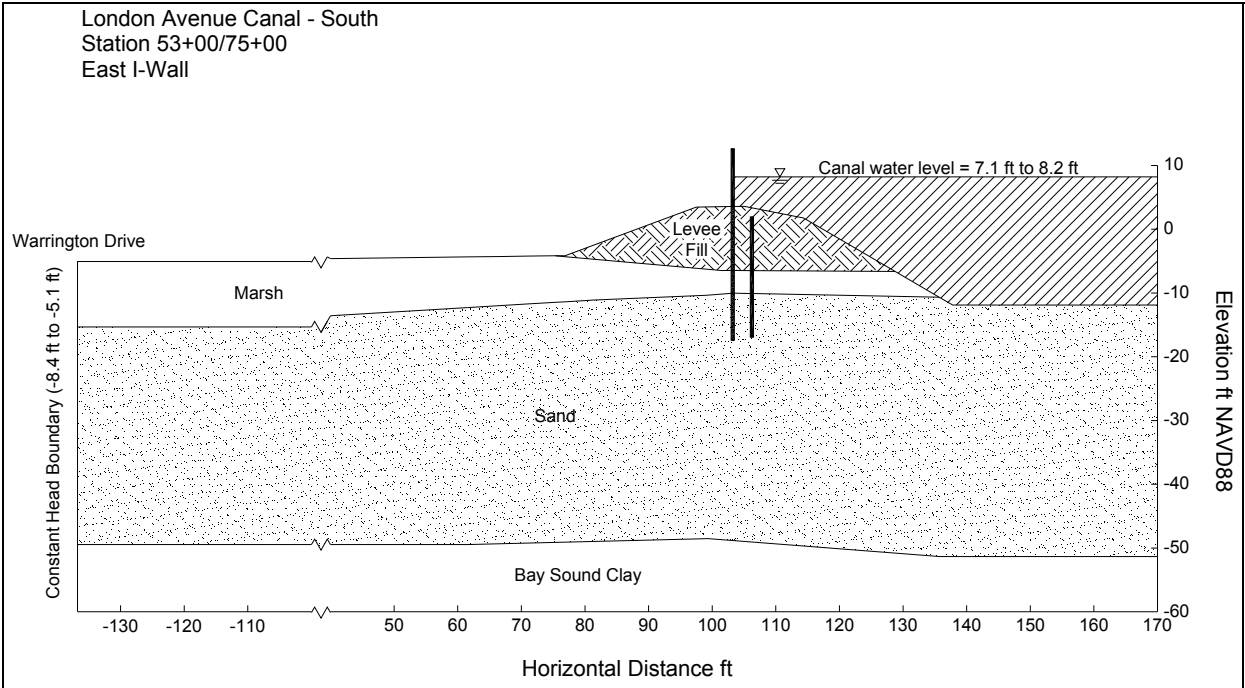


Figure 8-3. Schematic Cross Section at London South Breach, with Seepage Boundary Conditions

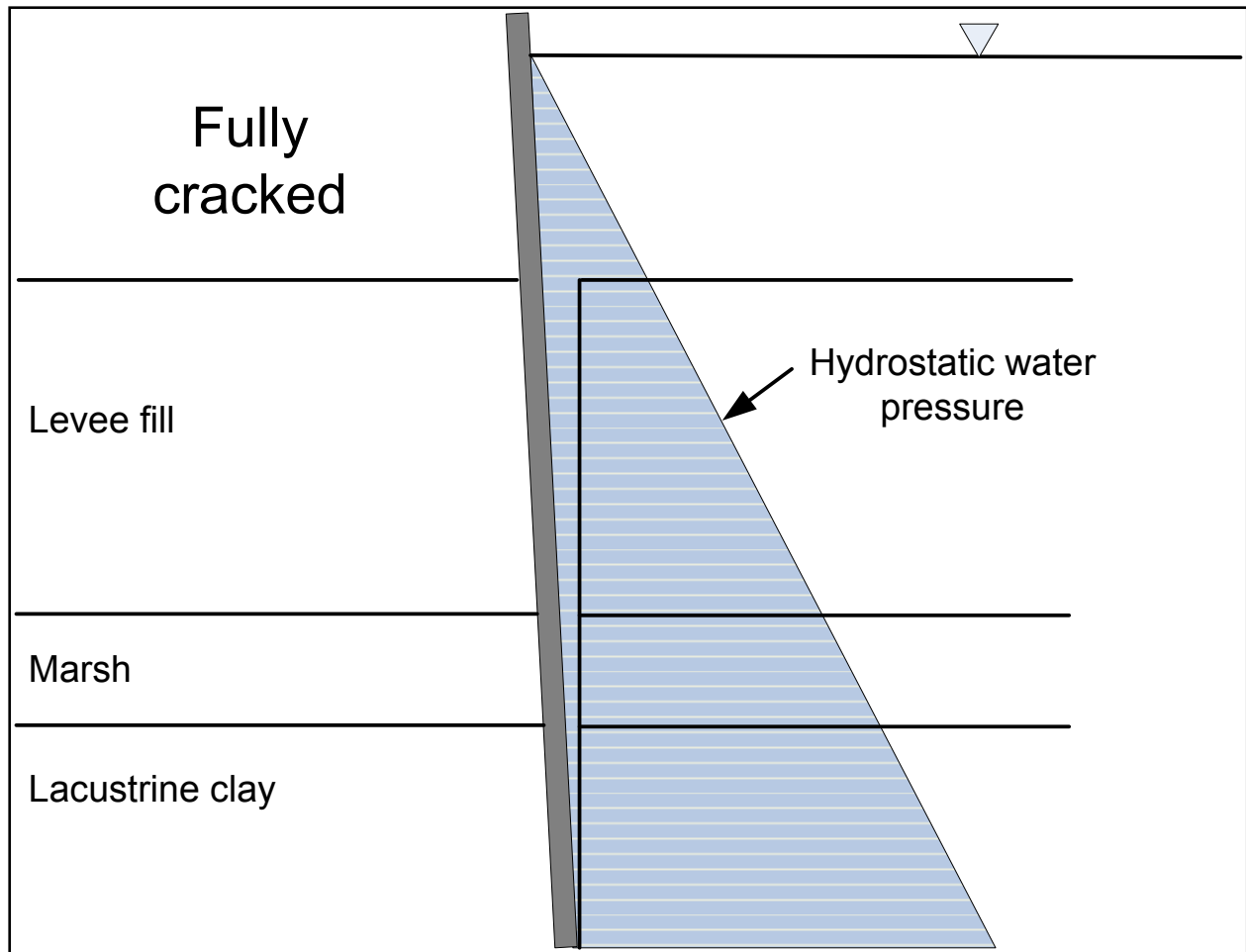


Figure 8-4. Schematic of Gap Used in 17th Street Canal Stability Analyses

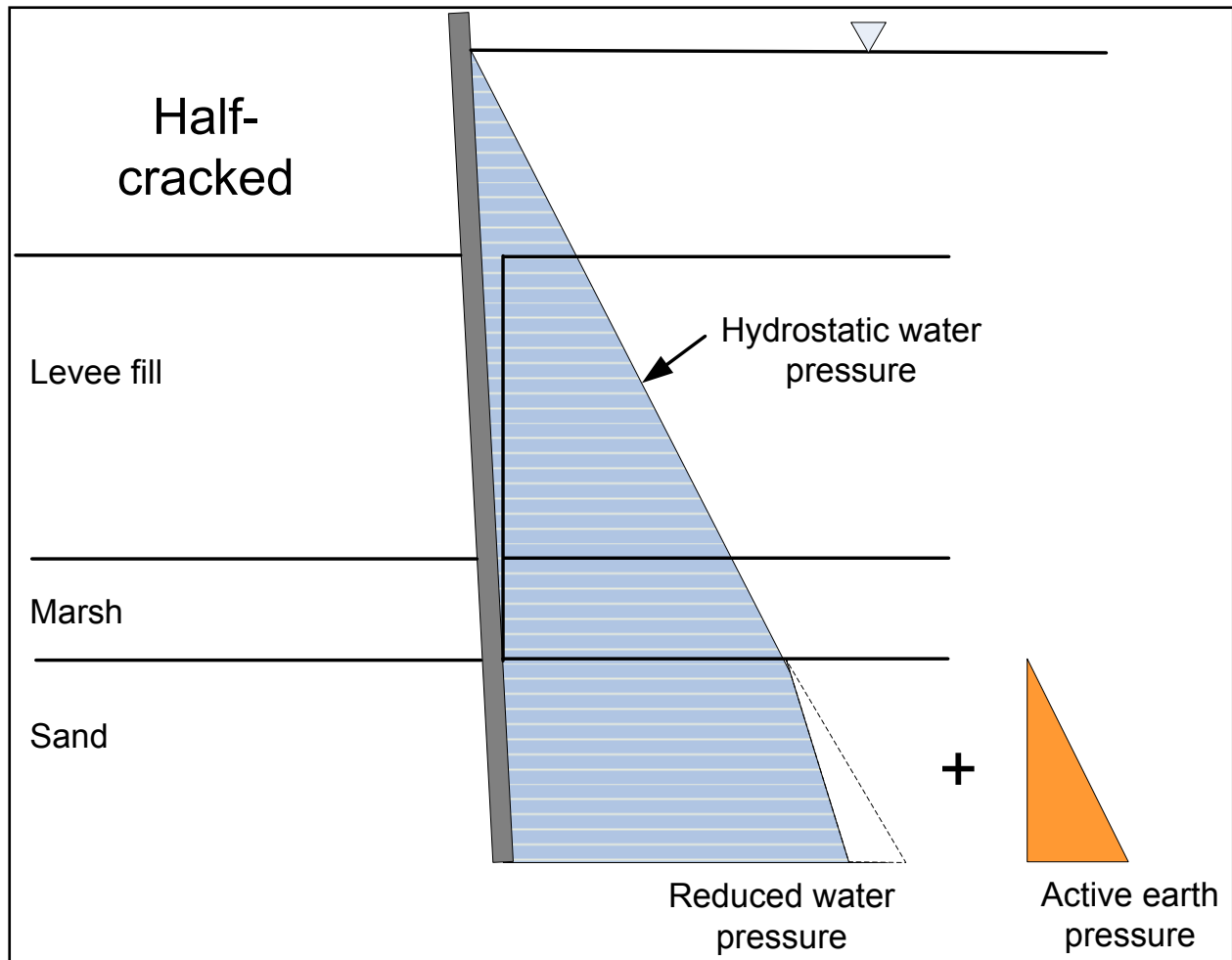


Figure 8-5. Schematic of Gap Used in London Avenue Canal Stability Analyses

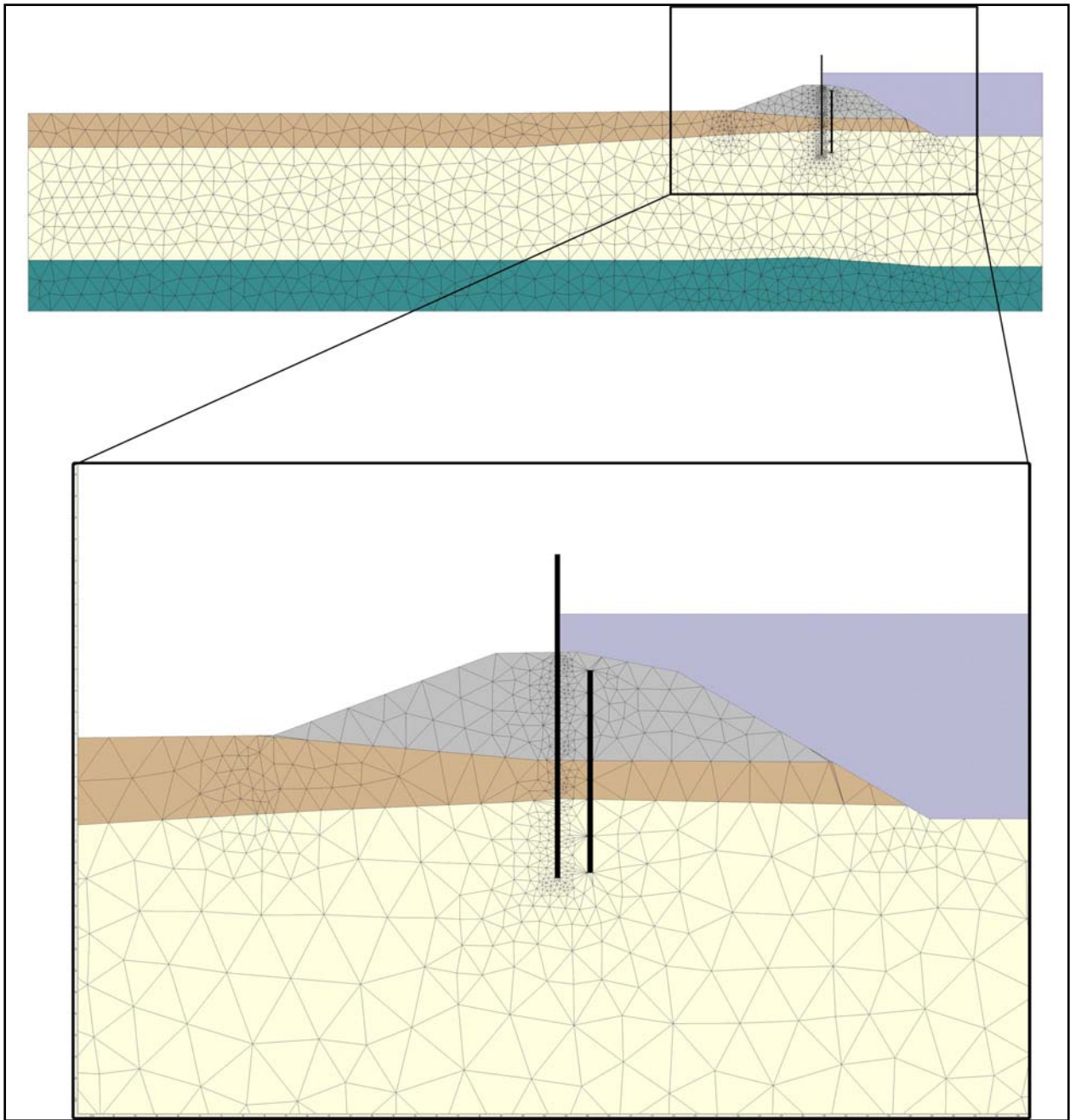


Figure 8-6. Finite Element Mesh Used for Seepage Analysis for London Avenue South Breach

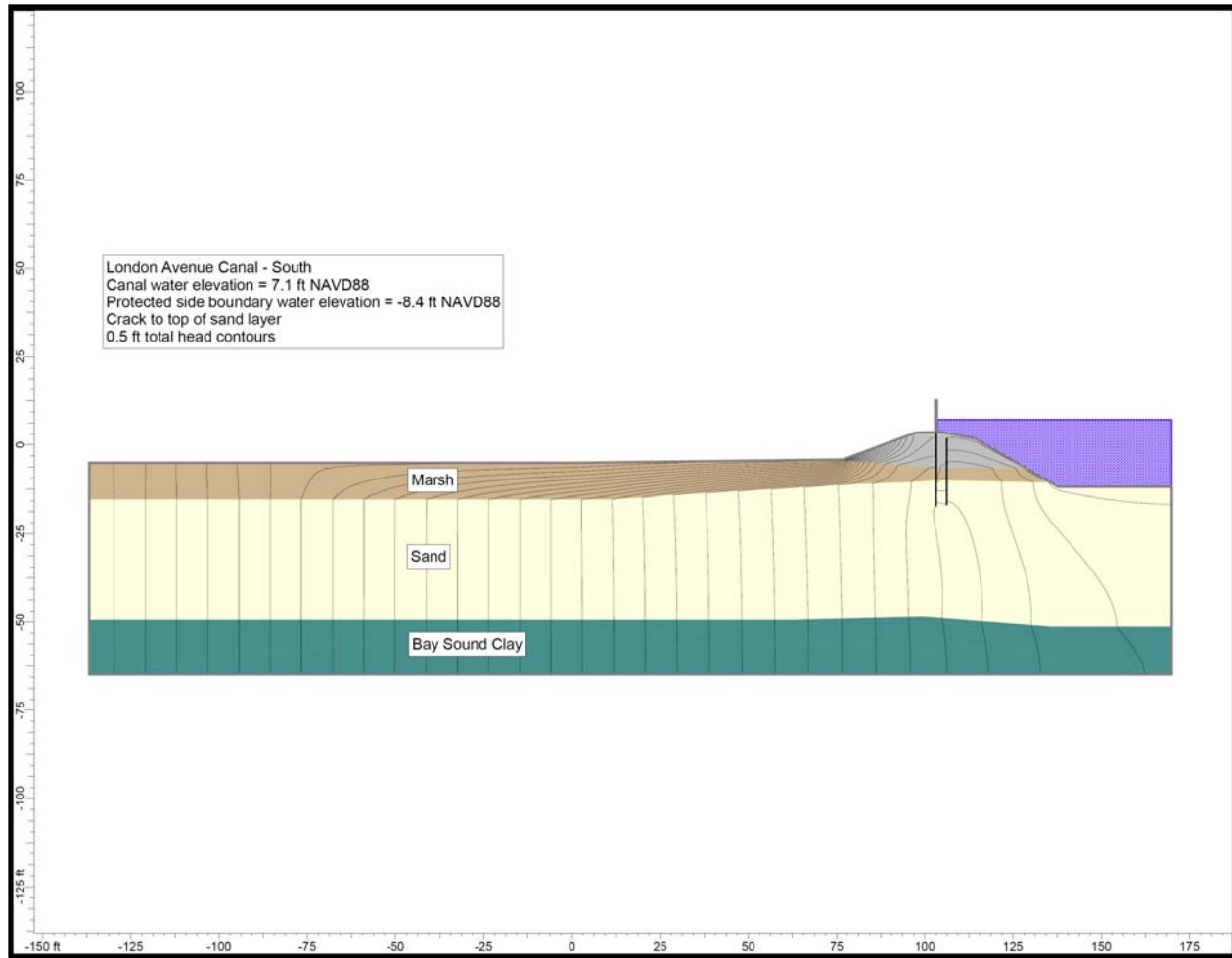


Figure 8-7. Total Head Contours Calculated for Seepage Analysis of London South Breach (Case 1)

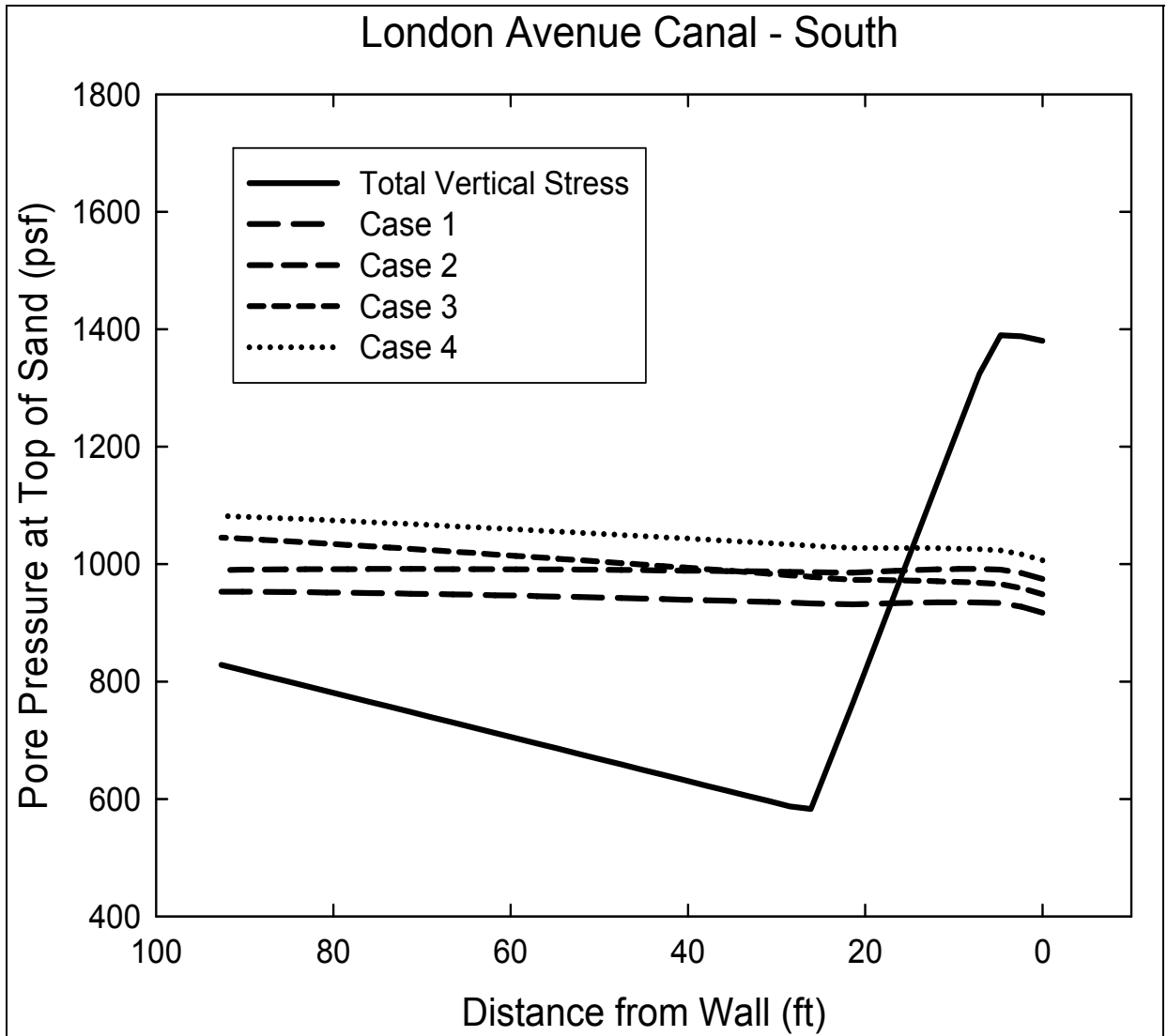


Figure 8-8. Calculated Uplift Pressures and Total Overburden Pressure for London South Breach

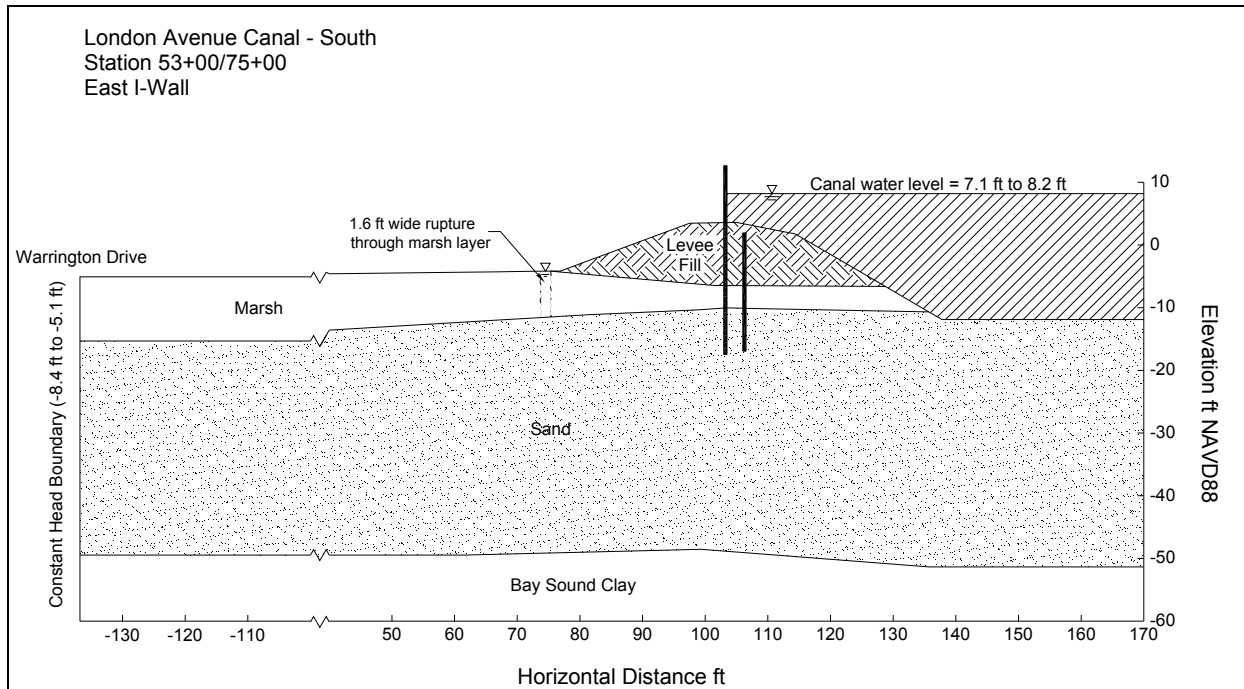


Figure 8-9. Schematic Cross Section at London South Breach, Showing Rupture Through Marsh Layer

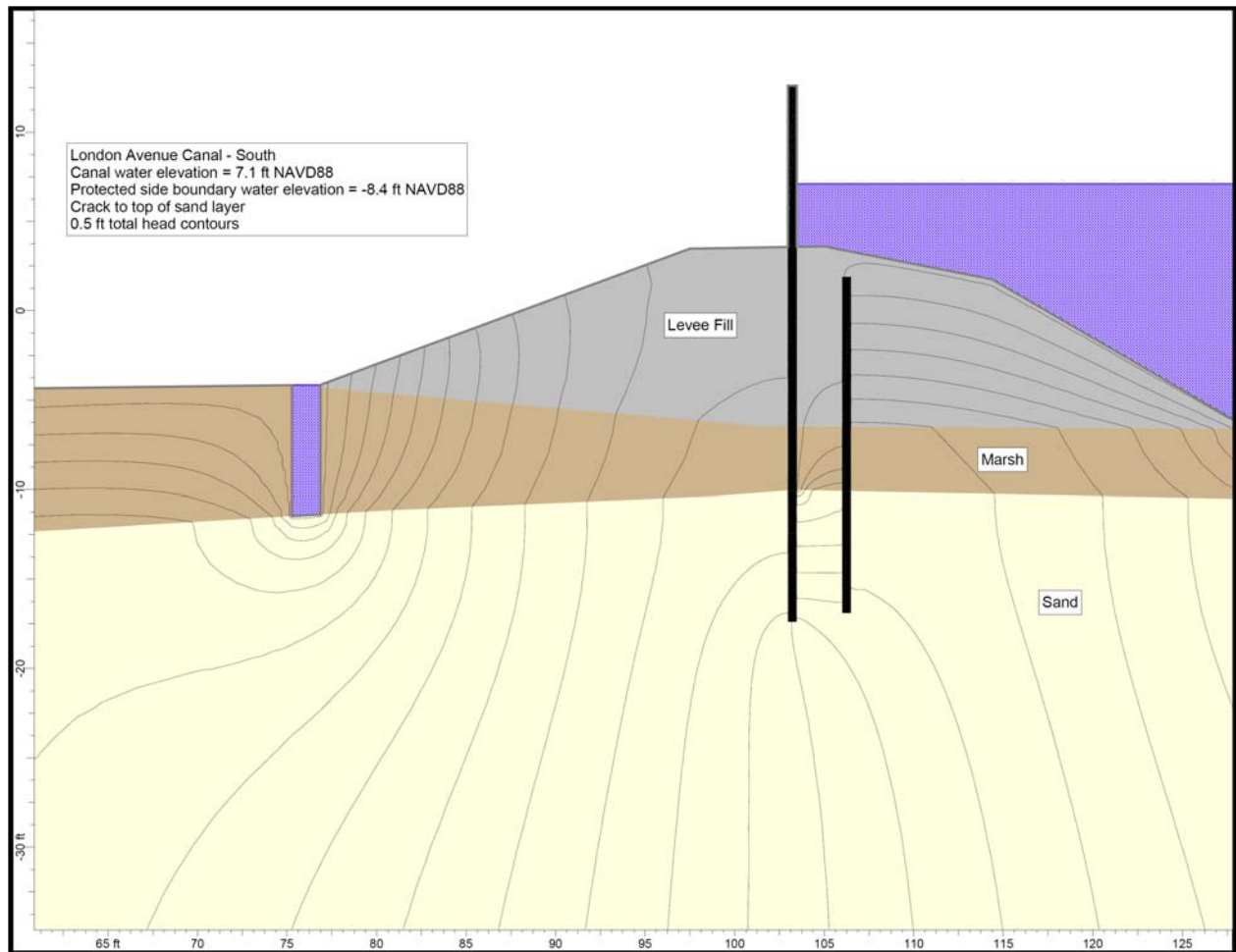


Figure 8-10. Total Head Contours in Vicinity of Rupture for London South Breach

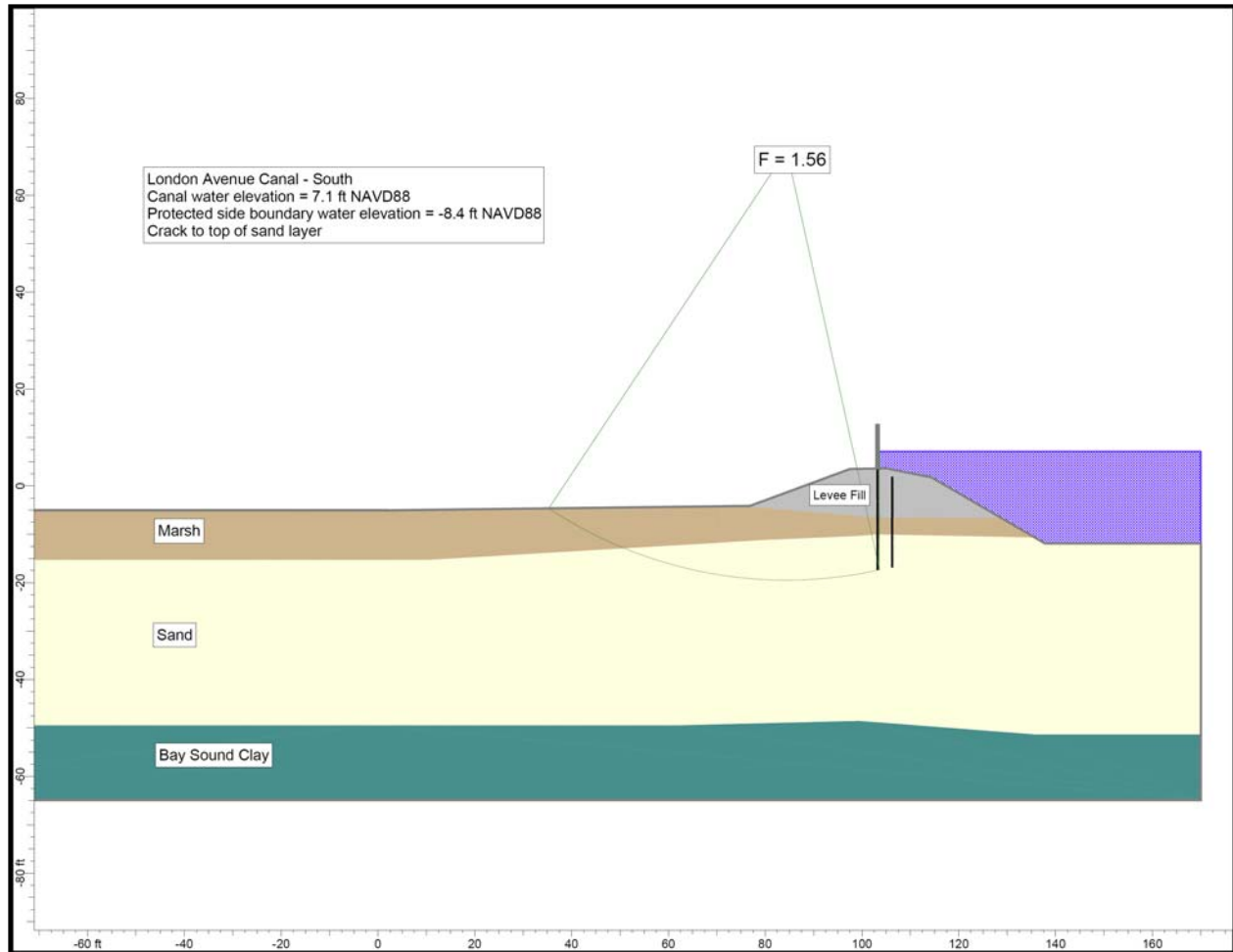


Figure 8-11. London South Breach Case 1 Stability Analysis

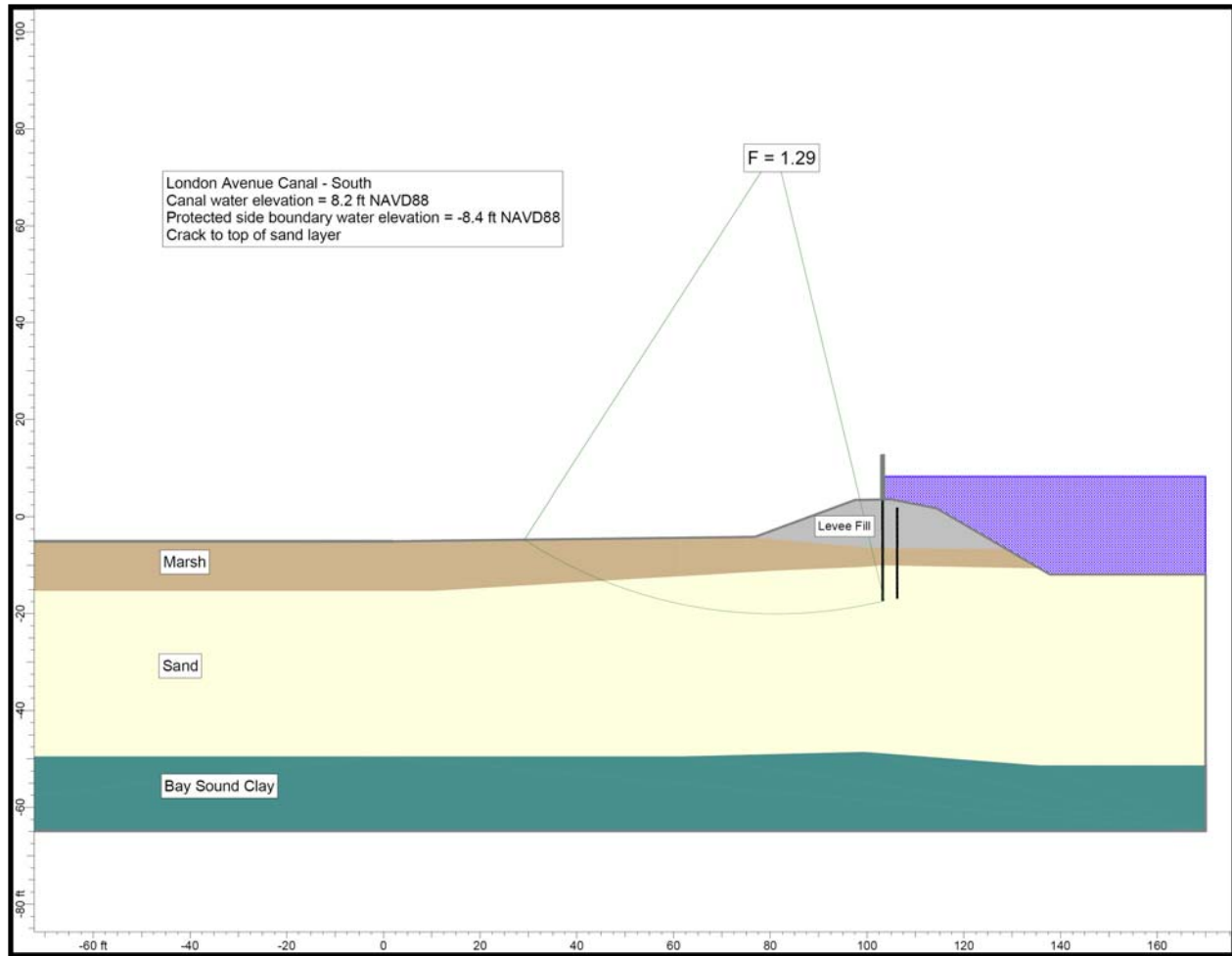


Figure 8-12. London South Breach Case 2 Stability Analysis

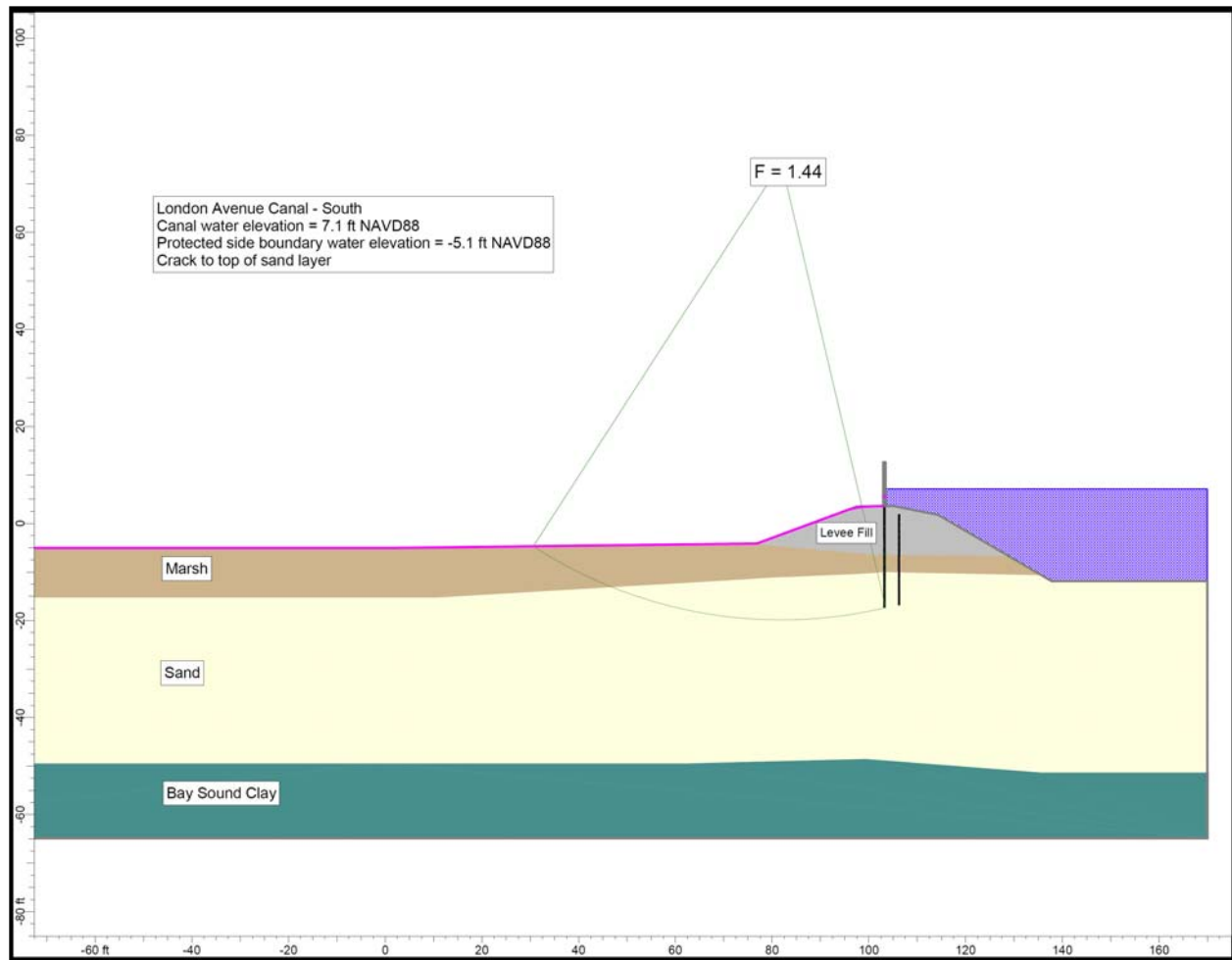


Figure 8-13. London South Breach Case 3 Stability Analysis

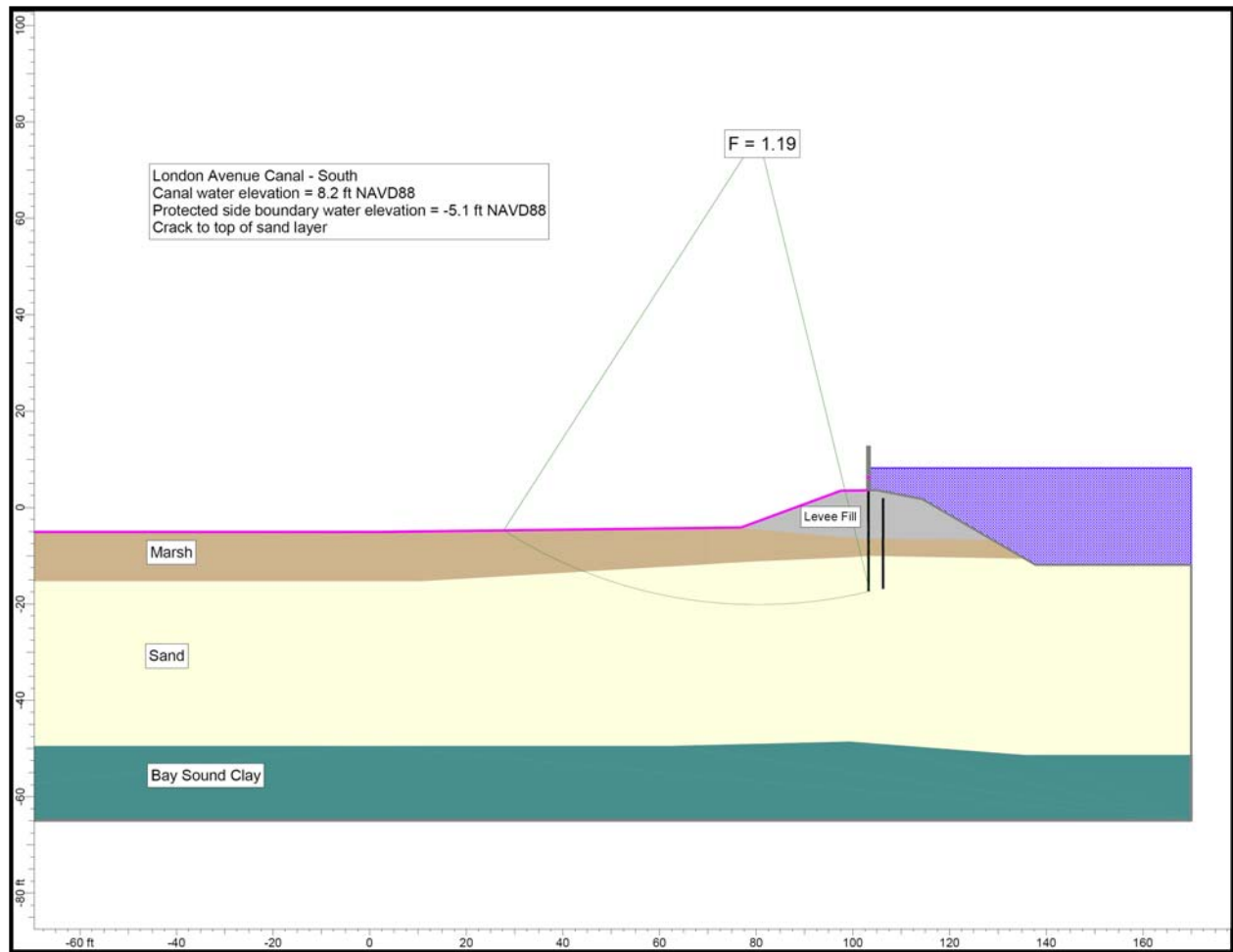


Figure 8-14. London South Breach Case 4 Stability Analysis

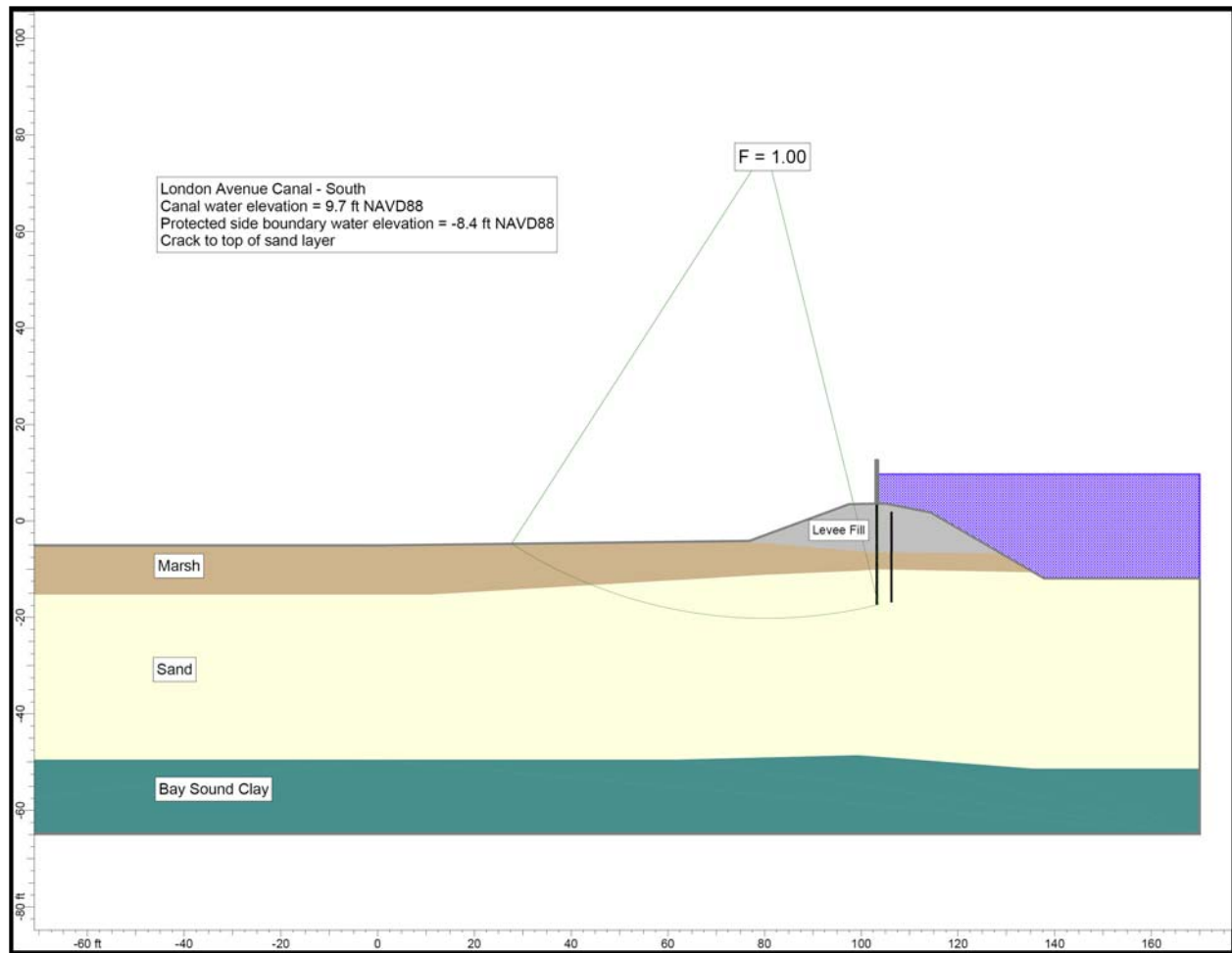


Figure 8-15. London South Breach Case 5 Stability Analysis

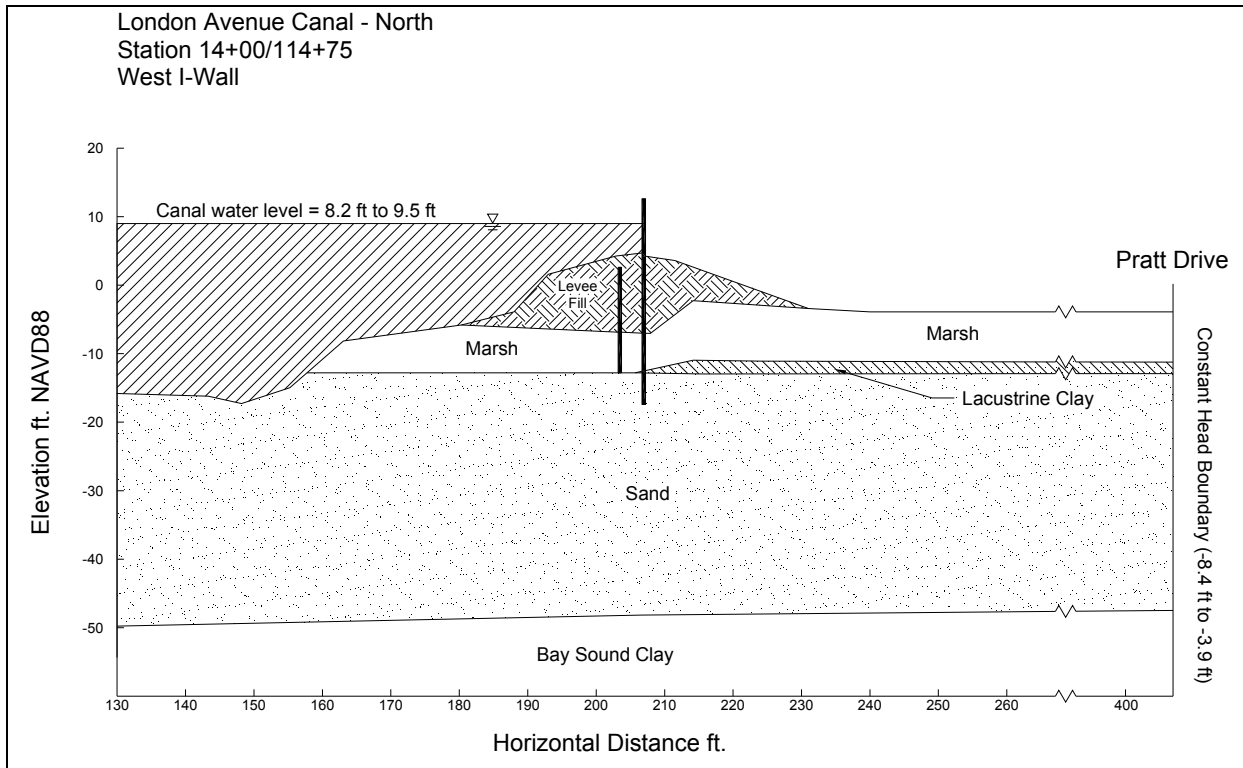


Figure 8-16. Schematic Cross Section at London North Breach, with Seepage Boundary Conditions

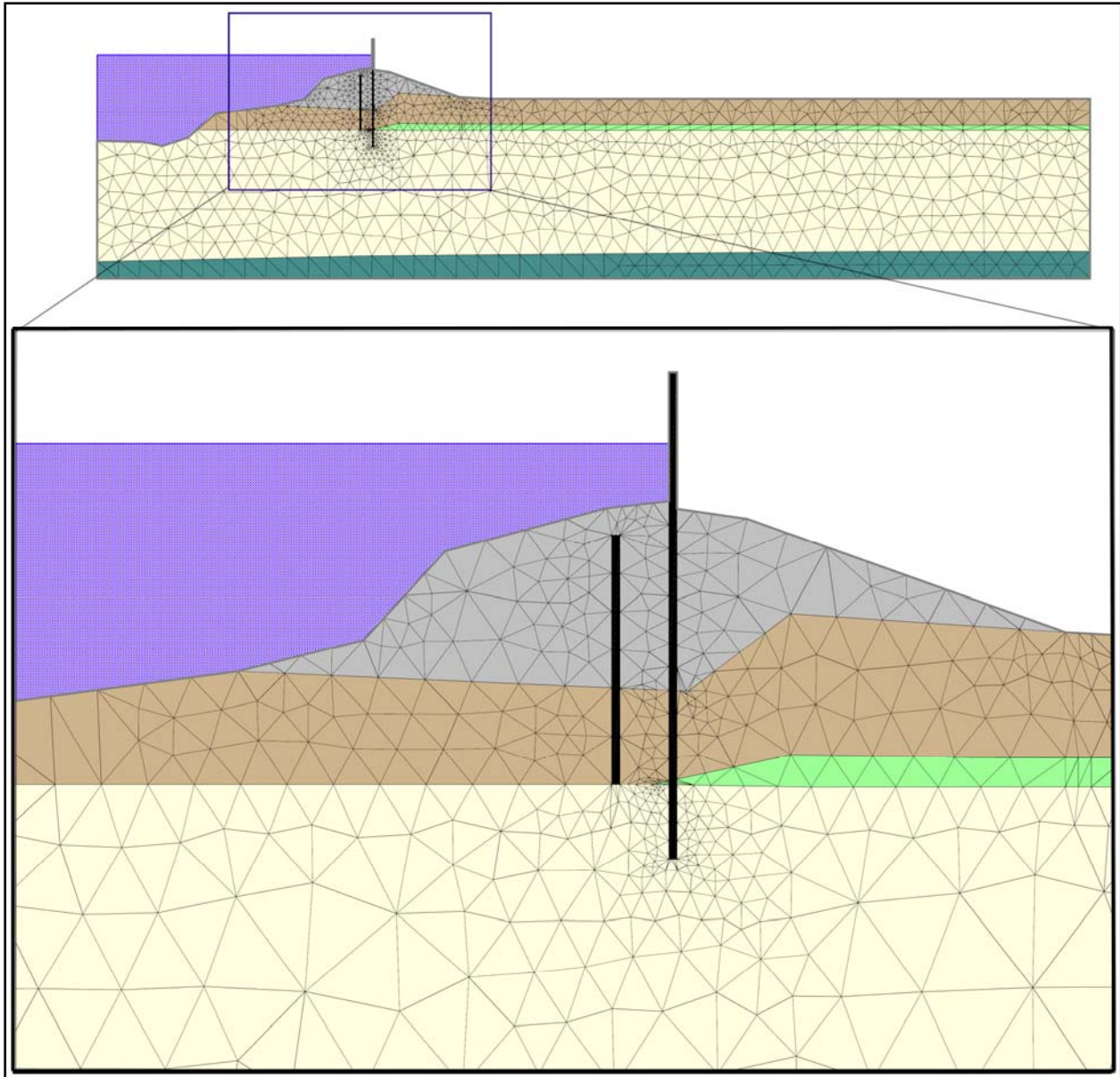


Figure 8-17. Finite Element Mesh Used for Seepage Analysis for London Avenue North Breach

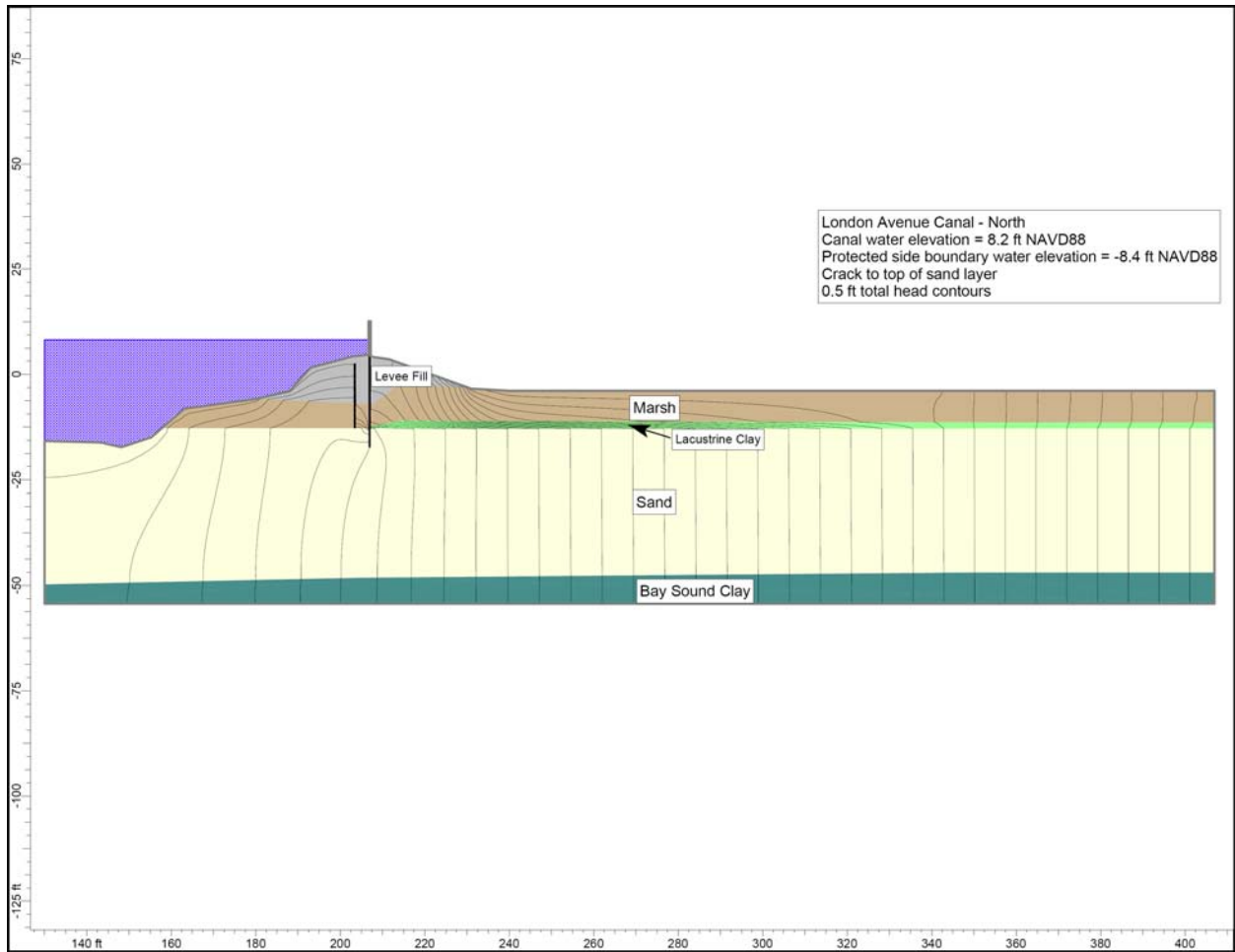


Figure 8-18. Total Head Contours Calculated for Seepage Analysis of London North Breach (Case 1)

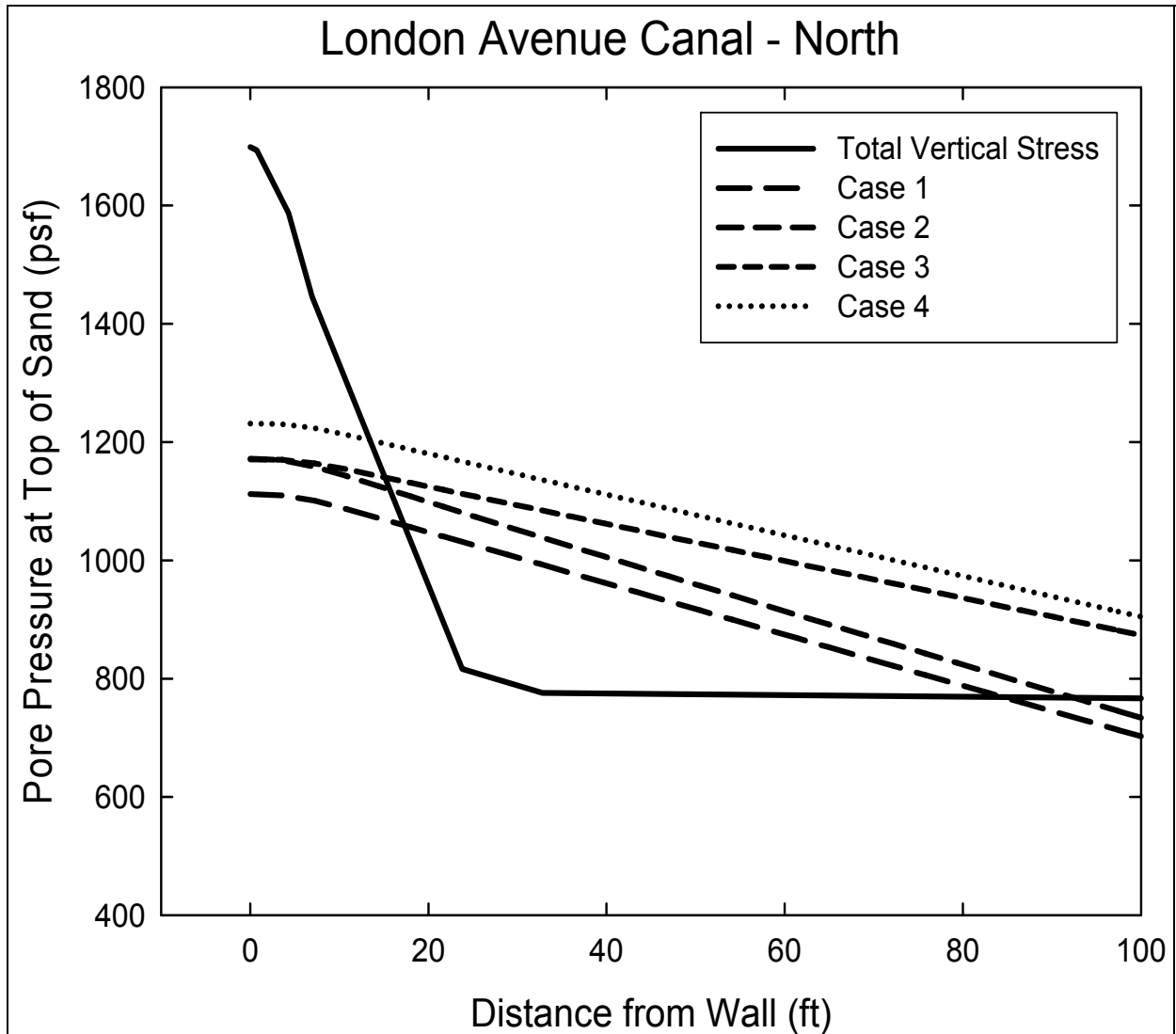


Figure 8-19. Calculated Uplift Pressures and Total Overburden Pressure for London North Breach

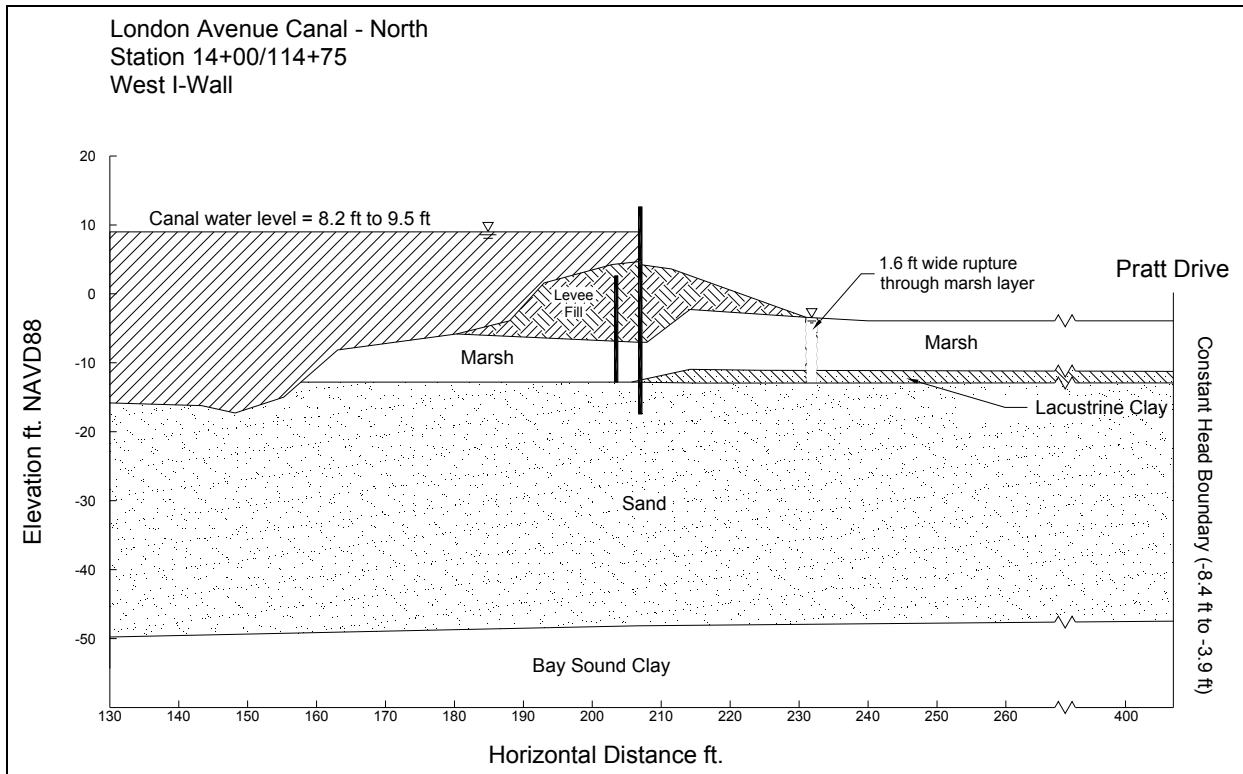


Figure 8-20. Schematic Cross Section at London North Breach, Showing Rupture Through Marsh Layer

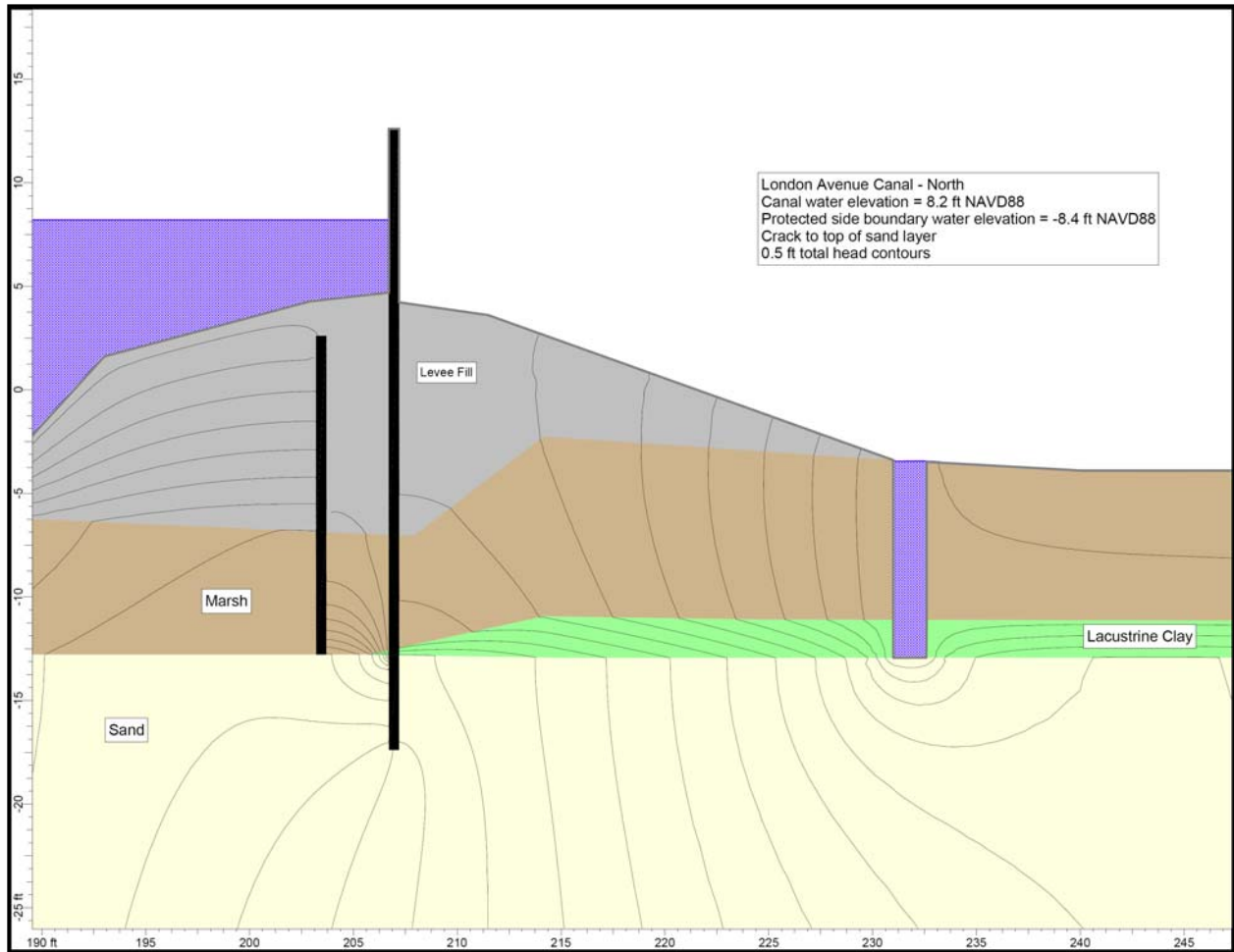


Figure 8-21. Total Head Contours in Vicinity of Rupture for London North Breach

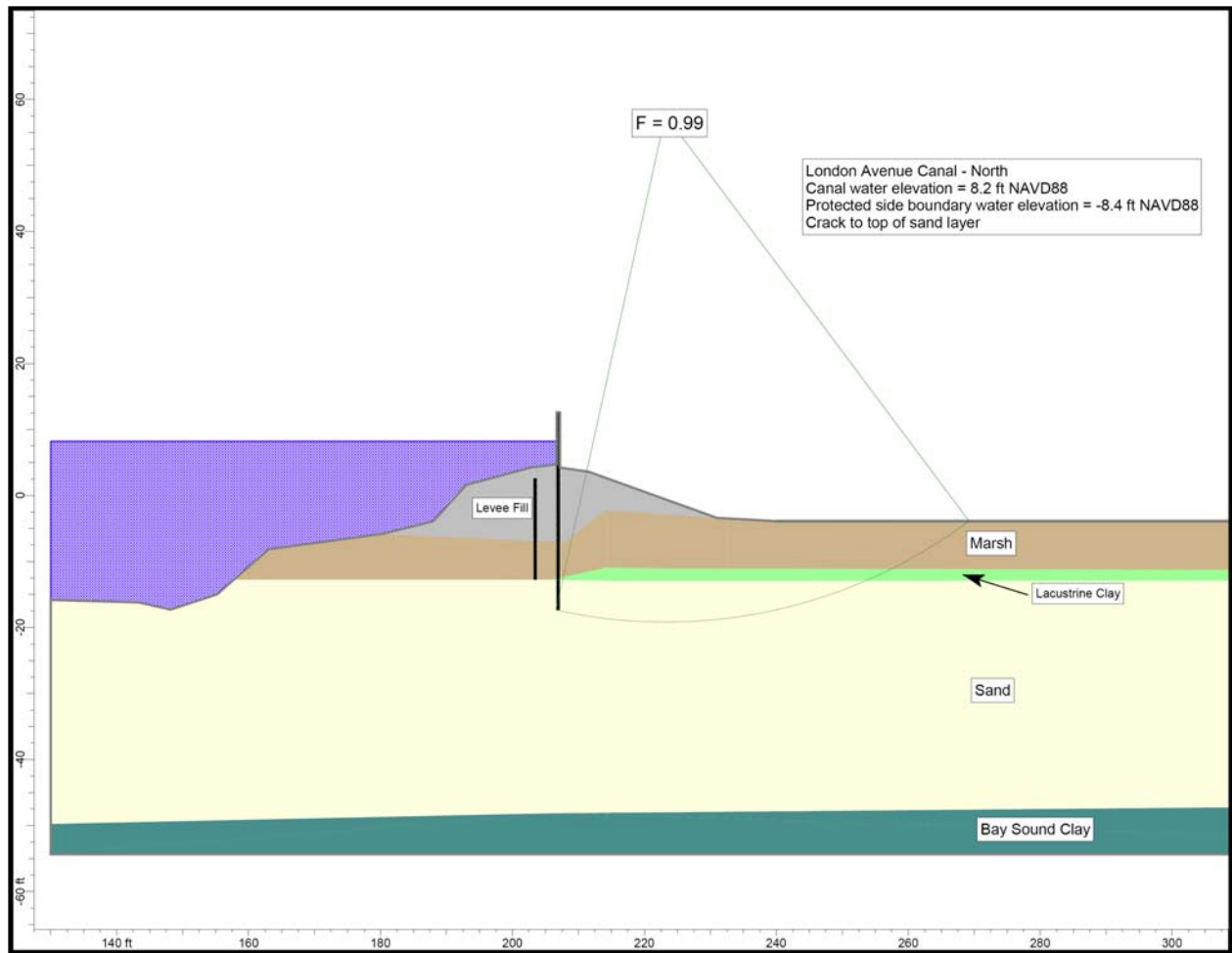


Figure 8-22. London North Breach Case 1 Stability Analysis

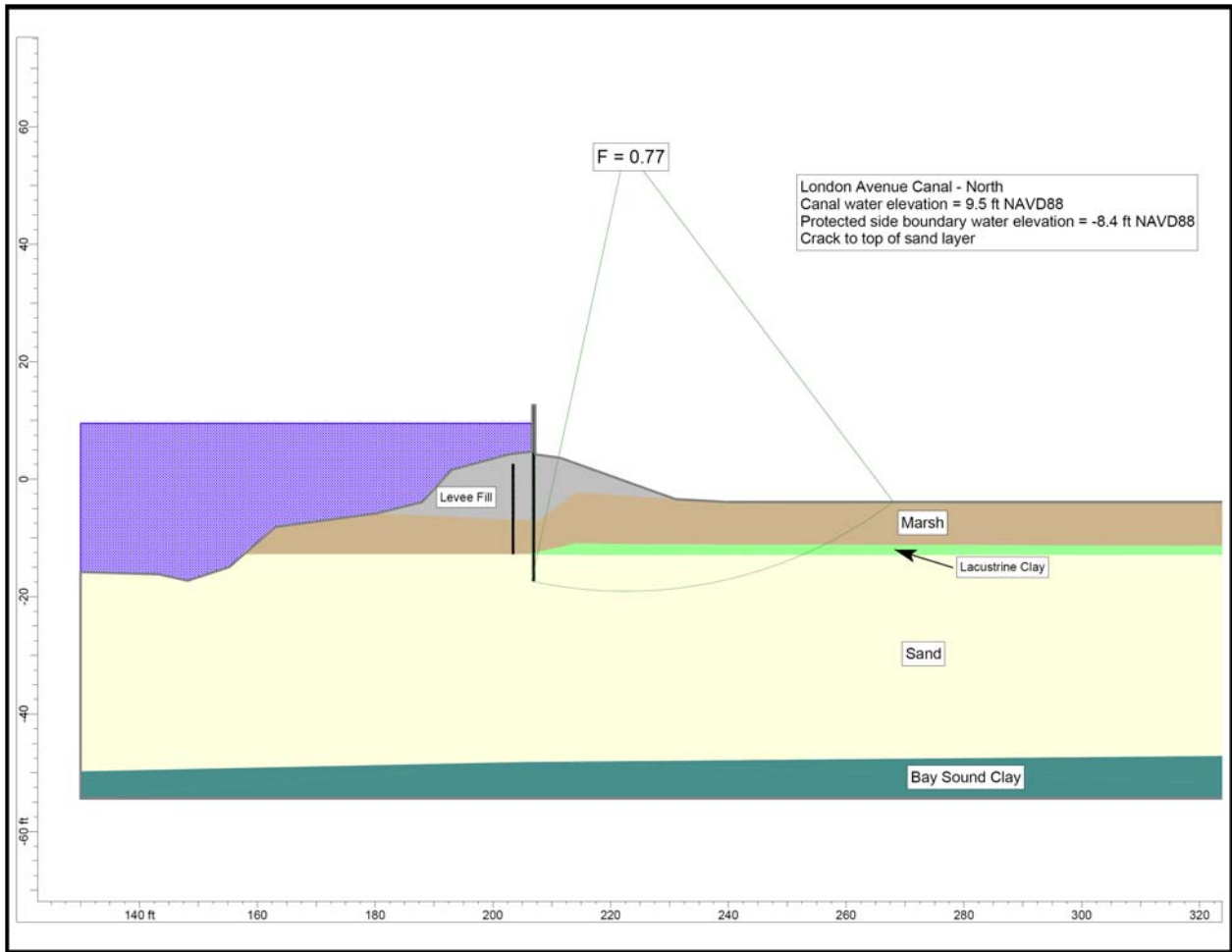


Figure 8-23. London North Breach Case 2 Stability Analysis

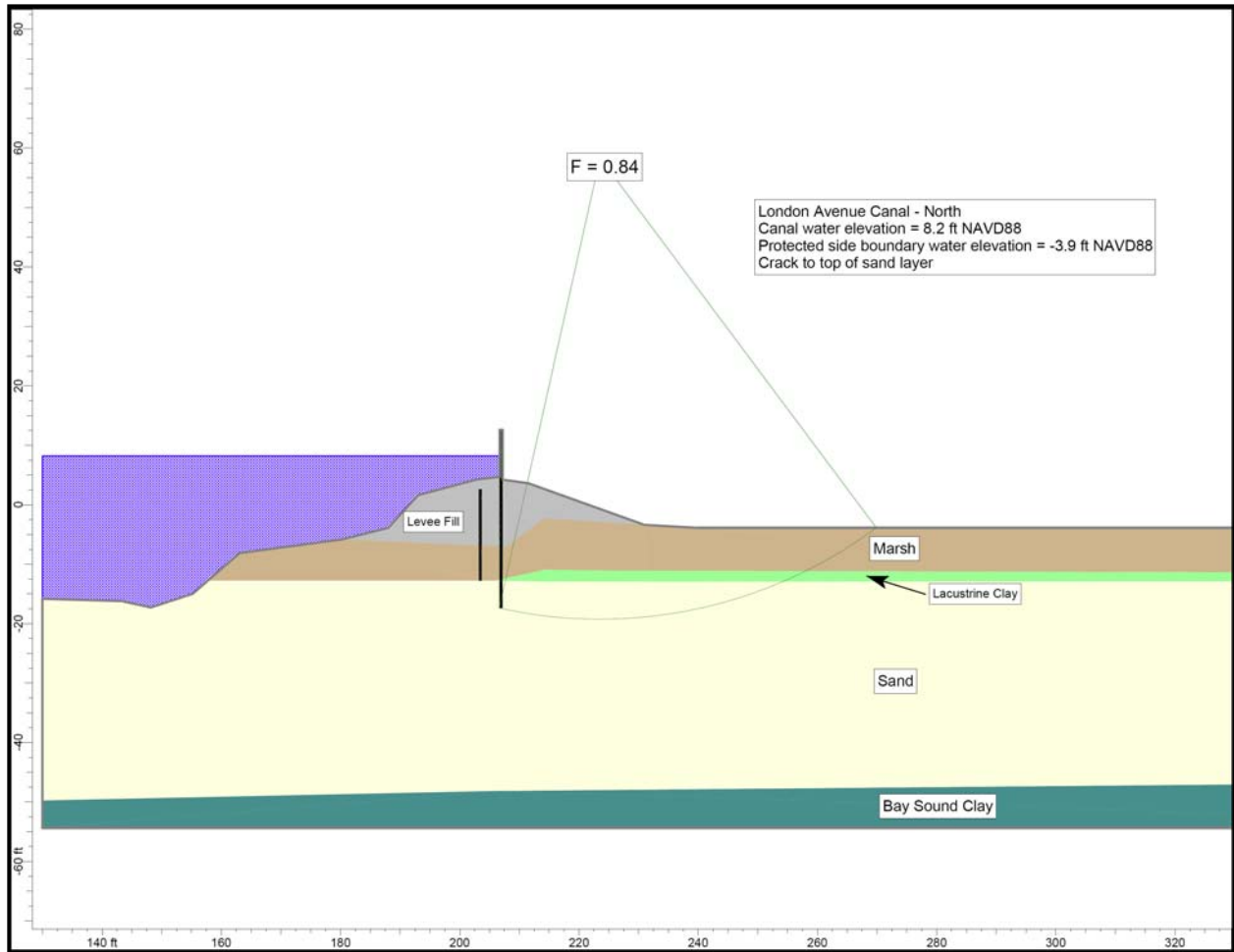


Figure 8-24. London North Breach Case 3 Stability Analysis

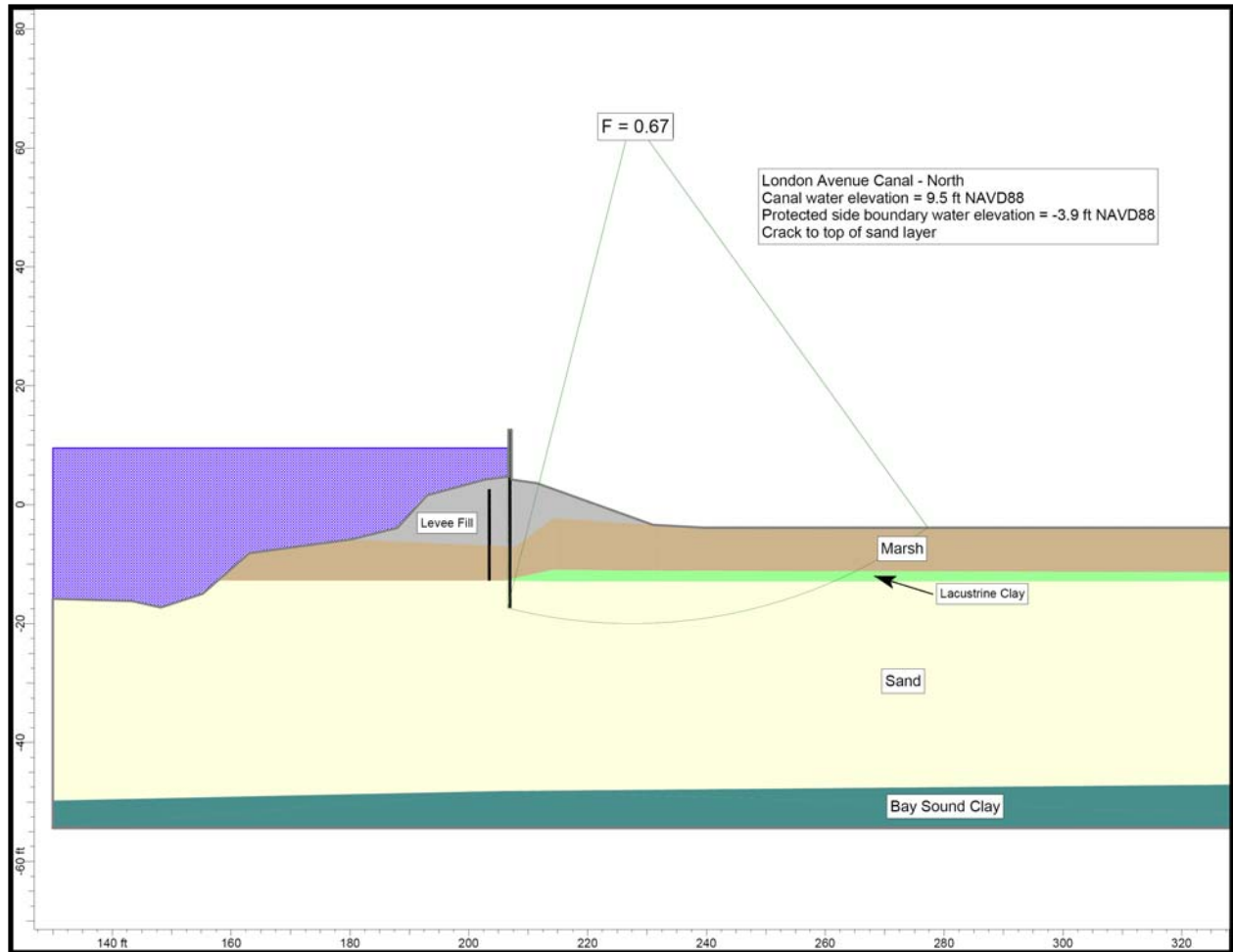


Figure 8-25. London North Breach Case 4 Stability Analysis

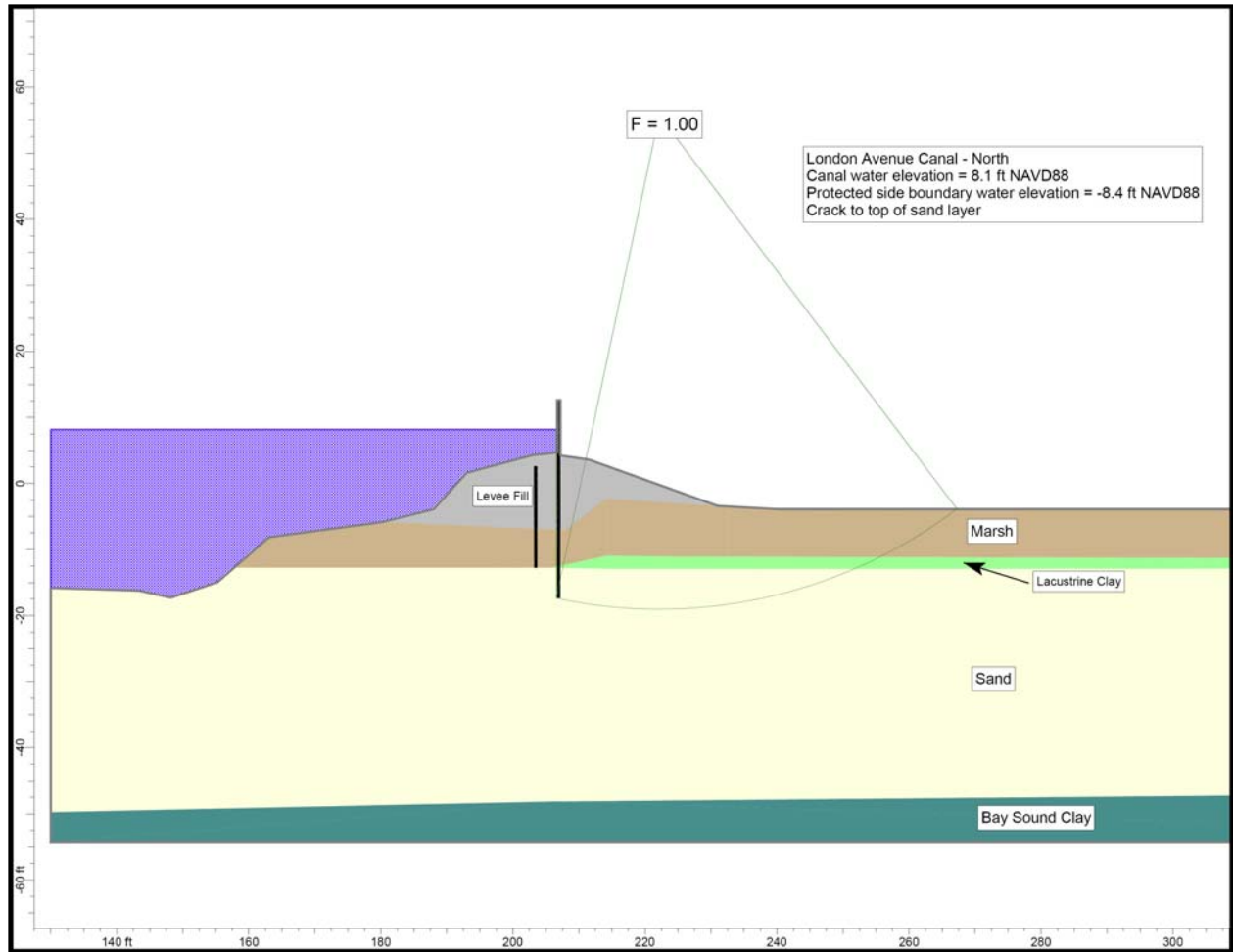


Figure 8-26. London North Breach Case 5 Stability Analysis

Appendix 9

Soil Structure Interaction Analysis of the Floodwalls at London Avenue Canal

This interim IPET report describes detailed soil-structure interaction finite element analysis of the two breaches that occurred at the London Avenue Canal. Finite element soil-structure interaction analyses were conducted to provide a third approach to development of a complete understanding of the London Avenue Canal breach mechanisms. The investigation of these breaches is an important step in IPET's system-wide investigation of floodwall and levee performance, and the findings illuminate a possible mechanism of failure that will be investigated system-wide for locations where sand underlies levees and floodwalls.

Soil-Structure Interaction Analysis of the London Avenue Canal North Breach (West Flood Wall at London at Station 14+00)

Introduction

This section describes a complete soil-structure interaction (SSI) analysis of an existing flood wall within London Canal using the PC-based finite element program Plaxis (2004). A two-dimensional cross section within the section of the West side, at Station 14+00 of the London Canal that failed during hurricane Katrina is the subject of this evaluation. Results of a complete nonlinear finite element analysis of a two dimensional (2-D) cross section during simulated flood loading are described.

Plaxis is a complete nonlinear finite element package geared towards geotechnical engineering applications that include soil-structure interaction issues such as those that occur between a sheet pile and the soils in which it is embedded. It allows for the nonlinear response of soils to flood loading as occurred at the London canal with an I-wall along the center line of the soil-founded levee. The Plaxis PC-based software comprises a visual pre-processor, a nonlinear finite element engineering analysis module, and a visual post-processor. All software components are combined into a single package. Computed results include not only soil stresses, but also structural (e.g. sheet pile and I-wall) bending moments, interaction stresses between sheet piling and the soil in which it is embedded, as well as soil (e.g., levee) and structural deformations. A complete SSI analysis is considered to provide the most reasonable estimate for

deformation response of a soil-structural system involving nonlinear material behavior. In a complete SSI analysis loads exerted by the canal water acting on the soils of the levee and then onto the sheet pile wall (below the I-wall) by means of a load transfer through the levee and foundation soils are generated automatically during the analysis (i.e., predetermined earth pressure force distributions between the soil and the embedded sheet pile are not specified).

Section Analyzed

The two-dimensional cross section within the failed section of the West side of the London Canal at Station 14+00 analyzed for flood loading is shown in Figure 9-1.¹ The 2-D section is 274-ft wide and extends from the center line of the canal at x equal to 133 ft to x-coordinate equal to 407 ft. The top of the I-wall is at El 13 and sheet pile tip is at EL -17.4. An older sheet pile is embedded in the levee on the canal side of the I-wall, approximately 5 feet in front of the I-wall (centerline-to-centerline). This old sheet pile used to be part of a shorter flood wall that was removed when the existing I-wall was installed. The old sheet piling extends from the ground surface to EL -12.9 (corresponding to the elevation of the top of the Beach sand layer).

The crest of the earthen levee on the protected (West) side of the I-wall is at El 4.4, with a crest width of approximately 5 feet. Note the I-wall extends above the crest of the soil founded levee. The protected side of the levee has a 1 on 3 side slope to approximately El -3.4. The protected side ground surface is assigned El -3.4 for this section. The crest of the earthen levee on the canal side of the I-wall is also at El 4.4. The upper 3.4 feet of the levee on the canal side of the I-wall is above normal canal water elevation. From El 4.4 to EL 1.6, the levee face has a 1 on 5 side slope. Between El 1.6 and El -4.1 the face of the levee has a 1 on 1 side slope. From El -4.1 to El -7.1 the face of the levee has a 1 on 5 side slope. From EL -7.1 to El -11.4 the peat is exposed to the canal water and has a 1 on 3 side slope. The deepest point in the canal is at canal center line (i.e., x = 133 ft in Figure 9-1), with a top of Canal bottom silt at El -12.4 at this location.

¹ All elevations cited are according to NAD88.

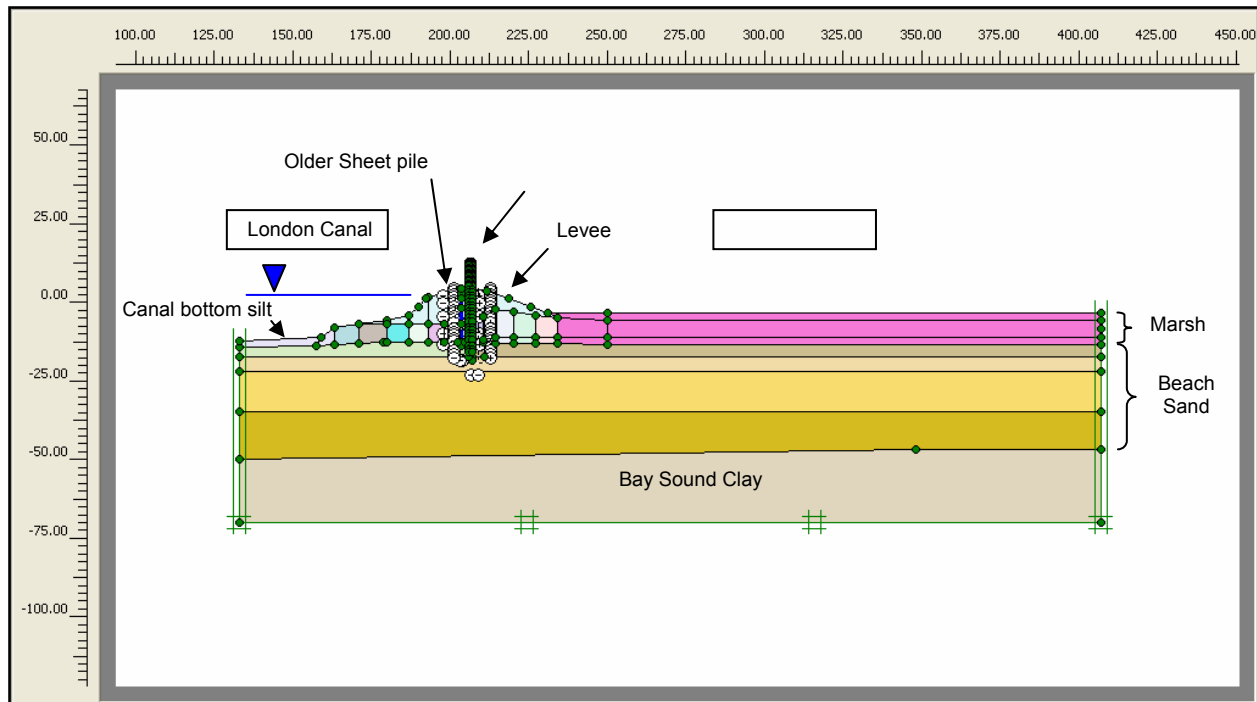


Figure 9-1. Two-Dimensional Cross Section Model used in the Complete SSI Analysis of Station 14+00 at London Canal – West Side

Proceeding from top to bottom in Figure 9-1, this cross section contains layers of Levee fill (clay), marsh (also referred to as peat), Beach sand, and Bay Sound clay. There is no Lacustrine clay contained within this cross section. The top of I-wall is at El 13 and the base of the Figure 9-1 cross-section is assigned to El -70. El -70 corresponds (approximately) to the bottom of the Bay Sound clay at Station 14+00. The soil layering is consistent with that used in the slope stability evaluations made for this cross section. The regions of uniform color in Figure 9-1 reflect the Plaxis “soil clusters” used to define the mesh and to assign soil regions with common properties.

Finite Element Mesh

Key Plaxis modeling features used in the plane strain analysis of London include the use of 15-node triangular elements to model the soil, plates (i.e., special beam elements) to model the bending of the newer I-wall/sheet pile wall as well as the older sheet pile wall, and interface elements to model soil-structure interaction between the sheet pile wall and the adjacent soil elements. A total of 33,208 nodes and 4,016 elements, containing 48,192 stress points, are used to define the Figure 9-2 mesh. Details regarding the quantity of each of the three types of plane strain elements used in the finite element model as well as select characteristics of each type of element are summarized in Table 9-1.

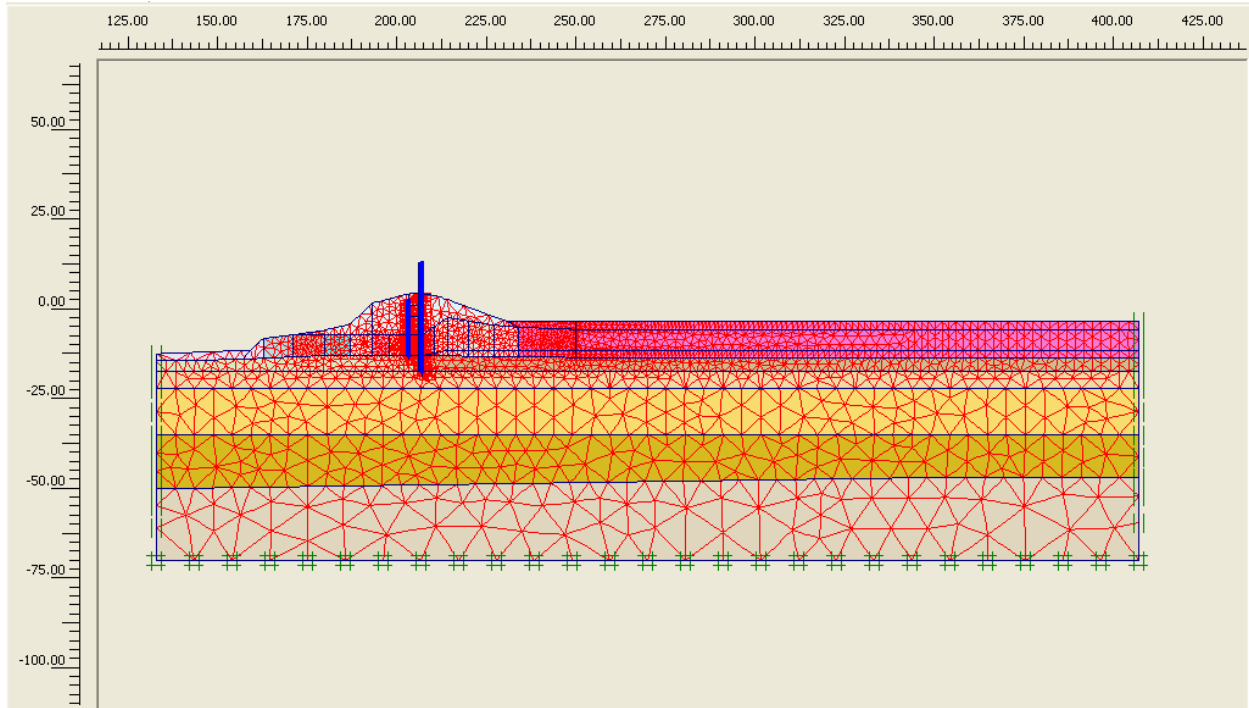


Figure 9-2. Finite Element Mesh used in the Complete SSI Analysis of Station 14+00 at London Canal – West Side

Table 9-1 Mesh Data Summary of Elements Used			
Type	Type of element	Type of integration	Total no.
Soil	15-Noded	12-point Gauss	4016
Plate	5-node line	4-point Gauss	76
Interface	5-node line	4-point Newton-Cotes	144

A zero horizontal displacement is specified along the left and right hand side vertical boundaries of the Figure 9-2 finite element mesh. However, these nodes are free to displace in the vertical direction. Along the bottom boundary of the mesh zero horizontal and vertical displacements are specified at these nodes.

Material Properties for the Soils and Flood Wall in the Complete Soil-Structure Interaction Analysis

The soil material properties used in this complete SSI analysis are the same as those used in the slope stability analyses of this cross section. Figure 9-2 shows the 76 soil clusters used to define the regions of common soil properties for the four primary categories of soil within the mesh (i.e., the marsh (or peat), Lacustrine clay, Beach sand, and Bay Sound clay). Note that each soil layer comprises many clusters, each of which is designated by a different color. Spatially varying soil properties are assigned in the slope stability analyses. Accordingly, multiple soil clusters are used in the nonlinear finite element mesh to assign material properties within each

soil layer to accommodate the spatially varying (i.e., vertically as well as horizontally) soil properties. Table 9-2 summarizes the engineering material properties and the corresponding to average stiffness values in the complete SSI analysis. Note that a range in engineering soil properties is reported for the Marsh layer. Table 9-3 summarizes the engineering material properties for the complete SSI analysis with increased values for soil stiffness of the Levee clay and the Marsh. This second set of soil stiffness values are used to assess the sensitivity in computed results to the stiffness of the protected side Levee clay and Marsh (i.e., peat).

Table 9-2 Material Characterization for Soils of Average Stiffness										
Soil type	Range in Elevation, NAD88	Total unit weight (pcf)	Constant S_u value in soil cluster (psf)	ϕ (deg)	Young's Modulus - Average					Hydraulic Conductivity (ft/hr)
					E^{ref}/S_u	E^{ref} (psf)	$(E^{ref})_{ur}/E^{ref}$	m	$R_{interface}$	
Levee clay	-	110	900	-	48	-	5	0.5	0.8	1.2E-04
Marsh (peat)	-	80	300 to 400	-	48	-	3	0.5	0.8	1.2E-04 to 1.2E-02
Beach Sand	-12 to -22	118	-	31	-	418,000	3	0.5	-	1.8
	-22 to -35	122	-	36	-	647,000	3	0.5	-	
	-35 to -47	118	-	32	-	438,900	3	0.5	-	
Bay Sound clay	-	102	779	-	68	-	3	1.0	-	1.2E-04

Note: $(E^{ref})_{50} = (E^{ref})_{oed} = E^{ref}$; $\psi = 0$ deg; $p_{ref} = 2116$ psf; $v_{ur} = 0.3$; $R_f = 0.9$

Table 9-3 Material Characterization for Soils of With Increased Stiffness										
Soil type	Range in Elevation, NAD88	Total unit weight (pcf)	Constant S_u value in soil cluster (psf)	ϕ (deg)	Young's Modulus - Stiff					Hydraulic Conductivity (ft/hr)
					E^{ref}/S_u	E^{ref} (psf)	$(E^{ref})_{ur}/E^{ref}$	m	$R_{interface}$	
Levee clay - canal side	-	110	900	-	48	-	5	0.5	0.8	1.2E-04
Levee clay - protected side	-	110	900	-	240	-	3	0.5	0.8	1.2E-04
Marsh (peat) - canal side	-	80	300 to 400	-	48	-	3	0.5	0.8	1.2E-04 to 1.2E-02
Marsh (peat) - protected side	-	80	300 to 400	-	240	-	3	0.5	0.8	1.2E-04 to 1.2E-02
Beach Sand	-12 to -22	118	-	31	-	418,000	3	0.5	-	1.8
	-22 to -35	122	-	36	-	647,000	3	0.5	-	
	-35 to -47	118	-	32	-	438,900	3	0.5	-	
Bay Sound clay	-	102	779	-	68	-	3	1.0	-	1.2E-04

Note: $(E^{ref})_{50} = (E^{ref})_{oed} = E^{ref}$; $\psi = 0$ deg; $p_{ref} = 2116$ psf; $v_{ur} = 0.3$; $R_f = 0.9$

Levee clay: A total unit weight of 110 pcf is assigned to the Levee clay soil clusters. A smaller data base of strength and stiffness tests results are available for London Canal Levee clay, as compared with 17th Street canal Levee clay. After a careful assessment of the test data on the Levee clay at London canal, an undrained shear strength (S_u) value of 900 psf is assigned. This is the same value for S_u that is assigned at 17th Street.

Stress-strain data for 17th Street canal Levee clay triaxial test specimens leads to the assignment of an average value for Young's modulus, E^{ref} , expressed in terms of (E^{ref}) normalized by S_u and equal to 48 (Table 9-2). This same value for Young's modulus is assigned to the London canal Levee clay. During the course of the complete SSI analysis of Station 14+00, an evaluation of the sensitivity in computed results to the value of Levee and Marsh stiffness is conducted. In this parametric study the protected side Levee clay E^{ref} is increased by a factor of five. It is expressed in Table 9-3 in terms of (E^{ref}) normalized by S_u and is set equal to 240 (i.e., = 5 times 48).

For the Plaxis nonlinear Hardening Soil (HS) model, the parameters $(E^{ref})_{50}$ and $(E^{ref})_{oed}$ are set equal to $[E^{ref}/S_u \text{ times } S_u]$. Additional HS parameters assigned are reference stress for stiffness, p_{ref} , equal to 2,116 psf, failure ratio $R_f = 0.9$, the exponent $m = 0.5$ and v_{ur} equals 0.3. For unload reload HS parameters, $(E^{ref})_{ur}$ is set equal to 5 times $(E^{ref})_{50}$ in the average modulus complete SSI analysis and set equal to 3 times $(E^{ref})_{50}$ in the sensitivity analysis using stiff clay properties. For Casteel CZ101 cold formed steel sheet piles to levee clay, the interface strength parameter $R_{interface}$ is set equal to 0.8 for Levee clay-to-steel interfaces (by the Potyondy, 1961, data).

Marsh (or peat): A smaller data base of strength and stiffness tests results are available for London Canal Marsh (or peat), as compared with 17th Street canal peat (or marsh). After a careful assessment of the test data on the Marsh at London canal, a range in values of undrained shear strength (S_u) of 300 psf to 400 psf is assigned. This is the same range in S_u values as is assigned for the 17th Street canal peat, which factored into the strength assessment made for this cross section. Below the I-wall and in the region of the greatest overburden, a value of S_u equal to 400 psf is assigned. With no overburden, the value for S_u is set equal to 300 psf in the Marsh. A shear strength value is assigned to each Marsh cluster based on the magnitude of the overburden for the center position of each Marsh cluster below the levee. There is no vertical variation in undrained shear strength for the Marsh layer. A total unit weight of 80 pcf is assigned to the Marsh soil clusters. Stress-strain data for 17th Street canal peat triaxial test specimens leads to the assignment of an average value for Young's modulus, E^{ref} , expressed in terms of (E^{ref}) normalized by S_u and set equal to 48 (Table 9-2). This same value for Young's modulus is assigned to the London canal Marsh. In the evaluation of the sensitivity in computed results to stiffness, the protected side Marsh E^{ref} is increased by a factor of five. It is expressed in Table 9-3 in terms of (E^{ref}) normalized by S_u and set equal to 240 (i.e., = 5 times 48).

For the Plaxis nonlinear Hardening Soil (HS) model the parameters $(E^{ref})_{50}$ and $(E^{ref})_{oed}$ are set equal to $[E^{ref}/S_u \text{ times } S_u]$. Additional HS parameters assigned are reference stress for stiffness, p_{ref} , equal to 2,116 psf, failure ratio $R_f = 0.9$ and the exponent $m = 0.5$. For unload reload HS parameters, $(E^{ref})_{ur}$ is set equal to 3 times $(E^{ref})_{50}$ and v_{ur} equals 0.3. For Casteel CZ101 cold formed steel sheet piles to Marsh interface, $R_{interface}$ is set equal to 0.8.

Beach Sand: The results from the field investigation indicate that the Beach sand is made up of three distinct layers based on the in-situ density of the sand. The upper layer of Beach sand extends from approximately El -12 to -22 and is a loose to medium sand. The middle layer extends from El -22 to -35 and is a medium sand. The lower layer extends from El -35 to -47 and is a loose to medium sand. Proceeding from the top layer down, total unit weights of 118 pcf, 120 pcf and 118 pcf are assigned to each of the three layers of Beach Sand soil clusters.

Standard Penetration Test and cone test results in the upper Beach sand layer (i.e., El -12 to -22) indicate an average value of 10 blows per ft depth for 60 percent of free-fall energy and corrected to an effective overburden pressure of 1 ton/ft² [i.e., $(N_1)_{60} = 10$]. For a fine sand with an average value of $(N_1)_{60} = 10$, the relative density (D_r) is 40 percent by Skempton's (1986) correlation. A $(N_1)_{60} = 10$ results in a value of 30 deg for the effective angle of internal friction by the Peck, Hanson and Thornburn (1974) correlation. For loose sand with D_r equal to 40 percent and using the correlations of Lengkeek and Vermeer and Shanz (cited in Brinkgreve, 2005, as well as in Plaxis course notes, 2006), the value of Young's modulus E^{ref} is set equal to 418,000 psf. For the Plaxis nonlinear Hardening Soil (HS) model, the parameters $(E^{\text{ref}})_{50}$ and $(E^{\text{ref}})_{\text{oad}}$ are set equal to 418,000 psf. Additional HS parameters assigned are reference stress for stiffness, p_{ref} , equal to 2,116 psf, failure ratio $R_f = 0.9$ and the exponent $m = 0.5$. For unload reload HS parameters, $(E^{\text{ref}})_{\text{ur}}$ is set equal to 3 times $(E^{\text{ref}})_{50}$ and v_{ur} equals 0.3. For Casteel CZ101 cold formed sheet piles to Beach sand, the interface strength parameter $R_{\text{interface}}$ is set equal to 0.8.

Standard Penetration Test and cone test results in the middle Beach sand layer (i.e., El -22 to -35) indicate an average value of 26 blows per ft depth for 60 percent of free-fall energy and corrected to an effective overburden pressure of 1 ton/ft² [i.e., $(N_1)_{60} = 26$]. For a fine sand with an average value of $(N_1)_{60} = 26$, the relative density (D_r) is 65 percent by Skempton's (1986) correlation. A $(N_1)_{60} = 26$ results in a value of 36 deg (approximately) for the effective angle of internal friction by the Peck, Hanson and Thornburn (1974) correlation. For medium sand with D_r equal to 65 percent and using the correlations of Lengkeek and Vermeer and Shanz (cited in Brinkgreve, 2005, as well as in Plaxis course notes, 2006), the value of Young's modulus E^{ref} is set equal to 647,000 psf. For the Plaxis nonlinear Hardening Soil (HS) model, the parameters $(E^{\text{ref}})_{50}$ and $(E^{\text{ref}})_{\text{oad}}$ are set equal to 647,000 psf. Additional HS parameters assigned are reference stress for stiffness, p_{ref} , equal to 2,116 psf, failure ratio $R_f = 0.9$ and the exponent $m = 0.5$. For unload reload HS parameters, $(E^{\text{ref}})_{\text{ur}}$ is set equal to 3 times $(E^{\text{ref}})_{50}$ and v_{ur} equals 0.3.

Standard Penetration Test and cone test results in the lower Beach sand layer (i.e., El -35 to -47) indicate an average value of 14 blows per ft depth for 60 percent of free-fall energy and corrected to an effective overburden pressure of 1 ton/ft² [i.e., $(N_1)_{60} = 14$]. For a fine sand with an average value of $(N_1)_{60} = 14$, the relative density (D_r) is 46 percent by Skempton's (1986) correlation. A $(N_1)_{60} = 14$ results in a value of 32 deg (approximately) for the effective angle of internal friction by the Peck, Hanson and Thornburn (1974) correlation. For loose sand with D_r equal to 46 percent and using the correlations of Lengkeek and Vermeer and Shanz (cited in Brinkgreve, 2005, as well as in Plaxis course notes, 2006), the value of Young's modulus E^{ref} is set equal to 438,900 psf. For the Plaxis nonlinear Hardening Soil (HS) model, the parameters $(E^{\text{ref}})_{50}$ and $(E^{\text{ref}})_{\text{oad}}$ are set equal to 438,900 psf. Additional HS parameters assigned are reference

stress for stiffness, p_{ref} , equal to 2,116 psf, failure ratio $R_f = 0.9$ and the exponent $m = 0.5$. For unload reload HS parameters, $(E^{ref})_{ur}$ is set equal to 3 times $(E^{ref})_{50}$ and v_{ur} equals 0.3.

Bay Sound clay: A smaller data base of strength and stiffness tests results are available for London Canal Bay Sound clay, as compared with 17th Street canal Bay Sound clay. After a careful assessment of the test data on the Bay Sound clay at London canal, a value of undrained shear strength (S_u) of 779 psf is assigned. This is the same S_u value assigned for the 17th Street canal Bay Sound clay, which factored into the strength assessment made for this cross section. A total unit weight of 102 pcf is assigned to the Bay Sound clay soil cluster. Stress-strain data for 17th Street canal Bay Sound clay triaxial test specimens leads to the assignment of an average value for Young’s modulus, E^{ref} , expressed in terms of (E^{ref}) normalized by S_u and set equal to 68 (Tables 9-2 and 9-3). This same value for Young’s modulus is assigned to the London canal Bay Sound clay.

For the Plaxis nonlinear Hardening Soil (HS) model, the parameters $(E^{ref})_{50}$ and $(E^{ref})_{oed}$ are set equal to $[E^{ref}/S_u \text{ times } S_u]$. Additional HS parameters assigned are reference stress for stiffness, p_{ref} , equal to 2,116 psf, failure ratio $R_f = 0.9$ and the exponent $m = 1.0$. For unload reload HS parameters, $(E^{ref})_{ur}$ is set equal to 3 times $(E^{ref})_{50}$ and v_{ur} equals 0.3.

Hydraulic Conductivity: Values for the hydraulic conductivity of the four soil types are listed in Tables 9-2 and 9-3. The hydraulic conductivity value assigned to the Beach sand is based on field pump tests while all other values are based on typical values found in the technical literature for soils of similar engineering material characteristics. For the Marsh material, data from Weber (1969) and others leads to the assignment of hydraulic conductivity values of 1.2×10^{-2} ft/hr for regions of lower overburden pressure and 1.2×10^{-4} ft/hr for regions of higher overburden, such as below the Levee. For canal bottom silts, a hydraulic conductivity value equal to 1.2×10^{-2} ft/hr is assigned.

Flood Wall: The flood wall comprises an exposed reinforced concrete I-wall, a reinforced concrete cap and Casteel CZ101 cold formed sheet pile. The 12-inch thick reinforced concrete I-wall extends from the top of protected levee (El 4.3) to El 13. At Station 14+00, the sheet pile tip is at El -17.4. The top of the Beach sand to Marsh interface is at El -12.9. Consequently, the sheet pile extends 4.5 ft into the Beach sand. The upper reach of pile is encased in a two-foot thick reinforced concrete cap extending below the surface of the protected side of the levee. Linear elastic material response was assumed in the complete SSI analysis. Engineering properties for the I-wall, cap and sheet pile are summarized in Table 9-4 for the zero thickness plate elements used in the finite element model.

Table 9-4 Material Characterization for the Flood Wall				
Identification	EA	EI	weight	v
	[lb/ft]	[lbft²/ft]	[lb/ft/ft]	[-]
Reinforced Concrete I-wall	4.32E8	3.6E7	150.00	0.20
Reinforced Concrete Cap	8.64E8	2.88E8	80.00	0.20
Sheet Pile (Hoesch 12)	9.77E7	1.31E7	9.15	0.30

Complete Soil-Structure Interaction Analysis

Introduction: Two sets of complete SSI analyses of the Figure 9-1 2-D cross section of Station 14+00 at London Canal are conducted in staged analysis using Plaxis. Both sets evaluate the response of the Station 14+00 cross-section to flood loading starting at canal water El 1.0 on through a series of incremental 0.6 to 3.4 feet raises in canal elevation. Table 9-5 summarizes the calculation phases of the first analysis set using average modulus values for the four soil types. More than 17 phases of calculations are used in this complete SSI analysis to a maximum canal water El 8. Table 9-6 summarizes the calculation phases of the second analysis set using stiff modulus values for the Levee clay and the Marsh on the protected side of the I-wall. More than 22 phases of calculations are used in this parametric SSI analysis to a maximum canal water El 8.

Table 9-5 Calculation Phases of the Nonlinear Finite Element Analysis Using Average Modulus Values			
Phase	PhaseNo.	Calculation type	Load input
Initial phase	0	-	-
Place Wall & Interface	1	Plastic analysis	Staged construction
Gravity (1.0)	2	Plastic analysis	Total multipliers
Water Table El -17.4	3	Plastic analysis	Staged construction
Water Table El +1	4	Plastic analysis	Staged construction
Canal Water El +4.4	5	Plastic analysis	Staged construction
Crack to El -3	6	Plastic analysis	Staged construction
Crack to El -5	7	Plastic analysis	Staged construction
Canal Water El +5	8	Plastic analysis	Staged construction
Crack to El -6	9	Plastic analysis	Staged construction
Canal Water El +6	10	Plastic analysis	Staged construction
Crack to El -7	11	Plastic analysis	Staged construction
Crack to El -10 Canal Water El +6,	12	Plastic analysis	Staged construction
Crack to El -12.9, linear phreatic surface	13	Plastic analysis	Staged construction
Canal Water El +7, linear phreatic surface	14	Plastic analysis	Staged construction
Canal Water El +7.5, linear phreatic surface	15	Plastic analysis	Staged construction
Canal Water El +8, linear phreatic surface	16	Plastic analysis	Staged construction
Phi-C Reductions	17 ⁺	Phi/c reduction	Incremental multipliers

**Table 9-6
Calculation Phases of the Nonlinear Finite Element Analysis Using Stiff Modulus Values for the Levee Clay and the Marsh on the Protected Side**

Phase	PhaseNo.	Calculation type	Load input
Initial phase	0	-	-
Place Wall & Interface	1	Plastic analysis	Staged construction
Gravity (1.0)	2	Plastic analysis	Total multipliers
Water Table El -17.4	3	Plastic analysis	Staged construction
Water Table El +1	4	Plastic analysis	Staged construction
Canal Water El +4.4	5	Plastic analysis	Staged construction
Crack to El -2	6	Plastic analysis	Staged construction
Crack to El -3	7	Plastic analysis	Staged construction
Canal Water El +5	8	Plastic analysis	Staged construction
Crack to El -4	9	Plastic analysis	Staged construction
Canal Water El +6	10	Plastic analysis	Staged construction
Crack to El -5	11	Plastic analysis	Staged construction
Crack to El -6	12	Plastic analysis	Staged construction
Canal Water El +7	13	Plastic analysis	Staged construction
Canal Water El +8	14	Plastic analysis	Staged construction
Crack to El -7	15	Plastic analysis	Staged construction
Canal Water El +8, Crack to El -12.9, linear phreatic surface	16	Plastic analysis	Staged construction
Canal Water El +4.4, Crack to El -12.9, Linear phreatic surface	17	Plastic analysis	Staged construction
Canal Water El +5, Crack to El -12.9, Linear phreatic surface	18	Plastic analysis	Staged construction
Canal Water El +6, Crack to El -12.9, Linear phreatic surface	19	Plastic analysis	Staged construction
Canal Water El +7, Crack to El -12.9, Linear phreatic surface	20	Plastic analysis	Staged construction
Canal Water El +7.5, Crack to El -12.9, Linear phreatic surface	21	Plastic analysis	Staged construction
Phi-C Reductions	22 ⁺	Phi/c reduction	Incremental multipliers

Loading phases 0 through 4 are used in both sets of complete SSI analyses to establish the initial total stress state condition existing prior to flooding. Loading phase 4 concludes with canal water at El 1, a steady state water elevation in the canal.

Loading phases 5 through 16 (Table 9-5) are used in the first analysis set with average modulus values for the four soil types to perform an incremental raise in the canal water to El 8, modeling the flood loading of the levee/I-wall system and the introduction of a crack along the canal-side face of the sheet pile in the Levee clay and in the Marsh/peat (eventually to the top of the Beach sand at El -12.9). The last of the loading phases (i.e., 17⁺) are used to compute the reserve capacity of the levee/I-wall system for different canal water elevations. This reserve capacity is expressed in terms of a Factor of Safety and is computed in a series of Plaxis phi/c reduction loading phases.

Loading phases 5 through 16 (Table 9-6) are used in the second analysis set with stiff modulus values assigned to the Levee clay and the Marsh on the protected side of the I-wall to perform an incremental raise in the canal water to El 8, modeling the flood loading of the levee/I-wall system and the introduction of a crack along the canal-side face of the sheet pile in the Levee clay and in the Marsh/peat (eventually to the top of the Beach sand at El -12.9). Loading phases 17 through 21 provide a data base used to determine the Factor of Safety for canal water El 8 and with a crack on the canal side of the sheet pile wall that extends from the top of the levee (El 4.4) to the top of the sand layer (El -12.9). The last of the loading phases (i.e., 22⁺) are used to compute the reserve capacity of the levee/I-wall system for different canal water elevations by phi/c reduction.

Initial steady state condition for canal water at EL 1: Loading phases 0 through 4 are used in the complete SSI analysis to establish the initial total stress state within the finite element mesh with a steady state canal water elevation at El 1. Gravity loading is applied in a single increment, followed by an incremental rising of the water table. In the Beach sand layer, the water table is established at El -8.4 on the right-hand, protected side of the mesh, at x-coordinate 407, by analysis phase 4 and is maintained at this elevation in all subsequent computation phases. Load input for gravity loading is specified in Plaxis by means of the total multiplier method and changes in water table are accomplished by staged construction and by steady state seepage analysis, unless stated otherwise.

The initial steady-state, total stress condition for the usual canal water elevation of 1 is established by using the average stiffness modulus values given in Table 9-2 in the Mohr-Coulomb soil model for loading phases 0 through 4 for both sets of complete SSI analyses. The results from the IPET Task 7 slope stability analyses for this usual canal elevation indicate a stable cross-section with an ample Factor of Safety, i.e., above 1.5. Consequently, an important aspect of the total stress regime achieved within the Figure 9-2 finite element mesh is that the mobilized shear stress at the strain integration points within the finite elements contained in the soil clusters shown in this figure be less than the shear strength of the soil. The resulting computed fraction of mobilized shear strength (referred to as relative shear stress in Plaxis output) from the resulting initial total stress condition is shown in Figure 9-3. The fraction of mobilized shear strength is less than or equal to 0.9 at the stress integration points for the four soil types.

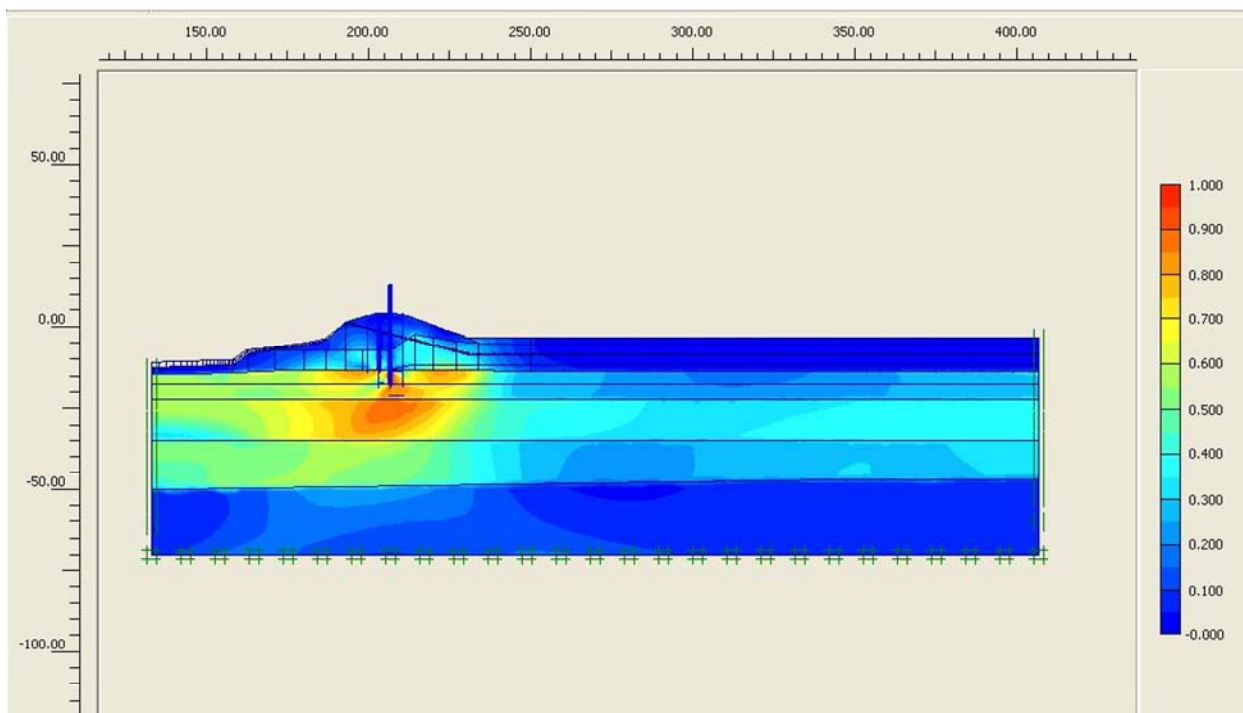


Figure 9-3. Fraction of Mobilized Shear Strength for Canal El 1

Flood loading: Modeling of flood loading commenced in the complete SSI analysis after the total initial stress state is established within the finite element mesh for steady state canal elevation (i.e., El 1). The hardening soil model with the Table 9-2 average stiffness material property values are assigned to each of the four types of soil regimes in the first complete SSI analysis set. Loading phases 5 through 16 (refer to Table 9-5) are used in the complete SSI analysis to perform an incremental raise in the canal water to El 8, modeling the flood loading of the levee/I-wall system. Load input for changes in canal water elevation is specified by staged construction. For canal water up to and including El 6 and for crack depths terminating above the top of the Beach sand layer (at El -12.9) on the canal side of the new sheet pile wall/I-wall, a steady state seepage analysis is used to establish the pore water pressure regime within the Beach sand layer for loading phases 5 through 12 (Table 9-5).

The results from first SSI set of analysis using Table 9-2 average soil stiffness values indicates that cracking commenced when Canal water reached the top of the Levee (i.e., El 4.4). Crack initiation occurs at the top of the Levee clay, on the canal side (at El 4.4) of the sheet pile wall when the total horizontal stress in the clay is less than the value for hydrostatic water pressure (i.e., γ_{water} times depth below canal water surface). This first occurs at Table 9-5 loading phase 5. Comparisons of values for hydrostatic water pressure, generated by hand computation, with the total horizontal stresses computed in the complete SSI analysis indicates a crack will extend from El 4.4 down to EL -5 in the Levee clay by loading phase 7. The line designated E_{average} in Figure 9-4 summarizes the Table 9-5 depth of cracking phases of analysis versus Canal water elevation. Depth of cracking to the top of Beach sand (El -12.9) occurs at Canal water El 6. Additional analyses using Table 9-2 E_{average} values are conducted for Canal water El's 7, 7.5, and 8 so as to establish the variation in Factor of Safety with Canal water elevation.

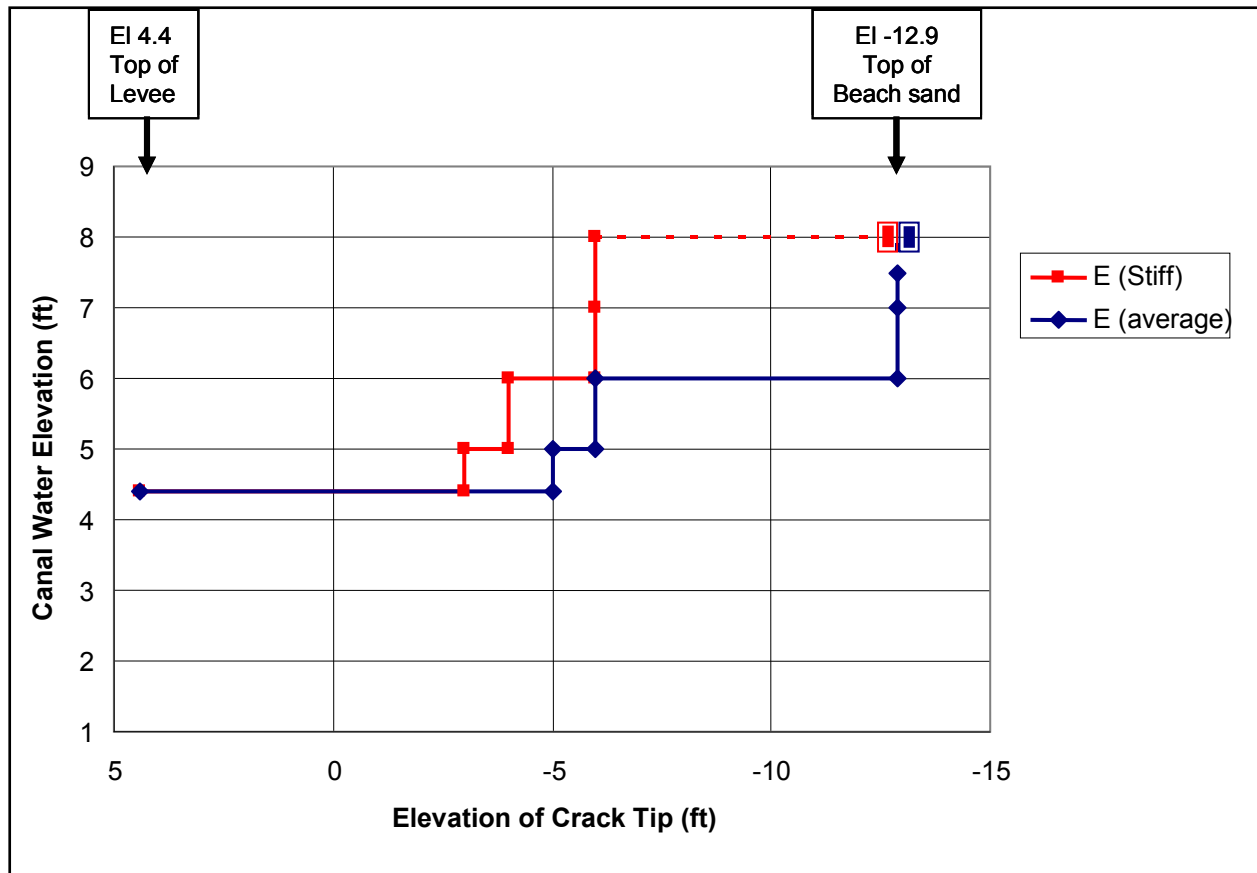


Figure 9-4. Elevation of Crack Tip Versus Canal Water Elevation

Due to numerical convergence issues, a linear phreatic surface assumption is used to establish the pore water pressures within the Beach sand for loading phases 13 through 16 (Table 9-5) of the first complete set of SSI analysis in which depth of cracking extends to the top of Beach sand layer (EL -12.9). This results in a less severe uplift pressure regime within the Beach sand below the toe of the protected side of the Levee as seen, for example, by comparing computed values and positions of equipotential lines for the Figure 9-5 steady state seepage results with the Figure 9-6 results for an analysis using a linear phreatic surface assumption. A linear phreatic surface assumption results in a less severe uplift pressure regime within the top of the Beach sand below and immediately beyond the toe of the protected side of the Levee. This results in a lower computed value for the Factor of Safety for the loading phases 13 through 16 in which this procedure is applied. Again, this compromise in accuracy is required in order to achieve convergence by Plaxis for these higher Canal water elevations with cracking to the top of the Beach sand.

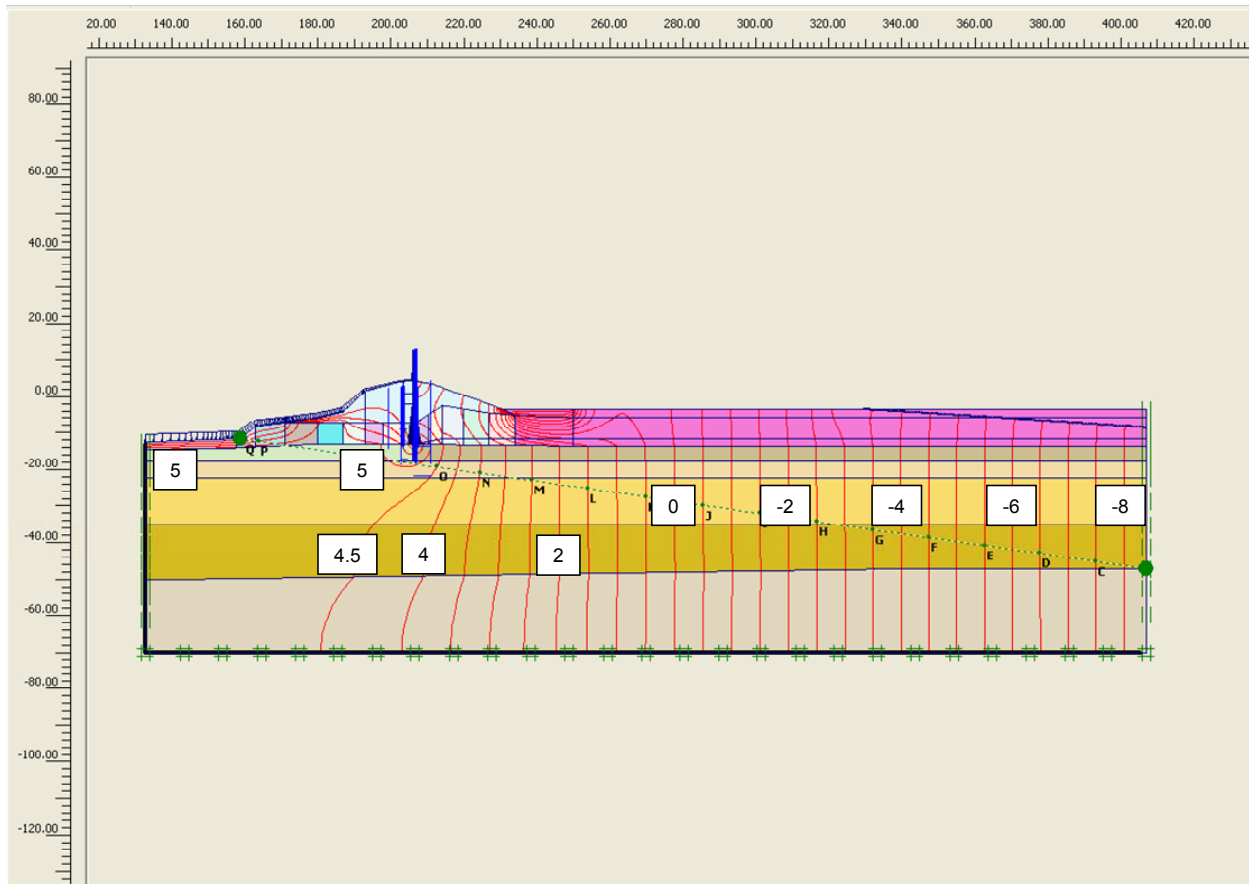


Figure 9-5. Equipotential Lines from a Steady State Seepage Analysis for Canal Water El 6 and a Crack to the Top of Beach Sand (El -12.9) on the Canal Side of the New Sheet Pile Wall



Figure 9-6. Equipotential Lines Based on a Linear Phreatic Surface for Canal Water El 6 and a Crack to the Top of Beach Sand (El -12.9) on the Canal Side of the New Sheet Pile Wall

Factor of Safety: Figure 9-7 summarizes the computed Factor of Safety versus Canal water elevation for the Table 9-2 average stiffness material property values. As the canal elevation rises, the factor of safety decreases in these results labeled E_{average} in this figure. Note that when the Canal water is raised to El 6, the Factor of Safety decreases from 2.5 to 1.84 with the crack tip progressing from El -6 to El -12.9 (i.e., the top of the Beach sand). With a crack tip at El -12.9 a new flow regime is established within the beach sand layer using a linear phreatic surface assumption as demonstrated in Figure 9-6 for Canal water El 6. (Note that for each subsequent rise in Canal water, a new linear phreatic surface is established based on the elevation of the Canal water in each analysis phase.) As the Canal water elevation rises to El 7, 7.5 and 8, the computed Factor of Safety decreases to 1.42, 1.25 and (approximately) 1. (Due to convergence issues in the ϕ/c reduction analysis, the Factor of Safety for Canal water EL 8 is established by extrapolation of the Figure 9-7 data.) Again, these computed Factors of Safety results labeled E_{average} are greater than the actual values for these last four loading phases due to the linear phreatic surface assumption used within the Beach sand.

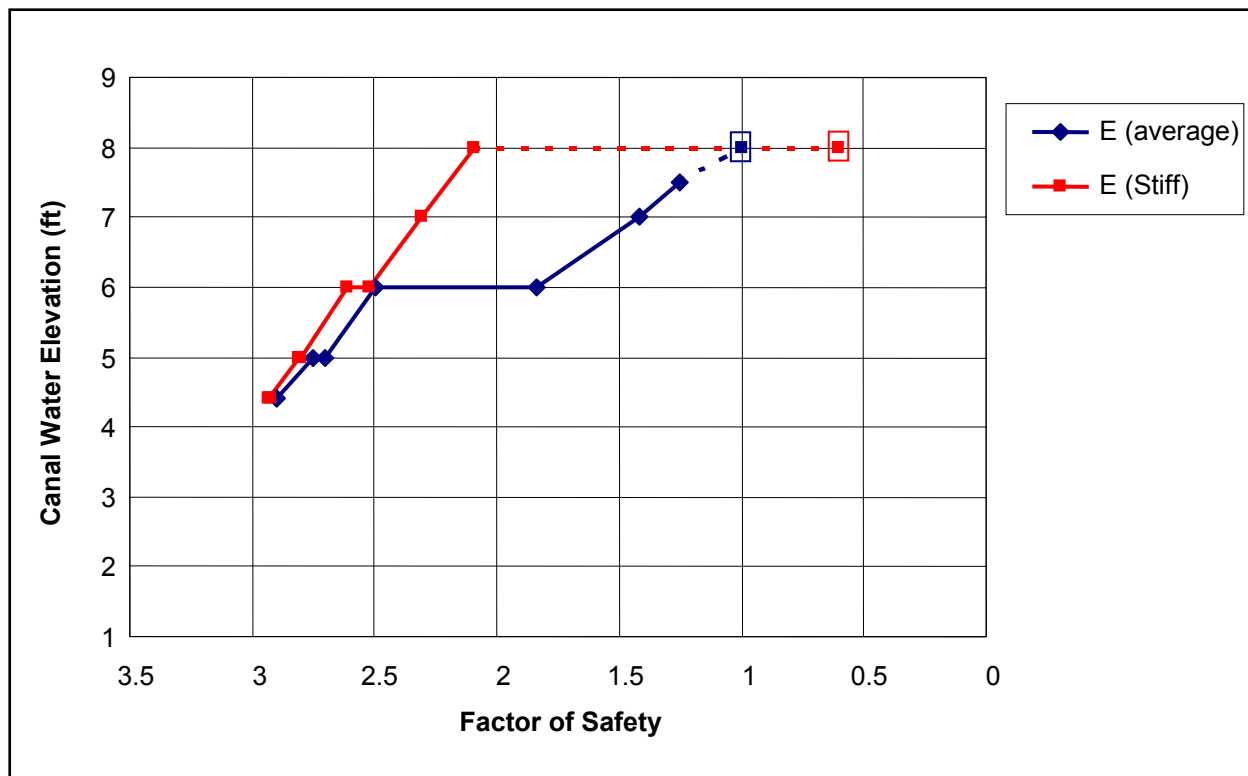


Figure 9-7. Factor of Safety Versus Canal Water Elevation

A second complete SSI analysis set with stiff modulus values (Table 9-3) assigned to the Levee clay and the Marsh on the protected side of the I-wall is conducted following the stages of loading listed in Table 9-6. Loading phases 5 through 16 (refer to Table 9-6) are used in the complete SSI analysis to perform an incremental raise in the canal water to El 8, modeling the flood loading of the Levee/I-wall system. Load input for changes in canal water elevation is specified by staged construction. For canal water up to and including El 7 in which crack depths terminate above the top of the Beach sand layer (at El -12.9) on the canal side of the new sheet pile wall/I-wall, a steady state seepage analysis is used to establish the pore water pressure regime within the Beach sand layer (i.e., loading phases 5 through 15 in Table 9-6).

The results from the second analysis set with stiff modulus values (Table 9-6) assigned to the Levee clay and the Marsh on the protected side of the I-wall indicates that cracking commenced when Canal water reached the top of the Levee (i.e., El 4.4). Crack initiation occurs at the top of the Levee clay, on the canal side (at El 4.4) of the sheet pile wall when the total horizontal stress in the clay is less than the value for hydrostatic water pressure (i.e., γ_{water} times depth below canal water surface). This first occurs at Table 9-6 loading phase 5. Comparisons of values for hydrostatic water pressure, generated by hand computation, with the total horizontal stresses computed in the complete SSI analysis indicates a crack will extend from El 4.4 down to EL -3 in the Levee clay by loading phase 7. The line designated E_{stiff} in Figure 9-4 summarizes the Table 9-6 depth of cracking phases of analysis versus Canal water elevation. Depth of cracking to the top of Beach sand (El -12.9) occurs at Canal water El 8. Additional analyses using

Table 9-3 E_{stiff} values are conducted for Canal water El's 4.4, 5, 6, 7 and 7.5 so as to establish the variation in Factor of Safety with Canal water elevation.

Computed results, summarized in Figure 9-4, shows that crack initiation occurs at the same Canal water EL of 4.4 in both sets of analyses. However, the progression of cracking is not as rapid in the E_{stiff} analyses set as it is for the $E_{average}$ analysis set. Additionally, the crack reached to top of Beach sand for a Canal water El 6 for the $E_{average}$ analysis set while the crack reached to top of Beach sand for a Canal water El 8 for the E_{stiff} analysis set; a difference of two feet.

Due to numerical convergence issues, a linear phreatic surface assumption is used to establish the pore water pressures within the Beach sand for loading phases 16 through 21 (Table 9-6) of the second analysis set with stiff modulus values assigned to the Levee clay and the Marsh on the protected side of the I-wall in which depth of cracking is specified to the top of Beach sand layer (EL -12.9). This results in a less severe uplift pressure regime within the Beach sand below the toe of the protected side of the Levee, as discussed previously. In turn, this results in a lower computed value for the Factor of Safety for the loading phases 16 through 21 in which this procedure is applied. Again, this compromise in accuracy is required in order to achieve convergence by Plaxis for these higher Canal water elevations with cracking to the top of the Beach sand.

Figure 9-7 also summarizes the computed Factors of Safety versus Canal water elevations for the Table 9-3 second analysis set with stiff modulus values assigned to the Levee clay and the Marsh on the protected side of the I-wall. These results are labeled E_{stiff} in this figure. This figure shows that as the canal elevation rises, the Factor of Safety decreases. Note that when the Canal water is raised to El 8, the Factor of Safety decreases from 2.09 to 0.6 (approximately) with the crack tip progressing from El -6 to El -12.9 (i.e., the top of the Beach sand). With a crack tip at El -12.9 a new flow regime is established within the beach sand layer and is computed using a linear phreatic surface assumption. The Plaxis phi/c reduction analysis for Canal water El 8, with depth of crack to EL -12.9 (i.e., top of beach sand), did not converge. In order to establish an estimate for the value of the Factor of Safety for this case, a series of phi/c reduction calculations for Canal water El's of 4.4, 5, 6, 7, and 7.5 are conducted with a fictitious depth of crack specified to EL -12.9 (i.e., top of beach sand) in each of these calculations (designated phase 17 through 21 in Table 9-6). These results are summarized in Figure 9-8. A Factor of Safety of 0.6 is estimated for Canal water El 8 by extrapolating the computed Factors of Safety results for these lower canal water elevations to canal water El 8. Additionally, this data shows that a Factor of Safety equal to unity occurs at Canal water El 7.7 (approximately). Again, recognize that these Figure 9-8 computed Factors of Safety results and the Figure 9-7 data point of Factor of Safety equal to 0.6 for Canal water El 8 on the E_{stiff} labeled curve, are greater than the actual values due to the linear phreatic surface assumption used within the Beach sand.

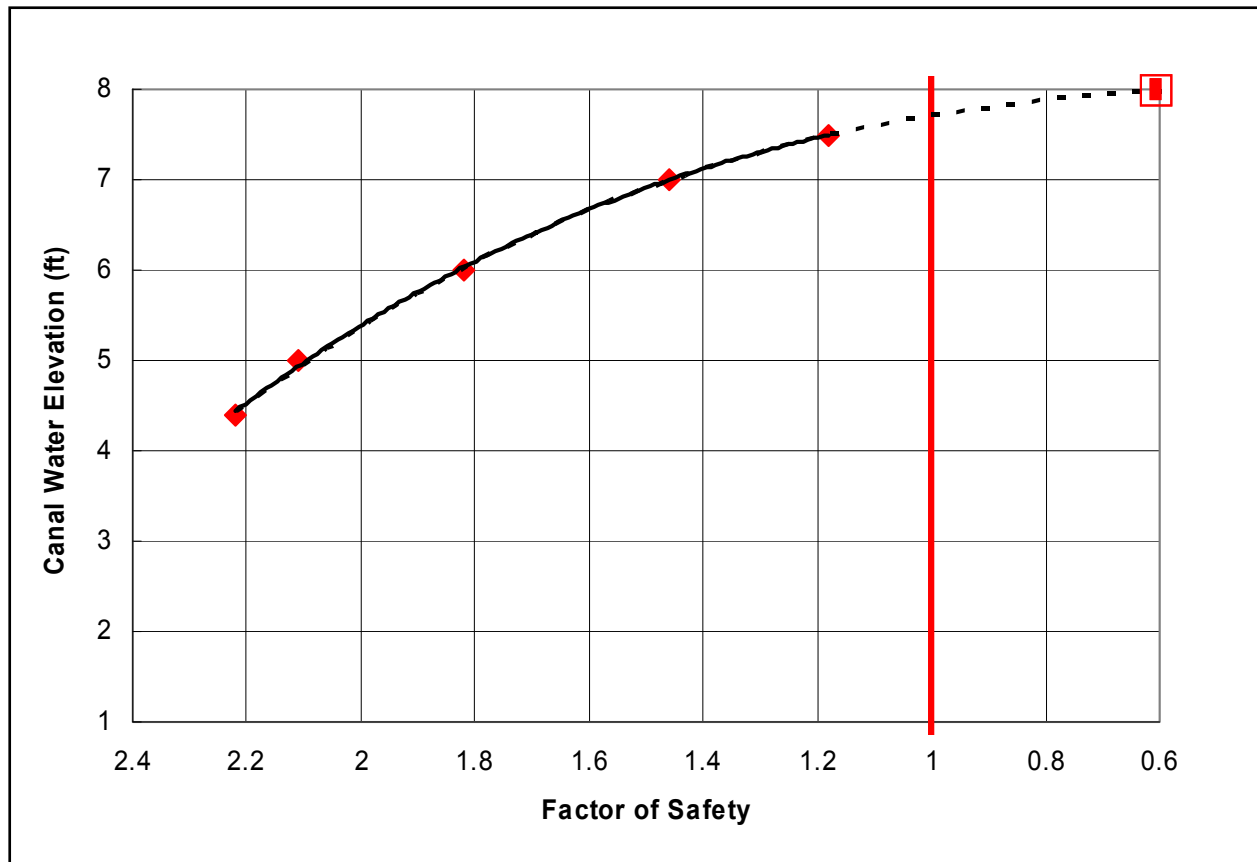


Figure 9-8. Factor of Safety Versus Canal Water Elevation, Computed With Crack to Top of Beach Sand El -12.9 and Using Stiff Modulus Values for the Levee Clay and Marsh on the Protected Side

Deformations: Figure 9-9 summarizes the computed deformations for the first analysis set with average modulus values, Canal El 6 and Crack to El -12.9 (i.e., top of Beach sand). Note the nodal deformations are magnified by a factor of 30 in order to show the deformed relative mesh relative to its position at canal water elevation of 1.0 (shown as a blue outline in this figure). The general trend is a rotational plowing of the protected side Levee clay by the I-wall/new sheet pile wall and a bulging of the Marsh beyond the toe of the Levee on the protected side. Recall that the computed Factor of Safety for this condition is 1.84 (for E_{average} values).

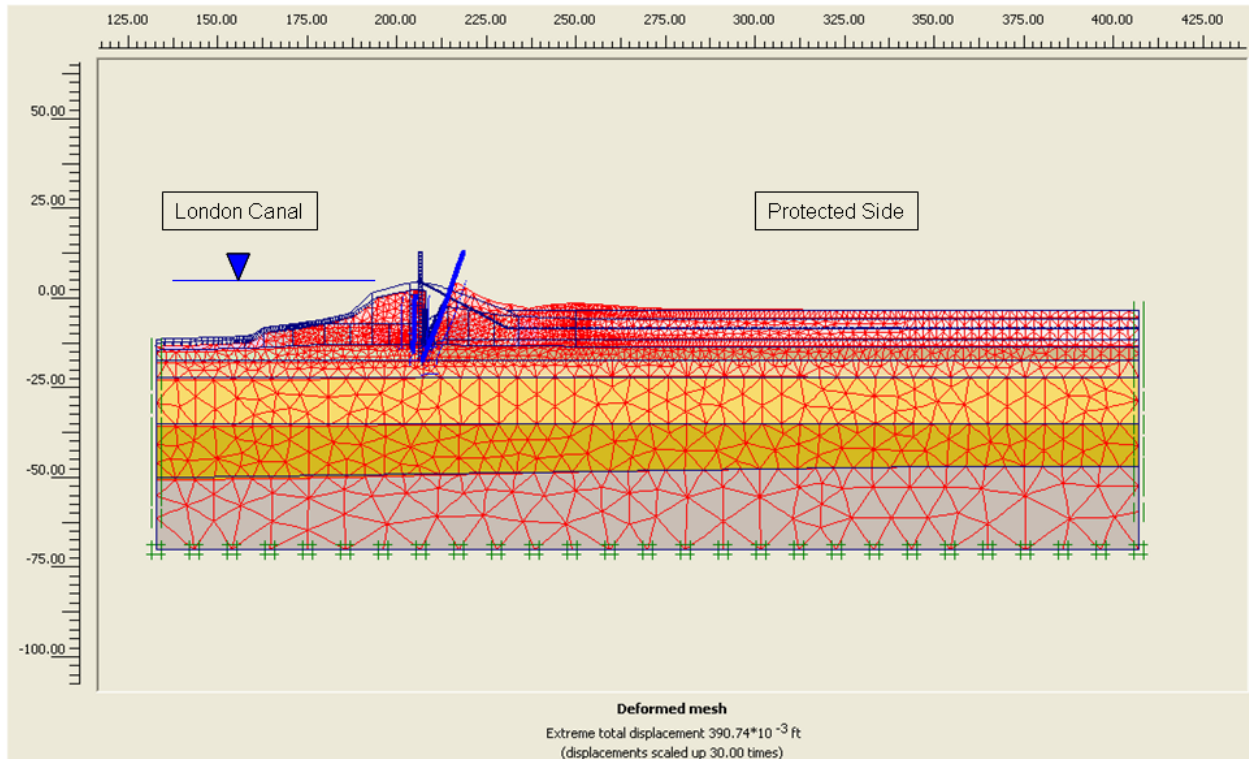


Figure 9-9. Deformed Mesh for Average Stiffness Values, Exaggerated by a Factor of 30, for Canal El 6 and Crack to El -12.9 (Note: Canal El not to scale in figure)

Figure 9-10 shows the horizontal displacements of the soil regions within the mesh, relative to their position at a canal water elevation of 1.0 for average stiffness values with Canal El 6 and Crack to El -12.9. This figure shows the horizontal deformations are concentrated within the protected region of the Levee and the Marsh immediately at the toe of the Levee on the protected side. The largest horizontal deformations are concentrated at the top of the Levee, on the protected side, approximately 0.29 ft (3½ inches).

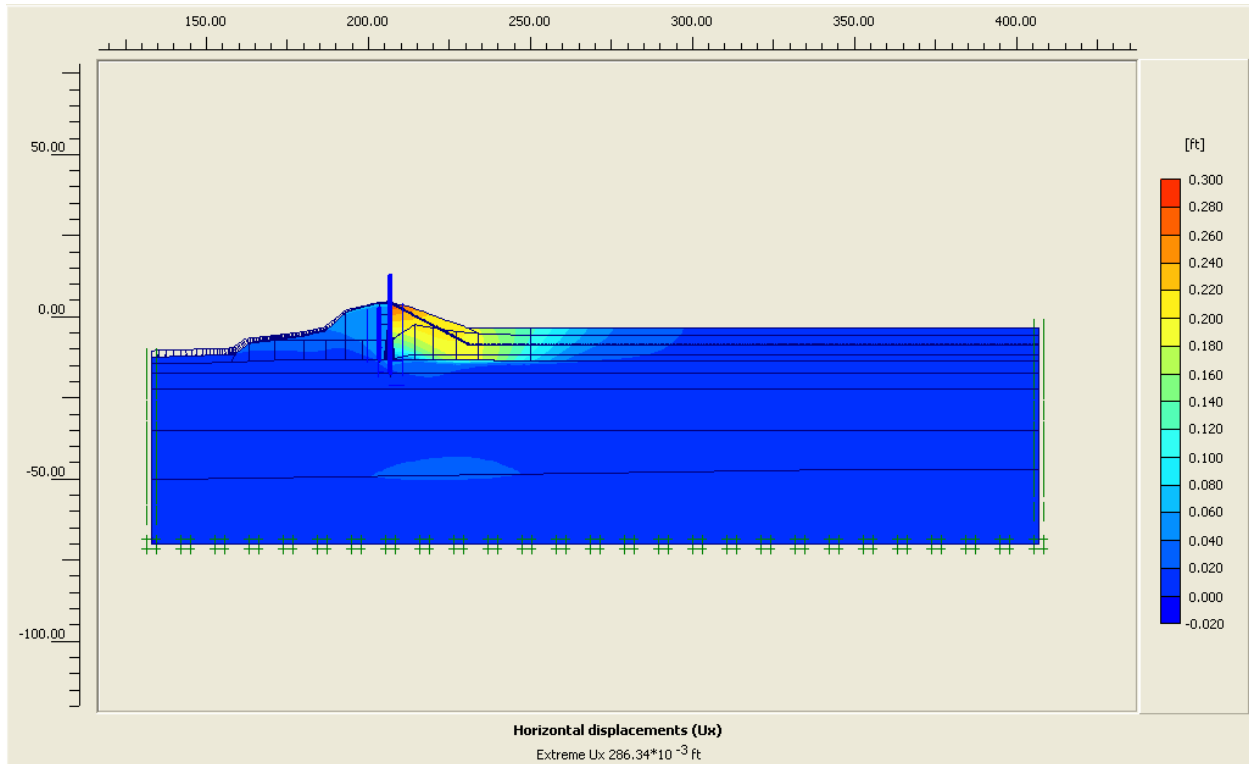


Figure 9-10. Horizontal Deformation Shadings for Average Stiffness Values with Canal EI 6 and Crack to EI -12.9 (Note: Canal EI not to scale in figure)

Figure 9-11 shows the variation in horizontal displacements of the sheet pile versus canal water elevation for average stiffness values. These displacements are relative to their position at a canal water elevation of 1.0 for average stiffness values. This figure shows the rotational nature of the I-wall/sheet pile wall deformations, with the toe of the sheet pile “anchored” in the Beach sand.

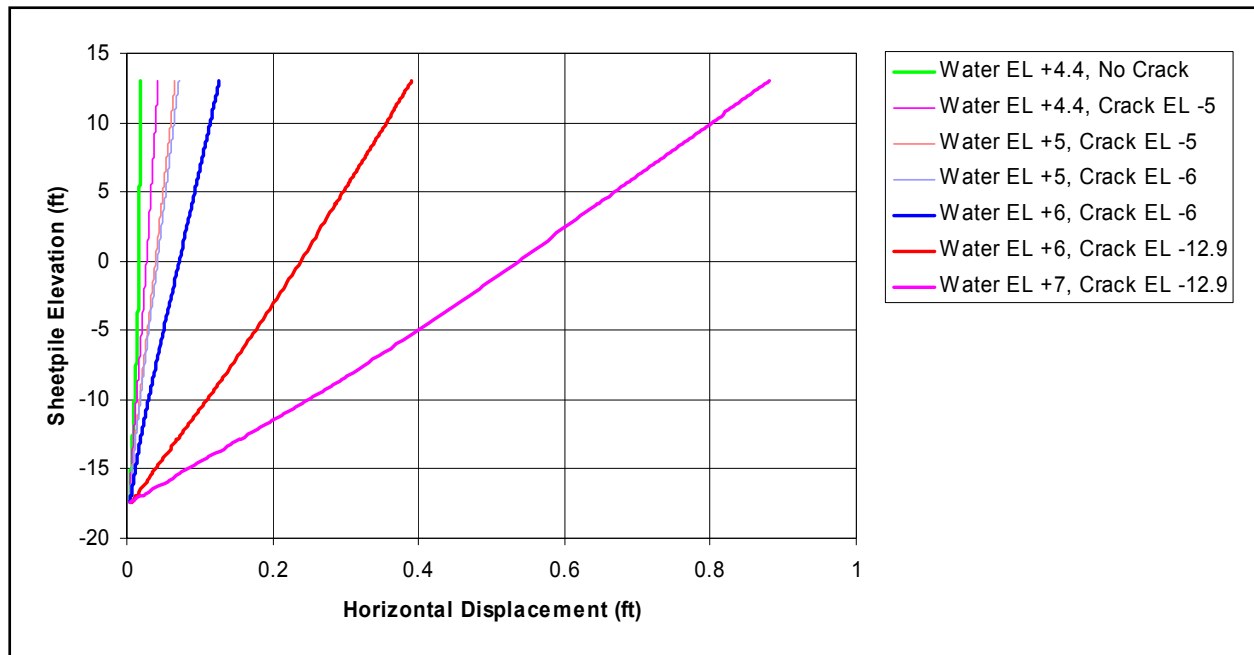


Figure 9-11. Horizontal Displacement of the I-Wall/Sheet Pile versus Canal Water El and Computed Using Average Stiffness Values

Figure 9-12 shows the horizontal displacements of three points within the flood wall, relative to its position at a canal water elevation of 1.0 for average stiffness values. The points monitored through the analysis are at the top of the I-wall (El 13), at El 4.4 (top of Levee) and at the sheet pile tip (El -17.4). Recall for Canal water El's of 6 and higher, the crack never extends into the Beach sand layer, it terminates at the top of the Beach sand layer (i.e., El -12.9). Note that there is a significant increase in horizontal deformations of the I-wall/sheet pile wall when the crack extends to El -12.9 at Canal El 6. Results in this figure shows the Beach sand is providing enough lateral support to prevent the sheet pile tip from moving laterally, therefore the deformation of the sheet pile is mostly a rotation about the sheet pile tip. Maximum horizontal movement at the top of the I-wall is 0.88 ft (10 ½ inches) for Canal Water El 7.

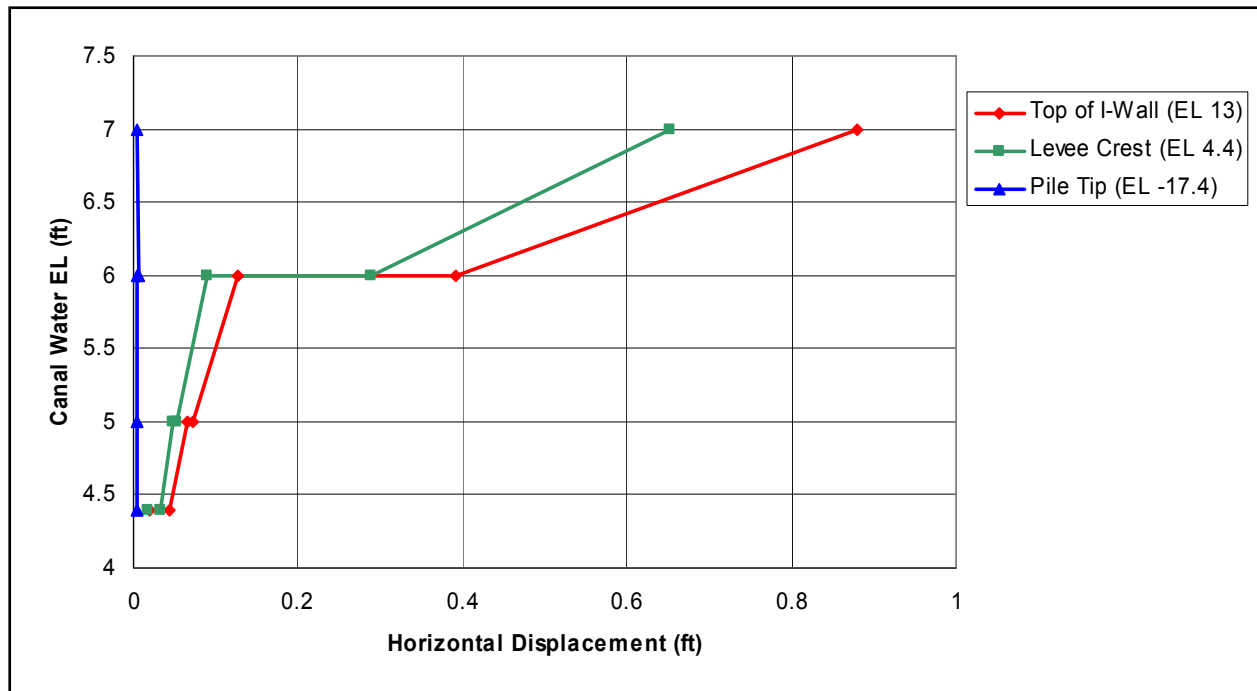


Figure 9-12. Horizontal Sheet Pile Deformations versus Canal Water El and Computed Using Average Stiffness Values

Figure 9-13 shows the vertical displacements of the soil regions within the mesh, relative to their position at a canal water elevation of 1.0 for average stiffness values with Canal El 6 and Crack to El -12.9. This figure shows the 0.07 ft (7/8 inch) uplift of the Marsh located beyond the toe of the Levee on the protected side.

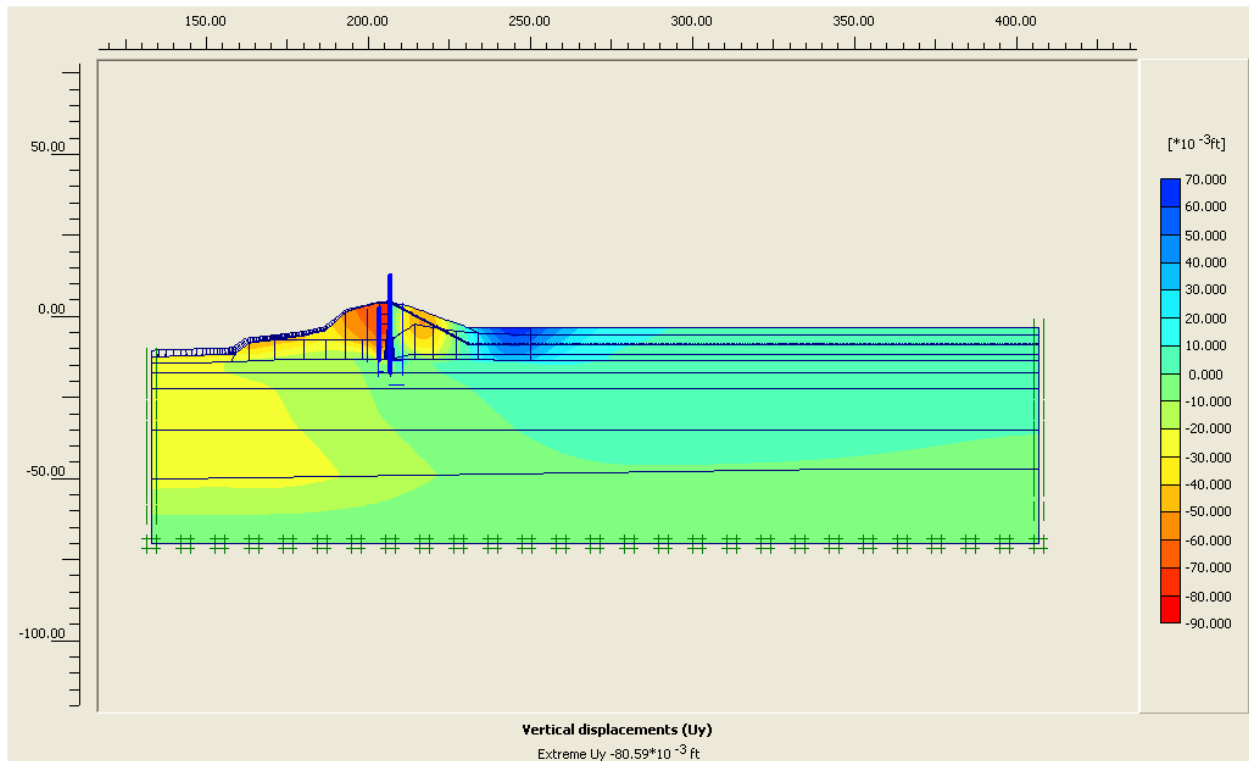


Figure 9-13. Vertical Deformation Shadings for Average Stiffness Values with Canal EI 6 and Crack to EI 12.9 (Note: Canal EI not to scale in figure)

Figure 9-14 shows the variation in horizontal displacements of the sheet pile versus canal water elevation for the second analysis set with stiff modulus values assigned to the Levee clay and the Marsh on the protected side of the I-wall. These displacements are relative to their position at a canal water elevation of 1.0 for average stiffness values. This figure shows the rotational nature of the I-wall/sheet pile wall deformations, with the toe of the sheet pile “anchored” in the Beach sand. The shape of the deformed wall is the same for both sets of E_{average} and E_{stiff} analyses. However the magnitude of the horizontal displacements in Figure 9-14 are less than the Figure 9-11 displacements for the first analysis set made using average stiffness values.

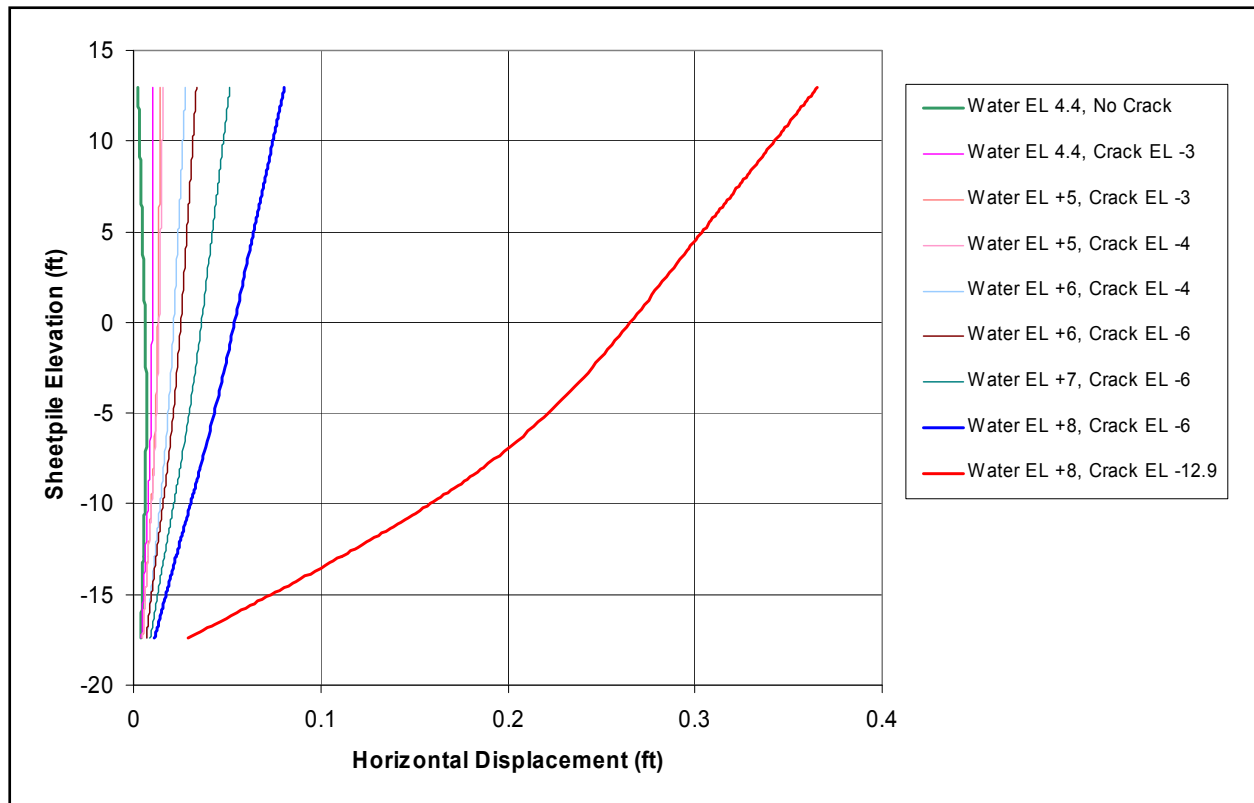


Figure 9-14. Horizontal Displacement of the Sheet Pile versus Canal Water El and Computed Using Stiff Modulus Values for the Levee Clay and Marsh on the Protected Side

Figure 9-15 shows the horizontal displacements of three points within the flood wall, relative to its position at a canal water elevation of 1.0 for average stiffness values. The points monitored through the analysis are at the top of the I-wall (El 13), at El 4.4 (top of Levee) and at the sheet pile tip (El -17.4). Recall for Canal water El 8, the crack never extends into the Beach sand layer, it terminates at the top of the Beach sand layer (i.e., El -12.9). Note that there is a significant increase in horizontal deformations of the I-wall/sheet pile wall when the crack extends to El -12.9 at Canal El 8. Results in this figure shows the Beach sand is providing enough lateral support to prevent the sheet pile tip from moving laterally, therefore the deformation of the sheet pile is mostly a rotation about the sheet pile tip for both sets of $E_{average}$ and E_{stiff} analyses. Maximum horizontal movement at the top of the I-wall is 0.36 ft (4 1/3 inches) for this analysis with Canal water El 8 and using E_{stiff} values. Contrast this result with the Figure 9-12 maximum displacement at the top of I-wall is 0.88 ft (10 1/2 inches) for Canal Water El 7 computed using average stiffness values. For each canal water elevation, the displacements in Figure 9-15 are less than half the Figure 9-12 displacements calculated for the first analysis set using average stiffness values.

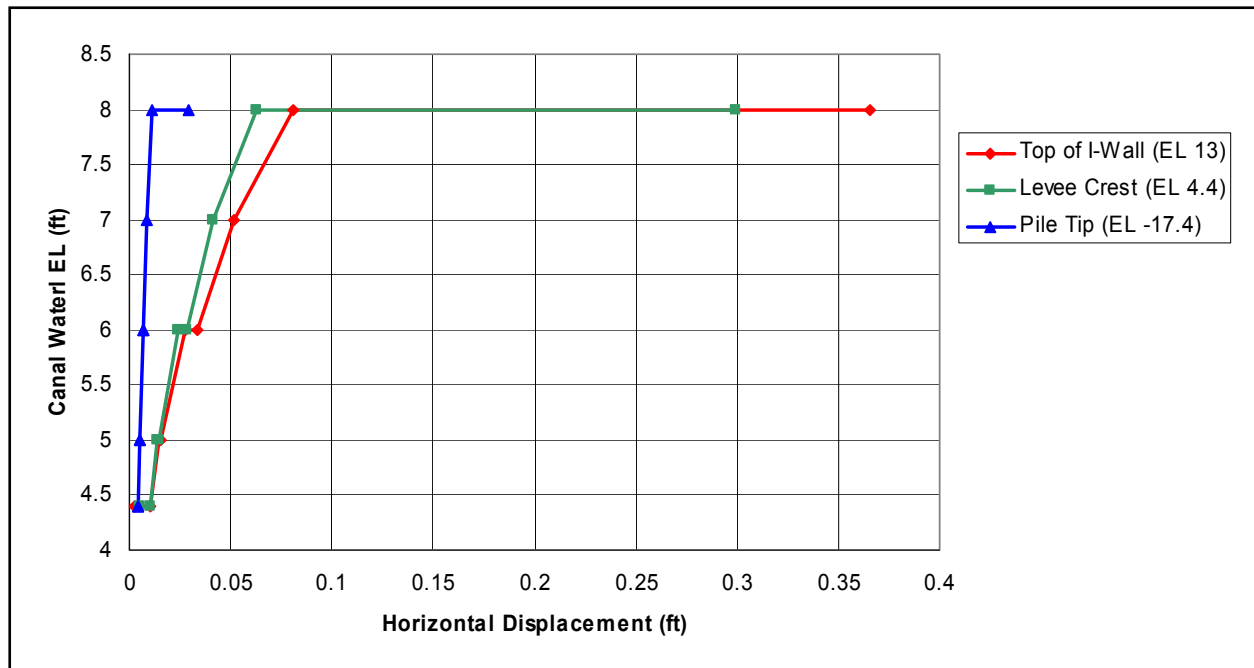


Figure 9-15. Horizontal Sheet Pile Deformations versus Canal Water El and Computed Using Stiff Modulus Values for the Levee Clay and Marsh on the Protected Side

Failure Mechanism: Figures 9-16 and 9-17 show that for the analysis using average stiffness values with Canal El 6 and Crack to El -12.9, there is a loss of effective vertical stress at the top of the Beach sand layer within the region beyond the toe of the Levee. This results in zero shear strength along the top of the Beach sand layer as demonstrated in the Figure 9-18 fraction of mobilized shear strength being equal to unity within this Beach sand region. Figure 9-19 shows that this, in turn, results in the beginning of the development of a mechanism as demonstrated by the concentration of large shear strains within this region for Canal water El 6 and crack to El -12.9. Figures 9-20 and 9-21 show the development of the ultimate mechanism (i.e., the failure mechanism) computed in a phi/c reduction analysis for Canal water El 6 and crack to El -12.9, with the computed Factor of Safety of 1.84. Note the vertical “bulging” in the Marsh beyond the toe of the Levee. The reaches of large shear strain shown in Figure 9-21 shows the complete failure wedge will form along the top of the Beach sand layer and “day light” beyond the toe of the Levee. All subsequent phi/c computations for higher canal water elevations and for the E_{stiff} analyses show this same Figures 9-20 and 9-21 failure mechanism to form.

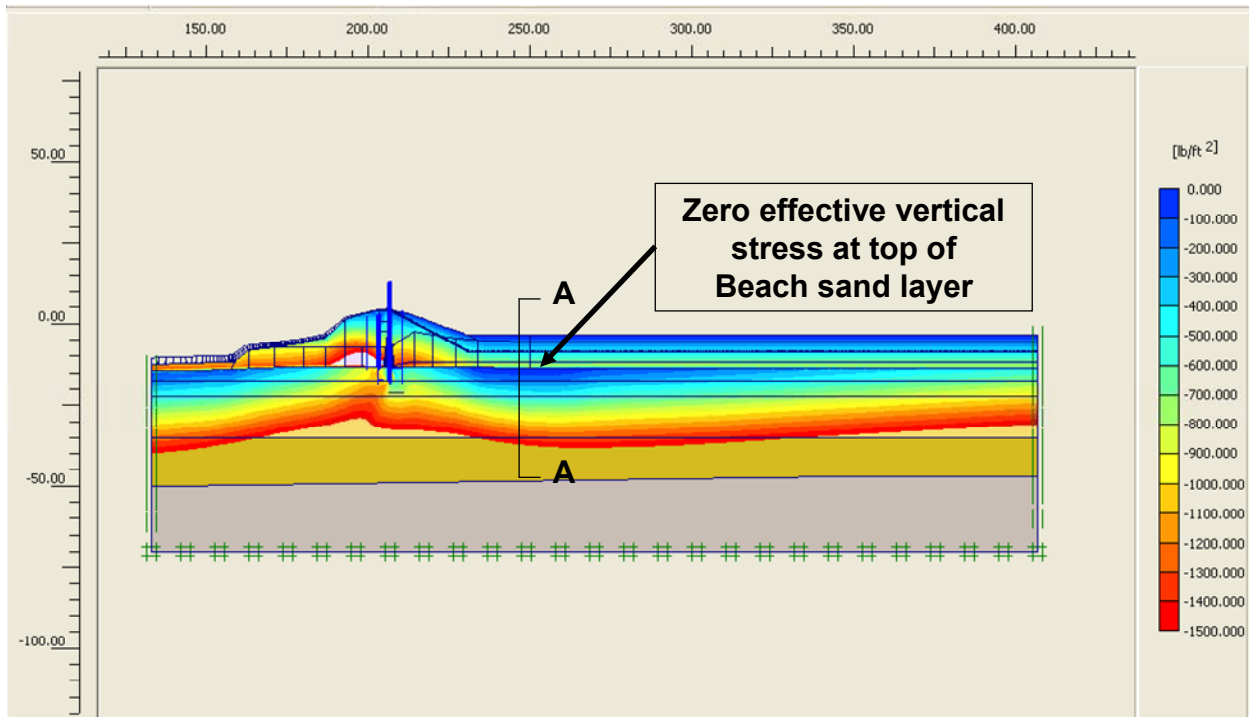


Figure 9-16. Shadings of Total Vertical Stress in the Levee Clay and Marsh and Effective Vertical Stress in the Beach Sand for the Analysis Using Average Stiffness Values with Canal EI 6 and Crack to EI -12.9

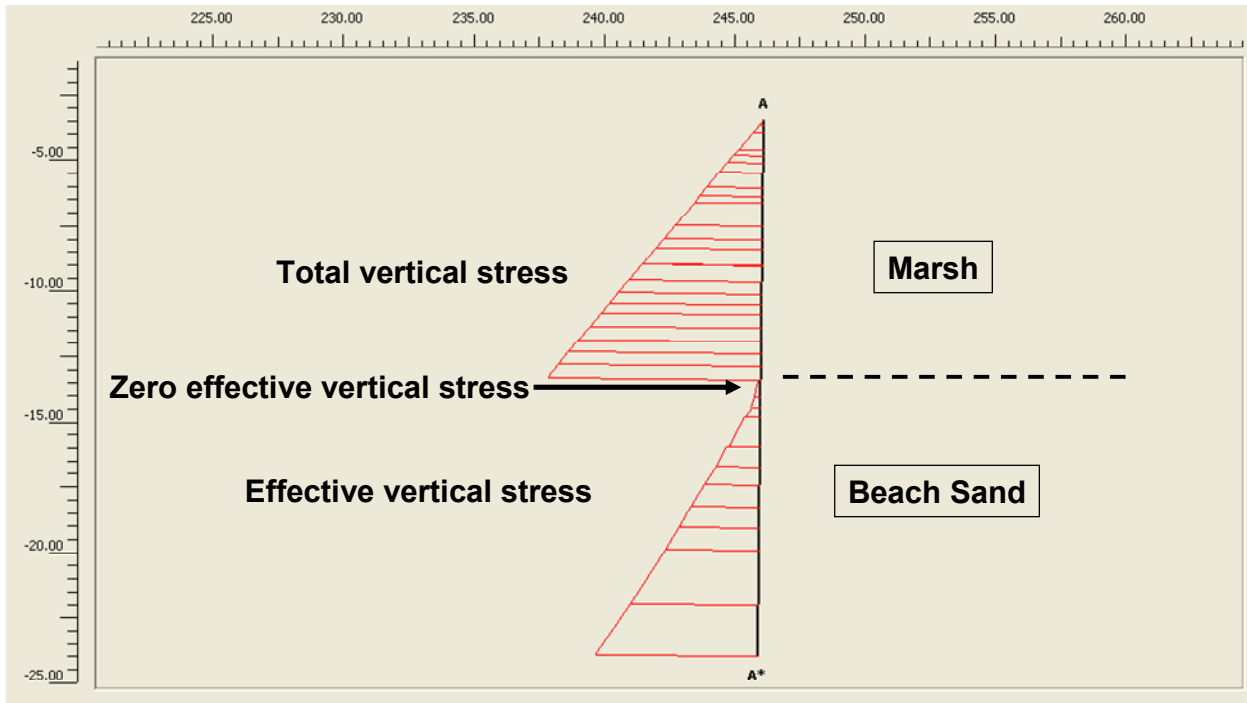


Figure 9-17. Vertical Section A-A Near the Toe of the Levee Showing Total Vertical Stress in the Marsh and Effective Vertical Stress in the Beach Sand for the Analysis Using Average Stiffness Values with Canal EI 6 and Crack to EI -12.9

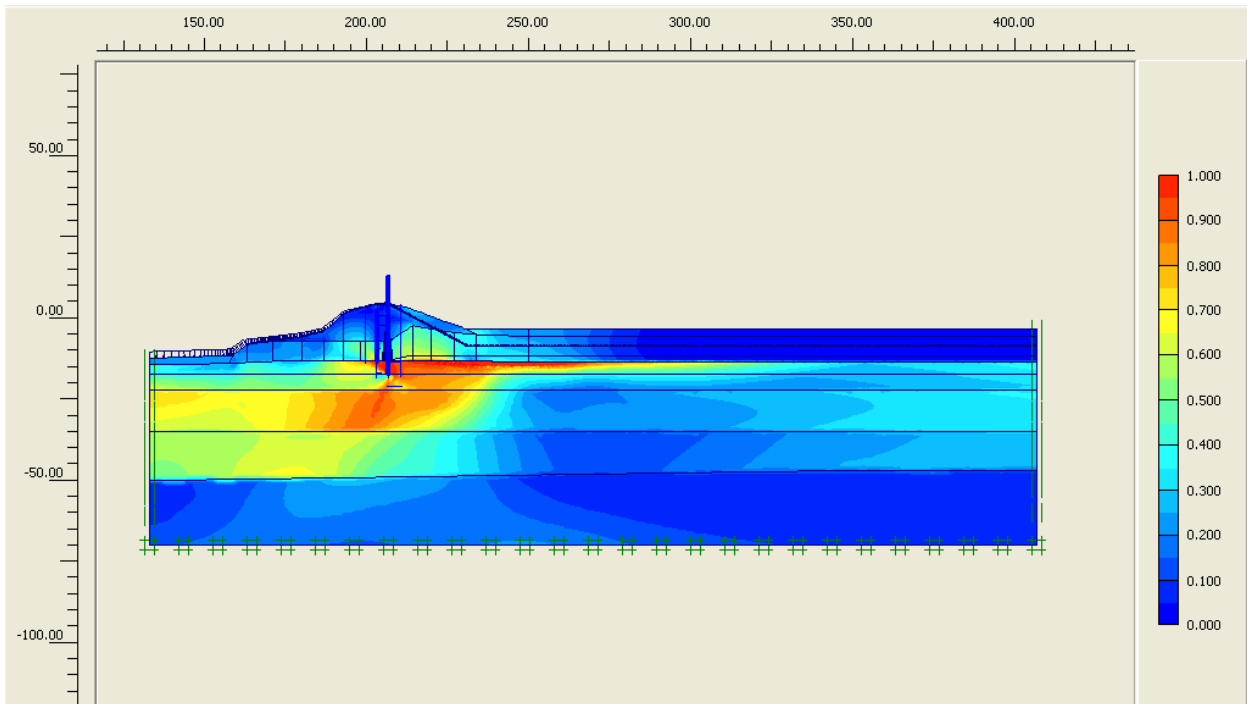


Figure 9-18. Fraction of Mobilized Shear Strength for the Analysis Using Average Stiffness Values with Canal EI 6 and Crack to EI -12.9

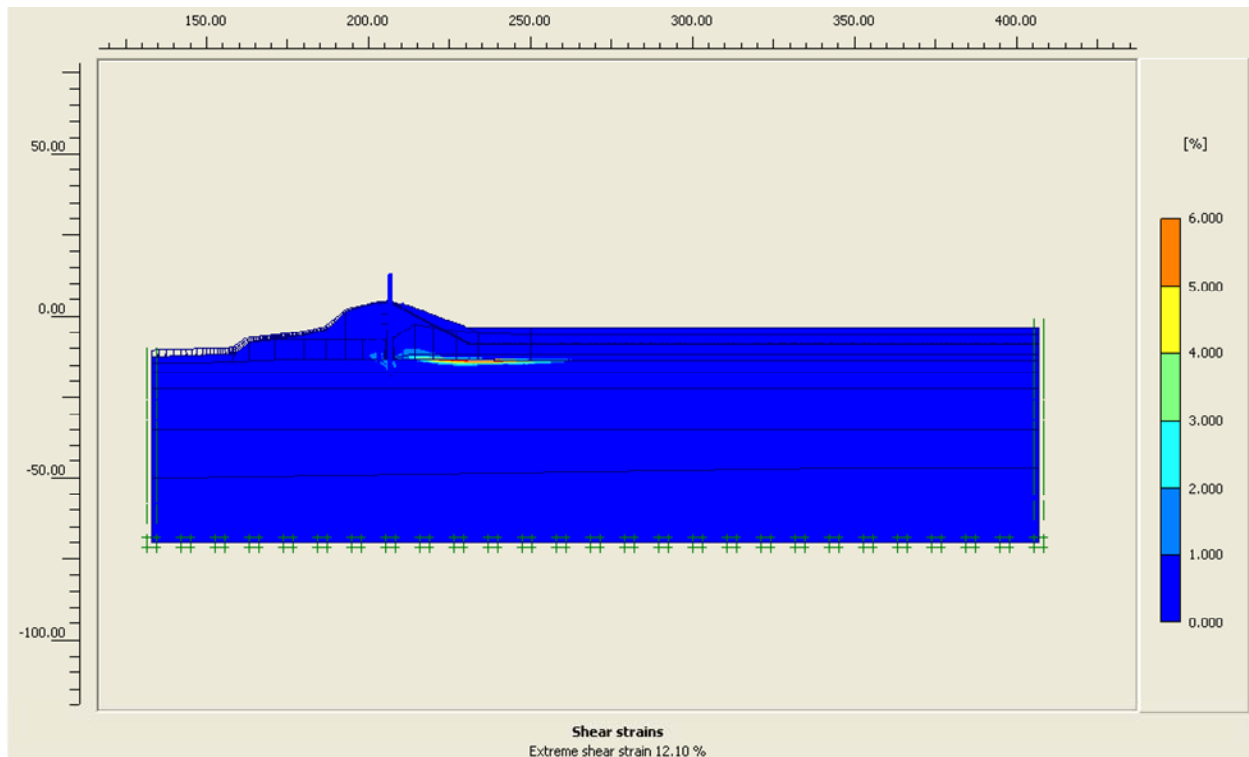


Figure 9-19. Reach of Large Shear Strains for the Analysis Using Average Stiffness Values with Canal EI 6 and Crack to EI -12.9

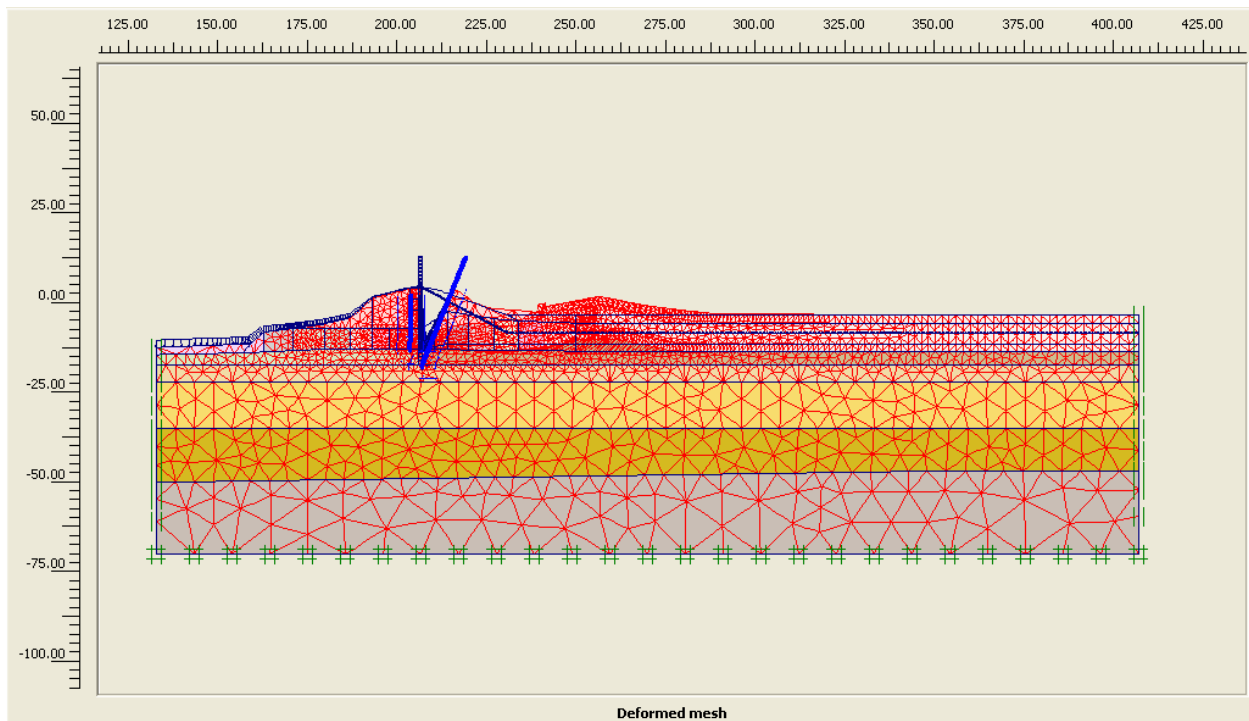


Figure 9-20. Ultimate Mechanism from Phi/C Reduction for the Analysis Using Average Stiffness Values with Canal EI 6 and Crack to EI -12.9

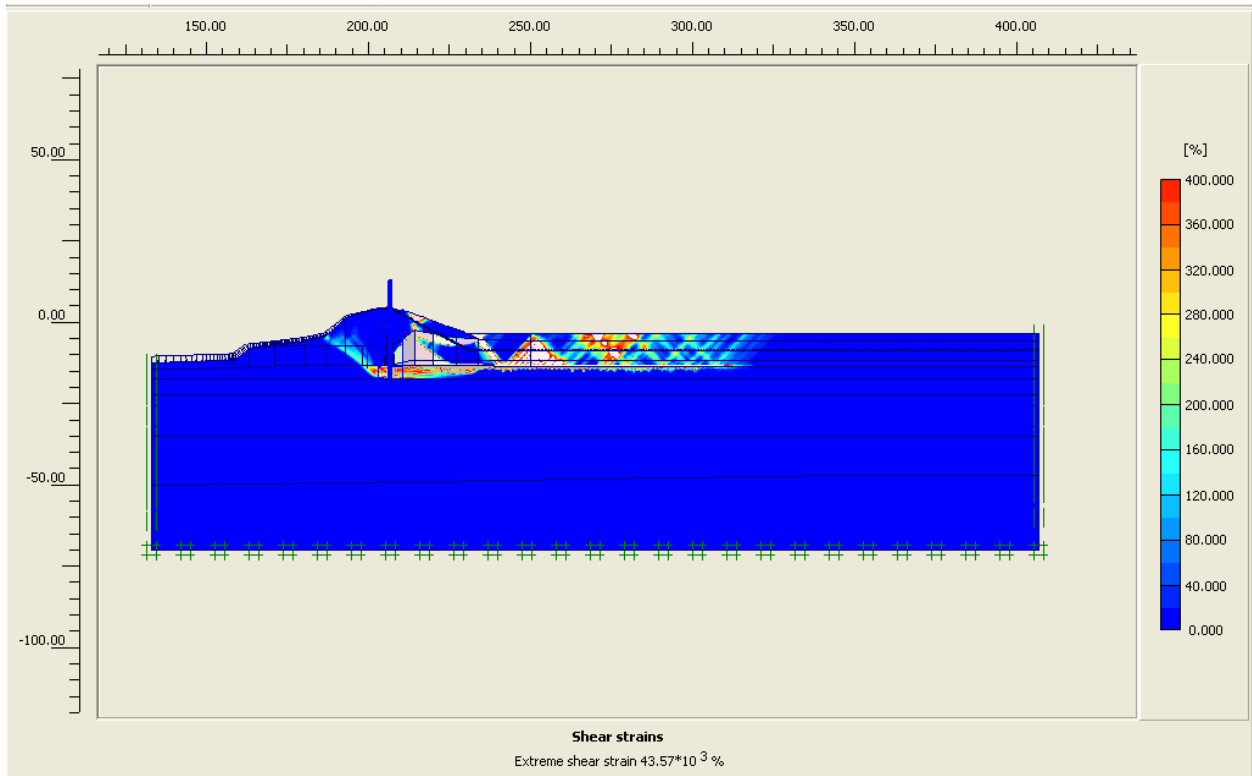


Figure 9-21. Reach of Large Shear Strains from the Phi/C Reduction Analysis Using Average Stiffness Values with Canal EI 6 and Crack to EI -12.9

Soil-Structure Interaction Analysis of the London Avenue Canal South Breach (East Flood Wall at London at Station 53+00)

Introduction

This section describes a complete soil-structure interaction (SSI) analysis of an existing flood wall within London Canal using the PC-based finite element program Plaxis (2004). A two-dimensional cross section within the section of the East side, at Station 53+00 of the London Canal that failed during hurricane Katrina is the subject of this evaluation. Results of a complete nonlinear finite element analysis of a two dimensional (2-D) cross section during simulated flood loading is described.

Plaxis is a complete nonlinear finite element package geared towards geotechnical engineering applications that include soil-structure interaction issues such as those that occur between a sheet pile and the soils in which it is embedded. It allows for the nonlinear response of soils to flood loading as occurred at the London canal with an I-wall along the center line of the soil-founded levee. The Plaxis PC-based software comprise a visual pre-processor, a nonlinear finite element engineering analysis module, and a visual post-processor. All software components are combined into a single package. Computed results include not only soil stresses, but also structural (e.g. sheet pile and I-wall) bending moments, interaction stresses between sheet piling and the soil in which it is embedded, as well as soil (e.g., levee) and structural deformations. A complete SSI analysis is considered to provide the most reasonable estimate for deformation response of a soil-structural system involving nonlinear material behavior. In a complete SSI analysis loads exerted by the canal water acting on the soils of the levee and then onto the sheet pile wall (below the I-wall) by means of a load transfer through the levee and foundation soils are generated automatically during the analysis (i.e., predetermined earth pressure force distributions between the soil and the embedded sheet pile are not specified).

Section Analyzed

The two-dimensional cross section within the failed section of the East side of the London Canal at Station 53+00 analyzed for flood loading is shown in Figure 9-22.² The 2-D section is 307-ft wide and extends from x-coordinate equal to -137 ft to the center line of the canal at x equal to 170 ft. The top of the I-wall is at El 13 and sheet pile tip is at EL -17.4. An older sheet pile is embedded in the levee on the canal side of the I-wall, approximately 3 feet in front of the I-wall (centerline-to-centerline). This old sheet pile used to be part of a shorter flood wall that was removed when the existing I-wall was installed. The old sheet piling extends from the ground surface to within the Beach sand layer, El -16.9.

The crest of the earthen levee on the protected (East) side of the I-wall is at El 3.6, with a crest width of approximately 4 feet. Note the I-wall extends above the crest of the soil founded levee. The protected side of the levee has a 1 on 3 and 1/3 side slope to El 1.1 with a 1 on 3 side slope to El -4.1. The protected side ground surface is assigned El -3.4 for this section. The crest

² All elevations cited are according to NAD88.

of the earthen levee on the canal side of the I-wall is also at El 3.6. There is a 2-ft wide crest on the canal side of the I-wall at El 3.6. The upper 2.6 feet of the levee on the canal side of the I-wall is above normal canal water elevation. From El 3.6 to EL 1.8, the levee face has a 1 on 5 side slope. Between El 1.8 and El -11.9 the face of the levee has an approximately 1 on 1-¾ side slope. From EL -6.4 to El -10.4 the peat is exposed to the canal water. The deepest point in the canal is at canal center line (i.e., x = 170 ft in Figure 9-22), with a top of Canal bottom silt at El -11.9 at this location.

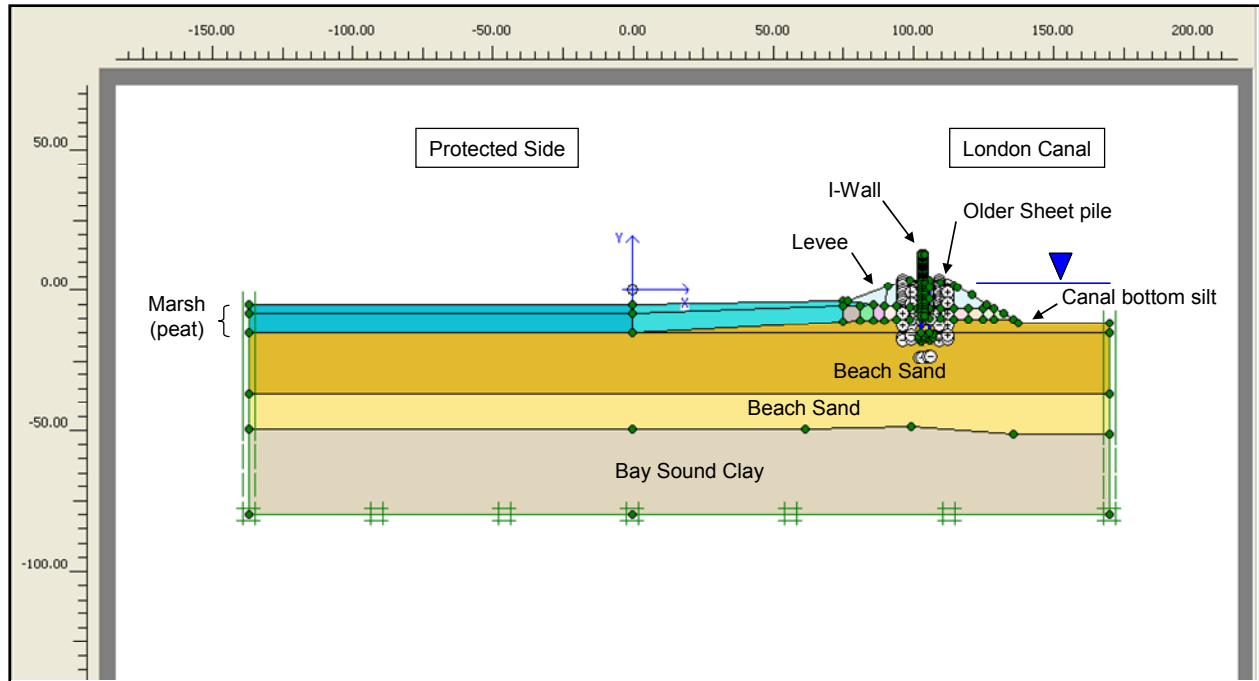


Figure 9-22. Two-Dimensional Cross Section Model used in the Complete SSI Analysis of Station 53+00 at London Canal – East Side

Proceeding from top to bottom in Figure 9-22, this cross section contains layers of Levee fill (clay), marsh (also referred to as peat), Beach sand, and Bay Sound clay. There is no Lacustrine clay contained within this cross section. The top of I-wall is at El 13 and the base of the Figure 9-22 cross-section is assigned to El -80. El -80 corresponds (approximately) to the bottom of the Bay Sound clay at Station 53+00. The soil layering is consistent with that used in the slope stability evaluations made for this cross section. The regions of uniform color in Figure 9-22 reflect the Plaxis “soil clusters” used to define the mesh and to assign soil regions with common properties.

Finite Element Mesh

Key Plaxis modeling features used in the plane strain analysis of London include the use of 15-node triangular elements to model the soil, plates (i.e., special beam elements) to model the bending of the newer I-wall/sheet pile wall as well as the older sheet pile wall, and interface elements to model soil-structure interaction between the sheet pile wall and the adjacent soil elements. A total of 31,272 nodes and 3,378 elements, containing 45,336 stress points, are used

to define the Figure 9-23 mesh. Details regarding the quantity of each of the three types of plane strain elements used in the finite element model as well as select characteristics of each type of element are summarized in Table 9-7.

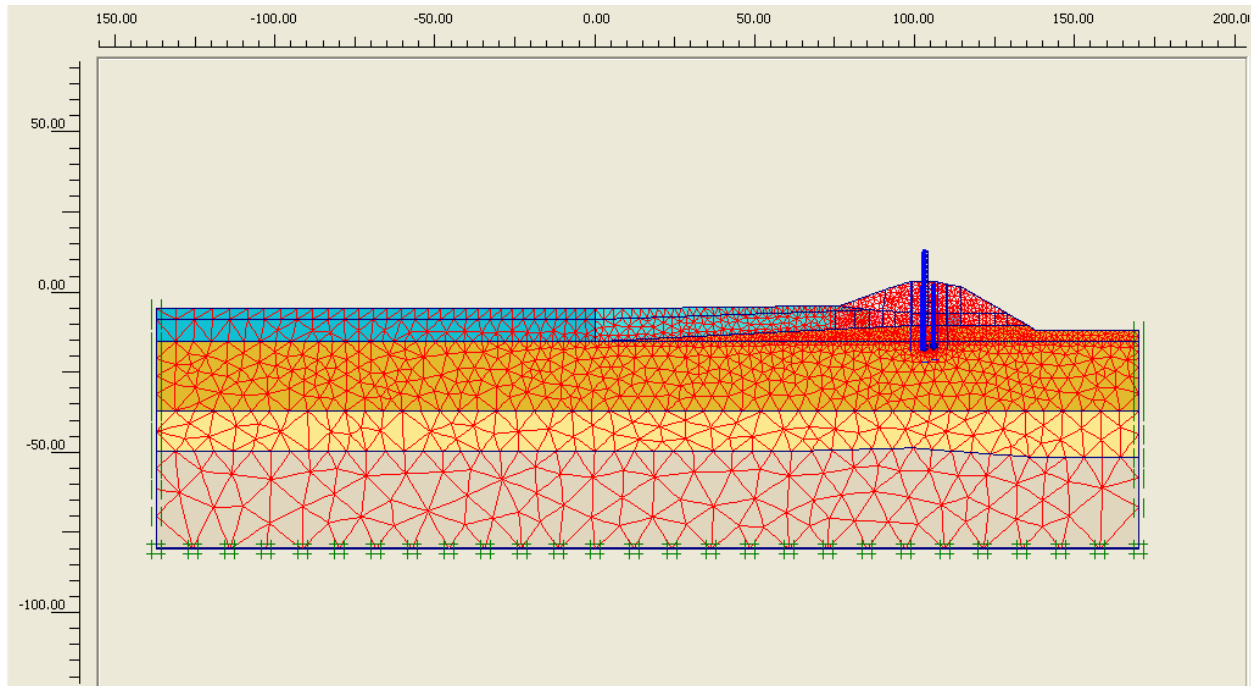


Figure 9-23. Finite Element Mesh used in the Complete SSI Analysis of Station 53+00 at London Canal – East Side

Table 9-7 Mesh Data Summary of Elements Used			
Type	Type of element	Type of integration	Total no.
Soil	15-Noded	12-point Gauss	3778
Plate	5-node line	4-point Gauss	75
Interface	5-node line	4-point Newton-Cotes	148

A zero horizontal displacement is specified along the left and right hand side vertical boundaries of the Figure 9-23 finite element mesh. However, these nodes are free to displace in the vertical direction. Along the bottom boundary of the mesh zero horizontal and vertical displacements are specified at these nodes.

Material Properties for the Soils and Flood Wall in the Complete Soil-Structure Interaction Analysis

The soil material properties used in this complete SSI analysis are the same as those used in the slope stability analyses of this cross section. Figure 9-23 shows the 41 soil clusters used to define the regions of common soil properties for the four primary categories of soil within the

mesh (i.e., the Levee clay, Marsh (or peat), Beach sand, and Bay Sound clay). Note that each soil layer comprises many clusters, each of which is designated by a different color. Spatially varying soil properties are assigned in the slope stability analyses. Accordingly, multiple soil clusters are used in the nonlinear finite element mesh to assign material properties within each soil layer to accommodate the spatially varying (i.e., vertically as well as horizontally) soil properties. Table 9-8 summarizes the engineering material properties and the corresponding to average stiffness values in the complete SSI analysis. Note that a range in engineering soil properties is reported for the Marsh layer. Table 9-9 summarizes the engineering material properties for the complete SSI analysis with increased values for soil stiffness of the Levee clay and the Marsh. This second set of soil stiffness values are used to assess the sensitivity in computed results to the stiffness of the protected side Levee clay and Marsh (i.e., peat).

Table 9-8 Material Characterization for Soils of Average Stiffness										
Soil type	Range in Elevation, NAD88	Total unit weight (pcf)	Constant S_u value in soil cluster (psf)	ϕ' (deg)	Young's Modulus - Average			m	$R_{interface}$	Hydraulic Conductivity (ft/hr)
					E^{ref}/S_u	E^{ref} (psf)	$(E^{ref})_{ur}/E^{ref}$			
Levee clay - canal side	-	109	900	-	24	-	5	0.5	0.8	1.2E-04
Levee clay - protected side	-	109	900	-	48	-	5	0.5	0.8	1.2E-04
Marsh (peat)	-	80	300 to 400	-	48	-	3	0.5	0.8	1.2E-04 to 1.2E-02
Beach Sand	-10 to -15.5	120	-	40	-	1,260,000	3	0.5	-	1.8
	-15.5 to -37	120	-	40	-	1,260,000	3	0.5	-	
	-37 to -50	120	-	36	-	647,000	3	0.5	-	
Bay Sound clay	-	102	779	-	68	-	3	1.0	-	1.2E-04

Note: $(E^{ref})_{50} = (E^{ref})_{oed} = E^{ref}$; $\psi = 0$ deg; $p_{ref} = 2116$ psf; $v_{ur} = 0.3$; $R_f = 0.9$

**Table 9-9
Material Characterization for Soils of With Increased Stiffness**

Soil type	Range in Elevation, NAD88	Total unit weight (pcf)	Constant S_u value in soil cluster (psf)	ϕ' (deg)	Young's Modulus - Stiff					Hydraulic Conductivity (ft/hr)
					E^{ref}/S_u	E^{ref} (psf)	$(E^{ref})_{ur}/E^{ref}$	m	$R_{interface}$	
Levee clay - canal side	-	109	900	-	48	-	5	0.5	0.8	1.2E-04
Levee clay - protected side	-	109	900	-	240	-	3	0.5	0.8	1.2E-04
Marsh (peat) - canal side	-	80	300 to 400	-	48	-	3	0.5	0.8	1.2E-04 to 1.2E-02
Marsh (peat) - protected side	-	80	300 to 400	-	240	-	3	0.5	0.8	1.2E-04 to 1.2E-02
Beach Sand	-10 to -15.5	120	-	40	-	1,260,000	3	0.5	-	1.8
	-15.5 to -37	120	-	40	-	1,260,000	3	0.5	-	
	-37 to -50	120	-	36	-	647,000	3	0.5	-	
Bay Sound clay	-	102	779	-	68	-	3	1.0	-	1.2E-04

Note: $(E^{ref})_{50} = (E^{ref})_{oed} = E^{ref}$, $\psi = 0$ deg; $p_{ref} = 2116$ psf; $v_{ur} = 0.3$; $R_f = 0.9$

Levee clay: A total unit weight of 109 pcf is assigned to the Levee clay soil clusters. A smaller data base of strength and stiffness tests results are available for London Canal Levee clay, as compared with 17th Street canal Levee clay. After a careful assessment of the test data on the Levee clay at London canal, an undrained shear strength (S_u) value of 900 psf is assigned. This is the same value for S_u that is assigned at 17th Street.

Stress-strain data for 17th Street canal Levee clay triaxial test specimens leads to the assignment of an average value for Young's modulus, E^{ref} , expressed in terms of $(E^{ref})_{50}$ normalized by S_u and equal to 48 (Table 9-8) on the protected side of the I-wall. This same value for Young's modulus is assigned to the London canal Levee clay. On the canal side of the I-wall, $(E^{ref})_{50}$ normalized by S_u is set equal to 24. During the course of the complete SSI analysis of Station 53+00, an evaluation of the sensitivity in computed results to the value of Levee and Marsh stiffness is conducted. In this parametric study the protected side Levee clay E^{ref} is increased by a factor of five. It is expressed in Table 9-9 in terms of $(E^{ref})_{50}$ normalized by S_u and is set equal to 240 (i.e., = 5 times 48).

For the Plaxis nonlinear Hardening Soil (HS) model, the parameters $(E^{ref})_{50}$ and $(E^{ref})_{oed}$ are set equal to $[E^{ref}/S_u \text{ times } S_u]$. Additional HS parameters assigned are reference stress for stiffness, p_{ref} , equal to 2,116 psf, failure ratio $R_f = 0.9$, the exponent $m = 0.5$ and v_{ur} equals 0.3. For unload reload HS parameters, $(E^{ref})_{ur}$ is set equal to 5 times $(E^{ref})_{50}$ in the average modulus complete SSI analysis and set equal to 3 times $(E^{ref})_{50}$ in the sensitivity analysis using stiff clay properties. For Casteel CZ101 cold formed steel sheet piles to levee clay, the interface strength

parameter $R_{\text{interface}}$ is set equal to 0.8 for Levee clay-to-steel interfaces (by the Potyondy, 1961, data).

Marsh (or peat): A smaller data base of strength and stiffness tests results are available for London Canal Marsh (or peat), as compared with 17th Street canal peat (or marsh). After a careful assessment of the test data on the Marsh at London canal, a range in values of undrained shear strength (S_u) of 300 psf to 400 psf is assigned. This is the same range in S_u values as is assigned for the 17th Street canal peat, which factored into the strength assessment made for this cross section. Below the I-wall and in the region of the greatest overburden, a value of S_u equal to 400 psf is assigned. With no overburden, the value for S_u is set equal to 300 psf in the Marsh. A shear strength value is assigned to each Marsh cluster based on the magnitude of the overburden for the center position of each Marsh cluster below the levee. There is no vertical variation in undrained shear strength for the Marsh layer. A total unit weight of 80 pcf is assigned to the Marsh soil clusters. Stress-strain data for 17th Street canal peat triaxial test specimens leads to the assignment of an average value for Young's modulus, E^{ref} , expressed in terms of (E^{ref}) normalized by S_u and set equal to 48 (Table 9-8). This same value for Young's modulus is assigned to the London Station 14+00 and the 17th Street canal Marsh. In the evaluation of the sensitivity in computed results to stiffness, the protected side Marsh E^{ref} is increased by a factor of five. It is expressed in Table 9-9 in terms of (E^{ref}) normalized by S_u and set equal to 240 (i.e., = 5 times 48).

For the Plaxis nonlinear Hardening Soil (HS) model the parameters $(E^{\text{ref}})_{50}$ and $(E^{\text{ref}})_{\text{oed}}$ are set equal to $[E^{\text{ref}}/S_u \text{ times } S_u]$. Additional HS parameters assigned are reference stress for stiffness, p_{ref} , equal to 2,116 psf, failure ratio $R_f = 0.9$ and the exponent $m = 0.5$. For unload reload HS parameters, $(E^{\text{ref}})_{\text{ur}}$ is set equal to 3 times $(E^{\text{ref}})_{50}$ and v_{ur} equals 0.3. For Casteel CZ101 cold formed steel sheet piles to Marsh interface, $R_{\text{interface}}$ is set equal to 0.8.

Beach Sand: The results from the field investigation indicate that the Beach sand is made up of three distinct layers based on the in-situ density of the sand. The upper layer of Beach sand extends from approximately El -10 to -15.5 and is a very dense sand. The middle layer extends from El -15.5 to -37 and is a very dense sand. The lower layer extends from El -37 to -50 and is a medium sand. Proceeding from the top layer down, a total unit weight of 120 pcf is assigned to each of the three layers of Beach Sand soil clusters.

Standard Penetration Test and cone test results in the upper Beach sand layer (i.e., El -10 to -15.5) indicate an average value of 46 blows per ft depth for 60 percent of free-fall energy and corrected to an effective overburden pressure of 1 ton/ft² [i.e., $(N_1)_{60} = 46$]. For a fine sand with an average value of $(N_1)_{60} = 46$, the relative density (D_r) is 87 percent by Skempton's (1986) correlation. A $(N_1)_{60} = 46$ results in a value of 40 deg for the effective angle of internal friction by the Peck, Hanson and Thornburn (1974) correlation. For very dense sand with D_r equal to 87 percent and using the correlations of Lengkeek and Vermeer and Shanz (cited in Brinkgreve, 2005, as well as in Plaxis course notes, 2006), the value of Young's modulus E^{ref} is set equal to 1,260,000 psf. For the Plaxis nonlinear Hardening Soil (HS) model, the parameters $(E^{\text{ref}})_{50}$ and $(E^{\text{ref}})_{\text{oed}}$ are set equal to 1,260,000 psf. Additional HS parameters assigned are reference stress for stiffness, p_{ref} , equal to 2,116 psf, failure ratio $R_f = 0.9$ and the exponent $m = 0.5$. For unload reload HS parameters, $(E^{\text{ref}})_{\text{ur}}$ is set equal to 3 times $(E^{\text{ref}})_{50}$ and v_{ur} equals 0.3. For Casteel

CZ101 cold formed sheet piles to Beach sand, the interface strength parameter $R_{\text{interface}}$ is set equal to 0.8.

Standard Penetration Test and cone test results in the middle Beach sand layer (i.e., El -15.5 to -37) indicate an average value of 60 blows per ft depth for 60 percent of free-fall energy and corrected to an effective overburden pressure of 1 ton/ft² [i.e., $(N_1)_{60} = 60$]. For a fine sand with an average value of $(N_1)_{60} = 60$, the relative density (D_r) is 99 percent by Skempton's (1986) correlation. A $(N_1)_{60} = 60$ results in a value of 40 deg (approximately) for the effective angle of internal friction by the Peck, Hanson and Thornburn (1974) correlation. For very dense sand with D_r equal to 99 percent and using the correlations of Lengkeek and Vermeer and Shanz (cited in Brinkgreve, 2005, as well as in Plaxis course notes, 2006), the value of Young's modulus E^{ref} is set equal to 1,260,000 psf. For the Plaxis nonlinear Hardening Soil (HS) model, the parameters $(E^{\text{ref}})_{50}$ and $(E^{\text{ref}})_{\text{oad}}$ are set equal to 1,260,000 psf. Additional HS parameters assigned are reference stress for stiffness, p_{ref} , equal to 2,116 psf, failure ratio $R_f = 0.9$ and the exponent $m = 0.5$. For unload reload HS parameters, $(E^{\text{ref}})_{\text{ur}}$ is set equal to 3 times $(E^{\text{ref}})_{50}$ and ν_{ur} equals 0.3.

Standard Penetration Test and cone test results in the lower Beach sand layer (i.e., El -37 to -50) indicate an average value of 28 blows per ft depth for 60 percent of free-fall energy and corrected to an effective overburden pressure of 1 ton/ft² [i.e., $(N_1)_{60} = 28$]. For a fine sand with an average value of $(N_1)_{60} = 28$, the relative density (D_r) is 66 percent by Skempton's (1986) correlation. A $(N_1)_{60} = 28$ results in a value of 36 deg (approximately) for the effective angle of internal friction by the Peck, Hanson and Thornburn (1974) correlation. For medium sand with D_r equal to 66 percent and using the correlations of Lengkeek and Vermeer and Shanz (cited in Brinkgreve, 2005, as well as in Plaxis course notes, 2006), the value of Young's modulus E^{ref} is set equal to 647,000 psf. For the Plaxis nonlinear Hardening Soil (HS) model, the parameters $(E^{\text{ref}})_{50}$ and $(E^{\text{ref}})_{\text{oad}}$ are set equal to 647,000 psf. Additional HS parameters assigned are reference stress for stiffness, p_{ref} , equal to 2,116 psf, failure ratio $R_f = 0.9$ and the exponent $m = 0.5$. For unload reload HS parameters, $(E^{\text{ref}})_{\text{ur}}$ is set equal to 3 times $(E^{\text{ref}})_{50}$ and ν_{ur} equals 0.3.

Bay Sound clay: A smaller data base of strength and stiffness tests results are available for London Canal Bay Sound clay, as compared with 17th Street canal Bay Sound clay. After a careful assessment of the test data on the Bay Sound clay at London canal, a value of undrained shear strength (S_u) of 779 psf is assigned. This is the same S_u value assigned for the 17th Street canal Bay Sound clay, which factored into the strength assessment made for this cross section. A total unit weight of 102 pcf is assigned to the Bay Sound clay soil cluster. Stress-strain data for 17th Street canal Bay Sound clay triaxial test specimens leads to the assignment of an average value for Young's modulus, E^{ref} , expressed in terms of (E^{ref}) normalized by S_u and set equal to 68 (Tables 9-8 and 9-9). This same value for Young's modulus is assigned to the London canal Bay Sound clay.

For the Plaxis nonlinear Hardening Soil (HS) model, the parameters $(E^{\text{ref}})_{50}$ and $(E^{\text{ref}})_{\text{oad}}$ are set equal to $[E^{\text{ref}}/S_u \text{ times } S_u]$. Additional HS parameters assigned are reference stress for stiffness, p_{ref} , equal to 2,116 psf, failure ratio $R_f = 0.9$ and the exponent $m = 1.0$. For unload reload HS parameters, $(E^{\text{ref}})_{\text{ur}}$ is set equal to 3 times $(E^{\text{ref}})_{50}$ and ν_{ur} equals 0.3.

Hydraulic Conductivity: Values for the hydraulic conductivity of the four soil types are listed in Tables 9-8 and 9-9. The hydraulic conductivity value assigned to the Beach sand is based on field pump tests while all other values are based on typical values found in the technical literature for soils of similar engineering material characteristics. For the Marsh material, data from Weber (1969) and others leads to the assignment of hydraulic conductivity values of 1.2×10^{-2} ft/hr for regions of lower overburden pressure and 1.2×10^{-4} ft/hr for regions of higher overburden, such as below the Levee. For canal bottom silts, a hydraulic conductivity value equal to 1.2×10^{-2} ft/hr is assigned.

Flood Wall: The flood wall comprises an exposed reinforced concrete I-wall, a reinforced concrete cap and Casteel CZ101 cold formed sheet pile. The 12-inch thick reinforced concrete I-wall extends from the top of protected levee (El 3.6) to El 13. At Station 53+00, the sheet pile tip is at El -17.4. The top of the Beach sand to Marsh interface is at El -10.2. Consequently, the sheet pile extends 7.2 ft into the Beach sand. The upper reach of pile is encased in a two-foot thick reinforced concrete cap extending below the surface of the protected side of the levee. Linear elastic material response was assumed in the complete SSI analysis. Engineering properties for the I-wall, cap and sheet pile are summarized in Table 9-10 for the zero thickness plate elements used in the finite element model.

Table 9-10 Material Characterization for the Flood Wall				
Identification	EA	EI	weight	v
	[lb/ft]	[lbft²/ft]	[lb/ft/ft]	[-]
Reinforced Concrete I-wall	4.32E8	3.6E7	150.00	0.20
Reinforced Concrete Cap	8.64E8	2.88E8	80.00	0.20
Sheet Pile (Hoesch 12)	9.77E7	1.31E7	8.94	0.30

Complete Soil-Structure Interaction Analysis

Introduction: Two sets of complete SSI analyses of the Figure 9-22 2-D cross section of Station 53+00 at London Canal are conducted in staged analysis using Plaxis. Both sets evaluate the response of the Station 53+00 cross-section to flood loading starting at canal water El 1.0 on through a series of incremental 0.5 to 2.6 feet raises in canal elevation. Table 9-11 summarizes the calculation phases of the second analysis set with stiff modulus values assigned to the Levee clay and the Marsh on the protected side of the I-wall. More than 13 phases of calculations are used in this parametric SSI analysis to a maximum canal water El 8. A similar set of analyses are conducted with average modulus values assigned to the four layers of soils. However, the discussion will focus on the results from the analysis set with stiff modulus values assigned to the Levee clay and the Marsh on the protected side of the I-wall.

Table 9-11 Calculation Phases of the Nonlinear Finite Element Analysis Using Stiff Modulus Values for the Levee Clay and the Marsh on the Protected Side			
Phase	PhaseNo.	Calculation type	Load input
Initial phase	0	-	-
Place Wall & Interface	1	Plastic analysis	Staged construction
Gravity (1.0)	2	Plastic analysis	Total multipliers
Water Table El +1	3	Plastic analysis	Staged construction
Canal Water El +3.6	4	Plastic analysis	Staged construction
Canal Water El +5,	5	Plastic analysis	Staged construction
Canal Water El +5, Crack to El -10.2, linear phreatic surface	6	Plastic analysis	Staged construction
Canal Water El +5.5, Crack to El -10.2, linear phreatic surface	7	Plastic analysis	Staged construction
Canal Water El +6, Crack to El -10.2, linear phreatic surface	8	Plastic analysis	Staged construction
Canal Water El +6.5, Crack to El -10.2, linear phreatic surface	9	Plastic analysis	Staged construction
Canal Water El +7, Crack to El -10.2, linear phreatic surface	10	Plastic analysis	Staged construction
Canal Water El +7.5, Crack to El -10.2, linear phreatic surface	11	Plastic analysis	Staged construction
Canal Water El +8, Crack to El -10.2, linear phreatic surface	12	Plastic analysis	Staged construction
Phi-C Reductions	13 ⁺	Phi/c reduction	Incremental multipliers

Loading phases 0 through 3 are used in both sets of complete SSI analyses to establish the initial total stress state condition existing prior to flooding. Loading phase 3 concludes with canal water at El 1, a steady state water elevation in the canal.

Loading phases 4 through 12 (Table 9-11) are used in the analysis set with stiff modulus values assigned to the Levee clay and the Marsh on the protected side of the I-wall for the four soil types to perform an incremental raise in the canal water to El 8, modeling the flood loading of the levee/I-wall system and the introduction of a crack along the canal-side face of the sheet pile in the Levee clay and in the Marsh/peat (eventually to the top of the Beach sand at El -10.2). The last of the loading phases (i.e., 13⁺) are used to compute the reserve capacity of the levee/I-wall system for different canal water elevations. This reserve capacity is expressed in terms of a Factor of Safety and is computed in a series of Plaxis phi/c reduction loading phases. A similar set of calculation phases (not listed) are conducted with the Table 9-8 average modulus values assigned to the four layers of soils.

Initial steady state condition for canal water at EL 1: Loading phases 0 through 3 are used in the complete SSI analysis to establish the initial total stress state within the finite element mesh with a steady state canal water elevation at El 1. Gravity loading is applied in a single increment, followed by a rising of the water table. In the Beach sand layer, the water table is

established at El -8.4 on the left-hand, protected side of the mesh, at x-coordinate -137, by analysis phase 3 and is maintained at this elevation in all subsequent computation phases. Load input for gravity loading is specified in Plaxis by means of the total multiplier method and changes in water table are accomplished by staged construction and by steady state seepage analysis, unless stated otherwise.

The initial steady-state, total stress condition for the usual canal water elevation of 1 is established by using the average stiffness modulus values given in Table 9-8 in the Mohr-Coulomb soil model for loading phases 0 through 3 for both sets of complete SSI analyses. The results from the IPET Task 7 slope stability analyses for this usual canal elevation indicate a stable cross-section with an ample Factor of Safety, i.e., above 1.5. Consequently, an important aspect of the total stress regime achieved within the Figure 9-23 finite element mesh is that the mobilized shear stress at the strain integration points within the finite elements contained in the soil clusters shown in this figure be less than the shear strength of the soil. The resulting computed fraction of mobilized shear strength (referred to as relative shear stress in Plaxis output) from the resulting initial total stress condition is shown in Figure 9-24. The fraction of mobilized shear strength is less than or equal to 0.9 at the stress integration points for the four soil types.

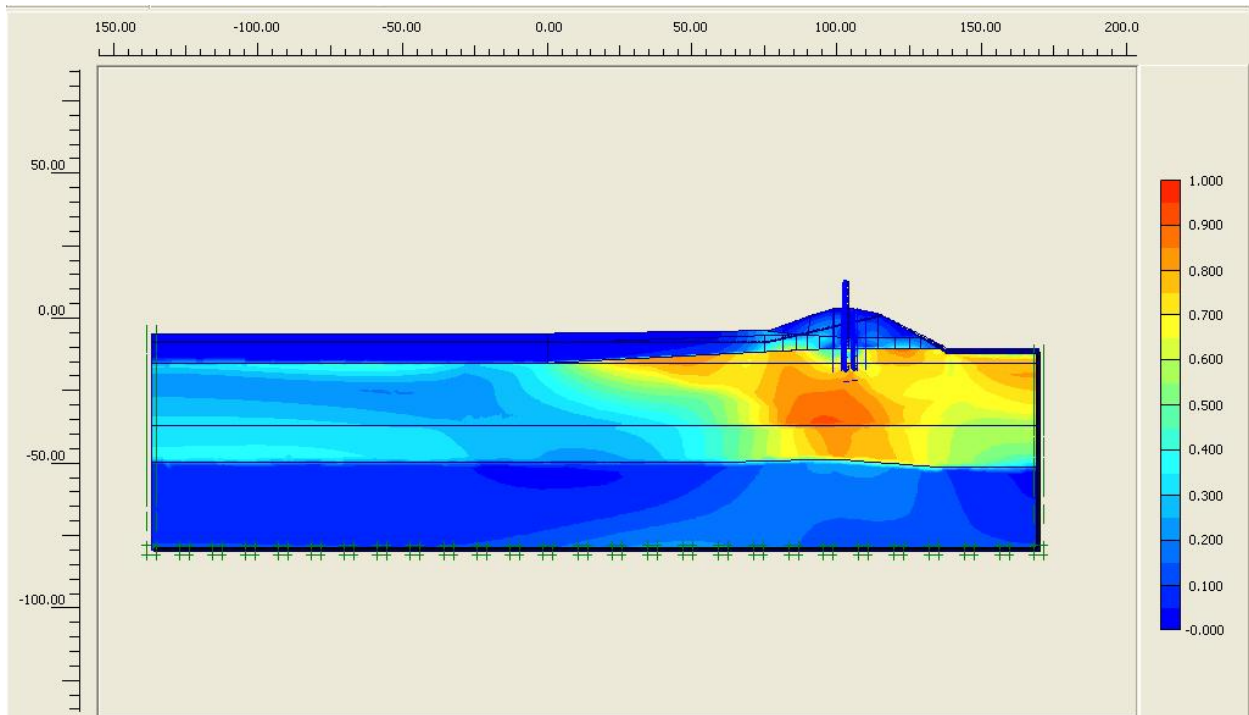


Figure 9-24. Fraction of Mobilized Shear Strength for Canal El 1

Flood loading: Modeling of flood loading commenced in the complete SSI analysis after the total initial stress state is established within the finite element mesh for steady state canal elevation (i.e., El 1). The hardening soil model with the Table 9-9 increased values for soil stiffness of the Levee clay and the Marsh are used in the analyses discussed in this section. Loading phases 4 through 12 (refer to Table 9-11) are used in the complete SSI analysis to

perform an incremental raise in the canal water to El 8, modeling the flood loading of the levee/I-wall system. Load input for changes in canal water elevation is specified by staged construction. For canal water up to and including El 5 and for crack depths terminating above the top of the Beach sand layer (at El -10.2) on the canal side of the new sheet pile wall/I-wall, a steady state seepage analysis is used to establish the pore water pressure regime within the Beach sand layer for loading phases 4 and 5 (Table 9-11).

The results from the SSI analysis set using the Table 9-9 increased values for soil stiffness of the Levee clay and the Marsh indicates that cracking commenced when Canal water reached El 5. Crack initiation occurs at the top of the Levee clay, on the canal side (at El 3.6) of the sheet pile wall when the total horizontal stress in the clay is less than the value for hydrostatic water pressure (i.e., γ_{water} times depth below canal water surface). This first occurs at Table 9-11 loading phase 5. Comparisons of values for hydrostatic water pressure, generated by hand computation, with the total horizontal stresses computed in the complete SSI analysis indicates a crack will extend from El 3.6 down to the top of the Beach sand layer (i.e., EL -10.2) in the Levee clay and Marsh in a single loading phase, phase no. 6. Subsequent analyses using Table 9-9 E_{stiff} values are conducted for Canal water El's 5.5, 6, 6.5, 7, 7.5 and 8 using a crack to EL -10.2 and a linear phreatic surface within the Beach sand.

Results (not shown) from the complete SSI analysis set for the Table 9-8 E_{average} analysis set indicates cracking will initiate at Canal water EL 4.5. Additionally, cracking will extend to the top of the Beach sand at this canal EL. Consequently, there is a 0.5 ft difference in Canal water elevation at which crack initiation occurs that can be directly attributed to the range in Tables 9-8 and 9-9 stiffness values.

Due to numerical convergence issues, a linear phreatic surface assumption is used to establish the pore water pressures within the Beach sand for loading phases 6 through 12 (Table 9-11) of the first complete set of SSI analysis in which depth of cracking extends to the top of Beach sand layer (EL -10.2). This results in a less severe uplift pressure regime within the Beach sand below the toe of the protected side of the Levee as discussed in the section describing the complete SSI analyses of London Canal Station 14+00. This results in a lower computed value for the Factor of Safety for the loading phases 6 through 12 in which this procedure is applied. Computed displacements are also affected in a similar fashion. Again, this compromise in accuracy is required in order to achieve convergence by Plaxis for these higher Canal water elevations with cracking to the top of the Beach sand.

Factor of Safety: The factor of safety is computed for flood loading of the I-wall/sheet pile wall using the phi/c reduction method of analysis in Plaxis by means of incremental multipliers. Problems with numerical convergence occurred in nearly all Phi/c reduction analyses of this cross-section, even for the Canal water El 5 flood loading case with a crack extending to El -10.2 (i.e., the top of the Beach sand layer). It is speculated by the authors of this document that these numerical problems stem from the change in the hydraulic boundary condition when a crack forms to the top of the Beach sand, resulting in new, higher uplift pressures at the top of the Beach sand layer, below and immediately beyond the toe of the Levee combined with the shallow (total) overburden pressure of the Marsh layer within this region. Converting from a steady state seepage analysis to a linear phreatic surface assumption with a head specified at

canal centerline as equal to the elevation of the canal was not sufficient to achieve numerical convergence as is the case for the complete SSI analyses of London Canal Station 14+00. The approach used in the Phi/c reduction analyses of this cross section with Canal water El 5 and a crack extending to the top of the Beach sand, is to maintain the Canal water El 5 but to conduct a series of Phi/c reduction analyses with different values assigned to the head within the Beach sand layer below the centerline of the canal, as depicted in Figure 9-26. Regrettably, Phi/c reduction only converged for linear phreatic surface analyses with canal centerline heads of EL 1.5 or less, as outlined in Figure 9-25. This is well below the centerline head of El 5 that would normally be assigned in a Phi/c reduction analysis. For a centerline head of El 1.5 the computed Factor of Safety is equal to 2.57. Using the data contained in Figure 9-25 it is speculated (in this figure) that for a centerline head at El 5 (corresponding to the canal water elevation), the Factor of Safety is likely to range in value from 1.0 to 2.1. Additionally, the computed Factors of Safety results shown in this figure are greater than the actual values due to the linear phreatic surface assumption used within the Beach sand (as compared to pore water pressures resulting from a steady state seepage analysis with a crack to the top of the Beach sand).

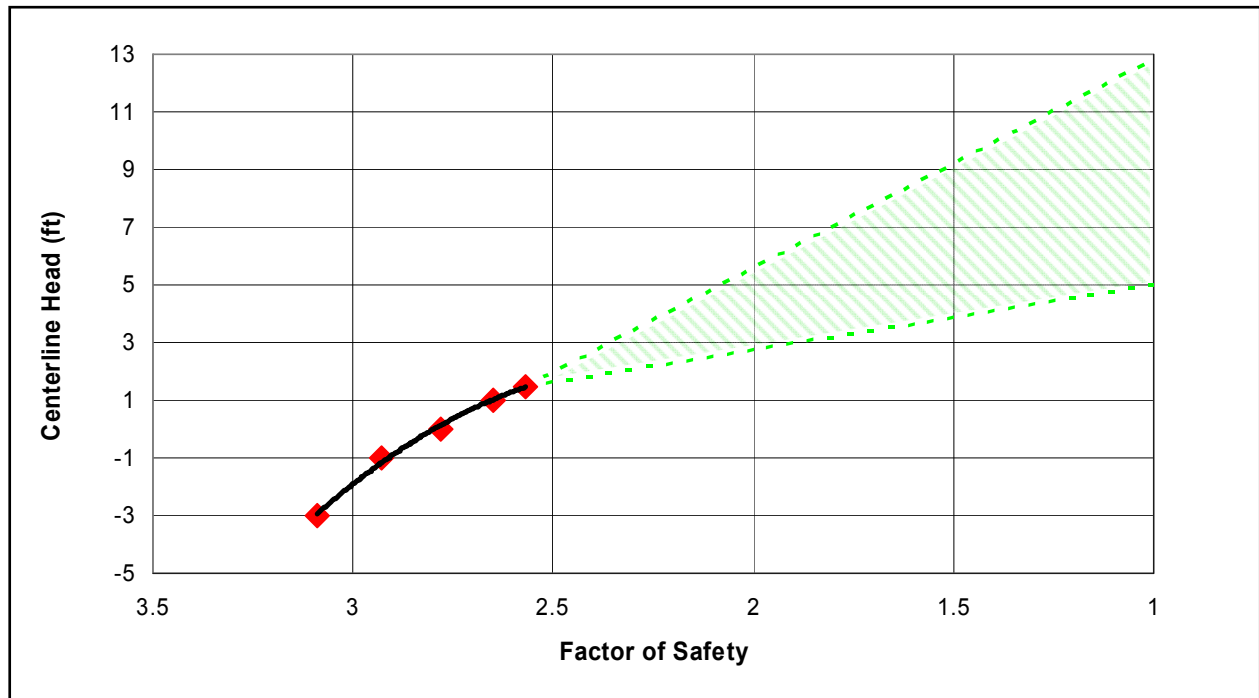


Figure 9-25. Factor of Safety Versus Centerline Head

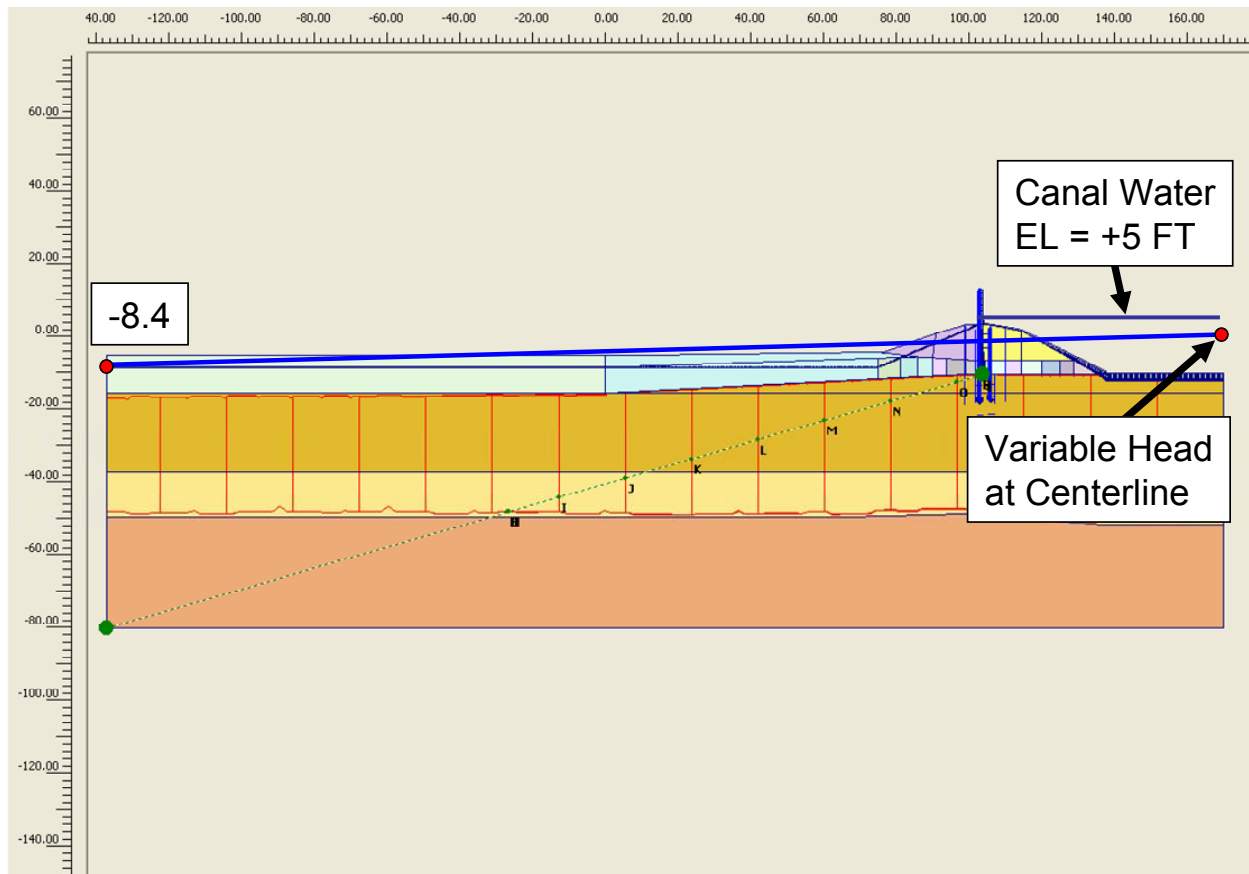


Figure 9-26. Graphical Definition of the Head at Canal Centerline for the Linear Phreatic Surface Assumption

Deformations: Figure 9-27 summarizes the computed deformations for the analysis set with stiff modulus values assigned to the Levee clay and the Marsh on the protected side of the I-wall, Canal water El 5 and crack to El -10.2 (i.e., top of Beach sand). Note the nodal deformations are magnified by a factor of 70 in order to show the deformed relative mesh relative to its position at canal water elevation of 1.0 (shown as a blue outline in this figure). The general trend is a rotational plowing of the protected side Levee clay by the I-wall/new sheet pile wall and a bulging of the Marsh beyond the toe of the Levee on the protected side.

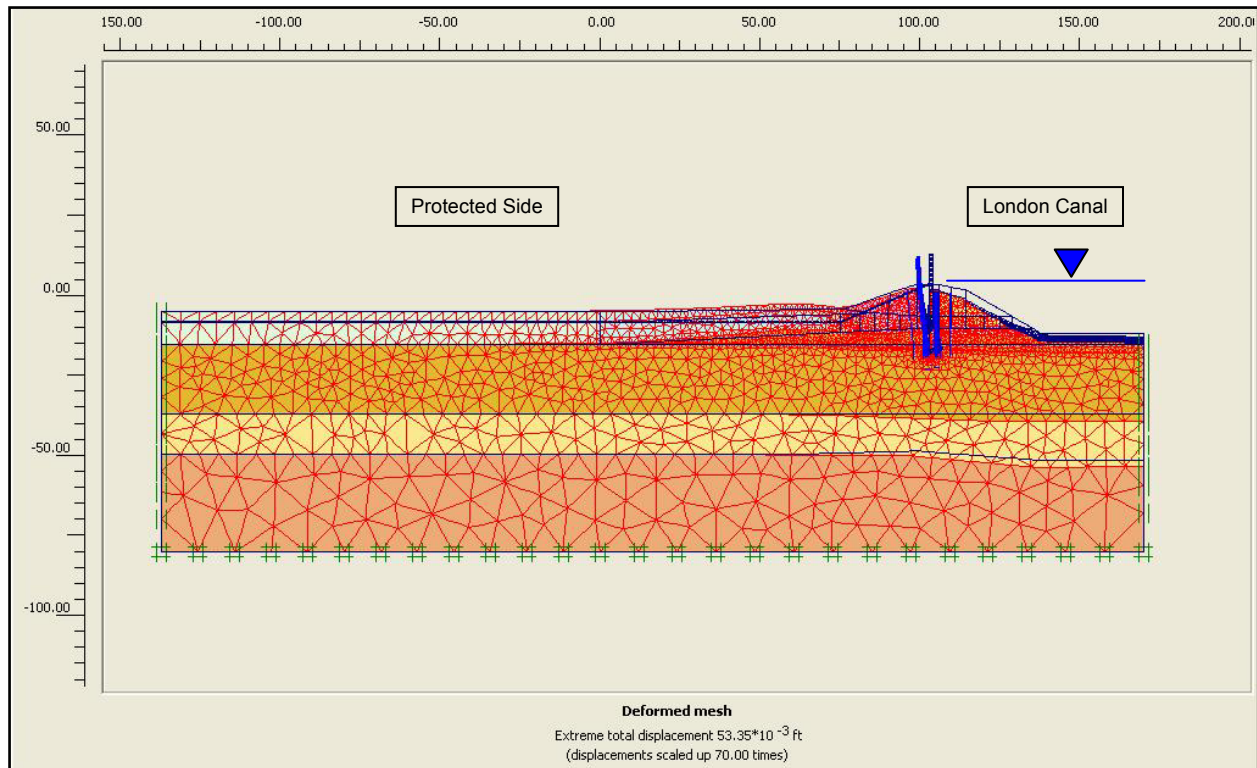


Figure 9-27. Deformed Mesh for Stiff Modulus Values for the Levee Clay and Marsh on the Protected Side, Exaggerated by a Factor of 70, for Canal EI 5 and Crack to EI -10.2 (Note: Canal EI not to scale in figure)

Figure 9-28 shows the horizontal displacements of the soil regions within the mesh, relative to their position at a canal water elevation of 1.0 for stiff modulus values assigned to the Levee clay and the Marsh on the protected side of the I-wall with Canal water EI 6 and crack to EI -10.2. This figure shows the horizontal deformations are concentrated within the protected region of the Levee and the Marsh immediately at the toe of the Levee on the protected side. The largest horizontal deformations are concentrated in the Marsh, on the protected side, (approximately) equal to 0.05 ft (5/8 inch).

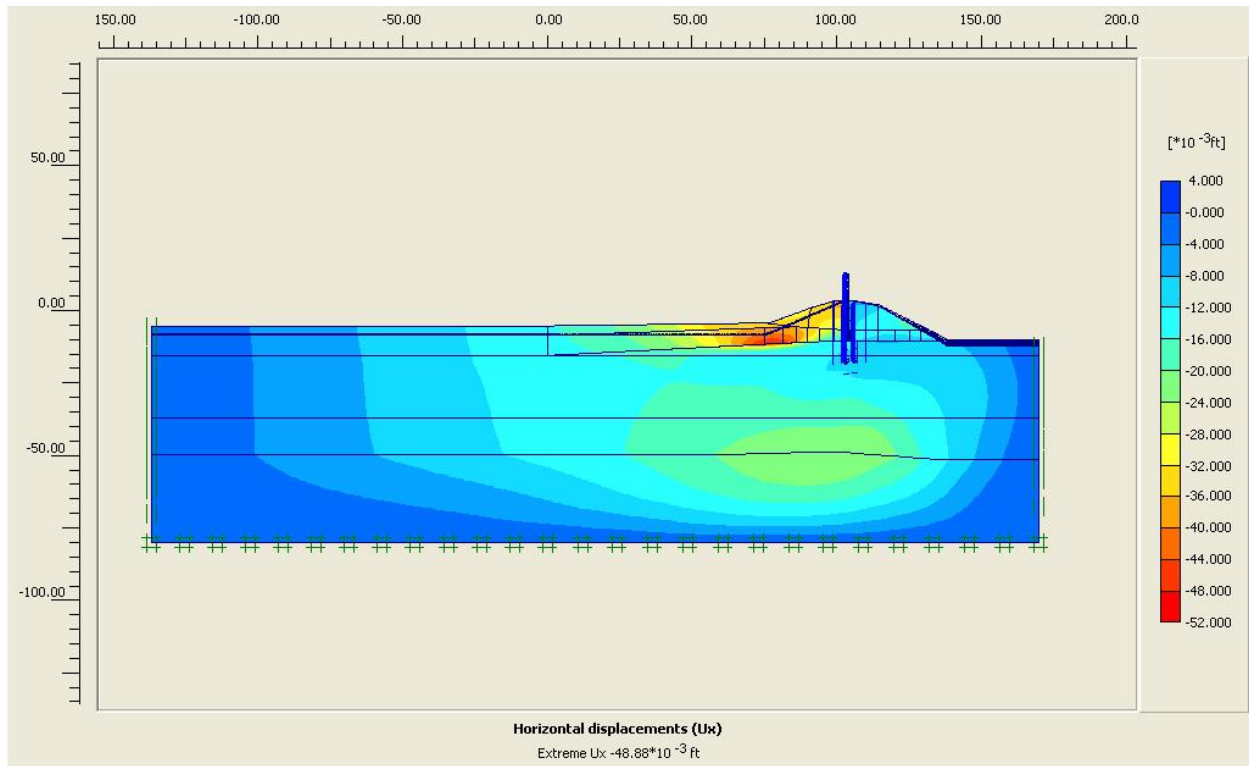


Figure 9-28. Horizontal Deformation Shadings for the Levee Clay and Marsh on the Protected Side with Canal EI 5 and Crack to EI -10.2

Figure 9-29 shows the variation in horizontal displacements of the sheet pile versus canal water elevation for the analysis set with stiff modulus values assigned to the Levee clay and the Marsh on the protected side of the I-wall. These displacements are relative to their position at a canal water elevation of 1.0. This figure shows the rotational nature of the I-wall/sheet pile wall deformations, with the toe of the sheet pile “anchored” in the Beach sand.

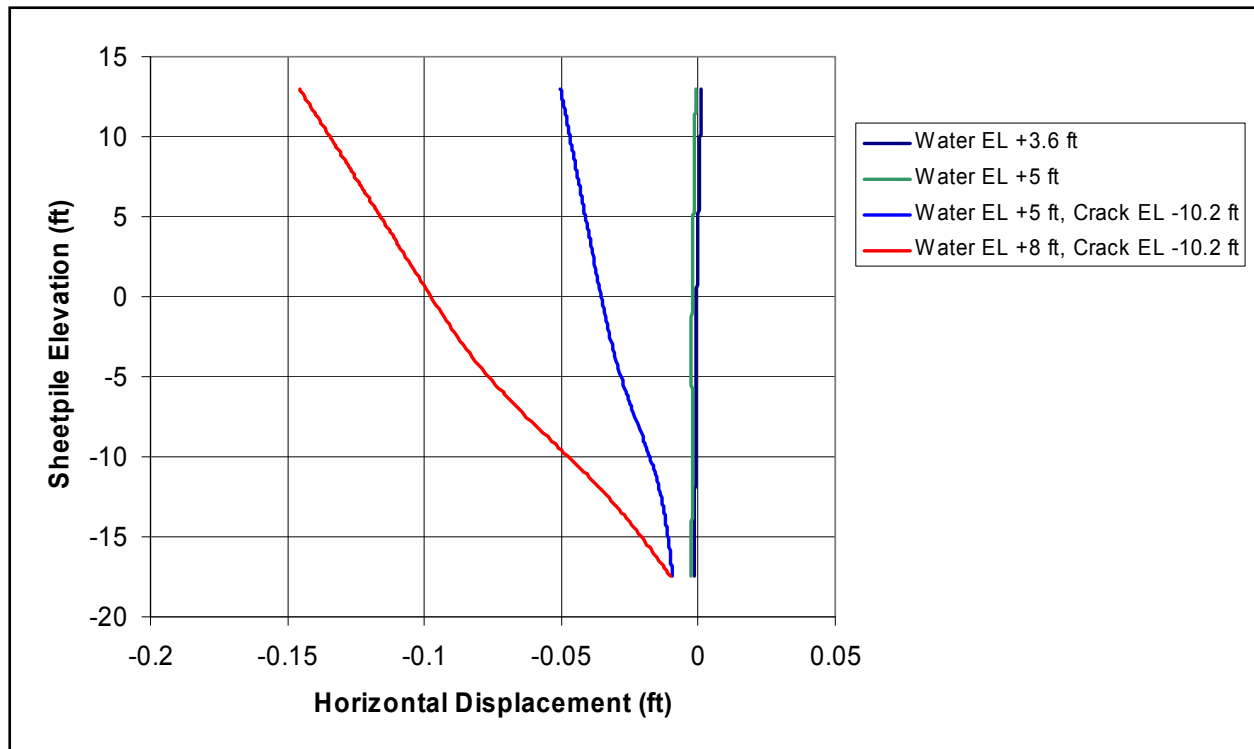


Figure 9-29. Horizontal Displacement of the I-Wall/Sheet Pile versus Canal Water El and Computed Using Stiff Modulus Values for the Levee Clay and Marsh on the Protected Side

Figure 9-30 shows the horizontal displacements of three points within the flood wall, relative to its position at a canal water elevation of 1.0 for stiff modulus values assigned to the Levee clay and the Marsh on the protected side of the I-wall. The points monitored through the analysis are at the top of the I-wall (El 13), at El 3.6 (top of Levee) and at the sheet pile tip (El -17.4). Recall for Canal water El's of 5 and higher, the crack never extends into the Beach sand layer, it terminates at the top of the Beach sand layer (i.e., El -10.2). Note that there is a significant increase in horizontal deformations of the I-wall/sheet pile wall when the crack extends to El -10.2 at Canal water El 5. Results in this figure shows the Beach sand is providing enough lateral support to prevent the sheet pile tip from moving laterally, therefore the deformation of the sheet pile is mostly a rotation about the sheet pile tip. Maximum horizontal movement at the top of the I-wall is 0.145 ft (1 3/4 inches) for Canal water El 8.

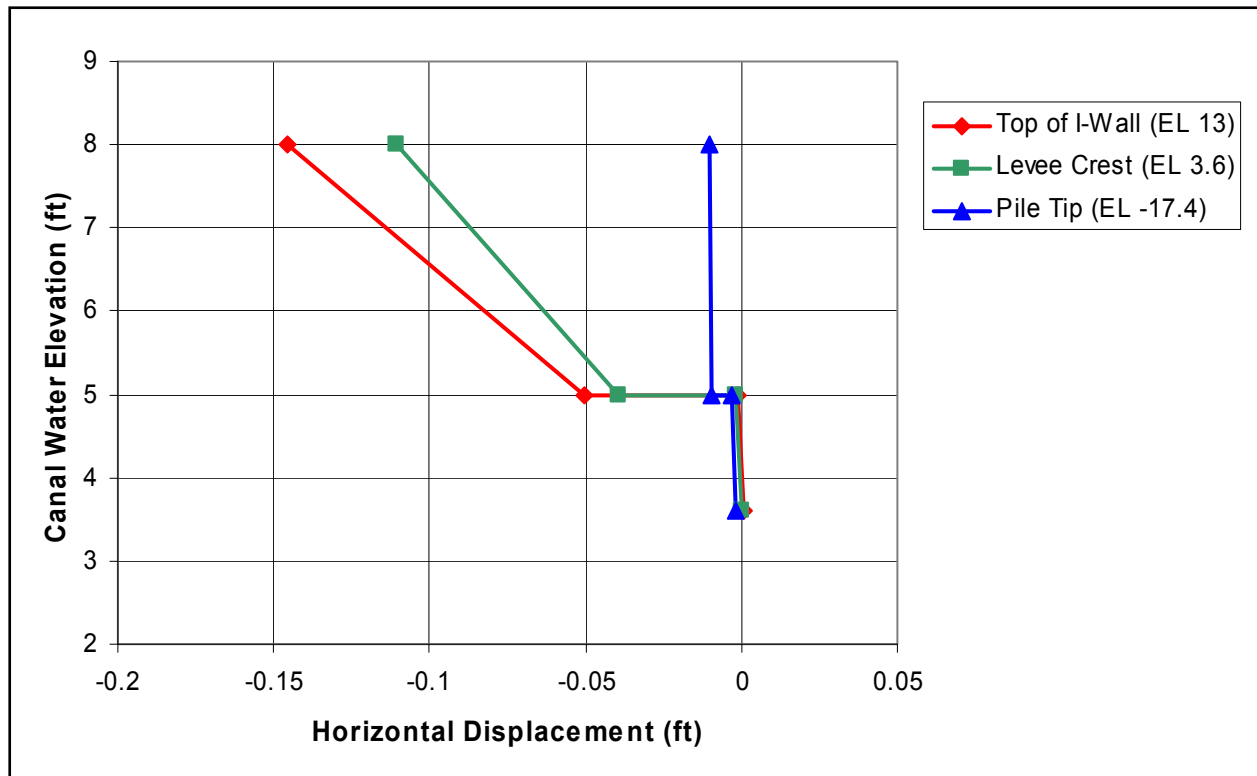


Figure 9-30. Horizontal Sheet Pile Deformations versus Canal Water El and Computed Using Stiff Modulus Values for the Levee Clay and Marsh on the Protected Side

Figure 9-31 shows the vertical displacements of the soil regions within the mesh, relative to their position at a canal water elevation of 1.0 for stiff modulus values assigned to the Levee clay and the Marsh on the protected side of the I-wall with Canal water El 5 and crack to El -10.2. This figure shows the 0.024 ft (1/4 inch) uplift of the Marsh located beyond the toe of the Levee on the protected side.

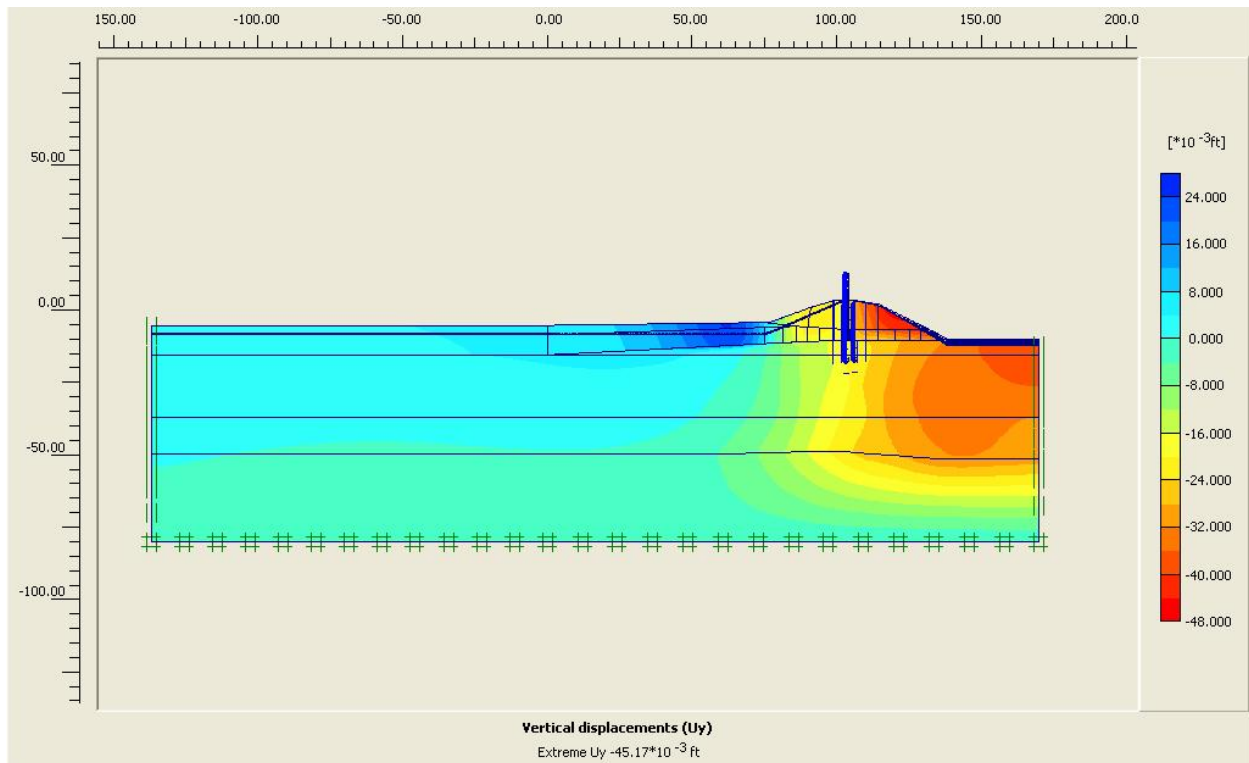


Figure 9-31. Vertical Deformation Shadings for Stiff Modulus Values for the Levee Clay and Marsh on the Protected Side with Canal El 5 and Crack to El -10.2

Failure Mechanism: Figures 9-32 and 9-33 show that for the analysis set using stiff modulus values assigned to the Levee clay and the Marsh on the protected side of the I-wall with Canal water El 5 and Crack to El -10.2, there is a loss of effective vertical stress at the top of the Beach sand layer within the region beyond the toe of the Levee. This results in zero shear strength along the top of the Beach sand layer as demonstrated in the Figure 9-34 fraction of mobilized shear strength being equal to unity within this Beach sand region. Figure 9-35 shows that this, in turn, results in the beginning of the development of a mechanism as demonstrated by the concentration of large shear strains within this region for Canal water El 5 and crack to El -10.2. Figure 9-36, with a close-up of the Levee region shown in Figure 9-37, and Figure 9-38 show the development of the ultimate mechanism (i.e., the failure mechanism) computed in a phi/c reduction analysis for Canal water El 5 and crack to El -10.2, for a linear phreatic surface Canal centerline head at El 0 with the computed Factor of Safety of 2.78 (actual value will be lower when the more realistic, larger pore water pressures are specified in an analysis). Note the vertical “bulging” in the Marsh beyond the toe of the Levee. The reaches of large shear strain shown in Figure 9-38 shows the complete failure wedge will form along the top of the Beach sand layer and “day light” beyond the toe of the Levee. All subsequent phi/c computations (that converged to a solution) for higher canal water elevations and for the E_{stiff} analyses show this same Figures 9-36, 9-37 and 9-38 failure mechanism to form.

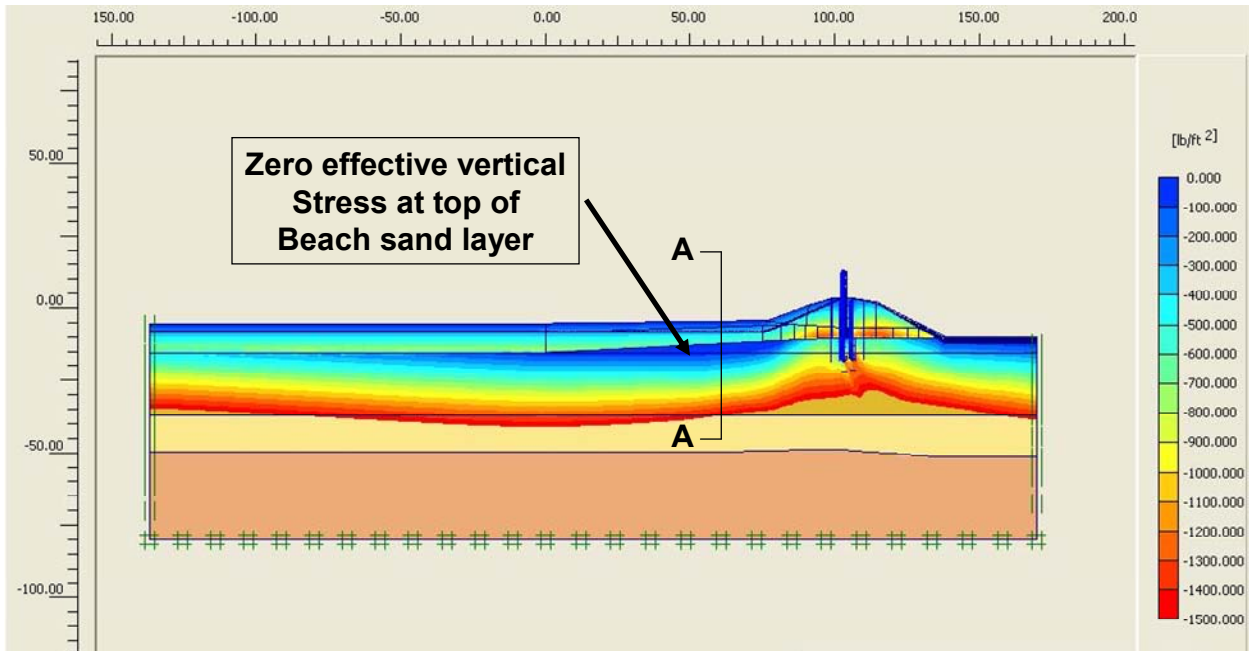


Figure 9-32. Shadings of Total Vertical Stress in the Levee Clay and Marsh and Effective Vertical Stress in the Beach Sand for the Analysis Using Stiff Modulus Values for the Levee Clay and Marsh on the Protected Side with Canal EI 5 and Crack to EI -10.2

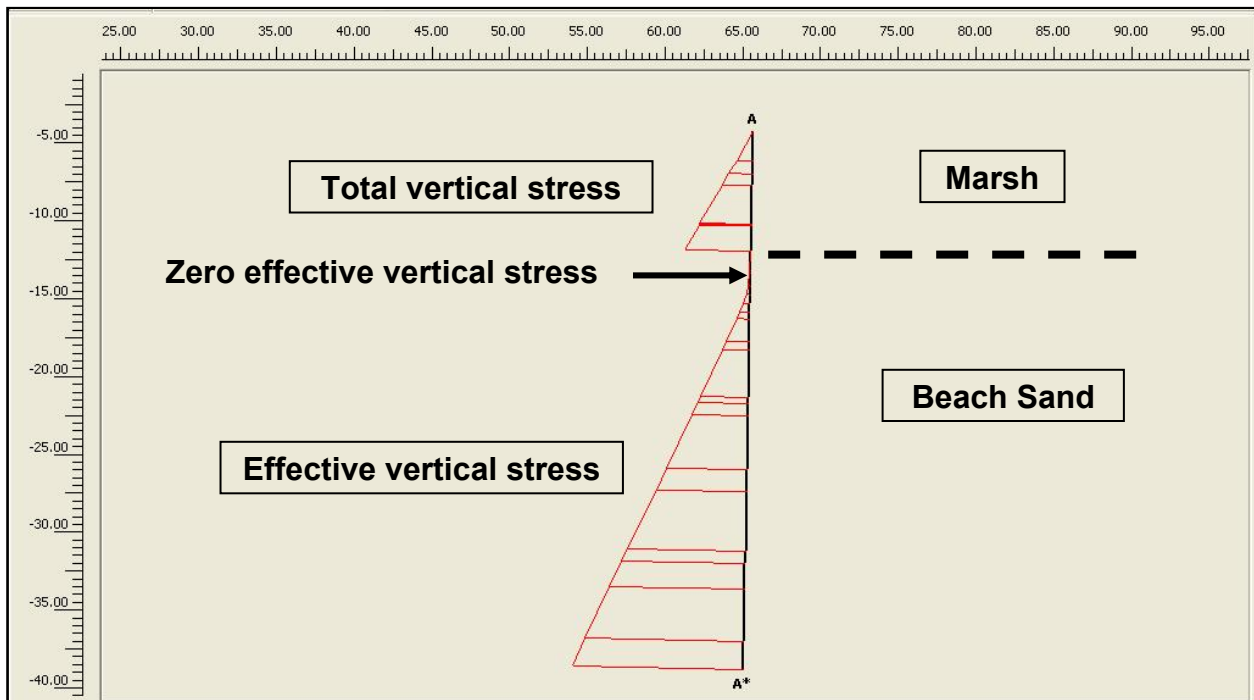


Figure 9-33. Vertical Section A-A Near the Toe of the Levee Showing Total Vertical Stress in the Marsh and Effective Vertical Stress in the Beach Sand for the Analysis Using Stiff Modulus Values for the Levee Clay and Marsh on the Protected Side with Canal EI 5 and Crack to EI -10.2

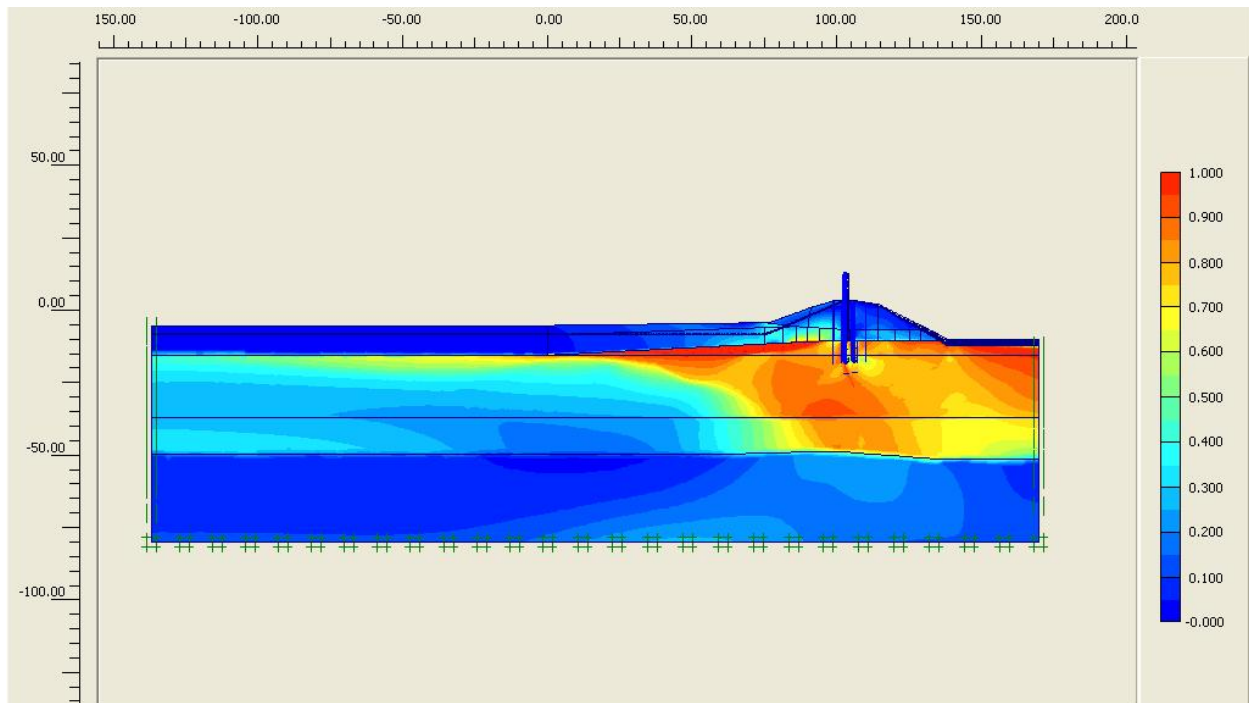


Figure 9-34. Fraction of Mobilized Shear Strength for the Analysis Using Stiff Modulus Values for the Levee Clay and Marsh on the Protected Side with Canal EI 5 and Crack to EI -10.2

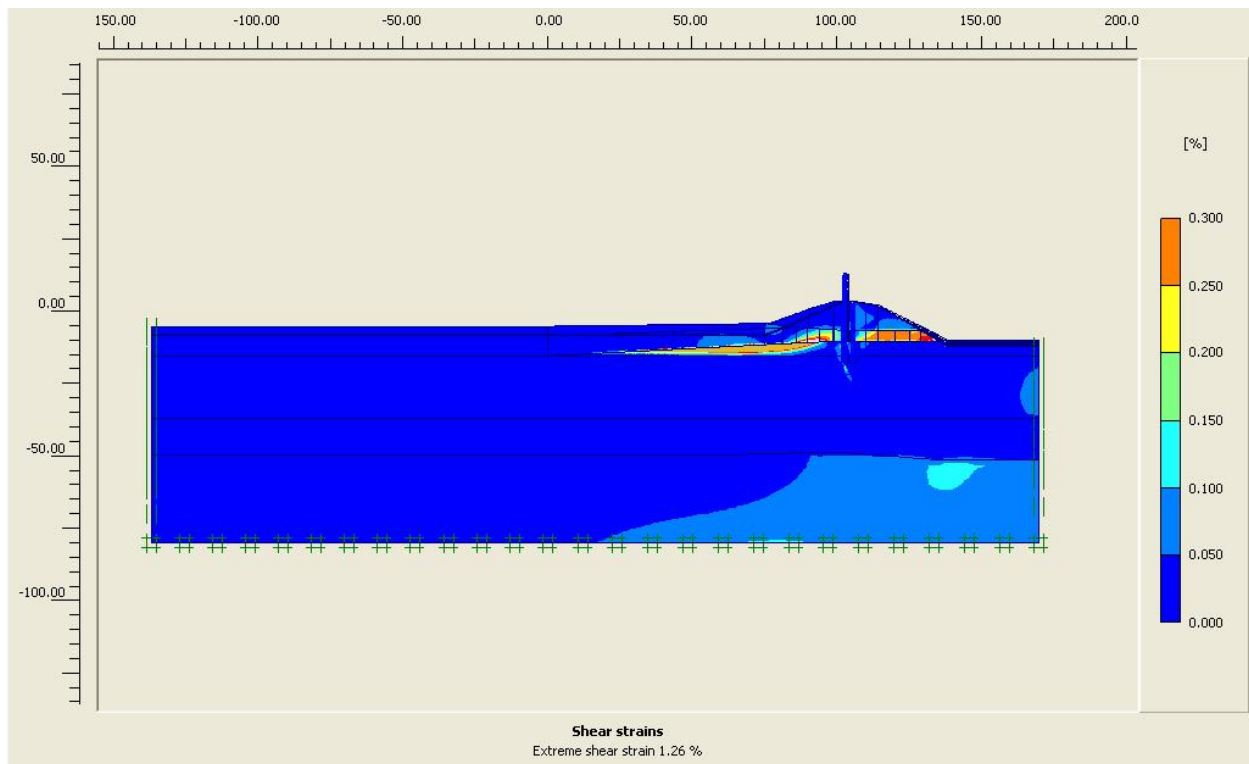


Figure 9-35. Reach of Large Shear Strains for the Analysis Using Stiff Modulus Values for the Levee Clay and Marsh on the Protected Side with Canal EI 5 and Crack to EI -10.2

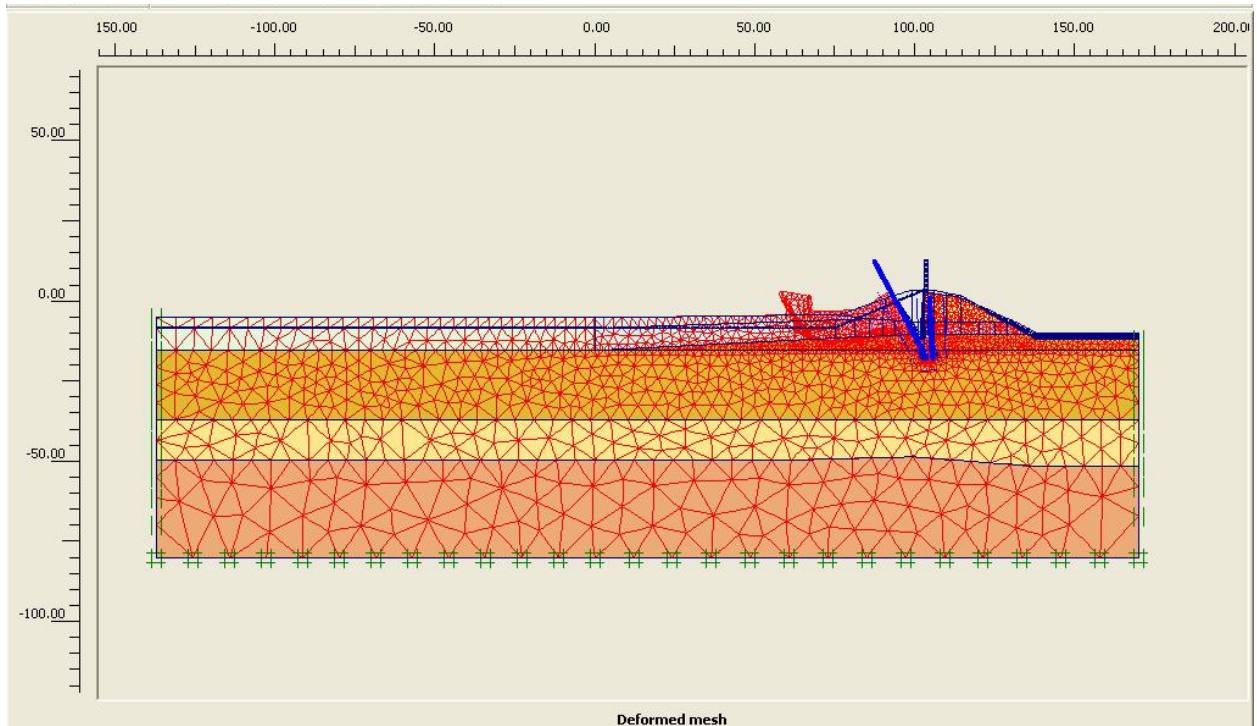


Figure 9-36. Ultimate Mechanism from Phi/C Reduction for the Analysis Using Stiff Modulus Values for the Levee Clay and Marsh on the Protected Side with Canal EI 5 and Crack to EI -10.2

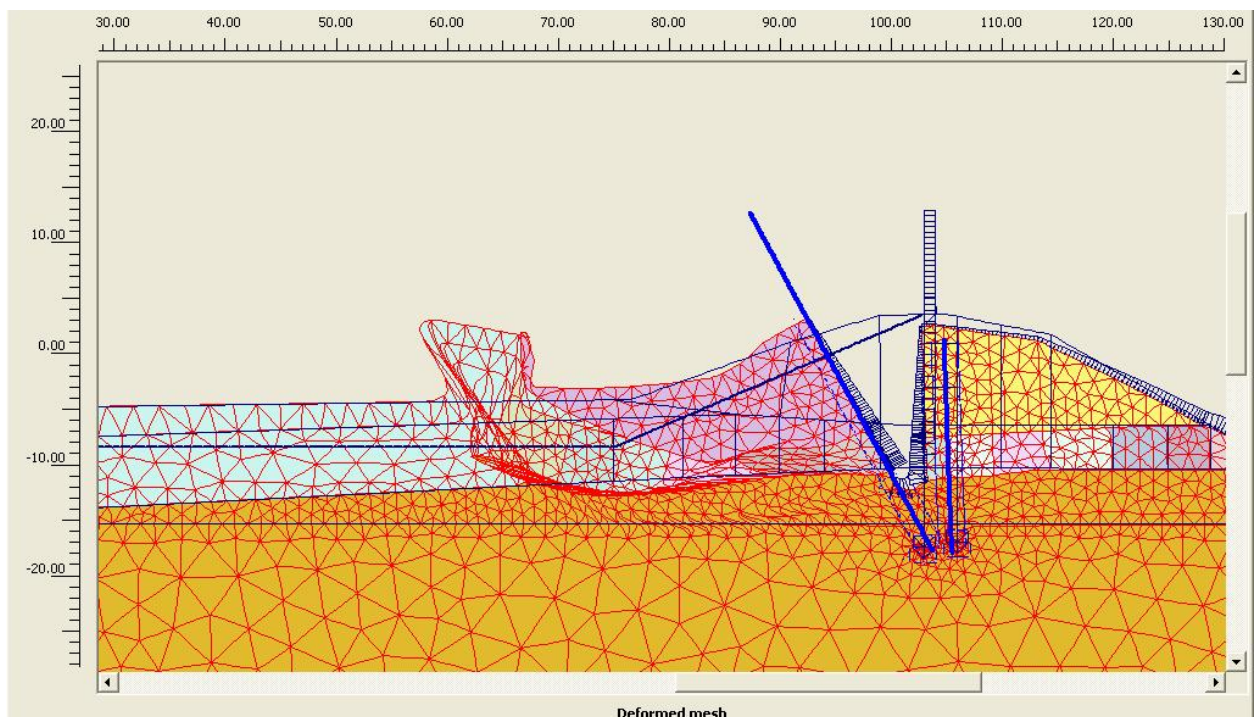


Figure 9-37. Close-up of the Ultimate Mechanism from Phi/C Reduction for the Analysis Using Stiff Modulus Values for the Levee Clay and Marsh on the Protected Side with Canal EI 5 and Crack to EI -10.2

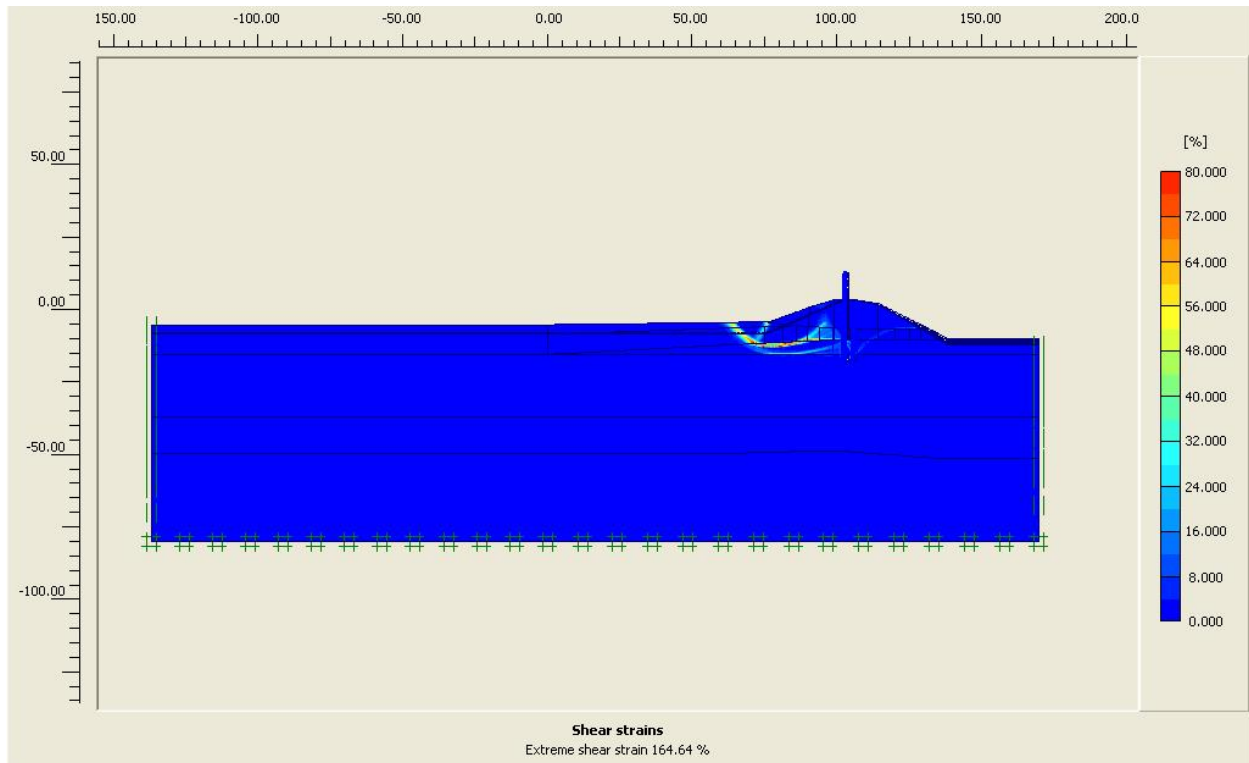


Figure 9-38. Reach of Large Shear Strains from the Phi/C Reduction Analysis Using Stiff Modulus Values for the Levee Clay and Marsh on the Protected Side with Canal EI 5 and Crack to EI -10.2

References

- Brinkgreve, R. B. J., W. Broere, and D. Waterman, ed. 2004. *Plaxis 2D – Version 8*. Plaxis B.V. The Netherlands: Delft University of Technology.
- Brinkgreve, R. B. J. 2005, Selection of Soil Models and Parameters for Geotechnical Engineering Application, ASCE Geotechnical Special Publication No. 128 Soil Constitutive Models; Evaluation, Selection, and Calibration, edited by J.A. Yamamuro and V. N. Kaliakin, pp. 69-98.
- Peck, R.B., Hanson, W. E., and Thornburn, T. H. 1974. *Foundation Engineering*, 2nd edition, New York, John Wiley and Sons, Inc., 514 p.
- Plaxis Short Course. 2006 (Jan). *Computational Geomechanics and Dynamics*, held at Polytechnic University Brooklyn, N.Y.
- Potyondy, J. G. 1961. Skin Friction Between Various Soils and Construction Materials, *Geotechnique*, Vol. II, pp. 339-353.
- Skempton, A. W. 1986. Standard Penetration Test Procedures and the Effects in Sands of Overburden Pressure, Relative Density, Particle Size, Ageing and Overconsolidation, *Geotechnique*, Vol. 36, No. 3, pp. 425-447.

Weber, W. G. 1969 (Jan). Performance of Embankments Constructed over Peat, ASCE Journal of the Soil Mechanics and Foundations Division, Vol. 95, No. SM1, pp. 53-76.

Appendix 10

Analysis of Performance of the Orleans Canal I-Walls

Purpose

The I-walls at the Orleans Canal did not fail, even though they were severely loaded. The purpose of the study described in this report was to determine if the analysis methods that indicated unstable conditions for the 17th Street Canal and London Avenue Canal I-walls, which did fail, would indicate stable conditions for the Orleans Canal I-walls, which did not fail.

The areas analyzed are shown in Figures 10-1 and 10-2. At the Orleans Canal south area (Station 8+61), the marsh layer beneath the levee is underlain by sand, as at the London Avenue breach locations. At the Orleans Canal north area (Station 64+27), the marsh layer beneath the levee is underlain by clay, as at the 17th Street Canal breach location. The geologic conditions at these two locations on the Orleans canal are thus directly comparable to the locations at the 17th Street Canal and the London Avenue Canal where breaches occurred.

Orleans South – Sand Underlying Levee and Marsh

Erosion and Piping

Steady state finite element analyses of seepage beneath the levee and I-wall were performed using the computer program SLIDE¹. The characteristics of the cross section analyzed are shown in Figure 10-3. The relevant materials are the sand, the overlying marsh (peat) layer, and the clayey levee fill. The Bay Sound clay at the base of the section has very low permeability, and acts like an impermeable boundary beneath the sand. Similar values of permeability were used for these materials as were used for the seepage analyses at the London Avenue Canal: $k_{\text{sand}} = 1 \times 10^{-2}$ cm/sec, $k_{\text{marsh}} = 1 \times 10^{-5}$ cm/sec, $k_{\text{levee fill}} = 1 \times 10^{-6}$ cm/sec, and $k_{\text{Bay Sound clay}} = 1 \times 10^{-6}$ cm/sec. The value of permeability for the sand was measured using a pumping test, and the other values of permeability are assumed. The most important factor governing the results of the seepage analyses is that the sand is much more permeable than the other materials in the cross section,

¹ Available from Rocscience Inc., 31 Balsam Avenue, Toronto, Ontario, Canada M4E 3B5

and the results of the seepage analyses would not be affected by moderate changes in the assumed values of permeability.

The hydraulic boundary conditions used in these analyses are shown in Figure 10-3. Two canal water levels were considered in the analyses: 11.1 ft (the highest canal water level reached on August 29th) and 13.2 ft (the elevation of the top of the I-wall). The design water elevation was 11.2 ft, essentially the same as the peak water level reached on August 29th. A constant-head boundary condition was imposed at the location of the drain beneath Marconi Drive. This head value was either -10.0 ft (the normal ground water level with pumps operating), or -3.0 ft (a higher level equal to the ground surface elevation, which might have occurred with pumps not operating).

Two possible conditions regarding cracking or formation of a gap behind the wall are illustrated in Figure 10-4. The first involves a gap to the bottom of the wall, as considered at the 17th Street Canal. The second involves continuation of this gap below the bottom of the wall, by hydraulic fracturing of the levee fill and marsh material below the wall.

Hydraulic fracturing is possible in any location where (1) water pressures exceed the total stress on a potential fracture plane, as would be the case for a vertical plane extending below the bottom of the wall, and (2) the soil has sufficient strength for the gap to remain open, supported by the water pressure. The maximum possible depth of a hydraulic fracture, or gap, is related to the strength of the soil by the following equation:

$$H_{\max \text{ crack}} = \frac{2s_u}{(\gamma_{\text{soil}} - \gamma_w)} \quad (10-1)$$

where $H_{\max \text{ crack}}$ = maximum possible gap depth, s_u = undrained strength of soil, γ_{soil} = total unit weight of soil, and γ_w = unit weight of water. For the conditions at Orleans south, the levee fill and marsh are strong enough to maintain a water-filled gap extending down to the marsh-sand interface². Water would fill this gap, loading the wall and the fracture plane below the wall, and introducing the canal head at the top of the sand.

Formation of a hydraulic fracture below the bottom of the wall would result in very severe loading on the wall for two reasons: (1) the gap would allow water to flow directly into the sand layer, increasing pore pressures and uplift pressures, and (2) the gap beneath the wall would extend the vertical face on which water pressures would act, thereby greatly increasing the water load acting on the plane of the wall. Although formation of a deeper gap by hydraulic fracturing has not been confirmed by field observation, it does appear to be feasible in soils as strong as the levee fill and marsh at Orleans south. Although occurrence of hydraulic fracturing is an extreme hypothesis, it is believed to be a condition that should be evaluated in this study of the performance of the Orleans south I-wall. Centrifuge model test results, and soil-structure

² The clay at the 17th Street Canal breach area is weaker than the marsh at Orleans. The clay at the 17th Street Canal is too weak to support a crack extending below the bottom of the wall.

interaction finite element analyses may help to confirm or refute the hydraulic fracturing at the Orleans Canal I-wall.

Six-node triangular elements were used for the seepage analyses. Seepage analyses were performed for eight different hydraulic boundary conditions, as shown in Table 10-1. An example finite element mesh (for Case 7) is shown in Figure 10-5. Computed total head contours for Case 7 are shown in Figure 10-6. It can be seen that the flow through the sand is predominantly horizontal, and that the total head on the landward side of the levee is above the ground surface, which is at elevation -3.0 ft. The head contours for the other cases had similar shapes, although the values of head were different, varying with the hydraulic boundary conditions.

Computed pore water pressures, or uplift pressures, at the base of the marsh layer are shown in Figure 10-7 for the eight cases analyzed, together with the total overburden pressure at the base of the marsh layer. For Cases 1 and 5, where the landside water level was -10 and the gap extended only to the bottom of the wall, the computed pore pressures are smaller than the total overburden pressure at the base of the marsh layer. In all other cases the computed pore pressures exceed the overburden pressure in some locations. This result indicates that in these cases the marsh layer would be heaved off the underlying sand by the uplift water pressures. A likely result of this heave would be rupture of the marsh layer at one or more weak points, and upward flow of water through the rupture through the marsh material. This flow would relieve the high water pressure locally, and create a new hydraulic boundary condition at the point of rupture.

Additional seepage analyses were performed to determine if the hydraulic gradients within the sand after rupture of the marsh layer would be large enough to cause erosion of the sand and begin a piping failure. For completeness, the same type of analysis was performed for Cases 1 and 5, although the uplift pressures did not exceed the overburden pressure. For these two cases the analyses correspond to existence of a pre-existing defect or void in the marsh layer, rather than a rupture caused by the uplift. The seepage boundary conditions used in these analyses are shown in Figure 10-8, where a rupture or pre-existing void extends upward through the marsh layer, from the top of the sand to the ground surface. As for the London Avenue seepage analyses, a rupture zone width equal to 1.6 ft was used in these analyses. In the real case, flow would converge in three dimensions rather than two dimensions, as represented in these two-dimensional seepage analyses. It therefore seems likely that the actual hydraulic gradients that might develop would be higher than the values discussed in the following sections, but the magnitude of this three-dimensional effect cannot be quantified.

The effect of the changed hydraulic boundary conditions caused by the rupture or void were analyzed by imposing a head at the base of the rupture that was equal to the elevation of the ground surface, simulating a condition where the water level within the rupture or void rises to the ground surface. An example of total head contours in the sand at the base of the hypothesized rupture (for Case 6) is shown in Figure 10-9. Values of vertical hydraulic gradient in this zone are shown in Table 10-2 for the six cases analyzed. The computed values of i range from 0.20 to 1.23 .

The value of hydraulic gradient that would cause erosion of the sand is:

$$i_{critical} = \frac{\gamma_b}{\gamma_w} = \frac{\gamma_s - \gamma_w}{\gamma_w} \quad (10-2)$$

where $i_{critical}$ = hydraulic gradient that would cause erosion of the sand, γ_b = buoyant unit weight of sand, γ_w = unit weight of water, and γ_s = saturated unit weight of sand. With γ_s for the sand assumed to be 120 pcf, the critical hydraulic gradient is 0.92.

Values of $F_{erosion} = i_{crit}/i$ are shown in Table 10-2 for all eight cases analyzed. For Cases 1 and 2, with the highest observed canal water level and a gap to the bottom of the wall, the computed factors of safety against erosion are 4.60 for the lower inland water level and 1.39 for the higher inland water level. For Cases 3 and 4, with the highest observed water level and a hydraulic fracture extending to the top of the sand, the factors of safety against erosion are 1.48 for the lower inland water level, and 0.89 for the higher inland water level. Thus, for the most severe condition of the highest maximum possible inland water level and hydraulic fracturing to the top of the sand, the computed factor of safety against erosion is less than 1.0, but for all other cases it is greater than 1.0.

Cases 5 through 8 involve water levels higher than the maximum reached at the Orleans Canal. Nevertheless, it is interesting to examine the factors of safety for these conditions, to determine if the I-wall could have withstood even higher water levels. The calculated factors of safety against erosion are greater than 1.0, except for Case 8, where a hydraulic fracture to the top of the sand is assumed, and the inland water level is at the highest possible elevation.

The probability of erosion was calculated for all eight cases, considering the variation in factor of safety caused by the uncertain landside water level and the uncertain depth of cracking. A simple method based on the Taylor Series³ was used for these calculations. The computed values of probability of erosion are shown in Table 10-3. For the canal water level at 11.1 ft, the maximum observed, the probability of erosion is 3% for a gap to the bottom of the wall, and nearly 30% for a gap down to the sand. For the canal water level at the top of the wall (13.2 ft), these probabilities of erosion are approximately twice as high.

The fact that no signs of erosion due to underseepage were reported in the Orleans south area after the flood neither confirms nor refutes these calculated probabilities. The analyses indicate a possibility of erosion, but this would not necessarily result in failure of the I-wall. Erosion, if it did occur beneath the marsh layer, might not result in visible manifestations at the ground surface, and might not move a sufficient quantity of sand to alter the cross section in any significant regard.

³ Wolff, T. F. (1994). "Evaluating the reliability of existing levees." Report, Research Project: Reliability of Existing Levees, prepared for U.S. Army Engineer Waterways Experiment Station Geotechnical Laboratory, Vicksburg, Miss.

Slope Instability

Slope stability analyses were performed for Cases 1 through 8 shown in Table 10-1. The critical circles and factors of safety for these cases are shown in Figures 10-10 through 10-17. The cross section shown in these figures is the same as that used in the seepage analyses. The analyses were performed using the computer program SLIDE¹, with Spencer's method.

Standard Penetration Tests performed in the Orleans south area showed that the sand had Standard Penetration Test blow counts (N_{SPT}) averaging about 40, which corresponds to a value of ϕ' in the range of 36 degrees to 40 degrees. Cone penetration tests in the area showed tip resistances that correspond to similar values of ϕ' . A value of $\phi' = 38$ degrees was used in the stability analyses.

The marsh layer was treated as undrained, with $s_u = 700$ psf and $\phi_u = 0$ beneath the levee crest, and $s_u = 450$ psf and $\phi_u = 0$ at the toe of the levee and beyond. These strength values, based on the available test results, are higher than the marsh strengths at the 17th Street Canal and the London Avenue Canal. The higher strengths at Orleans are likely due to the fact that the levee crest had been higher before the I-wall was constructed, and had compressed the marsh layer to a denser and stronger condition. The levee crest was degraded when the I-wall was built, and the marsh layer was overconsolidated as a result. A unit weight of 95 pcf was used for the marsh, based on available test results.

The levee fill was also treated as undrained, with $s_u = 1500$ psf, and $\phi_u = 0$. The slip circles do not intersect the levee fill, however, and the levee strength therefore has no influence on the calculated values of factor of safety. A value of unit weight = 109 pcf was used for the levee fill, based on available test results.

The analyses were performed using pore pressures in the sand from the finite element seepage analyses without a rupture or void through the marsh layer. The non-ruptured seepage analyses were used to determine pore pressures because a rupture or void would be of very limited size, not appropriate for inclusion in a two-dimensional cross section. At the bases of the slices where the pore pressures exceeded the overburden pressures near the top of the sand on the inland side, zero shear strength was assigned for the sand.

As discussed earlier, it was assumed in all analyses that deflection of the wall toward the land side would result in formation of a gap through the levee fill and the marsh in back of the wall, down to the bottom of the wall, or by hydraulic fracturing, down to the top of the sand. It was assumed that the gap would not extend below the top of the sand, because the sand is cohesionless, and would be expected to slump and fill any incipient gap. A gap to the bottom of the wall was assumed for Cases 1, 2, 5 and 6 (Figures 10-10, 10-11, 10-14 and 10-15), and a gap to the top of the sand was assumed for Cases 3, 4, 7, and 8 (Figures 10-12, 10-13, 10-16 and 10-17).

The critical circles extend to the bottom of the gap in all cases – to the bottom of the wall when the gap extends to that depth, and to the marsh/sand interface when the gap extends to that

depth. Hydrostatic water pressures act on the vertical plane of the gap, and the forces imposed by these pressures are the principal driving forces tending to cause instability.

The factors of safety calculated in these analyses are shown in Figures 10-10 through 10-17, and are summarized in Table 10-4. The values range from 1.38 to 2.71. Thus, even under the most severe conditions of water loading and possible gap formation considered here, the results of the analyses indicate that the wall would remain stable. For the highest water level observed at the Orleans south area, the lowest computed factor of safety is 1.86, which exceeds the minimum allowable for most conditions.

Probabilities of instability were computed considering uncertainties in gap depth, sand strength, and marsh strength, using the Taylor Series method³. The inland water level was varied from -10.0 ft to -3.0 ft, the sand friction angle was varied from 34 degrees to 42 degrees, and the marsh strength was varied by $\pm 25\%$ from its most likely average value. The results of the calculations are shown in Table 10-5.

For the canal water level at 11.1 ft, the calculated probability of instability is less than one in ten million for a gap extending to the bottom of the wall, and less than one in one million for a hydraulic fracture extending down to the sand. For the canal water level at the top of the wall (13.2 ft), the calculated probability of instability is less than one in one hundred thousand for a gap extending to the bottom of the wall, and less than one in one hundred for a hydraulic fracture extending down to the sand. Thus, for even the most severe conditions considered here, the calculations indicate that the probability of instability is small, and for the peak water level during the storm, it is very remote.

Orleans North – Clay Underlying Levee and Marsh

At the Orleans north area, the levee and I-wall are underlain by a marsh layer, which is in turn underlain by clay, and shown in Figure 10-18. As a consequence of the different soil conditions in this area, seepage effects are not important. The stability of the levee and I-wall are governed by the undrained shear strengths of the soils, most importantly, the clay.

The undrained strength of the clay was determined from the results of CPTU (piezocone) tests using Mayne's method⁴, which is applicable to clays that are overconsolidated, as well as to clays that are normally consolidated. The undrained shear strength is related to cone tip resistance by the equation

$$s_u = 0.091(\sigma'_v)^{0.2}(q_t - \sigma_v)^{0.8} \quad (10-3)$$

where s_u = undrained shear strength, σ'_v = effective vertical stress, q_t = total cone tip resistance adjusted for pore pressure effects, and σ_v = total vertical stress.

⁴ Mayne, P. W. (2003). "Class 'A' Footing Response Prediction from Seismic Cone Tests," Proceedings, Deformation Characteristics of Geomaterials, Vol. 1, Lyon, France.

The undrained shear strength calculated with this method is assumed to be equal to that measured using Direct Simple Shear (DSS) tests. This strength is lower than that measured by conventional triaxial compression tests and greater than that measured by triaxial extension tests. Ladd (1991)⁵ suggests that this is a reasonable average value for design purposes.

Results for three CPTU tests are shown in Figure 10-19. It can be seen that the results are very consistent. Some fill was removed from the top of the levee when the I-wall was constructed, and this left the underlying marsh and clay somewhat overconsolidated. Although overconsolidation increases the value of s_u/p for a clay, and might be expected to affect the rate of increase of undrained strength with depth, it was found that the strength within the lacustrine clay depth interval could be conservatively approximated by a rate of increase of undrained strength with depth of 11 psf per ft. This is the same rate of strength increase as found for the normally consolidated clay at the 17th Street Canal. Although somewhat surprising, this result was found to be a consequence of counteracting influences – the undrained strength ratio is increased by virtue of overconsolidation, but the overconsolidation ratio decreases with depth. It was concluded that the heavy straight line shown in Figure 10-19 is a sufficiently accurate, somewhat conservative, representation of the undrained strength of the lacustrine clay. The variation of undrained shear strength horizontally and vertically beneath the levee was estimated using the equation

$$\frac{s_u}{p} = 0.24(OCR^{0.8}) \quad (10-4)$$

where s_u = undrained shear strength, p = effective consolidation stress, and OCR = overconsolidation ratio. This equation was used to compute the undrained strength beneath the levee crest, beneath the toe, and beyond the toe of the levee. The resulting variation of undrained strength laterally and vertically within the cross section was represented in the stability analyses by means of the interpolation functions in SLIDE¹.

The marsh layer was treated as undrained, with $s_u = 650$ psf and $\phi_u = 0$ beneath the levee crest, and $s_u = 400$ psf and $\phi_u = 0$ at the toe of the levee and beyond. These strength values are based on the available test results. As noted above, the high strengths at Orleans are likely due to the fact that the levee crest had been higher before the I-wall was constructed, and the higher levee had compressed the marsh layer to a denser and stronger condition. A unit weight of 95 pcf was used for the marsh, based on available test results.

The levee fill was also treated as undrained, with $s_u = 1500$ psf, and $\phi_u = 0$. The slip circles do not intersect the levee fill, however, and the levee strength therefore has no influence on the calculated values of factor of safety. A value of unit weight = 109 pcf was used for the levee fill, based on available test results.

⁵ Ladd, C. C. (1991) "Stability Evaluation During Staged Construction," Terzaghi Lecture, ASCE Journal of Geotechnical Engineering, 117 (4), 540-615.

It was assumed in all of the Orleans north analyses that deflection of the wall toward the land side would result in formation of a gap through the levee fill and the marsh in back of the wall, down to the bottom of the wall.

The critical circles and factors of safety calculated in these analyses are shown in Figures 10-20 and 10-21, and the factors of safety are given in Table 10-6. The factors of safety are 1.62 for the highest observed water level (11.1 ft), and 1.47 for the water at the top of the wall (12.8 ft in this area). Thus, even under the most severe conditions of water loading and possible gap formation considered here, the results of the analyses indicate that the wall would remain stable. For the highest water level observed at the Orleans north area, the computed factor of safety is 1.62, which exceeds the minimum allowable for most conditions.

Probabilities of instability were computed considering uncertainties in clay strength and marsh strength, using the Taylor Series method³. The clay and marsh strengths were varied by $\pm 25\%$ from their most likely average values. The results of the calculations are shown in Table 10-7.

For the canal water level at 11.1 ft, the calculated probability of instability is less than one percent for a gap extending to the bottom of the wall. For the canal water level at the top of the wall (12.8 ft), the calculated probability of instability is 2.5%. Thus, for even the most severe conditions considered here, the calculations indicate that the probability of instability is small.

Design Analyses

The shear strengths, factor of safety criteria and stability analysis results are described in two Geotechnical Design Memoranda^{6,7}. The stability analyses were performed using the Method of Planes.⁸

For Stations 0+00 to 90+50 (which includes both the south and north sections analyzed in this report) lower undrained shear strengths were used for the clay beneath the toe of the embankment and beyond the toe than were used for the clay beneath the center of the levee. For sections further to the north, from Station 90+50 to Lake Pontchartrain, the same undrained shear strengths were used at the levee centerline, and at and beyond the toe of the levee.

The GDMs^{5,7} indicate a minimum acceptable factor of safety equal to 1.25 with the wall subjected to the design static water level and wave-load. The results of the stability analyses, summarized on Plate 48 for Stations 0+00 to 36+50 east (which includes to south section

⁶ Design Memorandum No. 19, General Design Vol. 1, *Orleans Avenue Outfall Canal*, Lake Pontchartrain, LA, and Vicinity, Lake Pontchartrain High Level Plan, Department of the Army, New Orleans District, Corps of Engineers, August 1988, Serial No. 53.

⁷ Design Memorandum No. 19, General Design Vol. 2, *Orleans Avenue Outfall Canal*, Lake Pontchartrain, LA, and Vicinity, Lake Pontchartrain High Level Plan, Department of the Army, New Orleans District, Corps of Engineers, August 1988, Serial No. 76.

⁸ A study of the Method of Planes, undertaken by IPET at the request of the New Orleans District Task Force Guardian, indicates that the Method of Planes gives lower factors of safety than more accurate methods of analysis, such as Spencer's method. The magnitude of the difference between the two varies from case to case.

analyzed in this report), and on Plate 54 for Stations 64+00 to 90+50 east (which includes the north section analyzed in this report), show that the lowest computed factors of safety were 1.30 in both cases. No gap behind the wall was considered in the analyses.

Consideration was given by the designers to the possibility that the water pressure in the Pine Island Beach sand beneath the marsh and lacustrine clay might be elevated during periods of high water level in the canal. Such water pressures would adversely affect stability, as was the case at the London Avenue south breach. The possibility of high water pressures in the Pine Island Beach sand formation was investigated by installing three piezometers near Station 18+10. These piezometers indicated no hydraulic communication between the water in the canal and the sand. Observations of other piezometer installations, in 1970 and 1971, also indicated that the buried beach sand was not hydraulically connected to the canal. The possibility that a hydraulic connection between the canal and the sand might result from dredging or erosion of the clay in the bottom of the canal was investigated by a test section at the 17th Street Canal, where the overlying impermeable materials were dredged to expose the beach sand in the bottom of the canal. Piezometer readings taken before and after the dredging showed no significant changes in piezometric levels due to dredging. On the basis of these studies, stability analyses were performed using water pressures in the Pine Island Beach sand that reflected normal groundwater elevations, unaffected by rise in the canal water level.

Summary

The analyses described here were performed as a test of the methods of analysis that were applied previously in investigations of the failures of the 17th Street Canal and London Avenue Canal I-walls. The objective was to determine if these same methods are capable of showing that failure should not occur, in cases where failure did not occur. The Orleans Canal south area, where the levee and marsh are underlain by sand, is directly comparable to the London Avenue Canal south breach area. The Orleans Canal north area, where the levee and marsh are underlain by clay, is directly comparable to the 17th Street Canal breach area.

The same type of seepage analysis and interpretation of results that showed high hydraulic gradients, factors of safety less than 1.0, and probability of erosion greater than 99% at the London Avenue south breach showed moderate hydraulic gradients, factors of safety larger than 1.0, and probabilities of erosion of 3% and 28% for the highest water level experienced on the Orleans Canal. The fact that no signs of erosion due to underseepage were observed in the Orleans south area after the flood neither confirms nor refutes these calculated probabilities. The analyses indicate a possibility of erosion, but this would not necessarily result in failure of the I-wall. Erosion, if it did occur beneath the marsh layer, might not result in visible manifestations at the ground surface, and might not move a sufficient quantity of sand to alter the cross section in any significant regard.

The same type of stability analyses and interpretation of results that showed factors of safety less than 1.0, and probabilities of instability varying from 70% to 97% at the London Avenue north breach showed factors of safety varying from 1.9 to 2.7 for the highest water level observed at the Orleans Canal, and probabilities of instability lower than one in one million.

These results show that the methods of stability analysis applied to conditions with sand beneath the levee and marsh layer are capable of modeling instability where it occurs, and stable conditions where they occur.

The same type of stability analyses and interpretation of results that showed factors of safety from 1.0 to 1.2, and probabilities of instability from 12% to 60% for the 17th Street Canal breach, showed factors of safety from 1.5 to 1.6 for the highest water level observed at the Orleans Canal, and probabilities of instability from 1% to 3%. These results show that the methods of stability analysis applied to conditions with clay beneath the levee and marsh layer are capable of modeling instability where it occurs, and stable conditions where they occur.

Table 10-1 Hydraulic Boundary Conditions for Seepage Analyses – Orleans South		
Case	Canal water level – CWL	Marconi Drive water level – LWL
1	11.1 ft	-10.0 ft
2	11.1 ft	-3.0 ft
3	11.1 ft	-10.0 ft
4	11.1 ft	-3.0 ft
5	13.2 ft	-10.0 ft
6	13.2 ft	-3.0 ft
7	13.2 ft	-10.0 ft
8	13.2 ft	-3.0 ft

Note:
Elevation datum = NAVD88
Crack to bottom of wall for Cases 1, 2, 5, and 6.
Crack to top of sand for Cases 3, 4, 7, and 8.

Table 10-2 Calculated Hydraulic Gradients and Factors of Safety Against Erosion – Orleans South				
Case	CWL	LWL	i = vertical hydraulic gradient	F_{erosion} = i_{crit}/i
1	11.1 ft	-10.0	0.20	4.60
2	11.1 ft	-3.0	0.60	1.39
3	11.1 ft	-10.0	0.62	1.48
4	11.1 ft	-3.0	1.03	0.89
5	13.2 ft	-10.0	0.34	2.71
6	13.2 ft	-3.0	0.80	1.15
7	13.2 ft	-10.0	0.82	1.12
8	13.2 ft	-3.0	1.23	0.75

Notes:
Crack to bottom of wall for Cases 1, 2, 5, and 6.
Crack to top of sand for Cases 3, 4, 7, and 8.
With $\gamma_{sat} = 120$ pcf, $i_{crit} = 0.92$

**Table 10-3
Calculated Probabilities of Erosion – Orleans South**

Case	CWL	LWL	F _{erosion}	ΔF	σ _F	F _{MLV}	COV _F	P _{erosion}
1	11.1 ft	-10.0 ft	4.60	3.21	1.60	3.00	56%	3%
2	11.1 ft	-3.0 ft	1.39					
3	11.1 ft	-10.0 ft	1.48	0.59	0.30	1.19	25%	28%
4	11.1 ft	-3.0 ft	0.89					
5	13.2 ft	-10.0 ft	2.71	1.56	0.78	1.93	40%	7%
6	13.2 ft	-3.0 ft	1.15					
7	13.2 ft	-10.0 ft	1.12	0.37	0.18	0.94	19%	66%
8	13.2 ft	-3.0 ft	0.75					

Notes:
 Crack to bottom of wall for Cases 1, 2, 5, and 6.
 Crack to top of sand for Cases 3, 4, 7, and 8.
 ΔF = change in F due to variation in parameter values
 σ_F = standard deviation of factor of safety for the variations considered
 F_{MLV} = most likely value of factor of safety
 COV_F = coefficient of variation of factor of safety
 P_{erosion} = probability of erosion

**Table 10-4
Factor of Safety Against Instability – Orleans South**

Case	CWL	LWL	F _{stability}
1	11.1 ft	-10.0 ft	2.71
2	11.1 ft	-3.0 ft	2.22
3	11.1 ft	-10.0 ft	2.29
4	11.1 ft	-3.0 ft	1.86
5	13.2 ft	-10.0 ft	2.35
6	13.2 ft	-3.0 ft	1.89
7	13.2 ft	-10.0 ft	1.74
8	13.2 ft	-3.0 ft	1.38

Note:
 Crack to bottom of wall for Cases 1, 2, 5, and 6.
 Crack to top of sand for Cases 3, 4, 7, and 8.

**Table 10-5
Probability of Instability – Orleans South**

Case	CWL (ft)	LWL (ft)	ϕ' (deg)	Su marsh Crest/toe psf	F	ΔF	σ_F	F_{MLV}	COV_F	$P_{instability}$
1	11.1	-10.0	38	700/450	2.71	0.49	0.42	2.47	17%	Less than 10^{-7}
2	11.1	-3.0	38	700/450	2.22					
1a	11.1	-10.0	38	875/563	2.96	0.54				
1b	11.1	-10.0	38	525/338	2.42					
1c	11.1	-10.0	34	700/450	2.51	0.41				
1d	11.1	-10.0	42	700/450	2.92					
3	11.1	-10.0	38	700/450	2.29	0.43	0.32	2.08	15%	Less than 10^{-6}
4	11.1	-3.0	38	700/450	1.86					
4a	11.1	-3.0	38	875/563	1.97	0.24				
4b	11.1	-3.0	38	525/338	1.73					
4c	11.1	-3.0	34	700/450	1.67	0.40				
4d	11.1	-3.0	42	700/450	2.07					
5	13.2	-10.0	38	700/450	2.35	0.46	0.35	2.12	17%	Less than 10^{-5}
6	13.2	-3.0	38	700/450	1.89					
6a	13.2	-3.0	38	875/563	2.11	0.47				
6b	13.2	-3.0	38	525/338	1.64					
6c	13.2	-3.0	34	700/450	1.78	0.22				
6d	13.2	-3.0	42	700/450	2.00					
7	13.2	-10.0	38	700/450	1.74	0.36	0.25	1.53	17%	Less than 10^{-2}
8	13.2	-3.0	38	700/450	1.38					
8a	13.2	-3.0	38	875/563	1.42	0.28				
8b	13.2	-3.0	38	525/338	1.14					
8c	13.2	-3.0	34	700/450	1.18	0.22				
8d	13.2	-3.0	42	700/450	1.40					

Notes:
 ΔF = change in F due to variation in parameters for the two conditions
 σ_F = standard deviation of factor of safety for the variations considered
 F_{MLV} = most likely value of factor of safety
 COV_F = coefficient of variation of factor of safety
 $P_{instability}$ = probability of instability

**Table 10-6
Factors of Safety Against Instability – Orleans North**

Case	CWL ft	Clay strength	Su marsh Crest/toe psf	F
1	11.1	$S_u/p = 0.24 \cdot OCR^{0.8}$	650/400	1.62
2	12.8	$S_u/p = 0.24 \cdot OCR^{0.8}$	650/400	1.47

**Table 10-7
Probability of Instability – Orleans North**

Case	CWL ft	Clay strength	Su marsh Crest/toe psf	F	ΔF	σ _F	F _{MLV}	COV _F	p _{instability}
1a	11.1	$S_u/p = 0.30 \cdot OCR^{0.8}$	650/400	1.91	0.59	0.31	1.62	19%	Less than 1 %
1b	11.1	$S_u/p = 0.18 \cdot OCR^{0.8}$	650/400	1.32					
1c	11.1	$S_u/p = 0.24 \cdot OCR^{0.8}$	813/500	1.73					
1d	11.1	$S_u/p = 0.24 \cdot OCR^{0.8}$	488/300	1.51					
2a	12.8	$S_u/p = 0.30 \cdot OCR^{0.8}$	650/400	1.73	0.52	0.28	1.47	19%	2.5%
2b	12.8	$S_u/p = 0.18 \cdot OCR^{0.8}$	650/400	1.21					
2c	12.8	$S_u/p = 0.24 \cdot OCR^{0.8}$	813/500	1.58					
2d	12.8	$S_u/p = 0.24 \cdot OCR^{0.8}$	488/300	1.36					



Figure 10-1. Aerial View of Orleans Avenue Canal – South (Station 8+61)



Figure 10-2. Aerial View of Orleans Avenue Canal – North (Station 64+27)

Orleans Avenue Canal - South
 Station 8+61
 East I-wall

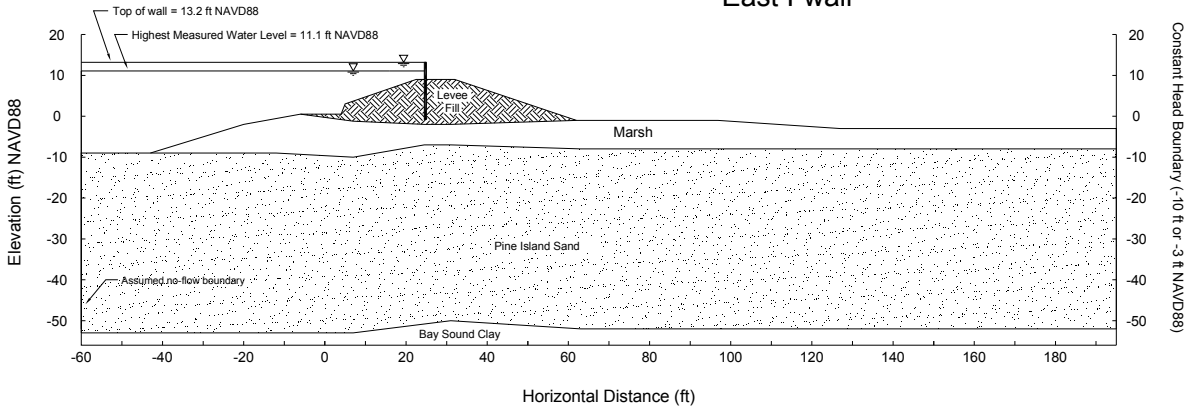


Figure 10-3. Schematic Cross Section at Orleans South, with Seepage Boundary Conditions

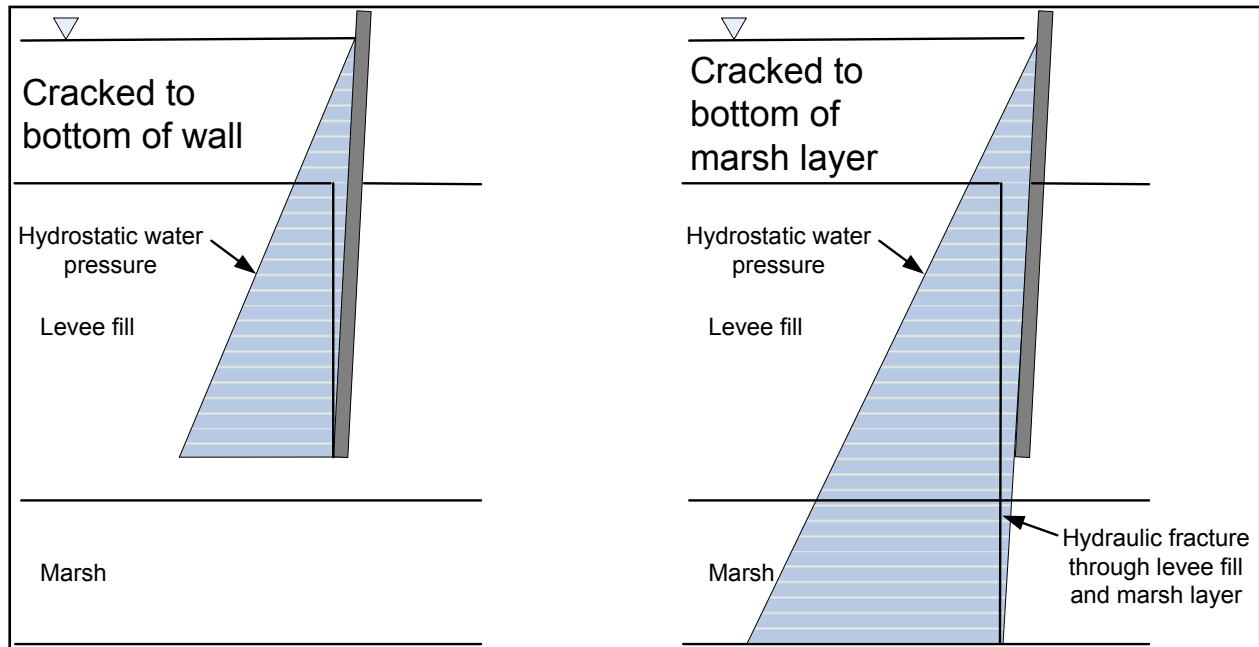


Figure 10-4. Schematic of Cracks Used in Orleans South Seepage and Stability Analyses

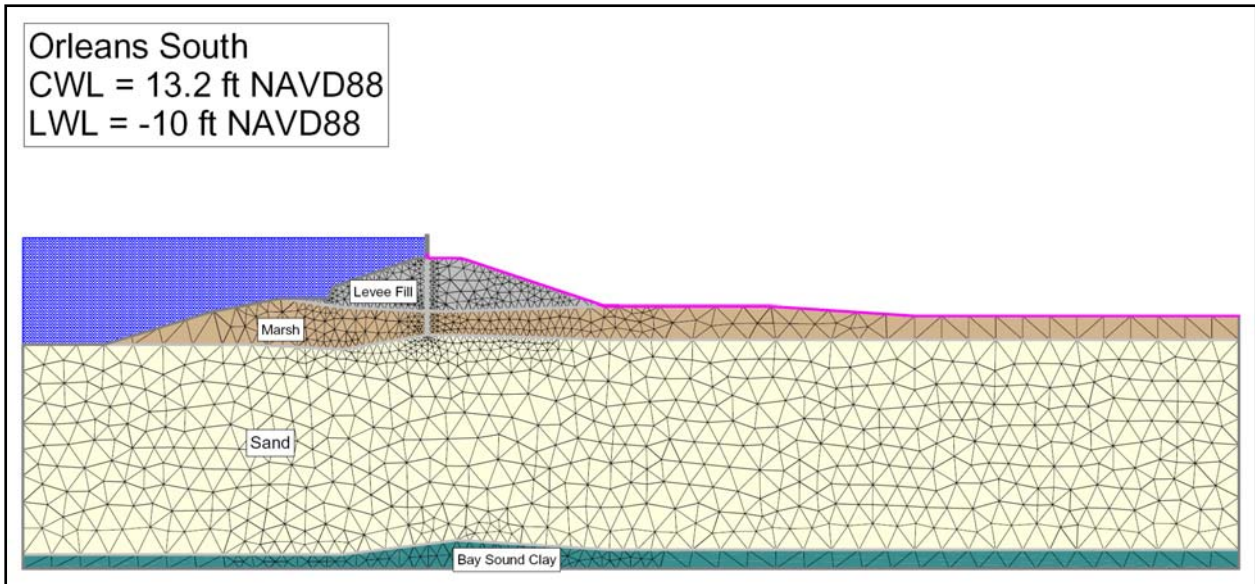


Figure 10-5. Finite Element Mesh Used for Seepage Analysis for Orleans South (Case 7)

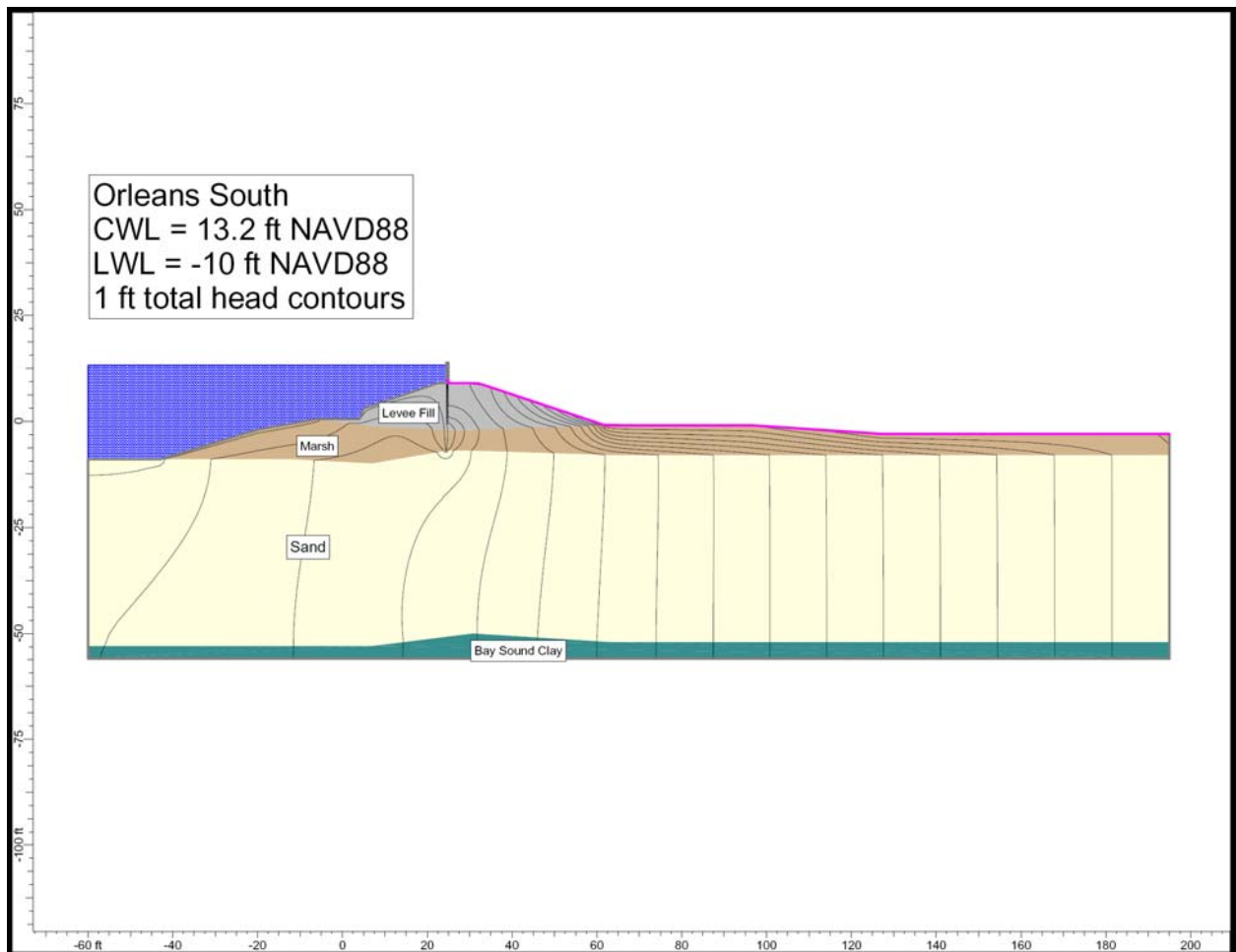


Figure 10-6. Total Head Contours for Orleans South (Case 7)

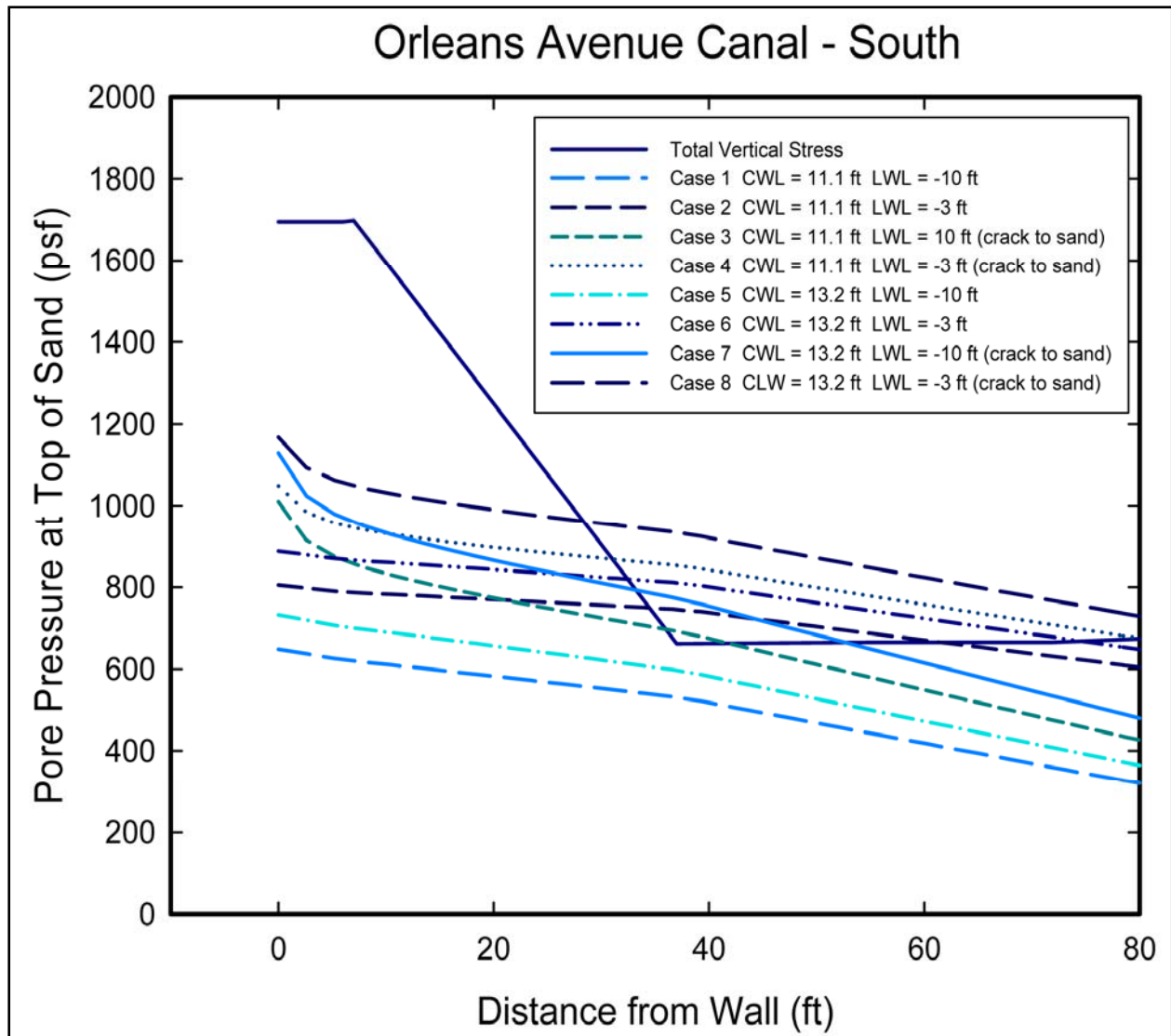


Figure 10-7. Calculated Uplift Pressures and Total Overburden Pressure for Orleans South

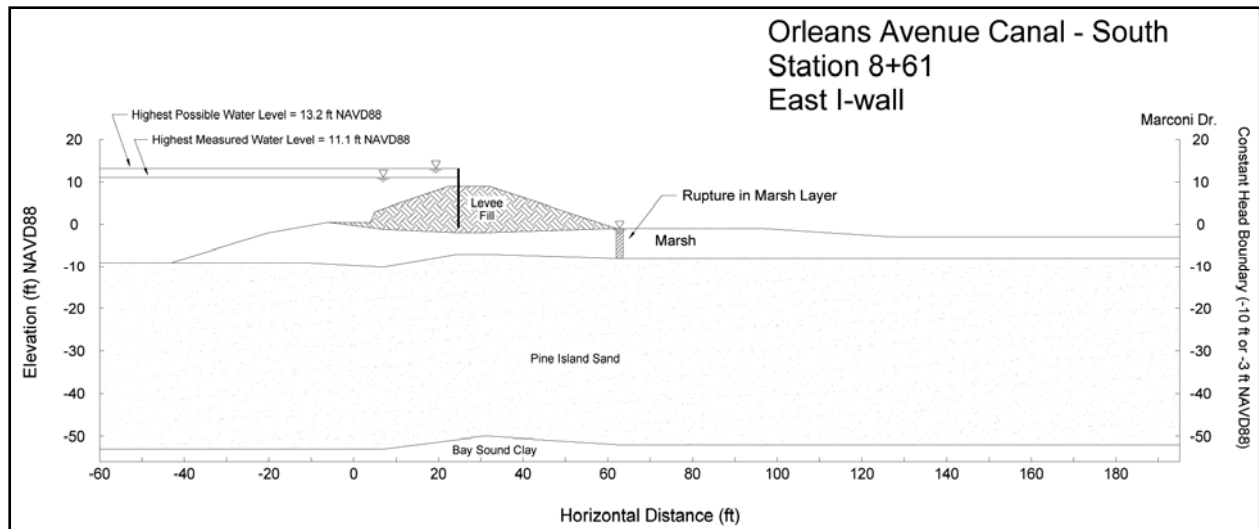


Figure 10-8. Schematic Cross Section for Orleans South, Showing Rupture Through Marsh Layer

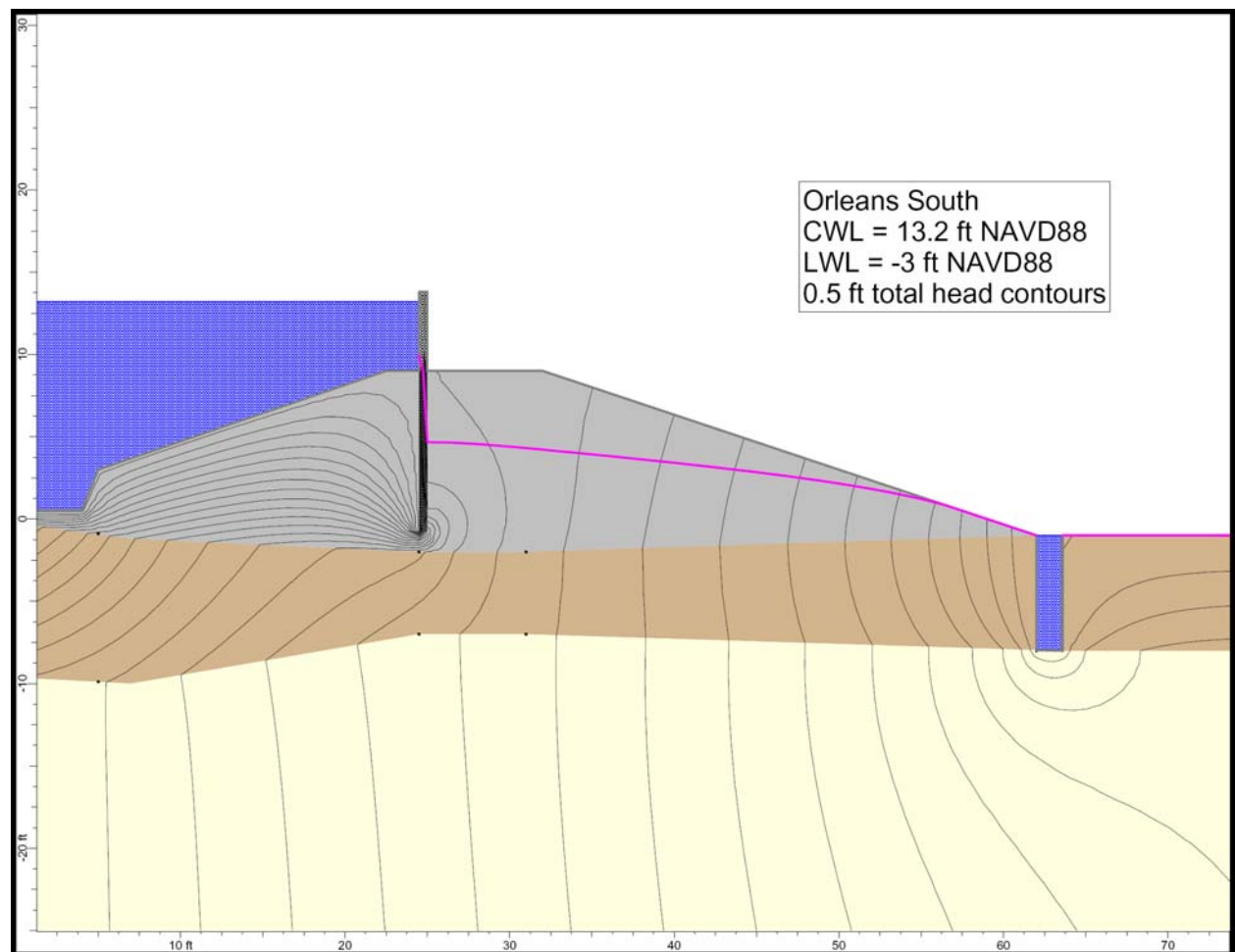


Figure 10-9. Total Head Contours in Vicinity of Rupture for Orleans South (Case 6)

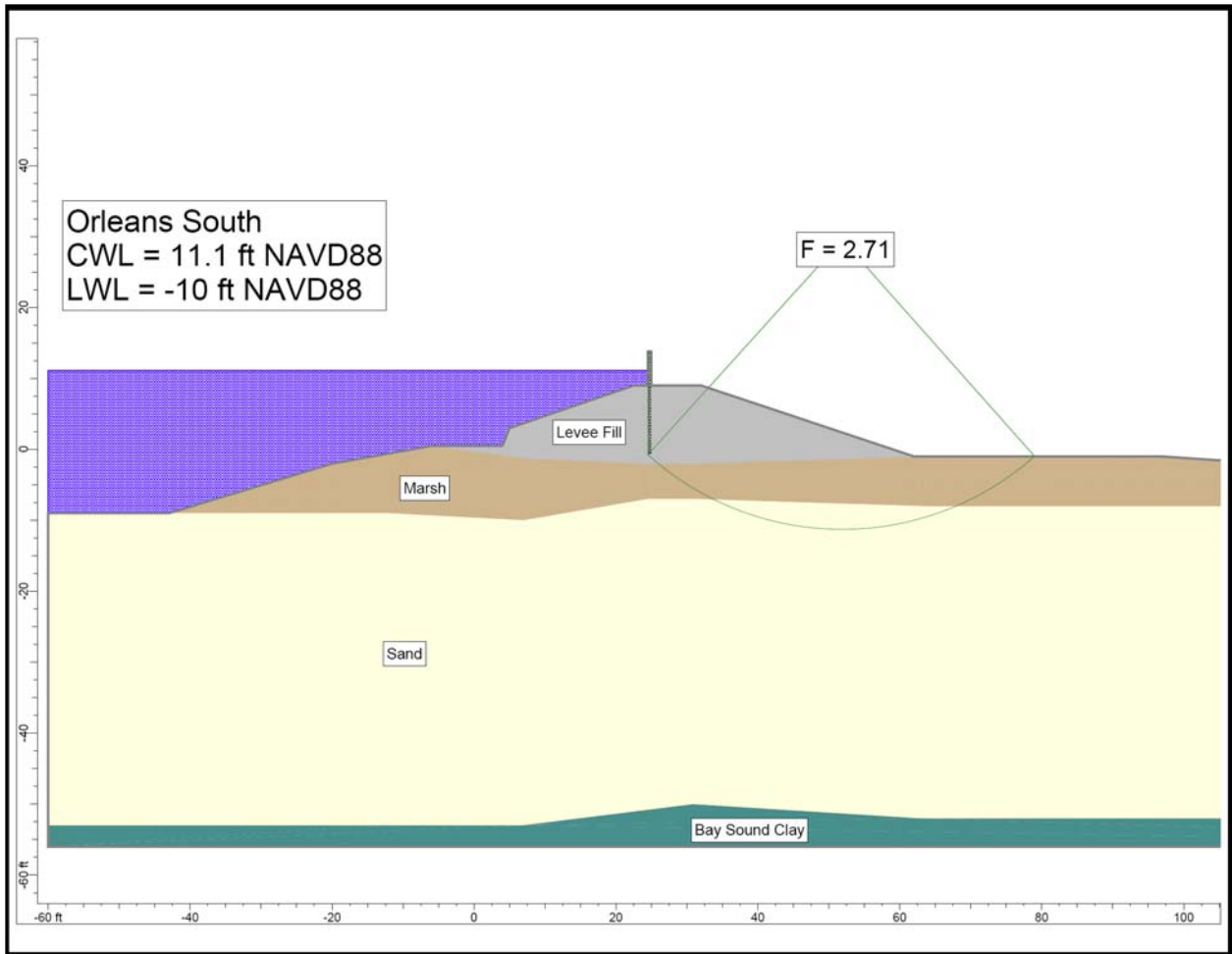


Figure 10-10. Orleans South Case 1 Stability Analysis

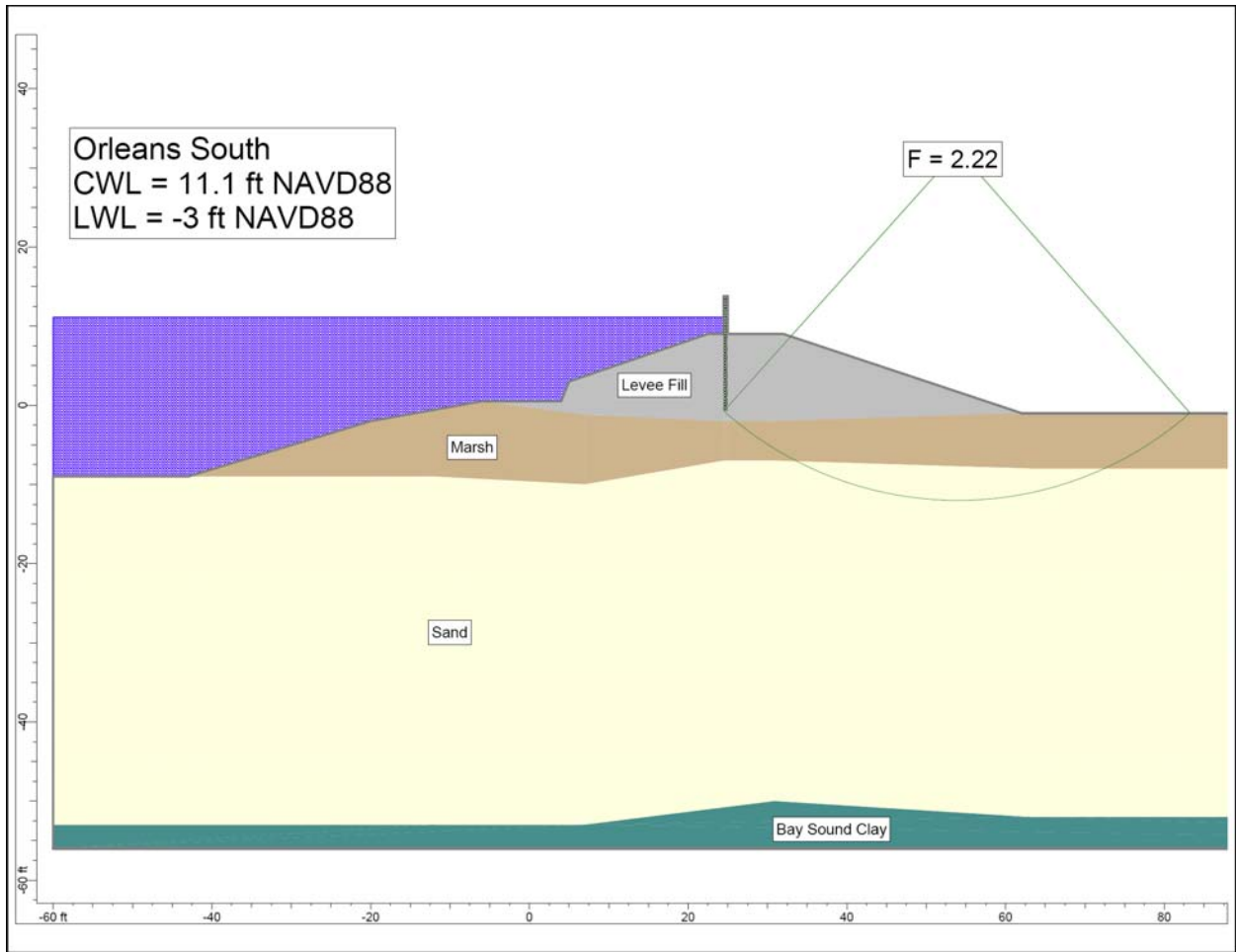


Figure 10-11. Orleans South Case 2 Stability Analysis

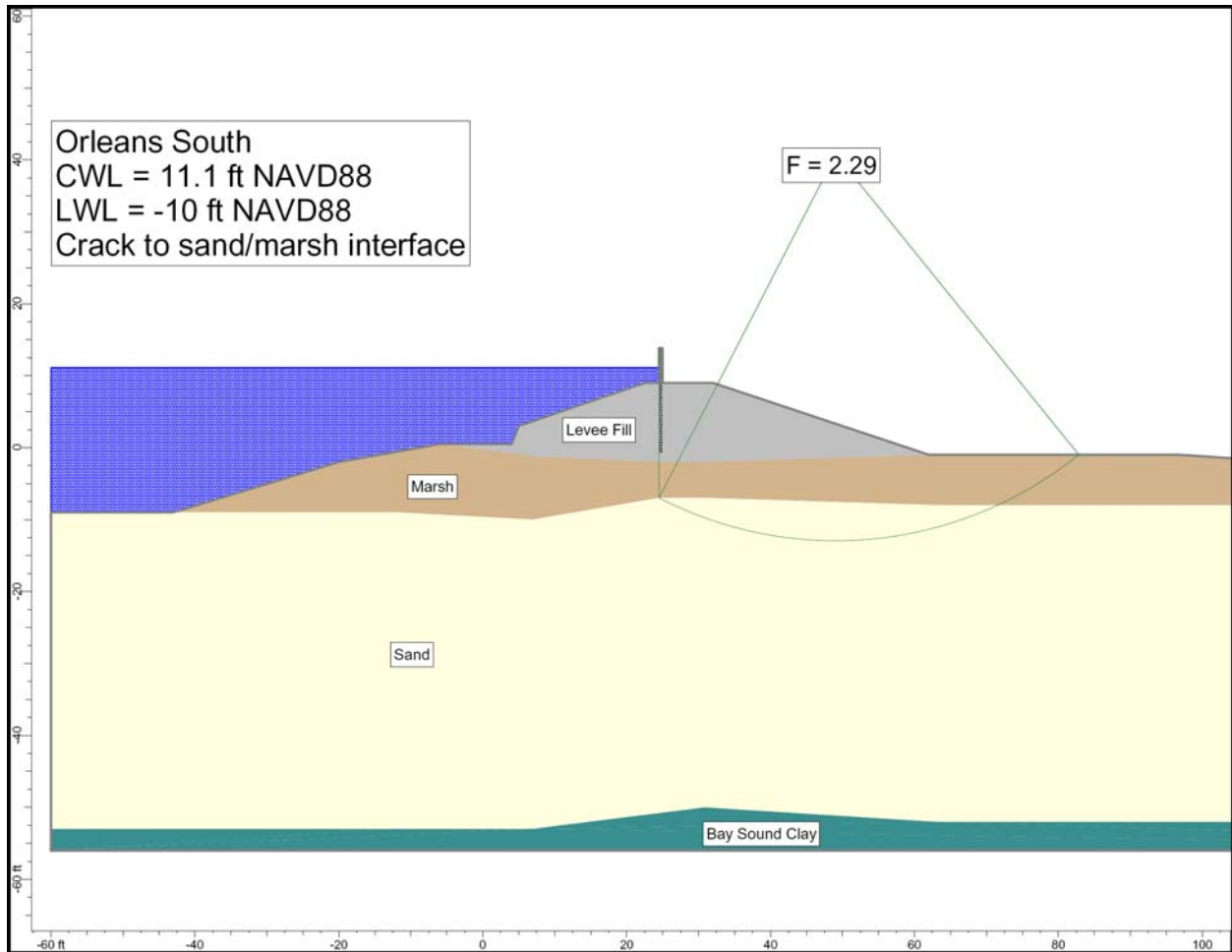


Figure 10-12. Orleans South Case 3 Stability Analysis

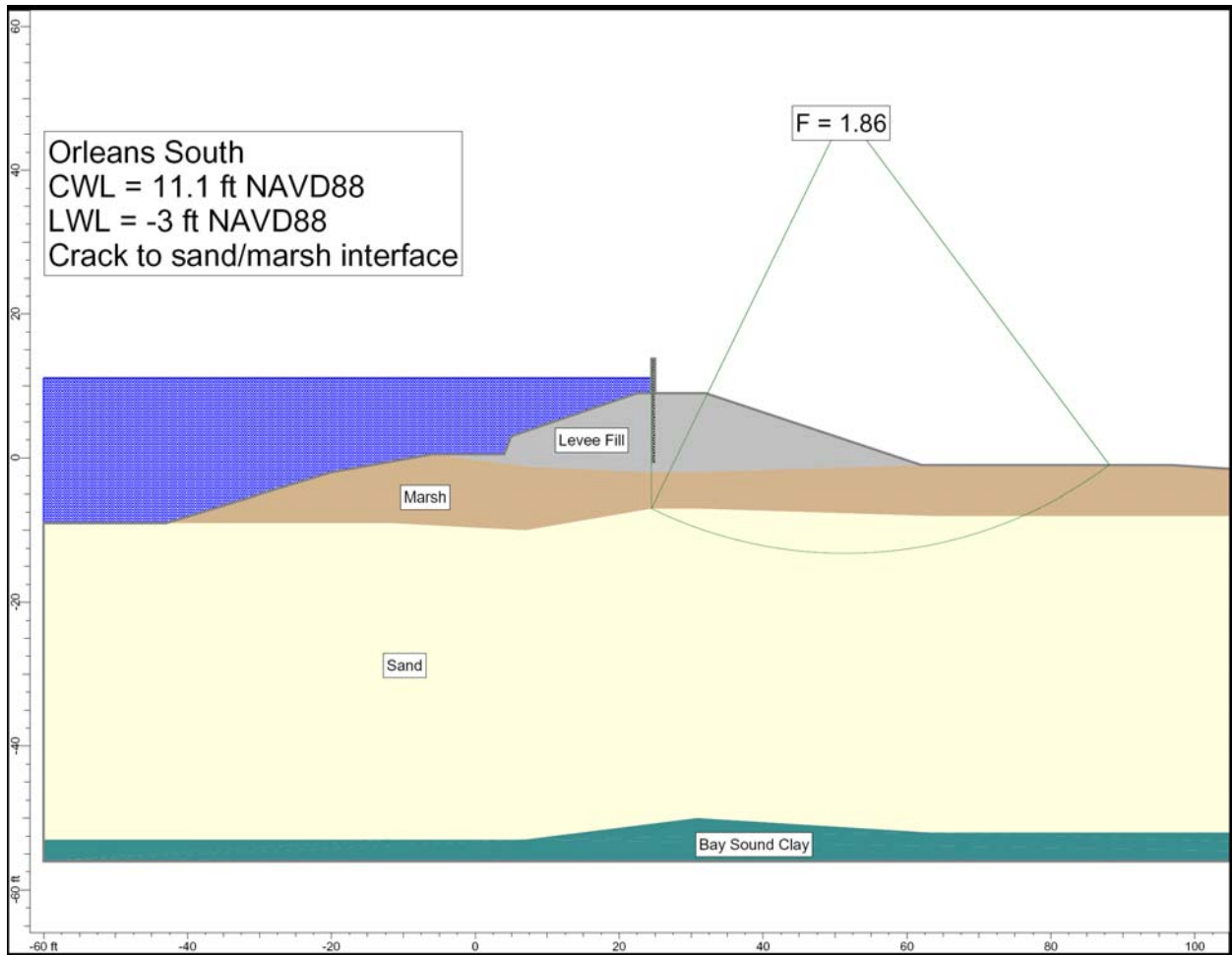


Figure 10-13. Orleans South Case 4 Stability Analysis

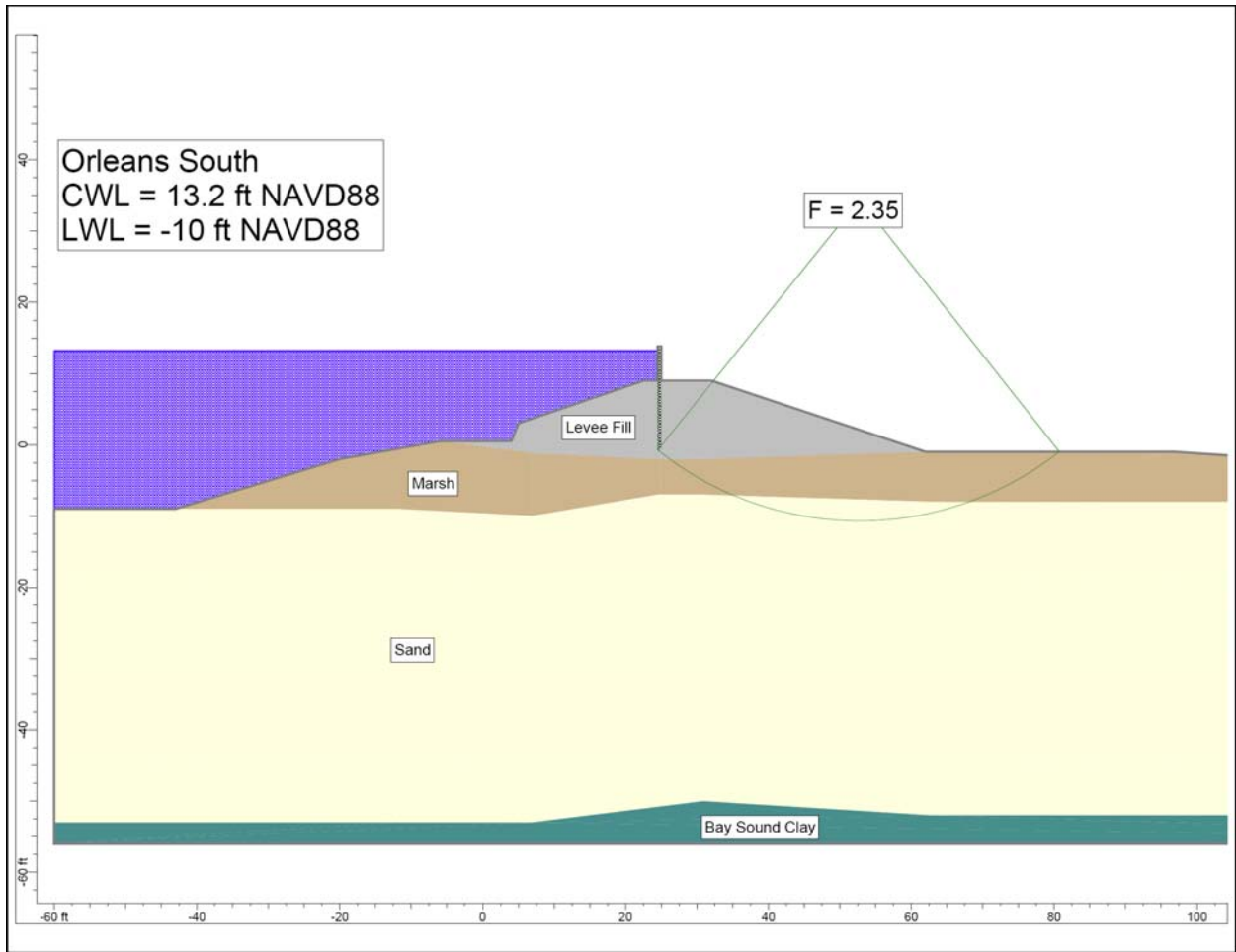


Figure 10-14. Orleans South Case 5 Stability Analysis

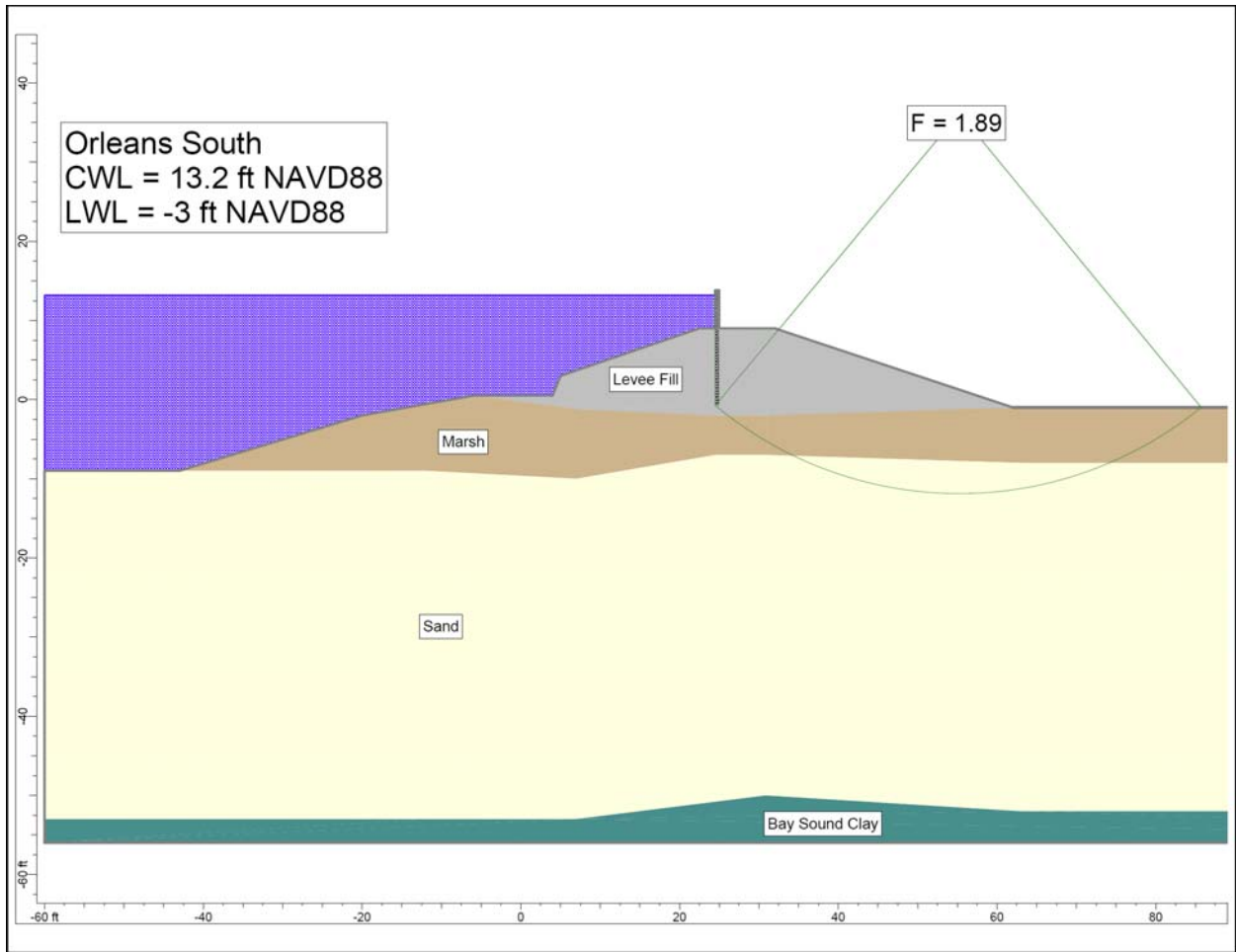


Figure 10-15. Orleans South Case 6 Stability Analysis

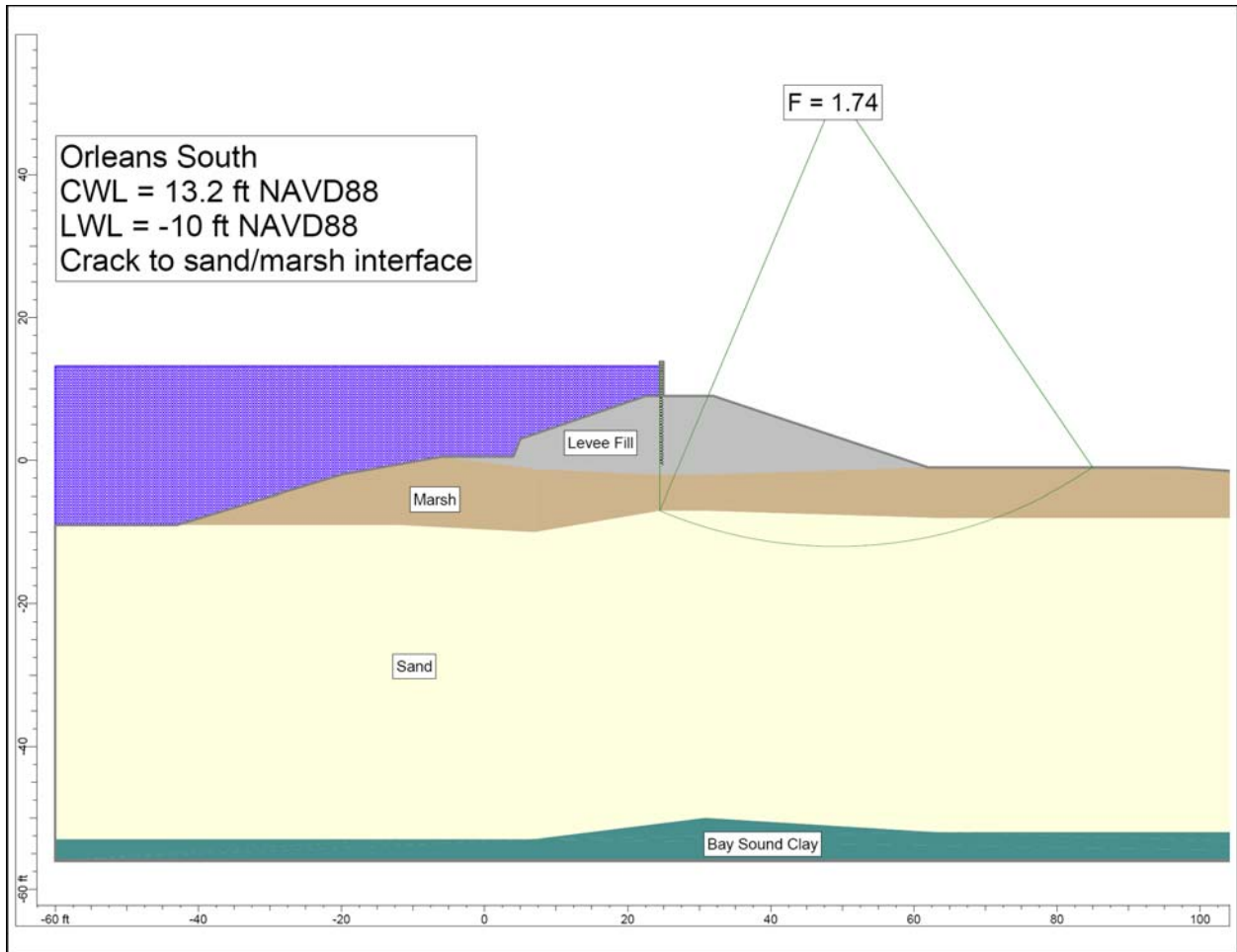


Figure 10-16. Orleans South Case 7 Stability Analysis

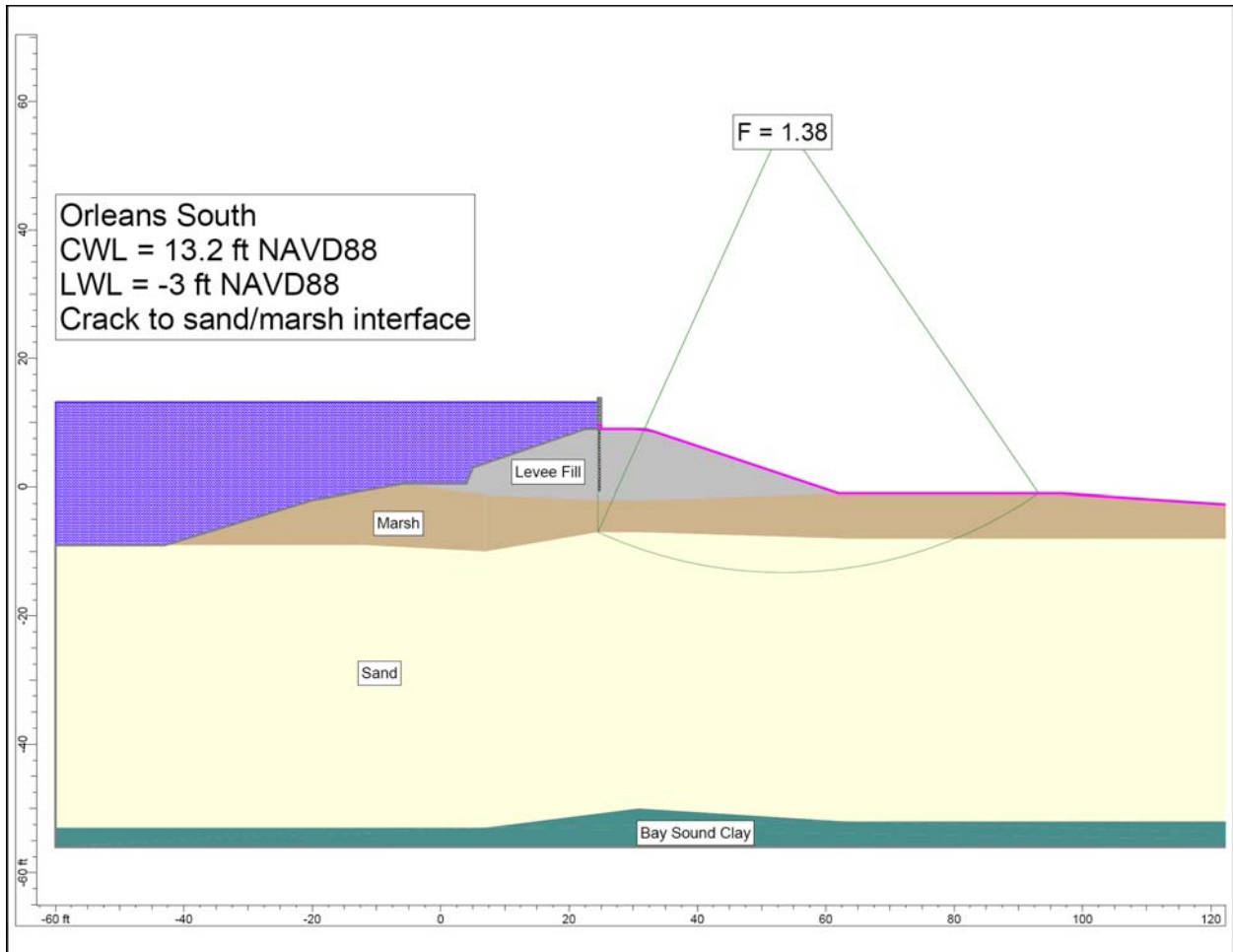


Figure 10-17. Orleans South Case 8 Stability Analysis

Orleans Avenue Canal - North
 Station 64+27
 East I-wall

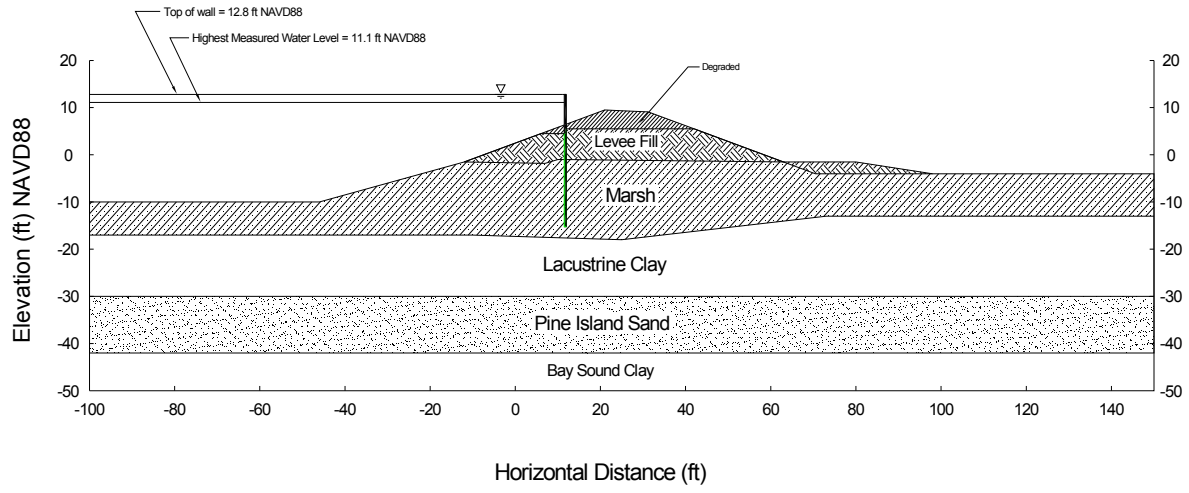


Figure 10-18. Schematic Cross Section of Orleans North

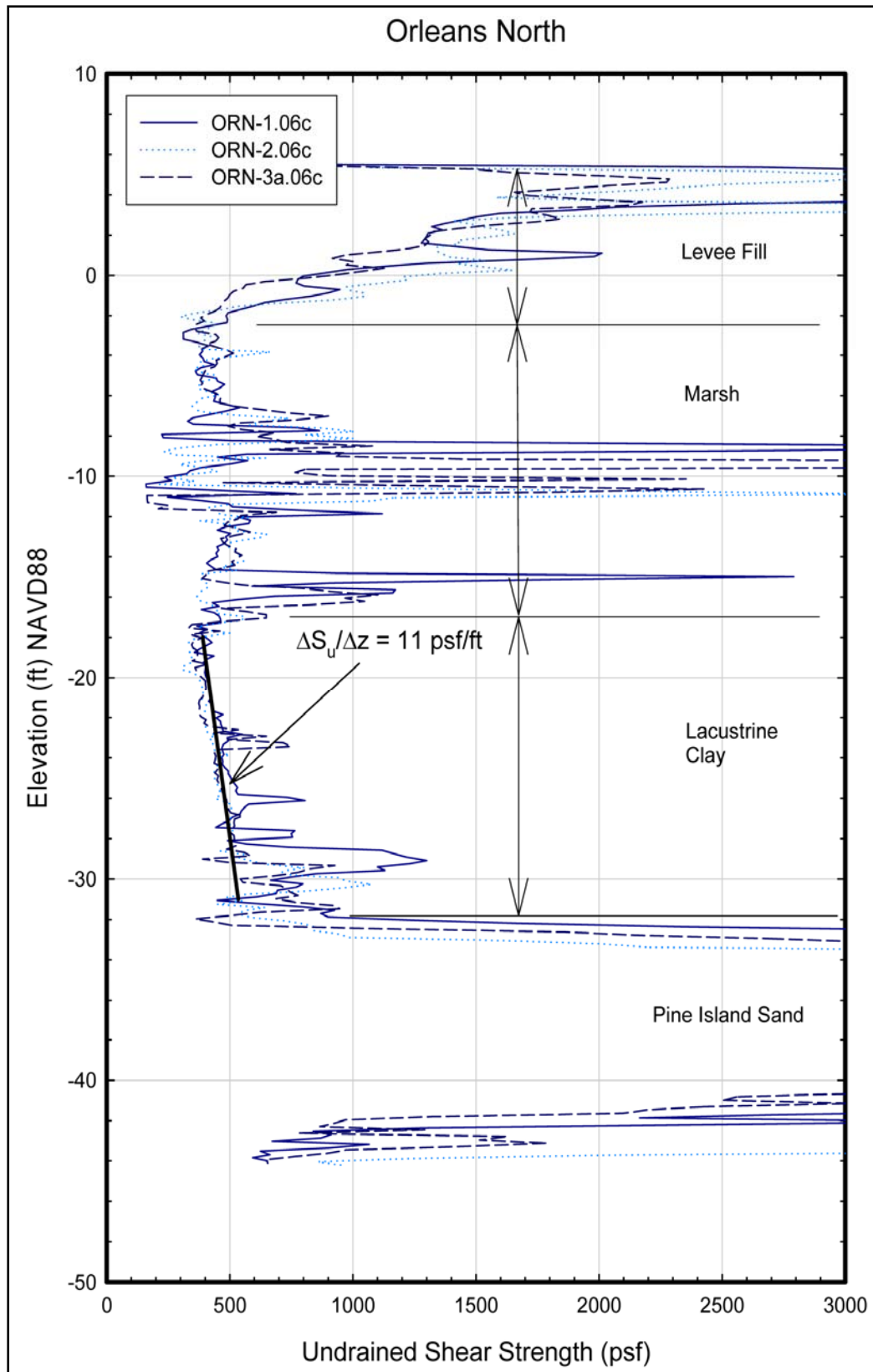


Figure 10-19. Undrained Shear Strength of Clay Calculated from CPTU Tests Using Mayne's Method

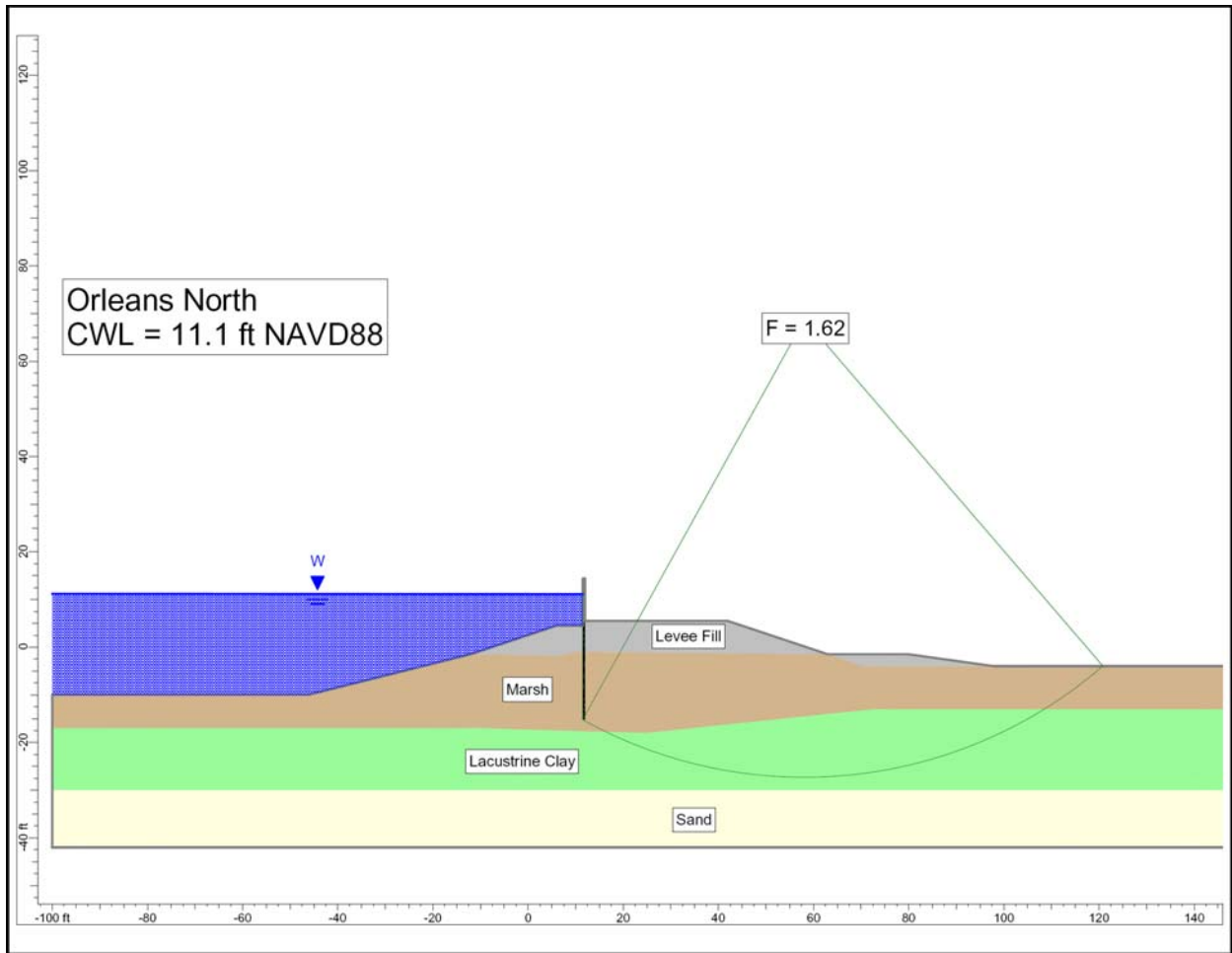


Figure 10-20. Orleans North Case 1 Stability Analysis

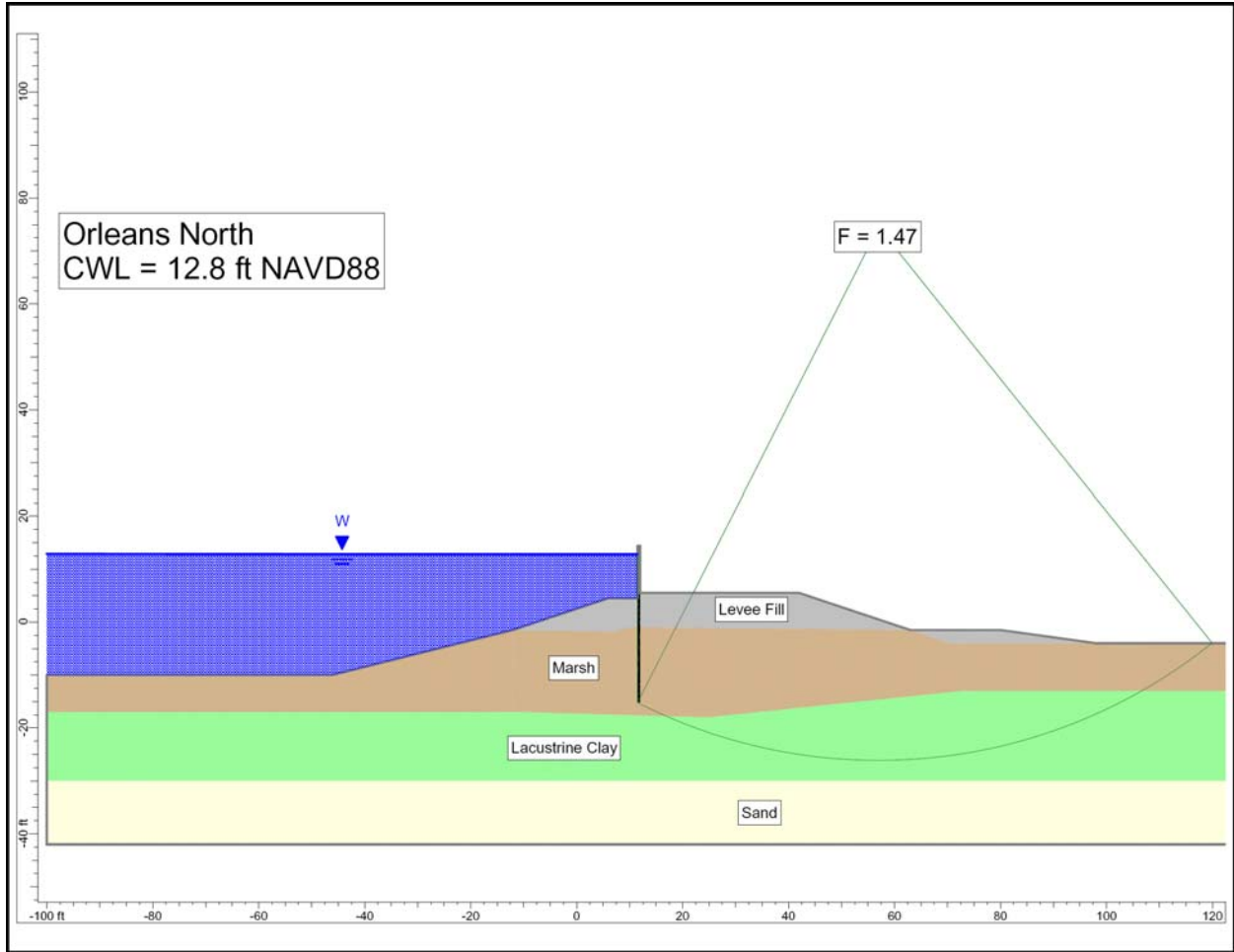


Figure 10-21. Orleans North Case 2 Stability Analysis